Talanta

The International Journal of Pure and Applied Analytical Chemistry

Publication information: *Talanta* (ISSN 0039-9140). For 2008, volumes 74–76 are scheduled for publication. Subscription prices are available upon request from the Publisher or from the Regional Sales Office nearest you or from this journal's website (http://www.elsevier.com/locate/talanta). Further information is available on this journal and other Elsevier products through Elsevier's website: (http://www.elsevier.com). Subscriptions are accepted on a prepaid basis only and are entered on a calendar year basis. Issues are sent by standard mail (surface within Europe, air delivery outside Europe). Priority rates are available upon request. Claims for missing issues should be made within six months of the date of dispatch.

Orders, claims, and journal enquiries: please contact the Customer Service Department at the Regional Sales Office nearest you:
Orlando: Elsevier, Customer Service Department, 6277 Sea Harbor Drive, Orlando, FL 32887-480 USA; phone: (+1) (877) 8397126 [toll free number for US customers], or (+1) (407) 3454020 [customers outside US]; fax: (+1) (407) 3631354; e-mail: usjcs@elsevier.com
Amsterdam: Elsevier, Customer Service Department, PO Box 211, 1000 AE Amsterdam, The Netherlands; phone: (+31) (20) 4853757; fax: (+31) (20) 4853432; e-mail: nlinfo-f@elsevier.com
Tokyo: Elsevier, Customer Service Department, 4F Higashi-Azabu, 1-Chome Bldg, 1-9-15 Higashi-Azabu, Minato-ku, Tokyo 106-0044, Japan; phone: (+81) (3) 5561 5037; fax: (+81) (3) 5561 5047; e-mail: jp.info@elsevier.com
Singapore: Elsevier, Customer Service Department, 3 Killiney Road, #08-01 Winsland House I, Singapore 239519; phone: (+65) 63490222; fax: (+65) 67331510; e-mail: asiainfo@elsevier.com

USA mailing notice: *Talanta* (ISSN 0039-9140) is published monthly by Elsevier B.V. (P.O. Box 211, 1000 AE Amsterdam, The Netherlands). Annual subscription price in the USA US$ 4,085 (valid in North, Central and South America), including air speed delivery. Application to mail at periodical postage rate is paid at Rathway, NJ and additional mailing offices.
USA POSTMASTER: Send address changes to *Talanta*, Publications Expediting Inc., 200 Meacham Avenue, Elmont, NY 11003.
AIRFREIGHT AND MAILING in the USA by Publications Expediting Inc., 200 Meacham Avenue, Elmont, NY 11003.

Talanta 76 (2008) 651–655

Contents lists available at ScienceDirect

Talanta

journal homepage: www.elsevier.com/locate/talanta

Monitoring the synthetic procedures of commercial drugs by ^{2}H NMR spectroscopy: The case of ibuprofen and naproxen

Daniela Acetti, Elisabetta Brenna*, Giovanni Fronza, Claudio Fuganti

Dipartimento di Chimica, Materiali, Ingegneria Chimica, Politecnico di Milano, and Istituto CNR per la Chimica del Riconoscimento Molecolare, Via Mancinelli 7, Milano I-20131, Italy

ARTICLE INFO

Article history:
Received 19 December 2007
Received in revised form 28 March 2008
Accepted 7 April 2008
Available online 16 April 2008

Keywords:
Ibuprofen
Naproxen
NMR
Isotope ratio
Patent infringement

ABSTRACT

We determined the D/H isotope ratios of some ibuprofen and naproxen samples by ^{2}H NMR spectroscopy. Some of these values were found to be useful for collecting hints on the synthetic procedures employed to prepare these drugs. Site-specific isotope ratio analysis shows great potentials in the fight against patent infringement.

1. Introduction

The history of pharma drugs is influenced by new achievements in the field of organic synthetic chemistry. During the last decades the synthetic procedures to even common drugs have been implemented and modified, according to criteria of waste reduction, yield increase, and environment preservation. After the launch of a new drug, a continuous work of research and development is performed, to obtain a low-cost manufacturing process able to compete with generic manufacturers after patent expiration. The new synthetic procedures are protected by process patents, usually expiring far after product patents. Great efforts are devoted to identify process patent infringement, in order to save all the work carried out in the field of research and development by pharma companies.

It is now established that synthetic procedures leave a definite fingerprint in the isotope ratios of the atoms of a molecular structure, and stable isotope analysis has become a well known method [1] to discriminate chemically identical molecules. The technique has been widely employed in food chemistry [2], and it has been now introduced in the pharmaceutical field. In this area most of the work has been carried out by using "bulk" isotope ratios, determined by EA-IRMS, in order to identify individual batches of synthetic drugs and to discriminate different manufacturers [3].

Isotope analysis can be carried out also by using D/H values determined by natural abundance deuterium NMR spectroscopy. This technique offers more punctual information because it allows to detect the effects of the synthetic path on each hydrogen atom of the molecule. Often only a few key positions of a molecule are involved in the reaction mechanism, and only the corresponding D/H ratios are therefore affected. The information on a single position can get lost when overall D/H values are evaluated. The analysis of site-specific isotope ratios can give hints on the particular reactions employed in a synthetic procedure, and not simply help in identifying the manufacturer. We have recently applied this technique to ecstasy [4], methamphetamine [5] and fluoxetine [6] samples.

Ibuprofen and naproxen are widely employed non-steroidal anti-inflammatory drugs (NSAID), and their syntheses have been implemented through the years. Recently, Jasper and collegues [7] have studied the stable isotope composition (δD, δ^{13}C, and δ^{18}O determined by IRMS) of several naproxen samples from six different manufacturers. Bivariate and trivariate isotope ratio graphs showed marked clustering of the data for five out six naproxen manufacturers.

We had in our hands some ibuprofen and naproxen samples. We recorded their deuterium NMR spectra and measured the site-specific deuterium isotope ratios. We now wish to discuss these data with reference to the known synthetic procedures.

* Corresponding author. Tel.: +39 02 23993027; fax: +39 02 23993080.
E-mail addresses: elisabetta.brenna@polimi.it (E. Brenna), giovanni.fronza@polimi.it (G. Fronza).

0039-9140/$ – see front matter © 2008 Elsevier B.V. All rights reserved.
doi:10.1016/j.talanta.2008.04.009

2. Experimental

2.1. Chemicals

The following commercial products were employed: (A) 4-isobutyl-α-methylphenylacetic acid, Aldrich, code 28,474–2, lot no. 04702HV; (B) (S)-(+)-ibuprofen, Fluka, code 58635, lot no. 357891/1; (C) the sample was obtained by acidification of ibuprofen sodium salt, Sigma, code I1892, lot no. 085K0716; samples (D–I) were extracted from the following preparations: (D) *Ibuprofen*, tablets 200 mg (Sunmark, lot no. 6FE0758); (E) *Brufen* 600 mg (Abbott s.p.a. – Campoverde di Aprilia, Italy, lot no. 14690TB21); (F) *Midol Cramps & Body Aches*, tablets 200 mg (Bayer, lot no.6FE0758); (G) *Motrin IB*, tablets 200 mg (McNeil, lot no. MCA186); (H) *Ibuprofen IB*, tablets 200 mg (Sunmark, lot no. 6FE0224) and (I) *Advil*, tablets 200 mg (Wyeth, lot no. B369940).

Sample J was prepared according to the Boots procedure reported in ref. [8]. Sample K was prepared by Ag_2O oxidation of aldehyde **2** prepared by Darzen reaction according to ref. [9].

Alcohol **3a** was obtained by reduction of ketone **1** with $NaBH_4$ at 0 °C in CH_2Cl_2–MeOH (2/1) solution. Alcohol **3b** was obtained by reduction of ketone **1** with $LiAlH_4$ in THF at room temperature. Alcohol **3c** was obtained by reduction of ketone **1** with molecular hydrogen according to ref. [10].

Naproxen samples were extracted from the following preparations: (L) *ALDRICH*, (+)-naproxen, not for drug use, code 28,478–5; (M) *Aleve*, tablets 220 mg, Roche Pharma – Madrid, lot no. E6952; (N) *Naprosyn*, suppositories 500 mg, Recordati – Milano, lot no. MO01; (O) *Momendol*, tablets 220 mg, Angelini Francesco – Roma, lot no. 180; (P) *Naproxene PLIVA* 500 mg, tablets 500 mg, Pliva Pharma – Milano, lot no. 6924. All naproxen samples were converted into the corresponding methyl ester by treatment with K_2CO_3 and CH_3I in acetone.

2.2. ^2H NMR measurements

The ^2H experiments were performed on a Bruker DRX 500 spectrometer equipped with a 10 mm probe head and a ^{19}F lock channel (C_6F_6), under CPD (Waltz 16 sequence) proton decoupling conditions at the temperature of 308 K. The spectra were recorded dissolving 0.5–0.6 g of material in ca. 3.0 mL of solvent adding ca. 40 μL of C_6F_6 for the lock. The ibuprofen samples were dissolved in CH_2Cl_2 using 130–160 mg of hexamethyldisiloxane as internal standard while the naproxen methyl ester samples were dissolved in C_6H_6 adding as internal standard a known quantity of certified TMU (tetramethylurea) (Institute for Reference Materials and Measurements, (D/H) 84.5 ppm). The solvent C_6H_6 was used also for the samples of alcohol **3** with hexamethyldisiloxane as standard. The (D/H) of hexamethyldisiloxane was determined by calibration against TMU (130.7 ppm).

The signal assignments of ibuprofen, naproxen methyl ester and alcohol **3** spectra, performed in the same conditions used for the deuterium spectra, are the following: ibuprofen (CH_2Cl_2, δ, ppm) 12.15 (1H, s br, COOH), 7.29 and 7.18 (4H, d, J = 7.9 Hz, phenylene hydrogens), 3.78 (1H, q, J = 7.5 Hz, CHMe), 2.52 (2H, d, J = 7.0 Hz, isobutyl CH_2), 1.91 (1H, m, isobutyl CH), 1.54 (3H, d, J = 7.1 Hz, CH_3), 0.97 (6H, d, J = 6.8 Hz, isobutyl CH_3); naproxen methyl ester (C_6H_6, δ, ppm) 7.61–6.90 (6H, m, naphthalene ring protons), 3.71 (1H, q, J = 7.2 Hz, CH), 3.40 (3H, s, OCH_3), 3.31 (3H, s, OCH_3 ester), 1.51 (3H, d, J = 7.2 Hz, CH_3); alcohol **3** (C_6H_6, δ, ppm) 7.21 and 6.99 (4H, d, J = 7.9 Hz, phenylene hydrogens), 4.65 (1H, q, J = 6.7 Hz, CHMe), 3.59 (1H, s br, OH), 2.36 (2H, d, J = 7.3 Hz, isobutyl CH_2), 1.77 (1H, m, isobutyl CH), 1.33 (3H, d, J = 6.7 Hz, CH_3), 0.85 (6H, d, J = 6.9 Hz, isobutyl CH_3). Two–three spectra were run for each sample collecting about 10,000 scans using the following parameters: 5.9 s acquisition time, 1380 Hz spectral width, 16 K time domain and 2 s delay. In these conditions the signal/noise ratio calculated for the CH peaks using a FID exponential multiplication of 1.0 Hz is always superior to 15. An estimation of the relaxation times (T_1) of the deuterium nuclei showed that the longest T_1 is that of the hexamethyldisiloxane reference material (ca. 1.0 s). Thus the total time of 7.9 s between successive pulses is sufficiently long to allow the complete nuclear relaxation. Each FID was repeatedly Fourier transformed with a line broadening of 1–2 Hz, manually phased and integrated after an accurate correction of the spectrum baseline. For partially overlapped signals the peak areas were determined through the deconvolution routine of the Bruker TopSpin NMR software using a Lorentzian line shape.

The absolute values of the site-specific (D/H) ratios were calculated according to the formula:

$$\left(\frac{D}{H}\right)_i = n_{WS} g_{WS} MW_L \; S_i \frac{(D/H)_{WS}}{n_i \; g_L \; (MW_{WS}) S_{WS}}$$

where WS stands for the working standard with a known isotope ratio $(D/H)_{WS}$ and L for the product under examination; n_{WS} and n_i are the number of equivalent deuterium atoms of the standard and of the ith peak; g_{WS} and g_L are the weights of the standard and the sample; MW_L and MW_{WS} are the corresponding molecular weights; S_i and S_{WS} are the areas of the ith peak and of the standard, respectively.

3. Results

3.1. Synthetic routes to ibuprofen and naproxen

Ibuprofen was first introduced in the UK in 1969 by the Boots Company PLC under the trade name Brufen, and it is now sold under several trade names such as Advil, Motrin and Nuprin.

The two most successful ways to obtain ibuprofen are the Boot process (Scheme 1) and the BHC process (Scheme 2). The first one was patented by the Boots Company in 1968 [8] and has been the method of election for the preparation of ibuprofen over the past decades. The second one was developed in the middle of the eighties [10] by the BHC company, a joint venture of the Hoechst Celanese corporation and the Boots Company. This three-step process won the prestigious Presidential Green Chemistry Challenge Award in 1997 [11]. It has been estimated that the plant operating on this process produces approximately 20–25% of the world's yearly supply of ibuprofen, which is sold to 25 pharmaceutical companies who market ibuprofen as generic [12].

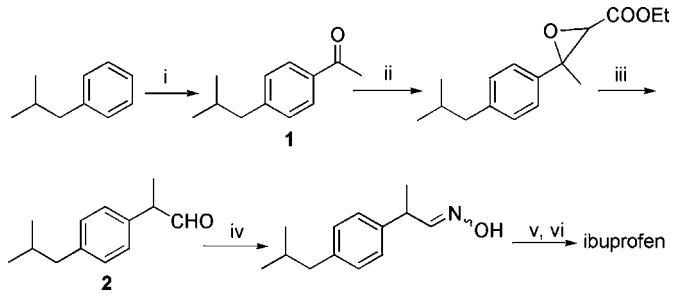

Scheme 1. (i) Ac_2O, $AlCl_3$, (ii) *t*-BuOK, $ClCH_2COOEt$, (iii) H_3O^+, Δ, (iv) NH_2OH, (v) Ac_2O, and (vi) OH^-, Δ.

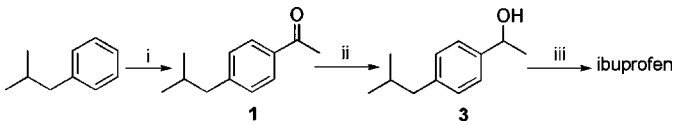

Scheme 2. (i) Ac_2O, $AlCl_3$, (ii) H_2 Ni-Raney, and (iii) CO, Pd – catalyst.

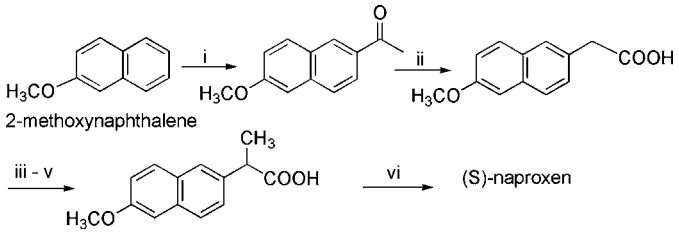

Scheme 3. (i) CH_3COCl, $AlCl_3$, (ii) morpholine, S, then H^+, (iii) H_2SO_4, MeOH, (iv) NaH, CH_3I, (v) NaOH, and (vi) cinchonidine.

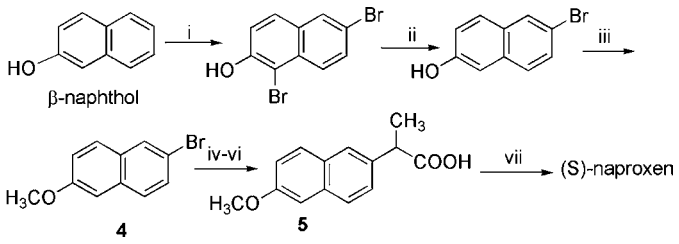

Scheme 4. (i) Br_2, (ii) $NaHSO_3$, (iii) CH_3Cl, base, (iv) Mg, (v) $ZnCl_2$, ethyl bromopropionate, (vi) base, and (vii) cinchonidine.

Both these routes employ isobutylbenzene as a starting material which is submitted to Friedel–Crafts acylation with acetic anhydride and aluminum chloride. The Boots process takes advantage of the Darzens reaction of ketone **1**, followed by hydrolysis and decarboxylation, to obtain aldehyde **2**, which is converted into the corresponding acid (ibuprofen) by the oxime route. The BHC process submits ketone **1** to hydrogen reduction to obtain alcohol **3**, which is then reacted with carbon oxide in the presence of a palladium catalyst.

(S)-Naproxen was introduced to the market by Syntex in 1976, and it is still commercialized in a single enantiomer form with the brand name of Naprosyn, Aleve, Anaprox, Naprogesic, Naprelan, Synflex. The first large scale synthesis [13] of Naproxen is depicted in Scheme 3. 2-Methoxynaphthalene was the starting material, and a final classical resolution step with cinchonidine was employed to obtain the right enantiomer.

The first manufacturing process working from 1972 to 1975 was completely different [14] (Scheme 4). β-Naphthol was the starting material and was brominated, reduced and alkylated with methyl chloride in basic medium, to afford compound **4**. This latter was converted into a Grignard reagent, transmetalated with zinc chloride and coupled with ethylbromopropionate, to afford compound **5**. This method was later improved and in the manufacturing process working from 1976 to 1993 the Grignard reagent obtained from **4** was coupled directly with a salt of bromopropionic acid, to give **5**. Improvements were also brought about in the following years in the final resolution step.

The actual Syntex resolution technology [14] is based on the racemisation of the unwanted enantiomer in basic medium and on the use of a N-alkylglucamine as a resolving agent.

In the eighties attempts were made to develop enantioselective synthesis of (S)-naproxen. One of the most outstanding example is the Zambon process [15] (Scheme 5). 2-Methoxy-6-propionylnaphthalene was prepared by Friedel-Crafts acylation of 2-methoxynaphthalene. Ketalization with (R,R)-dimethyl tartrate, bromination of the activated methylene, and ester hydrolysis afforded a 92:8 mixture of diastereoisomers **6**. This mixture of diastereoisomers was heated to 90 °C to produce an upgraded mixture of 1-bromonaproxen esters **7**. Reduction of the bromo substituent and ester hydrolysis afforded (S)-naproxen (ee >98%). An enantioselective hydrogenation of acrylic acid **8** by means of a tol-BINAP based catalyst was also described (Scheme 6) [16].

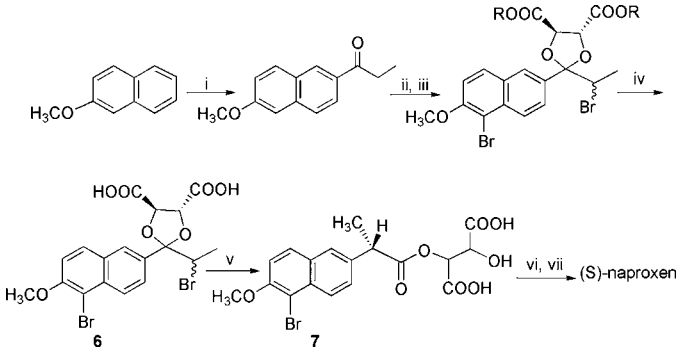

Scheme 5. (i) EtCOCl, $AlCl_3$, (ii) (R,R)-dimethyltartrate, (iii) Br_2, (iv) hydrolysis, (v) 90 °C, H_2O, (vi) H_2, and (vii) H_3O^+.

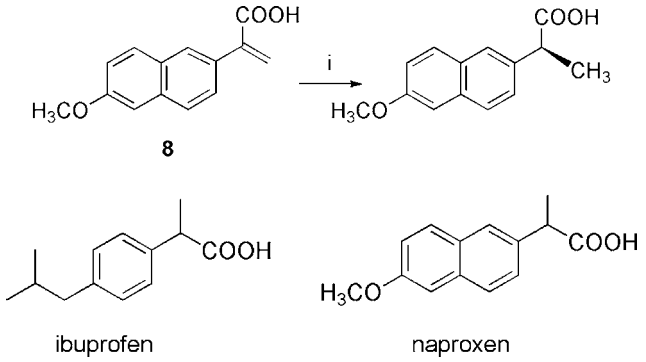

Scheme 6. (i) H_2 catalyst.

3.2. D/H Isotope ratios of ibuprofen samples

We collected 11 ibuprofen samples having the following origin (see also Section 2). Samples A and B were commercial products sold as chemicals not for drug use; sample C was prepared in our laboratory by acidification of a commercial ibuprofen sodium salt; samples D–I were extracted from commercial brand and generic drug tablets. Sample J was prepared in our laboratory following the Boots' process (Scheme 1), based on aldehyde **2** which was obtained through the Darzens route. Sample K was prepared by Ag_2O oxidation of same key aldehyde **2**. The 11 samples were submitted to ^2H NMR spectroscopy and the corresponding D/H values were evaluated (Table 1). The analysis of the data reported in Table 1 shows no significant variation of the D/H values for the aromatic hydrogens, determined as a whole, and for the hydrogens of the isobutyl moiety: isobutyl benzene is the starting material in both the main routes to commercial ibuprofen (Boots and BHC processes).

The analysis of the $D/H_{(CH3)}$ values show no great variation, excluding samples A, B, and K. The methyl group comes from isobutylacetophenone both in Boots and BHC process, and it is not submitted to variation in the course of the synthetic procedures.

In Fig. 1 the $D/H_{(CH)}$ values of ibuprofen samples are reported. The eleven samples can be grouped in three groups: (i) samples A–C, H and J, (ii) D–G and I, and (iii) K. The difference between the first two groups was found to be highly significant by two tails *t*-test ($p = 5 \times 10^{-5}$).

We can tentatively conclude that samples A, B, C, and H have been prepared like sample J through the Darzens and oxime route, while samples D–G, and I seem to come from the hydrogenation and carbonylation sequence. The mean value of $D/H_{(CH)}$ is 166 ppm for the first group and 116 ppm for the second one. This is in accordance with the fact that hydrogen atoms inserted by means of molecular hydrogen generally show a low deuterium content [4–6].

Table 1
$(D/H)_i$ isotope ratios (ppm) of ibuprofen samples

Sample	$D/H_{(aromatic)}$	$D/H_{(CH)}$	$D/H_{(CH3)}$	$D/H_{(CH2\text{-}isob)}$	$D/H_{(CH\text{-}isob)}$	$D/H_{(CH3\text{-}isob)}$
A	178.3 (1.6)	169.3 (4.6)	158.8 (1.9)	150.7 (1.7)	149.3 (2.5)	127.7 (0.5)
B	175.6 (1.5)	163.3 (4.3)	143.7 (0.8)	157.1 (1.9)	154.2 (3.4)	131.2 (1.1)
C	178.1 (1.7)	167.2 (5.1)	133.5 (3.1)	156.9 (3.0)	159.5 (3.3)	132.8 (1.4)
D	170.8 (2.4)	117 (5.2)	126.3 (2.6)	161.2 (1.9)	156.6 (3.7)	133.2 (1.4)
E	170.5 (1.9)	129.8 (4.4)	126.2 (2.1)	163.9 (1.4)	158.3 (4.7)	134.4 (1.0)
F	165.3 (1.6)	118.7 (1.0)	124.5 (1.7)	157.6 (2.2)	152.2 (4.7)	130.4 (0.7)
G	177.9 (2.6)	103.4 (4.4)	122.2 (1.1)	151.3 (1.4)	149.6 (5.8)	129.4 (1.4)
H	175.6 (0.9)	178.8 (3.1)	132.4 (0.6)	150.9 (2.5)	153.2 (3.6)	131 (1.0)
I	162.9 (2.1)	109.8 (5.8)	123.8 (0.6)	153.6 (2.3)	153.2 (3.9)	130.9 (0.4)
J	172.9 (1.2)	150.6 (3.3)	129.1 (1.0)	153 (1.2)	150.4 (1.2)	134.3 (2.0)
K	174.9 (1.0)	328.4 (2.7)	141.8 (0.9)	152.6 (0.9)	153.9 (1.6)	132.9 (0.4)

The $(D/H)_i$ standard deviations are reported within parentheses.

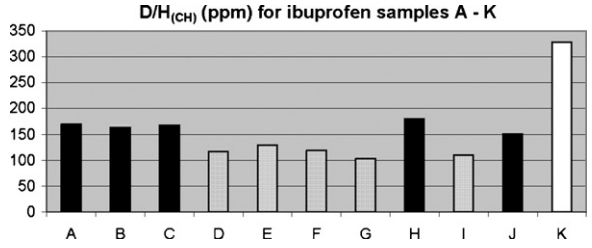

Fig. 1. $D/H_{(CH)}$ (ppm) for samples A–K.

These considerations are supported by the analysis of the D/H values of alcohol **3** (Table 2) prepared from isobutylacetophenone according to three different reduction procedures (see Section 2). Sample **3a** was obtained by $NaBH_4$ reduction; sample **3b** was prepared by reaction with $LiAlH_4$, and sample **3c** was obtained by hydrogenation with molecular hydrogen. As we had already observed and discussed [6], the reduction with molecular hydrogen or with $LiAlH_4$ gave the insertion of a deuterium depleted hydrogen atom in benzylic position ($D/H_{(CH)}$ = 53.9 ppm and 62 ppm), while the use of $NaBH_4$ brought to a much higher $D/H_{(CH)}$ value (144.6 ppm). $D/H_{(CH3)}$ values for alcohols **3a** and **3b** are similar to those calculated for most ibuprofen samples.

A surprisingly high value of $D/H_{(CH)}$ (328.4 ppm) was found for the benzylic position of sample K, obtained by Ag_2O oxidation of aldehyde **2**. This deuterium enrichment of the benzylic position seems to be due to isotope effects connected with the oxidation of the aldehydic moiety in basic medium.

3.3. D/H Isotope ratios of naproxen samples

We extracted five naproxen samples from commercial brand and generic drug tablets. The five samples were esterified with K_2CO_3 and CH_3I in acetone, submitted to ^2H NMR spectroscopy and the corresponding D/H values were evaluated (Table 3). D/H of aromatic hydrogens could not be determined because ^2H NMR spectra were recorded in benzene. Naproxen is sold as a single enantiomer and, in the synthetic sequences where classical resolution is employed, epimerisation of the unwanted enantiomer is exploited to enhance yields. Thus, the hydrogen atom in benzylic position of naproxen is submitted to equilibrium exchange and its deuterium content is strongly influenced by epimerisation conditions. No synthetic information can be obtained from the D/H_{CH} values. The analysis of D/H for the various positions of naproxen methyl ester shows that the only interesting data are those of the methoxy group of the naphthyl moiety. They clearly resemble the two possible origins of the methoxy group. The most common procedures to naproxen employ two possible starting materials, *i.e.* β-naphthol and 2-methoxy naphathalene. When β-naphthol is used, the methyl group is inserted by reaction with methyl chloride in basic medium. Methyl chloride is produced by chlorination of methane using large excess of methane to prevent multi halogenation. 2-Methoxynaphthalene is prepared by reaction of β-naphthol with dimethylsulphate [17], so that the methyl group derives from methanol, which comes ultimately from methane oxidation. Samples L, N, O, and P, showing similar values for the $D/H_{(OCH_3-napth)}$, seem to come from a common naphthyl starting material, while the higher deuterium content (189.4 ppm) of the OCH_3 group of sample M seems to trace back the synthesis to a different naphthyl precursor. In a recent work by Martin et al. [18] the D/H values of the OCH_3 group of commercial samples of anisole, guaiacol, *p*-anisaldehyde, and vanillin were evaluated and reported as mean values: 138. 1 ppm (anisole), 140.4 ppm (guaiacol), 126.1 ppm (*p*-anisaldehyde), 142.3 ppm (vanillin). These values are in accordance with the deuterium content found for the methoxy groups of samples L, N, O, and P.

Table 2
$(D/H)_i$ Isotope ratios (ppm) of alcohol samples **3a–c**

Sample	$D/H_{(CH)}$	$D/H_{(CH_3)}$	$D/H_{(CH_2\text{-}isob)}$	$D/H_{(CH\text{-}isob)}$	$D/H_{(CH_3\text{-}isob)}$
3a	144.6 (1.9)	119.9 (1.6)	156.3 (1.1)	158.3 (1.0)	133.8 (0.8)
3b	62 (1.0)	123.3 (1.6)	154.8 (1.5)	153.4 (1.5)	133.2 (0.4)
3c	53.9 (1.6)	–[a]	155.5 (1.0)	152.9 (2.1)	133.6 (0.7)

The $(D/H)_i$ standard deviations are reported within parentheses.
[a] Not determined.

Table 3
$(D/H)_i$ Isotope ratios (ppm) of naproxen samples

Samples	$D/H_{(CH)}$	$D/H_{(OCH_3)}$	$D/H_{(COOCH_3)}$	$D/H_{(CH_3)}$
L	150 (4.0)	142.1 (1.8)	132.3 (1.8)	140.0 (1.1)
M	165.5 (5.3)	189.4 (2.0)	135.3 (1.4)	132.5 (1.8)
N	201.0 (3.2)	155.0 (1.5)	133.1 (1.2)	145.1 (1.7)
O	151.4 (4.6)	147.0 (2.1)	134.0 (2.1)	137.9 (1.9)
P	139.3 (4.0)	149.3 (1.7)	133.5 (2.0)	132.0 (2.3)

The $(D/H)_i$ standard deviations are reported within parentheses.

4. Conclusions

Information on the synthetic sequence followed for the preparation of commercial drugs can be collected by the analysis of site-specific isotope ratios. Sometimes, only a few D/H isotope ratios are diagnostic, corresponding to the molecular positions effectively affected by the synthetic path. The recognition of the "isotope fingerprints" of a specific synthetic procedure is fundamental in order to identify patent infringement.

The analysis of $D/H_{(CH)}$ of ibuprofen samples seems to reflect the consideration that there are basically two convenient ways to prepare ibuprofen, while $D/H_{(OCH3)}$ values of naproxen samples are in accordance with two possible starting naphthyl precursors.

References

[1] W. Meier-Augenstein, Anal. Chim. Acta 465 (2002) 63;
S. Benson, C. Lennard, P. Maynard, C. Roux, Forensic Sci. Int. 157 (2006) 1;
S. Kelly, K. Heaton, J. Hoogewerff, Trends Food Sci. Technol. 16 (2005) 555;
J. Horita, Chem. Geol. 218 (2005) 171.

[2] E. Jamin, F. Martin, R. Santamaria-Fernandez, M. Lees, J. Agric. Food Chem. 53 (2005) 5130;
L.M. Reid, C.O. O'Donnell, G. Downey, Trends Food Sci. Technol. 17 (2006) 344;
E. Jamin, F. Martin, G.G. Martin, J. AOAC Int. 87 (2004) 621;
G. Calderone, C. Guillou, F. Reniero, N. Naulet, Food Res. Int. 40 (2007) 324;
H. Tamura, M. Appel, E. Richling, P. Schreier, J. Agric. Food Chem. 53 (2005) 5397;
E. Richling, C. Preston, D. Kavvadias, K. Kahle, C. Heppel, S. Hummel, T. König, P. Schreier, J. Agric. Food Chem. 53 (2005) 7925;
G. Fronza, C. Fuganti, C. Guillou, F. Reniero, D. Joulain, J. Agric. Food Chem. 46 (1998) 248;
G. Fronza, C. Fuganti, G. Pedrocchi-Fantoni, S. Serra, G. Zucchi, C. Fauhl, C. Guillou, F. Reniero, J. Agric. Food Chem. 47 (1999) 1150;
J. Aleu, G. Fronza, C. Fuganti, S. Serra, C. Fauhl, C. Guillou, F. Reniero, Eur. Food Res. Technol. 214 (2002) 63;
E. Brenna, G. Fronza, C. Fuganti, F.G. Gatti, V. Grande, S. Serra, C. Guillou, F. Reniero, S. Serra, J. Agric. Food Chem. 53 (2005) 9383.

[3] J.P. Jasper, L.E. Weaner, B.J. Duffy, J. Pharm. Biomed. Anal. 39 (2005) 66;
J.P. Jasper, B.J. Westenberger, J.A. Spencer, L.F. Buhse, M. Nasr, J. Pharm. Biomed. Anal. 35 (2004) 21;
J.P. Jasper, L.E. Weaner, J.M. Hayes, Pharm. Technol. 31 (2007) 68.

[4] S. Armellin, E. Brenna, G. Fronza, C. Fuganti, M. Pinciroli, S. Serra, Analyst 129 (2004) 130.

[5] S. Armellin, E. Brenna, S. Frigoli, G. Fronza, C. Fuganti, D. Mussida, Anal. Chem. 78 (2006) 3113.

[6] E. Brenna, G. Fronza, C. Fuganti, Anal. Chim. Acta 601 (2007) 234.

[7] A.M. Wokovich, J.A. Spencer, B.J. Westenberger, B.L. Fuhse, J.P. Jasper, J. Pharm. Biomed. Anal. 38 (2005) 781.

[8] J.S. Nicholson, S. S. Adams, to Boots Pure Drug Company Limited, US 3 385 886 (1968).

[9] to Boots Pure Drug Company Limited, FR 1545270 (1968).

[10] V. Elango, M.A. Murphy, US 4 981 995 (1991); D.D. Lindley, T.A.S. Curtis, to Hoechst Celanese Corp. US 5 068 448 (1991).

[11] http://www.chemistry.org/portal/a/c/s/1/acsdisplay.html?DOC=greenchemistryinstitute%5Cawards%5Cpresidential.html.

[12] M.C. Cann, M.E. Connelly, Real World Cases in Green Chemistry, American Chemical Society, Washington, DC, 2000.

[13] I.T. Harrison, B. Lewis, P. Nelson, W. Rooks, A. Roszkowski, A. Tomolonis, J.H. Fried, J. Med. Chem. 13 (1970) 203.

[14] P.J. Harrington, E. Lodewijk, Org. Proc. Res. Dev. 1 (1997) 72.

[15] C. Giordano, G. Castaldi, S. Cavicchioli, M. Villa, Tetrahedron 45 (1989) 4243.

[16] T. Ohta, H. Takaya, M. Kitamura, K. Nagai, R. Noyori, J. Org. Chem. 52 (1987) 3174.

[17] B. Voss, Justus Liebigs Ann Chem. 485 (1931) 258.

[18] G.J. Martin, G. Heck, R. Djamaris-Zainal, M.L. Martin, J. Agr. Food Chem. 54 (2006) 10120.

Talanta 76 (2008) 627–634

Contents lists available at ScienceDirect

Talanta

journal homepage: www.elsevier.com/locate/talanta

Direct sample introduction of wines in graphite furnace atomic absorption spectrometry for the simultaneous determination of arsenic, cadmium, copper and lead content

Zsolt Ajtony[a], Norbert Szoboszlai[b], Emőke Klaudia Suskó[a], Pál Mezei[c], Krisztina György[c], László Bencs[c,*]

[a] Institute of Food Science, University of West Hungary, H-9200 Mosonmagyaróvár, Lucsony u. 15-17., Hungary
[b] Loránd Eötvös University, Department of Inorganic and Analytical Chemistry, Institute of Chemistry, P.O. Box 32, H-1518 Budapest, Hungary
[c] Research Institute for Solid State Physics and Optics, Hungarian Academy of Sciences, P.O. Box 49, H-1525 Budapest, Hungary

ARTICLE INFO

Article history:
Received 16 November 2007
Received in revised form 29 March 2008
Accepted 7 April 2008
Available online 16 April 2008

Keywords:
Wine
Mineral content
Electrothermal atomic absorption spectrometry
ETAAS
SIMAA 6000
High sugar content
Hierarchical cluster analysis
Alcoholic beverage

ABSTRACT

A multi-element graphite furnace atomic absorption spectrometry (GFAAS) method was elaborated for the simultaneous determination of As, Cd, Cu, and Pb in wine samples of various sugar contents using the transversally heated graphite atomizer (THGA) with end-capped tubes and integrated graphite platforms (IGPs). For comparative GFAAS analyses, direct injection (i.e., dispensing the sample onto the IGP) and digestion-based (i.e., adding oxidizing agents, such as HNO_3 and/or H_2O_2 to the sample solutions) methods were optimized with the application of chemical modifiers.

The mixture of 5 μg Pd (applied as nitrate) plus 3 μg $Mg(NO_3)_2$ chemical modifier was proven to be optimal for the present set of analytes and matrix, it allowing the optimal 600 °C pyrolysis and 2200 °C atomization temperatures, respectively. The IGP of the THGA was pre-heated at 70 °C to prevent the sputtering and/or foaming of sample solutions with a high organic content, dispensed together with the modifier solution, which method also improved the reproducibility of the determinations.

With the digestion-based method, the recovery ranged between 87 and 122%, while with the direct injection method it was between 96 and 102% for Cd, Cu, and Pb, whereas a lower, compromise recovery of 45–85% was realized for As. The detection limits (LODs) were found to be 5.0, 0.03, 1.2, and 0.8 μg l^{-1} for As, Cd, Cu, and Pb, respectively. The characteristic mass (m_0) data were 24 pg As, 1.3 pg Cd, 13 pg Cu, and 35 pg Pb. The upper limits of the linear calibration range were 100, 2, 100, and 200 μg l^{-1} for As, Cd, Cu, and Pb, respectively. The precisions were not worse than 4.8, 3.1, 3.7, and 2.3% for As, Cd, Cu, and Pb, respectively. For arsenic, a higher amount of the modifier (e.g., 20 μg Pd plus 12 μg $Mg(NO_3)_2$) could be recommended to overcome the interference from the presence of sulphate and phosphate in wines. Although this method increased the sensitivity for As (m_0 = 20 pg), it also enhanced the background noise, thus only a slight improvement in the LOD of As (3.9 μg l^{-1}) was realized.

For the 35 red and white wine samples studied, the highest metal contents were observed for Cu ranging from 20 to 640 μg l^{-1} (average: 148 μg l^{-1}), followed by Pb from 6 to 90 μg l^{-1} (average: 32.3 μg l^{-1}), and Cd from 0.05 to 16.5 μg l^{-1} (average: 1.06 μg l^{-1}), whereas the As content was below the LOD. This wide fluctuation in the trace metal content could be associated with the origin of wines from various regions (i.e., different trace metal level and/or quality of soil, and/or anthropogenic impact), and with diverse materials (e.g., additives and containers) involved in the wine production processes. The Cu content of wine samples was significantly correlated with Pb, whereas its weak anti-correlation was found with Cd. Interestingly, the level of Pb was anti-correlated with the year of production of the wines. This is likely due to the gradual decrease in the Pb content of soils of vineyards by time, which certainly causes less Pb-uptake of the grape plant, thus a decrease in the Pb content of wines as well.

* Corresponding author. Tel.: +36 1 392 2222x1684; fax: +36 1 392 2223.
E-mail address: bencs@szfki.hu (L. Bencs).

0039-9140/$ – see front matter © 2008 Elsevier B.V. All rights reserved.
doi:10.1016/j.talanta.2008.04.014

1. Introduction

Wine is a popular and worldwide consumed alcoholic beverage, which has been well-known since the early periods of civilization. The moderate consumption of wine, especially the red wines, has been shown to improve health and longevity [1,2]. From analytical chemical points of view, wine is referred to as a complex matrix with a varying content of inorganic compounds (e.g., traces of dissolved alkaline and alkaline earth elements, and transition metals), as well as organic substances (e.g., polyphenols, polyhydroxy alcohols, proteins, amino acids, and polysaccharides) dissolved and/or dispersed in an aqueous solution of ethanol [3].

The concern about human exposure to the trace metal content of various beverages and dietary products, including wines, has received a raising attention, since the consumption of wines, – especially with fairly large volumes –, may significantly contribute to the daily dietary trace element intake by humans [3]. Moreover, some of these trace elements (e.g., Cu, Fe, and Mn) have an organoleptic effect at increased levels, and also contribute to the haze and taste of wines [4]. The regionally varying trace metal content of wines can also be used for source identification purposes, i.e., to verify the authenticity [3]. Considering all the above points, the determination of toxic (e.g., As, Cd, and Pb) and essential trace elements (e.g., Cu) in wines appears to be an important and challenging analytical task, which requires multi-element methods of good selectivity, sensitivity, and robustness. The origin of Cu in wines is associated with copper-based vineyard sprays, whereas the As, Cd, and Pb contents reflect the differences in grape variety, environmental factors (e.g., soil, climate), and the wine-processing methods [3].

According to a recent literature survey [3], a large set of analytical techniques have already been applied to quantify the trace metal content of wines, in particular attention to sample preparation for achieving good accuracy. For example, ion chromatography (IC) [5], stripping potentiometry [6], inductively coupled plasma mass spectrometry (ICP-MS) [7–9], inductively coupled plasma atomic emission spectrometry (ICP-AES) [10–12], flame atomic absorption spectrometry [10], and graphite furnace atomic absorption spectrometry (GFAAS) [10,13–15] were applied for this particular task.

Modern GFAAS systems generally meet the aforementioned requirements and also offer the possibility of multi-element analysis [16–19]. Thus they have been applied to the simultaneous determination of trace elements in complex material systems, for instance, optical crystal [20], foodstuff [21], seawater [22–25], mineral water [26], blood [27,28], urine [29–32], Al-alloy [33], aerosol [34], honey [35], and wine [14,15] samples.

The GFAAS literature reports mostly single element applications for the analysis of the mineral content in wines (e.g., As [36,37], Cd [13,38–40], Pb [13,38,40], and Cu [38,40–43]) and other kinds of alcoholic beverages (e.g., beers [42], aniseed spirits [44]). These methods comprise labour-intensive sample operation steps, such as acidic pre-treatment, digestion, and/or dilution, before sample dispension to the graphite furnace [10,13–15,36–44]. Besides, they are mainly based on the use of an end-heated graphite atomizer (EHGA) and deuterium-arc background correction (DBC), which techniques draw the problem of more intense physical and chemical interferences. These detrimental effects encounter particularly through evaporation and subsequent condensation of refractory sample components (e.g., carbonaceous pyrolysis products of organic constituents), as well as via their accumulation in the graphite furnace after each analytical cycle (i.e., memory/carry-over effects). On the other hand, the metal content of distilled alcoholic beverages has been often quantified with the application of EHGA and DBC techniques [44]. The selection of these experimental conditions can be reasonably justified by the much lower amounts of matrix components (i.e., pyrolysis residues) of these distilled products retained in the graphite furnace compared to wines. The analytical performance of these methods is also hampered by the aforementioned technical/methodological limitations for wine samples (e.g., low precision, narrow dynamic range of around one order of magnitude) [44]. In a quest of overcoming, or at least reducing these interference effects, the current GFAAS literature recommends the application of the transversely heated graphite atomizer (THGA) and Zeeman-effect background correction (ZBC) [45].

Considering all the above points, in the present study, a multi-element GFAAS method based on direct sample introduction into a THGA system equipped with ZBC and the application of chemical modifiers was elaborated for the simultaneous determination of As, Cd, Pb, and Cu in wines. Another aim of this work was to test the accuracy of the method over a wide range of wine samples with diverse organic matrix content, which may significantly affect the precision and accuracy of the determinations. For comparative GFAAS analyses, a digestion-based method (i.e., adding oxidizing agents, such as HNO_3 and/or H_2O_2 to the sample solution) was also studied with the application of chemical modifiers.

2. Experimental

2.1. Instrumentation

All the GFAAS experiments were performed on a Perkin-Elmer Model SIMAA 6000 atomic absorption spectrometer equipped with a transversely heated graphite atomizer, incorporating a longitudinal Zeeman-effect background (BG) corrector and an AS-72 autosampler (Perkin-Elmer, Überlingen, Germany). In the THGA, end-capped graphite tubes fitted with integrated graphite L'vov-platforms (IGPs) (Perkin-Elmer, Part No. B3 000653) were used. For the introduction of sample and modifier solutions, the IGP of the THGA was pre-heated at 70 °C. This condition prevented the sputtering and foaming of the organic content of wine samples during the drying and pyrolysis steps of the graphite furnace heating program, and moreover, it enhanced the reproducibility of the determinations. The details of the graphite furnace heating program are listed in Table 1.

The electrodeless discharge lamps of As, Cd, and Pb (Perkin-Elmer) were operated at 380, 200, and 450 mA currents, respectively, while the hollow-cathode lamp of Cu (Perkin-Elmer) at 15 mA current. Spectral lines of As 193.7 nm, Cd 228.8 nm, Pb 283.3 nm, and Cu 324.8 nm were selected for the determinations with a spectral bandpass of 0.7 nm. The BG corrected integrated absorbance (A_{int}) signals of As, Cd, Pb, and Cu were evaluated with signal integration times of 5, 3, 3, and 6 s, respectively. Each data in the tables and on the figures represents the average of three replicate determinations.

Table 1
Graphite furnace heating program for the direct injection and digestion-based methods

Step	Temperature (°C)	Ramp time (s)	Hold time (s)	Internal Ar flow rate ($cm^3\ min^{-1}$)
Drying 1	110	2	30	250
Drying 2	130	10	40	250
Pyrolysis 1	400	10	20	250
Pyrolysis 2	700	10	20	250
Atomization	2200	0	6	0
Cleaning	2450	1	2	250

Sample injection at 70 °C furnace temperature.

2.2. Reagents

All the chemicals were of analytical grade, or better quality. The 65% (v/v) HNO_3, and 30% (v/v) H_2O_2 (Merck, Darmstadt, Germany) were of Suprapur grade. The solutions were diluted with de-ionised (ultrapure) water (Milli-Q RG, Millipore) of 18 MΩ cm resistance. Standard solutions were prepared by dilution from a Perkin-Elmer GFAAS Mixed Standard (Überlingen, Germany) stock solution, which contains 5 μg ml^{-1} Cd, 50 μg ml^{-1} Cu, and 100 μg ml^{-1} As, Pb, as certified concentrations.

The Pd–Mg–nitrate chemical modifier was prepared by dilution from Perkin-Elmer palladium-modifier and magnesium-matrix-modifier solutions (Merck), which contain 1.0 ± 0.02% (m/v) Pd in ca. 15% (v/v) HNO_3 and 1.0 ± 0.02% (m/v) Mg in ca. 17% (v/v) HNO_3, respectively. The Pd (as nitrate) plus $Mg(NO_3)_2$ mixed chemical modifier was applied in either 5 μg Pd + 3 μg $Mg(NO_3)_2$, or 20 μg Pd + 12 μg $Mg(NO_3)_2$ amounts. All the sample containers and autosampler cups were thoroughly washed in 1:1 dilution of HNO_3, and after then, repetitively, in Milli-Q water.

2.3. Sample preparation

For the direct injection method, the sample was directly dispensed together with the chemical modifier, i.e., aliquots of 10 and 5 μl, respectively, onto and mixed on the IGP of the THGA. For the digestion-based method, 2.5–5.0 ml portion of each sample was added with some ml amounts of cc. H_2O_2 and cc. HNO_3 to decompose the high organic content of the matrix. Then each sample was diluted to 10 ml final sample volume with Milli-Q water. Sample and chemical modifier aliquots of 20 and 5 μl, respectively, were dispensed onto the IGP.

2.4. Statistical methods

To make statistical evaluation of the results, the SPSS software package (version 13.0, SPSS Inc.) was applied. Bivariate correlation analysis was performed with the assessment of the Pearson's correlation coefficient (r) at a two-tailed significance level (p). For the hierarchical cluster analysis (HCA), the concentration data were standardized with the Z-scores method, and after then the Ward's method of clustering was applied with the squared Euclidean distance as a measure.

3. Results and discussion

3.1. Optimization of the graphite furnace heating program

The ramp and length of the drying step was optimized to attain a smooth and complete evaporation/removal for the liquid part of each wine sample without sputtering. For the removal of the dry, residual sample constituents, a two-step pyrolysis was applied at 400 and 700 °C, which was especially necessary for wine samples with exceptionally high sugar content. Typical representatives of such types of wines are the Hungarian Tokaji Aszú and Sweet Szamorodni [12]. These optimization studies offered drying and pyrolysis steps of general applicability to the various wine samples both with the direct injection and the digestion-based methods (Table 1).

For the selection of compromise pyrolysis temperature (T_{pyr}) and atomization temperature (T_{at}), necessary for multi-element GFAAS determinations, the effects of various chemical modifiers (i.e., NH_4HPO_4–$Mg(NO_3)_2$, Pd, Pd–Mg, and permanent Ir) were studied using various types of Hungarian red and white wines with high organic (sugar) content. Amounts of 50–100 μg NH_4HPO_4 modifier combined with 3 μg $Mg(NO_3)_2$ was suitable only for the determination of three of the analytes studied, i.e., Cd, Cu, and Pb, for reasons explained below. The use of the permanent Ir modifier caused a lower sensitivity than the Pd-based modifiers. Regarding the thermal stabilization performance, the Pd modifier was similar to the Pd–Mg mixed modifier. However, for the best thermal stabilization performance, the near symmetrical shapes of the atomization transients, and the good ashing-aid/matrix removal efficacy, the Pd–Mg chemical modifier was applied in further experiments.

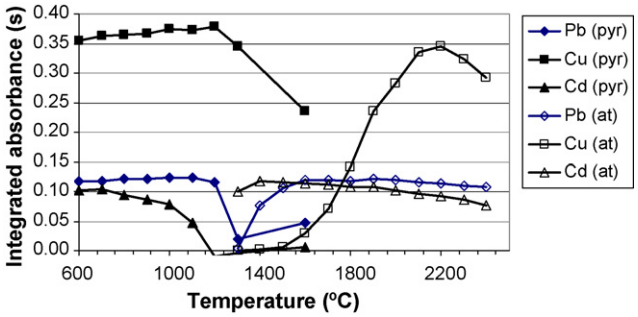

Fig. 1. Pyrolysis (pyr) and atomization (at) curves of 0.05 ng Cd, 0.5 ng Cu, and 1.0 ng Pb with sweet Tokaji Aszú on the addition of 5 μg Pd plus 3 μg $Mg(NO_3)_2$ mixed chemical modifier.

As the first step, the pyrolysis and atomization curves were determined for Cd, Cu, and Pb with the application of the high sugar content Aszú wine as a model matrix, representing the "worst case" (Fig. 1). After the pyrolysis of such wine samples, a carbonaceous residue remained in the graphite furnace, which significantly affected the precision and accuracy of the determinations. Adding 5 μg Pd and 3 μg $Mg(NO_3)_2$ to the Aszú sample resulted in the optimal T_{pyr} and T_{at} of 700 and 2200 °C, respectively (Fig. 1). On the other hand, by applying this modifier mass, a fairly high BG absorption was found on the analytical line of As, due to the sulphate and/or phosphate content of some wine samples. To overcome this interference, the amount of the modifier was increased to 20 μg Pd and 12 μg $Mg(NO_3)_2$, which resulted in the optimal T_{pyr} and T_{at} of 700 and 2100 °C, respectively (Fig. 2). Interestingly, the atomization curve of As developed two plateau sections between 1800 and 2000 °C and 2200–2300 °C, respectively (Fig. 2). These sections likely correspond to the vaporization–atomization of this element in two distinct chemical forms of diverse vaporization characteristics. Although As has not been detected in the studied samples, other brands of wines may contain it at higher amounts detectable with GFAAS, especially, wines originating from old copper distillation apparatus [36].

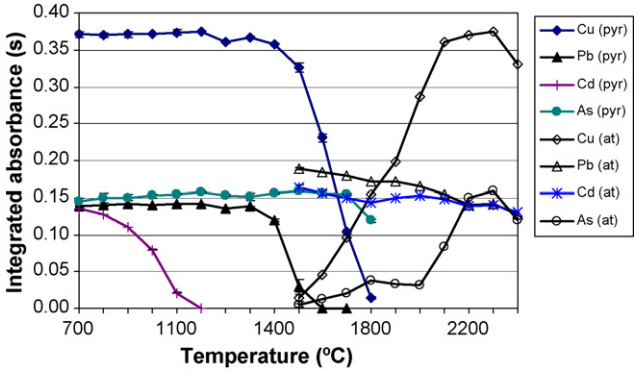

Fig. 2. Pyrolysis (pyr) and atomization (at) curves of 1.0 ng As, 0.05 ng Cd, 0.5 ng Cu, and 1.0 ng Pb with sweet Tokaji Aszú wine on the addition of 20 μg Pd plus 12 μg $Mg(NO_3)_2$ mixed chemical modifier.

Table 2
Calibration data with various amounts of the Pd–$Mg(NO_3)_2$ modifier

	Cu	Pb	Cd	As
Digestion-based method				
5 μg Pd + 3 μg $Mg(NO_3)_2$				
Slope (s l μg^{-1})	6.38×10^{-3}	2.39×10^{-3}	5.57×10^{-2}	3.60×10^{-3}
R	0.9997	0.9996	0.9997	0.9999
m_0 (pg)	13.8	36.8	1.6	24.5
LOD (μg l^{-1})	1.0	0.6	0.02	5.0
20 μg Pd + 12 μg $Mg(NO_3)_2$				
Slope (s l μg^{-1})	6.07×10^{-3}	2.49×10^{-3}	6.07×10^{-2}	4.28×10^{-3}
R	0.9996	0.9999	0.9998	0.9999
m_0 (pg)	14.5	35.3	1.4	20.6
LOD (μg l^{-1})	1.4	0.8	0.08	3.9
Direct injection method				
5 μg Pd + 3 μg $Mg(NO_3)_2$				
Slope (s l μg^{-1})	2.96×10^{-3}	1.25×10^{-3}	2.96×10^{-2}	–
R	0.9994	0.9993	0.9998	–
m_0 (pg)	13.5	35	1.3	–
LOD (μg l^{-1})	1.2	0.8	0.03	–

R: correlation coefficient; m_0: characteristic mass; LOD: limit of detection.

3.2. Effects of sample additives on the absorbance signals

For optimizing the digestion-based method, the effects of H_2O_2 and HNO_3 additives in the sample solutions were studied. The organic (mostly sugar) content of wines alters from brand-to-brand, and it can be high in several cases. This promotes the formation of the carbonaceous layer in the graphite furnace as aforementioned. Accumulation of this layer during subsequent measurement cycles certainly triggers memory effects, high BG levels, thus bad precision and inaccuracy. Moreover, it shortens the lifetime of the graphite tubes.

The HNO_3 additive had good removal efficiency on this residual pyrolysis product down to 2% (v/v) HNO_3 content. Below this concentration, generally, higher amounts of the pyrolysis products were retained in the graphite furnace, which certainly caused the drawbacks as above. Therefore, for samples of high sugar content (e.g., Aszú wines), a HNO_3 content of 4% (v/v) was found to be optimal for the matrix removal and for prolonging the lifetime of the graphite tubes. On the other hand, 10% (v/v) H_2O_2 also provided a similarly good ashing-aid for matrix removal, thus a better accuracy for wine samples of high sugar content.

Table 3
Recoveries for As, Cd, Cu, and Pb from various kinds of wine samples with the digestion-based method

Sample ID	Name of wine	Recovery (%)			
		Cd	Pb	Cu	As[a]
1	Bulls' blood of Eger	104.8	100.8	94.1	–
7	Kékfrankos	119.6	90.2	99.2	48.9
8	Pinot Noir	91.1	94.0	102.4	–
8	Pinot Noir	122.8	96.3	99.4	–
11	Tokaji Aszú (5-butt)	105.4	99.1	94.8	74.2
12	Furmint + hárslevelű	96.8	88.0	97.8	51.3
22	Ezerjó	94.8	89.5	97.2	71.5
24	Olasz riesling	95.2	96.0	99.6	81.2
27	Egri chardonnay	106.8	94.4	99.3	57.0
29	Zempléni Furmint	122.8	87.0	97.0	–
30	Mátraaljai Muscat	93.2	93.2	100.2	69.3
30	Mátraaljai Muscat	102.9	93.0	98.5	–
30	Mátraaljai Muscat	115.2	94.2	95.8	–
Average ± S.D.		105.4 ± 11	93.5 ± 4.1	98.1 ± 2.3	64.8 ± 12

Spikes for As, Cu, Pb, and Cd were 10, 5, 10, and 0.5 μg l^{-1}, respectively. S.D.: standard deviation; number of parallel determinations: $n = 3$.

[a] 20 μg Pd + 12 μg $Mg(NO_3)_2$.

In general, increasing the HNO_3 concentration from 0 to 8% (v/v) did not affect considerably the A_{int} signals of analytes concerned, neither for white, nor for red wines of high sugar content. However, a slight signal increase encountered for Cu at HNO_3 concentrations higher than 4% (v/v). This is due to the removal effect of HNO_3 on the organic content of the matrix, i.e., it significantly decreasing the amount of the carbonaceous residue in the furnace. This residue would otherwise form refractory carbides with Cu, thus slightly suppressing the analyte signal. Similar results have been found on the addition of H_2O_2 to white and red wine samples.

It has also been concluded that the HNO_3 content of the modifier solution together with the sample solution provides an appropriate ashing-aid for the removal of the organic content of wines. These experiments offered the possibility of direct sample insertion of wines into the graphite furnace.

3.3. Calibration and analytical performance data

The calibration was performed against simple, aqueous standard solutions on the addition of the Pd–Mg chemical modifier as in the case of samples. The analytical performance data are listed in Table 2. The correlation coefficient (R), resulted from linear fittings to the calibration points ($n = 7$), was better than 0.9993 for each element. The upper limit of the linear range of calibration was

Table 4
Recoveries for As, Cd, Cu, and Pb from various wine samples with the direct injection method

Sample ID	Name of wine	Recovery (%)			
		Cu	Pb	Cd	As
6	Tokaji Furmint	95.6	95.7	95.4	51.2
19	Olasz riesling	98.2	99.3	99.7	58.9
21	Rajnai riesling	106.6	99.6	96.5	62.4
24	Olasz riesling	100.0	97.2	99.3	–
25	Olasz riesling	104.4	99.2	95.5	70.2
27	Egri chardonnay	99.8	100.5	98.3	58.7
30	Mátraaljai Muskotály	101.2	99.4	97.9	70.4
32	Verdejo	101.3	97.4	99.6	61.2
33	Saint Émilion	98.6	92.5	90.8	45.9
34	Blaufranker	105.2	97.8	91.7	67.2
35	Huxelrebe	107.2	99.2	93.9	66.4
Average ± SD		101.7 ± 3.8	98 ± 2.3	96.2 ± 3.1	61.2 ± 8.0

Spikes for As, Cu, Pb, and Cd were 10, 5, 10, and 0.5 μg l^{-1}, respectively. S.D.: standard deviation ($n = 3$).

Table 5
Analytical results with quality control and certified reference materials

Reference sample	Analyte	Concentration (average ± S.D.) ($\mu g\,l^{-1}$)		
		Certified/assigned	Satisfactory range	Measured[a]
NIST SRM1643e water	As	60.45 ± 0.72	–	62.4 ± 1.9
NIST SRM1643e water	Cd	6.568 ± 0.073	–	6.56 ± 0.03
NIST SRM1643e water	Cu	22.76 ± 0.31	–	23.5 ± 0.5
NIST SRM1643e water	Pb	19.63 ± 0.21	–	19.5 ± 0.2
TMDA-51 fortified water	As	14.4	–	14.5 ± 1.0
TMDA-51 fortified water	Cd	36.6	–	33.2 ± 0.1
TMDA-51 fortified water	Cu	66.4	–	67.9 ± 1.0
TMDA-51 fortified water	Pb	66.6	–	63.3 ± 0.2
FAPAS T0777 white wine	Cd	69.3 (assigned)	38.8–99.7	62.3 ± 0.7
FAPAS T0777 white wine	Pb	260 (assigned)	158–361	237 ± 5.0

[a] $n = 3$, S.D.: standard deviation.

100, 2, 100, and 200 $\mu g\,l^{-1}$ for As, Cd, Cu, and Pb, respectively. For Cd, the calibration range could be extended up to 10 $\mu g\,l^{-1}$ by using second order fittings to the calibration points, which was a necessary approach for some wine samples with quite high Cd content. Alternatively, the dilution of the samples was also proposed for a few wines with metal content higher than the upper limit of the linear range of calibration.

The limit of detection (LOD) of the method, corresponding to 3σ confidence, was calculated from eleven repeated determination of a wine sample of low trace element content, called "Ezerjó". The LOD data were found to be 5.0, 1.2, 0.8, and 0.03 $\mu g\,l^{-1}$ for As, Cu, Pb, and Cd, respectively. The sensitivity of the determinations, expressed as the characteristic mass (m_0), was 1.3, 35, 24, and 13 pg for Cd, Pb, As, and Cu, respectively, with the application of 5 μg Pd and 3 μg $Mg(NO_3)_2$ modifier. The precision of the determinations, expressed as the relative standard deviation, were not worse than 4.7, 3.1, 3.7, and 2.3% for As, Cd, Cu, and Pb, respectively.

Table 6
Analytical results for various types of wines obtained with the direct injection method

Sample ID[a]	Name	Type	Year	Origin/winery/location	Average concentration ± S.D. ($\mu g\,l^{-1}$)		
					Cu	Pb	Cd
1	Bulls' blood of Eger	Dry red	2001	Egervin winery, Eger	104 ± 1.14	30.9 ± 0.30	0.54 ± 0.35
2	Blue portugueser	Red	2003	Szigetcsép, Pinceszer	291[b] ± 1.5	46.1 ± 0.20	0.05 ± 0.01
3	Badacsonytördemici Budaizöld	Dry white	2002	Badacsonytördemic, Samu Gy.	149[b] ± 0.04	46.7 ± 0.06	0.15 ± 0.00
4	House made	White	2004	Csepel, Budapest	55.1 ± 0.33	12.6 ± 0.20	0.68 ± 0.02
5	House made	Red	2004	Csepel, Budapest	64.7 ± 0.11	28.4 ± 0.14	0.42 ± 0.07
6	Tokaji Furmint	Semi-sweet white	1999	Bodnár cellary, Tokaj-Hegyalja	46.9 ± 0.22	37.6 ± 0.21	0.11 ± 0.06
7	Kékfrankos	Dry red	2001	Vince Béla, Old-Top, Eger	72.4 ± 0.67	11.0 ± 0.19	0.27 ± 0.06
8	Pinot Noir	Dry red	2003	BB Polgár, Balatonboglár	82.7 ± 0.01	17.4 ± 0.04	0.20 ± 0.02
9	Dél-dunántúli Kékfrankos	Semi-sweet red	2001	BB Polgár, Balatonboglár	192[b] ± 0.15	44.3 ± 0.08	0.11 ± 0.02
10	Olasz riesling	Dry white	2003	Dréher "Beer Garden", Győr	306[b] ± 2.32	25.5 ± 0.02	0.29 ± 0.01
11	Tokaji Aszú (5-butt)	Sweet white	2000	Tolcsva, Tokaj-Hegyalja region	78.4 ± 1.77	50.8 ± 0.46	0.85 ± 0.03
12	Furmint + hárslevelű	Dry white	2002	Woltz Márton	24.3 ± 1.82	48.6 ± 0.46	0.45 ± 0.01
13	Home-made	Dry red	2003	Woltz Márton	313[b] ± 2.64	28.1 ± 0.01	0.35 ± 0.03
14	Tokaji Édes Szamorodni	Sweet white	2001	Tolcsva, Tokaj-Hegyalja region	311[b] ± 2.36	39.1 ± 0.06	0.80 ± 0.04
15	Sárga muskotályos	Sweet white	2003	Tolcsva, Tokaj-Hegyalja region	427[b] ± 1.60	48.1 ± 0.03	0.51 ± 0.02
16	Hárslevelű + furmint	Dry white	2002	Tállya, Tokaj-Hegyalja region	85.9 ± 2.93	53.0 ± 0.87	0.44 ± 0.01
17	Hárslevelű + furmint	Dry white	2003	Tállya, Tokaj-Hegyalja region	66.3 ± 0.90	31.3 ± 0.28	16.5[b] ± 0.10
18	Home-made	Dry white	2003	Woltz Márton	108[b] ± 0.18	18.7 ± 0.29	0.23 ± 0.02
19	Olasz riesling	White	2003	Tramini bufette, Győr	20.3 ± 0.95	10.0 ± 0.35	0.27 ± 0.06
20	Olasz riesling	White	2003	Makk Hetes wine-shop	204 ± 0.04	29.1 ± 0.20	0.18 ± 0.03
21	Rajnai riesling	White	2003	"Gyógygödör" wine-shop, Csopak	642[b] ± 3.07	43.4 ± 0.07	0.19 ± 0.02
22	Ezerjó	Sweet white	2003	Bocskai restaurant, home-made	58.8 ± 0.42	23.5 ± 0.25	0.08 ± 0.01
23	Rajnai riesling	White	2003	Csopak wine-shop, Győr	254[b] ± 1.38	40.2 ± 0.43	0.09 ± 0.03
24	Olasz riesling	White	2003	Félhordó wine-shop, Győr	27.7 ± 1.97	6.0 ± 0.42	0.82 ± 0.02
25	Olasz riesling	White	2003	Mandula bufette, home-made	59.1 ± 0.32	26.0 ± 0.04	0.78 ± 0.01
26	Home-made	White	2003	Csepel, Budapest	36.0 ± 0.17	56.8 ± 0.30	12.2[b] ± 0.04
27	Egri chardonnay	Dry white	2002	Thummerer Vilmos, Noszvaj, Eger	21.8 ± 0.04	21.4 ± 0.04	0.42 ± 0.02
28	Igazi muskotály cuvée	Semi-sweet white	1999	Thummerer Vilmos, Noszvaj, Eger	108 ± 1.60	47.7 ± 0.34	0.15 ± 0.05
29	Zempléni Furmint	Dry white	2004	Tállya, Ráski cellary, Tokaj region	92.2 ± 0.98	34.3 ± 0.34	0.39 ± 0.04
30	Mátraaljai Muskotály	Dry white	2000	Gyöngyöspata, Mátraalja region	69.4 ± 0.72	25.1 ± 0.15	0.34 ± 0.03
31	Kékfrankos	Sweet red	2001	Bócsa, Dankó Weinhaus, Great Plain	293[b] ± 0.88	90.5 ± 0.97	0.74 ± 0.02
32	Verdejo	Red	2003	Castelo de Medina, Rueda, Spain	30.6 ± 1.2	8.7 ± 0.21	0.09 ± 0.006
33	Saint Émilion	Dry red	2003	Saint Émilion, Bordeaux, France	137[b] ± 0.07	8.0 ± 0.07	0.33 ± 0.003
34	Blaufranker	Dry red	2003	Dornfelder, Anselmann, Germany	150[b] ± 1.34	13.1 ± 0.22	0.09 ± 0.002
35	Huxelrebe	Dry red	2003	Dr. Hinkel, Germany	179[b] ± 12.0	27.6 ± 3.94	0.28 ± 0.06

S.D.: standard deviation ($n = 3$).
[a] Sample Nos. 1–31 is of Hungarian origin.
[b] Metal content obtained with 2–10-fold dilution of the sample.

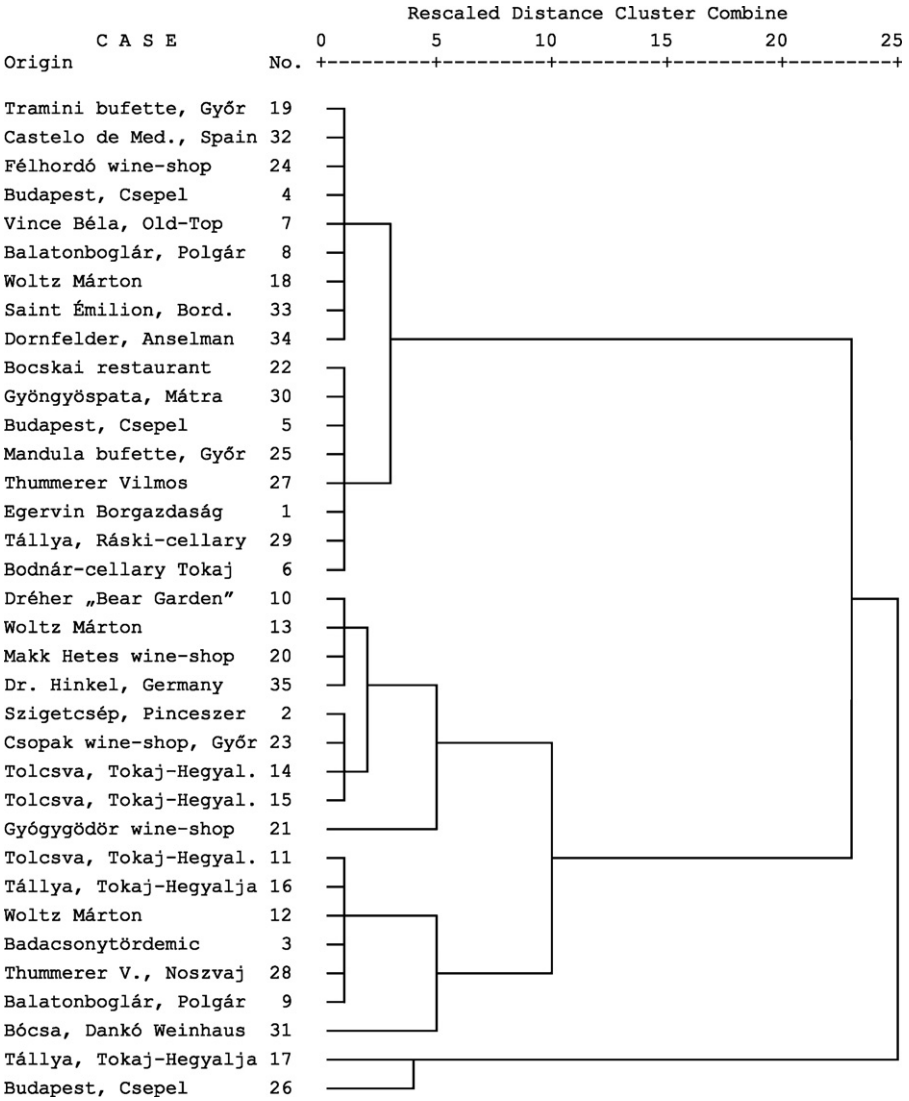

Fig. 3. Dendogram of the cluster analysis for the wine samples of various origin.

The determination of As was hampered by a high, structured BG absorbance, which could be expected to arise from the fairly high sulphate and/or phosphate content of some wines. These matrix components may cause co-vaporization interference on the determination of As [46], and likewise, they can also block the "active sites" of the Pd modifier [45]. In order to enhance the sensitivity of the determinations for As, the amount of chemical modifier was increased to 20 μg Pd + 12 μg $Mg(NO_3)_2$. Although this method provided better sensitivity (i.e., lower m_0 values, see Table 2), it was handicapped by a higher BG noise for the other analytes, due to the increased mass of the modifier. Thus it provided only slight improvement in the LOD of As (3.9 μg l^{-1}) compared to the method with the lower modifier amount.

The accuracy of both methods was first verified in spike experiments by adding aliquots of the diluted GFAAS Mixed Standard to a large set of wines of diverse brands. Using the digestion-based method, a fairly good recovery was found for each analyte, it being independent of the brand of the wine sample analyzed (Table 3). The recovery was found to range between 87 and 123% for Cd, Cu, and Pb, whereas it was a lower, compromise value for As, ranging from 65 to 70% for samples of 1:1 dilution, and 85% for samples diluted to four-fold. With the direct injection method, the recoveries for As, Cd, Cu, and Pb were obtained to be in the ranges of 45–70, 91–100, 96–107, and 93–101%, respectively (Table 4).

As an additional accuracy check, the analytes were also determined in certified reference materials of water (NIST SRM1643e and TMDA-51) and a quality control test material of wine (FAPAS T0777). As can be seen in Table 5, a good agreement has been found between the concentrations of analytes determined with the present GFAAS method and the certified/assigned values of the reference samples.

3.4. Evaluation of the analytical results

The analytical results for 35 wine samples obtained with the direct injection method are listed in Table 6. As a comparison, all of these wine samples were analyzed with the digestion-based method, which revealed a good agreement between the results of the two alternative approaches. The national legislation in Hungary, in line with OIV recommendations, allows the maximum level of 50 μg l^{-1} As, 20 μg l^{-1} Cd, 250 μg l^{-1} Pb, and 1000 μg l^{-1} Cu in wines (food products). The corresponding trace metal contents were below these limits in all wine samples studied. The

highest concentrations were observed for Cu ranging from 20 to 640 $\mu g\,l^{-1}$ (average: 148 $\mu g\,l^{-1}$), followed by Pb from 6 to 90 $\mu g\,l^{-1}$ (average: 32.3 $\mu g\,l^{-1}$), and Cd from 0.05 to 10.5 $\mu g\,l^{-1}$ (average: 1.06 $\mu g\,l^{-1}$). The Cu content of the studied wine samples was significantly correlated with Pb ($r = 0.364$, $p = 0.05$), whereas its weak anti-correlation was found with Cd ($r = -0.166$, $p = 0.05$). Interestingly, the level of Pb was anti-correlated with the year of production of the wines ($r = -0.363$, $p = 0.05$), showing a decreasing trend of the Pb content in wines by year. This is likely due to the gradual decrease in the Pb content of soil by time, which is the consequence of the banning of the Pb-containing fuel in Europe since 1995. As known in the literature [3], the concentrations of trace metals in wine also depend on the metal content in the vineyard soil, which primarily determines the degree of metal uptake by the grape plant. A decrease in the Pb content of vineyard soil certainly causes a decrease in the Pb concentration of wine.

According to the literature data, the Cd level ranged from 0.1 to 15.5 $\mu g\,l^{-1}$ in Spanish red wines [47], whereas other studies [48] reported lower levels (0.21–0.64 $\mu g\,l^{-1}$). In Brazilian red and white wines Cd was between 0.03 and 0.19 $\mu g\,l^{-1}$, whereas the Pb content fluctuated between 10.3 and 55 $\mu g\,l^{-1}$ [14]. In Slovenian wines, the Cd content was reported to be in the range of 0.2–0.5 $\mu g\,l^{-1}$, and the Pb content ranged between 18.4 and 31.3 $\mu g\,l^{-1}$ [13]. In German red wines, the Cu content was reported to be fairly high, it being ranged between 2700 and 3400 $\mu g\,l^{-1}$, whereas Pb was found to be between 324 and 477 $\mu g\,l^{-1}$ [7]. Other studies reported a bit lower levels of Pb and Cu for German (red and white) wines [6], ranged between 4 and 254, and 50 and 3940 $\mu g\,l^{-1}$, respectively, while the Cd content varied between 0.003 and 0.98 $\mu g\,l^{-1}$. In Argentinian red and white wines, the concentration of Cd fluctuated between 0.37 and 1.29 $\mu g\,l^{-1}$ and 0.8 and 2.2 $\mu g\,l^{-1}$, respectively [49]. For Australian white wines, the Cu content ranged between 170 and 1700 $\mu g\,l^{-1}$ [50].

The trace metal content of the studied Hungarian wine samples was generally lower than that of other European wines (e.g., German, Spanish, and French), but comparable with those found in Slovenian and South American wines. The high variation in the metal content of the present samples was due to their origin from different regions of Hungary with diverse quality of soil and/or anthropogenic impact. Some home-made wines (e.g., sample Nos. 13, 18, and 26 in Table 6), partly from diverse wine-shops/buffets (e.g., sample Nos. 20–25) have shown higher trace element content, possibly due to contamination during wine-making processes and/or mixing/storage originating from different containers, utensils, additives, etc. It is to be mentioned that As was not detected in the wine samples studied. On the other hand, this does not appear to be a flaw of the present methodology, since the LOD of the method acquired for As is an order of magnitude lower than the highest allowed concentration of this element in food products.

The results of HCA revealed five main clusters of wine samples based on their metal content, as it appears on the dendogram (Fig. 3). The first and the second clusters on the top of the dendogram are the largest groups, which represent mostly the dry category with low sugar content and low or low-to-medium metal content. On the contrary, the third and the fourth clusters downwards from the top of the dendogram show the rather sweet/semi-sweet category with medium-to-high metal content, although a few of the dry wines is also included in these groups. The fifth cluster includes the wines with medium Cu and Cd, but high Pb content. Only a few individual clusters are formed by wine samples of extremely high Cd or Cu content (sample Nos. 17, 21, 26, and 31), which is possibly due to contamination during the wine processing/storage.

4. Conclusions

The fast and simultaneous GFAAS determination of As, Cd, Cu, and Pb content in a large variety of wines can be accurately performed with the direct injection of the sample along with the Pd–Mg chemical modifier into a pre-heated graphite platform of the transversely heated graphite atomizer and with the use of aqueous standards for calibration. This method does not require any sample pre-treatment step, additionally, the acquired sensitivities and LODs are generally better than those for GFAAS methods published in the literature. Moreover, the dynamic range of the determinations for each element is extended to two orders of magnitude, which provides a very useful concentration range to cover the metal content of different brands/origins of wine samples with widely fluctuating mineral content. The Pb content of wines has been shown to be correlated with the year of production of the wine. This element might be utilized as an environmental marker, namely, an indicative of the actual Pb-content of the soil of the vineyard for the year of the grape harvest. The cluster analysis showed that there is some correlation between the sugar and metal contents of the wines.

This analytical method can be applied for the GFAAS analysis of material systems of similar organic matrix composition to the studied wine samples, e.g., other kinds of alcoholic beverages. It is to be noted that this methodology can also be implemented to the multi-element, continuum source GFAAS, a novel technique with good future prospects.

Acknowledgement

The support from the Hungarian Scientific Research Fund (OTKA) under the projects of F67647 and K68390 is gratefully acknowledged.

References

[1] D.M. Goldberg, I.L. Bromberg, Clin. Chim. Acta 246 (1996) 14–16.
[2] M. Gronbaek, M. Deis, T.I. Sorensen, U. Becker, P. Schnohr, P. Jensen, Br. Med. J. 10 (1995) 1165–1169.
[3] K. Pyrzyńska, Crit. Rev. Anal. Chem. 34 (2004) 69–83.
[4] K.A. Riganakos, P.G. Veltsistas, Food Chem. 82 (2003) 637–643.
[5] O. Zerbinati, F. Balduzzi, V. Dell'Oro, J. Chromatogr. A 881 (2000) 645–650.
[6] P. Ostapczuk, H.R. Eschnauer, G.R. Schollary, Fresenius J. Anal. Chem. 358 (1997) 723–727.
[7] M.M. Castiñeira, R. Brandt, A. Von Bohlen, N. Jakubowski, Fresenius J. Anal. Chem. 370 (2001) 553–558.
[8] C.M.R. Almeida, M.T.S.D. Vasconcelos, Anal. Chim. Acta 463 (2002) 165–175.
[9] C.M.R. Almeida, M.T.S.D. Vasconcelos, M. Barbaste, B. Medina, Anal. Bioanal. Chem. 374 (2002) 314–322.
[10] M. Aceto, O. Abollino, M.C. Buzzoniti, E. Mentasti, C. Sarzanini, M. Malandrio, Food Addit. Contam. 19 (2002) 126–133.
[11] Z. Murányi, L. Papp, Microchem. J. 60 (1998) 134–142.
[12] Z. Murányi, Zs. Kovács, Microchem. J. 67 (2000) 91–96.
[13] J. Kristl, M. Veber, M. Slekovec, Anal. Bioanal. Chem. 373 (2002) 200–204.
[14] G.P.G. Freschi, C.S. Dakuzaku, M. de Moraes, J.A. Nóbrega, J.A. Gomes Neto, Spectrochim. Acta Part B 56 (2001) 1987–1993.
[15] K.G. Fernandes, M. De Moraes, J.A.G. Neto, J.A. Nóbrega, P.V. Oliveira, Analyst 127 (2002) 157–162.
[16] B. Radziuk, G. Rödel, H. Stenz, H. Becker-Ross, S. Florek, J. Anal. At. Spectrom. 10 (1995) 127–136.
[17] B. Radziuk, G. Rödel, M. Zeiher, S. Mizuno, K. Yamamoto, J. Anal. At. Spectrom. 10 (1995) 415–422.
[18] M. Hoenig, A. Cilissen, Spectrochim. Acta Part B 52 (1997) 1443–1449.
[19] L. Bencs, O. Szakács, N. Szoboszlai, Zs. Ajtony, G. Bozsai, J. Anal. At. Spectrom. 18 (2003) 105–110.
[20] L. Bencs, O. Szakács, T. Kántor, I. Varga, G. Bozsai, Spectrochim. Acta Part B 55 (2000) 883–891.
[21] P.R.M. Correia, E. Oliveira, P.V. Oliveira, Anal. Chim. Acta 405 (2000) 205–211.
[22] P.G. Su, S.D. Huang, Spectrochim. Acta Part B 53 (1998) 699–708.
[23] P.G. Su, S.D. Huang, J. Anal. At. Spectrom. 13 (1998) 641–645.
[24] C.L. Chen, K.S.K. Danadurai, S.D. Huang, J. Anal. At. Spectrom. 16 (2001) 404–408.
[25] P.H. Li, K.S.K. Danadurai, S.D. Huang, J. Anal. At. Spectrom. 16 (2001) 409–412.

[26] V.R. Amorim Filho, K.G. Fernandes, M. de Moraes, J.A.G. Neto, J. Braz. Chem. Soc. 15 (2004) 28–33.
[27] A. Viksna, E.S. Lindgren, Anal. Chim. Acta 353 (1997) 307–311.
[28] P.R.M. Correia, P.V. Oliveira, J.A.G. Neto, J.A. Nóbrega, J. Anal. At. Spectrom. 19 (2004) 917–922.
[29] B.S. Iversen, A. Panayi, J.P. Camblor, E. Sabbioni, J. Anal. At. Spectrom. 11 (1996) 591–594.
[30] M.C. Hsiang, Y.H. Sung, S.D. Huang, Talanta 62 (2004) 791–799.
[31] P.V. Oliveira, E. Oliveira, Fresenius J. Anal. Chem. 371 (2001) 909–914.
[32] T.W. Lin, S.D. Huang, Anal. Chem. 73 (2001) 4319–4325.
[33] N. Carrión, A.M. Itriago, M.A. Alvarez, E. Eljuri, Talanta 61 (2003) 621–632.
[34] J.P. Pancras, J.M. Ondov, R. Zeisler, Anal. Chim. Acta 538 (2005) 303–312.
[35] Zs. Ajtony, L. Bencs, R. Haraszi, J. Szigeti, N. Szoboszlai, Talanta 71 (2007) 683–690.
[36] S. Galani-Nikolakaki, N. Kallithrakas-Kontos, A.A. Katsanos, Sci. Total Environ. 285 (2002) 155–163.
[37] S.N.F. Bruno, R.C. Campos, A.J. Curtius, J. Anal. At. Spectrom. 9 (1994) 341–344.
[38] M.E.R. Huguet, At. Spectrosc. 25 (2004) 177–184.
[39] J. Jaganathan, A.L. Reisig, S.M. Dugar, Microchem. J. 56 (1997) 221–228.
[40] R. Lara, S. Cerutti, J.A. Salonia, R.A. Olsina, L.D. Martinez, Food Chem. Toxicol. 43 (2005) 293–297.
[41] S. Catarino, I. Pimentel, A.S. Curvelo-Garcia, At. Spectrosc. 26 (2005) 73–78.
[42] M. Llobat-Estellés, A.R. Mauri-Aucejo, R. Marin-Saez, Talanta 68 (2006) 1640–1647.
[43] I. Karadjova, B. Izgi, S. Gucer, Spectrochim. Acta Part B 57 (2002) 581–590.
[44] J.M. Jurado, M.J. Martín, F. Pablos, A. Moreda-Piñeiro, P. Bermejo-Barrera, Food. Chem. 101 (2007) 1296–1304.
[45] B. Welz, M. Sperling, Atomic Absorption Spectrometry, third ed., Wiley-VCH, Weinheim, 1998.
[46] B. Welz, G. Schlemmer, J.R. Mudakavi, J. Anal. At. Spectrom. 3 (1988) 695–701.
[47] C. Mena, C. Cabrera, M.L. Lorenzo, M.C. Lopez, Sci. Total Environ. 181 (1996) 201–208.
[48] M.Y. Perez-Jordan, J. Soldevila, A. Salvador, A. Pastor, M. de la Guardia, J. Anal. At. Spectrom. 13 (1998) 33–39.
[49] R.F. Lara, R.G. Wuilloud, J.A. Salonia, R.A. Olsina, L.D. Martinez, Fresenius J. Anal. Chem. 371 (2001) 989–993.
[50] C. Wiese, G. Schwedt, Fresenius J. Anal. Chem. 358 (1997) 718–722.

Talanta 76 (2008) 591–596

Contents lists available at ScienceDirect

Talanta

journal homepage: www.elsevier.com/locate/talanta

Ion mobility spectrometry of volatile compounds from Iberian pig fat for fast feeding regime authentication

Ruth Alonso[a], Vicente Rodríguez-Estévez[c], Ana Domínguez-Vidal[b], Maria José Ayora-Cañada[b], Lourdes Arce[a], Miguel Valcárcel[a,*]

[a] Department of Analytical Chemistry, University of Córdoba, Annex C3 Building, Campus of Rabanales, E-14071 Córdoba, Spain
[b] Department of Physical and Analytical Chemistry, University of Jaén, E-23071 Jaén, Spain
[c] Department of Animal Production, University of Córdoba, Campus of Rabanales, E-14071 Córdoba, Spain

ARTICLE INFO

Article history:
Received 12 November 2007
Received in revised form 26 March 2008
Accepted 28 March 2008
Available online 8 April 2008

Keywords:
Ion mobility spectrometry
Volatile compounds
Iberian pig
Regimen authentication

ABSTRACT

Characteristic ion mobility spectra for volatile compounds present in fat were used to authenticate the feeding regime of Iberian pigs. Volatile compounds were obtained by heating the solid samples at 150 °C for 40 min. This produced a headspace that was introduced in the spectrometer ionization chamber by means of a highly purified nitrogen stream. The spectra thus, obtained for the fat samples were processed chemometrically in order to assess their usefulness for discriminating meat from free-range pigs fed on pasture and acorns and confined pigs fed with commercial feed including high-oleic acid products. Principal component analysis was used as both an exploratory tool and a variable reduction method, and linear discriminant analysis was employed to classify 65 subcutaneous fat samples according to pig feeding regime. Only 2.3% of the samples from pigs reared in confinement were misclassified. 95.5% of the free-range samples were correctly predicted.

1. Introduction

In recent times, consumer demand for natural and traditional foods, and free-range animal products (e.g. organic products), has risen by effect of the increasing concern with environment, animal welfare, food safety and food quality issues. This has raised the need for effective analytical methods for food authentication [1]. Vanguard methods capable of providing the analytical information required in the form of yes/no binary answers can be an effective, expeditious choice for this purpose [2].

The Iberian pig constitutes a breed of great economic importance in Spain and Portugal. In the traditional rearing system, pigs are free-reared in an expanse of land of variable area, using natural resources [mainly grass (*Quercus ilex*) and acorns (*Quercus suber*)] only [3]. Cured ham obtained from free-range pigs has gained widespread consumer acceptance and a high commercial value by virtue of it characteristic flavour; also, the high content in unsaturated fats of the ham has increased its appreciation as a healthy food [4]. The free-range rearing system departs considerably from the intensive farming regime, where pigs are confined and fattened with commercial feed. The Spanish official method for discriminating between pig feeding and rearing regimes determines the fatty acid composition of pig fat in terms of four fatty acids (FAs) (oleic, linoleic, palmitic and stearic) [5]. In recent years, however, new feed concentrates with high contents in unsaturated fats (oleic acid mainly) have been produced in order to mimic the healthier fat composition of meat from pigs reared on acorns and pasture [6]. Although this type of feeding improves the quality of meat from confined pigs, selling it as meat from free-range reared pigs would be a fraudulent practice. This activity is difficult to detect because the determination of the fatty acid profile using gas chromatography does not ensure identification of meat origin [7].

The volatile fraction of meat has proved decisive with a view to identifying the feeding regime used with pigs. The use of gas chromatographic techniques in combination with mass spectrometric detection (GC–MS) has allowed a variety of volatile compounds in meat to be identified and their usefulness for establishing meat provenance to be assessed [6,8,9]. Unfortunately, GC–MS techniques are extremely powerful but also time-consuming and expensive to implement, and hence impractical for the routine control of meat samples.

Ion mobility spectrometry (IMS) is a gas phase electrophoretic technique by which ions are separated by their relative mobility on the millisecond timescale. The underlying theory and detailed applications of this technique have been reviewed elsewhere [10,11]. IMS has been widely used for the rapid detection of explo-

* Corresponding author.
E-mail address: qa1meobj@uco.es (M. Valcárcel).

0039-9140/$ – see front matter © 2008 Elsevier B.V. All rights reserved.
doi:10.1016/j.talanta.2008.03.052

sives, chemical agents and toxic industrial chemicals, among others [12–16]. In addition, IMS can be useful in proteomic studies [17–19]. IMS equipment is robust and easy to miniaturize for field operation. IMS provides a very fast, sensitive, inexpensive tool for the efficient analysis and characterization of volatile compounds in samples of diverse nature [20–23].

The aim of this work was to assess the usefulness of the ion mobility spectrum for volatile compounds in subcutaneous fat samples with a view to identifying the feeding regime used with the pigs. The vast amount of data provided by IMS can be reduced by using statistical tools [24,25]. Here, principal component analysis (PCA) was used for this purpose and linear discriminant analysis (LDA) was employed for classification.

2. Experimental

2.1. Ion mobility spectrometer and conditions

Measurements were made with a portable UV–IMS instrument (35 cm × 35 cm × 15 cm, 5 kg) from Gesellschaft für analytische Sensorsysteme (Dortmund, Germany). The ionization source was a UV lamp of 10.6 eV. The instrument was operated at ambient pressure. The gas flow rate was controlled by means of an Alltech Digital Flow Check HR™ device from Chromatographie Service GMBH.

GASpector software was used to record spectra, which were acquired in the positive ion mode. A total of 25 spectra were continuously recorded for about 2 min per analysis, each spectrum being the average of 64 scans. The remaining instrumental settings used are summarized in Table 1.

2.2. Sample introduction

Fig. 1 shows the experimental set-up used. An amount of 1 g of subcutaneous fat sample was placed in a 10 mL glass vial which was then tightly sealed and heated at 150 °C in an Eco 1G thermoreactor (Velp Scientifica) for 40 min (volatilization step). Meanwhile, a stream of highly pure nitrogen from Abelló Linde (Barcelona, Spain) was passed through the UV–IMS system for cleaning and stabilization. After the 40 min, two stainless-steel selection valves (Selectomite®-7177G2Y, HOKE Incorporated, Spartanburg, SC) were actuated and the headspace vapours thus, formed in the vial swept out by the N_2 stream and transferred to the UV–IMS equipment for measurement (injection step).

Table 1
Instrumental settings used in the ion mobility spectrometer

Setting	
Spectrum length (points)	1024
Grid pulse width (μs)	500
Sampling frequency (kHz)	30
Repetition rate (ms)	50
Delay time (ms)	0.4
Sample flow-rate (mL min^{-1})	80
Drift flow-rate (mL min^{-1})	140
Electric field (V cm^{-1})	333
Tube length (cm)	12

2.3. Samples

Subcutaneous fat samples were obtained from 66 Iberian breed pigs of the Silvela Line from the 2004 to 2005 campaign. Two specimen types were considered. Type 1 ("free-range") specimens comprised 23 samples from pigs reared under the free-range regime and fed mainly on pasture and acorns for at least 2 months until reaching a weight of 160 kg in a *Q. ilex* dehesa in Fuenteobejuna (Córdoba, southern Spain). Type 2 specimens were obtained from 43 animals that were reared in confinement facilities and fed with commercial pig feed. The latter comprised two subgroups, namely: one consisting of fat samples from pigs fed with standard pig feed (type 2a, "standard feed", 20 samples) and the other of samples from animals fed with a special feed possessing an increased oleic acid content (type 2b, "high oleic acid feed", 23 samples).

All samples were analysed (Table 2) by using the Spanish official method of analysis [5], which involves gas chromatography (FID-GC) for the following fatty acids : palmitic (C16:0), stearic (C18:0), oleic (C18:1) and linoleic acid (C18:2).

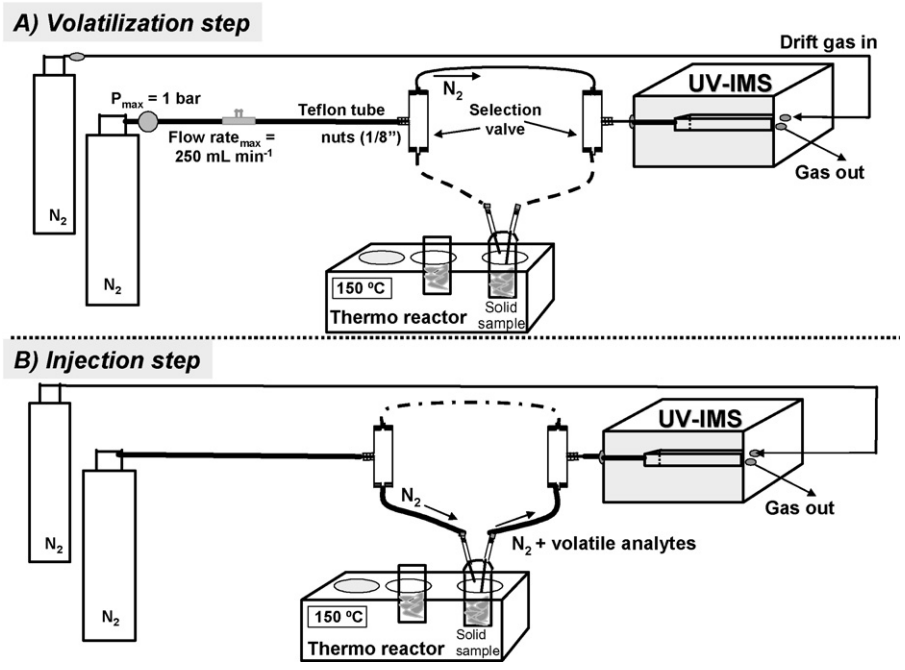

Fig. 1. Sample introduction system for the determination of volatile compounds by IMS.

Table 2
Fatty acid composition (%) of subcutaneous fat from pigs fed using various rearing methods

Samples	Type 1[a]	Type 2a[a]	Type 2b[a]	Reference[b]
C16:0	20 ± 1	21 ± 2	21.0 ± 0.2	≤21.3
C18:0	8 ± 1	12 ± 1	9.4 ± 0.5	≤9.8
C18:1	55 ± 3	42 ± 2	55 ± 1	≥54.0
C18:2	7 ± 1	8 ± 1	7 ± 1	≤9.8

[a] Mean value ± S.D. Type 1 (free range: 23 samples). Type 2a (standard feed: 20 samples). Type 2b (high oleic acid feed: 23 samples).
[b] Limits of fatty acids established for type 1 pigs (acorn classification) in Spanish legislation for the period 2004–2005.

2.4. Data analysis

Eleven spectra (5–15th) from the 25 recorded for each sample during the injection step were used to obtain an average spectrum for subsequent statistical analysis. The spectral range used spanned drift times from 16 to 32 ms (511 variables in all). Neither baseline correction nor smoothing was performed.

PCA and LDA were done with the SPSS 12.0 software package (SPSS Inc., Chicago, IL). PCA [26] is a data compression method which reduces the dimensionality of the original data matrix by constructing Principal Components (PCs) that are linear combinations of the original variables. The first few PCs capture much of the variability in the original data. Also, PCA is an unsupervised technique and allows relationships between variables and observations to be identified and structure in the data to be detected.

LDA [27] is a supervised classification technique that generates orthogonal linear discriminant functions from a set of samples for which class membership is known; the functions can then be applied to new samples of unknown class membership. The number of discriminant functions to be used is equal to the number of classes minus one.

In this work, the number of variables (511) was much greater than that of samples (66) and they were strongly correlated. This led us to use PCs scores instead of the original variables. Following the Kaiser criterion [28,29], only those PCs with eigenvalues greater than unity were retained. Stepwise discriminant analysis [27] was used to identify the most influential variables by using a statistical criterion to select the order of variable entry. Wilks' lambda [27] is a measure of separation quality that is computed as the determinant of the pooled within-class covariance matrix divided by the determinant of the covariance matrix for the whole set of samples. The smaller the result is, the better. In this work, variables were selected stepwise in terms of the largest decrease in Wilks' Lambda. The small number of samples available required that the models be evaluated using leave-one-out crossvalidation.

Table 3
Optimized parameter values for the sample introduction system

	Studied range	Optimum value
Sample weight (g)	0.1–2	1
Temperature (°C)	74–150	150
Heating time (min)	20–120	40
Teflon tube length (cm)	15–25	18

3. Results and discussion

The first step in the process of establishing the usefulness of IMS for authenticating the animal-feeding regime involved developing a simple procedure for introducing volatile compounds in subcutaneous fat into the IM spectrometer. An effective chemometric tool was needed to convert the chemical information contained in the ion mobility spectra into the required analytical information (i.e. the provenance of the meat in terms of animal feeding).

3.1. Sample introduction system (SIS)

A new sample introduction system was designed to extract volatile compounds from the solid fat samples and transfer them into the IM spectrometer. The system relies on the formation of a headspace which is created by encapsulating each sample in a glass vial that is carefully thermostated. The resulting gas phase is then introduced into the spectrometer by means of two selection valves (Fig. 1). Using such valves instead of injection syringes avoids errors arising from adsorption of sample components in syringes and minimizes the need to manipulate the sample.

The experimental variables optimized were the amount of sample, vial volume, temperature, heating time and tube length to the ionization chamber of the IMS equipment. Table 3 shows the selected value for each parameter.

One of the most crucial variables was the heating time, the effect of which was examined at 10 min intervals over the range 20–120 min. Tests were performed in duplicate on the three types

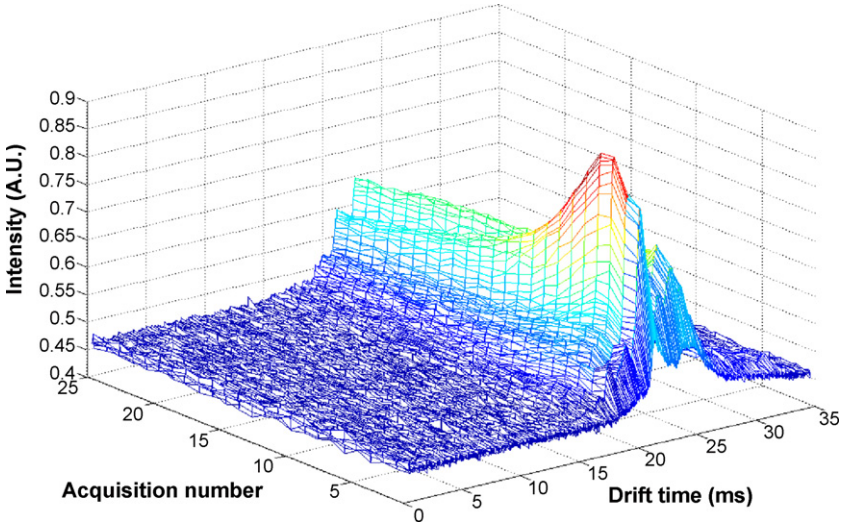

Fig. 2. Ion mobility spectra for a type 1 fat sample as recorded during the injection step.

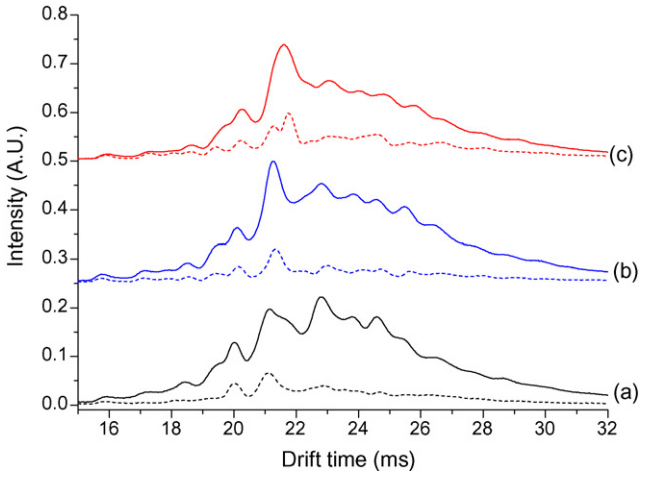

Fig. 3. Average spectra (solid lines) and standard deviation (dashed lines) for free-range (a, type 1), standard feed (b, type 2a) and high oleic acid feed (c, type 2b) fat samples.

of samples, using a constant temperature of 150 °C. Heating for up to 40 min was found to result in improved signals by effect of volatile compounds concentrating in the headspace, and also to maximize visual differences in the spectra for the different types of samples.

3.2. Ion mobility spectrometry of Iberian fat samples

Fig. 2 shows a typical IMS spectral profile. As can be seen, the signal appears shortly after the valves are switched, peaks and then decays in a virtually exponential manner. The relevant information is contained mainly in the spectral region from 16 to 32 ms drift time.

Although each measurement comprised 25 spectra, the average of 11 (5–15th) rather than a single scan at the maximum was used for chemometric treatment in order to ensure adequate reproducibility. In what follows, such an average spectrum is considered to be an IMS fingerprint from each fat sample.

Reproducibility was checked by measuring the same sample on 3 different days. The standard deviation thus, obtained in five replicates was 7%, which testifies to the robustness of the proposed approach.

Fig. 3 shows the average IMS spectra and standard deviations for subcutaneous fat samples from pigs reared under different feeding conditions. As can be seen, they exhibited many overlapped peaks. Also, although all types of samples gave some common peaks, each sample type could be distinguished from the others in the drift time region from 18 to 26 ms.

Identifying the individual compounds contributing to the IMS fingerprint of the fat samples is a complicated task owing to the high complexity of the data matrix; some useful conclusions can be drawn in this respect, however. Meat volatile compounds, which are stored mainly in adipose tissue by virtue of their lipophilic nature, have been widely studied as tracers of animal feeding systems. Thus, more than a hundred compounds have been identified in pig fat samples (especially aldehydes, aliphatic hydrocarbons, short-chain fatty acids and aromatic hydrocarbons).

Volatile compounds present in the studied fat samples must have an ionization energy bellow the energy of the UV ionization source used (10.6 eV) to be detected. Also, despite the absence of oxygen in the atmosphere of the proposed sample introduction system, the temperature rise during headspace generation probably caused the formation of compounds resulting from thermal degradation and heat-induced lipid oxidation.

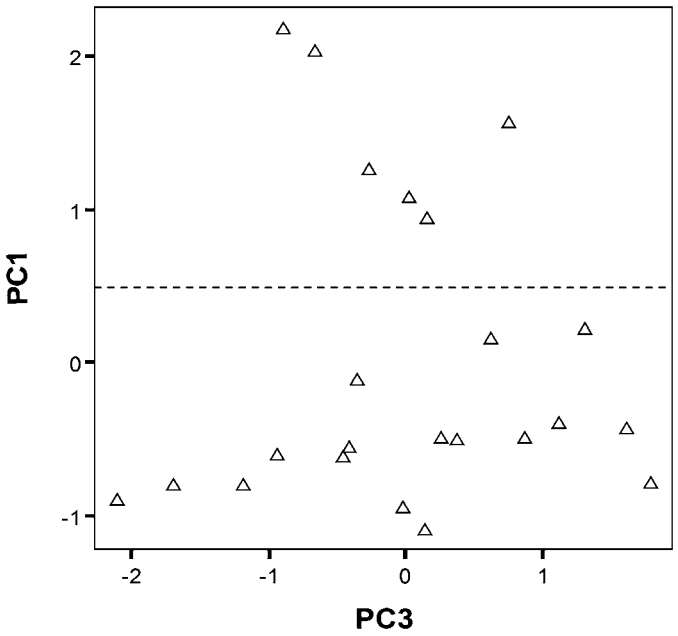

Fig. 4. PCA results (PC1 and PC3 scores plot) for the exploratory analysis of type 2b samples (23 samples).

The above-described differences between the IMS spectra for the fat samples from pigs fed in a free-range system (type 1) and pigs fed with commercial feed (type 2) testify to the potential of IMS for classifying fat samples according to pig feeding regime. However, further chemometric analysis was required in order to exploit this potential with a view to accurately classifying unknown samples. Principal component and discriminant analyses were used to this end.

3.3. Principal component analysis

PCA was performed separately on each sample group in order to detect potential outliers and groupings. Only one spectral outlier was found among type 1 samples. This free-range sample was discarded for further analysis. No clear-cut grouping pattern was observed within groups type 1 (free range samples) and type 2a (standard feed samples). However, PC1 seemingly split samples of high oleic acid feed (type 2b) into two different sub-groups. This can be seen in Fig. 4 which shows a scores plot of two PCs (PC1 and PC3) for type 2b samples. A sub-group of six samples showed much higher PC1 scores than the rest. In fact, these two subgroups corresponded to samples obtained from two different farms.

PCA was then performed on the whole data set (65 samples). Table 4 shows the cumulative variance explained by the different PCs. Surprisingly, even if type 1 and 2 (a and b) samples were examined jointly, the largest PC (67.7% of variance explained) was again that best resolving the above mentioned subgroups for type 2b samples. However, as can be seen in Fig. 5, the scores plot of PC2 and PC3 exhibited a tendency of the free-range class to separate from all other samples, even though there was a high degree of overlap between samples from animals fed with different types of commercial feed. Based on these results, the information contained in IMS spectra can be useful with a view to discriminating between fat samples from free-range pigs and confined pigs.

3.4. Discriminant analysis

The PCA scores of the first 15 PCs were considered to construct LDA models in order to reduce the dimensionality of the data.

Table 4
Cumulative variance of PCs with eigenvalues higher than one for the principal component analysis for the data set of 65 samples

Component	Cumulative variance (%)
1	67.711
2	77.389
3	83.355
4	88.656
5	91.385
6	92.778
7	93.913
8	94.925
9	95.773
10	96.355
11	96.806
12	97.238
13	97.552
14	97.843
15	98.045

One outlier sample has been removed.

Because the first few PCs are associated to the most important eigenvalues in the data covariance matrix, these are the directions with the greatest variance, but not necessarily those exposing the differences between the defined groups. Therefore, as shown in the previous exploratory analysis, the most discriminating directions need not be the first; in fact, the largest PC failed to discriminate between fat samples from free-range pigs and confined pigs, but accurately distinguished between two different origins of high oleic acid fat samples (type 2b). For this reason, stepwise feature selection was used to select the most discriminating PCs considering Wilks' Lambda.

As stated above, the main objective of this work was to distinguish fat samples from pigs reared outdoors from all other samples. A discriminant analysis considering these two groups (types 1 and 2) was required for this purpose. The second, third, fifth and tenth PC were thus, selected following the above-described procedure. The discriminant function constructed from these four components allowed 90.9% of the free-range samples to be accurately classified. The results of the classification tests are shown in Table 5. As can be seen, only one of the samples from confined pigs was misclassified as free-range fed on pasture and acorns.

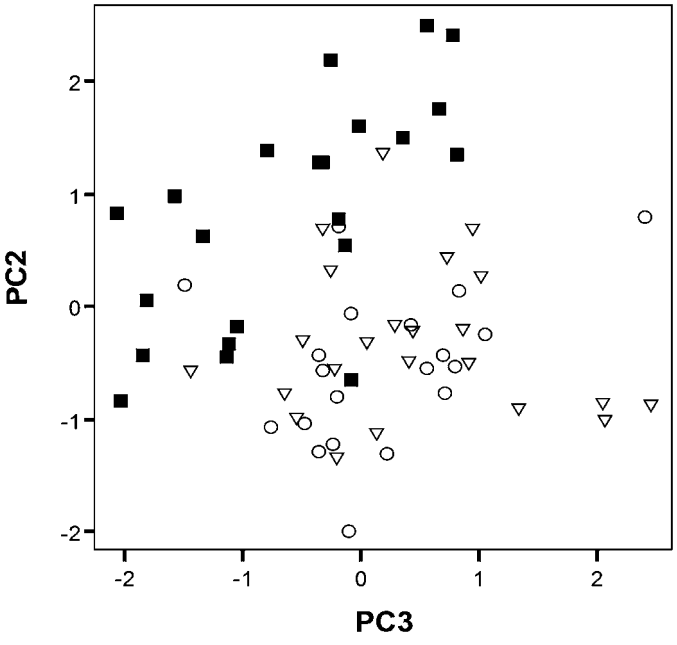

Fig. 5. PCA results (PC2 and PC3 scores plot) for the exploratory analysis of the whole sample set (65 samples). Samples: type 1 (■), type 2a (○) and type 2b (▽).

Table 5
Crossvalidation classification results for the discriminant analysis considering only two classes

Sample type	Predicted group membership		Total
	1	2	
Count			
1	20	2	22
2	1	42	43
%			
1	90.9	9.1	100.0
2	2.3	97.7	100.0

Type 1 (free-range) and type 2 (feed).

Interestingly, based on the results obtained with the official method (Table 2), type 2b fat samples (high oleic acid feed) are more similar to type 1 (free range) samples than to type 2a (standard feed) samples as regards the four major fatty acids. Therefore, type 2b samples cannot be distinguished from type 1 samples on the basis of these four fatty acids alone. However, other volatile compounds present in fat samples and detected by UV–IMS can be of assistance for this purpose.

In order to further investigate the possibility of discriminating among feeding regimes, a new discriminant analysis was performed on the "free range", "standard feed" and "high oleic acid feed" groups. The PCs previously selected with the stepwise procedure were also used to construct two discriminant functions to this end. Discrimination between type 1 samples and the others was quite accurate (90.9% such samples were correctly classified); however, the classification rules failed in the discrimination between samples from animals fed on standard feed (type 2a) and high oleic acid feed (type 2b) for which only 60% and 56.5%, respectively, were accurately classified.

The previously described PCA results in the exploratory analysis suggested the presence of two subgroups within the high oleic acid feed (type 2b) group. This could be the reason of the nonsatisfactory results of the classification. The possibility of splitting such samples in two classes according to their different farm origin, viz. types $2b_1$ (6 samples) and $2b_2$ (17 samples) was considered in the discrimination process with the aim of improving the classification results for feed samples. In this way, four classes were considered. Stepwise feature selection was again performed and PC1 was additionally selected as one of the most important discriminating features. Fig. 6 and Table 6 show the results of the analysis. As can clearly be seen from the figure, the six samples of class $2b_1$ were much more similar

Table 6
Crossvalidation classification results for the discriminant analysis considering four classes

Sample type	Predicted group membership				Total
	1	2a	$2b_1$	$2b_2$	
Count					
1	21	1	0	0	22
2a	0	14	2	4	20
$2b_1$	0	1	5	0	6
$2b_2$	1	1	0	15	17
%					
1	95.5	4.5	0.0	0.0	100.0
2a	0.0	70.0	10.0	20.0	100.0
$2b_1$	0.0	16.7	83.3	0.0	100.0
$2b_2$	5.9	5.9	0.0	88.2	100.0

Type 1 (free-range), type 2a (standard feed) and type $2b_1$ and $2b_2$ (two classes of high oleic acid feed).

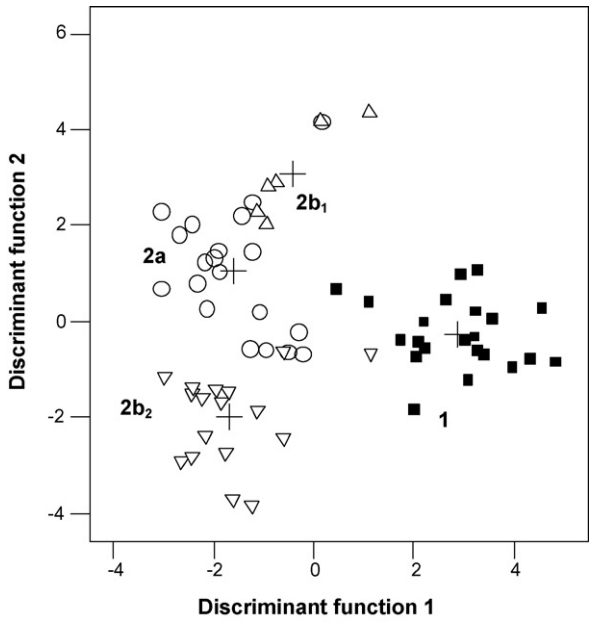

Fig. 6. Classification plot for the LDA as obtained by using four sample classes. Samples: type 1 (■); type 2a (○); type $2b_1$ (△) and type $2b_2$ (▽). Centroid groups are denoted by (+).

to the standard feed samples (2a) than to all others of high oleic acid feed. This is why discrimination between the latter two classes was impossible when all high oleic acid feed samples were included in a single group. The predictions of the different types of feed were acceptable (70.0%, 83.3%, and 88.2% for types 2a, $2b_1$ and $2b_2$, respectively), but reflected overlap between classes 2a and $2b_1$. The classification results for the free-range (type 1) samples obtained by using the four sample classes were slightly better (95.5% of accurate predictions) than those provided by only two classes. Classification errors occurred because some free-range samples were not recognized as such; expanding the calibration sample set with more samples can be expected to reduce this effect. Again, only one sample of high oleic acid feed was erroneously identified as belonging to free-range pigs fed on pasture and acorns. Interestingly, whereas the fatty acid profile considered in current regulations can be easily matched for high oleic acid feed (see Table 2), this sample type is correctly recognized by IMS.

4. Conclusions and outlook

A simple, reliable method for the extraction of volatile compounds from solid samples and their subsequent automatic introduction and detection in an ion mobility spectrometer was developed. Volatile compounds in subcutaneous fat samples from Iberian pigs can be accurately analysed by IMS. The proposed methodology allows the IMS fingerprint of subcutaneous fat samples from Iberian pigs to be obtained with a view to distinguishing pig feeding regimes.

The IMS data require chemometric processing. The combined use of UV–IMS and chemometrics enables accurate discrimination even when pigs are fed in a way that mimics the fatty acid profile of free-range pigs. For this reason, IMS provides an effective new tool for detecting potentially fraudulent attempts. This cannot be accomplished by simply using gas chromatography to detect only the four major fatty acids included in the Spanish official method. Further work with UV–IMS coupled to mass spectrometry may facilitate the identification of the specific volatile compounds responsible for the differences between samples obtained from pigs fed under each regime.

Acknowledgements

This work was funded by DGI, Spain's Ministry of Science and Technology, within the framework of Project CTQ2004-01220. The authors are also grateful to Turcañada, S.L. for providing fat samples.

References

[1] M. Lees, Food Authenticity and Traceability, Woodhead Publishing Ltd, Cambridge, U.K., 2003.
[2] M. Valcarcel, S. Cardenas, TrAC Trends Anal. Chem. 24 (2005) 67.
[3] C. Garcia, J.J. Berdague, T. Antequera, C. Lopez-Bote, J.J. Cordoba, J. Ventanas, Food Chem. 41 (1991) 23.
[4] R.O. Myer, D.D. Johnson, D.A. Knauft, D.W. Gorbet, J.H. Brendemuhl, W.R. Walker, J. Animal Sci. 70 (1992) 3734.
[5] BOE no. 283, November 24, 2004.
[6] M.L. Timon, L. Martin, M.J. Petron, A. Jurado, C. Garcia, J. Sci. Food Agric. 82 (2001) 186.
[7] L. Ninoles, G. Clemente, S. Ventanas, J. Benedito, Meat Sci. 76 (2007) 102.
[8] E. Muriel, T. Antequera, M.J. Petron, A.I. Andres, J. Ruiz, Meat Sci. 68 (2004) 391.
[9] V. Vasta, J. Ratel, E. Engel, J. Agric. Food Chem. 55 (2007) 4630.
[10] G.A. Eiceman, TrAC Trends Anal. Chem. 21 (2002) 259.
[11] C.S. Creaser, J.R. Griffiths, C.J. Bramwell, S. Noreen, C.A. Hill, C.L. Thomas, Analyst 129 (2004) 984.
[12] W.E. Steiner, B.H. Clowers, L.M. Matz, W.F. Siems, H.H. Hill, Anal. Chem. 74 (2002) 4343.
[13] A.B. Kanu, J. Hill, Talanta 73 (2007) 692.
[14] M.T. Jafari, T. Khayamian, V. Shaer, N. Zarei, Anal. Chim. Acta 581 (2007) 147.
[15] P. Dwivedi, L. Matz, D. Atkinson, H. Hill Herbert Jr., Analyst 129 (2004) 139.
[16] N. Budimir, D. Weston, C.S. Creaser, Analyst 132 (2007) 34.
[17] J.A. McLean, D.H. Russell, J. Proteome Res. 2 (2003) 427.
[18] S. Myung, Y.J. Lee, M.H. Moon, J. Taraszka, R. Sowell, S. Koeniger, A.E. Hilderbrand, S.J. Valentine, L. Cherbas, P. Cherbas, T.C. Kaufmann, D.F. Miller, Y. Mechref, M.V. Novotny, M.A. Ewing, C.R. Sporleder, D.E. Clemmer, Anal. Chem. 75 (2003) 5137.
[19] R.W. Purves, D.A. Barnett, B. Ells, R. Guevremont, J. Am. Soc. Mass Spectrom. 12 (2001) 894.
[20] J.I. Baumbach, S. Sielemann, Z. Xie, H. Schmidt, Anal. Chem. 75 (2003) 1483.
[21] G.M. Bota, P.B. Harrington, Talanta 68 (2006) 629.
[22] W. Vautz, J. Baumbach, E. Uhde, Anal. Bioanal. Chem. 384 (2006) 980.
[23] T. Keller, A. Miki, P. Regenscheit, R. Dirnhofer, A. Schneider, H. Tsuchihashi, Forensic Sci. Int. 94 (1998) 55.
[24] S. Bader, W. Urfer, J.I. Baumbach, Int. J. Ion Mobility 8 (2005) 1.
[25] S. Bader, W. Urfer, J.I. Baumbach, J. Chemometr. 20 (2006) 128.
[26] K.R. Beebe, R.J. Pell, M.B. Seasholtz, Chemometrics: A Practical Guide, 1st ed., Wiley Interscience, New York, USA, 1998.
[27] B.G.M. Vandeginste, D.L. Massart, L.M.C. Buydens, S. De Jong, P.J. Lewi, J. Smeyers-Verbeke, Handbook of Chemometrics and Qualimetrics: Part B, Elsevier, Amsterdam (The Netherlands), 1998.
[28] H. Kaiser, Educ. Psycholog. Meas. 20 (1960) 141.
[29] N.C. Thanasoulias, E.T. Piliouris, M.S. Kotti, N.P. Evmiridis, Forensic Sci. Int. 130 (2002) 73.

Talanta 76 (2008) 575–579

Contents lists available at ScienceDirect

Talanta

journal homepage: www.elsevier.com/locate/talanta

Simultaneous determination of Cd, Cu, Mn, Ni, Pb and Zn in nail samples by inductively coupled plasma mass spectrometry (ICP-MS) after tetramethylammonium hydroxide solubilization at room temperature: Comparison with ETAAS

Bruno L. Batista[a], Jairo L. Rodrigues[a], Juliana A. Nunes[a], Luciano Tormen[b], Adilson J. Curtius[b], Fernando Barbosa Jr.[a,*]

[a] *Laboratório de Toxicologia e Essencialidade de Metais, Depto. de Análises Clínicas, Toxicológicas e Bromatológicas, Faculdade de Ciências Farmacêuticas de Ribeirão Preto-USP, Avenida do Café s/n, Monte Alegre 14040-903, Ribeirão Preto-SP, Brazil*
[b] *Universidade Federal de Santa Catarina, Depto. Química, Campus Trindade, 88040900 Florianópolis, SC, Brazil*

ARTICLE INFO

Article history:
Received 14 February 2008
Received in revised form 24 March 2008
Accepted 26 March 2008
Available online 7 April 2008

Keywords:
ICP-MS
ETAAS
Nail samples
Trace elements
Rapid determination
Tetramethylammonium hydroxide

ABSTRACT

A simple method is described for the determination of Cd, Cu, Mn, Ni, Pb and Zn in nails by using inductively coupled plasma mass spectrometry (ICP-MS) or electrothermal atomic absorption spectrometry (ETAAS). Prior to analysis, 10–20 mg of nail samples were accurately weighed into (15 mL) conical tubes. Then, 1 mL of 25% (w/v) tetramethylammonium hydroxide (TMAH) solution was added to the samples, incubated at room temperature overnight and then further diluted to 10 mL with 1% (v/v) HNO_3. After that, samples were directly analyzed. Rhodium was used as internal standard for ICP-MS analysis. Method detection limits (3 s, $n = 20$) were 0.1, 3.0, 1.0, 4.5, 1.5, 5.0 ng g^{-1} for Cd, Cu, Mn, Ni, Pb and Zn, respectively for ICP-MS, and 24, 26, 30, 143, 130 and 1000 ng g^{-1}, respectively for ETAAS. The key issue addressed here is the elimination of the acid digestion prior to analysis. Moreover, with the use of the proposed method there is a considerable improvement in the sample throughput comparing to the traditional methods using microwave-assisted acid sample digestion prior to analysis. For validation purposes, six ordinary nail samples were solubilized and then directly analyzed by ICP-MS and ETAAS, with no statistical difference between the two techniques at 95% level on applying the *t*-test.

1. Introduction

Nail is a biological specimen that has some advantages as a biomarker for trace elements exposure, especially because its collection is noninvasive and simple and because nail samples are very stable after collection, not requiring special storage conditions [1,2]. Trace elements in nails reflect long-term exposure because this compartment remains isolated from other metabolic activities in the body [2,3]. Because toenails are less affected by exogenous environmental contamination than fingernails, they have been preferred for exposure to toxic metals [3]. Toenails have a slower growth rate than fingernails (up to 50% slower, especially in winter) and thus may provide a longer integration of the exposure [2–4].

Atomic absorption spectrometry (AAS) [5,6] and inductively coupled plasma emission spectrometry (ICP-OES) [7] are still the dominant analytical techniques used for trace element analysis in nail samples. However, the use of inductively coupled plasma mass spectrometry (ICP-MS) is becoming much more common in clinical laboratory analysis [3,8–12]. Compared to electrothermal atomic absorption spectrometry (ETAAS) or ICP-OES, this technique has some distinct advantages, including simultaneous multielement measurement capability coupled with very low detection limits [7]. Moreover, it offers a wider linear dynamic range which allows the determination of major and trace elements at same sample injection [8–10]. Additionally, compared to ICP-OES, ICP-MS provides simpler spectral interpretation and isotopic information [8].

Sample preparation is a critical and laborious step for chemical elements determination in biological samples [13–16]. In the case of nails, usually, samples are digested in acid medium prior to analysis. Wet digestion procedures in open [3] or closed vessels with microwave-assisted acid digestion [6,10] has been used for this purpose. However, both methods may be time-consuming for laboratories operating in routine with large amount of samples to be analyzed and require the use of concentrated acids and careful monitoring of digestion [11]. On the other hand, in clin-

* Corresponding author. Tel.: +55 16 36024701.
E-mail address: fbarbosa@fcfrp.usp.br (F. Barbosa Jr.).

0039-9140/$ – see front matter © 2008 Elsevier B.V. All rights reserved.
doi:10.1016/j.talanta.2008.03.046

ical laboratories, more attention has been given to methods of sample preparation with minimal handling and time consumption [17,18].

Nail is composed of keratin proteins. The sulfur in cysteine molecules in adjacent keratin proteins link together in disulfide chemical bonds. These disulfide bonds are very strong and very difficult to break apart. These disulfide chemical bonds linking the keratins together are the key factor in the durability and resistance of nail fiber. They are largely resistant to the action of acids but the disulfide bonds can be broken apart by alkali solutions, making the nail weak. Tetramethylammonium hydroxide (TMAH), an alkaline solution, has been previously used for sample pre-treatment as an attractive alternative to microwave-assisted acid digestion of biological materials for the determination of trace elements by different atomic spectrometry techniques [19–26]. For example, Pozebon et al. [24] used TMAH to dissolve biological samples for the determination of Tl, Pb, Ag, Hg and Cd by electrothermal vaporization inductively coupled plasma mass spectrometry (ETV-ICP-MS) and Moreton and Delves [25] used TMAH in one of their diluents for the determination of total Hg in whole blood by ICP-MS.

The aim of this study was to develop a simple method for the determination of five elements in nail samples by ICP-MS, that can also be applied for ETAAS analysis, using a sample solubilization with TMAH and then a dilute-and-shoot sample analysis.

2. Experimental

2.1. Reagents

All reagents used were of analytical-reagent grade (Sigma, St. Louis, MO, USA), except HNO_3 (Sigma, St. Louis, MO, USA) which was previously purified in a quartz sub-boiling stills (Kürner) before use. A clean laboratory and laminar-flow hood capable of producing class 100 were used for preparing solutions. High purity de-ionized water (resistivity 18.2 mΩ cm) obtained using a Milli-Q water purification system (Millipore, Bedford, MA, USA) was used throughout. All solutions were stored in high-density polyethylene bottles. Plastic bottles and glassware materials were cleaned by soaking in 10% (v/v) HNO_3 for 24 h, rinsing five times with Milli-Q water and dried in a class 100 laminar flow hood before use. All operations were performed in a clean bench.

For the ETAAS method, stock solutions containing 1000 mg L^{-1} of each element were obtained from PerkinElmer (PerkinElmer, Norwalk, CT, USA). Analytical calibration standards were prepared daily over the range of 5–40; 0.5–5; 1.0–50; 1.0–10; 5–50; 0.5–3.0 μg L^{-1} for Pb, Cd, Cu, Mn, Ni and Zn respectively by suitable serial dilutions of each stock solution in 2.5% (w/v) TMAH + 1% (v/v) HNO_3. For Cd and Pb determination, graphite tubes were previously coated with iridium according to the method proposed by Borges et al. [27]. The modifier solution was prepared by the suitable dilution of the 1000 mg L^{-1} Ir stock standard (PerkinElmer, Norwalk, CT, USA).

For the ICP-MS method, multielement stock solutions containing 1000 mg L^{-1} of each element were obtained from PerkinElmer (PerkinElmer, Norwalk, CT, USA). Analytical calibration standards were prepared daily over the range of 0–20 μg L^{-1} for all elements by suitable serial dilutions of multielement stock solution in 2.5% (w/v) TMAH + 1% (v/v) HNO_3. Rhodium was used as internal standard at the concentration of 10 μg L^{-1} Rh. The internal standard was diluted from 1000 mg L^{-1} stock standard (PerkinElmer, Norwalk, CT, USA). A rinse solution consisting of 0.005% (v/v) Triton X-100® in 2% (v/v) nitric acid was prepared before each run.

Table 1
Optimal heating programs for the determination of Cd, Cu, Mn, Ni, Pb and Zn in nails after TMAH solubilization (30 μL injection volume)

Temperature (°C)	Ramp (°C s^{-1})	Hold (s)	Gas flow rate (L min^{-1})
90	5	15	250
120	10	15	250
600[a]/700[b]/800[c]/1000[d,e,f]	20	15	250
20	1	3	250
1500[a]/1600[b,c]/2200[d,e]/2400[f]	0	5	0
1900[b,c]/2000[a]/2500[d,e,f]	1	5	250

[a] Zn.
[b] Cd.
[c] Pb.
[d] Cu.
[e] Ni.
[f] Mn.

2.2. Instrumentation

2.2.1. Electrothermal atomic absorption spectrometric method

Cadmium, copper, lead, manganese, nickel and zinc were determined in nails by using a AAnalyst 100 atomic absorption spectrometer (PerkinElmer, Norwalk, CT, USA), equipped with an HGA 800 longitudinally heated graphite tube atomizer and an AS-72 autosampler (PerkinElmer). Deuterium-arc background correction was employed to correct for non-specific absorption. All measurements were performed using integrated absorbance (peak area). Hollow cathode lamps for Cd, Pb, Ni, Mn, Cu and Zn (PerkinElmer) were operated at 4, 10, 25, 20, 15 and 15 mA, respectively, with a spectral bandwidth of 0.7, 0.7, 0.2, 0.2, 0.7 and 0.7 nm, respectively. The selected wavelengths were 228.8, 283.3, 232.0, 279.5, 324.8 and 213.9 nm for Cd, Pb, Ni, Mn, Cu, Zn, respectively. Argon 99.996% (White Martins, São Paulo, SP, Brazil) was used as protective and purge gas. Pyrolytic graphite coated polycrystalline electrographite tubes with total pyrolytic graphite platforms (PerkinElmer) were used throughout. Then, 30 μL of diluted samples was directly deposited onto the L'vov platform. The used heating programs used are given in Table 1.

2.2.2. Inductively coupled plasma mass spectrometry method

We used a PE ELAN DRC II ICP-MS instrument (PerkinElmer Life and Analytical Sciences) for the determination of elements in nails. Typical daily instrumental parameters are given in Table 2. Although this instrument can be used in the DRC mode to remove polyatomic interferences, we operated it solely in standard mode, i.e., with the DRC valve vented, for the determination of metals.

Table 2
ICP-MS operating conditions

PerkinElmer Elan DRC II	
Spray chamber	Cyclonic
Nebulizer	Meinhard®
RF power (W)	1100
Ar nebulizer gas flow (L min^{-1})	0.7–0.9 (optimized daily)
Measures	
Scan mode	Peak hopping
Resolution (amu)	0.7
Replicate time (s)	1
Dwell time (s)	50
Sweeps/reading	20
Integration time (ms)	1000
Replicates	3
Isotopes	^{63}Cu, ^{111}Cd, ^{208}Pb, ^{60}Ni, ^{55}Mn, ^{64}Zn
Correction equations	
Cadmium = $^{114}Cd - (0.027250 \times {}^{118}Sn)$	
Lead = $(^{204}Pb - [0.230074 \times {}^{202}Hg]) + {}^{206}Pb + {}^{207}Pb + {}^{208}Pb$	

Then, the proposed method can be used with simple quadrupole ICP-MS equipments. The ICP-MS was operated with Pt sampler and skimmer cones purchased from PerkinElmer. Argon 99.999% (White Martins, São Paulo, SP, Brazil) was used. The instrument conditions and measurement parameters used are listed in Table 2.

2.3. Specimen collection and washing

Fingernails were clipped with a stainless steel cutting instrument providing samples ranging in mass from 10 to 20 mg. Then, they were washed in 1% Triton X-100® and acetone and dried in a class 100 laminar-flow hood.

For comparison with literature data on background levels for metals in nails we also analyzed 35 human nail clippings collected from healthy and non-exposed subjects. These specimens had been obtained with informed consent from human subjects in accordance with procedures approved by our Institutional Review Board.

2.4. Specimen solubilization and dilution for GF AAS and ICP-MS analysis

For both ETAAS and ICP-MS methods, cleaned nail clippings (10–20 mg) were accurately weighed into (15 mL) conical tubes. Then, 1 mL of 25% (w/v) TMAH solution was added to the samples, incubated at room temperature overnight, vortexed for 5 min and then the volume made up to 10 mL with 1% (v/v) HNO_3. For ICP-MS analysis, rhodium was added as internal standard to get 10 $\mu g\,L^{-1}$ final concentration.

3. Results and discussion

Preliminary experiments were carried out to explore the feasibility of analyzing nail specimens (20 mg) incubated with 1 mL of 25% (w/v) TMAH solution at room temperature for 4 h and then the volume made up to 10 mL with MilliQ water. For this experiment, calibrations in TMAH medium were used for both ETAAS and ICP-MS analysis. However, there was a considerable instability of signals from the standard solutions, probably due the formation of metal hydroxides in basic pH conditions. To avoid this, nail specimens were incubated with TMAH and then diluted in acid medium to drop the pH. Nitric acid was selected for this experiment. Based on optimization studies, better conditions were attained after incubation of nail samples (20 mg) with 1 mL of 25 (w/v) TMAH and then the volume made up to 10 mL with 1% (v/v) HNO_3. All subsequent work utilized this sample preparation protocol for both techniques.

3.1. Solubilization time

The required time for clipping nail solubilization in TMAH medium was checked. For this study, ordinary nail clipping samples collected from one volunteer was used. In each of five tubes, a nail clipping sample (~20 mg) was diluted with 1 mL of 25% (m/v) TMAH; the tubes were incubated at room temperature for 1, 2, 4, 6, 8 h and overnight and then mixed (vortex) for 5 min. Only 4 h incubation time with TMAH at room temperature was good enough to solubilize nail clippings. However, in case of routine analysis with large amount of samples, we recommend that one might leave samples incubating overnight and in the next day dilute the samples with HNO_3 before the analysis. In this way, if ICP-MS is the technique of choice, at least 500 samples can be prepared and analyzed in 3 days.

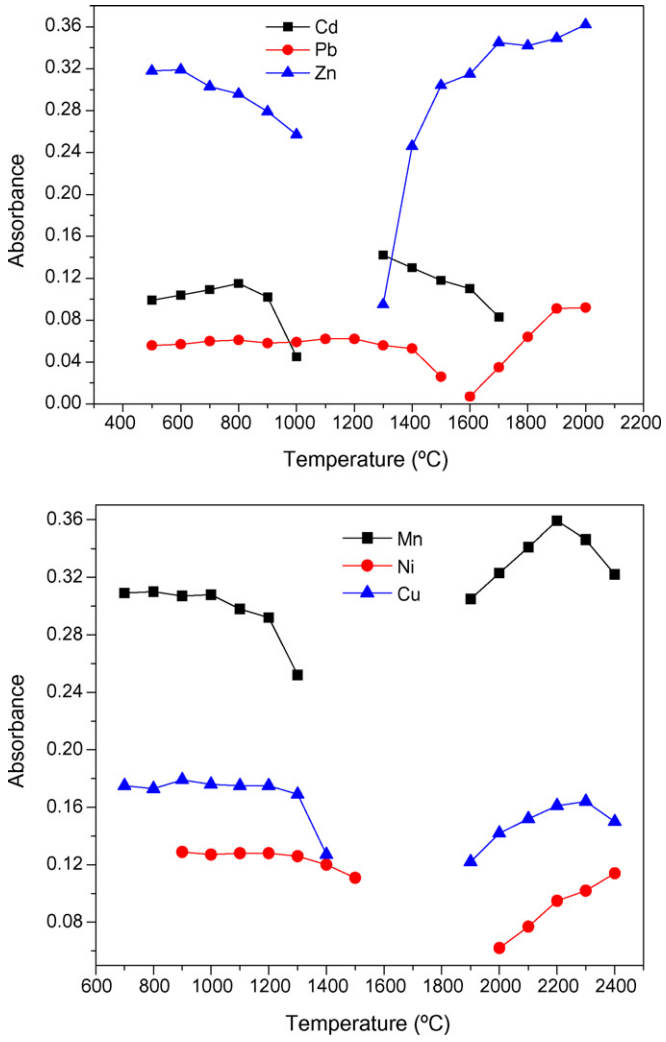

Fig. 1. Pyrolysis and atomization curves for Cd (20 pg), Pb (0.4 ng), Zn (20 pg), Mn (100 pg), Cu (100 pg), Ni (400 pg) and Zn (20 pg) in 2.5 (v/v) TMAH + 1.0% (v/v) HNO_3 medium.

3.2. Pyrolysis and atomization curves for the determination by ETAAS

Pyrolysis and atomization curves were used to find the optimum heating program for lead, cadmium, copper, manganese and nickel in ETAAS analysis. Fig. 1, shows the pyrolysis and atomization curves for, Cd (20 pg), Cu (100 pg), Mn (100 pg), Ni (400 pg) Pb (0.4 ng) and Zn (20 pg) diluted first with TMAH and then with HNO_3 on the same manner of solubilized samples. For Pb and Cd, graphite furnaces were previously coated with Ir (permanent modifier). Similar thermal behavior was also observed for the analytes in solubilized matrix. Based on the curves, the heating program shown in Table 1 was used for the determination of the analytes in nails by ETAAS.

3.3. Sample calibration

For both ICP-MS and ETAAS analysis, a simple method of calibration by using external standards to simplify the analysis and improve the sample throughput rate was applied. Standards were diluted in TMAH and HNO_3 (see Section 2). For ICP-MS analysis, the use of internal standards is recommended in routine analysis to compensate the possible drift during long-term runs.

Table 3
Trace elements in nail samples by ETAAS and ICP-MS methods ($n = 4$, mean ± S.D.)

Samples	Cu ($ng\,g^{-1}$)		Ni ($ng\,g^{-1}$)		Cd ($ng\,g^{-1}$)		Pb ($ng\,g^{-1}$)		Mn ($ng\,g^{-1}$)		Zn ($\mu g\,g^{-1}$)	
	ETAAS	ICP-MS	ETAAS	ICP-MS	ETAAS	ICP-MS	ETAAS	ICP-MS	ETAAS	ICP-MS	ETAAS	ICP-MS
1	4799 ± 106	4939 ± 130	580 ± 76	670 ± 83	<LOQ	23 ± 1	188 ± 28	153 ± 10	659 ± 7	675 ± 12	93 ± 3	101 ± 5
2	6190 ± 54	6355 ± 170	1221 ± 29	1090 ± 110	<LOQ	26 ± 2	218 ± 30	240 ± 16	646 ± 20	584 ± 49	81 ± 1	87 ± 4
3	5682 ± 63	5768 ± 110	813 ± 22	864 ± 40	<LOQ	32 ± 2	257 ± 33	266 ± 12	578 ± 10	519 ± 52	100 ± 4	103 ± 5
4	4523 ± 64	5120 ± 284	2098 ± 37	1823 ± 70	<LOQ	13 ± 1	<LOQ	112 ± 3	749 ± 4	684 ± 62	88 ± 1	89 ± 4
5	8723 ± 111	8721 ± 250	1978 ± 33	1839 ± 80	<LOQ	52 ± 3	277 ± 10	298 ± 20	646 ± 16	651 ± 30	109 ± 1	104 ± 3
6	6545 ± 26	6824 ± 180	2479 ± 66	2490 ± 80	<LOQ	39 ± 1	308 ± 20	276 ± 16	823 ± 25	795 ± 59	105 ± 2	101 ± 3

LOQ = limit of quantification were obtained as 10 s of the 20 consecutive measurements of the reagent blanks multiplied by the dilution factor used for sample preparation (20 mg of sample in 10 mL solution).

Table 4
Descriptive statistics for the trace elements concentration in fingernails ($\mu g\,g^{-1}$). Samples were analyzed by ICP-MS with the proposed method

	Cd	Pb	Mn	Cu	Ni	Zn
This study	(0.011–0.123)	(0.10–0.83)	(0.35–1.1)	(3.9–9.1)	(0.41–3.22)	(73–140)
Rodushkin and Axelsson [28]	(0.013–0.438)	(0.27–4.75)	(0.19–3.30)	(4.2–17)	(0.14–6.95)	(80–191)
Menezes et al. [29]	–	–	(1.2–1.7)	(3–46)	–	(57–290)
Mehra and Juneja [30]	(0.67–1.31)	–	(8.1–12.3)	(6.2–9.1)	–	(135–225)
Were et al. [31]	(0.01–3.70)	(5.5–77.5)	–	–	–	(34.4–317.0)
Mortada et al. [32]	(0.2–2.8)	(1.8–9.7)	–	–	–	–

Based on this, three internal standards, namely Rh, Ir and Y, were evaluated in this study. Rhodium showed to be the best internal standard (based on repeatability variation of the measurements) for the five analytes in study. Then, all nail samples and standards were prepared containing 10 $\mu g\,L^{-1}$ Rh for ICP-MS analysis.

3.4. Method validation

The recommended way to validate a method is to analyze a Standard Reference Material and/or to compare results obtained by two different techniques. However, no Certified Reference Material of nail is commercially available. Then, for validation purposes, six ordinary fingernail clippings (collected from three volunteers) were prepared according to the proposed method and then divided in two fractions, one was analyzed by ICP-MS and the other one by ETAAS. The results are shown in Table 3. No statistical differences at 95% level on applying the *t*-test were observed between values found in both techniques, demonstrating the accuracy of both methods.

3.5. Analytical characteristics

For the proposed solubilization procedure the method detection limits (MDLs) obtained were 0.1, 3.0, 1.0, 4.5, 1.5, 5.0 $ng\,g^{-1}$ for Cd, Cu, Mn, Ni, Pb and Zn, respectively for ICP-MS, and 24, 26, 30, 143, 130 and 1000 $ng\,g^{-1}$, respectively for ETAAS. The MDLs were obtained as 3 s of the 20 consecutive measurements of the reagent blanks multiplied by the dilution factor used for sample preparation (20 mg of sample in 10 mL solution).

3.6. Human nail analysis by ICP-MS method

For the purpose of comparing background levels of trace metals in nails of the Brazilian populations with the published ranges in other countries, we also analyzed 35 human fingernails clippings (the selected subjects were healthy and non-exposed to heavy metals). Samples were analyzed by ICP-MS by applying the proposed method. The obtained ranges are shown in Table 4 together with reference ranges published in other studies.

4. Conclusions

The proposed solubilization method showed to be reliable for the determination of Cd, Cu, Mn, Ni, Pb and Zn in nail samples either by inductively coupled plasma mass spectrometry or ETAAS. Moreover, the proposed method is simple, not requiring expensive instrumentation, heating or constant supervision of sample digestion. If ICP-MS is the technique of choice and considering the time for sample preparation (overnight) and the analysis, one technician can routinely analyzed at least 500 samples in three days. With our experience in large routine analysis of clinical specimens, with the use of commercially available microwave oven systems at least 15 days are necessary to digest 500 nail samples (one technician working 8 h/day). Then, with the proposed method there is a considerable improvement in the sample throughput comparing to the traditional methods using microwave-assisted acid sample digestion prior to analysis.

Acknowledgements

The authors are grateful to Fundação de Amparo à Pesquisa do Estado de São Paulo (FAPESP) and Conselho Nacional de Desenvolvimento Científico e Tecnológico (CNPq) for financial support and fellowships.

References

[1] F. Barbosa, J.E. Tanus-Santos, R.F. Gerlach, P.J. Parsons, Environ. Health Perspect. 113 (2005) 1669.
[2] H.C. Hoppes, Sci. Total Environ. 7 (1977) 71.
[3] M.J. Slotnick, J.R. Meliker, G.A. AvRuskin, D. Glosh, J.R. Nriagu, J. Toxicol. Environ. Health 70 (2007) 148.
[4] A. Sukumar, Rev. Environ. Contam. Toxicol. 185 (2005) 141.
[5] B. Nowak, J. Chmielnicka, Ecotox. Environ. Saf. 46 (2000) 265.
[6] M.J.L. Alonso, A.B. Barrera, J.A.C. de Juan, J.M.F. Bermúdez, P.B. Barrera, J. Trace Elem. Med. Biol. 19 (2005) 49.
[7] Y.C. Yoo, S.K. Lee, J.Y.J.Y. Yang, S.W. In, K.W. Kima, K.H. Chung, M.G. Chung, S.Y. Choung, J. Health Sci. 48 (2002) 186.
[8] P.J. Parsons, F. Barbosa, Spectrochim. Acta 62B (2007) 992.
[9] J.P. Goulle, L. Mahieu, J. Casternant, N. Neveu, L. Bonneau, G. Laine, D. Bouige, C. Lacroix, Forensic Sci. Int. 153 (2005) 39.
[10] I. Rodushkin, M.D. Axelsson, Sci. Tot. Environ. 250 (2000) 83.
[11] F. Barbosa, I. Ramires, M.H.C. Rodrigues, T.D. SaintïPierre, A.J. Curtius, M.R. Buzalaf, R.F. Gerlach, J.E. Tanus-Santos, Environ. Res. 102 (2006) 90.
[12] A. Schultz, I.A. Bergahl, A. Ekholm, S. Skerfving, Occup. Environ. Med. 53 (1996) 736.

[13] E.C. Lima, F. Barbosa, F.J. Krug, M.M. Silva, M.G.R. Vale, J. Anal. Atom. Spectrom. 15 (2000) 995.
[14] S.S. Souza, D. Santos, F.J. Krug, F. Barbosa, Talanta 73 (2007) 451.
[15] B.J. Bolann, R. Rahil-Khazen, H. Henriksen, R. Isrenn, R.J. Uluik, J. Scand, Clin. Lab. Invest. 67 (2007) 353.
[16] E.C. Lima, F. Barbosa, F.J. Krug, Anal. Chim. Acta 409 (2000) 267.
[17] C.D. Palmer, M.E. Lewis, C.M. Geraghty, F. Barbosa, P.J. Parsons, Spectrochim. Acta 61B (2006) 980.
[18] J.L. Rodrigues, J.A. Nunes, B.L. Batista, S.S. Souza, F. Barbosa, J. Anal. Atom. Spectrom. (2008) doi:10.1039/b800595h.
[19] F. Barbosa, C.D. Palmer, F.J. Kug, P.J. Parsons, J. Anal. Atom. Spectrom. 19 (2004) 1000.
[20] A.D. Ribeiro, A.J. Curtius, D. Pozebon, Microchem. J. 64 (2000) 105.
[21] G.H. Tao, S.N. Willie, R.E. Sturgeon, Analyst 123 (1998) 1215.
[22] R.G.L. Silva, S.N. Willie, R.E. Sturgeon, R.E. Stanelli, S.M. Sella, Analyst 124 (1999) 1843.
[23] D. Pozebon, V.L. Dressler, A.J. Curtius, J. Anal. Atom. Spectrom. 13 (1998) 1101.
[24] D. Pozebon, V.L. Dressler, A.J. Curtius, Talanta 51 (2000) 903.
[25] J.A. Moreton, H.T. Delves, J. Anal. Atom. Spectrom. 13 (1998) 659.
[26] J.A. Nobrega, M.C. Santos, R.A. de Sousa, S. Cadore, R.M. Barnes, M. Tatro, Spectrochim. Acta 61B (2006) 465.
[27] D.L.G. Borges, M.A.M.S. da Veiga, V.L.A. Frescura, B. Welz, A.J. Curtius, J. Anal. Atom. Spectrom. 18 (2003) 501.
[28] I. Rodushkin, M.D. Axelsson, Sci. Tot. Environ. 262 (2000) 21.
[29] M.A.B.C. Menezes, E.C.P. Maia, C.C.B. Albinati, C.V.S. Sabino, J.R. Batista, J. Radioanal, Nucl. Chem. 259 (2004) 81.
[30] R. Mehra, M. Juneja, J. Biosci. 30 (2) (2005) 253.
[31] F.H. Were, W. Njue, J. Murungi, R. Wanjau, Sci. Total Environ. 393 (2008) 376.
[32] W.I. Mortada, M.A. Sobh, M.M. El-Defraway, S.E. Farahat, Environ. Res. 90 (2002) 104.

Talanta 76 (2008) 621–626

Contents lists available at ScienceDirect

Talanta

journal homepage: www.elsevier.com/locate/talanta

Problems in the application of the three-step BCR sequential extraction to low amounts of sediments: An alternative validated route

Elena Ciceri, Barbara Giussani, Andrea Pozzi, Carlo Dossi, Sandro Recchia *

Dipartimento di Scienze Chimiche e Ambientali Università dell'Insubria, Via Valleggio 11, 22100 Como, Italy

ARTICLE INFO

Article history:
Received 18 October 2007
Received in revised form 2 April 2008
Accepted 7 April 2008
Available online 16 April 2008

Keywords:
Sediment analysis
Speciation of metals
BCR sequential extraction

ABSTRACT

Poor recoveries are obtained if the BCR three-step sequential extraction is applied to 100 mg specimens rather than to 1 g. It is observed that analytes are lost during each phase separation which is carried out via centrifugation and can be hardly quantitatively performed on 100 mg sediment specimens. An alternative procedure, which is carried out on a single empty SPE column and involves separation by filtration, is developed to solve this problem. The proposed method is validated on 100 mg samples of certified sediment (BCR-701), but could be potentially used for even lower sediment specimens. Problems related to pH stability during step 2 and its influence on recoveries is also reported.

1. Introduction

The study of the vertical distributions of heavy metals in lake sediments is a valuable issue because it can serve as an information archive of environmental changes, as heavy metals are persistent species [1]. In fact, sediments are an important storage compartment for metals being released to water bodies because of their ability to sequester them: they can thus reflect water quality and record the effects of anthropogenic emission [2].

Beside total concentration profiles, species distribution of trace metals can provide useful hints about the environment in which they were deposited, with a particular regard to oxic/anoxic conditions [3]. Moreover, trace metals mobility, bioavailability and eco-toxicity strongly depend on their chemical forms [4–8]. Apart from total concentration profiles, speciation studies of the binding forms of trace metals by sequential extraction procedures may add significant environmental information [9].

Single leaching and combined sequential extraction schemes have been developed to estimate the relative phase associations of sedimentary metals in various aquatic environments [10]. The two most widely utilised protocols were the Kersten/Forstner procedure [11,12] and the Tessier procedure [13,14]. However, as these procedures differ in the extraction sequences and in the operating conditions, it was quite difficult to compare data obtained with these two methods. In addition, the lack of suitable reference materials did not allow comparing the results obtained by different laboratories, independently from the adopted analytical protocol. These reasons prompted the European Community Bureau of Reference (BCR) to start a programme aimed at harmonizing the sequential extraction procedure for trace metal speciation in sediments [15–17]. As the result, a three-step procedure was optimized [18,19] together with the production of a Certified Reference Material (CRM 601) [20]. According to this procedure, the first extractable fraction is the exchangeable, the second is the reducible and the third is the oxidisable. Nevertheless, the application of the BCR procedure is not without difficulties and further studies were devoted to improve its reproducibility by determining the variables that could be source of uncertainty [21,22]. Another critical point of this protocol that was never evaluated so far concerns its applicability to sediments specimens significantly lower than 1 g that represent the amount normally required by the same protocol. This aspect is quite important especially if specimens coming from sediments cores have to be analysed, as 200–300 mg is normally the maximum available quantity for each core sub-sample.

As we will show in this paper, unexpected problems are encountered if the BCR protocol is scaled-down to work on 100 mg specimens. These problems, that could not be ascribed to a non-correct evaluation of the counting statistic of solids, are instead related to the entire operational procedure which must be strongly modified to work properly with such small samples specimens.

The aim of this work is to show the development of an alternative route to perform the BCR three-step sequential extraction which works correctly with 100 mg (and even lower) sediments specimens. The proposed method was validated against the BCR-701 reference material for Cd, Ni, Cr, Zn, Cu and Pb using inductively

* Corresponding author. Tel.: +39 0312386450; fax: +39 0312386449.
E-mail address: sandro.recchia@uninsubria.it (S. Recchia).

0039-9140/$ – see front matter © 2008 Elsevier B.V. All rights reserved.
doi:10.1016/j.talanta.2008.04.006

coupled plasma mass spectrometry (ICP-MS) for quantitative determination of the extracted metals.

2. Experimental

The BCR-701 was prepared from Lake Orta (Piemonte, Italy) sediments and was standardised by the Joint Research Centre, Ispra (Italy) [23].

2.1. Reagents

All solution manipulations were executed under an acid-resistant Class 100 laminar flow hood for the revised method only, while for the original method this condition was adopted only for ultrapure acids transferring operations. Ultrapure water from a Millipore MilliQ system (18 MΩ cm resistivity, <5 ppb TOC) was always used. Pure concentrated acids (HCl 36% and HNO_3 69% Suprapure from Fluka) were employed.

LDPE (low density polyethylene) sample and reagent bottles were used: bottles were cleaned by soaking in a detergent solution, rising with ultrapure water, soaking in 2% HNO_3, rinsing final storage was done in 2% HNO_3. Bottles were thoroughly rinsed with ultrapure water before use.

The extractant solutions were prepared in conformity with the following procedure:

Solution A (*acetic acid*, 0.11 mol L^{-1}): 2.5 mL of glacial acetic acid (Fluka, puriss. p.a., ACS reagent, ≥99.8%) were added to about 50 mL of water and made up to 100 mL with water. 25 mL of this solution (acetic acid 0.44 mol L^{-1}) was diluted to 100 mL to obtain a 0.11 mol L^{-1} acetic acid solution.

Solution B (*hydroxylamine hydrochloride*, 0.5 mol L^{-1}): 3.47 g of hydroxylamine hydrochloride (Fluka, puriss. p.a., for AAS, ≥99.0%) was dissolved in water; this solution was acidified with 2.5 mL of 2 mol L^{-1} nitric acid solution (prepared by adequate dilution of concentrate nitric acid) and made up to 100 mL. This solution was prepared on the same day of the extraction.

Solution C (*hydrogen peroxide*, 8.8 mol L^{-1}): no dilution was necessary; the hydrogen peroxide (Fluka, TraceSelectUltra, 30%) as supplied by the manufacturer was used.

Solution D (*ammonium acetate*, 1.0 mol L^{-1}): 7.708 g of ammonium acetate (Carlo Erba, ACS reagent, ≥97%) was dissolved in water, this solution was acidified with concentrate nitric acid to pH 2 and made up to 100 mL.

2.2. Certified sequential extraction procedure

The certified sequential extraction was performed in 12-mL test tubes scaling down all reagents in a proportional way. An orbital shaker (Ika-Ks 130 Basic) was used instead of the end-over-end shaker, because we have found that with the latter one samples are spread all over the inner wall of the small test tubes causing troubles during phases separation. As recommended by the BCR document, the target of shaking is to maintain the sediment sample in suspension and we have achieved this condition working at 480 rpm. As it will be clearly shown in the Section 3, this different shaking method has no effect in terms of extraction efficiency.

The extraction procedure is described below:

- *Step* 1: 0.1 g of sample (BCR-701) was transferred in a 12-mL test tube with a plastic spatula. 4 mL of solution A was added and shaken for 16 h at room temperature. The extraction solution was separated from the solid residue by centrifugation and decantation of the supernatant liquid. The latter is then removed with a pipette. The extracted fraction was transferred into a test tube and stored at 4 °C. The residue was washed by adding 2 mL of solution A, shaking for 15 min and the washing solution was separated from the residue as above mentioned, and stored at 4 °C. The residue was finally washed by adding 2 mL of ultrapure water, shaking for 15 min and the washing solution was separated from the residue and discharged.
- *Step* 2: 4 mL of solution B was added to the residue from step 1, and the extraction was performed as described in step 1. 2 mL of solution B was used to wash the residue. The residue was finally washed by adding 2 mL of ultrapure water, shaking for 15 min and the washing solution was separated from the residue and discharged.
- *Step* 3: 1 ml of solution C was added to the residue from step 2; the test tube was covered and left for 1 h to digest at room temperature. The digestion was continued for 1 h at 85 ± 2 °C in a water bath and then the volume was reduced by the further heating of the uncovered test tube. Another 1 mL aliquot of solution C was added and the covered test tube was heated again to 85 ± 2 °C and was digested for 1 h. Then the cover was removed and the volume reduced. 5 mL of solution D was added to the cool residue and the extraction was performed as described in step 1. 2 mL of solution D was used to wash the residue.

2.3. Revised sequential extraction procedure

The extraction with the revised BCR procedure was performed into a polypropylene special solid phase extraction (SPE) empty column with an appropriate valve put at the end of this column (see Fig. 2). The followed procedure was similar to the one reported in the previous section: anyhow, the system to separate the solid residue from the supernatant liquid was different and will be described in the result and discussion section. Even in this case an orbital shaker working at 480 rpm was used instead of the end-over-end shaker.

2.4. Determination of total metals concentration

Total metal concentrations were determined after microwave-assisted digestion (MLS-1200 Mega, Milestone) on sealed PTFE vessels with 1.5 mL HCl and 0.5 mL HNO_3 (for 50 mg of sample). The heating program is reported in Table 1. After cooling, the digested solution was diluted with ultrapure water.

It should be noted that this method is quite different from the one suggested in the BCR document. We have used this significantly more conservative approach in order to rule out any potential loss of analytes. In any case the total digestion is not a part of our revised protocol because we cannot validate it, as the data reported in the BCR document are only indicative.

2.5. Dry mass correction

All data are reported on a dry weight basis. The dry mass correction factor (w) was obtained with the moisture test and was calculated with the following formula (1). Three aliquots of BCR-701 were heated in an oven at 70 °C and were left until a constant

Table 1
Heating program for the microwave-assisted digestion

Time (minutes)	Power (W)	Temperature maximum (°C)
2	250	220
1	0	220
2	250	220
2	400	220
5	500	220
1	0	220
5	600	220

mass was achieved.

$$w = \frac{g_{end} - g_{empty}}{g_{beginning} - g_{empty}} \quad (1)$$

where g_{end} is the weight of the dry sample, g_{empty} is the weight of the vessel where the sample was put and $g_{beginning}$ is the weight of the sample (not dried).

2.6. Quantitative analyses

The determination of certified metals (Cd, Ni, Cr, Zn, Cu and Pb) was performed by inductively coupled plasma mass spectrometry (Thermo Elemental Mod. X-Series II). Optimization of the instrumental parameters was performed daily as recommended by the manufacturer with a 10 $\mu g\,L^{-1}$ multi-standard solution. The standard solutions used for external calibration were prepared by a proper dilution of 10 $mg\,L^{-1}$ multielement standard solution (Merck, ICP multi-element standard solution VI).

3. Results and discussion

3.1. Problems related to the BCR procedure

The extraction solutions of the BCR three-step procedure are shown in Table 2. Details about the entire procedure are reported in the BCR protocol [23]. The document reports the certified values of Cd, Cr, Cu, Ni, Pb and Zn in the BCR-701 for the three steps indicated in Table 2 and indicative values for the *aqua regia* extractable contents. The protocol involves the usage of 1 g of sediment for the entire sequential extraction: this amount of sample is normally not available in the analysis of sediment cores. In fact, it must be considered that when we deal with finely sampled cores the total available dried sample quantity is in the order of one or two hundreds of milligrams. This aspect causes serious problems because, as we mentioned earlier, the application of the BCR procedure on a 10-fold lower sample quantities cannot be easily faced with some simple modification of this validated analytical protocol.

We have tentatively tried to apply the BCR procedure on 100 mg of the certified sediment by simply maintaining the same sample:reagent ratios. Poor recoveries and high standard deviations were obtained with this strategy. We have thus tried to modify the original method with the introduction in each step of an additional extractant washing before the final water washing. Fig. 1 shows the data obtained in this way together with the corresponding certified ones. All the values (found and certified) are reported with their uncertainties (95% confidence intervals). As a general consideration these data are better than the ones (not shown) obtained with only one washing, although they are not acceptable yet.

A minor problem concerns the high concentrations obtained for Zn which are related to some external contaminations during the analytical procedure. This problem can be easily solved performing all manipulations, including the required 16 h-shakings, under a Class 100 laminar flow hood. In any case, it must be pointed out that the certified BCR procedure does not pose any requirement to take care of environmental contaminations during the analytical procedure.

Table 2
BCR three-step procedure

Step	Reagents and time	Target extractable fraction
1	0.11 M CH_3COOH, 16 h	Exchangeable ions Carbonates
2	0.1 M NH_2OHHCl at pH 1.5 HNO_3, 16 h	Fe and Mn oxides
3	(a) 30% H_2O_2 at pH 2–3 (HNO_3), 2 h at T = 85 °C	Sulphurs
	(b) 1 M CH_3COONH_4 at pH 2 (HNO_3), 16 h	Organic matter

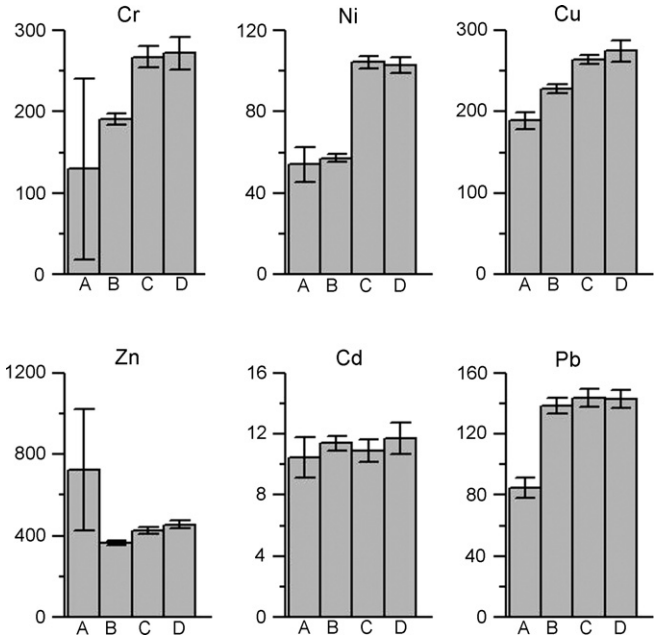

Fig. 1. Comparison between certified and experimentally determined concentrations obtained on four replicated independent extractions of 100 mg specimens (mg/kg). A: experimental sum of the three-step; B: sum of the three-step (as reported in the BCR document [23]); C: experimental total amount determined via *aqua regia* extraction; D: total amount determined via *aqua regia* extraction (as reported in the BCR document [23]). Note that only bar B reports certified values, while bar D reports indicative values.

It is, instead, evident that all the concentrations determined for the certified metals are noticeably lower than their certified values (refer to A and B bars of Fig. 1) when the BCR procedure is scaled down of 1 magnitude order. The amounts of all metals determined by total digestion fits well with the indicative values (compare C and D bars of Fig. 1) reported in the BCR document: we may thus suggest that the significantly lower total metal amount derived by the sequential extraction cannot be ascribed to the presence of some sort of bias in the final determination. In addition, the uncertainties experimentally obtained for bars C tell us that the data that comes from 50 mg specimens are sufficiently precise to be representative of the entire sediment.

Thus, it become fundamental to assess where and how analytes were lost during the steps of the sequential extraction, with the final aim to develop a new extraction protocol.

Additional insights came from the evidence that replications of the normal BCR procedure on 100 mg of certified sediment give error bars that are always sensibly higher than the certified ones, particularly for chromium, as discussed later, leading thus to an unexpectedly poor reproducibility.

This unexpected behaviour on a 100 mg specimen should be ascribed and rationalized in terms of the presence of critical points during phase separations, which take place at the end of each extraction step. In this respect, it should be recalled that the normal BCR procedure involves centrifugation and supernatant separation via pipette-picking. This operation can be done in a reproducible and almost quantitative way on 1 g of sediment, but on 100 mg the probability of washing out relevant portions of the solid residue is surely higher.

Inasmuch, all washing solutions were collected and analysed to establish if loss of analytes actually occurs during the separation steps. It then resulted that relevant percentages of all analytes

were found in the washing solutions. No data are reported because these results are operator-dependent, and solutions could not be standardized.

3.2. Developing the alternative procedure

It is now clear that attention must be focused on phase separation steps in order to revise the entire procedure. Preliminary attempts were directed to the utilisation of ultra-centrifugation but unsatisfactory results were gained.

An alternative route is to use filtration rather than centrifugation to perform the separation of the solid phase. In this respect the major drawback concerns the surely higher operational complexity of filtration if compared to separation by centrifugation, where all sample manipulations are performed in only one glass tube. This point is not of secondary importance: the more the operational complexity, the higher the sources of systematic and casual errors, overshadowing the advantages of filtration.

The challenge is thus to develop an operationally simple filtration protocol. Our attention was then driven in finding a way to avoid any transfer of the solid sample between steps: in other words, the challenge was to maintain the solid sample specimen always in the same vessel from the beginning to the end of the sequential extraction. A solution based on the utilisation of empty SPE cartridges (5 mL total volume) was finally developed and schematically sketched in Fig. 2.

With this simple system a weighted amount of the solid sample is loaded into a dry empty SPE column, and then the extraction solution for the first step is added. At this stage the bottom ON/OFF valve is in its closed position. After the 16 h shaking the extraction solution is separated by filtration from the solid residue by opening the ON/OFF valve and eventually applying a small over pressure to the top of the SPE column (using a an additional syringe and a proper adaptor). The extracted solid is then washed with water according to the BCR procedure, and the washing solutions are also removed by filtration. The extracted solid is now ready for the next step of the sequential extraction, which is performed in the same manner. All the operations are performed under a Class 100 laminar flow hood. The utilisation of commercially available 0.45 μm nitrocellulose membrane filters at the bottom of the system (E) is not mandatory: we normally use them if eluates have to be analysed by ICP-coupled techniques in order to prevent unwanted nebulisers cloggings.

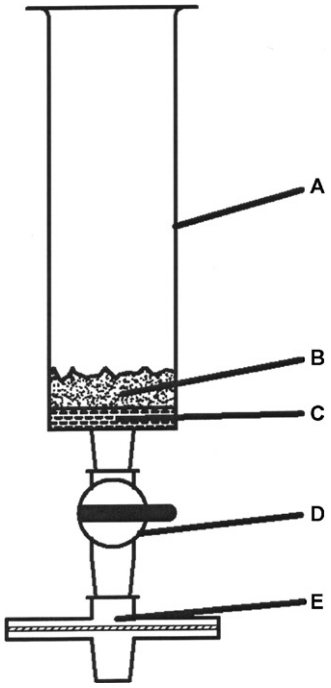

Fig. 2. Schematic representation of the extraction separation system used in the modified sequential extraction. A = empty SPE cartridge; B = sediment specimen; C = fritted disk; D = ON/OFF valve; E = 0.45 μm guard filter.

Table 3
LOD for the certified metals: three steps and total amount

Dry correction (mg kg^{-1})	Cr	Ni	Cu	Zn	Cd	Pb
Step 1	0.066	0.23	0.018	0.41	0.026	0.0059
Step 2	0.16	0.18	0.016	0.11	0.0069	0.0010
Step 3	0.50	0.14	0.023	0.76	0.0076	0.043
Total	4.2	0.22	0.0037	0.17	0.00065	0.0016

From an operational point of view this procedure is even simpler than the BCR procedure, as the separation steps can be performed without any centrifugation. Moreover the repeatability of separation by filtration is surely less dependent from the operator's skills than separation by centrifugation, leading to beneficial effects that can influence the overall precision. Finally, it should be noted that this procedure can intrinsically be used even with much lower sample quantities, providing that the bottom fritted disk pore are small enough to retain the solid sample.

This novel protocol was validated by both replicated blank extractions and replicated extractions over the certified sediment.

The detection limits (LOD) are reported in Table 3 and were calculated following the IUPAC rules [24]. Blank concentrations were obtained by the analysis of three blank extraction i.e. the three extraction steps and total determination procedures performed without the sediment sample.

Table 4 reports the data of three replicated blank extractions. The results were normalized to a sample weight of 100 mg, and show that the procedure and all disposables are clean, if compared to the certified metal concentrations.

The results obtained on a first trial of sequential extractions on the BCR-701 with the filtration systems showed that all recoveries are sensibly lower than 100%. This problem was easily solved by collecting the eluates of an additional washing performed with a 2 mL amount of the extraction solution used in each step. The revised separation sequence may be thus summarized as follows: (i) filter the extraction solution (collect eluates); (ii) wash the sediment with 2 mL of extraction solution, filter and collect eluates; (iii) wash the sediment with 5 mL of ultrapure water and filter (discharge eluates).

The data obtained for all the certified metals with this revised method are reported in Table 5.

Although there is no need to analyze independently the two collected eluates coming from each step, we have analysed them separately in order to critically evaluate the necessity of the additional extractant washing.

In Fig. 3 the relevancy of the found amounts in every collected extractant against the relative collected washing is shown. Uncertainties (95% confidence intervals) are reported as well.

This figure illustrates that the additional washing is definitely necessary to fully satisfy validation requirements. Moreover the precisions obtained on four replicates are comparable or better than the ones reported for the certified sediment. This could indicate that the better reproducibility of filtration exerts beneficial effects, even if a onefold lower sample quantity is used.

According to the data here reported we can thus suggest the utilisation of such a protocol to perform sequential extractions on small sediment quantities.

Table 4
Blank concentrations found for each certified element and for each step

Dry correction (mg kg^{-1})	Cr	Ni	Cu	Zn	Cd	Pb
Step 1	0.14 ± 0.020	0.24 ± 0.071	0.042 ± 0.0056	0.25 ± 0.12	0.260 ± 0.0079	0.005 ± 0.0018
Step 2	0.66 ± 0.047	0.15 ± 0.056	0.041 ± 0.0048	0.36 ± 0.034	0.007 ± 0.0021	0.1600 ± 0.00031
Step 3	3.2 ± 0.15	0.59 ± 0.041	0.087 ± 0.0071	1.2 ± 0.23	0.003 ± 0.0023	0.12 ± 0.013

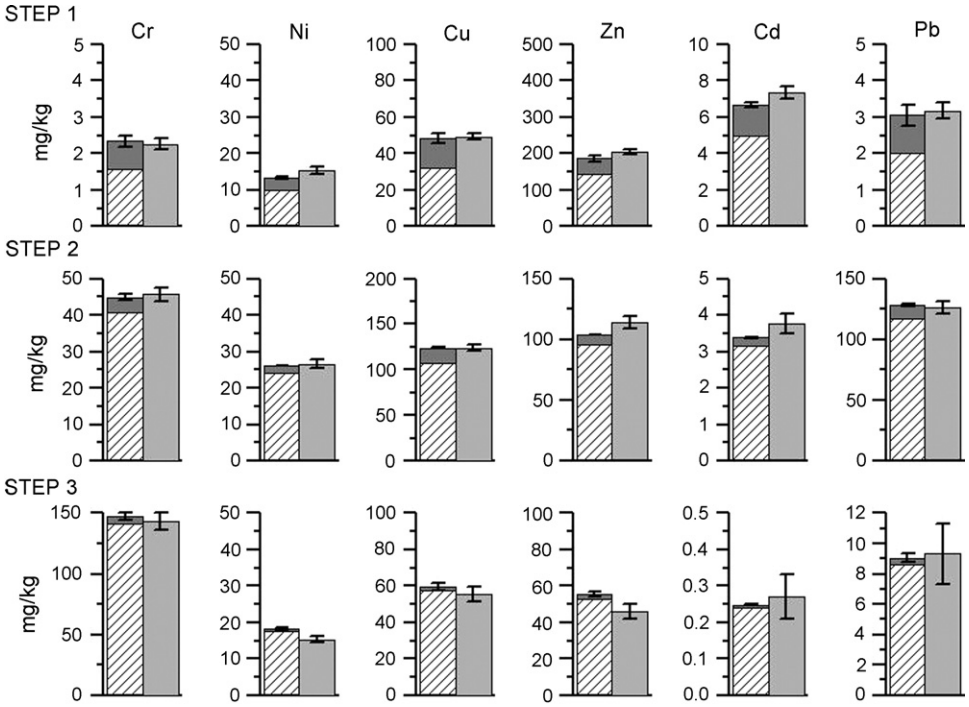

Fig. 3. Comparison between the found amount for each step (hatched) + the first wash (dark grey) in the first bar and the certified value (light grey) in the second bar.

It is noteworthy that the proposed methodology is able to solve all analytical problems with Cr. A poor reproducibility with the original procedure was instead found. In this respect we could only suggest that probably the problems related to the original procedure could be ascribed to a higher concentration of Cr related species in the tiny fraction of the certified sediment, which cannot be fully extracted when separation is done by centrifugation.

3.3. pH problems on step 2

As it was also shown in the literature [21], it is quite difficult to maintain under control the pH value of step 2. This fact is mainly due to the poor buffer capacity of the NH_2OHHCl extraction solution at pH 1.5, which is particularly stressed if sediments coming from a karst basin (or any sediment formed by relevant amounts of carbonatic rocks weathering) have to be analysed. Table 6 reports the pH values recorded during step 2 for some real sediment samples from Lake Como watershed (Italy).

It can be noticed how, in some cases, the extraction solutions reach quite high pH values (up to 5.16 after 1 h and up to 5.35 after 16 h). The impact on recoveries of these unpredictable increasing of pH is dramatic: in Table 7 are reported the data obtained on BCR-701 where only a 0.5 increase of pH was applied.

The data of Tables 6 and 7 are reported here only to give additional quantitative information to better assess the problems of step

Table 5
Concentrations obtained with the BCR revised procedure based on the analysis of four replicates of BCR-701

Dry correction (mg kg^{-1})	Cr	Ni	Cu	Zn	Cd	Pb
Step 1						
Found	2.34 ± 0.16	13.4 ± 0.4	48.5 ± 2.8	186 ± 9	6.64 ± 0.15	3.05 ± 0.28
Certified	2.26 ± 0.16	15.4 ± 0.9	49.3 ± 1.7	205 ± 6	7.34 ± 0.35	3.18 ± 0.21
Recovery	104	87	98	91	90	96
Step 2						
Found	45.0 ± 1	26.1 ± 0.08	124 ± 0.3	104 ± 0.2	3.38 ± 0.01	128 ± 1
Certified	45.7 ± 2	26.6 ± 1.3	124 ± 3	114 ± 5	3.77 ± 0.28	126 ± 3
Recovery	98	98	100	91	90	102
Step 3						
Found	148 ± 3	18.3 ± 0.3	59.5 ± 2	55.5 ± 1	0.25 ± 0.003	9.0 ± 0.3
Certified	143 ± 7	15.3 ± 0.9	55.2 ± 4	45.7 ± 4	0.27 ± 0.06	9.3 ± 2
Recovery	103	120	108	121	92	97

Table 6
pH values of step 2 solutions during extraction after 1 h and after 16 h of shaking, for seven different real samples

River	Coordinates (km)		pH extraction solution	pH after 1 h	pH after 16 h
	Longitude	Latitude			
Senagra	1,518,719	5,096,726	1.45	2.06	2.15
Meria	1,524,493	5,084,650	1.45	4.95	5.35
Livo	1,525,536	5,110,682	1.45	2.04	2.06
Rio Torto	1,528,745	5,078,323	1.45	2.19	2.37
Perlo	1,519,193	5,091,552	1.45	2.17	2.28
Breggia	1,505,672	5,075,748	1.45	2.14	2.18
Telo	1,510,008	5,087,929	1.45	5.16	5.21

For all samples the pH value of the initial extracting solution was 1.45.

Table 7
Concentrations of the BCR-701 for the step 2 obtained with the extraction solution at pH 2 and at pH 1.5

Dry correction (mg kg^{-1})	Cr	Ni	Cu	Zn	Cd	Pb
Found at pH 1.5	45.0 ± 1	26.1 ± 0.1	124 ± 0.3	104 ± 0.2	3.38 ± 0.01	128 ± 1
Recovery	98	98	100	91	90	102
Found at pH 2.0	20.6 ± 0.1	14.9 ± 0.5	56.7 ± 1	61 ± 1	2.49 ± 0.06	94 ± 3
Recovery	45	56	46	54	66	75

2. They should be then regarded only as a starting point for future developments of the three steps sequential extraction protocol.

4. Conclusions

A revised version of the BCR three-step sequential extraction procedure is proposed and validated. In this way, very small sample quantities, less then 100 mg, could be analyzed minimizing loss of analytes and external contamination. From the data here reported, in the case of BCR-701, the utilisation of a onefold lower sediment amount does not induce an increase of uncertainty related to sampling statistical fluctuations. Instead, the overall precision was enhanced and this should be ascribed to the better reproducibility of solid separation via filtration. Finally, this method can be downscaled to total sample amount lower that 100 mg, providing that problems related to sampling statistic are properly accounted for.

References

[1] L. El Bilali, P.E. Rasmussen, G.E.M. Hall, D. Fortin, Appl. Geochem. 17 (2002) 1171.
[2] U. Forstner, in: R. Baudo, J.P. Giesy, H. Mantau (Eds.), Sediments: Chemistry and Toxicity on In-place Pollutants, Lewis (1990) 61.
[3] K. Saeki, M. Okazaki, S. Matsumoto, Water Res. 27 (1993) 1243.
[4] M. Kaasalainen, M. Yli-Halla, Environ. Pollut. 126 (2003) 225.
[5] A. Lu, S. Zhang, X. Shan, S. Wang, Z. Wang, Chemosphere 53 (2003) 1067.
[6] C.M. Davidson, A.L. Duncan, D. Littlejohn, A.M. Ure, L.M. Garden, Anal. Chim. Acta 363 (1998) 45.
[7] H. Wang, C.X. Wang, Z.J. Wang, Z.H. Cao, Environ. Geochem. Health 26 (2004) 303.
[8] A. Tessier, P.G.C. Campbell, Hydrobiologia 149 (1987) 43.
[9] J.E. Rae, A. Parker, Appl. Geochem. 11 (1996) 211.
[10] W.F. Pickering, CRC Critical Rev. Anal. Chem. 12 (1981) 233.
[11] M. Kersten, U. Fortsner, Water Sci. Technol. 18 (1986) 121.
[12] W. Salomons, U. Forstner, Environ. Technol. Lett. 1 (1980) 506.
[13] A. Tessier, P.G.C. Campbell, M. Bisson, Anal. Chem. 51 (1979) 844.
[14] F. Rapin, A. Tessier, P.G.C. Campbell, R. Carignan, Environ. Sci. Technol. 20 (1986) 836.
[15] Ph. Quevauviller, G. Rauret, B. Griepink, Int. J. Environ. Anal. Chem. 51 (1993) 231.
[16] A.M. Ure, Ph. Quevauviller, H. Muntau, B. Griepink, Int. J. Environ. Anal. Chem. 51 (1993) 135.
[17] Ph. Quevauviller, H.A. Van der Sloot, A.M. Ure, H. Muntau, A. Gomez, G. Rauret, Sci. Total Environ. 178 (1996) 133.
[18] B. Griepink, H. Muntau, Ph. Quevauviller, A.M. Ure, Int. J. Environ. Anal. Chem. 51 (1993) 129.
[19] A.M. Ure, Ph. Quevauviller, H. Muntau, B. Griepink, Report EUR REPORT 14763 EN CEC Brussels (1993).
[20] Ph. Quevauviller, G. Rauret, J.F. Lopez-Sanchez, R. Rubio, A.M. Ure, H. Muntau, Sci. Total Environ. 205 (1997) 223.
[21] A. Sahuquillo, J.F. Lopez-Sanchez, R. Rubio, G. Rauret, R.P. Thomas, C.M. Davidson, A.M. Ure, Anal. Chim. Acta 382 (1999) 317.
[22] G. Rauret, J.F. Lopez-Sanchez, A. Sahuquillo, R. Rubio, C.M. Davidson, A.M. Ure, Ph. Quevauviller, J. Environ. Monit. 1 (1999) 57.
[23] G. Rauret, J.F. Lopez-Sanchez, D. Luck, M. Yli-Halla, H. Muntau, Ph. Quevauviller, Report EUR 19775 EN (2001).
[24] IUPAC, 1995, Pure Appl. Chem. 67 (1995) 1699.

Talanta 76 (2008) 548–556

Contents lists available at ScienceDirect

Talanta

journal homepage: www.elsevier.com/locate/talanta

Miniaturized electronic tongue with an integrated reference microelectrode for the recognition of milk samples

Patrycja Ciosek*, Wojciech Wróblewski

Department of Analytical Chemistry, Warsaw University of Technology, Noakowskiego 3, 00-664 Warsaw, Poland

ARTICLE INFO

Article history:
Received 29 October 2007
Received in revised form 20 March 2008
Accepted 25 March 2008
Available online 8 April 2008

Keywords:
Electronic tongue
PLS-DA
Milk recognition
Integrated sensor array

ABSTRACT

This work presents the application of a new construction of an electronic tongue for the classification of milk originating from various producers. Integrated array of microelectrodes was fabricated from epoxy-glass laminate. PVC membranes with various additives were used as chemosensitive layers. The developed device is capable of recognition of milk samples with high correctness. Moreover, the application of miniaturized reference electrode, integrated on the same substrate, also provided satisfactory results, which can be helpful in future constructions of hand-held electronic tongue systems.

1. Introduction

Usually the electronic tongue involves a fusion of separate sensors [1,2]. However, there have been few attempts to miniaturize that kind of device and to simplify its construction [3,4]. Miniaturization leads to the reduction of costs of the preparation of sensor arrays thanks to the lowering of the amount of chemicals and materials used. Moreover, smaller volumes of the samples can be analyzed.

There are two possible approaches in that task: to miniaturize single sensors, or to develop integrated sensor arrays, i.e. fabricated on a single substrate. Miniaturized single sensors for electronic tongue measurements were presented in our previous works [5–8]. Solid-state ion-selective microelectrodes fabricated on an epoxy-glass support were mounted in a flow-through cell in order to obtain a device capable of correct recognition of various foodstuffs. Solid-state ion-selective electrodes with plasticized PVC membranes were also proposed in [9–13] and with membranes based on polyurethane in [9,14]. Ion-selective field effect transistors (ISFETs) were applied in the system dedicated to the recognition of various brands of mineral waters [15]. Gardner et al. proposed a miniaturized total analysis taste system, based on SAW sensors, for the recognition of basic taste substances [16]. The device can be equipped with an additional micro-fluidic cell for more convenient measurements of liquids [17,18].

So far, there have been only a few attempts to develop electronic tongue based on integrated sensor array. The integration of sensors is advantageous—the set-up becomes simplified, and therefore the system is easier to operate and miniaturize. Toko et al. presented the so-called multichannel electrode, which was made of potentiometric microelectrodes with liquid inner solution and lipid–polymer membranes [19]. Another non-specific material was the basis of the integrated potentiometric system, which enabled to recognize various brands of mineral waters. The sensor array was fabricated in thick-film technology, where Ag, Au, Cu, Ni, RuO_2, Pt, and graphite pastes were used to obtain: transducers, active and insulating layers. The fusion of this device with PCA and neural networks led to the differentiation of the samples originating from various manufacturers [4]. An integrated potentiometric microsystem embracing carbon paste electrodes with chemosensitive layers for water, soft drinks, and beer recognition was presented by Lvova et al. [9].

De Saja et al. proposed a voltammetric integrated array for ET measurements [20]. Miniaturized, integrated array of ion-selective electrodes was described by Saurina et al. [21]. Recently, an integrated array of solid-state ion-sensitive microelectrodes applied for the construction of planar electronic tongue was also presented in our previous work [22]. The ion-selective sensor array was obtained by the deposition of PVC membranes, exhibiting different sensitivities towards various ionic species, on the surface of planar Au microelectrodes, fabricated using printed circuit board technol-

* Corresponding author. Tel.: +48 22 234 7873; fax: +48 22 234 7873.
E-mail address: pciosek@ch.pw.edu.pl (P. Ciosek).
URL: http://csrg.ch.pw.edu.pl (P. Ciosek).

0039-9140/$ – see front matter © 2008 Elsevier B.V. All rights reserved.
doi:10.1016/j.talanta.2008.03.051

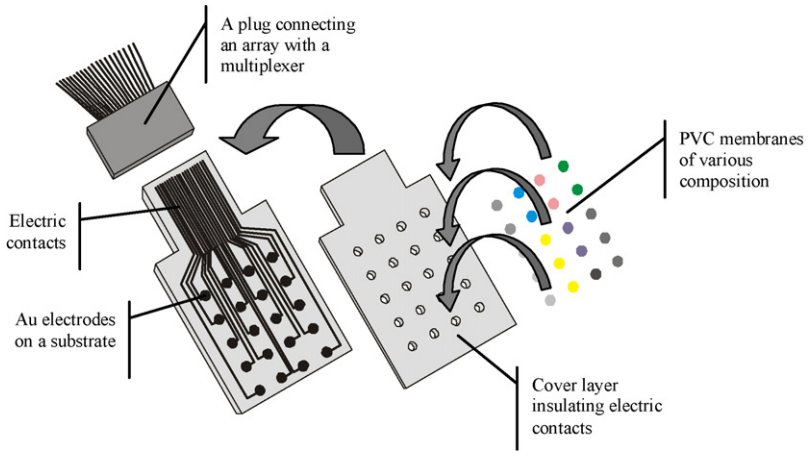

Fig. 1. The fabrication of integrated array of microelectrodes.

ogy. The miniaturized electronic tongue system was checked in the recognition of a brand of orange juice.

The miniaturization of a sensor array in potentiometric electronic tongue system demands not only the development of miniaturized sensors, but also the miniaturization and integration on the same substrate of the reference electrode. The design studies of the miniaturized reference electrode were undertaken by many research groups and they resulted in the development of pseudo-reference electrodes [23], liquid-junction reference electrodes [24,25], up to various kinds of all-solid-state (i.e. liquid-junction free) reference electrodes [26–30]. Recently, a novel construction of all-solid-state reference electrode with an ionic liquid (IL) introduced into plasticized PVC membrane was presented in our work [31]. The architecture of electrodes based on Ag/AgCl planar transducers covered with PVC membranes containing IL (1-dodecyl-3-methylimidazolium chloride) was adapted for flow-through analysis. It was found, that the developed miniaturized all-solid-state reference electrodes exhibited good potential stability, reproducibility, and long-term stability [31].

In this work, a novel construction of a sensor array is presented. An integrated array of microelectrodes, i.e. fabricated in one substrate, was tested in the classification of milk samples. The sensor array was prepared on the basis of printed circuit board (PCB) technology, which is simple, fast and non-expensive method. Moreover, the idea of a reference electrode with IL additive was applied to the construction of reference electrode on an integrated array. The aim of this work was also to compare the results of the recognition of milk samples on the basis of measurements performed with commercial Ag/AgCl electrode and miniaturized, integrated IL reference electrode. It was found, that they exhibit similar classification accuracy.

Table 1
Membrane components

Electrode type	Plasticizer	Lipophilic salt	Ionophore
Ca^{2+}	o-NPOE	KTFPB	ETH 1001
NH_4^+	BPPA	KTPClPB	Nonactine
Na^+/K^+	o-NPOE	KTPClPB	Ionophore X, valinomycin
Cl^-	o-NPOE	KTPClPB	TPPClMn
HCO_3^-	o-NPOE	TDMAC	ETH 6010
"Cation-selective" (CS)	DOS	KTPFPB	–
$F^-/H_2PO_4^-$	o-NPOE	TDAB	Ionophore $H_2PO_4^-$, ionophore F^-
Ionic liquid (IL)	DOS	1-Dodecyl-3-methyl-imidazolium chloride	–

2. Experimental

For all experiments redistilled water and chemicals of analytical-reagent grade were used. Fluoride ionophore and dihydrogen phosphate ionophore—uranyl salophene

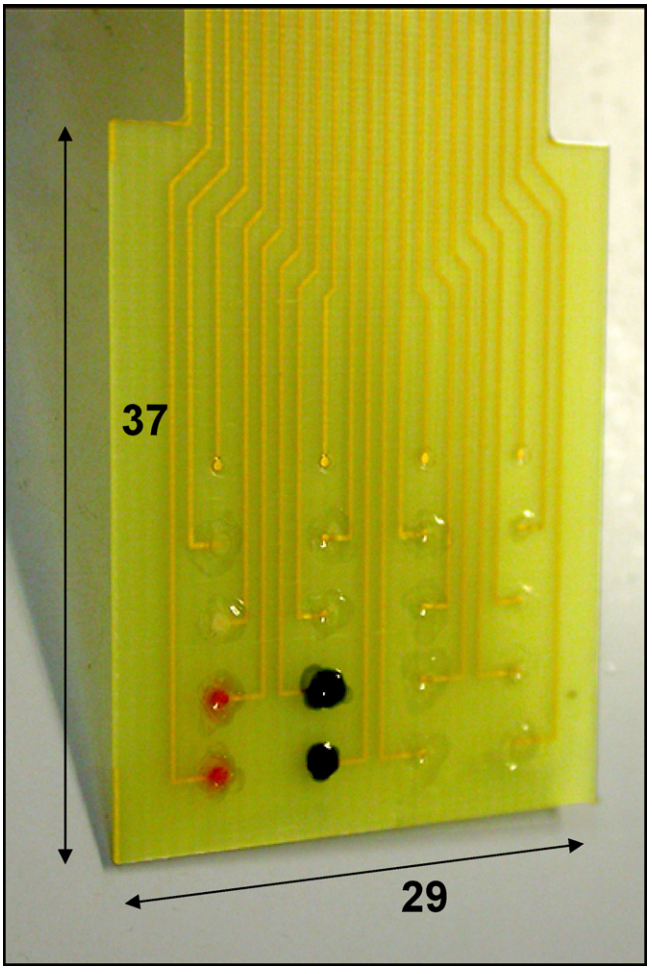

Fig. 2. Integrated array of microelectrodes.

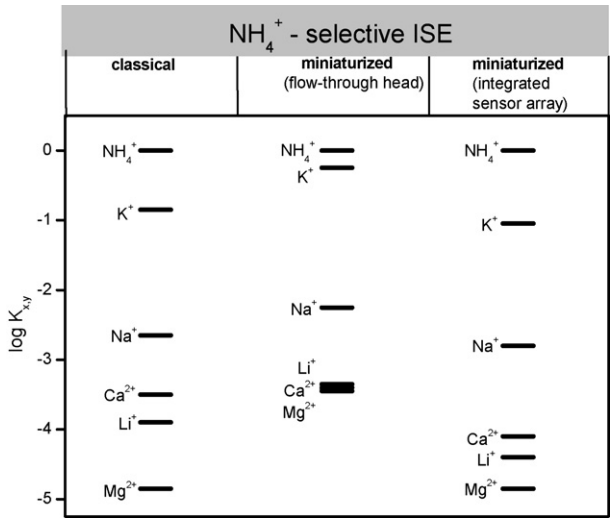

Fig. 3. The comparison of selectivity coefficients for ammonium-selective electrode [6,34].

derivatives were synthesized in Laboratory of SMCT, MESA+ Research Institute, University of Twente (The Netherlands) [32]. Ionic liquid—1-dodecyl-3-methyl-imidazolium chloride was supplied by Solvent Innovation GmbH (Koln). The membrane components were supplied by Fluka: o-NPOE (2-nitrophenyl octyl ether), BBPA (bis(1-butylpentyl)adipate), DOS (bis(2-ethylhexyl)sebacate), KTFPB (potassium tetrakis (3,5-bis(trifluoromethyl)phenyl) borate), KTPClPB (potassium tetrakis(4-chlorophenyl)borate), TDMAC (tridodecylmethylammonium chloride), TDAB (tetrakis(decyl)ammonium bromide), ETH 1001 (calcium ionophore I), nonactine (ammonium ionophore I), ionophore X (sodium ionophore X, 4-*tert*-butylcalix[4]arene-tetraacetic acid tetraethyl ester), valinomycin (potassium ionophore I), TPPClMn (chloride ionophore I, meso-tetraphenylporphiryn manganese (III)–chloride complex), ETH 6010 (carbonate ionophore I, heptyl 4-trifluoroacetylbenzoate).

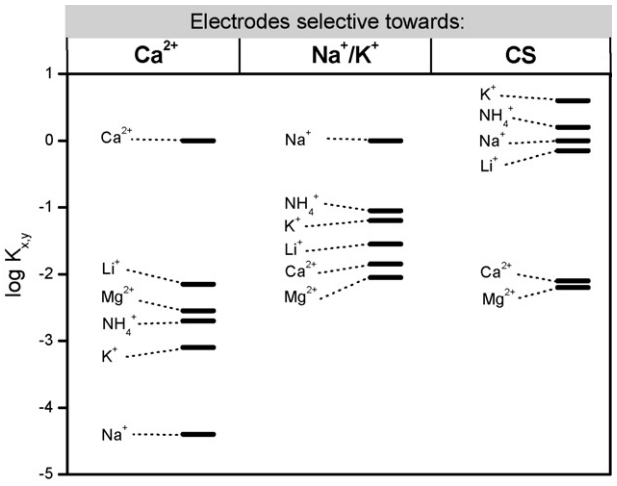

Fig. 4. Selectivity coefficients of cation-selective electrodes.

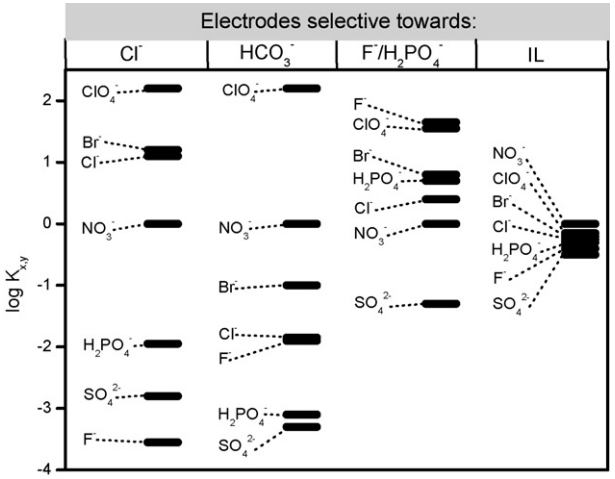

Fig. 5. Selectivity coefficients of anion-selective electrodes.

Table 2
Correlation between real and predicted values of milk classification

	Measurements performed with commercial Ag/AgCl reference electrode		Measurements performed with integrated reference microelectrode	
	Train set	Test set	Train set	Test set
Lowicz				
Intercept	0.002	0.056	0.004	0.115
Slope	0.988	0.720	0.979	0.426
Correlation coefficient	0.999	0.895	0.999	0.533
Laciate				
Intercept	0.008	0.023	0.004	0.036
Slope	0.958	0.884	0.979	0.818
Correlation coefficient	0.998	0.857	0.997	0.684
Biale				
Intercept	0.001	0.025	0.000	0.057
Slope	0.999	0.876	0.997	0.717
Correlation coefficient	0.999	0.871	0.999	0.851
Sielska Dolina				
Intercept	0.007	−0.017	0.009	−0.008
Slope	0.963	1.087	0.957	1.042
Correlation coefficient	0.994	0.764	0.999	0.823
Milko				
Intercept	0.009	−0.096	0.025	−0.092
Slope	0.955	1.479	0.876	1.461
Correlation coefficient	0.995	0.950	0.991	0.951
% of correct classifications	100	100	100	100

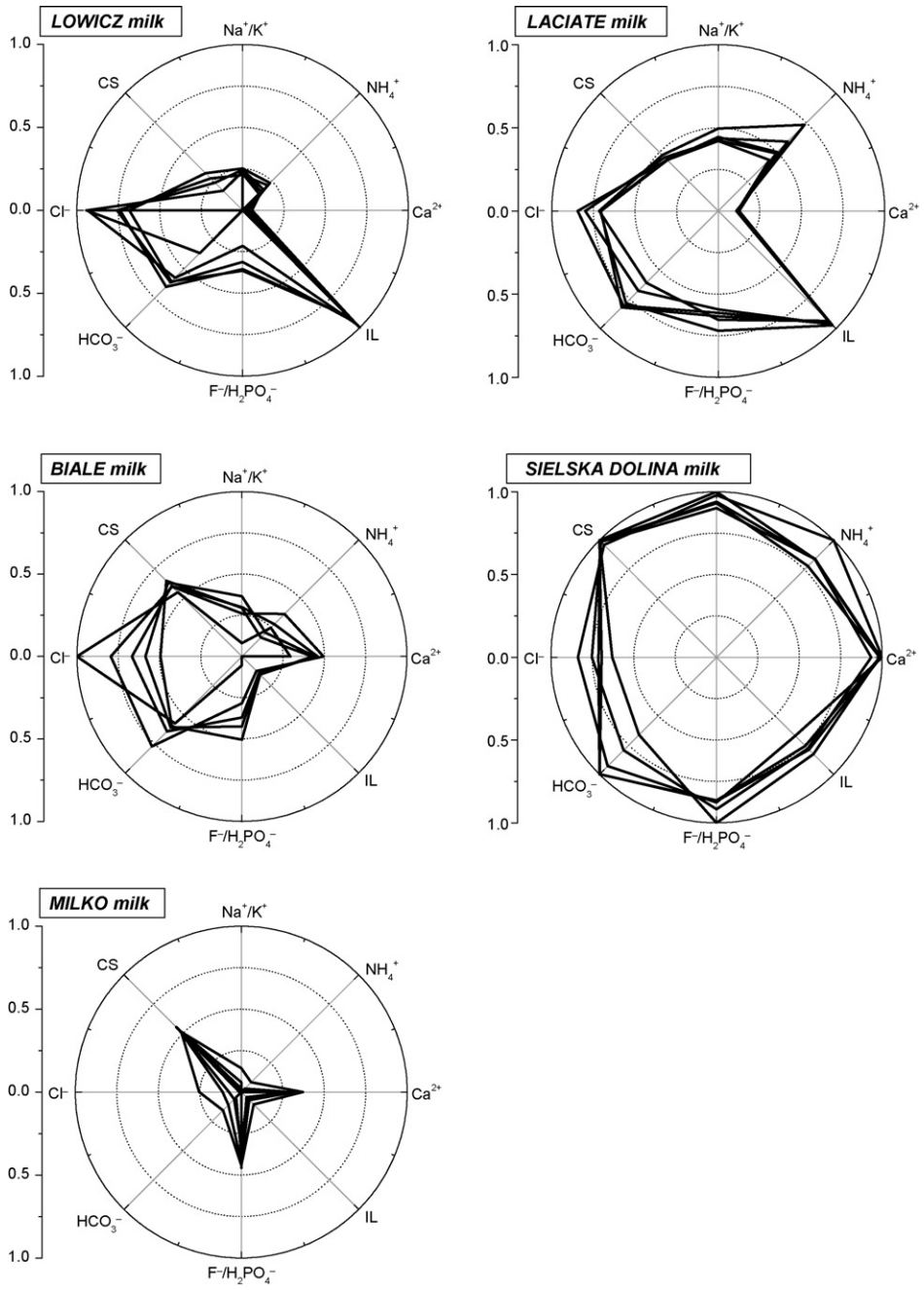

Fig. 6. Polar plots of milk measurements performed with commercial Ag/AgCl reference electrode.

The integrated array of solid-state microelectrodes was fabricated from epoxy-glass laminate (printed circuit board), covered with a gold layer forming the transducers in the shape of circles (diameter of 500 μm) and paths that are connecting the electrodes with the external plug. Transducer structure was covered with second epoxy-glass layer in order to insulate electric contacts of the microelectrodes. The holes drilled in the insulating layer (diameter of 1 mm), created compartments to be filled with membrane solutions ([22], Fig. 1).

The membranes contained appropriate ionophores, 20–50 mol% versus ionophore lipophilic salt, 61 wt.% plasticizer, and 31–33 wt.% high-molecular-weight PVC (Table 1). Membrane components (~100 mg) were dissolved in 0.5 ml of freshly distilled tetrahydrofuran (THF) to obtain membrane solutions. The membrane solutions were deposited on the surfaces of Au planar microelectrodes, cleaned thoroughly with distilled water and methanol. Two microliters of the membrane solution was cast on each electrode six times (each volume of the membrane solution was deposited after the formation of the previous layer), to achieve sufficient thickness of the final membrane (about 200–300 μm). For each membrane composition two electrodes were prepared (Fig. 2).

After membrane solvent evaporation, the sensor array was conditioned in the solution of 10^{-3} M KCl, 10^{-3} M NaCl, 10^{-3} M NH_4Cl for 24 h. All measurements were carried out with cells of the following type: Ag, AgCl; KCl 1 M/CH_3COOLi 1 M/sample solution//membrane//Au. EMF measurements were carried out using a potentiometric multiplexer (EMF 16 Interface, Lawson Labs Inc.,

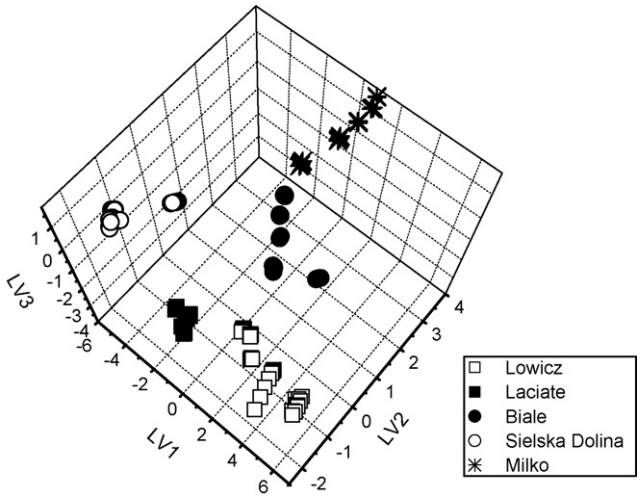

Fig. 7. 3D-PLS plot of milk measurements (commercial Ag/AgCl reference electrode).

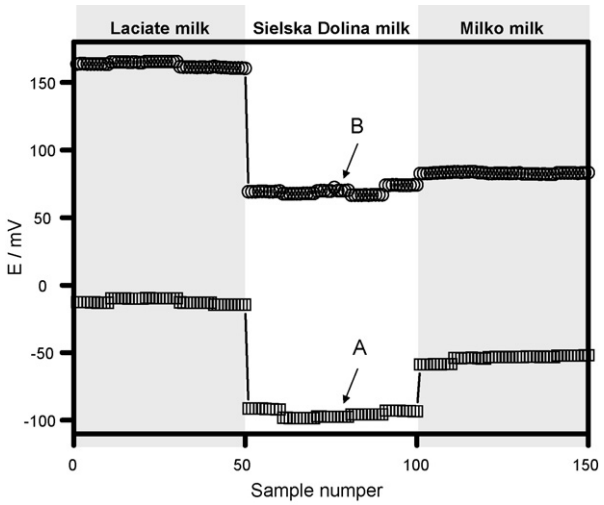

Fig. 9. Raw signals of Ca^{2+}-selective electrode obtained in the case of (A) commercial Ag/AgCl reference electrode; (B) IL reference electrode.

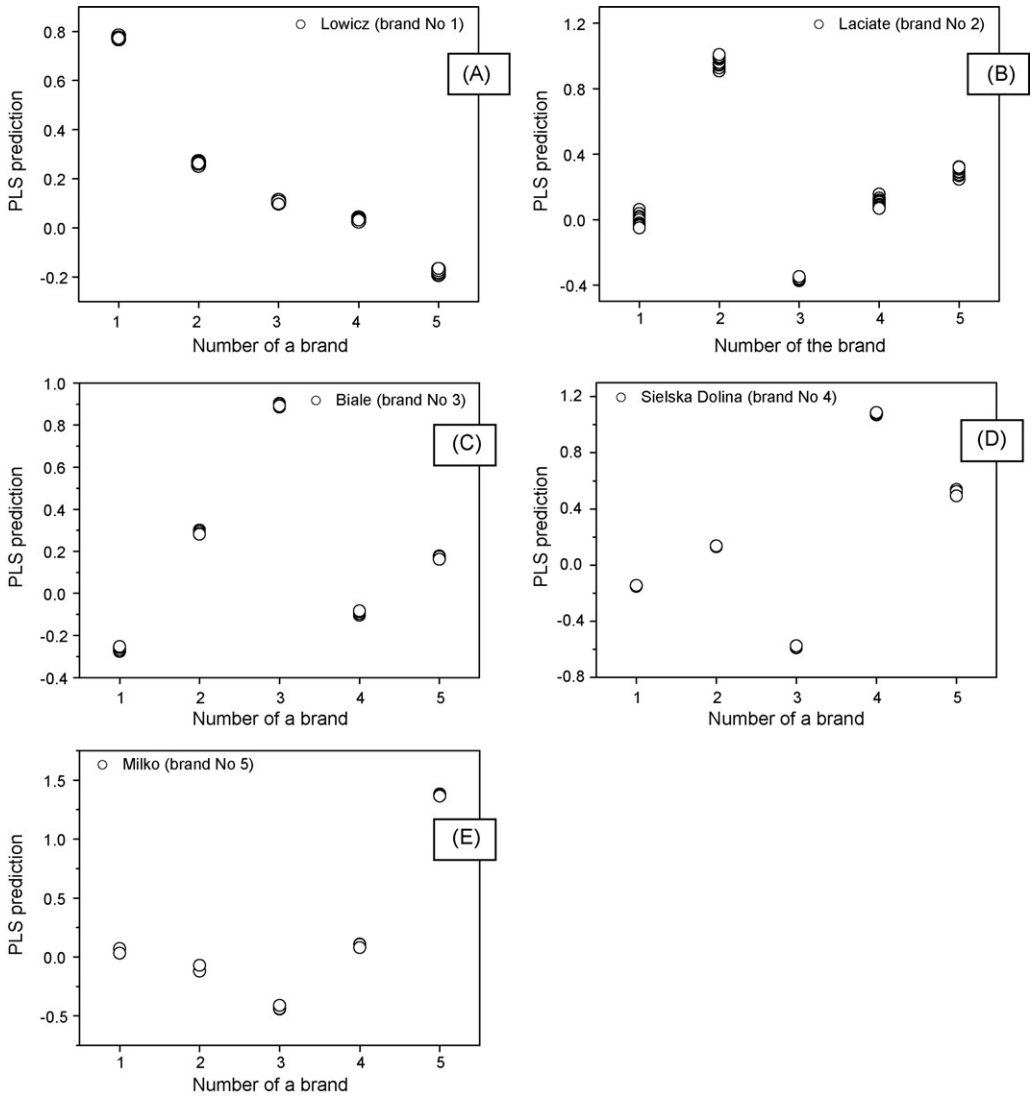

Fig. 8. PLS-DA prediction results for test set (commercial Ag/AgCl reference electrode): (a) Lowicz milk; (b) Laciate milk; (c) Biale milk; (d) Sielska Dolina milk; (e) Milko milk.

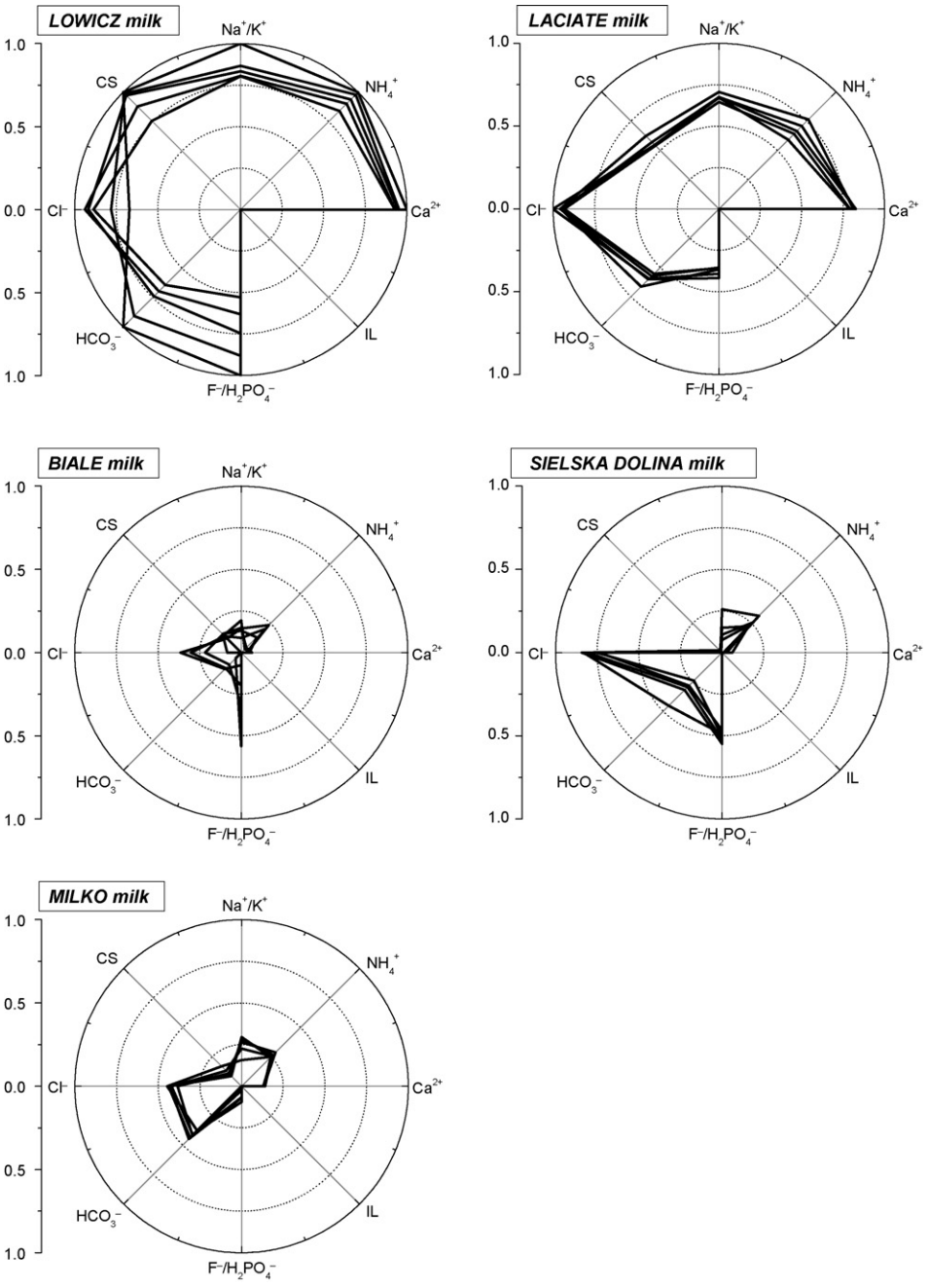

Fig. 10. Polar plots of milk measurements performed with IL reference electrode.

Malvern, USA). All data analysis was performed in MatLab (The MathWorks Inc., Natick, USA).

3. Results and discussion

3.1. The recognition of milk brand with an integrated sensor array and commercial Ag/AgCl reference electrode

Two kinds of sensitive materials: selective and partially selective polymeric membranes, were used in the integrated array. That approach was previously used for classical electrodes and high recognition ability in the classification of various foodstuffs and biological samples was noticed [5–8,33,34]. A sensor array consisted of eight types of electrodes: four ion-selective (NH_4^+, Cl^-, HCO_3^-, and Ca^{2+}), and four partially selective (Na^+/K^+, "cation-selective (CS)", $F^-/H_2PO_4^-$, and IL). Their performance in the integrated array was checked determining their selectivity coefficients. The comparison of the values of the selectivity coefficients of ammonium-selective electrodes in classical configuration (Philips body IS-561), their miniaturized version measured in flow conditions, and miniaturized electrodes on integrated sensor array is presented in Fig. 3. Similar selectivity pattern of NH_4^+-selective miniaturized electrodes on integrated sensor array and classical electrodes was noticed. The values of selectivity coefficients of the other cation-selective electrodes are presented in Fig. 4. The selectivity coefficients of Ca^{2+}-selective electrodes were in good accordance with literature data, whereas those obtained for Na^+/K^+-selective and "cation-selective" electrodes were in good

accordance with those previously obtained for miniaturized solid-state electrodes measured in flow conditions [6]. Selectivity of anion-selective electrodes is presented in Fig. 5. Also in this case the performance of electrodes on integrated sensor array was comparable to both classical electrodes and miniaturized solid-state electrodes measured previously [6,34]. IL-based electrodes exhibited low anion-selectivity, which was expected due to their application as reference electrodes (Fig. 5).

Samples of five brands of milk manufactured in Poland were tested with the use of the described microelectrode array. They were numbered in the following order: (1) Lowicz, (2) Laciate, (3) Biale, (4) Sielska Dolina, and (5) Milko. From each kind of milk five samples were collected. The signals were measured in each sample for 15 min (to ensure obtaining steady-state responses). From every sample and for each sensor 10 measurements in 5-s intervals were acquired. Data matrix consisted of 250 rows (5 brands of milk × 5 samples × 10 measurements) and 16 columns (16 electrodes). First, to check the ability of the system to distinguish between various brands of milk, the sensor array responses were scaled to [0,1] interval according to the formula:

$$x'_{i,j} = \frac{x_{i,j} - \mathrm{MIN}(x_i)}{\mathrm{MAX}(x_i) - \mathrm{MIN}(x_i)}$$

where $\boldsymbol{x'_{i,j}}$ is the scaled signal of ith sensor in jth measurement, $x_{i,j}$ is the signal of ith sensor in jth measurement, $\mathrm{MAX}(x_i)$ is the maximal value of ith sensor signal in all samples, and $\mathrm{MIN}(x_i)$ is the minimal value of ith sensor signal in all samples.

Then, the scaled responses were plotted on polar plots (Fig. 6). Polar plots are used for displaying a few series of multidimensional data and are very well suited to the visualization of multidimensional chemical images, according to easy comparison of their similarities and differences. In such graph every sensor is assigned with its own axis, on which the sensor signals are depicted. Finally, the drown points are linked together to form a closed shape, which presents a chemical image of a measured sample. The shapes can be compared—the more similar they are, the more similar are the respective samples. The response patterns in the case of the same milk samples were very similar, whereas for the samples originated from various diaries they were differentiated, i.e. the developed sensor array was capable of the recognition of the origin of milk.

Partial least squares-discriminant analysis (PLS-DA) procedure was used for the classification task. The data set was splitted into two parts: the train set (200 cases) and the test set (50 cases). In both sets the numbers of samples originating from the same producer was the same, i.e. in train set there were 40 measurements from each of five brands of milk, and in test set 10 measurements from each of five brands of milk. Every case belong either to train set, or test set, and their affiliation was chosen randomly.

PLS-DA was applied to train set with a target matrix composed of target vectors. Each target vector, characterizing a sample, was five-dimensional (five classes of milk) and it was composed of zeros and one. Each of the five outputs marked successive number of the sample (e.g. a target vector [0 0 1 0 0] was assigned to the sample belonging to the 3rd brand—Biale). The results of PLS analysis for train set are presented on 3D-PLS plot (see Fig. 7). The differentiation ability towards the recognition of various brands of milk was high—clusters of various classes were easily separable on 3D-PLS plot. To verify the performance of the whole system, the assignation to one of five brands of samples from test set was checked. The sample was assigned to that number of a class, on which the highest value in output vector was observed (e.g. output vector [0.1 0.8 0.4 0.0] assigned the sample to the 2nd class—Laciate milk). All output vectors are depicted in Fig. 8. Although the values are usually not ideal (they are not equal to ones and zeros), however, the classification results are still correct and evident. All samples were correctly recognized and percent of correct classifications reached 100, both for train set and test set. The correlation between real and predicted values of class membership is much better in the train set than in the test set (see Table 2), however, such result was expected since the test set samples were not included in the establishment of PLS-DA model (they are independent from train set). Thus, reliable validation of the system was performed and satisfactory results were obtained.

3.2. The recognition of milk brand with an integrated sensor array and miniaturized IL-based reference electrode

The second part of this study was dedicated to investigate the possibility of the replacement of commercial Ag/AgCl electrode with a miniaturized solid-state reference electrode, based on ionic liquid introduced in PVC membrane. That approach would be very advantageous for future applications of integrated sensor array—the developed reference microelectrode is compatible with ion-selective electrodes placed on the integrated sensor array. Moreover, the measurement set-up becomes simplified and smaller sample volumes can be analyzed.

The properties of the membranes containing IL were investigated in our previous article [31]. The aim of IL addition was to

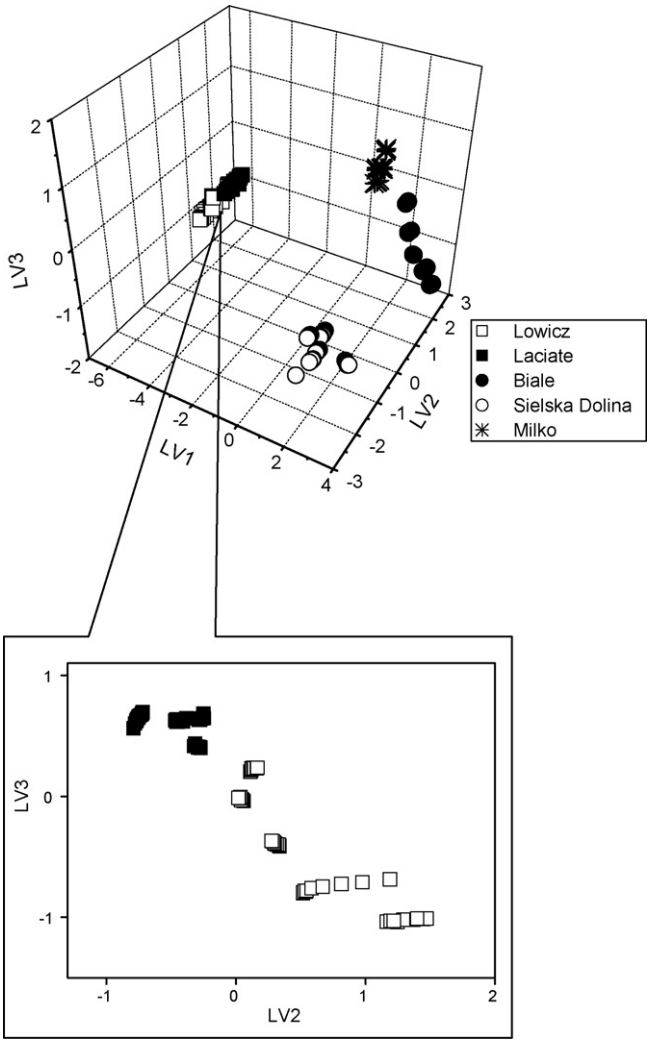

Fig. 11. 3D-PLS plot of milk measurements (IL reference electrode).

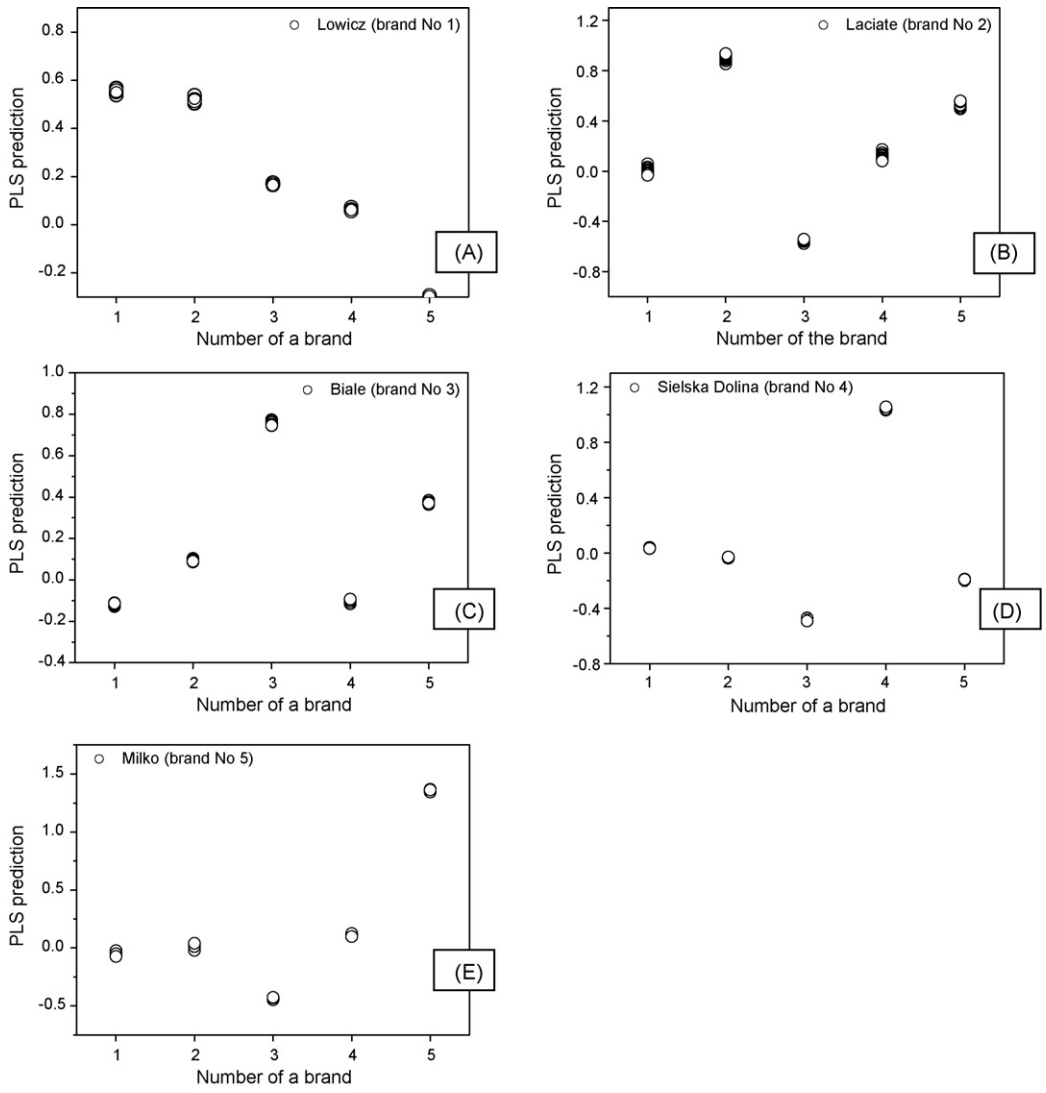

Fig. 12. PLS-DA prediction results for test set (IL reference electrode): (a) Lowicz milk; (b) Laciate milk; (c) Biale milk; (d) Sielska Dolina milk; (e) Milko milk.

provide non-selective polymeric layer being at the same time an internal solid electrolyte of constant chloride concentration. In this work, IL membrane was placed on Au transducer instead of Ag/AgCl. Despite low anion selectivity obtained for the reference microelectrodes (see Fig. 5), some differences in their signals measured in various brands of milk were observed (see Fig. 6). However, the variations of the IL-based electrode raw signals in various milk samples was significantly smaller in comparison with the other electrodes. According to that, IL-based electrode can be regarded as pseudo-reference electrode and as long as the distinguishing between various classes of a product is sufficient, the approach is satisfactory. The exemplary comparison of raw signals obtained with the use of commercial Ag/AgCl reference electrode and miniaturized IL-based reference electrode is presented in Fig. 9.

In order to check the performance of integrated sensor array with miniaturized reference electrode, the signals of sensors obtained during previous measurements were recalculated according to the formula:

$$x''_{i,j} = x_{i,j} - x_{\mathrm{IL},j}$$

where $x''_{i,j}$ is the signal of ith sensor in jth measurement versus IL reference electrode, $x_{i,j}$ is the signal of ith sensor in jth measurement versus commercial Ag/AgCl reference electrode, and $x_{IL,j}$ is the signal of IL electrode in jth measurement versus commercial Ag/AgCl reference electrode.

The procedure of data analysis was repeated for the data obtained in the second part of this study. Data matrix consisted of 250 rows as previously and 14 columns (seven types of microelectrodes). First, the response patterns of milk samples were checked and sufficient differences between various brands were found (see Fig. 10). The data were splitted into two parts—train (200 cases) and test set (50 cases). The assignation of each sample to either train set, or test set, was performed as in previous example. The similarity of the same kind of products was also visible on 3D-PLS plot (Fig. 11A). Even though two classes seem to overlap, there is a clear linear border between them, which can be observed when the 2nd and the 3rd Latent Variables are considered (see Fig. 11B). The similarity of Lowicz and Laciate milk (class 1 and class 2) causes the appearance of very high value on the second place of output vector, when Lowicz sample is investigated (see Fig. 12A), however, still the highest value occurs on the first place, which is correct (Lowicz samples form class 1). In the case of the other samples the recognition is even more evident, leading to 100% correct classifications both in train and test set (Fig. 12B–E). Correlations between real and predicted class memberships are comparable to those obtained in the

first part of this study, but smaller values of correlation coefficients are obtained in the case of measurements performed with the IL reference electrode (see Table 2).

4. Summary

This work presents the application of an integrated microelectrode array as a sensor array in potentiometric electronic tongue. The device was fabricated from epoxy-glass laminate where gold electrodes and their electric contacts were formed, and then covered by an insulating layer. The membranes were deposited on the Au electrodes and they formed selective and partially selective chemosensitive layers.

For data analysis PLS-DA was used. The system exhibited satisfactory classification abilities towards milks originating from various diaries. Moreover, the comparison of milk classification results obtained with the use of commercial Ag/AgCl electrode and miniaturized reference electrode based on ionic liquid (1-dodecyl-3-methyl-imidazolium chloride) showed, that it is possible to integrate the miniature reference electrode with ion-selective electrodes on the same substrate, which can be advantageous for the future constructions and applications of potentiometric electronic tongue. The presented integrated microelectrode array can form the base of hand-held electronic tongue.

Acknowledgments

This work was financially supported by the Ministry of Science and Higher Education, project No. N204 106 31/2448 (2006–2008). Patrycja Ciosek wishes to thank The Foundation for Polish Science for financial support.

References

[1] F. Winquist, E. Rydberg, S. Holmin, C. Krantz-Rülcker, I. Lundström, Anal. Chim. Acta 471 (2002) 159.
[2] A. Legin, A. Rudnitskaya, Y. Vlasov, C. Di Natale, E. Mazzone, A. D'Amico, Sens. Actuators B 65 (2000) 232.
[3] K. Toko, Mater. Sci. Eng. C 4 (1996) 69.
[4] R. Martínez-Máñez, J. Soto, E. Garcia-Breijo, L. Gil, J. Ibáñez, E. Llobet, Sens. Actuators B 104 (2005) 302.
[5] P. Ciosek, W. Wróblewski, Talanta 71 (2007) 738.
[6] P. Ciosek, W. Wróblewski, Talanta 69 (2006) 1156.
[7] P. Ciosek, Z. Brzózka, W. Wróblewski, Sens. Actuators B 118 (2006) 454.
[8] P. Ciosek, K. Brudzewski, W. Wróblewski, Meas. Sci. Technol. 17 (2006) 1379.
[9] L. Lvova, S.S. Kim, A. Legin, Y. Vlasov, J.S. Yang, G.S. Cha, H. Nam, Anal. Chim. Acta 468 (2002) 303.
[10] N. García-Villar, J. Saurina, S. Hernández-Cassou, Fresen. J. Anal. Chem. 371 (2001) 1001.
[11] J. Gallardo, S. Alegert, M. del Valle, Sens. Actuators B 101 (2004) 72.
[12] J. Gallardo, S. Alegret, R. Muñoz, L. Leija, P.R. Hernandez, M. del Valle, Electroanalysis 17 (2005) 348.
[13] J. Gallardo, S. Alegret, R. Muñoz, M. De-Roman, L. Leija, P.R. Hernandez, M. del Valle, Anal. Bioanal. Chem. 377 (2003) 248.
[14] J.D. Kim, H.G. Byun, D.J. Kim, Y.K. Ham, W.S. Jung, C.O. Yoon, Talanta 70 (2006) 546.
[15] L. Moreno, A. Merlos, N. Abramova, C. Jiménez, A. Bratov, Sens. Actuators B 116 (2006) 130.
[16] G. Sehra, M. Cole, J.W. Gardner, Sens. Actuators B 103 (2004) 233.
[17] S. Jacesko, J.K. Abraham, T. Ji, V.K. Varadan, M. Cole, J.W. Gardner, Smart Mater. Struct. 14 (2005) 1010.
[18] S.L. Jacesko, T. Ji, J.K. Abraham, V.K. Varadan, J. Gardner, Proceedings of the SPIE—The International Society for Optical Engineering, vol. 5055, 2003, p. 147.
[19] K. Toko, Sensors Update, vol. 3, Wiley–VCH, 1998.
[20] V. Parra, A.A. Arrieta, J.A. Fernández-Escudero, M.L. Rodríguez-Méndez, J.A. De Saja, Sens. Actuators B 118 (2006) 448.
[21] J. Saurina, E. López-Avilés, A. Le Moal, S. Hernández-Cassou, Anal. Chim. Acta 464 (2002) 89.
[22] P. Ciosek, R. Mamińska, A. Dybko, W. Wróblewski, Sens. Actuators B 127 (2007) 8.
[23] A. Simonis, H. Lüth, J. Wang, M.J. Schöning, Sens. Actuators B 103 (2004) 429.
[24] H. Suzuki, T. Hirakawa, S. Sasaki, I. Karube, Anal. Chim. Acta 387 (1999) 103.
[25] A. Van Den Berg, A. Grisel, H.H. Van Den Vlekkert, N.F. De Rooij, Sens. Actuators B B1 (1990) 425.
[26] D. Desmond, B. Lane, J.C. Alderman, J.D. Glennon, D. Diamond, D.W.M. Arrigan, Sens. Actuators B 44 (1997) 389.
[27] Tymecki, E. Zwierkowska, R. Koncki, Anal. Chim. Acta 526 (2004) 3.
[28] P.J. Kinlen, J.E. Heider, D.E. Hubbard, Sens. Actuators B 22 (1994) 13.
[29] I.Y. Huang, R.S. Huang, L.H. Lo, Sens. Actuators B 94 (2003) 53.
[30] E. Bakker, Electroanalysis 11 (1999) 788.
[31] R. Mamińska, A. Dybko, W. Wróblewski, Sens. Actuators B 115 (2006) 552.
[32] K. Wojciechowski, W. Wróblewski, J. Przygorzewska, G. Rokicki, Z. Brzózka, Chem. Anal. 47 (2002) 335.
[33] P. Ciosek, B. Pokorska, E. Romanowska, W. Wróblewski, Electroanalysis 18 (2006) 1266.
[34] P. Ciosek, E. Augustyniak, W. Wróblewski, Analyst 129 (2004) 639.

Talanta 76 (2008) 564–574

Contents lists available at ScienceDirect

Talanta

journal homepage: www.elsevier.com/locate/talanta

Classification of genomic data: Some aspects of feature selection

Tomasz Czekaj[a], Wen Wu[b], Beata Walczak[a,*]

[a] Department of Chemometrics, Institute of Chemistry, The University of Silesia, 9 Szkolna Street, 40-006 Katowice, Poland
[b] Bioinformatics Science & Technology, GlaxoSmithKline, Gunnels Wood Road, Stevenage, Hertfordshire SG1 2NY, UK

ARTICLE INFO

Article history:
Received 28 January 2008
Received in revised form 21 March 2008
Accepted 25 March 2008
Available online 4 April 2008

Keywords:
PLS
UVE-PLS
Continuum power regression
GA
Stepwise MLR regression
Microarrays

ABSTRACT

Feature selection, while working with genomic data sets, is of particular interest, not only for classification (diagnostics) improvement, but also for the data interpretability. Application of the multivariate feature selection approaches allows an efficient reduction of data dimensionality, but as demonstrated in our study, sets of the selected variables depend on the objective function of the classifier. It is possible to select different subset of genes for classification due to the correlation of genes but their interpretation ought to be cautiously made.

1. Introduction

1.1. Microarray technology

Microarrays offer a potential of simultaneous examining the transcription level of expression for all genes in a genome. The basic concept hidden behind microarrays is a global scale (large-scale) extension of hybridization methods (e.g., the Northern blot) [1]. Thus, mRNA extracted from a collection of cells is hybridized on the array, which consists of the probe set for the target genes of interest. Each probe (separate hybridization) has its own, well-defined place on the microarray, and it is called a spot or a variable. It is possible to measure up to 20,000 genes in one step [2]. Identification of an individual hybridization is possible, thanks to labeling of mRNA. In this manner, one obtains complex signals that reveal identity (and concentration) of each labeled target in a solution. This result is then compared across a set of samples. For certain kind of microarrays, it is possible to apply two fluorescent tags on a single array (using, e.g., cyanine 3—Cy3 and cyanine 5—Cy5) [3]. Thus a possibility is offered to perform direct comparison of the two samples, e.g., one being a reference, and the other one an experimental sample. After scanning of the microarray's surface, digital signals for the both colors (channels) are recorded separately for each spot.

1.2. Analysis of microarrays

On the spotted cDNA chip, the gene expression profiling can present a wealth of the data containing information not only about the absolute expression of a large amount of genes, but also about the potential interactions and regulation among the genes [4–6]. To fully explore the potential of the genome-scale experiments to alter our understanding of cellular biology, the analysis of the DNA microarray data is usually multi-objective. After the image processing and standardization procedures, a natural first step in extracting information from the genomics data is to examine genes with a significant differential expression in the two (or more) groups of studied samples or in a time series, after a given treatment. This step is usually followed by an unsupervised pattern recognition and classification [4]. The pattern discovery techniques include a variety of the dimension-reduction methods (which allow data visualization and help in revealing data structure), as well as the various 'clustering' techniques [4]. Cluster analysis of microarray data aims to find coherent patterns of gene expression [7], i.e., to detect groups of co-expressed genes, in an attempt to draw some inferences about the underlying regulatory networks or response mechanisms. In contrast to unsupervised pattern discovery, supervised pattern recognition methods are designed to classify objects

* Corresponding author. Tel.: +48 32 359 21 15; fax: +48 32 259 99 78.
E-mail address: beata@us.edu.pl (B. Walczak).

0039-9140/$ – see front matter © 2008 Elsevier B.V. All rights reserved.
doi:10.1016/j.talanta.2008.03.045

into the known groups. The goal may be diagnostics or prediction of a clinical outcome.

1.3. Feature selection

As microarray data is highly correlated (redundant) and contains many irrelevant variables, one of the main problems in its exploration is feature selection. The three principal reasons for feature selection in genomics are usually formulated as [4,8,9]:

(1) finding co-expressed genes to build metabolic pathways,
(2) biological relevance of individual genes for clinical diagnosis and
(3) enhancement of the classifier performance.

As an additional benefit of the variable selection one can also mention facilitation of data visualization, reduction of the measurements and storage requirements and time reduction of data processing.

The available feature selection methods can be divided into univariate, stepwise and multivariate. In the univariate approach, each feature is evaluated individually in the preprocessing step. It ought to be stressed that the different criteria of the genes scoring lead to the different subsets of significant genes [8,10] and it is believed, that certain insight into the significance of genes can be gained, based on the performance of a classifier trained on these subsets [4,11–13]. However, the univariate methods that score variables individually and independent of each other are unable to determine, which combination of the variables would give the best performance of a classifier.

In the stepwise approach, subset selection is performed by combining the forward selection with backward elimination, both yielding the nested variable subsets [8]. Approaches of this type do not guarantee selection of the optimal subset of the variables. Weaker subsets are found by the forward selection, because the importance of the variables is not assessed in the context of the other variables not yet included.

The multivariate variable selection approaches only take into account the joint influence of the features' subset on the classifier performance, which seems of a particular interest for the determination of interactions and regulation among the genes. To this class belongs the uninformative variable elimination-partial least squares (UVE-PLS) approach [14], and genetic algorithm (GA)-based approaches (e.g., [15]).

From the biological point of view, the elementary question is to what a degree the subsets of genes with high discrimination power can be used to draw any conclusions about the underlying regulatory networks or response mechanisms. Some insight into the discussed problem can be gained by comparing the results of the continuum regression (CR) approach, in which the objective function is modified in a continuous manner. This approach was enhanced by the feature selection procedure, based on stability of the regression coefficients, which can be considered as modification of the UVE approach [14].

2. Theory

2.1. Notation

The studied microarray data sets contain m profiles, each measuring the expression level of n genes, $\mathbf{X}$ (m, n). The term 'gene' (meaning the variable or feature) is used instead of the cDNA clones for the sake of simplicity. Each data set consists of the two groups of samples coded in vector $\mathbf{y} \in \{-1, 1\}$.

2.2. Partial least squares

In the PLS method, set of latent variables is constructed to maximize the covariance of latent variable $\mathbf{t} = \mathbf{Xc}$ and $\mathbf{y}$ data. This relation can be expressed as follows:

$$\text{maximize the function}: \quad R^2(\mathbf{y}, \mathbf{Xc})\mathrm{Var}(\mathbf{Xc}) \tag{1}$$

where R denotes the correlation, Var denotes the variance and $\mathbf{c}$ represents the direction which maximizes a given above criterion and $|\mathbf{c}| = 1$.

Optimization of the number of latent variables can be performed in several ways and one possible approach is cross-validation (CV). Optimal complexity of the PLS model corresponds to the number of factors, where the minimum CV error appears.

2.3. Continuum regression and continuum power regression

The concept of continuum regression (CR), introduced by Stone and Brooks [16], embraces ordinary least squares (OLS), PLS, and principal component regression (PCR). The construction rule of CR can be expressed, as follows:

$$\text{maximize the function}: \quad R^2(\mathbf{y}, \mathbf{Xc})\mathrm{Var}(\mathbf{Xc})^{\gamma/(1-\gamma)} \tag{2}$$

where γ is the parameter, that changes from 0 to 1. For $\gamma \in [0, 1]$, the vector of the regression coefficients is determined by a simple regression of $\mathbf{y}$ on a one-dimensional regressor $\mathbf{Xc}$.

In the case of OLS, $\gamma = 0$, the squared correlation between $\mathbf{y}$ and $\mathbf{Xc}$ is maximized. In the case of PLS, $\gamma = 0.5$, the covariance between $\mathbf{y}$ and $\mathbf{Xc}$ is maximized, and for PCR, $\gamma = 1$, the sample variance of $\mathbf{Xc}$ is maximized.

For PLS and PCR, the maximization is subject to the following constrain: $|\mathbf{c}| = 1$, in order to avoid trivial results.

In our study, the continuum power regression method, CPR [17], is used. CPR, like CR, also encompasses OLS, PLS, and PCR. The advantage of this approach is that it is very fast. In this method, data matrix $\mathbf{X}$ is decomposed via the singular value decomposition (SVD) as $\mathbf{X} \equiv \mathbf{USV}^{\mathrm{T}}$ (where $\mathbf{U}$ denotes normalized score matrix; $\mathbf{V}$ denotes loadings and $\mathbf{S}$ is diagonal matrix, containing singular values) and appears as $\mathbf{X}^{\gamma/(1-\gamma)} \equiv \mathbf{US}^{\gamma/(1-\gamma)}\mathbf{V}^{\mathrm{T}}$, followed by the ordinary PLS.

2.4. Uninformative variable elimination in latent variable approaches

Stability of the regression coefficients, $s(\mathbf{b}_j)$, can be defined as the absolute value of the ratio of its value and the standard deviation:

$$s(\mathrm{b}_j) = \left| \frac{\bar{\mathrm{b}}_j}{\mathrm{std}(\mathrm{b}_j)} \right| \tag{3}$$

where $\bar{\boldsymbol{b}}_j$ and std denote the mean and the standard deviation of the regression coefficients, respectively, and $j = 1, \ldots, n$.

Nowadays, it is theoretically possible to calculate standard deviation of the regression coefficients for the latent variable models, constructed within the CR frame [18], although the problem becomes intractable for the data sets containing more than 10,000 variables, due to the calculation time requirements. Standard deviation of the regression coefficients can be, however, well estimated, based on the cross-validation procedure (the study performed for the data sets with a smaller number of variables strongly supports this statement). For the data set of the dimensionality $m \times n$, the leave-one-out cross-validation (LOOCV) procedure allows to calculate m vectors of the regression coefficients and thus to calculate standard deviation of n individual regression coefficients.

As proposed by Centner et al. [14], the original data set can be augmented with the artificial random variables (having a very small amplitude, to prevent their influence on the regression model), and their stability can be indicative of the values, which can be reached by the uninformative experimental variables. All variables with stability smaller than the maximum value s, obtained for the artificial variables, can be considered uninformative and eliminated from the original data set. The higher the number of the artificial random variables, the better is the estimation of the cut-off level. In our study, as a default 5000 random variables are added to the original data matrix.

To avoid high dependence of the cut-off value on the distribution of the stabilities of the regression coefficients of the augmented random variables, it is recommended [14] not to eliminate all the variables with the stability lower than the maximal stability of the noise variables, $\max|s_{\text{artif}}|$, but to use a more robust criterion. Namely, the elements of the stability vector associated with the noise are ranked and the cut-off level is defined as a value that corresponds with the predefined quantile, e.g., 95 or 99%. Depending on the quantile applied, the following notation is used: b_w-α-95 and b_w-α-99, respectively. In our study, the 95% quantile (b_w-α-95) is applied.

After elimination of uninformative variables, the final model can be constructed. However, if the new set of the retained variables is again augmented with the random variables and calculations of the regression coefficients stability are repeated, it appears that among the retained variables there are still the variables uninformative for the actual model. Thus, in order to obtain the model with the stable regression coefficients for all the retained variables, it is necessary to repeat the whole procedure several times (usually from two to four times). This leads to a stable model with low complexity and a relatively small set of variables.

2.5. Validation of classification models

Optimization of the complexity of the latent variable model can be performed by k-fold cross-validation (k-fold CV) or Monte Carlo cross-validation (MCCV).

In k-fold CV, the data set is split into the k subsets and each subset is used as the test set, while the remaining ones are in the model set. It means that each sample is drawn into the test set only once. A variant of the k-fold CV when k is equal to the number of samples in the data set is called leave-one-out CV (LOOCV).

In MCCV, a fixed number (p) of randomly selected samples is left out and prediction of their **y** is based on the remaining samples. Theoretically, the fewer samples are in the model set, the more repetitions (t) are needed [19].

The complexity of the model is evaluated based on the so-called root mean square error of cross-validation (RMSECV), defined as:

$$\text{RMSECV}(f) = \sqrt{\frac{\sum_{i=1}^{a}(y_i - \hat{y}_i(f))^2}{a}} \tag{4}$$

where $a = m$ in the k-fold CV method, whereas $a \times pt$ in the case of MCCV; $\hat{y}_i(f)$ is the prediction of y_i based on the model built with f factors.

In our study, the RMSECV was calculated for MCCV with $p = 5$–30% of the samples and $t = 100$ iterations.

The prediction power of the final model was calculated, based on the independent test set and expressed as

$$\text{RMStest}(f) = \sqrt{\frac{\sum_{i=1}^{a}(y\text{test}_i - \hat{y}\text{test}_i(f))^2}{a_{\text{test}}}} \tag{5}$$

where $\hat{y}\text{test}_i(f)$ denotes the predicted value of the independent variables and a_{test} is the number of samples in the test set.

2.6. Classification and regression tree (CART)

Using CART [20], we can derive the binary decision tree, which partitions input space of a data into the mutually exclusive regions, containing the homogenous subsets of data. CART is based on a recursive partitioning scheme, i.e., initially all objects are stored in the root node and then they are recursively split with the aim of obtaining the nodes which contain objects with similar properties. The CART algorithm searches for each potential split point in the data and chooses the split which minimizes some impurity measure of the node. For the classification purpose, the most popular impurity measure (cost function) is the entropy function. To construct a tree with the good generalization property, tree pruning is applied and the tree predictive power is evaluated, based on the 10-fold cross-validation.

2.7. Stepwise multiple linear regression (stepwise MLR)

The objective of stepwise MLR regression [21] is to construct a multivariate model for the dependent variable, **y**, based on a few deliberately selected explanatory variables. In stepwise regression, the first selected explanatory variable has the highest correlation with **y**. Then, explanatory variables are consecutively added to the model in a forward selection procedure, based on their correlation with the **y**-residuals. The significance of the model improvement is evaluated using the statistical F-test [21] and each time a new variable is included into the model, the backward elimination step follows in which the F-test detects variables that can be removed from the model without changing the residuals significantly. The variable selection procedure terminates, when no additional variable significantly improves the given model.

2.8. Genetic algorithm MLR (GA-MLR)

Genetic algorithm is a global optimization procedure, based on the principles of natural evolutionary process [22]. It is a general approach, which however requires definition of the problem-dependent 'fitness function'. In our study, the fitness function is defined as an inverse of RMSEP of the MLR model containing no more than 23 features. In the version of GA-MLR, published by Leardi [23], GA alternates with the cycles of backward stepwise selection of features and the most important parameters are the following ones: deletion groups: 5, population size: 100; uniform cross-over, mutation probability 1%, stop criterion: 500 reproduction steps.

2.9. Data pretreatment

The experimental microarray data can be visualized in many different ways. One of the most convenient methods of visualization is the so-called RI plot, in which the log-intensity ratio $R = \log_2(\text{Cy5}/\text{Cy3})$ versus the log-intensity product $I = \log_2\sqrt{\text{Cy3}\cdot\text{Cy5}}$ is plotted (see Fig. 1).

In an ideal case, most points on the RI-plot should fall along a horizontal line [24]. However, due to the different effects from the non-biological sources (like differences in labeling, in detection efficiencies for the fluorescent labels, and in the quantity of the initial RNA from the two samples [25]), data deviate from the natural, horizontal trend (see Fig. 1a). This non-horizontal trend should be removed before drawing the conclusions about the relative levels of the gene expression [24]. Removal of such trends

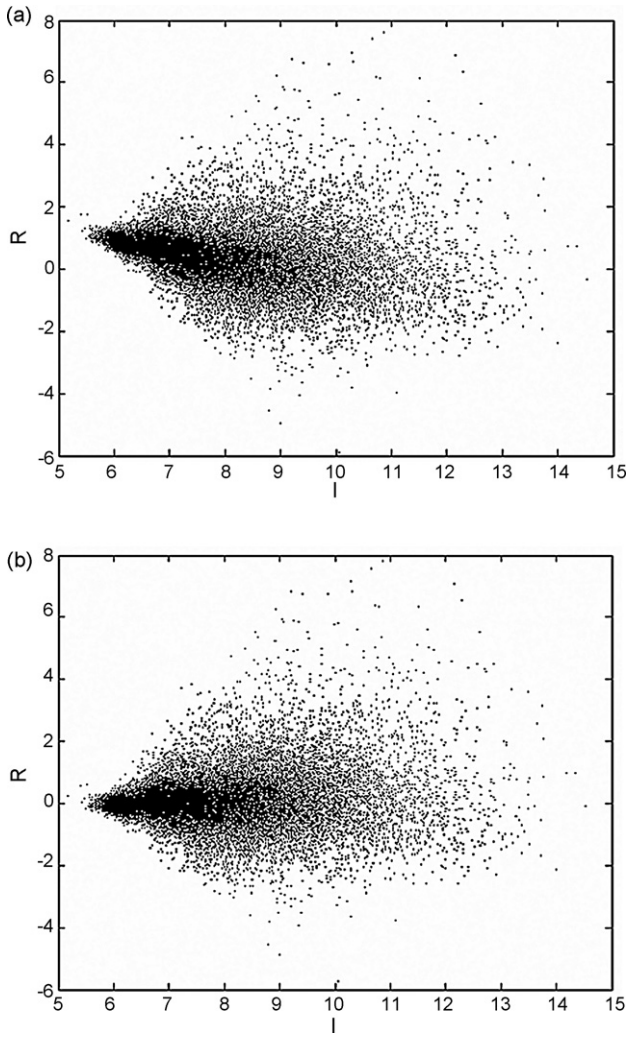

Fig. 1. Scatterplots of the microarray data (a) before and (b) after normalization, using the P-splines approach, where $R = \log_2(\text{Cy5}/\text{Cy3})$ and $I = \log_2\sqrt{\text{Cy3}\cdot\text{Cy5}}$.

is called normalization and plays a crucial role in the preparation of data for the further analysis. The most frequently used normalization methods are lowess [26] and loess [27]. Both methods use locally weighted linear regression to smooth the data. In our study, the approach, proposed by Eilers [28] was applied. It allows a fast and efficient estimation of signals trends, obtained from a microarray. This method uses P-splines, which are a combination of the regression on a B-splines basis with a penalty term, which determines the roughness of the regression coefficients [29]. The method described allows removal of the systematic trend, what is visible in Fig. 1b, where the normalized data are presented.

2.10. Design of training and test sets

All training sets were selected after the data normalization, using the Kennard and Stone algorithm [30].

The Kennard and Stone design selects a set of objects in the n-dimensional space, which are "uniformly" distributed over the space defined by the candidates. All m objects from the given data matrix $\mathbf{X}$ $(m \times n)$ are considered as candidates for the training set. As the object which is nearest to the mean of the $\mathbf{X}$ data can be considered as the most representative for the given data set, it is

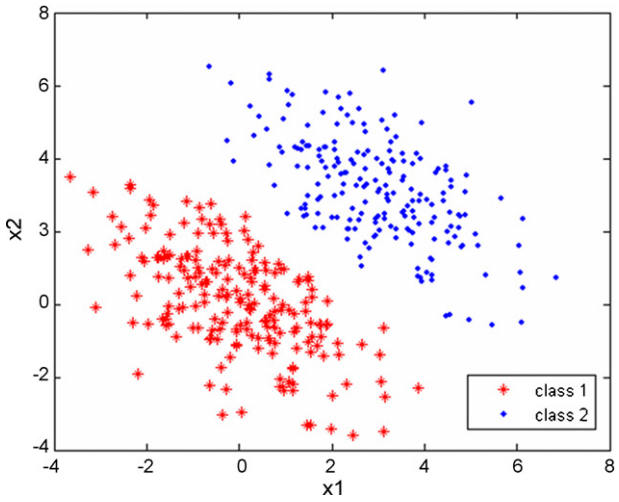

Fig. 2. Distribution of objects of the two-dimensional data set. Individual variables have no discrimination power, but their linear combination allows proper classification of the studied objects.

included as the first point in the training set. Let us denote it as O_1. The consecutive objects are chosen sequentially, based on their squared distance from the points that have already been assigned to the training set. The squared distance from the ith to the jth object

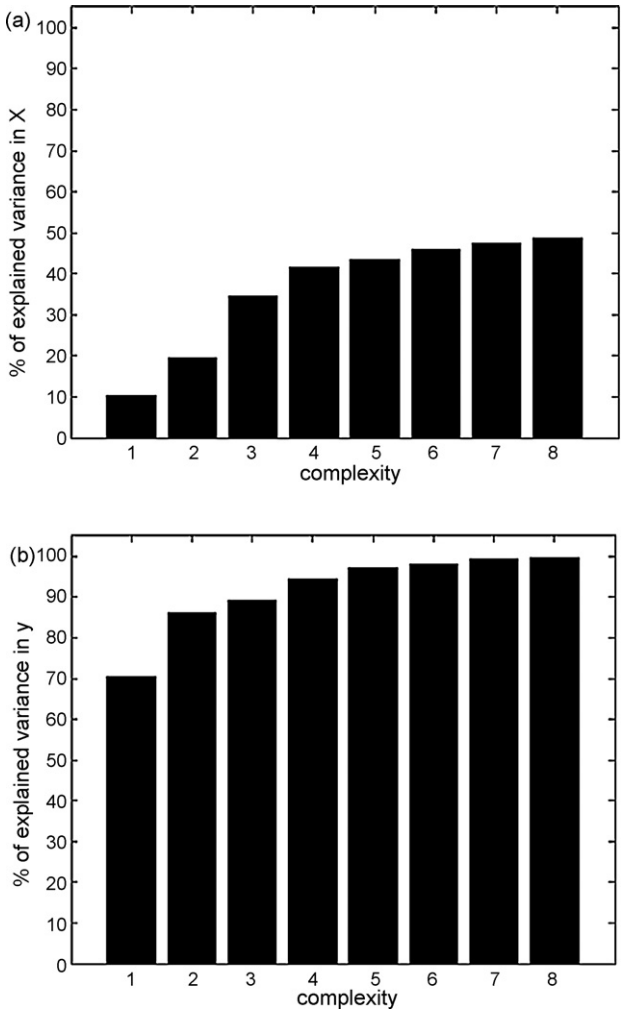

Fig. 3. Data set 1—percentage of variance, described by the PLS model, in (a) $\mathbf{X}$ and (b) $\mathbf{y}$.

is defined as

$$d_{ij}^2 = ||\mathbf{x}_i - \mathbf{x}_j|| = \Sigma_k (x_{ik} - x_{jk})^2 \quad (6)$$

Thus, the second object for the training set is the one situated farthest away from O_1. The third object is chosen which is farthest away from both O_1 and O_2, etc.

Generally, the main steps of the Kennard and Stone algorithm can be presented as follows:

Let $O_1, O_2, \ldots, O_k$ (where $k < m$) denote k objects that have already been assigned to the training set. We are looking for the $(k+1)$st object from the remaining $(m-k)$ candidates that is farthest away from an existing training set using the criterion:

$$D_{k+1}^2 = \max(D_v^2(k)) \quad \text{for } v = k+1, \ldots, m \quad (7)$$

where $D_v^2(k) = \min(d_{1v}^2, d_{2v}^2, \ldots, d_{kv}^2)$

3. Data

3.1. Data set 1

The original data set available at [31] contains gene expression of 157 samples (microarrays), where 82 and 75 samples correspond to the diseased and the healthy cells, respectively. Originally, each sample is characterized by 24,192 variables, denoting a mean fluorescent intensity of a microarray spot, without subtracting the background. Due to the presence of empty spots and repetitions, the number of variables was reduced to 22,413. One non-tumor object with the experimental ID number 15,019 was excluded from further analysis. Originally, this sample has twice as many spots (variables), as the remaining microarrays. All zero values were replaced by a minimal value of the signals of these variables, for the objects belonging to the same classes. For each spot, the fluorescence intensity ratio of the experimental to the reference signal was computed (Cy5/Cy3). To produce a continuous spectrum of the values and treating the up- and down-regulated genes in a similar fashion [32], the logarithm base 2 transformation of the signal ratio, $\log_2$(Cy5/Cy3), was computed and normalized according to the above described procedure and used for further analysis.

The training set contains 100 samples (50 from each class), whereas the independent test set contains 32 and 24 objects from class one and class two, respectively.

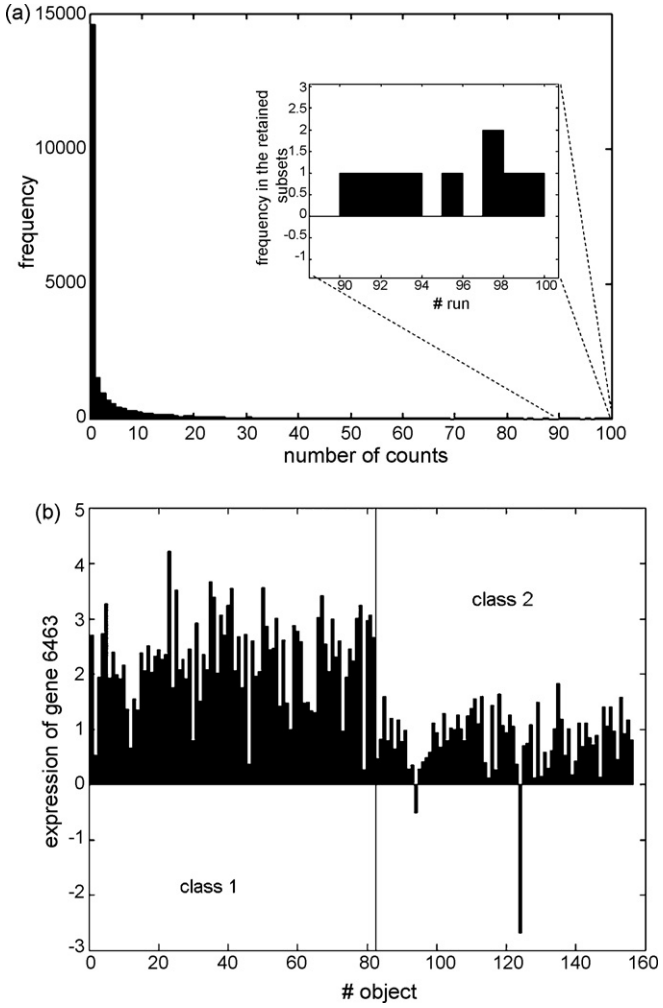

Fig. 4. Data set 1: (a) histogram of the vector $(1 \times m)$, elements thereof representing how many times the individual variables appeared in 100 selected subsets and (b) illustration of the discrimination power of gene 6463.

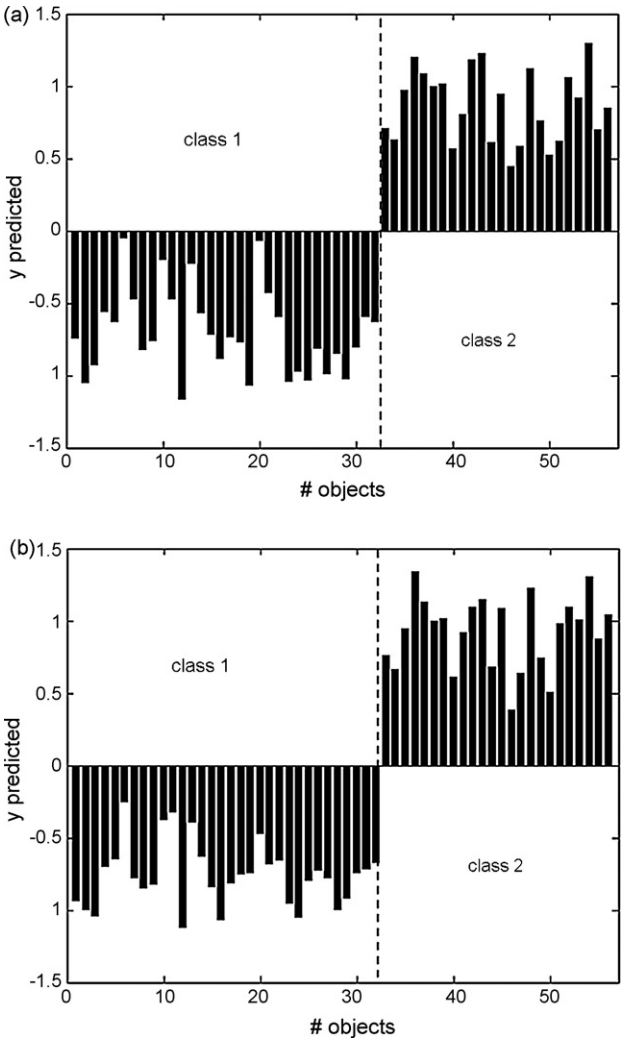

Fig. 5. Data set 1—y predicted by the PLS models: (a) before and (b) after feature selection.

3.2. Data set 2

The original data set [33] contains gene expression of 120 samples (microarrays), where 60 and 60 samples correspond,

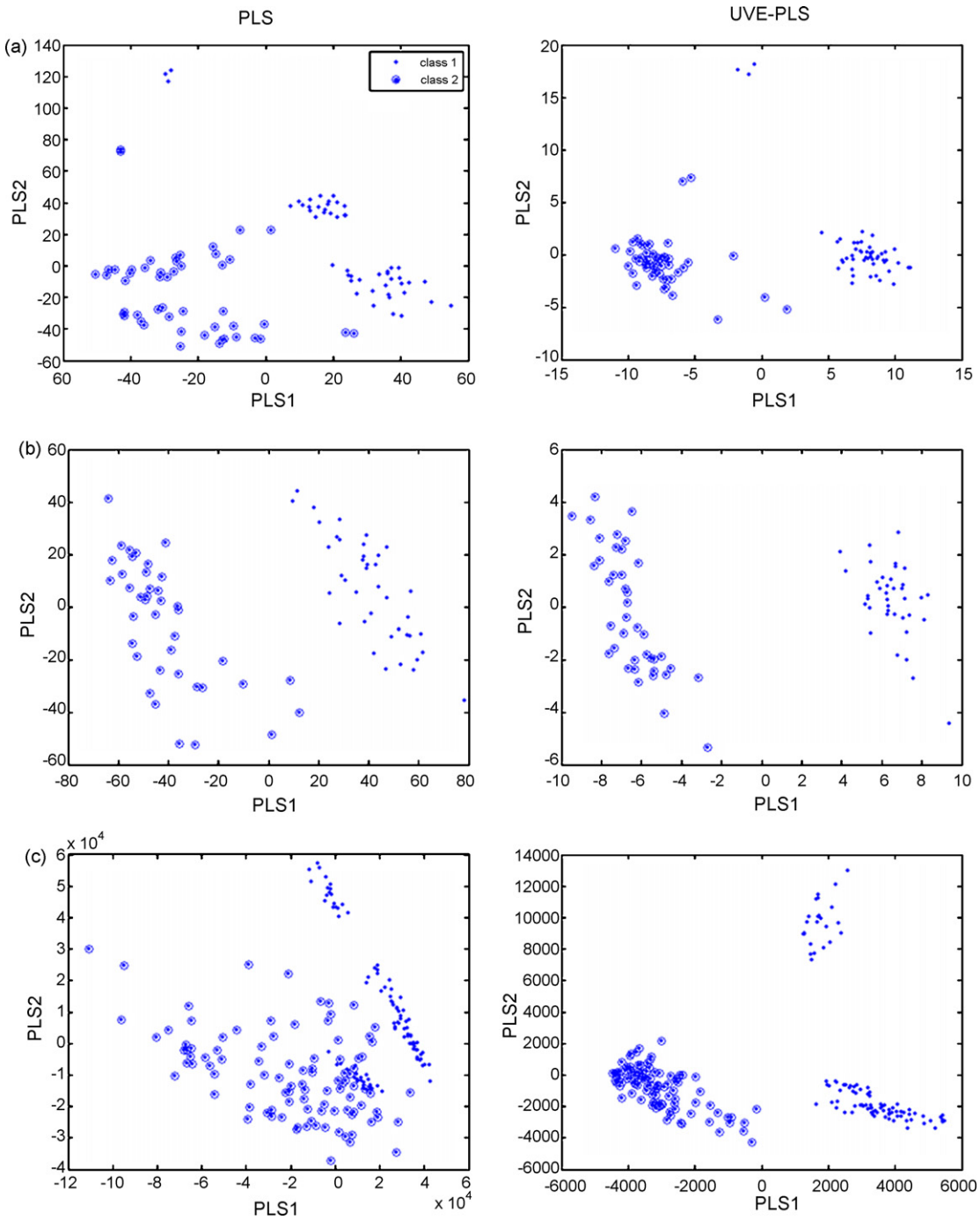

Fig. 6. Data sets 1–3: score plots of the PLS and the UVE-PLS models on the planes defined by the first two factors.

respectively, to the treated and the non-treated (with the adjuvant tamoxifen monotherapy) breast tumor cells. For each object, 22,575 variables were measured. All the data are available in the GEO database [34] with the accession numbers GSE1378 and GSE1379. In our study, the original fluorescence intensity ratios of the experimental Cy5 to the reference Cy3 signals were logarithmically transformed $\log_2$(Cy5/Cy3) and normalized by the above described method.

The training set contains 80 samples (40 from each of the two classes), whereas in the test set there are 40 objects (20 from each class).

3.3. Data set 3

The original data set [35] contains gene expression of 336 samples, corresponding to the normal B cells, B primary tumors cells, and the experimentally manipulated B cells. In our study, 186 primary tumor samples and 125 experimentally manipulated cells were used to the further analysis. For each of them, 12,600 variables were measured in accordance with the protocol recommended by Affymetrix. The gene expression values were determined and normalized by the Affymetrix Microarray Suite 5.0 software, using the Global Scaling option [35]. Data set is

Table 1
The results of the discriminant PLS (D-PLS) for the data sets studied

Data set	Complexity	RMS	RMSECV	RMStest
Data set 1	5	0.2539 (0)	0.3970 (2)	0.3575 (0)
Data set 2	4	0.1121 (0)	0.2922 (1)	0.2769 (0)
Data set 3	8	0.1161 (0)	0.2218 (1)	0.1789 (0)

The numbers of the misclassified objects are given in parenthesis.

available at the GEO database [34], with the accession number GSE2350.

The data set studied was divided into the test set and the training set, containing 200 (100 from each class) and 111 (86 from class 1 and 25 from class 2) samples, respectively.

4. Results and discussion

The main aim of our study is to construct stable classification models, which allow proper assignment of the new sample to the healthy or the diseased class, based on its genes expression. Additionally, we would like to focus on the different aspects of the feature selection, to gain certain insight into co-expression of genes, and possibly to find the minimal subsets of genes, necessary for medical diagnostics.

In the arsenal of classification methods there are many very efficient tools, but the choice of a classifier is always data-dependent (i.e., determined by the data dimensionality and the problem complexity). As the genomic data sets are highly dimensional and contain more irrelevant than relevant variables, many classifiers can work properly only after a feature pre-selection. Among the known classifiers there are, however, the methods well suited for this type of the data such as, e.g., PLS. PLS does not require feature pre-selection, so that the doubtful univariate features ranking can be avoided.

Just to remind the reader how inefficient the univariate approaches can be, let us have a look of Fig. 2, where the distribution of the objects from the two-dimensional data set is visualized. As illustrated in Fig. 2, even if the individual variables, **x1** and **x2**, have no discrimination power, their linear combination can lead to very effective classification of the considered two-dimensional data set.

Moreover, the multivariate feature selection can easily be embedded into the PLS classifier, so that the subset of the variables, significant for the classification purpose, can be found. This subset will contain the correlated, i.e., co-expressed, genes and can furnish a good starting point for estimation of the minimal subset of genes, necessary for medical diagnostics.

4.1. PLS models

The results of classification of the data sets studied, expressed as the root mean square errors describing the model fit (RMS) and its predictive power (RMSECV and RMStest) are summarized in Table 1.

Let us have a closer look of the classification model constructed for data set 1. Plots of the percentage of the explained variance in **X** and **y** versus the number of factors (see Fig. 3) reveal that a very small fraction of the **X** data only is significant for the classification purpose. The same observation remains valid for the remaining data sets also.

Table 2
Data set 1: the mean value of the cut-off, its standard deviation and the number of the retained variables calculated, based on 100 runs of UVE-PLS with the different subsets of the random variables

b_w-α-	Cut-off ± std (cut-off)	Number of retained variables
100	14.52 ± 2.09	480 ± 222
99	9.81 ± 0.51	1657 ± 232
95	7.24 ± 0.25	3587 ± 276

Table 3
The results of UVE-PLS for the studied data sets

Data set	Complexity	Features[a]	RMS[b]	RMSECV[b]	RMStest[b]
Data set 1	4	186 (50%)	0.1578 (0)	0.2407(0)	0.2952 (0)
Data set 2	2	131 (100%)	0.1332 (0)	0.1529 (0)	0.2139 (0)
Data set 3	5	132 (95%)	0.1460 (0)	0.1670 (0)	0.1789 (0)

[a] The percent of the frequency of appearance of the same variables taken to build the model.
[b] The number of the misclassified objects.

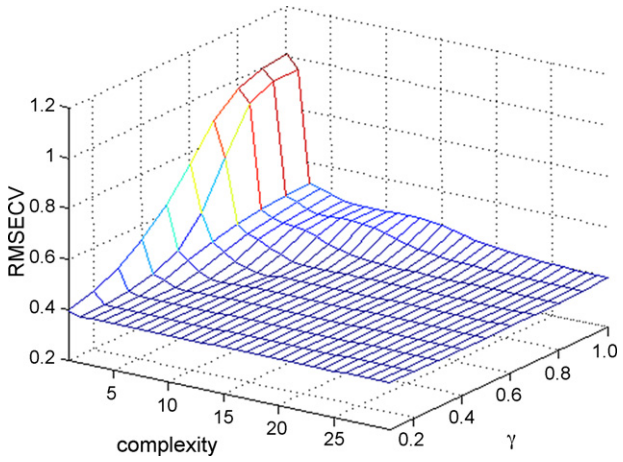

Fig. 7. Data set 1: RMSECV as a function of γ parameter and the model complexity.

4.2. UVE-PLS models

The approach proposed by Centner et al. [14] allows the multivariate feature selection and it seems of particular interest with the classification of the genomic data sets that contain more irrelevant than relevant features, for modeling of the class belongingness.

We faced, however, certain problems when applying UVE-PLS to the studied data set, and namely, due to small differences in the stability of the regression coefficients, a small change in the cut-

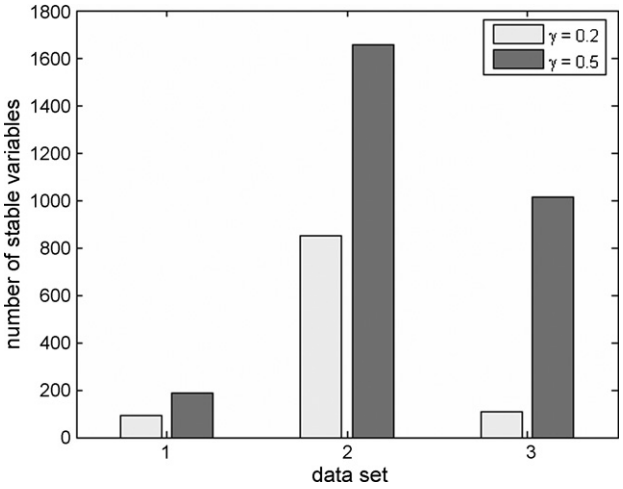

Fig. 8. Data sets 1–3: the numbers of stable features selected in UVE-CPR for $\gamma = 0.2$ and $\gamma = 0.5$.

off value results in a significantly different number of the retained variables (see Table 2).

The cut-off value is determined by stability of the random variables, added to the experimental data, and it varies from one run to another. Of course, the variations are most significant for b_w-α-100, and smaller for b_w-α-99 and b_w-α-95. However, the lower the α, the lower is also the number of the eliminated, insignificant variables. To stabilize the whole procedure, we decided to re-run it 100 times, in each run augmenting the experimental data with the new noise variables, and within each run, feature elimination was repeated with b_w-α-95, till the regression coefficients of all the retained variables became stable.

For the construction of the final model, features were selected, based on the frequency of their presence in the retained subsets. For an illustrative purpose, the histogram of the variables selected from all Monte Carlo (MC) runs and obtained for data set 1 is presented in Fig. 4a.

For this data set, the majority of the variables (14,603 variables) were never selected as stable ones and hence, they can be eliminated from the further studies. In the retained set of variables, there is only one variable (gene no. 6463) that appears in each subset of the retained features. Its discrimination power is illustrated in Fig. 4b.

The PLS model constructed for these variables, which at least once appear in the subsets of the retained variables has the predictive power similar to the initial PLS model with all the variables. When the number of the variables is limited to those selected more than 50 times (186 variables for data set 1), the model and its predictive power are improved and all the objects are classified properly (see Fig. 5 and Table 3).

The two classes of objects are already well separated on the plane defined by the first two PLS scores (see Fig. 6a), and the two subsets of the variables responsible for this discrimination can be identified, based on the corresponding loading plot.

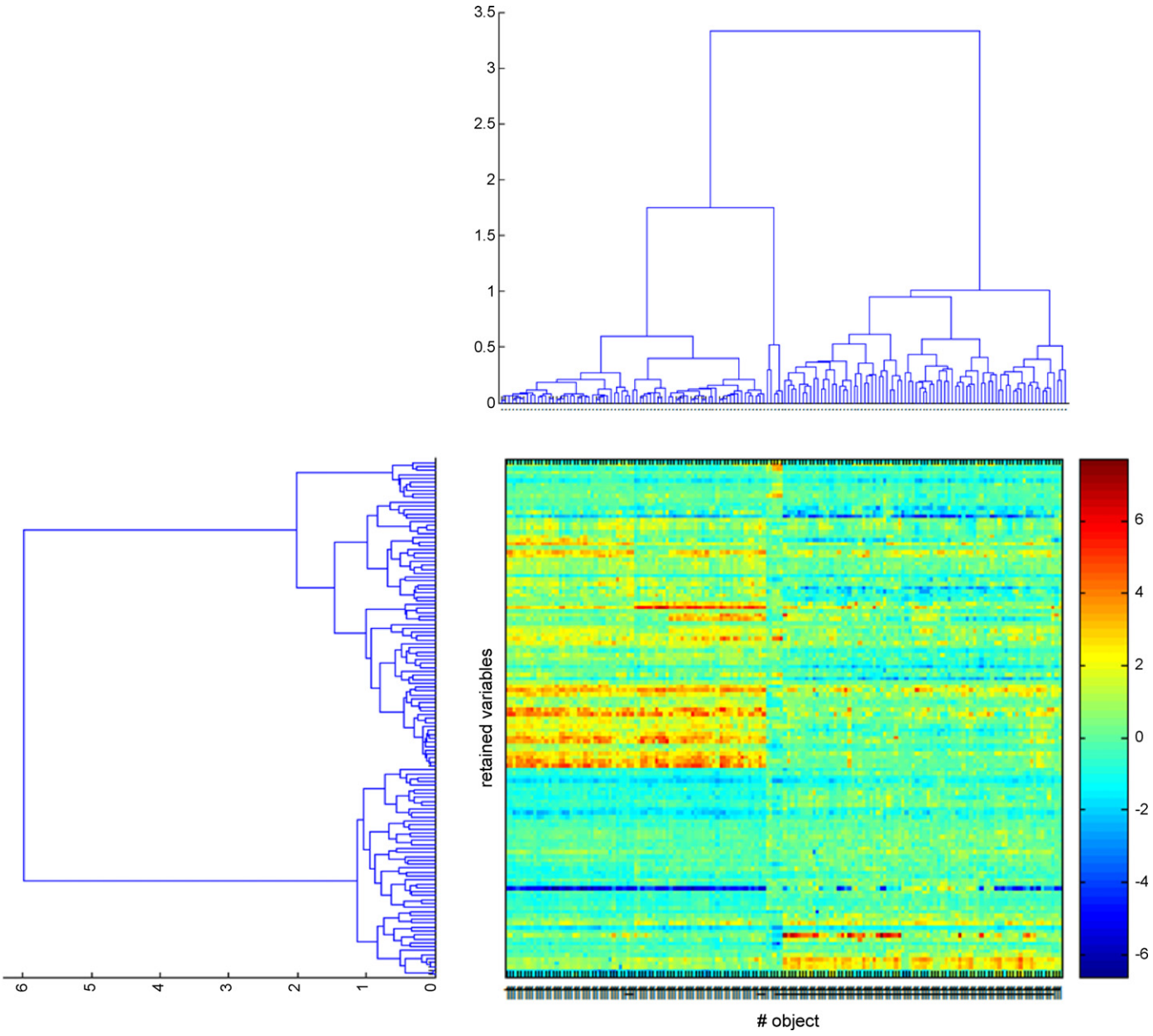

Fig. 9. Data set 1: dendrogram (based on correlation) of objects and variables, determined as stable in the UVE-PLS model, and the corresponding color map of the data.

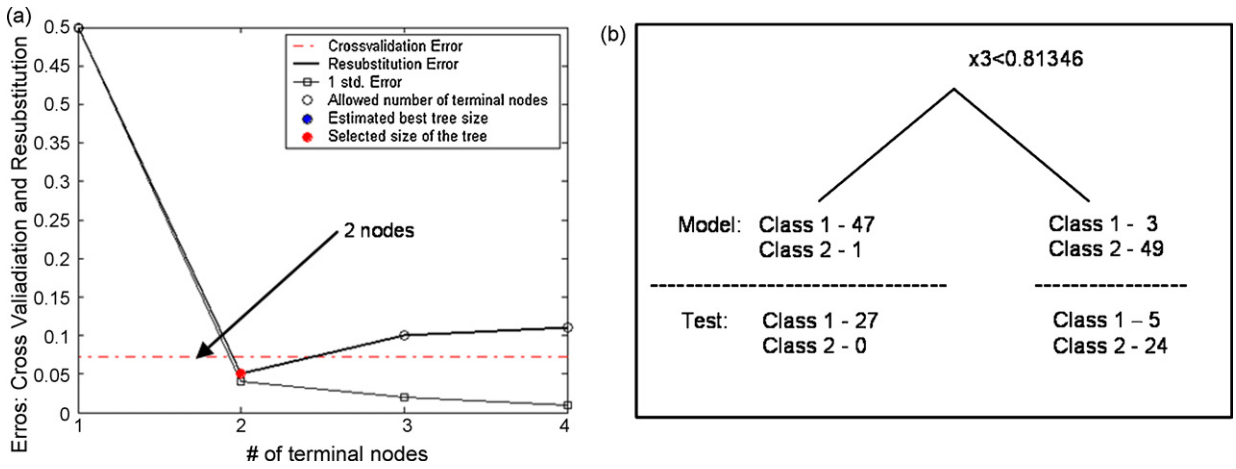

Fig. 10. Data set 1—the results of CART: (a) RMSCV versus the number of the terminal nodes and (b) the constructed optimal tree.

An improvement of the model performance (i.e., of its predictive power) after elimination of the irrelevant variables is observed also for data set 2 (see Table 3 and Fig. 6b). For this data set, there are 131 stable variables, which appear in all the selected subsets of stable variables.

For data set 3, the UVE-PLS model has lower complexity than the PLS model, but its predictive power is not improved.

4.3. Uninformative variable elimination-continuum power regression (CPR)

To demonstrate, how the subset of the relevant genes depends on the applied classifier, the procedure of feature elimination was embedded into CPR, in which the objective function can vary continuously.

As presented in Fig. 7, RMSECV reaches similar values for all the CPR models (10 models with $\gamma = 0.1, 0.2, \ldots, 1$), but these models significantly differ in their complexity. The higher the value of γ, the more complex is the model.

When the procedure of the uninformative variable elimination is implemented into the CPR scheme, different subsets of stable variables are retained in the consecutive models. They significantly differ in the number of the retained features. For the sake of example, the number of the variables, which appear in the subsets of stable features more than 50 times, are presented for the studied data sets in Fig. 8. For data set 1, the subset of the significant variables for the model with $\gamma = 0.2$ contains 93 variables only, whereas the subset selected for the model with $\gamma = 0.5$, contains 186 variables (65 variables are in the both subsets). The highest difference is observed for data set 3. For this data set there are almost 10 times less variables in the model with $\gamma = 0.2$ than in the model with $\gamma = 0.5$ (107 and 1011 variables, respectively, and 95 are observed in the both subsets).

All subsets of the retained variables are highly redundant and can be considered as the subsets of co-expressed genes, selected according to the objective function of the classifier.

4.4. Selection of a minimal subset of variables for medical diagnostics

Let us again focus on data set 1. As presented in Fig. 9, the set of the retained variables that are stable in the UVE-PLS model, contains correlated genes. They form two subgroups: one subgroup contains genes with higher expression for the objects from class 1 than those from class 2, whereas the genes in the second subgroup reveal lower expression for class 1 than for class 2.

Further reduction of the number of features can be performed in many ways. In our study, the following approaches were considered: classification and regression trees (CART) [20], stepwise multiple linear regression (stepwise MLR) [21], and genetic algorithms MLR (GA-MLR) [23,36].

CART is one of the most popular methods for classification of the genomic data and feature selection is embedded in it. When applied to the data sets studied, it does not perform very well though. Based on the CV procedure, the trees with two nodes were constructed for data sets 1–3 (the results for data set 1 are presented in Fig. 10).

As shown in Fig. 10b, variable no. 3 was selected as the most discriminant one, and all samples with **x3** lower than 0.813 form one subgroup, whereas those with **x3** higher than 0.813, form the second subgroup of similar objects. Among the samples from the model set there are 47 samples from class 1 and 1 sample (sample no. 1) from class 2. In the same subgroup there are 27 samples from the test set, belonging to class 1. In the second subgroup there are 3 samples from class 1 and 49 samples from class 2 for the model set, and 5 samples from class 1 and 24 samples from class 2 for the test set. Percentage of the correctly classified objects from the test sets equals to 91, 90 and 85.6% for data sets 1–3, respectively.

Stepwise MLR and genetic algorithm MLR allow further reduction of variables, without deterioration of the models. For data set 1, the stepwise approach, applied to the subset of 186 variables, selects 23 of them as significant (the significance level equals

Table 4
The minimal subsets of the variables found according to GA-MLR, ccr—the correct classification rate

Data set	Selected features	ccr (test)
Data set 1	5327, 18,364, 1434, 11,714, 10,259, 18,124, 3810, 14,364, 3045, 13,899, 5169, 16,872, 3810, 14,364, 3045, 13,899, 5169, 16,872, 19,270, 21,952, 5509, 1951, 15,908	100%
Data set 2	17,861, 17,946, 2453, 5727, 18,653, 14,872, 511, 22,317, 17,321, 8395, 10,817, 3556, 9072	100%
Data set 3	10,463, 6858, 8013, 7128, 11,143, 273, 9357, 6618, 8331, 11,651, 8527, 10,203, 9178	100%

to 0.5%) for the MLR model. The best subset of 23 variables can also be selected, basing on the genetic algorithm (see Fig. 11). These subsets are, however, completely different. Although there are only two common variables (variables nos. 26 and 86, corresponding to the genes 22,403 and 22,134, respectively) in these two subsets, their predictive power is mutually comparable (see Fig. 12).

For all the data sets studied it was possible to find different minimal subsets of variables with a comparable predictive power. For data sets 2 and 3, the minimal subsets, leading to 100% correct classification rate (ccr), contain 13 variables each. Examples of the minimal subsets of variables are presented in Table 4. These subsets can be used for classification, but interpretation of the selected variables (genes) must be cautious. They can be considered as representatives of the groups of co-expressed genes only.

Summing up, due to high redundancy (correlation) of the genomic data, in the cases when individual genes with a high discrimination power are lacking, many subsets of genes can be found as valid for classification (diagnostics). The methods were also applied to a GlaxoSmithKline dataset and the similar conclusion was obtained although the results are not published here due to confidential reason.

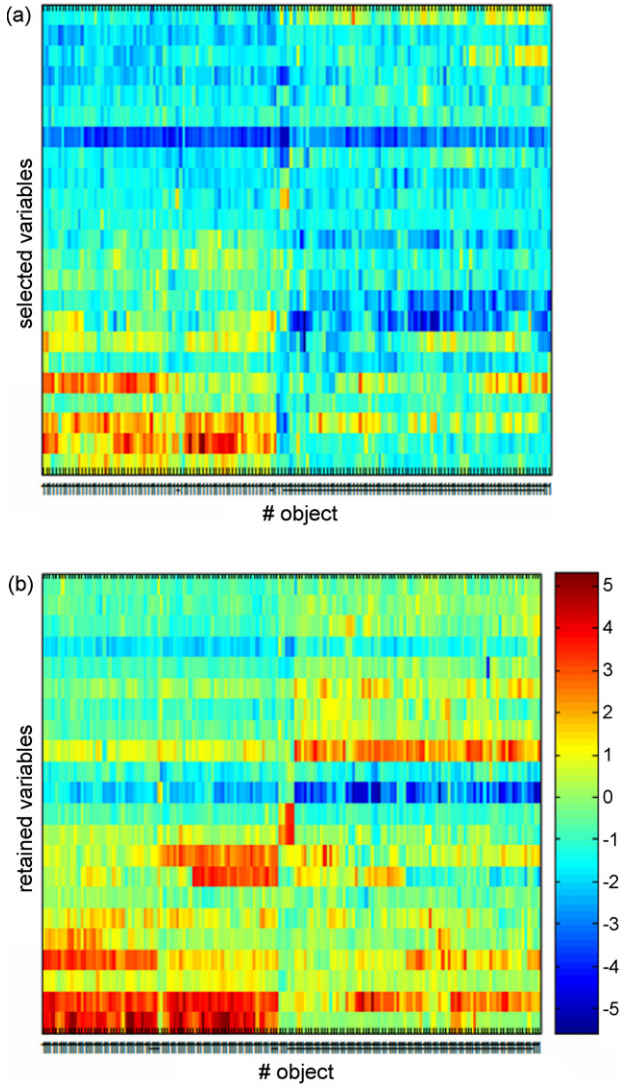

Fig. 11. Data set 1—expression of the selected 23 genes (out of 186 genes) based on (a) the stepwise MLR and (b) GA-MLR.

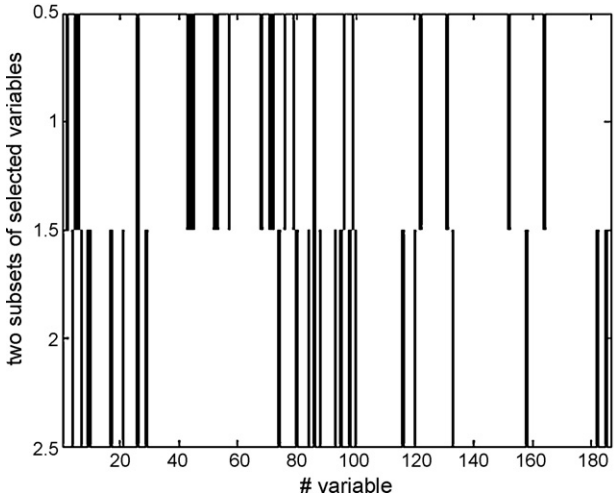

Fig. 12. Data set 1—RMStest for the MLR models based on the 23 variables, selected by (a) the stepwise MLR and (b) GA-MLR.

5. Conclusions

The genomic data sets contain highly correlated variables, many of them being irrelevant for the classification purpose. Although the feature selection methods can identify these irrelevant variables, it ought to be stressed that the term relevant (or irrelevant) has a meaning only in the context of the objective function of the applied classifier. As demonstrated in our study, the selected subsets of significant genes can vary in cardinality, and due to the redundancy (correlation) of genes, it is possible to select different minimal subsets of genes, necessary for classification. Although these subsets can be efficiently used for this purpose, their interpretation ought to be cautiously made.

Acknowledgements

Richard J. Stephens and Chris L. Clayton are acknowledged for presenting such challenging problem and also providing one test dataset. Mike Lutz is acknowledged for his useful comments.

References

[1] M.B. Eisen, P.O. Brown, Method Enzymol. 303 (1999) 179–205.
[2] D.P. Berrar, W. Dubitzky, M. Granzow, Practical Approach to Microarray Data Analysis, Kluwer, New York, USA, 2003, pp. 306–325.
[3] R.L. Steras, T. Martinsky, M. Schena, Nat. Med. 9 (2003) 140–145.
[4] D.K. Slonim, Nat. Genet. 32 (2002) 502–508.
[5] C. Yoo, V. Thorsson, G.F. Cooper, Discovery of causal relationships in a gene regulation pathway from a mixture of experimental and observational DNA microarray data, in: Proceedings of the Pacific Symposium on Biocomputing, Lihue, Hawaii, USA, 2002, pp. 498–509.
[6] B. Walsh, D. Henderson, J. Anim. Sci. 82 (2004) E292–E299, E Supplement.
[7] M.B. Eisen, P.T. Spellman, P.O. Brown, D. Botstein, Proc. Natl. Acad. Sci. 95 (1998) 14863–14868.
[8] I. Guyon, A. Elisseeff, J. Mach. Learn. Res. 3 (2003) 1157–1182.
[9] G. Stolovitzky, in: T.S. Deisboeck, J.Y. Kresh (Eds.), Complex Systems Science in BioMedicine, Springer-Verlag, USA, 2006, pp. 679–699.
[10] A.Y. Kim, J.W. Lee, I.S. Sohn, Stat. Methods Med. Res. 15 (2006) 3–20.
[11] L. Joos, E. Eryüksel, M.H. Brutsche, Swiss Med. Weekly 133 (2003) 31–38.
[12] C.A. Afshari, Endocrinology 143 (2002) 1983–1989.
[13] T.K. Jenssen, W.P. Kuo, T. Stokke, E. Hovig, Hum. Genet. 111 (2002) 411–420.
[14] V. Centner, D.L. Massart, O.E. de Noord, S. de Jong, B. Vandeginste, C. Sterna, Anal. Chem. 68 (1996) 3851–3858.
[15] R. Leardi, in: J. Devillers (Ed.), Genetic Algorithms in Molecular Modeling, Academic Press, 1996, p. 67.
[16] M. Stone, R.J. Brooks, J. Roy. Stat. Soc. B52 (1990) 237–269.
[17] S. de Jong, B.M. Wise, N.L. Ricker, J. Chemometr. 15 (2001) 85–100.
[18] S. Serneels, P. Filzmoser, C. Croux, P.J. Van Espen, Chemometr. Intell. Lab. Syst. 76 (2005) 197–204.
[19] Q.-S. Xu, Y.-Z. Liang, Chemometr. Intel. Lab. Syst. 56 (2001) 1–11.

[20] L. Breiman, J.H. Friedman, R.A. Olshen, C.J. Stone, Classification and Regression Trees, Wadsworth, Monterey, 1984.
[21] D.L. Massart, B.G.M. Vandeginste, L.M.C. Buydens, S. De Jong, P.J. Lewi, J. Smeyers-Verbeke, Handbook of Chemometrics and Qualimetrics, Part A, Elsevier, Amsterdam, 1997.
[22] D.E. Goldberg, Genetic Algorithms in Search, Optimisation and Machine Learning, Addison-Wesley, Massachusetts, 1989.
[23] R. Leardi, J. Chemometr. 8 (1994) 65–79.
[24] X. Cui, M.K. Kerr, G.A. Churchill, Stat. Appl. Genet. Mol. Biol. 2 (2003), Article 4.
[25] J. Quackenbush, Nat. Rev. Genet. 2 (2001) 418–427.
[26] W.S. Cleveland, LOWESS: a program for smoothing scatterplots by robust locally weighted regression, Am. Stat. (1981) 35–54.
[27] W.S. Cleveland, E. Grosse, W.M. Shyu, Local regression models, in: J.M. Chambers, T.J. Hastie (Eds.), Statistical Models in S, Wadsworth & Brooks/Cole, 1992 (Chapter 8).
[28] P.H.C. Eilers, Fast Computation of Trends in Scatterplots, vol. 71, Kwantitatieve Methoden, 2004, 38–45.
[29] P.H.C. Eilers, B.D. Marx, Stat. Sci. 11 (1996) 89–121.
[30] R.W. Kennard, L.A. Stone, Technometrics 11 (1969) 137–148.
[31] http://genome-www5.stanford.edu/cgi-bin/publication/viewPublication.pl?pub_no=107, Stanford Microarray Database (SMD), accessed January 25, 2008.
[32] J. Quackenbush, Nat. Genet. 32 (2002) 496–501.
[33] X.J. Ma, Z. Wang, P.D. Ryan, S.J. Isakoff, A. Barmettler, A. Fuller, B. Muir, G. Mohapatra, R. Salunga, J.T. Tuggle, Y. Tran, D. Tran, A. Tassin, P. Amon, W. Wang, W. Wang, E. Enright, K. Stecker, E. Estepa-Sabal, B. Smith, J. Younger, U. Balis, J. Michaelson, A. Bhan, K. Habin, T.M. Baer, J. Brugge, D.A. Haber, M.G. Erlander, D.C. Sgroi, Cancer Cell 5 (2004) 607–616.
[34] http://www.ncbi.nlm.nih.gov/geo/, NCBI. Gene Expression Omnibus (GEO), accessed January 25, 2008.
[35] K. Basso, A.A. Margolin, G. Stolovitzky, U. Klein, R. Della-Favera, A. Califano, Nat. Genet. 37 (2005) 382–390.
[36] R. Leardi, R. Boggia, M. Terrile, J. Chemometr. 6 (1992) 267–281.

Talanta 76 (2008) 580–590

Contents lists available at ScienceDirect

Talanta

journal homepage: www.elsevier.com/locate/talanta

First interlaboratory exercise on non-steroidal anti-inflammatory drugs analysis in environmental samples

M. Farré[a], M. Petrovic[a,b], M. Gros[a], T. Kosjek[c], E. Martinez[a], E. Heath[c], P. Osvald[d], R. Loos[e], K. Le Menach[f], H. Budzinski[f], F. De Alencastro[g], J. Müller[h], T. Knepper[h], G. Fink[i], T.A. Ternes[i], E. Zuccato[j], P. Kormali[k], O. Gans[l], R. Rodil[m], J.B. Quintana[m], F. Pastori[n], A. Gentili[n], D. Barceló[a,*]

[a] *Department of Environmental Chemistry, IIQAB-CSIC, C/Jordi Girona 18-26, 08034 Barcelona, Spain*
[b] *Institucio Catalana de Recerca i Estudis Avanzats (ICREA), Barcelona, Spain*
[c] *Jozef Stefan Institute, Ljubljana, Slovenia*
[d] *Environmental Institute, Kos, Slovak Republic*
[e] *Institute for Environment and Sustainability, JRC, Ispra, Italy*
[f] *CNRS, LPTC, Université Bordeaux 1, Talence, France*
[g] *ENAC-ISTE-Central Environmental Laboratory EPF Lausanne, Switzerland*
[h] *Europa Fachhochschule Fresenius, University of Applied Science, Idstein, Germany*
[i] *Federal Institute of Hydrology (BFG), Koblenz, Germany*
[j] *Mario Negri Institute for Pharmacological Research, Milan, Italy*
[k] *Pesticide Residues Laboratory, General Chemical State Laboratory, Athens, Greece*
[l] *Umweltbundesamt GmbH, Abt. Umweltwirksame Stoffe und Metaboliten, Wien, Austria*
[m] *IUMA, University Institute of Environment University of A Coruña, A Coruña Spain*
[n] *Universita "La Sapienza" di Roma, Italy*

ARTICLE INFO

Article history:
Received 10 August 2007
Received in revised form 25 March 2008
Accepted 28 March 2008
Available online 16 April 2008

Keywords:
Non-steroidal anti-inflammatory drugs (NSAIDs)
Ketoprofen
Naproxen
Ibuprofen
Diclofenac
LC–MS/MS
GC–MS
Wastewater
River water
Interlaboratory

ABSTRACT

Comparability of monitoring data are essential for any meaningful assessment and for the management of environmental risks of emerging pollutants. The reliability and comparability of data at European level is often limited, because analytical methods for emerging pollutants are often not fully validated, not harmonized or not suitable for all relevant matrices.

This paper describes a collaborative interlaboratory exercise for the analysis of non-steroidal anti-inflammatory drugs (NSAIDs) residues in freshwater and wastewater, held in the framework of the EU project "Network of reference laboratories for monitoring of emerging environmental pollutants" (NORMAN). The NSAID compounds selected in this study were ketoprofen, naproxen, ibuprofen and diclofenac.

Thirteen laboratories distributed along nine European Countries (Austria, France, Germany, Greece, Italy, Slovak Republic, Slovenia, Spain, and Switzerland) took part in this exercise, 126 samples were analyzed and a total number of 473 values in duplicate were collected.

Samples selected in this study include environmental water (river water and waste water) and artificial water (fortified environmental and distilled water) with different ranges of complexity.

Two analytical methods were proposed by the organiser; one is based on the use of solid phase extraction (SPE) followed by liquid chromatography–tandem mass spectrometry (LC–MS/MS) and the second one is based on SPE followed by gas-chromatography–mass spectrometry (GC–MS), however, in the first round some different approaches were also admitted.

The main goals of this interlaboratory comparison were to evaluate the available analytical schemes for NSAID analysis in natural waters, to evaluate the repeatability (r) and reproducibility (R) between participating laboratories, and to evaluate the influence of the analytical method and sample matrices on the results.

1. Introduction

Human and veterinary pharmaceutical compounds are a source of increasing environmental concern as they are used in large quantities and their physical and chemical properties make them likely

* Corresponding author. Tel.: +34 93 400 61 00; fax: +34 93 204 59 04.
E-mail address: dbcqam@cid.csic.es (D. Barceló).

0039-9140/$ – see front matter © 2008 Elsevier B.V. All rights reserved.
doi:10.1016/j.talanta.2008.03.055

to be transported into hydrologic systems, where their effects on human health and aquatic ecosystems are mostly unknown.

Pharmaceuticals are in general, after intake and absorption into humans or animal blood system, a subject of metabolic degradation processes. However, significant fractions of the original substances are excreted in un-metabolized form or as active metabolites via urine or faeces to be emitted into raw sewage, which may or may not be treated [1,2]. Yet, some pharmaceuticals are not degraded in waste treatment plants and enter the environment in their original form [3,4]. In addition to metabolic excretion, disposal by flushing of unused or expired medication and drug-containing waste from manufacturing facilities can also contribute to environmental contamination [2]. Flushing unused medicines down the drain appears to be of minor importance, while patient excretion following therapy is widely considered to be the primary pathway to the environment [5]. Even posthumously, the drugs administered in the closing phases of our lives likely leach into cemeteries and groundwater [6].

Different studies carried out in Europe [7,8], Canada [9], and USA [10] during the last decade show that one of the most common group of pharmaceuticals found in wastewater, river water and even in drinking water are non-steroidal anti-inflammatory drugs (NSAIDs) representatives, because they are commonly used in treatment of mild to moderate pain, and chronically in treatment of rheumatic diseases. Moreover, some of them are available as non-prescription pharmaceuticals. A number of reservoirs tapped for drinking water have been monitored along the Lergue River in Southern France, where pharmaceuticals and other wastewater-related dominant contaminants such as paracetamol, diclofenac, and carbamazepine were found [11]. Other examples have been reported; Zuccato et al. reported the presence of clofibric acid and diazepam in treated drinking water [3], in Italy; Heberer et al. [12] have reported the presence of diclofenac in the drinking water of Berlin; Loraine and Pettigrove identified and quantified ibuprofen (0.93 μg/L) and ibuprofen methyl ester (4.95 μg/L) in treated water [13].

Due to that, several methods have been developed for the determination of NSAIDs and their metabolites in water in the lower ng/L range using solid phase extraction (SPE) coupled to gas chromatography–mass spectrometry (GC–MS) based methods [14]. However, due to the elevated polarity and acidic nature of NSAIDs, with pK_a values between 4 and 4.5, liquid chromatography–mass spectrometry (LC–MS) and LC–tandem MS have experienced an impressive progress during the last years, both in terms of technology development and application, avoiding the derivatization step required by GC–MS methods. Recently, both groups of analytical techniques, i.e. LC–MS/MS and GC–MS have been used for the trace analysis of acidic drugs in environmental samples [15].

However, there is need for harmonization and validation of analytical methods for NSAID residue analysis. According to new EU recommendations, validation of analytical methods should be conducted in step-by-step processes with different levels of verification, and the achievements in each step should be evaluated by interlaboratory studies. In the present work, we performed the first level of verification, and the quality of the existing methods of analysis was evaluated, and a selection of more suitable methods to be validated in a second step was carried out. In this sense, this interlaboratory study was organised by the Environmental Chemistry Department, IIQAB-CSIC in Barcelona (Spain) under the frame of NORMAN EU project. The study was performed using either LC–MS/MS or GC/MS, both of which employed SPE as purification and concentration step.

During the exercise, three series of three samples each were analyzed. Every batch of samples consisted of three natural wastewater samples, three fortified river samples and three fortified deionised water samples. In total, every laboratory received nine samples for analysis. The samples were prepared by the Environmental Chemistry Department, IIQAB-CSIC in Barcelona, Spain.

In this round, 14 participations were carried out in 13 laboratories in Austria, France, Germany, Greece, Italy, Slovak Republic, Slovenia, Spain, and Switzerland.

The main goals of this study were to compare the results using different analytical methods, to evaluate the quality of individual approaches, to evaluate the accuracy and quality parameters in different aqueous matrices and to assess variations between different approaches (LC–MS/MS, GC/MS) and different laboratories.

2. Experimental

2.1. Experimental design, sample collection and handling

A total number of 126 samples corresponding to 14 participations were distributed in 13 laboratories (one laboratory participate twice, a LC–MS/MS based method and also using a method based on GC/MS). Three series of samples were analyzed in three batches, and every batch was composed by an effluent sample of a wastewater treatment plant (WWTP), a fortified Ebro river water and a fortified deionised water. Table 1 shows sample codification. The environmental samples were selected according to their expected NSAID concentration and matrix complexity, and a wastewater effluent sample from a WWTP near Barcelona (Spain) fitted well these criteria. Ebro river samples were collected near the area of Amposta (Barcelona, Spain). In all cases, samples were collected in Pyrex borosilicate glass containers, previously rinsed with tap and high-purity water. The samples were transported at 4 °C to the laboratory in Barcelona. In order to minimize the sources of variation, all samples were collected, transported, homogenised and prepared at the same time in a central laboratory (Environmental Chemistry Department, IIQAB-CSIC, Barcelona).

After sampling, the water samples were filtered through 2.7 and 0.45 μm glass micro-fibre filters to remove suspended matter and homogenised in a polyethylene bucket. The samples were transported refrigerated, and each participant received approximately 1.1 L of each sample. Participants were requested to measure and note the temperature of each sample at reception, in order to check that all samples were received in similar conditions for all participants. Then, all laboratories were requested to keep the samples under freezing conditions until the extraction of each batch. Water samples were allowed to reach room temperature and were spiked with surrogate standard. Samples were then extracted and analyzed during the same dates by the participants and the total duration of the exercise was 4 months.

In order to maintain the anonymous character of all participants, an identification number was provided to every laboratory. This number was requested to be used later for the presentation of results.

Table 1
Sample codes table

Batch 1	A1 (fortified river water)	B1 (wastewater)	C1 (fortified MilliQ water)
Batch 2	A2 (wastewater)	B2 (fortified MilliQ water)	C2 (fortified river water)
Batch 3	A3 (fortified MilliQ water)	B3 (fortified river water)	C3 (wastewater)

Table 2
List of participants in alphabetical order and the main characteristics of the analytical methods involved in the exercise

Participant	Pre-treatment	Extraction	Extract reconstitution	Chromatography	Column	Derivatization	Reference
CNRS, LPTC, Université Bordeaux 1,Talence, France	Neutral pH	Oasis HLB (60 mg, 3 mL), Waters	Ethyl acetate	GC–MS	Capillary column 30 m, 0.25 μm film thickness	MTBSTFA (MSTFA)	[23]
Environmental Institute, Kos, Slovak Republic	Neutral pH	Oasis HLB (60 mg, 3 mL), Waters	Ethyl acetate	GC–MS	Capillary column 30 m, 0.25 μm film thickness	MTBSTFA (MSTFA)	[22]
EPF Lausanne, Switzerland	Acidification pH 2	ENVI-18 reverse phase	Toluene	GC–MS	RTX-capillary column 60 m, 0.25 μm film thickness	Pentafluorobenzyl bromide	[18]
Europa Fachhochschule Fresenius, University of Applied Science, Idstein, Germany	Acidification pH 2	Oasis MCX 3cc (60 mg), Waters	Hexane	GC–MS	Capillary column 30 m, 0.25 μm film thickness	Diazomethane	[18]
Federal Institute of Hydrology (BFG), Koblenz, Germany	Acidification pH 2	Oasis MCX 3cc (60 mg), Waters	100 μg methanol + 400 μg water, 0.1 M formic acid	LC-ESI (−) MS/MS	Zorbax Eclipse XDB-C8	–	[19]
General Chemical State Laboratory (Athens, Greece)	Acidification pH 3	SPE Oasis HLB 6cc, 200 mg, Waters	Water 0.3% formic acid	LC-ESI (+) MS/MS	Xterra® Waters	–	[20]
IIQAB-CSIC, Barcelona, Spain	Neutral pH	Oasis HLB (60 mg, 3 mL), Waters	Methanol:water (25:75, v/v)	LC-ESI (−) MS/MS	Purosphere Star RP-18 endcapped column	–	[7]
Institute for Environment and Sustainability, JRC, Ispra, Italy	Neutral pH	Oasis HLB (60 mg, 3 mL), Waters	Methanol:water (25:75, v/v)	LC-ESI (−) MS/MS	Purosphere Star RP-18 endcapped column	–	[7]
IUMA, University Institute of Environment University of A Coruña, Spain	Neutral pH	Oasis HLB (60 mg, 3 mL), Waters	Ethyl acetate	GC–MS	Capillary column 30 m, 0.25 μm film thickness	MTBSTFA	[21]
Jozef Stefan Institute, Ljubljana, Slovenia		Oasis HLB (60 mg, 3 mL), Waters	Ethyl acetate	GC–MS	Capillary column 30 m, 0.25 μm film thickness	MTBSTFA	[22]
Mario Negri Institute for Pharmacological Research, Milan, Italy	Acidification pH 3	Oasis MCX 3cc (60 mg), Waters	Methanol, 2% NH_4^+, 0.2% NaOH in methanol	LC-ESI (−) MS/MS	Zorbax Eclipse XDB-C8	–	[23]
Umweltbundesamt GmbH, Abt. Umweltwirksame Stoffe und Metaboliten, Wien, Austria	Neutral pH	Oasis HLB (60 mg, 3 mL), Waters	Methanol:water (25:75, v/v)	LC-ESI (−) MS/MS	Purosphere Star RP-18 endcapped column	–	[21]
Umweltbundesamt GmbH, Abt. Umweltwirksame Stoffe und Metaboliten, Wien, Austria	Acidification pH 2	Oasis HLB (60 mg, 3 mL), Waters	Ethyl acetate	GC–MS	Capillary column 30 m, 0.25 μm film thickness	MTBSTFA	[22]
Universita “La Sapienza” di Roma, Italy	Acidification pH 3	Oasis HLB (500 mg), Waters	Methanol:water (25:75, v/v)	LC-ESI (−) MS/MS	Alltima C18 (4.6 × 250 mm; 5 μm)	–	[24]

Table 3
Statistical values corrected after the outlier exclusion for each compound in the different types of water

Group	No. of accepted results	Mean	Standard deviation	Standard error of mean	Median	Minimum value	Maximum value	95% Confidence interval		No. of outliers
								From	To	
Ketoprofen										
Wastewater										
Batch 1	13	678.77	282.23	78.27	800.00	25	1090	508.21	849.33	0
Batch 2	12	601.08	235.24	67.91	620.95	112	897	451.61	750.54	1
Batch 3	13	642.55	303.61	84.21	662.00	144	1200	459.06	826.03	1
Fortified river water (fortification 290 ng/L)										
Batch 1	13	238.73	121.08	33.58	200	73	461	165.56	311.90	0
Batch 2	13	297.92	134.13	37.20	260	62	538	216.85	378.98	0
Batch 3	12	241.39	92.317	26.65	230	106.2	420	182.74	300.05	1
Fortified MilliQ water (fortification 83 ng/L)										
Batch 1	12	164.24	99.52	28.73	133.5	64	365	101	227.47	0
Batch 2	11	101.71	40.52	12.22	100.0	60	208.8	74.49	128.93	1
Batch 3	11	97.35	33.96	10.24	91.00	37	151	74.54	120.17	0
Naproxen										
Wastewater										
Batch 1	12	913.18	744.55	214.93	848.00	18	2140	440.11	1386.3	1
Batch 2	13	858.17	635.68	176.31	887.00	77	1790	474	1242.3	0
Batch 3	13	818.54	603.27	167.32	930.00	77	1800	153.95	1183.1	0
Fortified river water (fortification 1124 ng/L)										
Batch 1	13	1109.0	845.51	234.50	1430.0	53	24.37	598.01	1620	0
Batch 2	12	1088.9	746.59	215.52	1047.5	308	2446	614.51	15.63	1
Batch 3	13	1066.6	764.33	211.99	1230.0	53.5	2325	604.69	1528	0
Fortified MilliQ water (fortification 266 ng/L)										
Batch 1	11	174.32	96.214	29.010	200.00	51	330	109.68	238.95	2
Batch 2	12	158.83	96.254	27.786	165.00	33.5	327	97.68	219.99	1
Batch 3	12	201.96	106.87	30.850	225.00	24	369	134.06	269.86	1
Ibuprofen										
Wastewater										
Batch 1	13	1834.2	640.75	177.71	1980.0	233	2680	1446.9	2221.4	1
Batch 2	14	1777.6	589.47	157.54	1715.5	645	2951.5	1437.3	2117.9	0
Batch 3	13	1918.3	385.03	106.79	1904.0	1124	1685.5	1685.6	2151.0	1
Fortified river water (fortification 675 ng/L)										
Batch 1	14	536.04	278.79	74.510	508.75	22	1067.1	375.1	699.0	0
Batch 2	13	523.73	156.46	43.395	484.00	310	875.0	429.2	618.3	1
Batch 3	13	542.74	190.58	52.859	603.00	278	811.1	427.6	657.9	1
Fortified MilliQ water (fortification 225 ng/L)										
Batch 1	13	260.46	139.51	38.693	215.00	66	621	176.15	344.8	1
Batch 2	13	253.15	102.87	28.532	246.00	165	547	190.97	315.3	1
Batch 3	13	206.12	45.461	12.609	203.00	96	265	178.65	233.6	1
Diclofenac										
Wastewater										
Batch 1	14	1482.2	784.75	209.73	1545.0	92	2557	1029.2	1935.2	0
Batch 2	14	1476.4	919.93	245.86	1564.5	177	2920	945.29	2007.4	0
Batch 3	14	1503.8	982.03	262.46	1457.0	177	3343	936.84	2070.7	0
Fortified river water (fortification 398 ng/L)										
Batch 1	11	400.36	198.83	59.951	340.00	133	767	266.79	533.93	1
Batch 2	11	408.27	145.78	43.955	457.00	129	609	310.34	506.21	1
Batch 3	12	392.88	157.37	45.428	400.00	154	705	292.89	492.86	2
Fortified MilliQ water (fortification 200 ng/L)										
Batch 1	13	205.71	109.18	30.280	193.00	61	483.2	139.73	271.69	1
Batch 2	14	167.43	79.237	21.177	156.00	61.4	284	121.69	213.17	0
Batch 3	14	150.51	71.030	19.700	148.00	33	320	107.58	193.43	1

All samples included in the study were delivered to each participating laboratory at 4 °C. An aliquot of each sample was kept in the laboratory in Barcelona, in order to perform an additional study and check whether the samples were stable when kept under unfavourable conditions. For this test, a set of samples was extracted immediately after sampling, i.e. within 24 h after sampling. Another two sets of samples were kept refrigerated and were extracted and analyzed 1 week and 10 days after sampling, respectively. Two more sets of samples were stored at room temperature and were extracted and analyzed also within 1 week, and 10 days after sampling. The results for the different sets extracted after different periods of time and under various conditions were compared with those extracted immediately after sampling (24 h). In all cases, no significant differences in NSAID concentrations were quantified and the stability of samples was confirmed in all situations. Finally, the homogeneity of the samples was checked and

confirmed by analyzing three randomly selected samples for each type. The NSAID concentrations were compared between the samples and no significant differences were found, with the coefficients of variation lower than 10%, in all cases.

2.2. Chemicals

Ibuprofen, naproxen, ketoprofen, and diclofenac used were of the highest purity available (>99%), and were kindly supplied by Jescuder (Rubí, Spain).

Deuterated d3 ibuprofen was used as the internal standard. Individual stock standard solutions used for spiked samples were prepared on a weight basis in methanol and stored at −20 °C.

2.3. Statistical parameters

For each series, the mean value (X), the standard deviation (σ), variance (σ^2), upper warning limit (UWL) value, lower warning limit (LWL) value, number of outlier values, repeatability (r), reproducibility (R) and coefficient of variation (CoV) were calculated.

The formulae used to calculate the UWLs, and the LWLs as were UWL = ($X + 2\sigma$) and LWL = ($X - 2\sigma$), respectively.

As acceptance criteria for each result were used, the Z-score function according with the IUPAC [16,17] following the AOAC, and ISO directives.

The Z-values where calculated according to

$$Z = \frac{X_{\text{lab}} - X}{\sigma}$$

where X_{lab} is the result for a laboratory, X the mean value of all laboratories values, and σ the standard deviation in the correspondent population (taking into account the results obtained for the different laboratories in a series for a type of sample).

The results whose Z-value was over 3 were directly excluded. For the results whose Z-score values were a number between 2 and 3 the Dixon test was applied with a 5% of significance level.

In order to follow the stability of samples along the test, it was necessary to study whether the mean concentrations difference between series were significant. Therefore, the analysis of variance (ANOVA) was applied to the results. First of all, it was necessary to prove whether the groups of data followed Gaussian distributions and if the differences between standard deviations of the groups were significant to select a parametric or non-parametric procedure. The normality test of the Kolmogorov and Smirnov method was applied, while the Bartlett's test was performed to establish if the differences among the standard deviations were significant. Finally, was selected the Kruskal–Wallis test, a non-parametric ANOVA.

The measurement of precision of each laboratory to repeat the measurements on a sample at different intervals, reproducibility

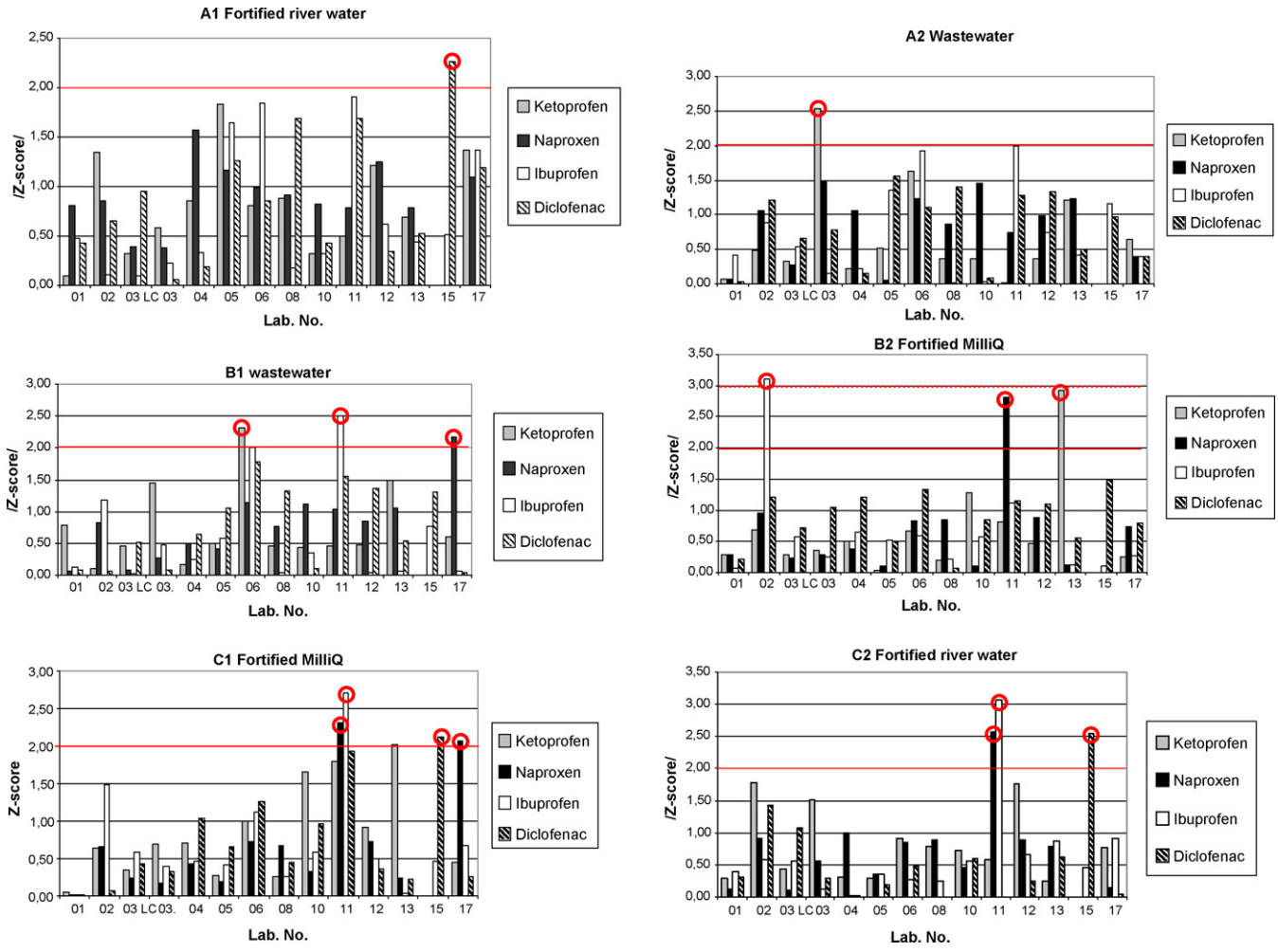

Fig. 1. Z-score absolute values.

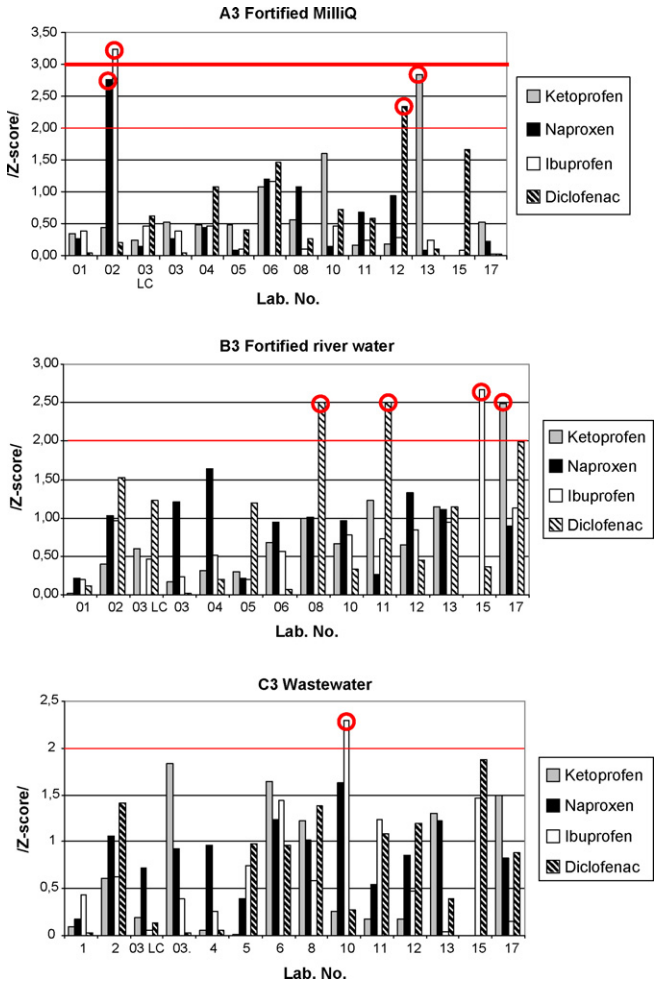

Fig. 1. (*Continued*).

(R) was calculated in terms of dispersion (D) as

$$D = R^{-1} = \frac{\Sigma r_{lab}}{N} = \frac{\Sigma(2 \times 2^{1/2})\sigma_{lab}}{N}$$

where $r^{-1}{}_{lab} = \sum(2 \times 2^{1/2})\sigma_{lab}$, N is the number of samples (only results for stable samples were included), and σ_{lab} is the standard deviation between results from the same laboratory on a stable sample at different intervals.

The hierarchical cluster analysis was based on the *similarity* matrices. The *similarity* measures were the *squared Euclidean* distances between the results obtained for a compound. The average linkage method was used as clustering approach.

2.4. Analytical methods

In the first round of this Interlaboratory exercise on the determination of NSAID residues in environmental water samples, a set of rules was proposed for the pre-concentration, extraction, and analysis of the samples. Analytical techniques utilized were based on liquid, or gas chromatography. Table 2 lists the participant laboratories in alphabetical order, as well as the main characteristics of the analytical methods used by each of them.

2.4.1. Extraction

Polymeric Oasis HLB 60 mg/3 mL (Waters) cartridges were proposed for off-line SPE extraction.

2.4.1.1. SPE protocol for LC–MS/MS analysis. Conditioning was carried out using 5 mL of methanol followed by 5 mL of deionised water (HPLC grade) at a flow rate of 1 mL/min. The samples (500 mL of ground and river water, and 200 mL of WWTP effluent) at neutral pH were allowed to percolate through the cartridges at a flow rate of 10 mL/min. Then the cartridges were rinsed with 5 mL of HPLC-grade water and dried under vacuum to remove excess of water for 15–20 min. Finally, the cartridges were eluted with 2×4 mL of methanol at 1 mL/min, evaporated under nitrogen stream, and reconstituted with 1 mL methanol–water (25:75, v/v).

2.4.1.2. SPE protocol for GC–MS analysis. Cartridges were conditioned using 3 mL of ethyl acetate followed by 3 mL of methanol and 3 mL of deionised water (HPLC grade) at a flow rate of 1 mL/min. The samples (500 mL of ground and river water, and 200 mL of WWTP effluent) were allowed to percolate through the cartridges at a flow rate of 10 mL/min, rinsed, and dried under vacuum to remove excess of water for 15–20 min. Finally, the cartridges were eluted with 3×1 mL of ethyl acetate and concentrated to 1 mL under a stream of nitrogen.

An off-line SPE method based on the extraction of the pre-filtered samples at neutral pH using polymeric cartridges Oasis HLB (60 mg, 3 mL) was proposed by the organisation based on next steps: condition of the SPE cartridges with 5 mL of methanol and 5 mL of deionised water (HPLC grade) at a flow rate of 1 mL/min, followed of the percolation of water samples (500 mL of ground and

river water, and 200 mL of WWTP effluent) through the cartridges at a flow rate of 10 mL/min, rinsing with 5 mL of HPLC-grade water, and drying under vacuum for 15–20 min, to remove excess of water. Finally, cartridges elution with 2 × 4 mL of methanol at 1 mL/min, evaporated under nitrogen stream and reconstitution with 1 mL methanol–water (25:75, v/v) for LC–MS/MS analysis, and with 1 mL of ethyl acetate for GC–MS. However, for the first round of the interlaboratories the participants were allowed to modify the proposed method (acidification, cartridge selection, temperature programme and elution conditions). During the Second round of the interlaboratory study, variations in the whole analytical procedures will not be allowed.

All the methods included in this exercise were based on the use of polymeric cartridges. Eight of the participants applied optimized methods that included acidification of the sample during extraction. The reconstitution of the sample extracts was also performed in different manners either according to the mobile phases in the case of LC or according to the derivatization procedure in the case of GC. Details of the various procedures for sample treatment are summarized in Table 2.

2.4.2. LC–ESI-tandem MS analysis

The LC analyses were performed using a RP-18 column. The method proposed outliner the analysis to be performed under negative ion conditions. The mobile phase was methanol as eluent A and MilliQ water as eluent B. Other mobile phases were also admitted. Two SRM transitions for each compound were acquired where possible; one was used for identification and one for quantification.

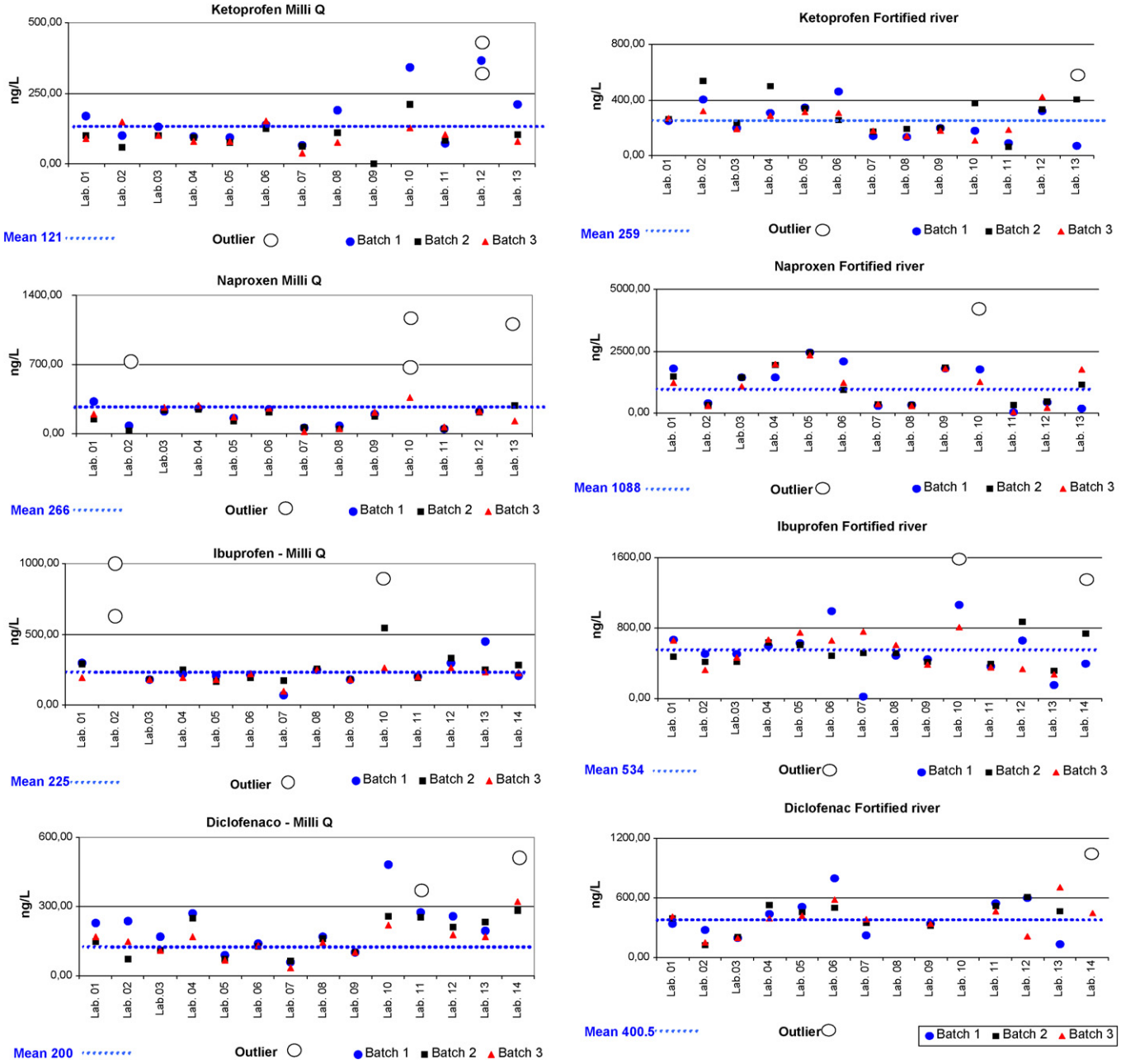

Fig. 2. Results obtained for each participant for naproxen, ibuprofen, diclofenac and ketoprofen expressed in ng/L in the different samples, and mean value of results (blue line). (For interpretation of the references to color in this figure legend, the reader is referred to the web version of the article.)

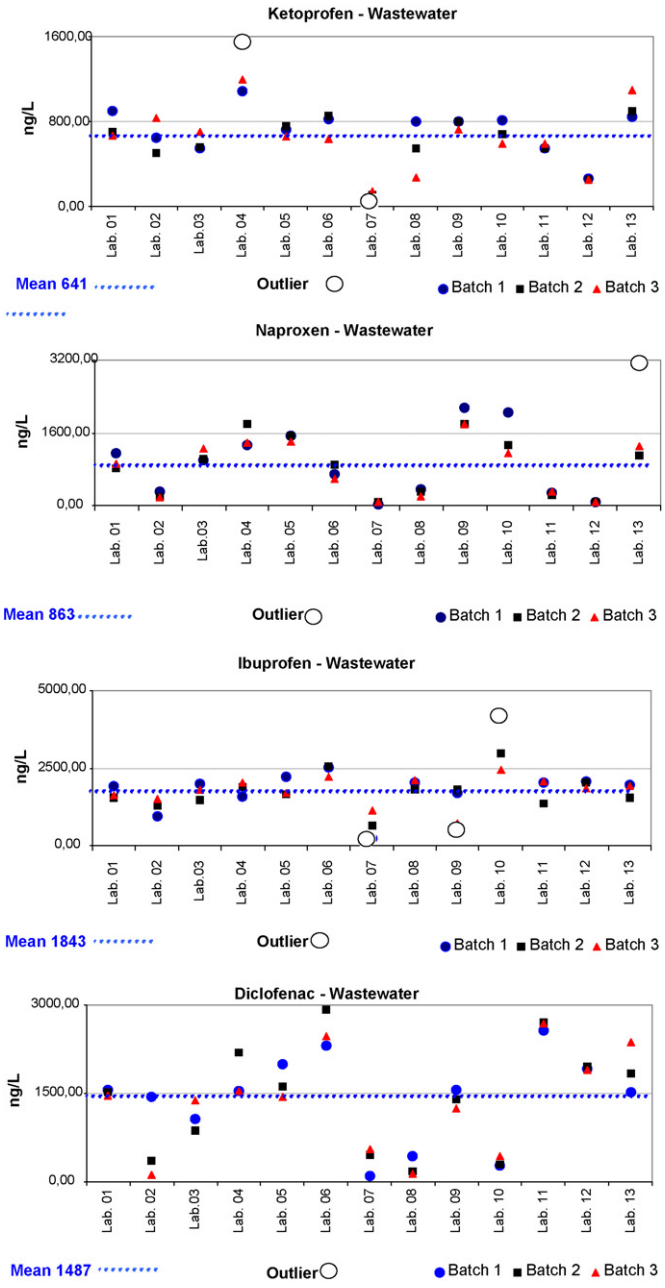

Fig. 2. (*Cntinued*).

Further chromatography and spectrometric conditions were optimized by the participants according to the available equipments and skills.

2.4.3. Gas chromatography–mass spectrometry

The method suggested by the organiser was derivatization with *N*-methyl-*N*-trimethylsilyl-trifluoracetamide (MTBSTFA) for 1 h at 60 °C. For GC–MS analysis, 1 μL of sample was injected in a split-less mode, at 250 °C; The GC oven was programmed as follows: 2 min at 65 °C, first ramp at rate 30°/min to 180°, rate 5°/min to 300 (hold 12 min). The target ions chosen were ibuprofen: *m*/*z* 263, naproxen: *m*/*z* 287, ketoprofen: *m*/*z* 311, diclofenac: *m*/*z* 352 and 354.

Most of the participants using GC followed this method, although the capillary columns were purchased from different suppliers and differences especially in the oven programme were introduced according to the different equipments available in the different laboratories.

3. Results

A total number of 14 participations took part of this study: 7 participations using a method based on GC–MS, and 7 participations using LC–MS/MS.

A total number of 486 results were collected. The mean values, standard deviations (σ), variances (σ^2), standard error of mean, median and upper and lower warning limits (UWL and LWL) between results from the participant laboratory at different intervals were calculated.

Z-score values and the Dixon test were used to calculate the outliers within the results. The calculation gave 24 outliers (4.9% of the

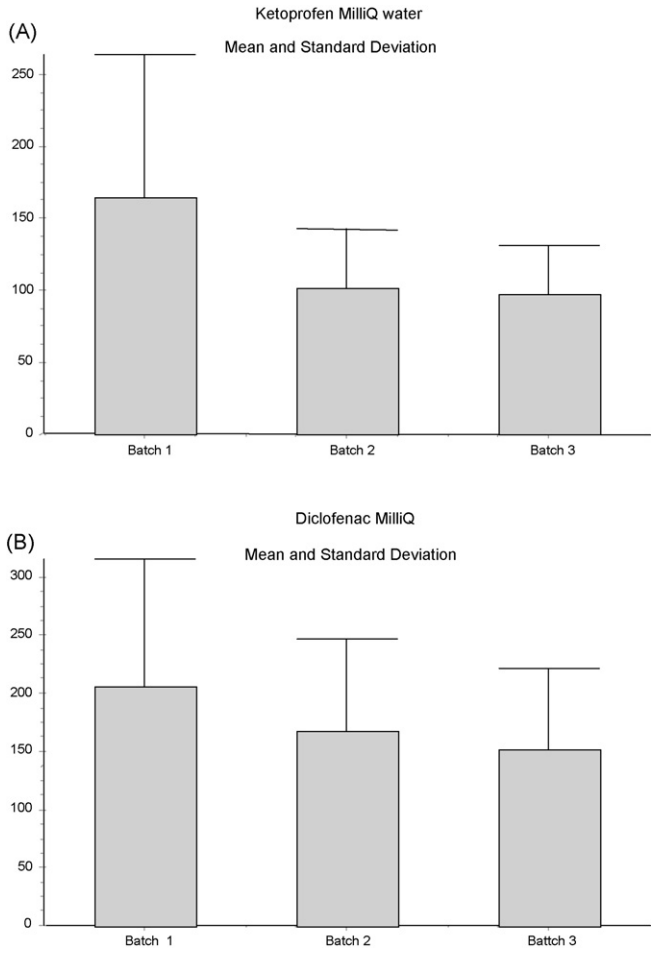

Fig. 3. Representation of the mean values and their standard deviations obtained for ketoprofen and diclofenac during the different intervals of time (Batch 1, Batch 2, Batch 3), for fortified MilliQ water.

total number of results). In the group of results obtained by GC–MS 15 outliers were obtained from 216 results (a 6.9% of total results). In the case where LC–MS/MS was utilized nine outliers (corresponding to 3.3%) were obtained. Fig. 1 presents the absolute values of *Z*-score. According to the range of concentrations measured during the exercise, the complexity of the wastewater sample and the differences of the analytical methods used, the number of outliers obtained in this exercise can be considered low. The fact that more outliers were obtained by GC was expected due to the additional derivatization step in the sample preparation.

The distribution of outlier values for the different compounds resulted in similar percentages. The sample matrix with the higher number of outliers was deionised water. On the other hand, wastewater had the highest concentrations of the analytes. Since this was the most complex sample matrix, higher levels of variability between participants were obtained.

The coefficients of variation were high, as it was expected, because the selected compounds are emerging pollutants and different analytical methods were compared.

The outlier values were excluded of the final data treatment and the statistical parameters (mean values (X_i), standard deviation (σ_i), variance (σ_2), coefficient of variation (CoV) were recalculated. Table 3 shows the corrected statistical values (after outlier exclusion) obtained for each compound in the different types of samples along the exercise.

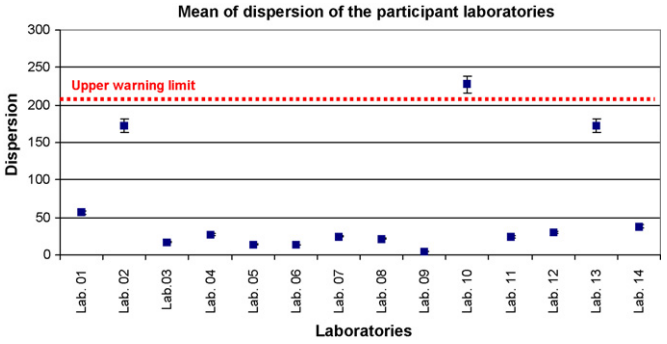

Fig. 4. Reproducibility (*R*) expressed as the inverse of dispersion (*D*). Dispersion mean values for the participants analyzing the selected compounds along the exercise are represented. Dotted line means the dispersion upper warning limit.

Results for the different samples expressed in ng/L and mean values are plotted in Fig. 2.

In order to establish the stability of samples along this intercomparison test, differences between variances obtained for every type of sample at different intervals were evaluated. In all cases the distribution of results followed a Gaussian distribution.

In two cases, ketoprofen and diclofenac in deionised water, the results from Bartlett's test suggested that the differences among standard deviation were significant along the exercise. Fig. 3 represents the mean values and the standard deviations along the

Table 4
Repeatability and reproducibility (*R*) expressed through r^{-1} and dispersion (*D*) values of each laboratory for ketoprofen, naproxen, ibuprofen and diclofenac in wastewater (A) and river water (B)

Laboratory codes, chromatographic method	Ketoprofen	Naproxen	Ibuprofen	Diclofenac
(A)				
01, LC	356	488	546	113
02, GC	455	186	805	1978
03, LC	237	386	747	727
04, GC	220	704	645	1086
05, GC	133	233	898	792
06, LC	335	436	565	900
07, LC	174	96	1261	684
08, GC	752	217	495	469
09, GC	131	572	200	453
10, LC	311	1366	1018	253
11, LC	66	94	1166	226
12, LC	14	0	307	85
13, GC	368	412	621	1218
14, LC	0	0	309	1492
D	254	371	684	748
(B)				
01, LC	28	795	314	888
02, GC	308	143	257	726
03, LC	75	613	128	361
04, GC	328	891	99	281
05, GC	49	191	211	597
06, LC	298	1704	733	2074
07, LC	59	149	1065	3013
08, GC	92	61	169	478
09, GC	33	65	97	273
10, LC	397	997	512	1448
11, LC	178	462	47	133
12, LC	153	368	773	2188
13, GC	656	2242	235	664
14, LC			700	1980
D	204	668	381	1079

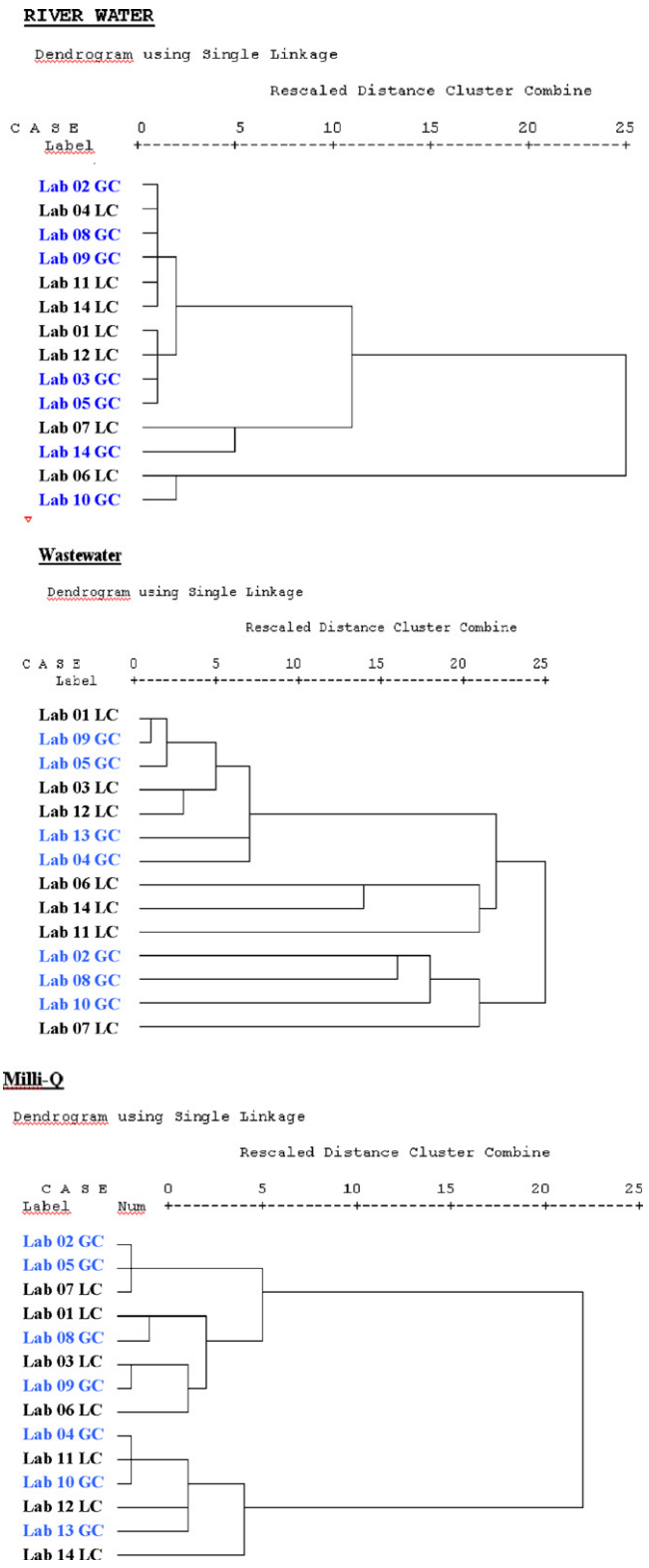

Fig. 5. Cluster analysis representation. Two-dimensional dendograms using the single linkage method for the three types of samples: (A) river; (B) wastewater; (C) MilliQ.

exercise for these compounds in MilliQ water. As can be seen, in these cases an important decrease in the measured concentrations was produced after the first batch of analysis, whereas good stability was obtained for wastewater and river water.

Repeatability data for river water and wastewater are summarized in Table 4A and B. Reproducibility may be expressed quantitatively in terms of the dispersion characteristics of the results. Fig. 4 shows the dispersion mean values for the participants analyzing the selected compounds along the exercise are represented. The dotted line represents the UWL, over which the reproducibility of a participant is considered to be significantly lower in comparison to the others. Therefore, it can be concluded that overall the reproducibility was quite low.

The possible interrelation between results was studied using the hierarchical cluster analysis. So, as all the results for each type of water were studied together and the results for each participant were grouped, first according the Average Linkage Cluster method, and second according to the Nearest Neighbour Cluster method. In both cases, the measured interval between results was the squared Euclidean distance. In Fig. 5 dendograms corresponding to the cluster analyses using the single linkage method are represented.

Both cluster analyses concluded that the results of the participating laboratories are independent of the analytical method used for the analysis of the samples (LC or GC). In addition, no relation was obtained between the results and the temperature of the samples at reception in the range of temperatures studied.

4. Conclusions

The number of participants that initiated this interlaboratory exercise was 17, and the final number of participants was 13 (77%). The final number of results collected was 486 and 24 values were outliers (4.9%) and discarded.

The number of outlier values by liquid chromatography was 9 (3.3% of results), whereas the number of outlier using GC–MS was superior than 15 (6.9%), probably due to an additional step in the sample preparation (derivatization).

Four laboratories obtained the higher number of outlier values and can be associated to samples handling and calculation errors. The sample with the highest number of outliers was the fortified deionised water, possibly because of the lowest concentration applied in the sample.

The second sample having a high number of outlier values was wastewater, most probably due to the complexity of the matrix. For this matrix higher levels of variability were also observed.

The stability of the samples was followed along the exercise by means of the ANOVA. In all cases the ANOVA test showed good stability for the NSAIDs selected in this study, and the variations among means were not significantly greater than expected by chance, with the exception of ketoprofen and diclofenac in MilliQ water.

A generally good agreement was obtained between the concentrations of fortification and the mean values reported by the participants. However, the precision of individual participants was quite low along the exercise, although only one participant showed a significantly low level of reproducibility. In order to minimize sources of variation in future validation steps, a protocol for sample treatment should be unified, and it should be clearly stated how to pre-treat the samples prior to analysis, e.g. how to defreeze de samples.

The hierarchical cluster analysis showed that no relation can be found between the results and if the chromatographic method is based on GC or LC.

Acknowledgements

This work has been supported by the EU through the project NORMAN (contract no. 018486).

Marinella Farré thanks the support from the MINISTERIO DE EDUCACIÓN y CIENCIA through the I3P program. J.B. Quintana acknowledges Xunta de Galicia ("Isidro Parga Pondal"research program"). R. Rodil acknowledges "Ministerio de Educación y Ciencia"("Juan de la Cierva"research program").

This article reflects only the author's views and the EU is not liable for any use that maybe made of the information contained therein.

References

[1] B. Halling-Sorensen, S.N. Nielsen, P.F. Lanzky, F. Ingerslev, H.C.H. Lutzhoft, S.E. Jorgersen, Chemosphere 36 (1998) 357.
[2] C.G. Daughton, T.A. Ternes, Environ. Health Perspect. 107 (1999) 907.
[3] E. Zuccato, D. Calamari, M. Natangelo, R. Fanelli, Lancet 355 (2000) 1789.
[4] K.J. Kummerer, Antimicrob. Chemother. 54 (2004) 311.
[5] T. Heberer, Toxicol. Lett. 131 (2002) 5.
[6] C.G. Daughton, Environ. Health Perspect. 111 (2003) 757.
[7] M.J. Gómez, M. Petrovic, A.R. Fernández-Alba, D. Barceló, J. Chromatogr. A 1114 (2006) 224–233.
[8] N.M. Vieno, T. Tuhkanen, L. Kronberg, Environ. Sci. Technol. 39 (2005) 8220.
[9] W.C. Lin, H.C. Chen, W.H. Ding, J. Chromatogr. A 1065 (2005) 279.
[10] B.W. Brooks, T.M. Riley, R.D. Taylor, Hydrobiologia 556 (2006) 365.
[11] M. Rabiet, A. Togola, F. Brissaud, J.L. Seidel, H. Budzinski, F. Elbaz-Poulichet, Environ. Sci. Technol. 40 (2006) 5282.
[12] T. Heberer, B. Fuhrmann, K. Schmidt-Baumler, D. Tsipi, V. Koutsouba, A. Hiskia, in: C.G. Daughton, T.L. Jones-Lepp (Eds.), Pharmaceuticals and Personal Care Products in the Environment: Scientific and Regulatory Issues, American Chemical Society, Washington, DC, 2001.
[13] G.A. Loraine, M.E. Pettigrove, Environ. Sci. Technol. 40 (2006) 687.
[14] T.A. Ternes, Trends Anal. Chem. 20 (2001) 419.
[15] M. Farré, M. Petrovic, D. Barceló, Anal. Bioanal. Chem. 387 (2007) 1203.
[16] International Union of Pure and Applied Chemistry (IUPAC), The international harmonized protocol for the proficiency testing of (chemical) analytical laboratories, Pure Appl. Chem., 2004. http://www.iupac.org/projects/2001/2001-009-1-500Draft040317.pdf.
[17] AOAC, ISO, IUPAC, "Z-Scores". Laboratory Accreditation & Audit Protocol: Food Inspection Directorate, Agriculture Canada, March 1987.
[18] T.P. Knepper, F. Sacher, F.T. Lange, H.J. Brauch, F. Karrenbrock, O. Roerden, K. Lindner, Waste Manage. 19 (1999) 77.
[19] M. Hilton, K.V. Thomas, J. Chromatogr. A 1015 (2003) 129.
[20] V. Koutsouba, Th. Heberer, B. Fuhrmann, K. Schmidt-Baumler, D. Tsipi, A. Hiskia, Chemosphere 51 (2003) 69–75.
[21] I. Rodrıguez, J.B. Quintana, J. Carpinteiro, A.M. Carro, R.A. Lorenzo, R. Cela, J. Chromatogr. A 985 (2003) 265.
[22] T. Kosjek, E. Heath, A. Krbavcic, Environ. Int. 31 (2005) 679.
[23] E. Zuccato, S. Castiglioni, R. Fanelli, J. Hazard. Mater. 122 (2005) 205–209.
[24] S. Marchese, D. Perret, A. Gentili, R. Curini, F. Pastori, Chromatographia 58 (2003) 263–269.

Talanta 76 (2008) 503–508

Contents lists available at ScienceDirect

Talanta

journal homepage: www.elsevier.com/locate/talanta

Determination of Sn(II) and Sn(IV) after mixed micelle-mediated cloud point extraction using α-polyoxometalate as a complexing agent by flame atomic absorption spectrometry

M.B. Gholivand[a,*], A. Babakhanian[a], E. Rafiee[b]

[a] Islamic Azad University – Kermanshah Branch, Iran
[b] Department of Chemistry, Razi University, Kermanshah, Iran

ARTICLE INFO

Article history:
Received 24 November 2007
Received in revised form 31 January 2008
Accepted 19 March 2008
Available online 16 April 2008

Keywords:
Mixed micellar medium
α-Polyoxometalate
Cloud point extraction
Tin

ABSTRACT

The cloud point extraction behavior of Sn(II) and Sn(IV) using α-polyoxometalate and mixed surfactants solution was investigated. The mixture of a nonionic surfactant (Triton X-100) and a cationic surfactant (CTAB) was utilized as a suitable micellar medium for preconcentration and extraction of tin complexes. Sn(II) in the presence of Sn(IV) was extracted with α-polyoxometalate, 0.3% (w/v) Triton X-100 and 3.5×10^{-5} mol L^{-1} CTAB at pH 1.2. Whereas the pH value of 3.7 were used for the individual determination of Sn(II) and Sn(IV) and also for total tin determination at the same conditions. Enrichment factors of 100 were obtained for the preconcentration of both metal ions. Under the optimal conditions, linearity was obeyed in the ranges of 55–670 μg L^{-1} of Sn(II) and 46–750 μg L^{-1} of Sn(IV) ion concentration. The detection limit of the method was also found to be 12.6 μg L^{-1} for Sn(IV) and 8.4 μg L^{-1} for Sn(II). The relative standard deviation of seven replicate determination of 100 μg L^{-1} both metal ions were obtained about 2.4%. The diverse ion effect of some anions and cations on the extraction efficiency of target ions were tested. Finally, the optimized conditions developed were successfully utilized for the determination of each metal ion in various alloy, juice fruit, tape and waste water samples with satisfactory results.

1. Introduction

Tin is a toxic metal which could gather in a human's body and the tissue of animals [1] and high concentration of tin, brings serious interference to the metabolism of zinc [2]. Tinplate is widely used in food industry and for the production of beverage cans. The use of tinplate for food and beverage packaging will result in some tin dissolving into the food content [3,4]. Therefore, the determination of tin has become an important task because of the wide industrial use of tin compounds in the past decades and their diverse effects on human health. Cloud point extraction (CPE) is an impressive alternative to conventional solvent extraction because it produces high extraction efficiencies and preconcentration factors, and uses inexpensive, lower toxicity reagents. To carry out the separation and preconcentration of the tin species, mixed micelle-mediated extraction (mixed-MME) system was used in this study. Separation and preconcentration based on mixed-MME methods are becoming an important and practical application of surfactants in analytical chemistry [5–7]. It was reported that the CP of nonionic surfactant increased on adding small amounts of ionic surfactant [8] and was also used to the preconcentration of organic compounds [9,10] and metal cations [11,12]. In this paper a cationic surfactants in combination with nonionic surfactant has been used for the preconcentration and determination of tin species. Polyoxometalates (POMs) are a large and rapidly growing class of compounds that have attracted much attention in catalysis, medicine, bioanalysis and materials science owing to their chemical, structural and electronic versatility [13–15]. One of the most important properties of POMs is their ability to form complex with variety of heavy metal ions [16–17]. Recently, some analytical applications of POMs such as capillary electrophoretic determination of Sc(III) and Y(III), liquid-type carbon paste electrode construction and chemometric analysis of lanthanide(III) ions have been reported [18–20]. To the best of our knowledge, there is no report to apply polyoxometalate as a reagent in separation techniques, especially CPE. In view of the prominent properties of our newly synthesized α-polyoxometalate($K_7PMO_2W_9O_{39}{\cdot}H_2O$), we tried to utilize the α-polyoxometalate as a complexing agent for the cloud point extraction and preconcentration of Sn(II) and Sn(IV) in various alloy, juice fruit, tape and waste water samples. The method was based on the complexation of Sn(II) and Sn(IV) with α-polyoxometalate and then their CPE in the presence of mixed surfactants (CTAB and Triton

* Corresponding author. Tel.: +98 831 4274557; fax: +98 831 4274559.
E-mail address: mbgholivand@yahoo.com (M.B. Gholivand).

0039-9140/$ – see front matter © 2008 Published by Elsevier B.V.
doi:10.1016/j.talanta.2008.03.057

X-100) as an ionic and nonionic surfactants and then determination by FAAS.

2. Experimental

2.1. Apparatus

A Shimadzu flame atomic absorption spectrometer model AA-670 was used for recording absorbance. A tin hollow cathode lamp was used as radiation source at 286.3 nm. The absorbance measurements were carried out under the manufacturer's recommendations. A HANA ion analyzer 302 pH/mV meter with a combined glass electrode was utilized for pH measurements at $25.0 \pm 0.1\,^{\circ}C$. A thermo stated bath maintained at the desired temperature was applied to obtain cloud point preconcentration. A centrifuge and calibrated centrifuge tubes were used to accelerate the phase separation process.

2.2. Reagents

All reagents were of analytical grade, and deionized water was used throughout. $SnCl_2{\cdot}2H_2O$, $SnCl_4{\cdot}5H_2O$, polyoxyethylene-9.5-octylphenylether (Triton X-100), cetyltrimethylammonium bromide (CTAB) and 37% HCl were purchased from Merck and were used without further purification. A Stock solution of Tin(II) was prepared by dissolving 190.0 mg of $SnCl_2{\cdot}2H_2O$ in 10 mL of concentrated HCl. After addition of 5 mL of 0.1 mol L^{-1} hydrazine chloride it was diluted to the mark in 100 mL volumetric flask. The stock solution containing 2.5×10^{-3} mol L^{-1} of Tin(IV) was also prepared by dissolving appropriate a mount of stannic chloride in 2 mol L^{-1} HCl and was standardized by known method [21]. These solutions were prepared daily and were stable during the day. α-Polyoxometalate was synthesis according to previous report [22,23]. A solution of 2.5×10^{-3} mol L^{-1} of α-polyoxometalate was prepared by dissolving of the appropriate amount of compound in water and utilized as chelating extract ant agent during experiments. A buffer solution of pH 3.7 was prepared by mixing an appropriate volume of 0.1 mol L^{-1} acetic acid and 0.1 mol L^{-1} sodium acetate. Also a mixture of 25 mL of 0.2 mol L^{-1} KCl and 42.5 mL of 0.2 mol L^{-1} HCl was used for adjusting of pH 1.2. The materials and vessels used for trace analysis were kept in 10% nitric acid for at least 48 h and subsequently washed four times with deionized water before use.

2.3. General procedure

2.3.1. Determination of Sn(II) or Sn(IV) or total tin

For the individual determination of tin species or total tin, aliquots of 10 mL of the solution containing the analyte (Sn(II) or Sn(IV) or mixture of both), 0.3% (w/v) of Triton X-100, 3.5×10^{-5} mol L^{-1} of CTAB and 6.5×10^{-5} mol L^{-1} of α-polyoxometalate solution, buffered at pH 3.7, were mixed and left in the thermostatic bath ($55\,^{\circ}C$) for 15 min. Then the phase separation was accelerated by centrifugation for 15 min at 3800 rpm. The surfactant-rich phase became viscous. Then, the aqueous phases can be separated in an easy way by only inverting the tubes. Later, in order to decrease the viscosity and facilitate sample handling, 300 μL of DMF was added to the surfactant-rich phase. The samples were introduced by conventional aspiration into a flame atomic absorption spectrometer.

2.3.2. Determination of Sn(II) in the mixture of tin species

The same procedure mentioned above (except adjusting the pH at 1.2) was used for determination of Sn(II) in the presence of Sn(IV).

2.4. Digestion procedures

2.4.1. Juice samples

Five milliliters of sample juice was transferred into a 250 mL Erlenmeyer flask and 10 mL concentrated HCl was added. After heating, the mixture was diluted to about 75 mL by distilled water. The solution was cooled and filtered. The filtrated solution was made up to 100 mL with doubly distilled water in a standard flask. The tin content was so low that its determination was not possible with the proposed method. Therefore, tin was spiked to the juice solution in order to obtain a solution with the final concentration of 300 μg L^{-1}. The total tin content of juice was determined using standard addition method.

2.4.2. Alloy sample

A 1.0 g sample of the standard alloys was completely dissolved in 10–15 mL of hydrochloric acid (1:1) by heating on a water-bath and then 2–3 mL of 30% (v/v) hydrogen peroxide were added to it. The excess of peroxide was decomposed by heating the sample. The solution was cooled and filtered. The filtrated solution was made up to 100 mL with doubly distilled water in a standard flask. The total tin content was determined using standard addition method.

3. Result and discussion

It is reported that α-polyoxometalate can form complexes with tin species. Their tetrabutylammonium salts of resulted complexes were used as a catalyst for oxidation of a variety of organic compounds [22,24,25]. In the primary experiment, it was found that the addition of some equivalent of Sn(II) and Sn(IV) to aqueous solution of α-polyoxometalate resulted in a fast change in the color of the solution to yellow and purple, respectively. So, this tendency encouraged us to carry out the preconcentration and separation of tin species using α-polyoxometalate as complexing agent. Due to advantages of CPE, it was used for separation and preconcentration of tin species. Thus, for finding the optimum conditions, the influence of various parameters on extraction efficiency was investigated.

3.1. Effect of pH on extraction efficiency

Tin(II) and Tin(IV) reacts with α-polyoxometalate in acidic medium and form $[PSnMo_2W_9O_{39}]^{5-}$ and $[PSnMo_2W_9O_{39}]^{3-}$ Keggin-type complexes which in the presence of CTAB are subsequently trapped in the surfactant micelles (e.g. Triton X-100) and separated from the aqueous phase. The pH was the first critical parameter evaluated for its effect on the determination of tin. CPE of tin species was performed in different buffer solutions. The separation of metal ions by CPE method involves the formation of a complex with a sufficient hydrophobicity to be extracted into a small volume of surfactant-rich phase. The extraction yield depends on the pH at which complex formation occurs. Thus, the effect of pH on extraction efficiency of Sn(II) and Sn(IV) were evaluated and the results are shown in Fig. 1. As can be seen the best interval of pH for Sn(II), Sn(IV) and total tin maximum extraction efficiency was 2.2–4.8. In more acidic solutions, absorbance decreased may be attributed to some hydronium ions trapped in cage of α-polyoxometalate which avoid interaction between metal ion and α-polyoxometalate. On the other hand, when the pH of solution is higher than 5.0, the signal intensity of analyte is decreased obviously due to the degradation of α-polyoxometalate complexing

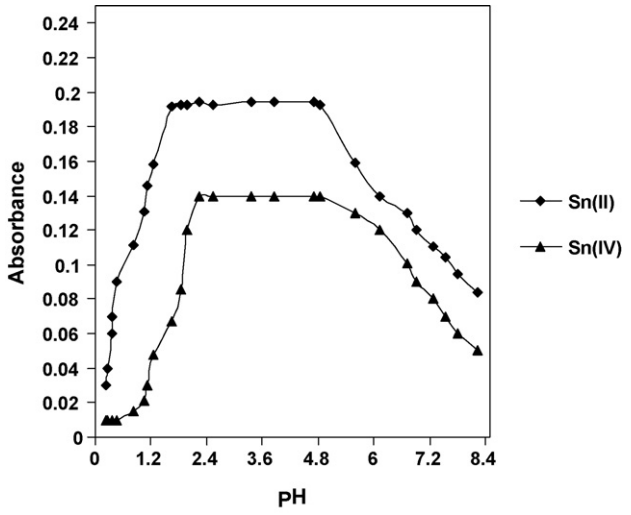

Fig. 1. Effect of pH variations over extraction efficiency. Condition: CTAB, 2.0×10^{-5} mol L^{-1}; Triton X-100, 0.4% (w/v); ligand, 4.0×10^{-6} mol L^{-1}; Sn(II), 400 μg L^{-1}; Sn(IV), 400 ng m L^{-1}; incubation time, 15 min; centrifuge time, 15 min; temperature, 55 °C.

agent [23]. Thus, the pH value of 3.7 was selected as the working value for the individual determination of Sn(II) and Sn(IV) and also total tin detection. As it is seen from Fig. 1, Sn(II) can be determined in the presence of Sn(IV) if the pH of the solution was adjusted at 1.2. In spite of decreasing of the sensitivity of determination of Sn(II) in comparison to that obtained in pH 3.7, the pH 1.2 was chosen for determination of Sn(II) in the presence of Sn(IV). At this pH the interference of Sn(IV) on determination of Sn(II) is negligible.

3.2. Effect of surfactants concentration on extraction efficiency

In the preliminary experiments it is observed that the addition of the neutral surfactant such as Triton X-100 to ternary complex of tin ion–α-polyoxometalate–CTAB and heating, makes the solution turbid. This shows that the ternary complex of Sn(II) or Sn(IV)–α-polyoxometalate–CTAB can be extracted by CPE method. Therefore, the effect of CTAB and nonionic surfactant (Triton X-100) concentration on the analytical response of 400 μg L^{-1} (3.4×10^{-6} mol L^{-1}) of each metal ion (Sn(II) and Sn(IV)) were investigated. The results are shown in Figs. 2 and 3. As it is seen the measured absorbance reached its maximum at more than 0.3% (w/v) of Triton X-100 and 2.8×10^{-5} mol L^{-1} of CTAB, indicating that quantitative extraction by cloud point method was obtained. Therefore, 3.5×10^{-5} mol L^{-1} and 0.3% (w/v) were selected as the optimum amounts of ionic and nonionic surfactants for subsequent uses. Thus, by using Triton X-100 and CTAB as a mixed surfactant agent, the test solution could be separated easily into two phases and the bulk aqueous phase could be decanted after centrifugation. No cooling step was needed due to the appropriate cloud point temperature (55 °C) of the surfactant. Under this circumstance, the satisfactory results were obtained.

3.3. Effect of the salting out reagent

Several concentrations of sodium chloride were tested to examine its contribution to the extraction efficiency of the proposed scheme. It was found that the addition of up to 0.02 mol L^{-1} sodium chloride resulted in the quantitative isolation of up to 400 μg L^{-1} tin species. The salting out effect was also tested in the presence of other salts like sodium fluoride, potassium nitrate, potassium bromide and potassium iodide. Provided that clouding is achieved,

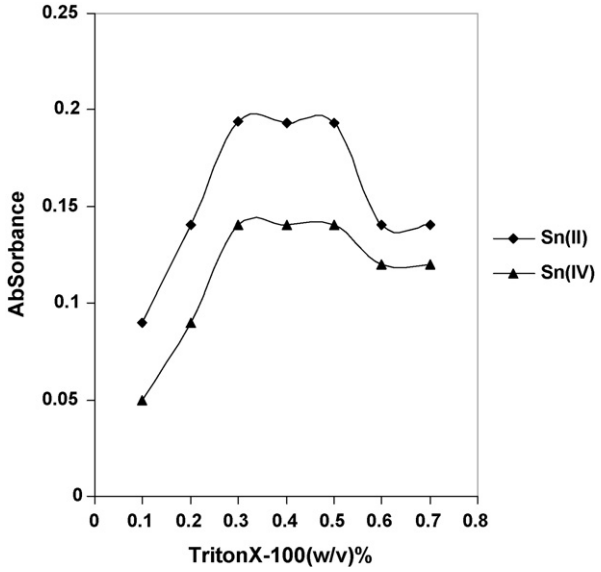

Fig. 2. Effect of concentration of Triton X-100 over extraction efficiency. Condition: CTAB, 2.0×10^{-5} mol L^{-1}; ligand, 4.0×10^{-6} mol L^{-1}; Sn(II), 400 μg L^{-1}; Sn(IV), 400 μg L^{-1}; incubation time, 15 min; centrifuge time, 15 min; temperature, 55 °C; pH 3.7.

Table 1
Effect of ionic strength on CPE of 400 μg L^{-1} of Sn(II) and or Sn(IV) ion

Salt	Concentration range (mol L^{-1})	Absorbance Sn(II)	Absorbance Sn(IV)
NaF	2×10^{-5}–6×10^{-2}	0.195–0.200	0.144–0.149
NaCl	1×10^{-5}–2×10^{-2}	0.195–0.199	0.145–0.148
KNO_3	1×10^{-5}–5×10^{-2}	0.197–0.198	0.147–0.149
KBr	1×10^{-6}–6×10^{-2}	0.193–0.200	0.146–0.147
KI	5×10^{-6}–8×10^{-2}	0.194–0.198	0.144–0.148

the nature of the salt had no effect on the extraction ability of the proposed method (Table 1).

3.4. Effect of α-polyoxometalate concentration

In general, the concentration of the chelating reagent has a remarkable influence on the extraction efficiency. In order

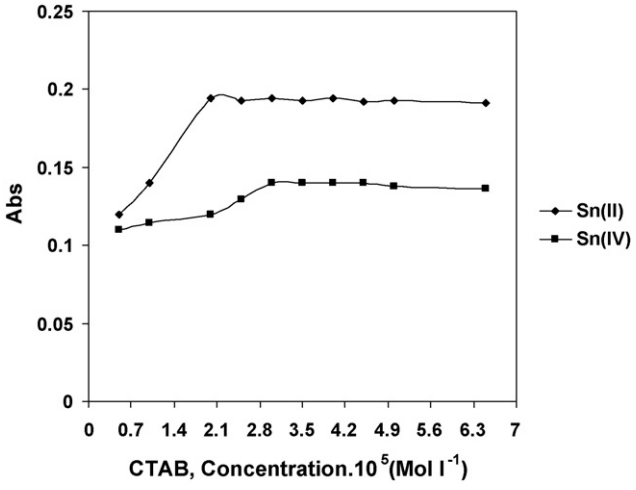

Fig. 3. Effect of concentration of CTAB on cloud point extraction process. Condition: Triton X-100, 0.3 % (w/v); ligand, 4.0×10^{-6} mol L^{-1}; Sn(II), 400 μg L^{-1}; Sn(IV), 400 μg L^{-1}; incubation time, 15 min; centrifuge time, 15 min; temperature, 55 °C; pH 3.7.

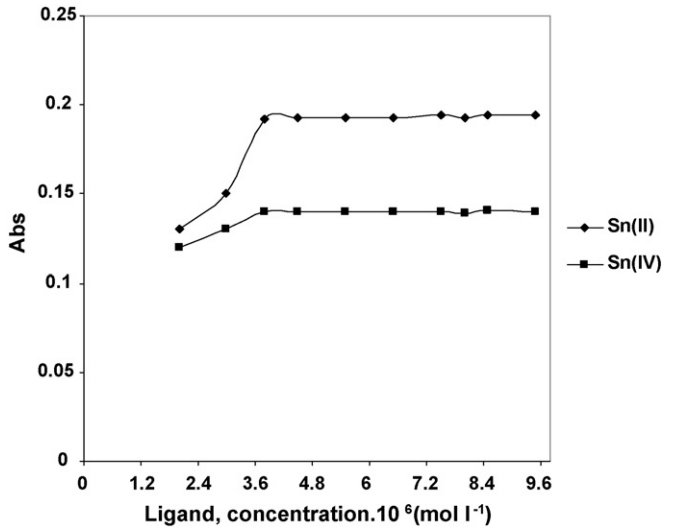

Fig. 4. Effect of concentration of α-polyoxometalate complexing agent on cloud point extraction process. Condition: Triton X-100, 0.3% (w/v); CTAB, 3.5×10^{-5} mol L^{-1}; Sn(II), 400 μg L^{-1}; Sn(IV), 400 μg L^{-1}; incubation time, 15 min; centrifuge time, 15 min; temperature, 55 °C; pH 3.7.

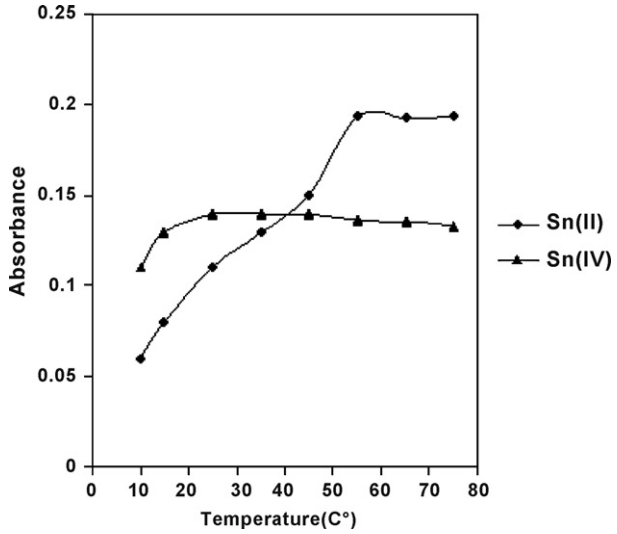

Fig. 5. Effect of equilibration temperature on cloud point extraction process. Condition: Triton X-100, 0.3% (w/v); CTAB, 3.5×10^{-5} mol L^{-1}; Sn(II), 400 μg L^{-1}; Sn(IV), 400 μg L^{-1}; incubation time, 15 min; centrifuge time, 15 min; pH 3.7.

to select the optimal concentration of α-polyoxometalate, with the other experimental parameters remaining constant, the effect of concentration of α-polyoxometalate (in the range of 2.0×10^{-6}–9.5×10^{-6} mol L^{-1}) on analytical response of 400 μg L^{-1} (3.4×10^{-6} mol L^{-1}) of each metal ion (Sn(II) and Sn(IV)) was investigated. Results are presented in Fig. 4. For both Sn(II) and Sn(IV)-substituted of α-polyoxometalate, higher analytical signals were obtained when α-polyoxometalate concentrations are equal or greater than 4.0×10^{-6} mol L^{-1}. At this initial point of the plateau, a total complexation was attained. Thus, a 6.5×10^{-5} mol L^{-1} of α-polyoxometalate complexing agent was used in subsequent studies.

3.5. Effects of the incubation time, equilibration temperature and centrifugation time

The equilibration temperature above the CPT and the incubation time were the next parameters considered. It was desirable to employ the shortest incubation time and the lowest possible equilibration temperature, which compromise completion of the reaction and efficient separation of phases. The dependence of extraction efficiency upon equilibration temperature and time was studied in a range of 10–90 °C and 5–25 min, respectively. The results showed that an equilibration temperature of 55 °C (Fig. 5) and a time of 15 min were adequate to achieve quantitative extraction for both cases. In general, centrifugation time hardly ever affects micelle formation but accelerates phase separation in the same sense as in conventional separations of a precipitate from its original aqueous environment [26]. Therefore, a centrifugation time of 15 min at 3800 rpm was selected for subsequent uses.

3.6. Analytical characteristics

Calibration graphs for Sn(II) and Sn(IV) were obtained by preconcentrating of 10 mL of different concentrations of standard solutions of $SnCl_2$ and $SnCl_4$ in the presence of 0.3% Triton X-100 and 3.5×10^{-5} mol L^{-1} CTAB in a medium buffered at pH 3.7. After separation of the surfactant-rich phase, it was introduced into the flame by conventional aspiration following the addition of 300 μL of DMF. In both cases, linear relationships between the absorbance measured and the concentration of tin species in solution were obtained. Table 2 gives the calibration parameters, the relative standard deviation obtained for five samples subjected to the complete procedure, and the detection limits. Preconcentration of only 10 mL of sample in the presence of 0.3% Triton X-100 permitted the detection of 8.4 μg L^{-1} Sn(II) and 12.5 μg L^{-1} Sn(IV). The enhancement factors, calculated as the ratio of absorbance of preconcentrated samples to that obtained without preconcentration, were 100 for both tin ions.

3.7. Determination of Sn(II) in the presence of Sn(IV)

At pH 1.2, the calibration curve that was constructed for Sn(II) in the presence of maximum amount of Sn(IV) (750 μg L^{-1}) was linear in the range of 65–670 ng mL^{-1} ($A = 0.0003\ C\ \mu g\ L^{-1} + 0.0743$, correlation coefficient of 0.996). The detection limit was 8.4 μg L^{-1}.

3.8. Interferences

In view of the high selectivity provided by flame atomic absorption spectrometry, the only interferences studied were those related to the preconcentration step: cations that may react with α-polyoxometalate or anions that may form complexes with metal ions and decrease extraction efficiency. Thus, the effect of foreign ions on the determination of 100 μg L^{-1} of each tin species by the proposed method was investigated. An ion was considered to interfere when its presence produced a variation in the absorbance of the sample of more than 5%. The results are summarized in Table 3. As the results show common cations and anions do not interfere on the determination of trace quantities of tin species that may be due to high selectivity tendency of the α-polyoxometalate as chelating agent with Sn(II) and Sn(IV).

3.9. Analytical application

The proposed method for the determination of tin ions were applied to some water, juice and alloy samples. The analysis of real samples (except alloys) showed that total tin was not detectable in them, so they were spiked with a standard tin ion solutions, and total tin were obtained (pH 3.7) and

Table 2
Analytical features of the proposed method

Analytical parameter	Sn(II)	Sn(IV)
Linear range[a]	55–670 ($\mu g\,L^{-1}$)	46–750 ($\mu g\,L^{-1}$)
Regression equation[a]	$A = 3 \times 10^{-4}\,C\,\mu g\,L^{-1} + 0.0768$	$A = 2 \times 10^{-4}\,C\,\mu g\,L^{-1} + 0.0735$
R^2[a]	0.994	0.996
Linear range[b]	5.50–67.50 ($\mu g\,mL^{-1}$)	5.06–82.50 ($\mu g\,mL^{-1}$)
Regression equation[b]	$A = 3 \times 10^{-6}\,C\,\mu g\,mL^{-1} + 0.0698$	$A = 2 \times 10^{-6}\,C\,\mu g\,mL^{-1} + 0.0735$
R^2[b]	0.994	0.996
EF[c]	100	100
R.S.D. ($C = 100\,\mu g\,L^{-1}$, $n = 5$)	2.5	2.4
LOD (3 Sb/m, $\mu g\,L^{-1}$)	8.4	12.6
LOQ (10 Sb/m, $\mu g\,L^{-1}$)	27.9	41.8

[a] With preconcentration at pH 3.7.
[b] Without preconcentration at pH 3.7.
[c] Enhancement factors (EF) at pH 3.7.

Table 3
Tolerance limit of diverse ions on the individual determination of 100 $\mu g\,L^{-1}$ of Sn(II) and Sn(IV)

Interfering ion	Interfering ion/Sn(II) ($\mu g\,L^{-1}$)	Recovery of Sn(II) (%)	Interfering ion/Sn(IV) ($\mu g\,L^{-1}$)	Recovery of Sn(IV) (%)
Ni^{2+}, Zn^{2+}, Cu^{2+}, Fe^{3+}	27	103.6	24	97.4
Al^{3+}, Cr^{3+}, Ce^{3+}	38	97.7	38	97.9
Cd^{2+}, Pb^{2+}, Mn^{2+}	25	103.6	23	97.1
Ti^{4+}, Co^{2+}	9.5	104.5	9.3	104.3
SO_4^{2-}, Br^-, F^-, CH_3COO^-, $S_2O_3^{2-}$	600	102.5	600	102.7
Hg^{2+}, Pd^{2+}	40	97.5	37	97.3
Li^+, K^+, Na^+	65	98.2	65	98.4
Zr^{4+}, Y^{3+}, Bi^{3+}	70	97.7	68	102.3
Mg^{2+}, Sr^{2+}, Ca^{2+}	45	97.2	45	102.6
NO_3^-, PO_4^{3-}, SCN^-, NH_4^+	700	102.3	700	102.6

Table 4
Individual determination of Sn(II) and Sn(IV) in the water samples (pH 3.7, $n = 5$).

Sample	Sn(II) added ($\mu g\,L^{-1}$)	Sn(II) found ($\mu g\,L^{-1}$)	Recovery Sn(II) (%)	Sn(IV) added ($\mu g\,L^{-1}$)	Sn(IV) found ($\mu g\,L^{-1}$)	Recovery Sn(IV) (%)
Tap water	100.0	96.7 ± 4.0	96.7	100.0	97.7 ± 3.7	97.7
	150.0	153.3 ± 2.5	102.2	150.0	146.5 ± 3.7	97.7
	200.0	196.00 ± 3.4	98.0	200.0	197.5 ± 3.2	98.7
Wastewater (oil refinery)	100.0	97.00 ± 3.0	97.0	100.0	96.7 ± 3.2	96.7
	150.0	146.3 ± 2.5	97.5	150.0	147.7 ± 3.2	98.5
	200.0	196.3 ± 2.5	98.2	200.0	196.5 ± 3.7	98.3

Table 5
Analysis of tin content in standard alloy and juice fruit samples by the proposed method at pH over 3.7 ($n = 5$)

Sample	Composition (w/w, %)	Certified value (w/w, %)	Found value (w/w, %)	Recovery (%)
NKK No. 916	Si, 0.41; Mg, 0.10; Cr, 0.05; Fe, 0.54; Ni, 0.06; Ti, 0.10; Pb, 0.04; Cu, 0.27; V, 0.02; B, 0.0006; Bi, 0.03; Co, 0.03; Mn, 0.11; Zr, 0.050; Sb, 0.01	0.050	0.048 ± 0.003	96
NKK No.1021	Si, 5.56; Mg, 0.29; Cr, 0.03; Ni, 0.14; Ti, 0.04; Pb, 0.18; Sb, 0.01; Bi, 0.01; V, 0.007; Ca, 0.004; Mn, 0.11; Cu, 2.72; Fe, 0.99, Zr, 0.010	0.100	0.097 ± 0.003	97.4
Orange juice	–	300.00[a] ($\mu g\,L^{-1}$)	296.50 ± 3.84 ($\mu g\,L^{-1}$)	98.83
Pineapple juice	–	300.00[a] ($\mu g\,L^{-1}$)	291.50 ± 3.74 ($\mu g\,L^{-1}$)	97.16

[a] Spiked tin amount.

Table 6
Analysis of synthetic Sn(II)–Sn(IV) mixture solution at varying proportion ($n = 5$)

Sn(II)/Sn(IV) in mixture ($\mu g\,L^{-1}$)	Sn(II), found[a] ($\mu g\,L^{-1}$)	Recovery of Sn(II) (%)	Sn(IV), found[b] ($\mu g\,L^{-1}$)	Recovery of Sn(IV) (%)
100.0/0.0	98.3 ± 2.5	98.4	–	–
100.0/100.0	102.3 ± 3.0	102.3	96.6 ± 3.8	96.6
100.0/200.0	97.7 ± 3.4	97.7	205.5 ± 3.2	102.7
100.0/300.0	98.3 ± 4.0	98.3	294.5 ± 2.4	98.2

[a] pH 1.2.
[b] pH 3.7.

the results were given in Tables 4 and 5. As could be seen, the recoveries of the spiked samples were in the acceptable range (96.6–102%). The speciation of Sn(II) and Sn(IV) were tested using the different synthetic sample solutions containing both target ions at different ratio, and their results are shown in Table 6. The obtained results revealed that the proposed mixed-MME method was quite quantitative, precise and accurate.

4. Conclusion

Cloud point using mixed micelles is a very promising methodology for the establishment of a new analytical procedure. The extent of extraction is influenced by the presence of the surfactant concentrations, the complexing agent used and its concentration and the pH of the medium. The small volume of the surfactant-rich phase obtained by using the proposed cloud point methodology permitted to design a extraction strategy presenting robustness, low cost, good extraction efficiency and lower toxicity than those using organic solvents. Environmental pollution is limited to a small amount of surfactant. This fact is particularly attractive, because the "green chemistry" concept can be employed here. The results of this work clearly show the potential and versatility of this method, which could be applied for monitoring the total tin and individual tin species (Sn(II) and Sn(IV)). The proposed method permits analysis and quantification of tin species at $\mu g\,L^{-1}$ levels in different samples with FAAS. The proposed CPE method gives low LOD, good R.S.D. and solvent-free extraction of the tin from its initial matrix without previous treatment. The method was verified with real samples and applied satisfactory to the determination of tin in different samples.

References

[1] M.E. Malla, M.B. Alvarez, D.A. Batistoni, Talanta 57 (2002) 277.
[2] X. Zhang, Toxic. Det. Tin Sanit. Res. 31 (2002) 324.
[3] S.M. Lee, Metals in Food: A Literature Survey, Leatherhead Food RA, 1990.
[4] Codex Alimentarius Commission-Codex Committee on Food Additives and Contaminants, Position Paper on Tin, Food and Agriculture Organization of the UN/World Health Organization, Rome, 1998.
[5] J. Chen, T.K. Chuan, Anal. Chim. Acta 434 (2000) 325.
[6] A. Afkhami, T. Madrakian, A. Maleki, Anal. Biochem. 347 (2005) 162.
[7] A. Afkhami, M. Bahram, S. Gholami, Z. Zand, Anal. Biochem. 336 (2005) 295.
[8] T. Gu, P.A. Galera-G'omez, Colloids Surf. A 104 (1995) 307.
[9] E.J. Kim, D.O. Shah, Langmuir 18 (2002) 10105.
[10] J.W. Kang, G. De Reymaeker, A. Van Schepdael, E. Roets, J. Hoogmartens Electroph. 22 (2001) 1356.
[11] E.K. Paleologos, A.G. Vlessidis, M.I. Karayannis, N.P. Evmiridis, Anal. Chim. Acta 477 (2003) 223.
[12] D.L. Giokas, J. Antelo, E.K. Paleologos, F. Arce, M.I. Karayannis, J. Environ. Monit. 4 (2002) 505.
[13] D.E. Katsoulis, Chem. Rev. 98 (1998) 359.
[14] T. Yamase, Chem. Rev. 98 (1998) 307.
[15] W.E. Klmperer, C.G. Wall, Chem. Rev. 98 (1998) 297.
[16] C.G. Yuan, G.B. Jiang, B. He, J.F. Liu, Microchim. Acta 150 (2005) 329.
[17] L. Wang, Y.Q. Cai, B. He, C.G. Yuan, D.Z. Shen, J. Shao, G.B. Jiang, Talanta 70 (2006) 47.
[18] S. Himeno, E. Kitano, M. Kanaya, M. Takamoto, Talanta 71 (2007) 822.
[19] H. Liu, P. He, Z. Li, C. Sun, L. Shi, Y. Liu, G. Zhu, J. Li, Electrochem. Commun. 7 (2005) 1357.
[20] B.S. Valaulikar, C.J. Manohar, J. Colloids Interface Sci. 108 (1985) 403.
[21] W.W. Scott, Standard Methods of Chemical Analysis, vol. 1, 6th ed., 1963.
[22] S. Tangestaninejad, B. Yadollahi, Chem. Lett. 512 (1998).
[23] R. Massart, R. Contant, J.M. Fruchart, J.P. Ciabrini, M. Fournier, Inorg. Chem. 16 (1997) 296.
[24] E. Rafiee, S. Tangestaninejad, M. Habibi, H. Mirkhani, V. Russ, J. Org. Chem., in press, 2008.
[25] L.C.W. Baker, D.C. Glick, Chem. Rev. 98 (1998) 3.
[26] E.K. Paleologos, D.L. Giokas, M.I. Karayannis, Trends Anal. Chem. 24 (2005) 426.

Talanta 76 (2008) 669–673

Contents lists available at ScienceDirect

Talanta

journal homepage: www.elsevier.com/locate/talanta

Cloud point extraction for cobalt preconcentration with on-line phase separation in a knotted reactor followed by ETAAS determination in drinking waters

Raúl A. Gil[a,b], José A. Gásquez[a], Roberto Olsina[a,b], Luis D. Martinez[a,b], Soledad Cerutti[b,*]

[a] *Área de Química Analítica, Facultad de Química Bioquímica y Farmacia, Universidad Nacional de San Luis, Chacabuco y Pedernera, San Luis, C.P. 5700, Argentina*
[b] *Instituto de Química San Luis, INQUISAL-CONICET, Chacabuco y Pedernera, San Luis, C.P. 5700, Argentina*

ARTICLE INFO

Article history:
Received 13 February 2008
Received in revised form 3 April 2008
Accepted 7 April 2008
Available online 12 April 2008

Keywords:
Cloud point extraction
On-line phase separation
Cobalt determination
Knotted reactor
STPF–ETAAS

ABSTRACT

A novel method for cobalt preconcentration by cloud point extraction with on-line phase separation in a PTFE knotted reactor and further determination by electrothermal atomic absorption spectrometry (ETAAS) is proposed.

The cloud point system was formed in the presence of non-ionic micelles of polyethyleneglycolmono-*p*-nonylphenylether (PONPE 7.5) and it was retained on the inner walls of a knotted reactor (KR). The surfactant rich-phase was removed from the knotted reactor with 75 μL of methanol acidified with 0.8 mol L^{-1} nitric acid, directly into the dosing hole of the L'Vov graphite tube. An enrichment factor of 15 was obtained with a preconcentration time of 60 s, with respect to the direct determination of cobalt by ETAAS in aqueous solutions. The value of the detection limit for the preconcentration of 5 mL of sample solution was 10 ng L^{-1}. The precision, expressed as the relative standard deviation (R.S.D.), for 10 replicate determinations at 0.5 μg L^{-1} Co level was 4.5%. Verification of the accuracy was carried out by analysis of a standard reference material (NIST SRM 1640e "Trace elements in natural water"). The method was successfully applied to the determination of cobalt in drinking water samples.

1. Introduction

The toxicity of cobalt is low and it is considered as an essential element, which is required in the normal human diet in the form of vitamin B_{12} (cyanocobalamin). For this reason, Co has been used in the treatment of anemia [1]. However, the ingestion or inhalation of large doses of this analyte may lead toxic effects [2,3]. Since one of the routes of incorporation of cobalt into the human body is by ingestion [4], its determination in drinking water becomes important. Cobalt concentration levels are very low in water samples, and therefore sensitive analytical techniques are required to carry out its detection.

Electrothermal atomic absorption spectrometry (ETAAS) is one of the most sensitive techniques with low volumes of sample required for a large number of elements with detection limits in the μg L^{-1} to ng L^{-1} range, and therefore it is often chosen for the determination of analytes at trace levels [5]. However, in real samples of complex composition, matrix effects can significantly impact on the performance of ETAAS. While interferences may be overcomed to various degrees by applying the "stabilized-temperature platform furnace" (STPF) concept [6], separation of the analyte element from the matrix is undoubtedly even more effective in avoiding matrix effects. The on-line coupling of a flow injection (FI) preconcentration and separation technique with ETAAS has proved to be a powerful technique for ultratrace determination of a variety of elements [3–5].

During the past years, cloud point extraction (CPE) has become one of the most preferred preconcentration methodologies to enhancing the sensitivity in metal analysis thanks to its potential, benefits and versatility offered by this particular technique [6–10]. The principles and relevant applications of this separation methodology have already been discussed [6–10]. CPE is based on surfactant aggregates which together with ionic liquids have been recognized as the solvents of a modern era [11]. Both bulk solvent-soluble and solvent-insoluble species can reversibly interact with and bind to the micellar assembly. Sparingly soluble or non-water-soluble materials can be solubilized in water due to their binding to the micelles in solution [3]. This explains the fact that many analytical and other applications of surfactant micellar media have been based upon their analyte solubilization proficiencies. It has

* Corresponding author.
E-mail address: ecerutti@gmail.com (S. Cerutti).

0039-9140/$ – see front matter © 2008 Elsevier B.V. All rights reserved.
doi:10.1016/j.talanta.2008.04.004

Table 1
Experimental conditions for Co determination in CPE extracts by ETAAS

Stage	Ramp (s)	Hold (s)	Temperature (°C)	Internal gas flow (L min^{-1})	Sensitivity
Drying	10	–	200	1.0	No
	5		400	1.0	No
Pyrolysis	–	20	800	1.0	No
	–	3	800	0.0	Yes
Atomization	–	4	2200	0.0	Yes
Cleaning	–	2	2700	1.0	No

been demonstrated that non-ionic surfactant micelles provide the best general solubilization medium for the widest variety of solutes [10–19].

For the determination of trace elements by on-line combination of CPE with atomic spectrometry, the use of a salting-out agent to induce cloud point phase separation online may present serious problems because the introduction of high concentration of salts is unfavorable for atomic spectrometric detection. Also, the incorporation of a heating device within the FIA manifold may complicate the system design.

Our research group has reported an on-line phase separation methodology which included the dysprosium preconcentration by CPE followed by the retention of the micelle-rich phase onto a cotton-filled conical minicolumn and ICP OES detection [17]. Similar strategies were carried out by Li et al. [20] and Nan et al. [21].

In this work, to the best of our knowledge, for the first time the coupling of a cloud point extraction preconcentration system with the on-line phase separation by sorption of the micelle-rich phase into the inner walls of a PTFE knotted reactor (KR) has been performed. This methodology was associated to ETAAS determination with STPF by mounting the KR in the arm of the auto sampler. In order to optimize the proposed methodology, all variables which may affect the analytical performance were studied, including buffer pH, reagents concentration, pyrolysis and atomization temperatures, among others. Additionally, for the cobalt–CPE system, the use of a complexing reagent and the heating system requirement to reach the phase separation were unnecessary. All these mentioned features are a very important contribution because the majority of the methodologies reported in the literature need a heating step, a complexing reagent, and consequent higher sample manipulation to carry out the cloud point extraction process [8,20,21]. In this case, all those drawbacks were solved by implementing the proposed on-line phase separation due to: (i) Co was extracted by PONPE 7.5 without the use of a complexing reagent, (ii) the cloud point temperature for PONPE 7.5 is around 25 °C and (iii) the separation was made directly into the PTFE-KR.

2. Experimental

2.1. Apparatus

The measurements were performed with a Shimadzu Model AA-6800 atomic absorption spectrometer (Tokyo, Japan), equipped with a 6500-electrothermal atomizer and an ASC-6100 autosampler. L'Vov platform graphite tubes (Shimadzu, Tokyo, Japan) were used in all experiments. A cobalt hollow-cathode lamp (Hamamatsu, Photonics K.K., Japan) was employed as radiation source, the 242.5 nm spectral line was used. Other ETAAS instrumental and operating conditions are listed in Table 1.

A Minipulse peristaltic pump (Gilson (Villiers, Le-Bell, France)) and Tygon-type pump tubing (Ismatec, Cole-Parmer, Vernon Hills, IL, USA) were employed to propel reagents and solutions. Sample injection was achieved using a Rheodyne (Cotati, CA, USA), model 50, four-way injection valve.

For sorption of the cloud point system, a knotted reactor was made from a PTFE tubing of 0.5 mm internal diameter by tying interlaced knots of approximately 5 mm diameter loops.

2.2. Reagents and solutions

All reagents used were of high purity and analytical reagent grade. Working standard solutions were prepared by stepwise dilution from a 1000 mg L^{-1} Co stock standard solution (Sigma–Aldrich, St. Louis, USA) immediately before use. As it is not possible to obtain a real aqueous solution of the surfactant polyethyleneglycolmono-*p*-nonylphenylether (PONPE 7.5, Tokyo Kasei Industries, Chuo-Ku, Tokyo, Japan); it was experimentally convenient to prepare a stock surfactant solution (A-solution) as follows: 20 g of PONPE 7.5, and 40 mL of ethanol (Carlo Erba, Milan, Italy) were mixed and made up to 100 mL with ultrapure water. A buffer solution was prepared by diluting a 3.0 mol L^{-1} ammonium hydroxide solution adjusted to pH 10.0 with a hydrochloric acid solution. Ultrapure water was obtained from an EASY pure RF (Barnstedt, IA, USA).

2.3. Sample preparation

The water samples were filtered through 0.45 μm pore size membrane filters immediately after sampling, and were adjusted to pH 10.0 with buffer solution immediately before use. All the instruments used were previously washed with a 10% (v/v) nitric acid/water solution and then with ultrapure water.

2.4. Preconcentration procedure and determination

A scheme of the preconcentration manifold is shown in Fig. 1. At the beginning of the preconcentration/determination cycles, tubing lines were prepared for preconcentration with 10 mL of a

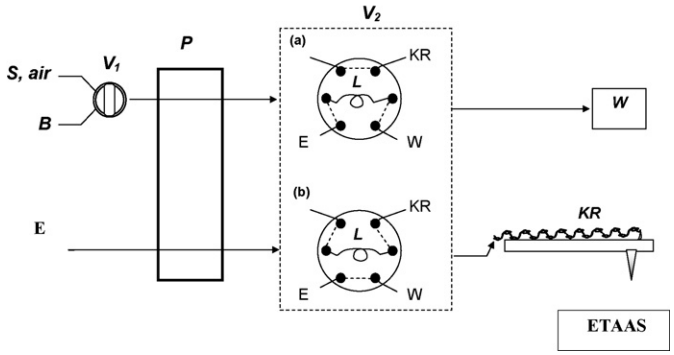

Fig. 1. Schematic diagram of the instrumental setup: **V_1**, two-way rotary valve; **V_2**, six port rotary valve ((**a**), load position; (**b**), injection position); **L**, eluent loop; **S**, sample; **B**, buffer; **E**, eluent; **P**, peristaltic pump; **KR**, knotted reactor; **W**, waste.

1.0 mol L^{-1} HNO_3 solution, washed with ultrapure water and finally conditioned at the correct pH value with buffer solution (valve **V_1** in position **B**).

2.4.1. Sample conditioning

Two milliliters of A-solution plus 2 mL of ammonia buffer were added to 50 mL of cobalt solution (standard or sample solutions) in order to form the micellar cloud point.

2.4.2. On-line phase separation

After the solution became turbid, 5 out of 50 mL were passed through the KR at a flow rate of 5.0 mL min^{-1} with valve **V_1** in position **S** and valve **V_2** in load position (**a**). This step allowed the phase separation due to the micelles, which contained the analyte, were retained in the inner walls of the KR. While the CPE solution was loaded, the injection loop (75 μL) was filled with the eluent solution (1:1 water:ethanol solution acidified with 0.6 mol L^{-1} of nitric acid).

2.4.3. Injection

After the loading time, sample line (**S**) was emptied. The peristaltic pump (**P**) was stopped and the injection valve **V_2** was switched to the injection position (**b**). Finally, the arm of the furnace autosampler was automatically moved to the dosing hole of the graphite tube and the retained metal was eluted with 75 μL eluent directly into the platform of the graphite furnace at 0.2 mL min^{-1}.

2.4.4. Reading

After the injection step, the autosampler arm was moved back to the on-line phase separation position and the temperature program was started. During this period, the KR was washed with eluent solution and conditioned at the correct pH. The absorbance measurements (peak area) were proportional to the cobalt concentration in the sample and were used for all the measurements.

The operating conditions were established and the determination was carried out. Measurements were corrected against a blank solution previously prepared.

3. Results and discussion

3.1. Study of the CPE system variables

The optimal temperature was selected according to available data [11]. Accordingly, we choose 25 °C as the working temperature.

The effect of pH upon the Co extraction was studied within the range of 5–12. The results showed that the metal extraction began at pH 6.0 and remained almost constant up to pH 11.0. Thus a pH value of 10 (obtained by adding ammonia solution) was selected for further experiments.

Under appropriate conditions, PONPE 7.5 may form a complex with Co^{2+} through its polyoxyethylene groups; thereby the metal can be extracted into the surfactant-rich phase. Complex formation between ether linkage of some non-ionic surfactants and cations such as Co^{2+} has also been reported by other researchers [22,23]. Working at pH 10, the variation of extraction efficiency upon the surfactant concentration was examined within the range: 0.025–1.5% (v/v). Quantitative extraction was observed for a surfactant concentration higher than 0.07% (v/v); however, at surfactant concentrations greater than 1.2%, the background signal increased significantly. Therefore, to attain a favorable enrichment factor, a 0.8% (v/v) surfactant concentration was chosen.

In order to optimize the on-line phase separation step, some variables were optimized carefully, e.g. knotted reactor length, eluent composition, and also volume and concentration of eluent.

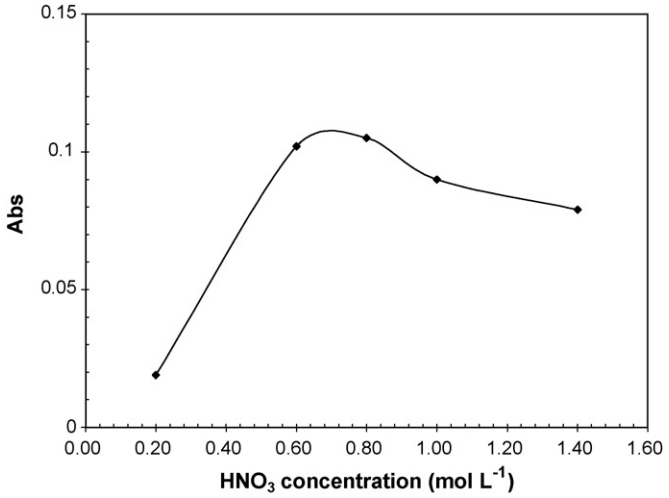

Fig. 2. Effect of the nitric acid concentration in the eluent solution upon the Co signal.

As a first step, several eluent compositions such as acids (nitric or hydrochloric acid), organic solvents (acetonitrile, methanol or ethanol), and also, mixtures of solvents (ethanol acidified with nitric acid among others) were tested. It was found that best Co signal was achieved when a solution 1:1 water:ethanol acidified with nitric acid was employed as eluent solution. This eluent composition provides good surface tension to form defined drops inside the graphite tube and could easily elute the micellar phase in a discrete volume. Based on the results, the concentration of nitric acid in the hydro-ethanolic mixture was studied. As depicted in Fig. 2, the concentration of nitric acid had a positive effect upon the Co signal in a range between 0.60 and 0.80 mol L^{-1}. When the concentration of nitric acid reached higher levels, the signal decreased, the increment of the background signal leading to an overcorrection of the Co absorbance could be attributed as the reason for such behavior. According to the experimental results, a concentration of nitric acid of 0.60 mol L^{-1} was selected.

While studying the effect of the KR length, the sample loading flow rate was fixed at 5.0 mL min^{-1}, and the KR length was varied up to 3 m. As shown in Fig. 3, a reactor length of 2 m sufficed to obtain the best phase separation, and thus the best enrichment factor.

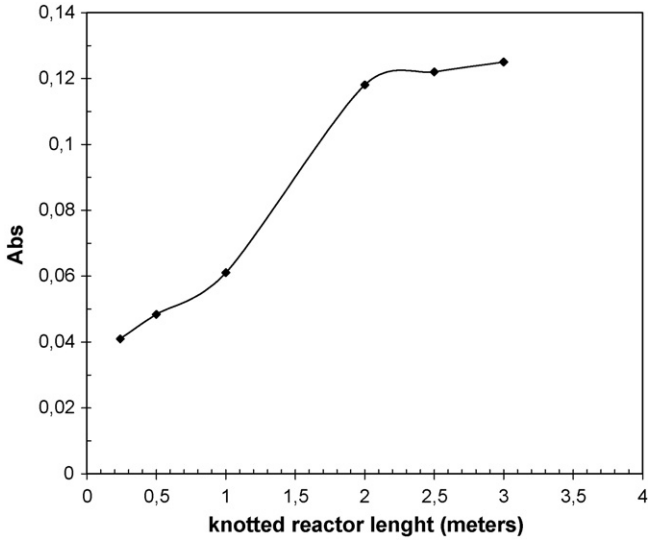

Fig. 3. Effect of the knotted reactor length upon the Co signal.

The loading flow rate is one of the most important variables when the time of analysis is evaluated. The retention mechanism in KRs involves changes in the flow direction caused by the knots, creating a secondary flow with some centrifugal force that pushes the particles toward the tubing walls. Considering these facts, the loading flow rate may strongly influence the retention of the micelles. Thus, the sample flow rate was studied in the range between 1.0 and 15.0 mL min^{-1}. The best Co signal was observed around loading flow rates of 5.0 mL min^{-1}, which was selected for further experiments.

3.2. Graphite furnace temperature programs

The study of the best conditions for the graphite furnace temperature program was carried out by optimizing the pyrolysis and atomization steps, and the hold times as well. For this purpose, cloud point systems prepared from aqueous solutions containing 0.5 μg L^{-1} of Co were employed. A 5 mL volume of the cloud point mixture was loaded on the KR and the surfactant phase was eluted later onto the platform of the graphite furnace with 75 μL of the eluent solution. With the purpose of obtaining the most suitable temperatures and hold times, the usual way of working with an AAS graphite furnace was followed.

3.2.1. Pyrolysis and atomization temperatures

Pyrolysis temperatures lower than 400 °C demonstrated that could not be used since concomitants were not eliminated efficiently and the background signal was considerable high. This originated, in some cases, and over-correction and erroneous absorption values for the analyte response. The ramp time for the pyrolysis stage was carefully adjusted to allow gradual elimination of the matrix, avoiding any analyte loss by a sudden increase in temperature.

Fig. 4 shows the optimization of pyrolysis and atomization temperatures and also the pyrolysis hold time. Curve A shows a significant increase in the Co signal was achieved when the pyrolysis temperature reached 800 °C. As illustrated in curves A and B when the pyrolysis time increased, the Co signal increased accordingly.

For the atomization step (curve C in Fig. 4), the atomization temperature was varied in the range between 1400 and 2600 °C and the optimum atomization temperature was selected as 2200 °C. In addition, a hold time of 4 s was chosen for this step. No peak tailing or differences between standards and samples were observed under the mentioned above conditions.

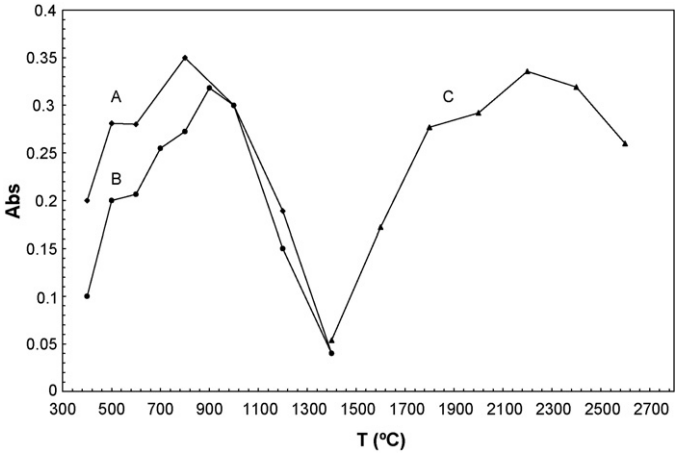

Fig. 4. Pyrolysis and atomization curves. (A) Study of the pyrolysis curve with a hold time of 18 s; (B) study of the pyrolysis curve with a hold time of 23 s; (C) study of the atomization temperature with a hold time of 4 s. *Conditions*: Five milliliters of the cloud point mixture containing 0.5 μg L^{-1} of Co were loaded on the KR and the surfactant phase was eluted later onto the platform of the graphite furnace with 75 μL 1.0 mol L^{-1} nitric acid.

Table 2
Concentrations of cobalt in drinking water (95% confidence interval, $n = 6$)

Sample	Co concentration (μg L^{-1})
A (1st week)	0.20 ± 0.02
B (2nd week)	0.19 ± 0.01
C (3rd week)	0.17 ± 0.01
D (4th week)	0.22 ± 0.02

The drinking water samples were collected at different times in our laboratory.

A temperature of 2700 °C and a hold time of 2 s were selected for the cleaning step.

No significant changes in the graphite tube performance were observed under the proposed temperature settings.

3.3. Interferences

The effects of potentially interfering species (at the concentration levels at which they may occur in the sample) were tested under the optimal preconcentration conditions. Thus Cu^{2+}, Zn^{2+}, Pb^{2+}, Ni^{2+}, Mn^{2+} and Fe^{3+} could be tolerated up to at least 2500 μg L^{-1}. Commonly encountered matrix components such as alkali and alkaline earth elements were not CPE-extractable or retained onto the KR walls under the working conditions used here.

3.4. Analytical performance

The overall time required for preconcentration of 5.0 mL of sample (1 min, at flow rate of 5 mL min^{-1}), and elution (approximately 0.8 min, at flow rate of 0.2 mL min^{-1}) was about 1.8 min, ETAAS analysis time (approximately 0.7 min); the throughput sample was about 24 determinations per hour. An enrichment factor of 15-fold was obtained with respect to the direct Co determination by ETAAS.

The precision for 10 replicate determinations at 0.5 μg L^{-1} Co level was 4.5% relative standard deviation (R.S.D.), calculated from the peak areas obtained. The detection limit (DL), calculated as the concentration of cobalt required to yield a net peak equal to three times the standard deviation of the blank signal (3σ), was 0.01 μg L^{-1} for the preconcentration of 5 mL of sample solution

3.5. Accuracy verification and application to real samples

The accuracy of the proposed method was evaluated by analyzing a standard reference material, NIST SRM 1640e "Trace elements in natural water", with a reported Co content of 20.28 ± 0.31 μg kg^{-1}, and a density of 1.0015 ± 0.0005 g mL^{-1} at 22 °C. Using the proposed methodology the Co content determined in this SRM was 20.12 ± 0.11 μg kg^{-1}. Finally, the procedure was applied to the cobalt determination in drinking water samples (Table 2).

4. Conclusions

An on-line CPE procedure coupled with KR preconcentration of cobalt in drinking water was for the first time performed with a simple FI system, which was easily coupled to ETAAS.

One of the most distinct features of the proposed methodology is the use of a knotted reactor for the on-line retention of the analyte-entrapped micelles, greatly simplifying the system design

by avoiding the need for a heating device and a salting-out agent for phase separation. Another important feature is that all operations for the micelle-mediated preconcentration are performed in on-line mode.

This preconcentration system can be adapted for other analytes and coupled to other detection techniques with simple modifications.

Acknowledgments

This work was supported by Consejo Nacional de Investigaciones Científicas y Técnicas (CONICET); Agencia Nacional de Promoción Científica y Tecnológica (FONCYT) (PICT-BID); and Universidad Nacional de San Luis (Argentina).

References

[1] E.J. Underwood, Trace Elements in Human and Animal Nutrition, Academia, London, 1971.
[2] P. Bratter, P. Schramel, Trace elements in Analytical Chemistry, Medicine and Biology, Walter de Gruyter, New York, 1980.
[3] D.L. Tsalev, Z.K. Zaprianov, Atomic Absorption in Occupational and Environmental Health Practice, Analytical Aspects and Health Significance, vol. 11, CRC Press, Boca Raton, FL, 1983.
[4] H.G. Seiler, A. Siegel, H. Siegel, Handbook on Metals in Clinical and Analytical Chemistry, Marcel Dekker, New York, 1994.
[5] B. Welz, M. Sperling, Atomic Absorption Spectrometry, 3rd ed., Wiley-VCH, Weinheim, 1999.
[6] W. Slavin, D.C. Manning, G.R. Carnrick, Anal. Chem. 53 (1981) 1504.
[7] Z.L. Fang, Flow Injection Atomic Absorption Spectrometry, John Wiley & Sons, Chichester, 1995.
[8] Z.L. Fang, Spectrochim. Acta Part B 53 (1998) 1371.
[9] X.P. Yan, Y. Jiang, Trends Anal. Chem. 20 (2001) 552.
[10] F.H. Quina, W.L. Hinze, Ind. Eng. Chem. Res. 3 (1999) 4150.
[11] M.F. Silva, S. Cerutti, L.D. Martinez, Microchim. Acta 155 (2006) 349.
[12] W.L. Hinze, E. Pramauro, Crit. Rev. Anal. Chem. 24 (1993) 133.
[13] G.L. McIntire, Crit. Rev. Anal. Chem. 21 (1990) 257.
[14] Z.S. Ferrera, C.P. Sanz, C.M. Santana, J.J.S. Rodriguez, Trends Anal. Chem. 23 (2004) 469.
[15] E.K. Paleologos, D.L. Giokas, M.I. Karayannis, Trends Anal. Chem. 24 (2005) 426.
[16] S. Rubio, D. Perez-Bendito, Trends Anal. Chem. 22 (2003) 470.
[17] C. Ortega, S. Cerutti, R.A. Olsina, M.F. Silva, L.D. Martinez, Anal. Bioanal. Chem. 375 (2003) 270.
[18] M.G.A. Korn, J.B. de Andrade, D.S. de Jesus, V.A. Lemos, M.L.S.F. Bandeira, W.N.L. dos Santos, M.A. Bezerra, F.A.C. Amorim, A.S. Souza, S.L. Costa Ferreira, Talanta 69 (2006) 16.
[19] C.D. Stalikas, Trends Anal. Chem. 5 (2002) 343.
[20] Y. Li, B. Hu, Z. Jiang, Anal. Chim. Acta 576 (2006) 207.
[21] J. Nan, Y. Jiang, X.P. Yan, J. Anal. At. Spectrom. 18 (2003) 946.
[22] G.C. Na, B.O. Yuan, H.J. Stevens, B.S. Weekley, N. Rajagopalan, Pharm. Res. 16 (1999) 562.
[23] H. Schott, A.E. Royce, J. Pharm. Sci. 73 (1984) 793.

Talanta 76 (2008) 662–668

Contents lists available at ScienceDirect

Talanta

journal homepage: www.elsevier.com/locate/talanta

Simultaneous determination of adenosine and inosine using single-wall carbon nanotubes modified pyrolytic graphite electrode

Rajendra N. Goyal*, Vinod K. Gupta, Sanghamitra Chatterjee

Department of Chemistry, Indian Institute of Technology Roorkee, Roorkee 247667, India

ARTICLE INFO

Article history:
Received 5 February 2008
Received in revised form 7 April 2008
Accepted 7 April 2008
Available online 16 April 2008

Keywords:
Single-wall carbon nanotubes
Adenosine
Inosine
Osteryoung square wave voltammetry

ABSTRACT

Voltammetric determination of adenosine and inosine has been carried out at single-wall carbon nanotubes (SWNTs) modified pyrolytic graphite electrode (PGE) at pH 7.2 using Osteryoung square wave voltammetry (OSWV). The modified electrode exhibits remarkable electrocatalytic properties towards adenosine and inosine oxidation with a peak potential of ~1229 mV and 1348 mV, respectively. Linear calibration curves are obtained over the concentration range 0.5 μM to 1.0 mM in adenosine and 10 μM to 1.0 mM in inosine with sensitivity of 1.0 μA μM^{-1} and 1.9 μA μM^{-1} for adenosine and inosine respectively. The limit of detection for adenosine and inosine was found to be 0.51×10^{-7} M and 2.04×10^{-7} M, respectively. The proposed method was also used to estimate these compounds in human blood plasma and urine samples and the method was validated using HPLC.

1. Introduction

Adenosine (**I**) known as 6-amino-9-β-D-ribofuranosyl-9-H-purine is an endogenous purine nucleoside occurring in all cells of the human system. It is recognized as a molecule that has wide-ranging biological importance and plays a vital role in biochemical processes. It is a potent anti-inflammatory and antiarrhythmic agent which is important in the control of coronary and cerebral blood flow [1–5]. It regulates the renal function [6] and is an inhibitory neurotransmitter [7] which plays a role in promoting sleep and suppressing arousal [8]. It has anti-epileptic effects on the central nervous system, anti-secretory effect in the stomach, anti-diuretic effect [9] and is an endogenous vasodilating agent [10]. Adenosine is administered for the treatment of gastrointestinal diseases [11]. Inosine (**II**) is a nucleoside which is formed when hypoxanthine is attached to a ribose ring via a β-N_9-glycosidic bond. It is used to treat irregular heart beat, heart attacks, Tourette's syndrome, inflammation, ischemic diseases and is better known as a performance enhancer for athletes [12–14].

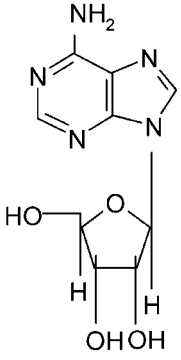

(I)

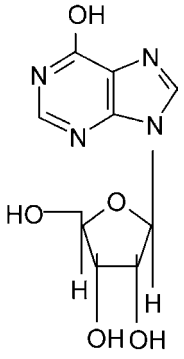

(II)

Adenosine is converted to inosine in biological systems by hydrolytic deamination and the enzyme adenosine deaminase is involved in purine metabolism [15,16]. The conversion is site specific and takes place in the mRNA of the cell [17] and specifically enhances deep sleep and slow wave activity during sleep [18]. Plasma adenosine concentration increases in patients with septic shock [19], severe preeclampsia [20] vasoplegia and post-operative severe systemic inflammatory response [21] and in the third trimester of normal pregnancy [22]. The adenosine level also increases significantly in the pericardial fluid of patients suffering from valvular heart disease and coronary artery disease [23]. Sim-

* Corresponding author. Tel.: +91 1332 285029 (O)/91 1332 274454 (R).
E-mail address: rngcyfcy@iitr.ernet.in (R.N. Goyal).

0039-9140/$ – see front matter © 2008 Elsevier B.V. All rights reserved.
doi:10.1016/j.talanta.2008.04.011

ilarly, inosine levels increase remarkably in the coronary sinus of patients undergoing cardiac artery bypass grafting surgery (CABG) [24]. The increase in the plasma adenosine and inosine concentration affects the metabolic pathway occurring in the human system which led to the need of simultaneous determination of adenosine and inosine.

In view of the importance of adenosine and inosine in human physiology, various attempts have been made to determine them individually in body fluids by different voltammetric techniques [25–28] and concentrations as low as 10^{-10} M/L have been determined. However, simultaneous determination of adenosine and inosine has attracted little attention using voltammetric techniques. One of the reasons for this is the close oxidation potential of the two compounds. During the last few years, several analytical methods have been developed for the determination of adenosine and inosine in presence of each other [29–34]. The chromatographic methods have high operational cost and involve time-consuming extraction steps. To the best of our knowledge, simultaneous determination of adenosine and inosine has not been carried out voltammetrically. The electrooxidation of these compounds require a relatively high oxidation potential at conventional electrodes which results in the merging of the signal current with the background discharge current. Carbon nanotubes (CNTs) with their extraordinary mechanical and unique electrochemical properties have garnered much attention in the past 5 years. The CNT based electrodes are generally prepared by casting SWNTs suspension on conventional electrode surface [35–38]. In the present study, SWNTs modified pyrolytic graphite electrode (PGE) has been used for the simultaneous determination of adenosine and inosine using Osteryoung square wave voltammetry (OSWV) procedure. The recovery of adenosine and inosine in biological samples and interfering effects of common biological metabolites have also been studied.

2. Experimental

2.1. Reagents

Adenosine was obtained from Merck (Germany) and inosine from Sigma (USA) and were used as received without further purification. Single-wall carbon nanotubes (SWNTs) of purity >95% was purchased from Bucky, USA. All other solvents and chemicals used were of analytical grade. For voltammetric experiments, a 0.1 M phosphate buffer solution (PBS) at pH 7.2 was used as supporting electrolyte. Freshly prepared solutions of adenosine and inosine were prepared in double distilled water each day before starting each set of experiments.

2.2. Apparatus and procedure

The square wave voltammetric experiments were carried out using a three electrode single compartment cell equipped with SWNT modified pyrolytic graphite electrode or bare pyrolytic graphite electrode as the working electrode, platinum wire as the counter electrode and an Ag/AgCl (3M NaCl) reference electrode (BAS Model MF-2052 RB-5B). The pyrolytic graphite electrode ($\sim$6 mm^2) used as the working electrode for the electrooxidation studies was prepared in the laboratory by the reported method [39]. Experiments were performed using a BAS CV-50W voltammetric analyzer (Bioanalytical Systems, West Lafayette, IN, USA). All the potentials quoted are versus Ag/AgCl electrode at an ambient temperature of 25 $\pm$ 2 °C. Phosphate buffers of different pH were prepared from analytical grade chemicals (NaH_2PO_4 and Na_2HPO_4 from Merck) according to the reported method [40]. The pH measurements were carried out using a Century India Ltd. Digital pH-meter (Model CP-901) after due standardization with 0.05 M potassium hydrogen phthalate (pH 4.0 at 25 °C) and 0.01 M borax (pH 9.2 at 25 °C). Optimized square wave voltammetry parameters used were: initial E: 400 mV, final E: 1400 mV, square wave amplitude (E_{sw}): 25 mV, potential step (E): 4 mV, square wave frequency (f): 15 Hz. HPLC studies were performed on Agilent 1100 series system with RP-18e (5 μm) column. The mobile phase used for HPLC experiment was a mixture of 0.01 M NaH_2PO_4:methanol (60:40) at a flow rate of 0.5 mL min^{-1} and detection was carried out at 260 nm.

Working solutions of adenosine and inosine were prepared by adding required volumes of the respective stock solution to the phosphate buffer solution and then the voltammograms were recorded. Human blood samples from three healthy volunteers were obtained from the Institute hospital. The blood samples from the third trimester of normal pregnant woman were obtained from a local pathology lab. The sample with EDTA as anticoagulant was centrifuged and the supernatant was taken for analysis. Urine samples received from laboratory personnel were used after fifty times dilution with buffer.

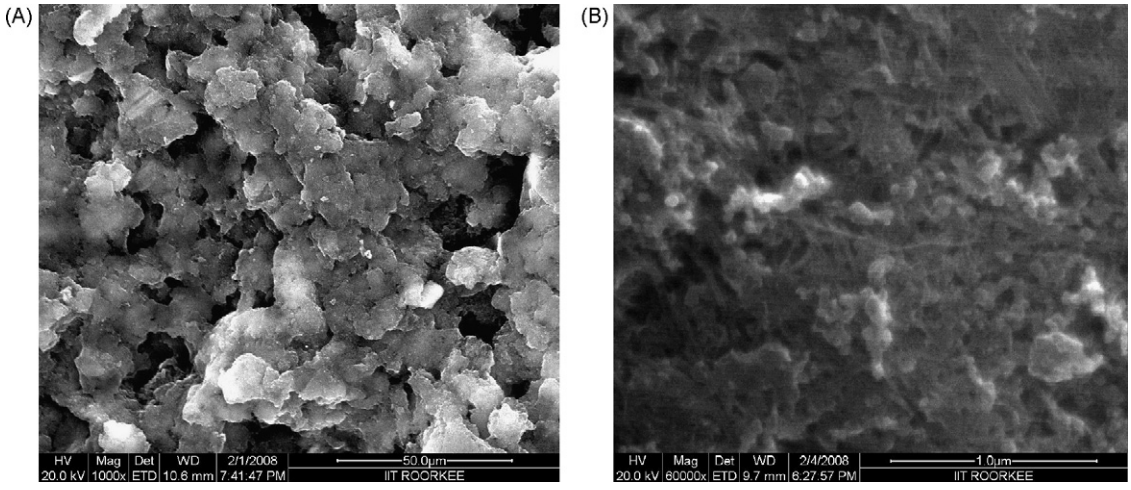

Fig. 1. (A) A typical FE-SEM image of SWNT modified pyrolytic graphite electrode and (B) high resolution image of (A).

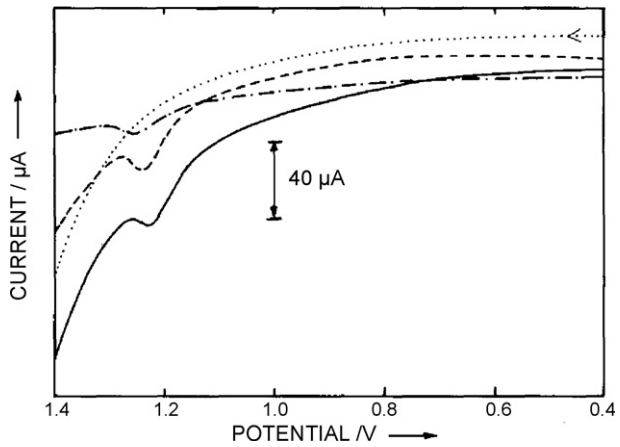

Fig. 2. A comparison of square wave voltammograms of 0.05 mM adenosine at pH 7.2 at SWNTs modified PGE (—), edge-plane graphite electrode (– – – –), basal-plane graphite electrode (–·–·–), background PBS (pH 7.2) at SWNTs modified PGE (·····).

2.3. Preparation of the modified electrode

The bare pyrolytic graphite electrode was rubbed on the emery paper and then washed with double distilled water. It was then touched softly with tissue paper. A 0.5 mg/mL suspension was prepared by dispersing 0.5 mg SWNTs in 1.0 mL *N*,*N*-dimethylformamide (DMF). A known volume (40 μL) of this suspension was coated onto the surface of the bare pyrolytic graphite electrode and dried in a stream of hot air. The working electrode surface with a well-coated layer of SWNT was then ready for use. The surface morphology of modified electrode was studied by recording SEM images as shown in Fig. 1. The images clearly indicate the deposition of SWNT at the surface of the electrode.

3. Results and discussion

3.1. Electrooxidation of adenosine

Fig. 2 compares typical Osteryoung square wave voltammograms of 0.05 mM adenosine in 0.1 M phosphate buffer solution at pH 7.2 recorded at three different working electrodes (SWNTs modified PGE, edge-plane pyrolytic graphite (EPPG) and basal-plane pyrolytic graphite (BPPG) electrodes). A poorly defined peak was observed at BPPG electrode because lesser number of edge-plane sites are exposed. At EPPG electrode the voltammetric response improves and the peak is shifted to lower oxidation potential. Under identical conditions, a well-defined oxidation peak is observed at SWNTs modified PGE where the peak shifted negatively to 1229 mV and the peak current increased remarkably. The significant enhancement in current response followed by a decrease in peak potential indicates that SWNTs modified PGE acts as a promoter to enhance the electrochemical reaction, considerably accelerating the rate of electron transfer. It also indicates that the observed voltammetric response at the SWNTs modified PGE is not due to the edge-plane sites on the SWNTs. The presence of significant amount of metal impurities within the nanotubes are likely responsible for electrocatalytic activity of SWNTs [41].

The calibration curve for adenosine was measured by using OSWV mode and the plot of i_p versus concentration (Fig. 3A) was linear in the range 0.5 μM to 1.0 mM at pH 7.2. The graph passed through the origin and the dependence of peak current (after subtracting background current) can be represented by the equation:

$$i_p(10^{-4}\text{A}) = 0.01C(\mu\text{M})$$

where C is the concentration of adenosine having a sensitivity of 1.0 μA μM^{-1} and a correlation coefficient of 0.9977. This indicated that adenosine can be safely estimated in the given concentration range. The detection limit of adenosine was found to be 0.51×10^{-7} M.

The effect of pH was studied on the peak potential (E_p) of oxidation peak of 0.05 mM adenosine in the range 3.3–10.9 (Fig. 3B) at a square wave frequency of 15 Hz. The peak potential was found to be dependent on pH and shifted to less positive potentials with increasing pH. The linear dependence of the peak potential of oxidation peak of adenosine on pH can be represented by the relation:

$$E_p(\text{pH}\,3.3-10.9) = [1533 - 42.57\text{pH}]\,\text{mV} \text{ versus Ag/AgCl}$$

having correlation coefficient 0.9978.

The effect of OSWV frequency on peak current and peak potential of adenosine was studied in the range 5–200 Hz. The peak current increases with an increase in OSWV frequency and the peak potential shifted to more positive values with increasing frequency. The plot of E_p versus log v was linear with a correlation coefficient of 0.9939 and this behavior was consistent with the EC nature of the reaction in which the electrode reaction is coupled with irreversible follow-up chemical reactions [42]. The variation of E_p with log v can be expressed by the equation:

$$E_p(\text{mV}) = 54.334 \log v + 1162.1$$

3.2. Electrooxidation of inosine

The voltammetric behavior of inosine was similarly studied at SWNTs modified PGE, EPPG and BPPG electrodes as illustrated in Fig. 4. A small bump was noticed at BPPG with a high oxidation peak potential. At EPPG, the peak potential shifted slightly to a lower value and at SWNTs modified PGE a well-defined oxidation peak was observed at 1348 mV with a significant increase in cur-

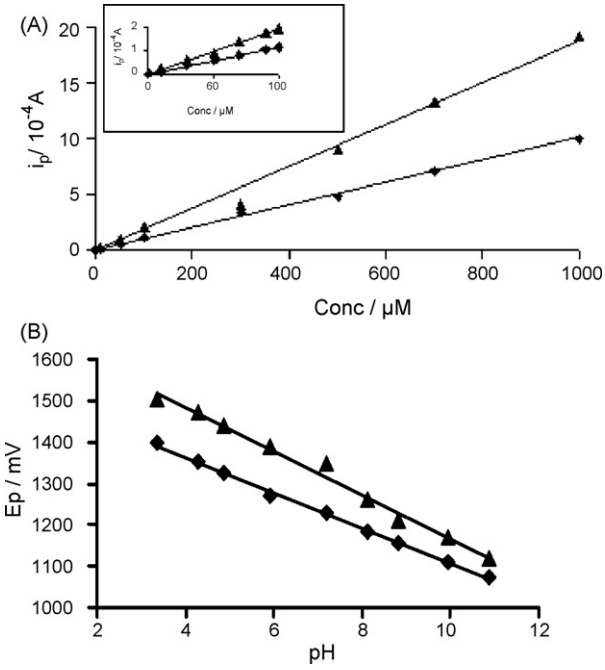

Fig. 3. (A) Dependence of observed peak current (i_p) against concentration of adenosine (■) and inosine (▲) at the SWNTs modified PGE at pH 7.2. (B) Observed dependence of peak potential (E_p) on pH for 0.05 mM adenosine (■) and inosine (▲) at the SWNTs modified PGE.

rent response. The shift of the oxidation potential to less positive values along with a remarkable increase in peak current further supported the electrocatalytic effect of SWNTs modified pyrolytic graphite electrode.

The peak current (i_p) of the oxidation peak (after correction of background current) increased with the increase in concentration of inosine at pH 7.2 as depicted in Fig. 3A. The plot was linear in the range 0.01–1.0 mM with a correlation coefficient of 0.9911. The linear regression equation is

$$i_p(10^{-4}\text{A}) = 0.0187C(\mu\text{M})$$

where C is the concentration of inosine having a sensitivity of 1.8 μA μM^{-1}. The detection limit of inosine at pH 7.2 was calculated by using the formula $3\sigma/b$, where σ is the standard deviation of the blank and b is the slope of the calibration curve and was found to be 2.04×10^{-7} M.

The peak potential of 0.05 mM inosine at modified electrode was dependent on pH and shifted to less positive potential with increase in pH (Fig. 3B). The dependence of E_p on pH can be expressed by the relation:

$$E_p(\text{pH } 3.3 - 10.9) = [1696 - 52.90\text{pH}]\,\text{mV versus Ag/AgCl}$$

with a correlation coefficient of 0.9900.

The E_p of inosine was also dependent on the square wave frequency and shifted towards more positive potential with increasing frequency. The nature of the plot of E_p versus log v was linear having a correlation coefficient of 0.9954 and is expressed by the relation:

$$E_p(\text{mV}) = 36.513 \log v + 1307.2$$

This suggested the nature of the electrode reaction as EC in which charge transfer is followed by irreversible chemical reactions. It was found that the peak current increased linearly with an increase in the square wave frequency.

3.3. Simultaneous determination of adenosine and inosine

The main aim of present study is to investigate the electrochemical responses when adenosine and inosine co-exist using the SWNTs modified pyrolytic graphite electrode. Fig. 5 shows square wave voltammograms for different concentrations of inosine keeping the concentration of adenosine constant (0.05 mM). It clearly depicts that inosine signal increases with increase in its concentration without affecting the adenosine signal. Similarly, Fig. 6 shows

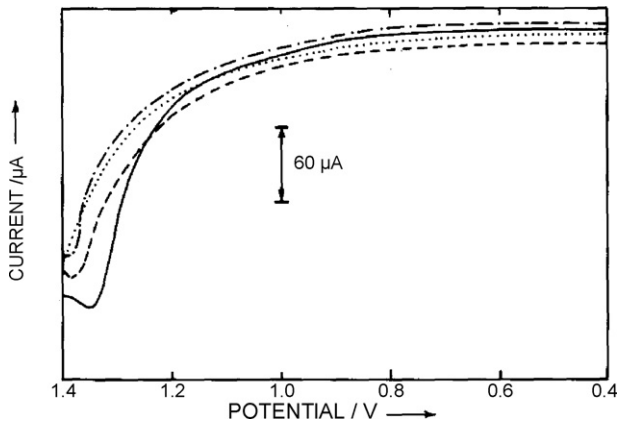

Fig. 4. A comparison of square wave voltammograms of 0.05 mM inosine at pH 7.2 at SWNTs modified PGE (—), edge-plane graphite electrode (– – – –), basal-plane graphite electrode (– – –), background PBS (pH 7.2) at SWNTs modified PGE (· · · · · ·).

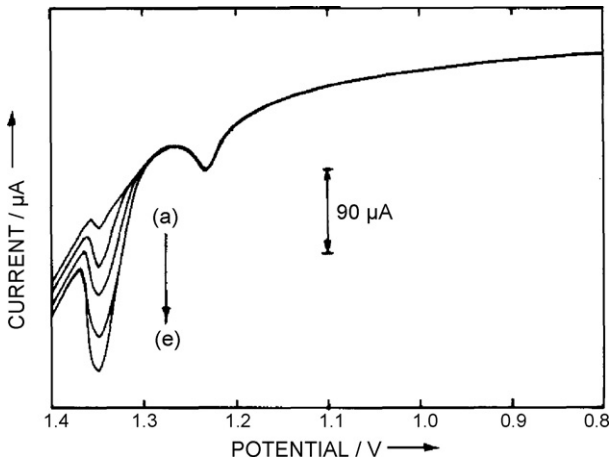

Fig. 5. Square wave voltammograms of a mixture of adenosine and inosine at SWNTs modified pyrolytic graphite electrode at pH 7.2. Concentration of inosine was changed (a) 0.01, (b) 0.03, (c) 0.05, (d) 0.07 and (e) 0.09 mM, keeping the concentration of adenosine constant (0.05 mM).

square wave voltammograms obtained by varying the concentration of adenosine keeping the concentration of inosine constant (0.05 mM). It was found that the voltammetric peak of inosine was unaltered and the peak current remained almost constant. The voltammetric signal of adenosine increased with increase in its concentration. Individual voltammetric curves of adenosine and inosine are identical to the voltammetric curves observed in the mixture of both the compounds. It was found that neither adenosine nor inosine interfere with the oxidation signals of each other and thus, the proposed method can be successfully used for the simultaneous quantitative determination of adenosine and inosine.

3.4. Stability and reproducibility of the modified electrode

The long-term stability of the SWNTs modified PGE was evaluated by measuring the voltammetric current response of fixed concentration of adenosine (0.05 mM) and inosine (0.05 mM) after the modified electrode was stored for approximately 1 week. Only a minimal decrease of current sensitivity with a relative standard deviation (R.S.D.) of about 3.82% for adenosine and 4.45% for inosine was observed which can be attributed to the excel-

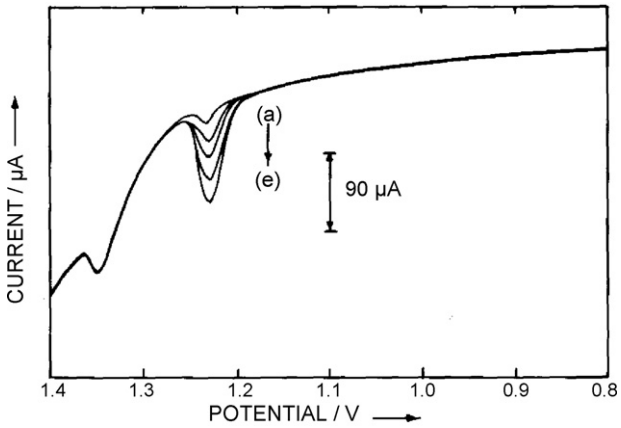

Fig. 6. Square wave voltammograms of a mixture of adenosine and inosine at SWNTs modified pyrolytic graphite electrode at pH 7.2. Concentration of adenosine was changed keeping the concentration of inosine constant [(inosine) = 0.05 mM; (adenosine): (a) 0.01, (b) 0.03, (c) 0.05, (d) 0.07 and (e) 0.09 mM].

lent stability of the modified electrode. The reproducibility of the modified electrode has also been investigated. The intra-day precision of the method was evaluated by repeating six experiments in the same solution containing 0.05 mM of adenosine and 0.05 mM of inosine taken separately using the same SWNTs modified PGE. The R.S.D. was found to be 0.74% and 1.26% for adenosine and inosine, respectively, indicating excellent reproducibility of the modified electrode. Further, inter-day precision was investigated by measuring the current response of the modified electrode for 6 consecutive days for the same concentration of adenosine (0.05 mM) and inosine (0.05 mM) taken separately and the respective relative standard deviations were found to be 1.37% and 2.43%. Thus, it demonstrated the good reproducibility of the method at the SWNTs modified pyrolytic graphite electrode.

3.5. Effect of the amount of SWNTs

The effect of different quantity of SWNTs on the peak current response of adenosine and inosine was studied. Different volumes of the suspension prepared by dispersing SWNTs in *N*,*N*-dimethylformamide were casted on the electrode surface. It was observed that up to 40 μL there was an increase in the peak current response of 0.1 mM of both the compounds. At SWNTs volume more than 40 μL, the peak current response of both the nucleosides became almost constant. Therefore, it can be stated that the optimum amount of SWNTs required to catalyze the oxidation of these nucleosides is 40 μL and is used in these studies.

3.6. Effect of interferents

Ascorbic acid, uric acid, xanthine and hypoxanthine are common biological metabolites present in living systems which can interfere in the electrochemical studies of adenosine and inosine by influencing their peak potential and peak current response. The effect of these metabolites on the voltammetric peak response of 0.05 mM adenosine and 0.05 mM inosine was studied. It was observed that up to 10-fold excess of each of the interferents there was no remarkable change in the peak current response. However, uric acid and hypoxanthine showed >10% change in peak current of inosine when present at concentrations greater than 10-fold excess. The variation in peak current response of adenosine and inosine on adding different amounts of interferents is summarized in Table 1.

Table 1
Influence of interferents on i_p value of adenosine and inosine

Interferent	Concentration of interferents (mM)	Change in i_p of adenosine		Change in i_p of inosine	
		(10^{-5} A)	(%)	(10^{-5} A)	(%)
Ascorbic acid	0.05	0.022	0.39	0.080	0.89
	0.10	−0.008	0.14	0.074	0.83
	0.25	−0.034	0.61	0.026	0.29
	0.50	0.096	1.71	0.008	0.09
	0.75	0.130	2.32	0.610	6.82
Uric acid	0.05	−0.033	0.59	0.013	0.14
	0.10	−0.033	0.59	0.022	0.25
	0.25	−0.050	0.89	−0.013	0.14
	0.50	0.090	1.60	0.326	3.65
	0.75	0.458	8.17	1.242	13.89
Xanthine	0.05	0.010	0.18	0.000	0.00
	0.10	0.009	0.16	0.062	0.69
	0.25	0.026	0.46	0.065	0.73
	0.50	0.058	1.03	0.179	2.00
	0.75	0.384	6.85	0.328	3.58
Hypoxanthine	0.05	−0.056	1.00	−0.037	0.41
	0.10	−0.030	0.53	−0.037	0.41
	0.25	0.009	0.16	−0.039	0.44
	0.50	0.072	1.28	−0.237	2.65
	0.75	0.120	2.14	−0.951	10.64

Table 2
Recovery of adenosine and inosine added to human blood plasma

	Spiked (μM)	Detected (μM)	Recovery (%)
Adenosine			
Sample 1	10.0	10.15	101.50
	50.0	52.30	104.60
	90.0	89.92	99.91
Sample 2	10.0	9.88	98.80
	50.0	50.60	101.20
	90.0	92.17	102.41
Sample 3	10.0	10.25	102.50
	50.0	49.95	99.90
	90.0	91.32	101.47
Inosine			
Sample 1	30.0	30.34	101.13
	60.0	59.86	99.77
	90.0	91.24	101.38
Sample 2	30.0	30.09	100.30
	60.0	61.37	102.28
	90.0	90.80	100.89
Sample 3	30.0	30.96	103.20
	60.0	61.14	101.90
	90.0	91.65	101.83

3.7. Real sample analysis

3.7.1. Human blood plasma

The utilization of the SWNTs modified pyrolytic graphite electrode for the determination of adenosine and inosine in a real sample was tested by measuring their concentration in three human blood plasma samples. Purines present in the blood can pass through the cell membrane and enter the blood stream and thus can be measured in plasma. Literature survey reveals that adenosine concentration in normal human blood plasma ranges between 0.05 μM and 0.1 μM [43–45] which is very low. Inosine concentration in human blood plasma is also very low. However, their concentrations increase in the case of diseases such as septic shock, etc. Hence, it was decided to detect the concentration of adenosine and inosine in human blood plasma by standard addition method. The samples were diluted 10 times with pH 7.2 phosphate buffer solution before analysis. The concentration of adenosine and inosine in the plasma was calculated after spiking the samples with a measured amount of their standard solutions. The results obtained are presented in Table 2. It was observed that in majority of cases the amount of inosine recovered was higher than the spiked one. The recoveries were found to be 98.80–104.60% for adenosine and 99.77–103.20% for inosine.

3.7.2. Human urine

The practical analytical application of the method was further established by the selective measurement of adenosine and inosine in human urine without any preliminary treatment. Two human urine samples obtained from laboratory personnel were used for determination and were diluted 50 times with pH 7.2 phosphate buffer solution prior to analysis to minimize the complexity of matrix. Then, the samples were spiked with certain amounts of adenosine and inosine subsequently followed by recording their Osteryoung square wave voltammograms. The results are summarized in Table 3. The recovery rates ranged from 95.80 to 101.50% for adenosine and 99.69–101.39% for inosine, respectively.

Table 3
Analytical recovery of adenosine and inosine added to urine samples

	Added (μM)	Found (μM)	Recovery (%)
Adenosine			
Sample 1	10.0	10.12	101.20
	40.0	40.60	101.50
	60.0	59.94	99.90
Sample 2	10.0	9.58	95.80
	40.0	40.04	100.10
	60.0	58.98	98.30
Inosine			
Sample 1	50.0	50.04	100.08
	70.0	69.82	99.74
	90.0	91.25	99.90
Sample 2	50.0	51.18	101.39
	70.0	70.08	100.11
	90.0	89.72	99.69

3.8. Validation of the method

The results of the voltammetric determination were cross-validated with HPLC analysis. For this purpose, various concentrations of adenosine and inosine were analyzed using HPLC and the peak area under the peak was calculated. The calibration curve was obtained by plotting the peak area ratio of the analyte peaks relative to that of the dexamethasone as internal standard (1.0 g/100 mL) against the analyte concentration. The concentration of adenosine and inosine in the blood plasma of pregnant women in their third trimester was determined. Fig. 7 shows a typical HPLC chromatogram of blood plasma and five peaks are observed at R_t ~3.225, 3.469, 3.717, 4.349 and 4.879 min. The peak at R_t ~3.225 min is found to be due to adenosine and that at R_t ~4.349 min is due to inosine. No attempt was made to identify other peaks. As concentration of insoine in these blood plasma samples is expected to be very low, the actual concentration is determined by spiking the samples. A comparison of the concentration of adenosine and inosine obtained by HPLC and proposed method (Table 4) clearly indicate that the results obtained by the two methods are in good agreement and close to the values reported in literature [22].

Table 4
A comparison of observed concentration of adenosine and inosine in blood plasma of pregnant women in third trimester at SWNTs modified PGE and by using HPLC

Added (μM)	Found (μM)	Diluted concentration (μM)[a]	Actual concentration (μM) by	
			Modified PGE	HPLC
Adenosine				
Sample 1				
0.00	0.05	0.05	0.50	0.51
0.50	0.56	0.06	0.60	0.60
1.00	1.55	0.05	0.50	0.54
Sample 2				
0.00	0.04	0.04	0.40	0.50
1.00	1.04	0.04	0.40	0.46
1.50	2.55	0.05	0.50	0.54
Inosine				
Sample 1				
0.0	–	–	–	0.24
2.50	2.52	0.02	0.20	0.20
5.00	7.53	0.03	0.30	0.26
Sample 2				
0.0	–	–	–	0.26
2.50	2.53	0.03	0.30	0.28
4.00	6.52	0.02	0.20	0.28

[a] Blood plasma were diluted ten times before analysis.

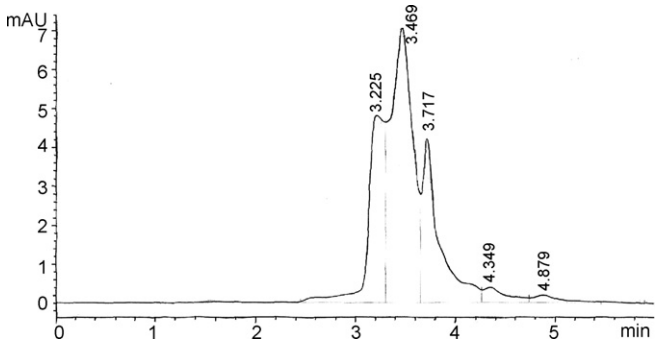

Fig. 7. A typical HPLC chromatogram observed for blood plasma (Sample 1) of pregnant woman in her third trimester.

4. Conclusions

The single-wall carbon nanotubes modified pyrolytic graphite electrode exhibited remarkable electrocatalytic effects on the oxidation of adenosine and inosine by increasing their oxidation peak currents and lowering their oxidation peak potentials. The modified electrode showed a marked increase in the sensitivity of adenosine and inosine by accelerating the rate of electron transfer of these compounds. It successfully separated the voltammetric signals of adenosine and inosine which are ~119 mV apart. The molecular electrochemistry of adenosine and inosine has already been reported in literature at pyrolytic graphite electrode [42,46] and products of oxidation have been identified. The present investigation demonstrates the simultaneous determination of both the biomolecules with a detection limit of 0.51×10^{-7} M for adenosine and 2.04×10^{-7} M for inosine. The detection limit of adenosine found in the present method is about six times lower than previously reported in literature [47] using fullerene-C_{60}-modified glassy carbon electrode and slightly lower as compared to nanogold modified indium tin oxide electrode (0.70×10^{-7} M) [48].

The electrode showed good sensitivity, selectivity, reproducibility and high stability with remarkable electrocatalytic properties. The method described above requires less time and is easy to perform. The utility of the proposed method was demonstrated by the determination of adenosine and inosine in human blood plasma and urine samples. The plasma level of adenosine increases in patients with septic shock (~8 μM) [19], vasoplegia and postoperative severe systemic inflammatory response (~1.6 μM) [21], severe preeclampsia (~0.72 μM) [20], and in the third trimester of normal pregnancy (~0.59 μM) [22]. The concentration of adenosine also increases significantly in the pericardial fluid of patients suffering from coronary artery disease (~1.5 μM) and valvular heart disease (~0.7 μM) [23] which lie in our detectable range. The plasma and urine levels of inosine have been found to increase to 5 μM in case of inborn errors of metabolism [49]. Similarly, inosine levels increase remarkably in the coronary sinus of patients undergoing CABG (~2 μM) [24] which can be easily detected by the proposed method. The present method can also be applied to determine alteration of these nucleotides level in traumatic head injury, acute myocardial infarction, stroke, etc. [49]. Thus, in the present study an electroanalytical approach for the simultaneous determination of adenosine and inosine using single-wall carbon nanotubes modified pyrolytic graphite electrode is reported with application in biological samples also and the proposed method is comparable to HPLC.

Acknowledgments

One of the authors (S. Chatterjee) is thankful to the Council of Scientific and Industrial Research, New Delhi for the award of Junior Research Fellowship. Financial assistance for this work was provided by the Council of Scientific and Industrial Research, New Delhi vide Grant no. 01/2045/06-EMR-II.

References

[1] A.M. Tesch, Modulation of chondrocyte activity via cell surface receptor stimulation, 2004, 166.
[2] M. Pritchard, J. Ouzman, E. Savory, G. Brown, Int. Appl. (2005) 81.
[3] K. Vijayalakshmi, V.J. Whittaker, B. Kunadian, J. Graham, R.A. Wright, J.A. Hall, A. Sutton, M.A. de Belder, Heart 92 (2006) 1278.
[4] E.O. Feigl, Am. J. Physiol. 287 (2004) 1891.
[5] J.W. Phillis, Crit. Rev. Neurobiol. 16 (2004) 237.
[6] A. Nishiyama, M. Rahman, E.W. Inscho, Hypertens. Res. 27 (2004) 791.
[7] Harry E. Gruber, US Patent 5,030,623, 1991.
[8] R. Basheer, T. Porkka-Heiskanen, R.E. Strecker, M.M. Thakkar, R.W. McCarley, Biol. Signals Recept. 9 (2000) 319.
[9] A. Sollevi, US Patent 5,449,665, 1995.
[10] C. Martin, M. Leone, X. Viviand, M.L. Ayem, R. Guieu, Crit. Care Med. 28 (2000) 3198.
[11] E.K. Jackson, US Patent 6,566,371, 2003.
[12] L. Schneider, M. Pietschmann, W. Hartwig, M.S. Sevillano, T. Hackert, Martha-Maria Gebhard, W. Uhl, M.W. Buchler, J. Werner, Am. J. Surg. 191 (2006) 510.
[13] A.L. Salzman, C. Szabo, US Patent 6,958,324, 2005.
[14] D. Farthing, D. Sica, T. Gehr, B. Wilson, I. Fakhry, T. Larus, C. Farthing, H. Thomas Karnes, J. Chromatogr. B 854 (2007) 158.
[15] D. Laxminarayana, K.S. O'Rourke, S. Mass, I. Olorenshaw, Immunology 121 (2007) 359.
[16] S. Heptinstall, A. Johnson, J.R. Glenn, A.E. White, J. Thromb. Haemost. 3 (2005) 2331.
[17] E.Y. Levanon, E. Eisenberg, R. Yelin, S. Nemzer, M. Hallegger, R. Shemesh, Z.Y. Fligelman, A. Shoshan, S.R. Pollock, D. Sztybel, M. Olshansky, G. Rechavi, M.F. Jantsch, Nat. Biotechnol. 22 (2004) 1001.
[18] J.V. Retey, M. Adam, E. Honegger, R. Khatami, U.F.O. Luhmann, H.H. Jung, W. Berger, H.P. Landolt, Proc. Natl. Acad. Sci. U.S.A. 102 (2005) 15676.
[19] C. Martin, M. Leone, X. Viviand, Crit. Care Med. 28 (2000) 3198.
[20] Y. Yoneyama, S. Suzuki, R. Sawa, K. Yoneyama, G.G. Power, T. Araki, Obstet. Gynecol. 100 (2002) 1266.
[21] F. Kerbaul, F. Collart, R. Giorgi, Z. Ibrahim, J.C. Guillen, J.M. Gil, A. Saadjian, A. Mouly-Bandini, G. Habib, F. Gouin, R. Guieu, Crit. Care Med. 34 (2006) 640.
[22] Y. Yoneyama, S. Suzuki, R. Sawa, Y. Otsubo, G.G. Power, T. Araki, Am. J. Obstet. Gynecol. 182 (2000) 1200.
[23] L. Fazekas, F. Horkay, V. Kekesi, E. Huszar, E. Barat, R. Fazekas, T. Szabo, A. Juhasz-Nagy, A. Naszlady, Life Sci. 65 (1999) 1005.
[24] B.F. Becker, S. Zahler, T. Freyholdt, P. Massoudy, Drug Dev. Res. 45 (1998) 159.
[25] B.J. Venton, S. Cechova, Abstracts, 59th Southeast Regional Meeting of the American Chemical Society, Greenville, SC, United States, October 24–27, 2007.
[26] B.E.K. Swamy, B.J. Venton, Anal. Chem. 79 (2007) 744.
[27] Y. Yang, L. Shi, Fenxi Huaxue 28 (2000) 219.
[28] L. Liu, J. Song, P. Yu, B. Cui, Electrochem. Commun. 8 (2006) 1521.
[29] A. Mei David, J. Gross Garrett, K. Nithipatikom, Anal. Biochem. 238 (1996) 34.
[30] F.Q. Yang, J. Guan, S.P. Li, Talanta 73 (2007) 269.
[31] F.Q. Yang, S. Li, P. Li, Y.T. Wang, Electrophoresis 28 (2007) 1681.
[32] H.F. Tzeng, C.H. Hung, J.Y. Wang, C.H. Chou, H.P. Hung, J. Chromatogr. A 1129 (2006) 149.
[33] L. Yu, J. Zhao, S.P. Li, H. Fan, M. Hong, Y.T. Wang, Q. Zhu, J. Sep. Sci. 29 (2006) 953.
[34] Y.X. Gong, S.P. Li, P. Li, J.J. Liu, Y.T. Wang, J. Chromatogr. A 1055 (2004) 215.
[35] F. Valentini, A. Amine, S. Orlanducci, M.L. Terranova, G. Palleschi, Anal. Chem. 75 (2003) 5413.
[36] J. Wang, M. Musameh, Y. Lin, J. Am. Chem. Soc. 125 (2003) 2408.
[37] C.H. Wang, C.Y. Li, C.F. Wang, Microchim. Acta 152 (2006) 233.
[38] J. Wang, M. Li, Z. Shi, N. Li, Z. Gu, Anal. Chem. 74 (2002) 1993.
[39] F.J. Miller, H.E. Zittel, Anal. Chem. 35 (1963) 1866.
[40] G.D. Christian, W.C. Purdy, J. Electroanal. Chem. 3 (1962) 363.
[41] C.E. Banks, A. Crossley, C. Salter, S.J. Wilkins, R.G. Compton, Angew. Chem. Int. Ed. 45 (2006) 2533.
[42] R.N. Goyal, A. Sangal, J. Electroanal. Chem. 521 (2002) 72.
[43] Z. Csoma, E. Huszar, E. Vizi, G. Vass, Z. Szabo, I. Herjavecz, M. Kollai, I. Horvath, Eur. Respir. J. 25 (2005) 873.
[44] E. Vizi, E. Huszar, Z. Csoma, G. Boszormenyi-Nagy, E. Barat, I. Horvath, I. Herjavecz, M. Kollai, J. Allergy Clin. Immunol. 109 (2002) 446.
[45] P. Dolezalova, J. Krijt, J. Chladek, D. Nemcova, J. Hoza, Rheumatology 44 (2005) 74.
[46] R.N. Goyal, A. Tyagi, Electrochim. Acta 51 (2006) 5095.
[47] R.N. Goyal, V.K. Gupta, M. Oyama, N. Bachheti, Talanta 71 (2007) 1110.
[48] R.N. Goyal, M. Oyama, S.P. Singh, Electroanalysis 19 (2007) 575.
[49] B. Tavazzi, G. Lazzarino, P. Leone, A.M. Amorini, F. Bellia, C.G. Janson, V.D. Pietro, L. Ceccarelli, S. Donzelli, J.S. Francis, B. Giardina, Clin. Chem. 38 (2005) 997.

Talanta 76 (2008) 656–661

Contents lists available at ScienceDirect

Talanta

journal homepage: www.elsevier.com/locate/talanta

Separation of chromium(III) and chromium(VI) by ion chromatography and an inductively coupled plasma mass spectrometer as element-selective detector

Harald Hagendorfer, Walter Goessler*

Institute of Chemistry-Analytical Chemistry, Karl-Franzens University Graz, Universitaetsplatz 1, 8010 Graz, Austria

ARTICLE INFO

Article history:
Received 14 January 2008
Received in revised form 1 April 2008
Accepted 7 April 2008
Available online 16 April 2008

Keywords:
Chromium(III)
Chromium(VI)
Chromium speciation
HPLC–ICPMS
Chromate

ABSTRACT

Due to its extensive use in industrial processes, large quantities of chromium compounds are discharged into the environment. Common approaches for the speciation of Cr employ the determination of Cr(VI) and total Cr. The focus of the present work was a separation of Cr(III) and Cr(VI) species, with a minimum of sample preparation, by keeping an eye on the more relevant and toxic Cr(VI). For the successful simultaneous separation of both chromium species we implemented a RSpak NN-814 4DP (PEEK, 4 mm × 150 mm) multi-mode column using an eluent containing 90 mM ammonium sulfate and 10 mM ammonium nitrate, adjusted to pH 3.5. At a flow of 0.3 mL min^{-1} the separation of both Cr species was possible within 8 min.

Further the octopole reaction system of the inductively coupled plasma mass spectrometer was systematically studied and optimised to reduce the influence of polyatomic interferences.

The major advantage of the developed method compared to published methods is that a derivatisation of the Cr(III) species – an invasion in the speciation – is not required. With the used multi-mode column both chromium species are retained. Furthermore the pH of the mobile phase (pH 3.5) prevents reduction of Cr(VI) as well as precipitation of Cr(III) during the analysis.

A limit of determination of ~0.5 μg L^{-1} for both chromium species with an injection volume of 25 μL was obtained. The optimised method was successfully applied to the determination of Cr(VI) in cement samples as well as chromium speciation analysis in homeopathic drugs.

1. Introduction

Chromium is used in several industrial processes and products like electroplating, dyes and pigments, additives in cooling water, leather and wood preservation and cement manufacturing. As a consequence chromium is emitted into the environment. The toxicity as well as the mobility and bioavailability of chromium, depend on its chemical form [1,2]. Thus, a detailed knowledge of the speciation rather than the total chromium level is required to evaluate physiological and toxicological effects of chromium. As a result of the ambivalent nature of chromium the development of speciation techniques with high sensitivity and sufficient selectivity is a challenge for analytical chemists.

Besides ICPMS other detectors such as UV-VIS spectrometry [3–5], fluorescence spectrometry [6,7], thermal lens spectroscopy [8], and ICPOES [9] have been used. The low detection limits and wide linear range of ICPMS make it superior to the above mentioned detectors. A drawback of ICPMS is the occurrence of polyatomic interferences on the two most abundant isotopes, ^{52}Cr and ^{53}Cr. At m/z 52 the most severe interference arises from carbon (e.g. $^{40}Ar^{12}C$). Also chlorine influences the measurement due to polyatomics such as $^{35}Cl^{16}O^{1}H$ and $^{37}Cl^{16}O$ at masses 52 and 53.

For the preservation and separation of the chromium species already at the sampling cation-exchange resins have been employed [10,11]. Other separation modes described in the literature include a flow injection on-line desalter [12], reversed-phase chromatography [13,14] and selective extraction methods [15].

Most commonly ion chromatography is used for the separation of the chromium species. Powell and Boomer [16] used a microcolumn, specially packed with an anion-exchange resin for Cr speciation. Unlike the other methods presented, Pantsar-Kallio and Manninen [17] worked with a coupled column system consisting of a cation- and an anion-exchange column. Vonderheide et al. [18] used high performance chelation ion chromatography with 2,6-pyridine dicarboxylic acid as chelating agent for the separation of both chromium species. Byrdy et al. [19], Inoue et al. [20], as well as Gürleyük and Wallschläger [21], used an anion-exchange column for the separation of Cr(III) and Cr(VI). In order to retain

* Corresponding author. Tel.: +43 316 380 5302; fax: +43 316 380 9845.
E-mail address: walter.goessler@uni-graz.at (W. Goessler).

0039-9140/$ – see front matter © 2008 Elsevier B.V. All rights reserved.
doi:10.1016/j.talanta.2008.04.010

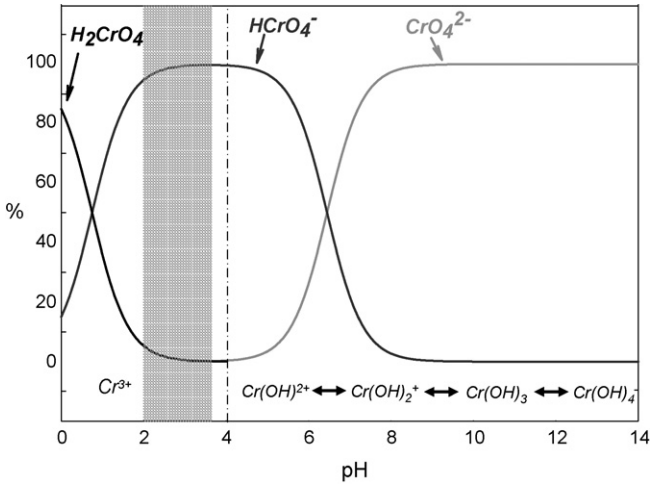

Fig. 1. Species distribution diagrams of Cr(III) and Cr(VI) in an aqueous system.

Cr(III) on the anion-exchange column, a pre-column chelation step with ethylenediamine-tetraacetic-acid (EDTA) and heating was used.

Although the complexation of Cr(III), for example with EDTA, seems to overcome the issue of different charged chromium species, an intervention in the sample system is given and thus the original speciation is changed. To avoid this problem, Barnowski et al. [22] as well as Seby et al. [23] used a column which showed anion- and cation-exchange properties. Like stated from the authors, the main problem of the reported methods is the use of nitric acid as mobile phase. Increasing the nitric acid concentration, necessary to elute all analytes, results in the formation of H_2CrO_4—a strong oxidizing agent. In consequence species conversion during the analysis was reported.

The aim of the present work was the development of a chromatographic separation in which Cr(III) as well as Cr(VI) species are retained without the use of chelating agents like ethylenediamine-tetraacetic-acid (EDTA) or similar compounds. Furthermore the used chromatographic conditions should guarantee the stability as well as the solubility of both chromium species (Fig. 1) during the analysis.

A metal-free chromatographic system together with a multimode Shodex RSpak NN-814 4DP PEEK column was used for this purpose. Aqueous solutions of ammonium sulfate/ammonium nitrate adjusted to pH 3.5 served as mobile phases and an ICPMS equipped with collision/reaction cell technology was applied for detection.

With the optimised method Cr(VI) in cement, regulated by the European Union [24], was determined. Additionally we investigated the Cr speciation in extracts of a homeopathic drug containing potassium dichromate.

2. Experimental

2.1. Chemicals

All solutions were prepared in 18 MΩ cm pure water. For a 1000 mg Cr(III) L^{-1} solution 775.4 mg $Cr(NO_3)_3 \cdot 9H_2O$ (p.a., Merck, Darmstadt) were dissolved with water in a 100 mL volumetric flask. For the 1000 mg Cr(VI) L^{-1} solution 285.2 mg $K_2Cr_2O_7$ (p.a., Merck, Darmstadt) were dissolved with water in a 100 mL volumetric flask.

The pH of the Cr(III) and Cr(VI) stock solutions was adjusted to pH 1 by adding an amount of 0.7 mL 65% w/w of nitric acid to guarantee long time stability. The Cr(III) and Cr(VI) concentration of the stock solutions were measured by FAAS. The used apparatus was a GBC Avanta Σ (GBC Scientific Equipment PTY LTD, Australia) flame atomic absorption spectrometer. The standards for calibration were made by dilution of a certified standard solution (Peak Performance CRM, Cr in 2% HNO_3; P/N S4400-1000121) with a certified chromium concentration of 1000 ± 3 μg mL^{-1}.

All chemicals used were of pro analysis or better grade. For the mobile phase 99.999% ammonium nitrate (Alfa Aesar, Puratronic, Karlsruhe, Germany) and 99.5% ammonium sulfate (Fluka Chemie GmbH, Traceselect, Buchs, Switzerland) were used. For pH adjustment of the mobile phase double distilled 65% w/w nitric acid (Merck, Darmstadt) was used. All standards for method development were diluted with eluent solution or 18 MΩ cm water.

2.2. Chromatography

For method development a Shodex RSpak NN-614 steel column (6 mm × 150 mm) and an Agilent 1100 HPLC System (Agilent, Waldbronn, Germany) was used.

The final chromatographic setup consisted of an IC 25 chromatograph, a LC 25 chromatography oven and an AS 50 autosampler (Dionex, Sunnyvale, USA). All parts of the chromatographic system were connected with PEEK (polyether-ether-ketone) capillaries. The pump and the injector were built without any metal parts to ensure that no chromium contamination from the chromatographic system was possible. With this metal-free system a custom made Shodex PEEK column (NN-814 4DP) with a dimension of 4 mm × 150 mm was used. The columns were packed with polyhydroxymethacrylate with trace amounts of sulfo-groups. The stationary phase ensured reversed-phase separation as primary chromatographic mode. However, due to the sulfo-groups cation interaction may also take place. Due to the producer the column also shows an ion-exclusion mode.

2.3. ICPMS instrumentation

Typical settings for the ICPMS and the chromatographic system are given in Table 1. Detection took place on an Agilent 7500ce ICPMS with ORS (octopole reaction system). The sampler cone was made from copper with platinum tips, the skimmer cone was made from nickel. For sample introduction a Polycarb-400 and a PFA-100, both microflow nebulisers purchased from CPI International (CPI International, Amsterdam, Netherlands), were used. For total determination of chromium also the PFA-100 nebuliser was used.

Table 1
Typical ICPMS and chromatographic system settings used

Instrument	Agilent 7500ce
Nebuliser	Polycarb 400/PFA 100
RF-Power	1500 W
Carrier gas flow	0.74 L min^{-1}
Make-up flow	0.25 L min^{-1}
Plasma gas flow	15 L min^{-1}
Collision gas type and flow	He, 4.0 mL min^{-1}
Cell entrance	−32 V
Cell exit	−40 V
Octopole bias	−15 V
Quardupole bias	−19 V
Spray chamber temperature	2 °C
Integration time per amu	100 ms
Monitored amu	*m/z* 52; *m/z* 53
Column	Shodex Rspak NN-814 4DP
Mobile phase	90 mM ammonium sulfate + 10 mM ammonium nitrate; pH 3.0–3.5
Flow rate	0.3 mL min^{-1}
Temperature	40 °C
Injection volume	25 μL

To minimize the background arising from the mobile phase and the column on m/z 52 and m/z 53 He was used as collision gas.

For data acquisition the isotopes ^{52}Cr and ^{53}Cr with an integration time of 100 ms per isotope were chosen. The ratio of ^{52}Cr and ^{53}Cr was always used to check for spectral interferences.

2.4. Sample preparation for cement

For determination of water soluble chromium in cement, an extraction procedure for Cr(VI) released by the federal institute for occupational safety and health of Germany (TRGS 613) [25] was used. After extraction the samples were centrifuged, filtered (0.45 μM) and further diluted with water (1 + 24).

2.5. Sample preparation for homeopathic drugs

Total chromium determinations in the samples were carried out by ICPMS after mineralisation with nitric acid in an UltraCLAVE II microwave digestion system (EMLS, Leutkirch, Germany). After microwave digestion, the samples were diluted with deionised water. For quality control the certified standard material NIST-SRM 8418 (Wheat gluten) was available to us.

Samples for determination of both chromium species by HPLC–ICPMS were prepared by dissolving one tablet (0.25 g) in 10 g deionised water or 0.1 M HCl (simplified gastric juice) and shaking for about 10 min. For chromatographic measurement the solution was further diluted (1 + 9) with deionised water or 0.1 M HCl and filtered trough a 0.45 μm Nylon membrane filter.

3. Results and discussion

3.1. Method development

From the species distribution diagrams depicted in Fig. 1 it can be clearly seen that there is only a small pH-range (shaded area) were both chromium species are present in ionic form. At pH-values above 4 Cr(III) starts to form insoluble hydroxo-aqua complexes, pH-values below 2 are not recommended for the column as well as formation of H_2CrO_4.

3.2. Steel column

In a first attempt a Shodex RSpak NN-614 steel column was used for the separation of Cr(III) and Cr(VI) which has been successfully used for the separation of anionic, neutral, and cationic arsenic compounds [26]. First we used the published conditions (8 mM nitric acid/5 mM ammonium nitrate, flowrate of 0.4 mL min^{-1}; pH 2.1) for the separation of the chromium species. The injection of 25 μL of a 50 μg Cr(III) L^{-1} and 50 μg Cr(VI) L^{-1} standard solution produced no signal within 60 min. Higher flow rates were not possible due to the pressure limits for the column (2×10^6 Pa). In order to elute the chromium species we raised the ionic strength to 30 mM ammonium nitrate and adjusted the pH to 3.5 with nitric acid. Cr(III) eluted after 20 min but Cr(VI) still did not elute within 60 min. With a 40 mM ammonium sulfate solution, Cr(III) eluted but was split into two peaks at 6 and 22 min. Cr(VI) was not eluted within 30 min. Using a mixed solution of 60 mM ammonium sulfate and 40 mM ammonium nitrate resulted in a separation of both chromium species within 10 min.

Thereafter, the influence of the temperature on the separation was studied. Higher temperatures shortened the retention times for Cr(VI) and improved its signal width. The retention time for Cr(III) was not influenced by the temperature but the signals became also sharper. In order to get a clear separation, the ammonium sulfate and ammonium nitrate concentrations had to be readjusted. With a mobile phase of 70 mM ammonium sulfate and 30 mM ammonium nitrate a successful separation at 40 °C was obtained.

After optimizing the chromatographic separation, the detection conditions using ICPMS were systematically investigated. Irrespective of the tuning conditions on the ICPMS, high background signals at m/z 52 and m/z 53 were obtained. Therefore, we speculated that some parts in our experimental setup (conventional HPLC, column) and polyatomic interferences were contributing to the high background at m/z 52 and m/z 53.

To assess a possible contamination from the HPLC system the column was mounted into a full PEEK chromatographic system (IC25A Dionex, Sunnyvale, USA). Surprisingly the background decreased only about 10%. Thus, we speculated that the high background arose from the steel body of the column and/or due to polyatomic interferences from the sulfur containing mobile phase (e.g. $^{34}S^{18}O$, $^{34}S^{18}O^{1}H$).

3.3. PEEK column

To see the contribution of the columns steel body to the background signal, we replaced the steel column by a custom made metal-free PEEK column. The Shodex RSpak NN-814 4DP was filled with the same stationary phase as the RSpak NN-614, but had a different column diameter (4 mm instead of 6 mm). Because of the lower inner diameter, better peak-shapes at lower flow rates were anticipated. Additionally the lower flow rate is of benefit for microflow nebulisers as flow splitting is not necessary.

Replacing the steel column with the NN-814 4DP metal-free PEEK column resulted in a six fold decrease of the background. However, although the RSpak NN-814 4DP PEEK column is filled with exactly the same stationary phase as the steel column, separation with a 70 mM ammonium sulfate and 30 mM ammonium nitrate mobile phase was not successful. Therefore, the mobile phase composition was reoptimised for the NN-814 4DP PEEK column. A mixture of 10 mM ammonium nitrate and 90 mM ammonium sulfate was found as the optimum mobile phase composition. The influence of various concentrations of ammonium nitrate and ammonium sulfate on the retention behaviour of Cr(III) and Cr(VI) is shown in Fig. 2.

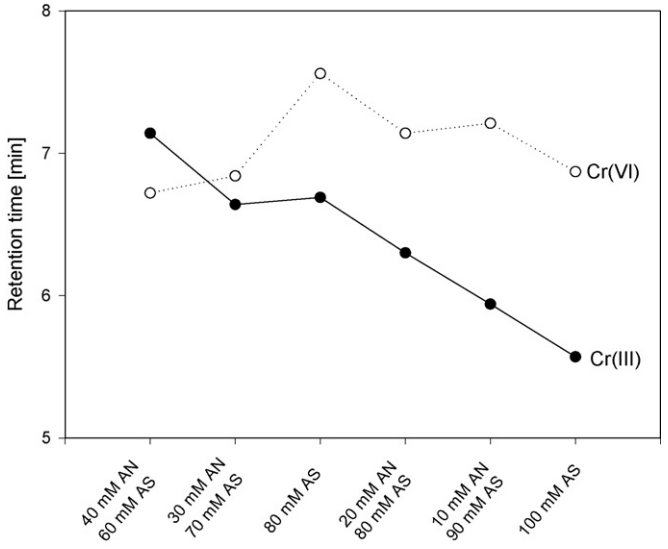

Fig. 2. Retention behaviour of Cr(III) and Cr(VI) at various mobile phase compositions (AN = ammonium nitrate; AS = ammonium sulfate); column: RSpak NN-814 4DP; flow = 0.3 mL min^{-1}; column temperature = 40 °C.

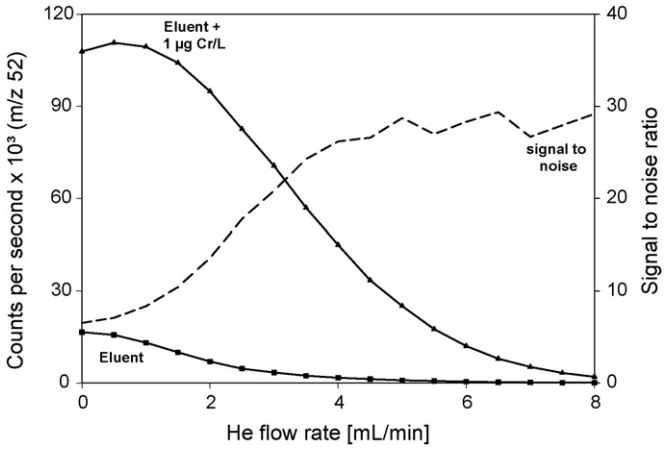

Fig. 3. Graphical evaluation of the optimum He flow rate.

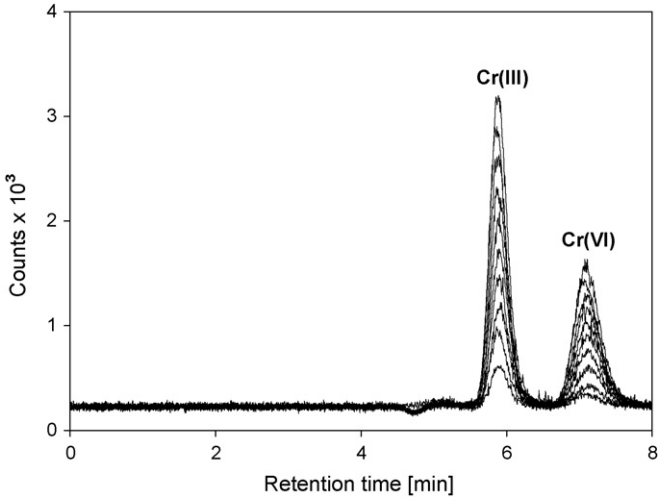

Fig. 4. Chromatogram of 0.5–5 µg Cr(III) L^{-1} and Cr(VI) L^{-1}; column: RSpak NN-814 4DP, mobile phase: 90 mM AS + 10 mM AN, pH 3.0, column temperature = 40 °C, flow = 0.3 mL min^{-1}, injection volume: 25 µL, monitored isotope: *m*/*z* 52.

3.4. Optimization of the octopole reaction system (ORS)

Unfortunately the background of both chromium signals was still higher than we expected (around 1500 counts on *m*/*z* 52). Further the ratio of *m*/*z* 52 to *m*/*z* 53 was higher than the theoretical value of 8.8. We assumed that polyatomic interferences from the sulfur containing mobile phase raised the background and the ratio *m*/*z* 52 to *m*/*z* 53. To minimize the background on both observed isotopes and in consequence to improve the signal to noise ratio, we decided to use the ORS and He as collision gas. At a He flow rate above 4 mL min^{-1} the signal to noise ratio remains constant but the sensitivity on *m*/*z* 52 decreases by increasing the He flow rate. To guarantee both, a high sensitivity and a high signal to noise ratio, a He flow rate of 4–4.5 mL min^{-1} was chosen. Fig. 3 provides the graphical evaluation of the collision gas optimization.

3.5. Method validation

The optimised method was validated according to the DIN 32645 guidelines [27]. Calibration solutions in the range of 1–5 µg Cr(III) L^{-1} and Cr(VI) L^{-1} (1 order of magnitude higher than the expected detection limit) in steps of 0.5 µg L^{-1} were prepared five times. For each batch a complete dilution step with water starting from the stock solution was performed. For validation of the data the Microsoft Excel based macro-sheet "ValiData", Version 3.02.54ger was used.

The limit of decision, detection, and determination was calculated with the calibration method. The validation was performed conforming to standards based on a variance-test on 99% level. The limit of decision was 0.18 µg Cr(VI) L^{-1} and 0.14 µg Cr(III) L^{-1}. The limit of determination was 0.62 µg Cr(VI) L^{-1} and 0.47 µg Cr(III) L^{-1} (Fig. 4). The calibration was linear up to 1.00 mg L^{-1} (but not further investigated). Accuracy and precision was not investigated due to the lack of a suitable certified reference material. The column recovery was typically between 95% and 105% for Cr(VI) and between 90% and 110% for Cr(III).

3.6. Application of the method

3.6.1. Chromium in cement—comparison of three methods

The aqueous extracts from the cements samples have been used for the determination of total soluble chromium and chromium speciation. For this we used an in-house developed anion-exchange chromatographic method [28]. These results were compared with the above mentioned optimised method.

The total chromium concentrations in the aqueous extracts ranged from 2.8 to 9.0 mg Cr kg^{-1} (Table 2) which is well above the current limit of 2 mg Cr(VI) kg^{-1} for manually processed cement set by the EU [23]. With the in-house method only Cr(VI) could be determined in these extracts. The results are in good agreement with the total water soluble chromium concentrations. In order to see water soluble Cr(III) species we investigated the aqueous extract with our newly developed method (Fig. 5). The results as shown in Table 2 indicate that all the extractable chromium is present as Cr(VI).

3.6.2. Chromium in homeopathic drugs

A homeopathic pharmaceutical called Tonsiotren produced by the "Deutsche Homöopathie Union, Karlsruhe" (DHU), contains 7.0 ± 0.4 mg Cr(VI) kg^{-1} according to declaration of the producer. Further compounds of the drug next to some homeopathic ingredients are poly(1-vinyl-2-pyrollidone), hexadecanole, calcium arachinate, talcum, lactic acid, and saccharose. With the developed method the chromium speciation in the Tonsiotren tablets was

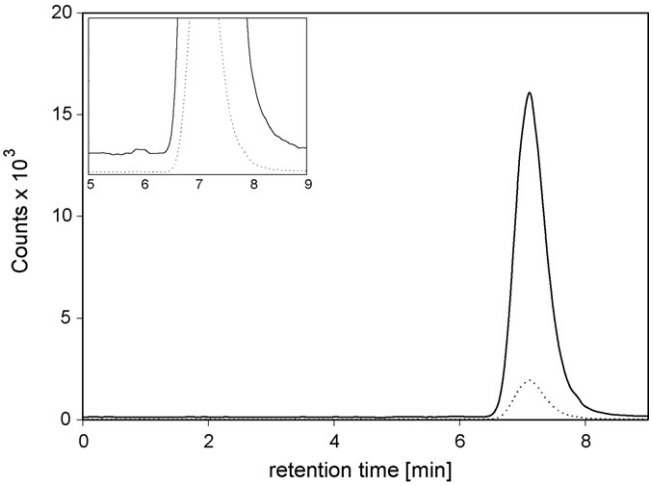

Fig. 5. Chromatogram obtained for a cement sample; column: RSpak NN-814 4DP, mobile phase: 90 mM AS + 10 mM AN, pH 2.9, column temperature = 40 °C, flow = 0.3 mL min^{-1}, He: 4.5 mL min^{-1}, injection volume: 25 µL, measured isotopes: *m*/*z* 52 (full line) and *m*/*z* 53 (dotted line).

Table 2
Comparison of total water soluble Cr, Cr(III) and Cr(VI) concentration with different methods in five cement samples determined after TRGS 613; $n = 3$

Sample name	Total water soluble Cr		With in-house method		This work		
	Mean Cr (mg kg^{-1})	SD Cr (mg kg^{-1})	Mean Cr(VI) (mg kg^{-1})	SD Cr(VI) (mg kg^{-1})	Mean Cr(VI) (mg kg^{-1})	SD Cr(VI) (mg kg^{-1})	Mean Cr(III) (mg kg^{-1})
m/*z* 52							
Cement 1	6.0	0.9	5.8	0.6	5.9	0.6	n.d.
Cement 2	2.8	1.0	2.9	0.9	2.8	1.1	n.d.
Cement 3	9.0	1.0	8.5	0.6	8.4	0.6	n.d.
Cement 4	5.0	0.7	4.8	0.5	4.5	0.9	n.d.
Cement 5	7.0	0.4	6.7	0.2	6.8	0.2	n.d.
m/*z* 53							
Cement 1	5.8	0.6	5.9	0.5	5.9	0.6	n.d.
Cement 2	2.8	0.9	2.8	0.8	2.8	1.1	n.d.
Cement 3	8.5	0.6	8.6	0.8	8.4	0.7	n.d.
Cement 4	4.8	0.5	4.9	0.5	4.5	0.8	n.d.
Cement 5	6.7	0.2	6.6	0.3	6.8	0.1	n.d.

determined and compared with the total amount of chromium and the amount of Cr(VI) determined with the EPA 3060a [29] extraction procedure.

The total chromium concentration determined after microwave digestion agrees well with the declared value. For the certified reference material SRM 8418 we found 0.047 ± 0.004 mg kg^{-1} ($n = 3$, certified concentration 0.053 ± 0.013). With the EPA 3060a procedure only 10% (0.7 ± 0.2 mg kg^{-1}, $n = 4$) of the total chromium was extracted. The chromatographic results obtained for Cr(VI) from the water extracts (0.9 ± 0.3 mg kg^{-1}, $n = 4$) show good agreement with the results determined by the EPA extraction method.

In Fig. 6a a chromatogram of one tablet (0.25 g) diluted 1 + 399 with water is presented. Two signals can be observed at retention

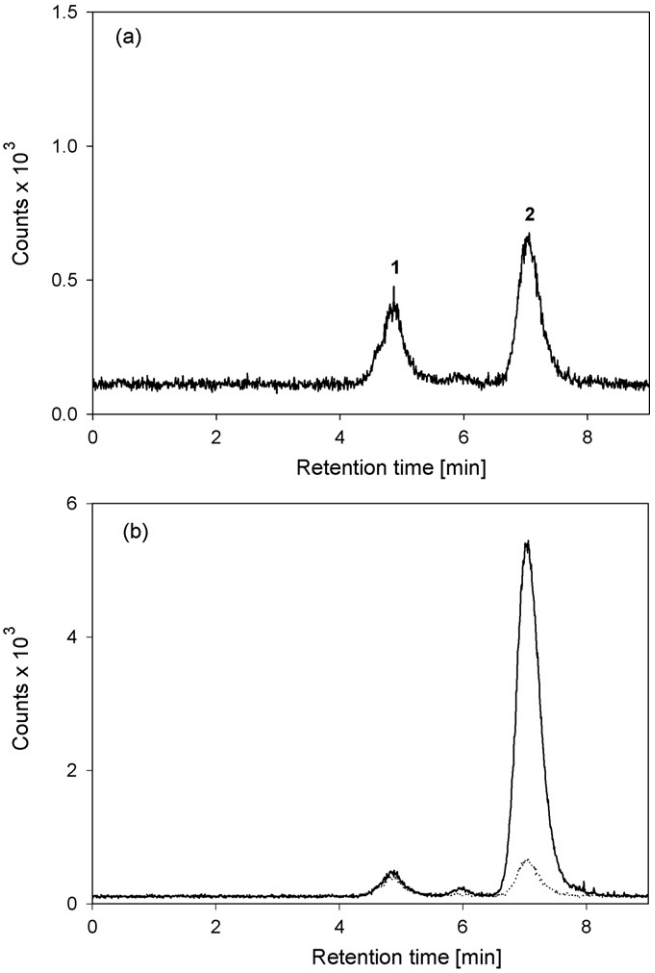

Fig. 6. (a) Chromatogram of Tonsiotren in water—(1) assumed Cr(III) complex; (2) Cr(VI) 2.2 μg/kg; total dilution: 1 + 399; (b) solid line: spike of 20 μg L^{-1} Cr(VI). Column: RSpak NN-814 4DP, mobile phase: 90 mM AS + 10 mM AN, pH 2.9, column temperature = 40 °C, flow = 0.3 mL min^{-1}, injection volume: 25 μL, monitored isotope: *m*/*z* 52.

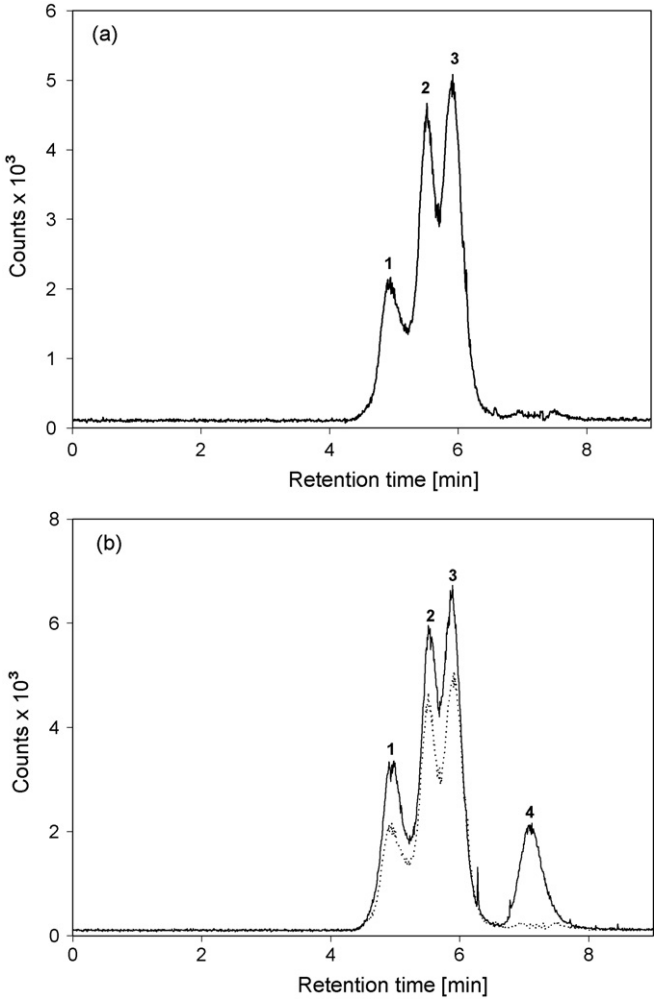

Fig. 7. (a) Chromatogram of Tonsiotren in gastric juice (0.1 M HCl); (1–3) assumed Cr(III) compounds, (4) Cr(VI), total dilution: 1 + 399; (b) solid line: spike of 20 μg L^{-1} Cr(VI). Column: RSpak NN-814 4DP, mobile phase: 90 mM AS + 10 mM AN, pH 2.9, column temperature = 40 °C, flow = 0.3 mL min^{-1}, injection volume: 25 μL, monitored isotope: *m*/*z* 52.

times of 4.9 and 7.1 min. The signal at 7.1 min matched well with Cr(VI). Although originally chromium was added by the producer as potassium dichromate (Kalium bichromicum), it seems that Cr(VI) was already reduced to Cr(III) complexes (signal at 4.9 min) and most likely precipitated as $Cr(OH)_3$. Adding 20 $\mu g\,L^{-1}$ of the Cr(VI) standard to the diluted aqueous extracts of Tonsiotren showed that the Cr(VI) species are stable under the analytical conditions employed (Fig. 6b).

To investigate the behaviour of Tonsiotren tablets in gastric juice, we dissolved one tablet in 0.1 M HCl (simplified gastric juice). Fig. 7a shows a chromatogram of one tablet (0.25 g) dissolved in 0.1 M HCl (1 + 399). We observed three signals at retention times of 4.9, 5.5 and 6.0 min in this extract.

From the retention times it was clear that these signal cannot be Cr(VI) which would elute at ~7 min. All three signals might be Cr(III) complexes of unknown composition. The third signal elutes at the same retention time as the Cr(III) standard. It appeared that all the Cr(VI) was reduced to Cr(III) during the extraction with HCl, which was checked by spiking the extract with Cr(VI) at a concentration of 20 $\mu g\,L^{-1}$. Even when the spiked extract was chromatographed immediately, only one-third of the added Cr(VI) was detectable (Fig. 7b). In contrast all the signals attributed to Cr(III) complexes increased. Chromatography of the spiked extract 10 min after the extraction with HCl, revealed that all the added Cr(VI) was converted to Cr(III) complexes.

4. Conclusions

The developed method allows the determination of Cr(III) and Cr(VI) species without derivatisation of one of the chromium species. This ensures a minimum of sample preparation and almost no intervention in the "sample system" which is a prerequisite for speciation analysis. The method was successfully used for the determination of Cr(III) and Cr(VI) in cement samples, as well as for the speciation analysis of chromium in homeopathic drugs. A determination limit of ~0.5 μg Cr(VI) and Cr(III) per litre at an injection volume of 25 μL was achieved.

The determination of chromium in homeopathic drugs revealed several unknown signals for Cr(III) complexes depending on the extraction procedure employed. It is evident, that the chromatographic resolution is not good enough for separating all chromium species. Changing the mobile phase composition (ammonium-nitrate and sulfate ratio) with emphasis on Cr(III) complexes or gradient elution will certainly improve the separation of the unknown compounds.

Most of the Cr(VI) originally present in the homeopathic drugs is reduced quickly in the aqueous extract. Using HCl as extracting agent reduced the originally present Cr(VI) completely, which is certainly important with respect to human health.

Acknowledgements

Showa Denko Europe GmbH, especially Mr. Thomas Orthmann, is kindly acknowledged for providing their columns.

References

[1] G. Darrie, in: L. Ebdon, L. Pitts, R. Cornelis, H. Crews, O.F.X. Donard, Ph. Quevauviller (Eds.), Trace Element Speciation for Environment, Food and Health, Royal Society of Chemistry, Cambridge, 2001, pp. 315–328, chapter 22.
[2] J. Kotas, Z. Stasicka, Environ. Pollut. 107 (2000) 263–283.
[3] United States Environmental Protection Agency, Method 218.6, October 1999, Revision 3.4.
[4] D.H. Thomas, J.S. Rohrer, P.E. Jackson, T. Pak, J.N. Scott, J. Chromatogr. A 956 (2002) 255–259.
[5] E. Pobozy, E. Wojasinska, M. Trojanowicz, J. Chromatogr. A 736 (2006) 141–150.
[6] B. Gammelgaard, Y. Liao, O. Jones, Anal. Chim. Acta 354 (1997) 107–113.
[7] H.G. Beere, P. Jones, Anal. Chim. Acta 293 (1994) 237–243.
[8] M. Sikovec, M. Novic, V. Hudnik, M. Franko, J. Chromatogr. A 706 (1995) 121–126.
[9] J. Prokisch, B. Kovacs, Z. Györi, J. Loch, J. Chromatogr. A 683 (1994) 253–260.
[10] J.W. Ball, R.B. McCleskey, Talanta 61 (2003) 305–313.
[11] S.A. Steiner, M.D. Porter, J.S. Fritz, J. Chromatogr. A 1118 (2006) 62–67.
[12] Y.C. Sun, C.Y. Lin, S.F. Wu, Y.T. Chung, Spectrochim. Acta Part B 61 (2006) 230–234.
[13] D.Y. Sarica, A. Turker, E.E. Rehber, J. Sep. Sci. 29 (2006) 1600–1606.
[14] C.Y. Kuo, S.J. Jiang, A.C. Sahayam, JAAS 22 (2007) 636–641.
[15] E.H. Borai, E.A. El-Sofany, A.S. Abdel-Halim, A.A. Soliman, Trends Anal. Chem. 21 (2002) 741–745.
[16] M.J. Powell, D.W. Boomer, Anal. Chem. 67 (1995) 2474–2478.
[17] M. Pantsar-Kallio, P.K.G. Manninen, J. Chromatogr. A 750 (1996) 89–95.
[18] A.P. Vonderheide, J. Meija, K. Tepperman, A. Puga, A.R. Pinhas, J.C. States, J.A. Caruso, J. Chromatogr. A 1024 (2004) 129–137.
[19] F.A. Byrdy, L.K. Olson, N.P. Vela, J.A. Caruso, J. Chromatogr. A 712 (1995) 311–350.
[20] Y. Inoue, T. Sakai, H. Kumagai, J. Chromatogr. A 706 (1995) 127–136.
[21] H. Gürleyük, D. Wallschläger, J. Anal. At. Spectrom. 16 (2001) 926–930.
[22] C. Barnowski, N. Jakubowski, D. Stuewer, J.A.C. Broekaert, J. Anal. At. Spectrom. 12 (1997) 1155–1161.
[23] F. Seby, S. Charles, M. Gagean, H. Garraud, O.F.X. Donard, J. Anal. At. Spectrom. 18 (2003) 1386–1390.
[24] European Union Directive 2003/53/EC, OJ L 178/24, 17.7.2003.
[25] TRGS 613, Federal Institute for Occupational Safety and Health of Germany, October 2002.
[26] N. Tsunoda, FARUAW 34 (1998) 1237–1241.
[27] DIN 32645, Chemical analysis; decision limit; detection limit and determination limit; estimation in case of repeatability; terms, methods, evaluation.
[28] H. Hagendorfer, Diploma thesis, Karl-Franzens University Graz, 2005.
[29] United States Environmental Protection Agency, Method 3060a, 1996.

Talanta 76 (2008) 597–601

Contents lists available at ScienceDirect

Talanta

journal homepage: www.elsevier.com/locate/talanta

Advantages of pentafluorophenylpropyl stationary phase over conventional C18 stationary phase—Application to analysis of triamcinolone acetonide

Lucie Havlíková, Ludmila Matysová, Renata Hájková, Dalibor Šatínský, Petr Solich*

Department of Analytical Chemistry, Faculty of Pharmacy, Charles University, Heyrovského 1203, 500 05 Hradec Králové, Czech Republic

ARTICLE INFO

Article history:
Received 27 November 2007
Received in revised form 25 March 2008
Accepted 28 March 2008
Available online 8 April 2008

Keywords:
Degradation product
C18 columns
HPLC
Pentafluorophenylpropyl stationary phase
Triamcinolone acetonide

ABSTRACT

A pentafluorophenylpropyl (PFPP) stationary phase was for the first time tested for the simultaneous determination of triamcinolone acetonide, its degradation product triamcinolone and two preservatives, methylparaben, and propylparaben. A new simple isocratic reversed phase HPLC method with UV detection, using estradiol hemihydrate as an internal standard, has been developed and validated. Chromatography was performed on a Discovery HS F5 column (150 mm × 4.6 mm, 5 μm) using a binary mobile phase composed of acetonitrile and water 45:55 (v:v). The flow-rate was 0.6 mL/min, the column temperature 25 °C and the UV detection was accomplished at 240 nm.

The chromatography results using PFPP stationary phase were compared with those obtained using conventional C18 columns.

1. Introduction

Pentafluorophenylpropyl (PFPP) stationary phase has been recently introduced and has been applied in areas like pharmaceutical, toxicological, and clinical analysis. Fluorinated, silica-based stationary phases are becoming popular alternatives to traditional alkyl phases [1]. The pentafluorophenyl ring structure is attached to the silica over a propyl chain. The PFPP stationary phase provides separations that are different from C18 because the PFPP stationary phase shows increased retention. Compounds which elute too closely to void volume on the C18 column, are sufficiently retained by PFPP stationary phase [2]. Mixed reversed- and normal-phase retention mechanisms give unique selectivity. This allows isocratic separation of polar and non-polar compounds in the same run, and provides benefits for LC/MS [3]. The relationship between the amount of organic modifier and the logarithm of the retention factor was observed for basic analytes [4]. The importance of a combined ion-exchange and non-ionic mechanism on retention of basic compounds, at high percentages of organic modifier, on a fluorinated stationary phase was described by Bell and Jones [5]. "U-shaped" retention as a function of mobile phase acetonitrile content was more dramatic on a PFPP column when compared to C18. These findings suggest ion-exchange mechanisms strongly influence the retention of basic analytes in the high acetonitrile realm on the PFPP [5]. In a later study the authors investigated the relationship between retention and temperature. Using a fluorinated stationary phase, with a high percentage of organic modifier, it was observed that with increased temperature, greater retention was achieved. This observation could be based on the reduction in the solvating power of the solvent with increasing temperature [1]. Studies dealing with the comparison of chromatography performance of fluorinated and C18 stationary phases have been published [6,7].

HPLC applications of PFPP stationary phase so far reported include: analysis of phenethylamine alkaloids in citrus products [8], pentacyclic triterpenoid [9], and ciprofloxacin in plasma [10]. The ion-exchange mechanism characteristic for a fluorinated phase was explored for the analysis of ephedrine alkaloids [1]. There have been investigations into the advantages of utilizing phenyl ring structures in stationary phases for the HPLC/ESI-MS analysis of cocaine, and its metabolite ecgonine methyl ester, in human urine [11], beta-blockers, and tricyclic antidepressants [12,13], for *S*-adenosylmethionine and *S*-adenosylhomocysteine [14] and for the analysis of paclitaxel and related taxanes [15].

Triamcinolone acetonide (chemically 9α-fluoro-16α-hydroxyprednisolone 16α,17α-acetonide) is a neutral synthetic corticosteroid. It is administered either as an oral metered-dose inhaler for the treatment of asthma, as a topical preparation for the skin or as a nasal spray or inhaler for relieving symptoms of rhinitis [16]. Topical corticosteroids are indicated for the relief of the inflammatory and pruritic manifestations of corticosteroid-responsive dermatoses [17]. Recently a novel analytical method, using conventional C18 stationary phase, for

* Corresponding author. Tel.: +420 495067294; fax: +420 495067164.
E-mail address: petr.solich@faf.cuni.cz (P. Solich).

0039-9140/$ – see front matter © 2008 Elsevier B.V. All rights reserved.
doi:10.1016/j.talanta.2008.03.048

determination of triamcinolone acetonide (active substance), triamcinolone (degradation product), methylparaben, and propylparaben (preservatives) have been developed and reported by our team [18]. This method was applied for stability tests of triamcinolone cream 1% (triamcinolone acetonide, active compound; methylparaben and propylparaben, preservatives) in quality control laboratory.

The aim of the present study was to test the separation performance of an analytical column, containing PFPP stationary phase, for the analysis of triamcinolone acetonide (TCA), triamcinolone (TC), methylparaben (MP), and propylparaben (PP) and for analysis of Triamcinolone cream 1%. These results were then compared with those obtained using conventional C18 columns.

2. Experimental

2.1. Chemicals and reagents

Working standards of triamcinolone acetonide (the active substance), triamcinolone (degradation product), estradiol hemihydrate (ES) (internal standard), and both preservatives methylparaben and propylparaben were used in this study. Standards were supplied by Sigma–Aldrich (Prague, Czech Republic). Acetonitrile Chromasolv for HPLC gradient grade was supplied by Sigma–Aldrich (Prague, Czech Republic) too. Triamcinolone cream 1% and its placebo (cream without the active substance and preservatives) were supplied by Herbacos–Bofarma (Bochemie Group, Pardubice, Czech Republic). HPLC grade water was prepared by Milli-Q reverse osmosis Millipore (Bedford, MA, USA), pH 5.2.

2.2. Chromatography

A Shimadzu LC-2010 C system (Shimadzu, Kyoto, Japan) with a built-in UV–VIS detector was used. Class VP 6.12 chromatographic software (Shimadzu, Kyoto, Japan) was used for the data collection and evaluation. A Discovery HS F5 column (150 mm × 4.6 mm, 5 μm) and Discovery C18 columns (125 mm × 4.6 mm, 5 μm; 250 mm × 4.6 mm, 5 μm) were purchased from Sigma–Aldrich (Prague, Czech Republic). A Hypersil ODS column (250 mm × 4.6 mm, 5 μm) was purchased from Thermo Fisher Scientific, Inc. (Waltham, USA). Optimal chromatography was performed on a Discovery HS F5 column (150 mm × 4.6 mm, 5 μm) using a binary mobile phase composed of acetonitrile and water 45:55 (v:v). The flow-rate was 0.6 mL/min, the column temperature 25 °C and the UV detection was accomplished at 240 nm. The injection volume was 10 μL. Estradiol hemihydrate was applied as internal standard for the analysis on Discovery HS F5 column.

2.3. Reference standard preparation

Reference standard solution for triamcinolone acetonide analysis was prepared in 100 mL volumetric flask by dissolving 2.5 mg of triamcinolone acetonide, 0.5 mg of triamcinolone, 5.0 mg of methylparaben, and 1.25 mg of propylparaben in acetonitrile. Next, 10.0 mL of internal standard estradiol hemihydrate stock solution was added and the remaining volume was made up with acetonitrile. The stock solution of internal standard, estradiol hemihydrate, was prepared by dissolving of 50 mg of estradiol hemihydrate in 100.0 mL of acetonitrile. Working solution of internal standard was prepared by diluting 10.0 mL of the internal standard stock solution in acetonitrile to a volume of 100.0 mL. The final concentration of the internal standard solution was always approximately 50 mg/L.

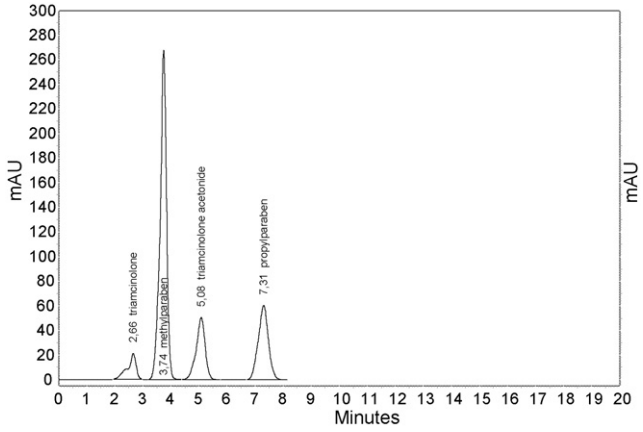

Fig. 1. Chromatogram: analysis performed on Discovery C18 (125 mm × 4.6 mm, 5 μm) triamcinolone acetonide standard solution, mobile phase: acetonitrile–water (40:60 v:v), 0.6 mL/min, UV 240 nm, 25 °C. TCA 25 mg/L, TC 5 mg/L, MP 50 mg/L, PP 12.5 mg/L, ES (IS) 50 mg/L.

2.4. Sample preparation

0.5 g of the Triamcinolone cream 1% was accurately weighed and transferred into a centrifuge flask. Then 20.00 mL of working solution of internal standard, estradiol hemihydrate, was added. The mixture in centrifuge flask was sonicated for 10 min. It was then centrifuged for 15 min at 1300 × *g* using laboratory centrifuge EBA 21 (Hettich, Tuttlingen, Germany). 10 μL of the supernatant was injected into the chromatographic system.

3. Results

The original chromatographic separation [18] was performed on a Discovery C18 column (125 mm × 4 mm, 5 μm) under the following conditions: acetonitrile and water 40:60 (v:v), flow-rate of 0.6 mL/min, column temperature of 25 °C, detection wavelength 240 nm (Fig. 1). Triamcinolone co-eluted with column hold-up time, hydrocortisone (internal standard) was to close to co-elution with methylparaben. An impurity of the extraction procedure co-eluted with methylparaben and was not detected on chromatograms. Therefore three other columns were chosen with the aim to improve the separation. Firstly the chromatography was per-

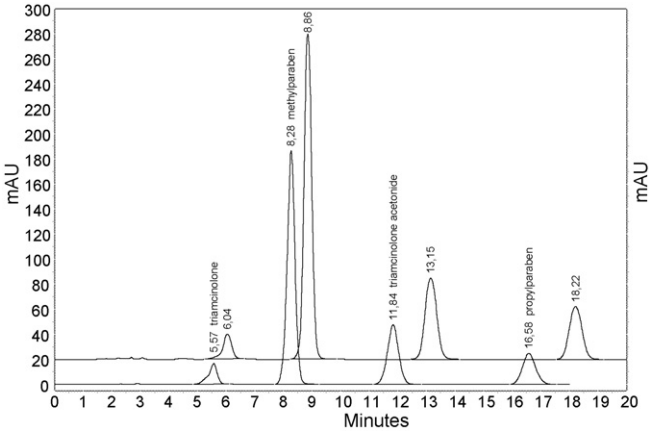

Fig. 2. Chromatogram: comparison of analyses of triamcinolone acetonide standard solution performed on Hypersil ODS (250 mm × 4.6 mm, 5 μm) and Discovery C18 (250 mm × 4.6 mm, 5 μm)—upper curve. Mobile phase: acetonitrile–water (40:60 v:v), 0.6 mL/min, UV 240 nm, 25 °C, TCA 25 mg/L, TC 5 mg/L, MP 50 mg/L, PP 12.5 mg/L, ES (IS) 50 mg/L.

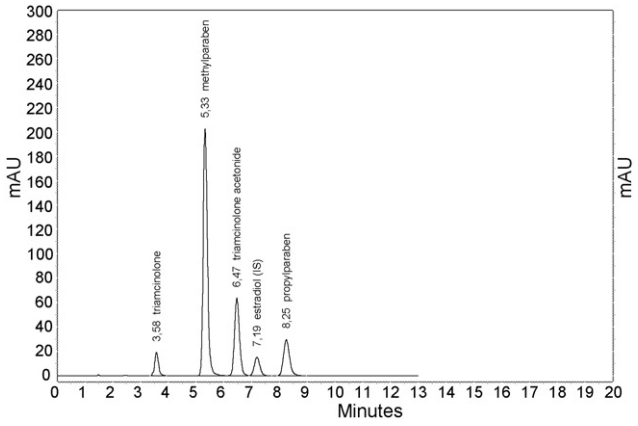

Fig. 3. Chromatogram: analysis performed on Discovery HS F5 (150 mm × 4.6 mm, 5 μm), triamcinolone acetonide standard solution, mobile phase: acetonitrile–water (45:55 v:v), 0.6 mL/min, UV 240 nm, 25 °C. TCA 25 mg/L, TC 5 mg/L, MP 50 mg/L, PP 12.5 mg/L, ES (IS) 50 mg/L.

formed on Discovery C18 (250 mm × 4.6 mm, 5 μm), and Hypersil ODS (250 mm × 4.6 mm, 5 μm) columns (Fig. 2) using similar conditions to those described above. For the third tested column, a Discovery HS F5 (PFPP bonded), the composition of the mobile phase was changed. The acetonitrile portion was increased to ratio acetonitrile–water 45:55 (v:v) for a higher resolution between analytes and faster separation of compounds (Fig. 3). System suitability data of all columns were determined and compared. The results are shown in Table 1.

3.1. System suitability test (SST)

The samples of standard solution underwent six lots of injections into the chromatographic system. Mean values and standard deviations of retention time, number of theoretical plates, asymmetry (symmetry factor), resolution, and repeatability of analytical run were calculated according to the European Pharmacopoeia [19]. To make a comparison of column efficiency the high equivalent of theoretical plates (HETP) parameter was used. The number of theoretical plates depends on column length. A longer column has a larger plate number. Therefore, the term high equivalent of theoretical plates has been introduced to measure how efficiently columns have been packed. HETP (μm) is calculated as the ratio of the column length (μm) to the number of theoretical plates (N). The lower the plate height and the higher the number of theoretical plates the more efficient the chromatographic column [20]. The retention was evaluated using retention time and capacity factor k'. The capacity factor was calculated using the following equation:

$$k' = \frac{t_R - t_0}{t_0} \quad (1)$$

t_R is the retention time of the analyte and t_0 is the column hold-up time. The hold-up time was estimated by monitoring the first signal disturbance upon injection for the HS F5 column [5] and by using potassium iodide (Sigma–Aldrich) for C18 columns, respectively.

The time of analysis was about 20 min using Discovery C18 (250 mm × 4.6 mm, 5 μm) and Hypersil ODS column (250 mm × 4.6 mm, 5 μm) and 10 min on Discovery C18 (125 mm × 4.6 mm, 5 μm) and Discovery HS F5 column (150 mm × 4.6 mm, 5 μm),

Table 1
System suitability test data

SST		Discovery HS F5 150 mm × 4.6 mm, 5 μm		Discovery C 18 125 mm × 4.6 mm, 5 μm		Discovery C18 250 mm × 4.6 mm, 5 μm		Hypersil ODS 250 mm × 4.6 mm, 5 μm	
		ACN–H_2O = 45:55, 0.6 mL/min		ACN–H_2O = 40:60, 0.6 mL/min		ACN–H_2O = 40:60, 0.6 mL/min		ACN–H_2O = 40:60, 0.6 mL/min	
Triamcinolone									
k'	k' R.S.D. (%)	2.25	0.14	–	–	4.81	0.08	1.06	0.25
t_R R.S.D. (%)	A R.S.D. (%)	0.05	0.15	–	–	0.16	0.40	0.13	0.73
N	N R.S.D. (%)	6174	0.89	–	–	2022	0.98	2153	1.79
HETP	HETP R.S.D. (%)	43.25	0.90	–	–	123.68	0.98	116.16	1.82
R_i	R_i R.S.D. (%)	11.79	0.72	–	–	2.69	0.85	8.03	0.05
T	T R.S.D. (%)	1.17	0.88	–	–	0.82	2.44	0.78	0.91
Methylparaben									
k'	k' R.S.D. (%)	3.85	0.29	1.52	0.22	7.52	0.09	2.07	0.34
t_R R.S.D. (%)	A R.S.D. (%)	0.22	0.17	0.68	0.51	0.08	0.52	0.23	0.31
N	N R.S.D. (%)	5989	0.70	1576	0.25	4969	0.28	4611	1.46
HETP	HETP R.S.D. (%)	25.05	0.72	79.32	0.26	50.31	0.28	54.23	1.38
R_i	R_i R.S.D. (%)	6.67	0.93	2.58	1.18	4.89	0.28	5.66	0.74
T	T R.S.D. (%)	1.19	0.91	0.85	1.06	1.03	0.82	0.96	1.36
Triamcinolone acetonide									
k'	k' R.S.D. (%)	4.88	0.14	2.48	0.08	11.65	0.08	3.38	0.07
t_R R.S.D. (%)	A R.S.D. (%)	0.16	0.17	0.23	0.25	0.07	0.20	0.10	0.10
N	N R.S.D. (%)	6256	0.91	1393	0.91	4702	0.38	4702	0.38
HETP	HETP R.S.D. (%)	23.98	0.88	89.74	0.90	53.17	0.38	40.25	0.73
R_i	R_i R.S.D. (%)	3.74	0.31	3.07	0.49	4.55	0.16	5.94	0.08
T	T R.S.D. (%)	1.14	0.38	0.85	0.88	1.28	0.79	1.08	0.77
Propylparaben									
k'	k' R.S.D. (%)	6.50	0.18	4.04	0.13	16.53	0.11	5.15	0.31
t_R R.S.D. (%)	A R.S.D. (%)	0.29	0.39	0.27	0.25	0.10	0.14	0.26	0.19
N	N R.S.D. (%)	7017	0.80	2206	1.59	7540	0.27	6212	0.73
HETP	HETP R.S.D. (%)	20.66	0.80	56.68	1.55	33.15	0.26	40.25	0.73
R_i	R_i R.S.D. (%)	2.78	0.81	3.89	1.80	4.37	0.19	5.94	0.08
T	T R.S.D. (%)	1.19	0.96	0.96	0.93	1.34	0.42	1.08	0.77

t_R: retention time (min); R.S.D. (%): relative standard deviation; A: area; HETP: height equivalent of theoretical plates (μm); R_i: peak resolution; N: number of theoretical plates; T: asymmetry; six repetitions of standard solution for each condition.

respectively. Discovery C18 (125 mm × 4.6 mm, 5 μm) produces a retention time of triamcinolone which is too close to the column hold-up time. The repeatability of the analytical run was evaluated for retention time and for peak area. Relative standard deviations, both of retention time and area, do not exceed 1%. The height equivalents of theoretical plates of analytes on Discovery HS F5 column (150 mm × 4.6 mm, 5 μm) compared to analyses performed on Discovery C18 column, and Hypersil ODS column were lower, the separation efficiency of HS F5 column was higher. The peak resolution parameter was used for characterizing compound separation. A resolution greater than 1.5 corresponds to baseline separation [19]. There is no statistical difference between the symmetry factors for analytes and analyses performed on tested columns in exception to the analysis performed on Hypersil ODS—the symmetry factor of triamcinolone did not meet the requirement of the European Pharmacopoeia (0.8–1.5) [19].

Triamcinolone was separated from the column hold-up time using the Discovery HS F5 column and both 250 mm columns. Results of system suitability test for Discovery HS F5 and Discovery 250 mm were comparable.

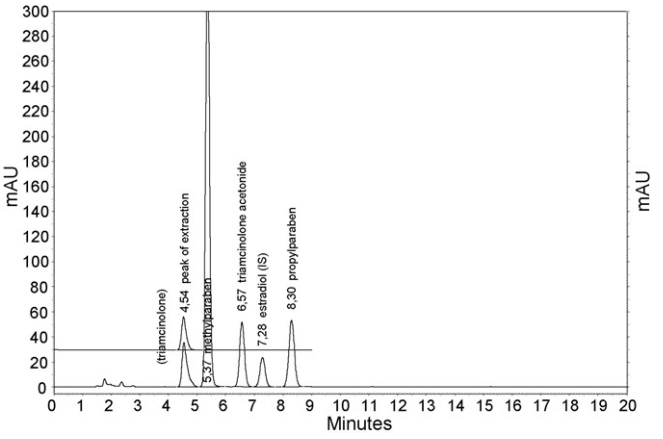

Fig. 4. Chromatogram: analysis of compounds in topical pharmaceutical preparation, and placebo analysis to demonstrate method selectivity. Discovery HS F5 column (150 μm × 4.6 mm, 5 μm), mobile phase: acetonitrile–water (45:55 v:v), 0.6 mL/min, UV 240 nm, 25 °C.

3.2. Analysis of topical cream

The analysis of a topical pharmaceutical cream containing triamcinolone acetonide, methylparaben and propylparaben was performed on tested columns. ODS Hypersil column was not suitable for the analysis because of the co-elution of a peak from the cream extraction, with the peak of the methylparaben. This problem also occurred for analysis on the Discovery C18 250 mm column. The retention characteristics for each of the tested compounds were measured from 30% to 90% acetonitrile in 10% increments using the PFPP stationary phase, Hypersil ODS and Discovery C18 250 mm columns. The samples of Triamcinolone cream 1% spiked with triamcinolone were injected in triplicate into the chromatographic system. Changing of the acetonitrile content did not lead to the separation of methylparaben and the peak of extraction. The increase of acetonitrile content caused co-elution of analytes. The decrease of acetonitrile content caused extended time of analysis. Changing of pH (phosphoric acid 0.085% and/or ammonium phosphate pH 7.0) did not influence the separation of methylparaben and the peak of extraction. The retention of triamcinolone and triamcinolone acetonide were not significantly influenced; the capacity factor ranged from 2.3 (pH 7.0) to 2.2 (pH 2.1) and from 4.9 (pH 7.0) to 4.6 (pH 2.0) for triamcinolone and triamcinolone acetonide, respectively, using Discovery HS F5 column. Similar results were achieved for parabens.

Methylparaben and of the extraction procedure peak (retention time 4.54 min) were separated from all tested compounds using a Discovery HS F5 (150 mm × 4.6 mm, 5 μm) column and water–acetonitrile 45:55 (v/v) mobile phase. The flow-rate was 0.6 mL/min and column temperature was 25 °C (Fig. 4).

Discovery HS F5 (150 mm × 4.6 mm, 5 μm) column was used for the analysis and method validation.

3.3. Method validation

Within the method validation, the system suitability test (SST) and some chosen validation parameters were measured and evaluated in accordance with ICH guidelines recommendations [21] and guidelines followed in our laboratory. The SST parameters were calculated according to the European Pharmacopoeia [19].

Table 2
Method validation results

Parameter		Triamcinolone	Triamcinolone acetonide	Methylparaben	Propylparaben	Criteria
SST						[19]
Repeatability retention time[a]	R.S.D. (%)	0.05	0.16	0.22	0.29	$X < 1\%$
Repeatability area[a]	R.S.D. (%)	0.15	0.17	0.17	0.39	$X < 1\%$
Theoretical plates[a]		6174	6256	5989	7017	$N > 1500$
Resolution[a]		11.79	3.74	6.67	2.78	$R_{ij} > 1.5$
Asymmetry[a]		1.17	1.14	1.19	1.19	$T = 0.8–1.5$
Validation						
Precision[b]	R.S.D. (%)	0.95	0.62	0.95	0.91	$X < 5\%$
Linearity[c]	Correlation coefficient (r)	0.99998	0.99987	0.99993	0.99981	$r > 0.9990$
	Calibration equation	0.6 + 0.003	0.68–0.014	0.52–0.052	0.59–0.002	
	Intercept	0.003 ± 0.0008	−0.014 ± 0.019	−0.052 ± 0.029	−0.002 ± 0.014	
	Slope	0.60 ± 0.0049	0.68 ± 0.0049	0.52 ± 0.0029	0.59 ± 0.0059	
Accuracy[b]	Recovery (%)	97.66	97.92	97.75	97.85	$X = 100 \pm 5\%$
	R.S.D. (%)	0.94	0.47	0.48	0.30	$X < 5\%$
LOD (mg/L)		0.0102	–	–	–	
LOQ (mg/L)		0.0341	–	–	–	
Selectivity		No interference	No interference	No interference	No interference	

[a] Made in six replicates.
[b] Six samples injected three times each.
[c] Linearity at six concentration levels in the range of 19.5–58.5 mg/L for triamcinolone acetonide, 25–75 mg/L for methylparaben, 6.5–18.5 mg/L for propylparaben, and 0–8.2 mg/L for triamcinolone.

SST covers six injections of standard solutions and calculation of following parameters: repeatability of retention times (t_R) and peak area (A), number of theoretical plates, asymmetry factor, and resolution. Repeatability was expressed as the relative standard deviation (%R.S.D.). Method validation was accomplished on topical pharmaceutical preparation containing triamcinolone acetonide, and methylparaben and propylparaben, and included: determination of precision, accuracy, linearity, and detection and quantitation limits of degradation product triamcinolone (LOD, LOQ). Method Precision (% of R.S.D.) was investigated using sample preparation procedure for six real samples of Triamcinolone cream 1%. Recovery (accuracy) was determined by spiking placebo with standard additions of standard solution. Linearity was measured at six concentrations levels for each analyte. Each solution was injected three times. The method of linear regression was used for data evaluation. Linearity was described by a calibration equation and by the determination of a correlation coefficient. Selectivity was verified by injection of standard solution, placebo of pharmaceutical preparation and pharmaceutical preparation treated according to sample preparation procedure. No interferences were observed. The limit of detection (LOD) was defined as the compound concentration that produced a signal-to-noise ratio greater than three and the limit of quantitation (LOQ), was evaluated as the concentration equal to 10 times the value of the signal-to-noise ratio. The results are shown in Table 2.

4. Conclusion

Pentafluorophenylpropyl stationary phase was firstly introduced for the simultaneous determination of triamcinolone acetonide, its degradation product triamcinolone, and two preservatives methylparaben and propylparaben. The results were compared with those obtained using conventional C18 columns. The retention characteristics of analyzed compounds using PFPP stationary phase (Discovery HS F5 150 mm × 4.6 mm; 5 μm) are comparable with results performed on Discovery C18 (250 mm × 4.6 mm; 5 μm) column. The new optimized method was applied for analysis of topical preparation Triamcinolone cream 1%. The positive outcome is the separation of the unknown peak (of the separation procedure) from methylparaben using the PFPP stationary phase. Furthermore, the degradation product was better separated from the column hold—up time using the PFPP stationary phase in comparison with the analysis using Discovery C18 (125 mm × 4.6 mm; 5 μm). The Discovery HS F5 column (150 mm × 4.6 mm; 5 μm) was an alternative to the traditional alkyl phase for the analysis of triamcinolone acetonide and related compounds.

Acknowledgement

The authors gratefully acknowledge the financial support of the Research Project MSM 0021620822.

References

[1] D.D.S. Bell, H.M. Cramer, A.D. Jones, J. Chromatogr. A 1095 (2005) 113.
[2] https://www.sigmaaldrich.com/Brands/Supelco_Home/Spotlights/Discovery_HPLC/HS_F5.html (accessed 09/07).
[3] Bulletins Sigma–Aldrich T103938, Sigma–Aldrich Co., USA, 2003.
[4] M.R. Euerby, A.P. McKeown, P. Petersson, J. Sep. Sci. 26 (2003) 295.
[5] D.S. Bell, A.D. Jones, J. Chromatogr. A 1073 (2005) 99.
[6] M.R. Euerby, P. Petersson, J. Chromatogr. A 994 (2003) 13.
[7] M. Reta, P.W. Carr, P.C. Sadek, S.C. Rutan, Anal. Chem. 71 (16) (1999) 3484.
[8] F. Pellati, S. Benvenuti, J. Chromatogr. A 1165 (1–2) (2007) 58–66.
[9] B. Büchele, W. Zugmaier, F. Genze, T. Simmet, J. Chromatogr. B 829 (1–2) (2005) 144.
[10] Z. Vybíralová, M. Nobilis, J. Zoulová, J. Květina, P. Petr, J. Pharm. Biomed. Anal. 37 (5) (2005) 851.
[11] S.R. Needham, P.R. Brown, K. Duff, Rapid Commun. Mass Spectrom. 13 (1999) 2231.
[12] S.R. Needham, P.M. Jeanville, P.R. Brown, E.S. Estape, J. Chromatogr. B: Biomed. Sci. Appl. 748 (1) (2000) 77.
[13] S.R. Needham, P.R. Brown, K. Duff, D. Bell, J. Chromatogr. A 869 (2000) 159.
[14] K.A. Burren, K. Mills, A.J. Copp, N.D.E. Greene, J. Chromatogr. B 844 (1) (2006) 112.
[15] Application Notes Sigma–Aldrich, T303174, Sigma–Aldrich Co., USA, 2003.
[16] http://www.medicinenet.com/triamcinolone_acetonide_nasal_inhaler-spray/article.htm (accessed 09/07).
[17] http://www.rxlist.com/cgi/generic/triamcinolone-cream_ids.htm (accessed 09/07).
[18] L. Matysová, R. Hájková, J. Šícha, P. Solich, Anal. Bioanal. Chem. 376 (2003) 440.
[19] Council of Europe European (EDQM), European Pharmacopoeia, sixth ed., Strasbourg Cedex, 2007, p. 72.
[20] Z. Kazachevich, H. McNair, Textbook on High Performance Liquid Chromatography, 2008.
[21] http://www.ich.org/LOB/media/MEDIA417.pdf (accessed 02/08).

Talanta 76 (2008) 698–702

Contents lists available at ScienceDirect

Talanta

journal homepage: www.elsevier.com/locate/talanta

Analytical application of poly{methyl[3-(2-hydroxy-3,4-difluoro)phenyl] propyl siloxane} as a QCM coating for DMMP detection

Wei He[a,*], Zhongxiang Liu[a], Xiaosong Du[a], Yadong Jiang[a], Dan Xiao[b]

[a] State Key Lab of Electronic Thin Films and Integrated Devices, University of Electronic Science and Technology of China (UESTC), Chengdu 610054, PR China
[b] College of Chemistry, Sichuan University, Chengdu 610065, PR China

ARTICLE INFO

Article history:
Received 15 December 2007
Received in revised form 9 April 2008
Accepted 12 April 2008
Available online 20 April 2008

Keywords:
Poly{methyl[3-(2-hydroxy-3,4-difluoro)phenyl]propyl siloxane}
DMMP
QCM
Selectivity

ABSTRACT

A new material—poly{methyl[3-(2-hydroxy-3,4-difluoro)phenyl]propyl siloxane}(PMDFPS) sensitive to toxic organophosphate vapor was synthesized with 2,3-difluorophenol, allyl bromide and poly (methyl hydrosiloxane) as raw materials, via *O*-alkylation, Claisen rearrange reaction and hydrosilylation reaction. This novel material was then coated on a quartz crystal microbalance (QCM) to investigate its gas sensitive properties to the nerve agent simulant dimethyl methylphosphonate (DMMP) vapor, as well as known interfering vapors. When tested with competing vapors, the sensor was more than 10 times sensitive to DMMP than to other interfering vapors. Thus, high selectivity of poly{methyl[3-(2-hydroxy-3,4-difluoro)phenyl]propyl siloxane} to DMMP was demonstrated. The poly{methyl[3-(2-hydroxy-3,4-difluoro)phenyl]propyl siloxane}-QCM sensor responded linearly to DMMP vapor with a slope of 14 Hz/ppm in the 1–50 ppm range with a detection limit of 0.21 ppm (S/N = 3).

1. Introduction

Organophosphate compounds (Ops) are significant environmental and food chain pollutants because of their widespread use as pesticides and insecticides [1,2]. Additionally, several Ops have been demonstrated to be potent nerve agents and have thus been used as chemical warfare agents [3]. Nerve agents exert their effects by the inhibition of enzyme acetylcholinesterase (AChE), leading to the excessive accumulation of the neurotransmitter acetylcholine (ACh) at cholinergic synapses. Enzyme inhibition can occur extremely rapidly making nerve agents both highly toxic and extremely dangerous [4]. Traditionally, the most commonly used methods for nerve agent detection are gas chromatography [5,6], liquid chromatography [7], atomic emission detection [8], gas chromatography-mass spectrometry coupled method [9] and ion chromatography [10]. These methods can give precise and reliable analytical results, but they require expensive instrumentation and highly trained personnel, as well as time-consuming analysis. Both of these requirements are unsuitable for on-line process monitoring. Therefore, there is a strong demand to develop detection methods that are both rapid and reliable for nerve agent detection.

Among the various types of gas sensors investigated in previously, surface wave acoustic (SAW) sensors and quartz crystal microbalance (QCM) sensors have generated considerable interest due to their simplicity, ease of use and high sensitivity and selectivity. The SAW sensor and QCM sensor comprise of thin sorbent layers of a chemically selective material to collect and concentrate analyte of interest. Collection of analyte increases the mass of the sensor, resulting in a change in resonant frequency. The selectivity and sensitivity of both sensors to a specific vapor analyte are highly dependent on the chemical natures and physical properties of the coated polymers. To date, many sensitive polymers for nerve agents detection have been synthesized, including poly(styrene-co-vinyl benzyl hexafluorodimethyl carbinol) [11], fluoropolyol [12], hybrid organic/inorganic polymers [13] and functionalized polysiloxane [14,15]. During the development of these sensitive materials, functionalized polysiloxane incorporating hexafluoroisopropanol groups was a focal point of the research due to its high selectivity, efficient reversibility, and stability. However, polysiloxane incorporating hexafluoroisopropanol groups exhibited high sensitivity to water molecules as well nerve agents. According to linear solvation energy relationships [16–18], the solubility properties of the chemoselective polymer for nerve agents detection should be both strongly dipolar/polarisable and hydrogen-bond acidic to complement the dipolar and hydrogen-bond basic properties of nerve agents, thus, polysiloxane functionalized with difluorophenol groups could be a promising sensitive material for nerve agent

* Corresponding author. Tel.: +86 28 83203218; fax: +86 28 83203218.
E-mail address: hewei999@vip.sina.com (W. He).

0039-9140/$ – see front matter © 2008 Elsevier B.V. All rights reserved.
doi:10.1016/j.talanta.2008.04.022

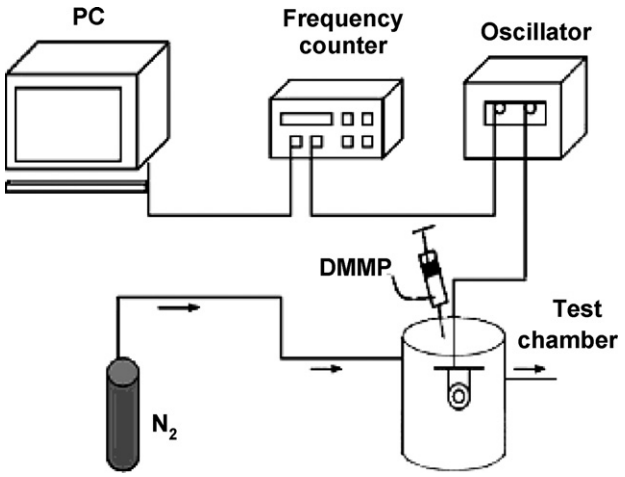

Fig. 1. Schematic diagram of the measurement system.

detection, and it may also exhibit a significantly lower response to water molecules because of the effect of polarizable aromatic groups [19]. To our knowledge, such compounds have not been synthesized or used for nerve agent detection.

In this study, a new sensitive material incorporating 2,3-difluorophenol groups has been synthesized via *O*-alkylation, Claisen rearrangement reaction and hydrosilylation reaction using 2,3-difluorophenol, allyl bromide and poly (methylhydrosiloxane) as raw materials. This new material was then coated on a QCM sensor to investigate its gas sensitive properties to dimethyl methylphosphonate (DMMP) vapor, a simulant of nerve agents, as well its response to interfering vapors.

2. Experimental

2.1. Reagents and instrumentations

2,3-Difluorophenol was purchased from AstaTech (Chengdu) Pharmaceutial Co., Ltd., poly(methylhydrosiloxane) was purchased from Sihai Chemical Factory, NaOH, CH_2Cl_2, C_2H_5OH, $CHCl_3$ were purchased from Chengdu Kelong Chemical reagent Factory. DMMP was purchased from Aldrich. All of the above chemicals were used without further purification.

^{1}H NMR assays were performed on an AVANCE 300 NMR spectrometer (BRUKER). Mass Spectra were recorded on a LCQ^{DECA} mass spectrometer (Finnigan). IR spectra were recorded on an MX-1E FT-IR spectrometer (NICOLET). AT-cut 8 MHz quartz crystals with Ag electrodes of 4 mm diameter on both sides were purchased from Benyue Technology Ltd.

All measurements of the sensitive features of sensitivity material films were carried out in a homemade cell as shown in Fig. 1. The measurements were conducted in a 100 ml sealed glass vessel. The QCM gas sensors were attached at the inner side of the glass vessel lid. The resonance frequency shifts of QCM sensors due to gas adsorption were measured by the counter, and the recorded data were transferred to the computer versus GPIB (general purpose interface bus) interface. QCM-5 Oscillator was used to excite the QCM device. The calibration gases were prepared by Static Volumetric Method. The testing gases were injected into the chamber with a syringe. And to desorb the testing vapor out of a polymer film (regeneration of the sensor), a flow of high-purity nitrogen was purged through the cell. The backshift of the frequency to its initial position was monitored as an indication of full desorption.

2.2. Synthesis of sensitivity material

The molecular structure and synthetic route of sensitivity material production is shown in Fig. 2.

One equivalent of 2,3-difluorophenol was reacted with one equivalent of allyl bromide in the presence of alcohol and sodium hydroxide at 65 °C, and the product (I) of this reaction was heated to 170 °C, undergoing a Claisen rearrangement. Then intermediate product (II) was reacted with poly(methylhydrosiloxane) with toluene as solvent, platinum-1,3-divinyltetramethyldisiloxane as catalyst at 100 °C for 4 h to yield the target product (III) – poly{methyl[3-(2-hydroxy-3,4-difluoro)phenyl]propyl siloxane}. The target product was obtained as yellow oil in 42.17% yield. FT-IR (thin film): ν (cm^{-1}) 3580, 3439 (OH), 3032 (Ar–H), 2957 (CH_3), 2926 (–CH_2–), 2866, 1622, 1509, 1476, 1408, 1342, 1258, 1212, 1090

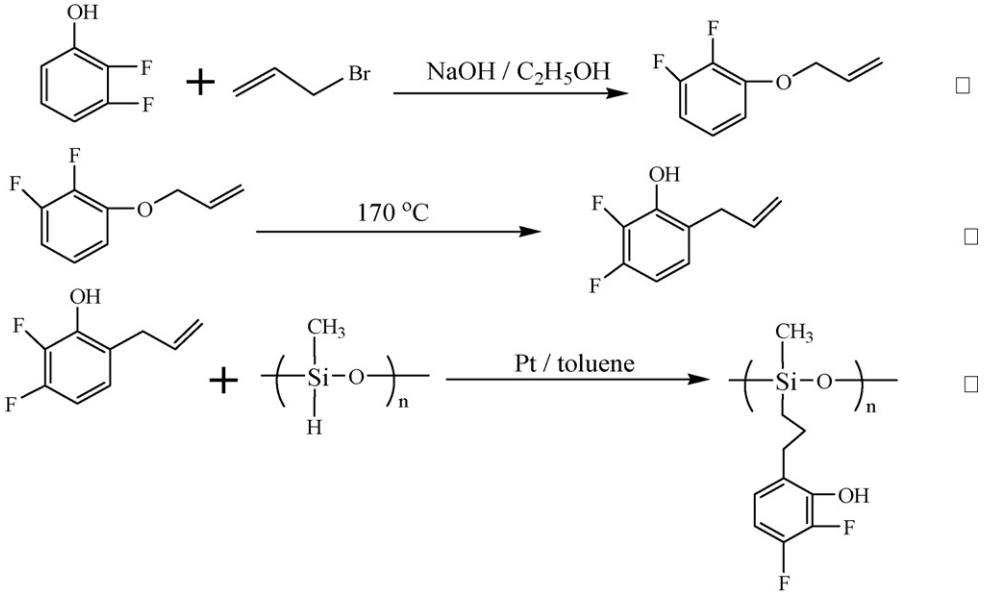

Fig. 2. The molecular structure and synthetic route of sensitivity material production.

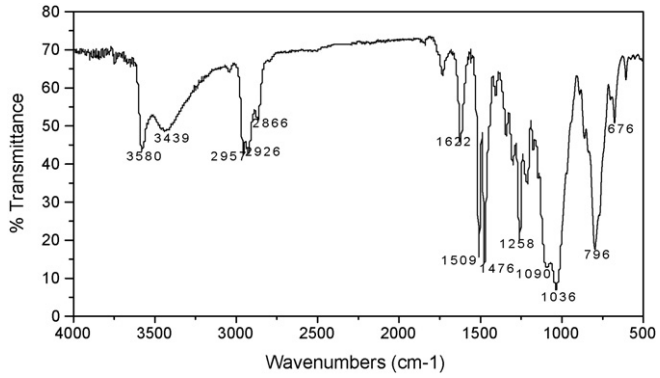

Fig. 3. FT-IR spectrum of poly{methyl[3-(2-hydroxy-3,4-difluoro)phenyl]propyl siloxane} thin film.

(Si–O), 1036, 969, 861, 796, 676. ^{1}H NMR ($CDCl_3$, TMS): δ (ppm) 0.024–0.205 (m, Si–CH_3), 0.491(m, 2H, Si–CH_2), 1.562–1.771 (m, 2H, –CH_2), 2.507 (m, 2H, –CH_2), 6.521–6.701 (m, 2H, Ar–H).

2.3. DMMP vapor tests

A small amount of poly{methyl[3-(2-hydroxy-3,4-difluoro)phenyl]propyl siloxane} was dissolved in $CHCl_3$, and the solution was subsequently added dropwise onto the center of the QCM electrode by a 20 μL microsyringe. The coated QCM was then baked at 50 °C for 0.5 h to obtain stable films. After the solvent had evaporated, a solid film was deposited on the electrode surface. The thickness of the films was determined to be 250 nm by the Sauerbrey equation [20]. The testing gases were then injected into the chamber, and the resonant frequencies of the QCM sensors were recorded.

3. Results and discussion

3.1. Synthesis of poly{methyl[3-(2-hydroxy-3,4-difluoro)phenyl]propyl siloxane}

Poly{methyl[3-(2-hydroxy-3,4-difluoro)phenyl]propyl siloxane} was obtained by treating the intermediate product (II) with poly(methylhydrosiloxane) using platinum-1,3-divinyltetramethyldisiloxane as the catalyst. The disappearance the Si–H group (2127 cm^{-1}) of poly(methylhydrosiloxane) was monitored by FT-IR, as shown in Fig. 3. It was observed that after 4 h, the Si–H signal had disappeared, indicating complete conversion of poly (methylhydrosiloxane) into poly {methyl[3-(2-hydroxy-3,4-difluoro)phenyl]propyl siloxane} had occurred. The formation of this polymer was also confirmed through ^{1}H NMR by observing the disappearance of signals characteristic to the Si–H proton of poly(methylhydrosiloxane) (δ: 4.7 ppm) and the allylic group of protons from the intermediate product (II).

3.2. Sensitivity to DMMP vapor

After the deposition of poly{methyl[3-(2-hydroxy-3,4-difluoro)phenyl]propyl siloxane} film on the QCM, the resonant frequencies of the sensors were measured. The results of the QCM sensors response to different concentrations of DMMP are shown in Fig. 4. It is obvious that as the concentration of the analyte increases, the frequency shifts increases proportionately. Furthermore, it is shown that the QCM sensor exhibits a rapid response, negligible baseline drift, and excellent reversibility. And from the presented data in Fig. 4, it seems that the sensor's response time is inversely proportional to the concentration of DMMP and seems to be quite long for the lowest concentration below 10 ppm. This is ascribed to the rate of diffusion of DMMP increases as the concentration increases, thus, the time of the absorptive reaching the equilibrium increases as the concentration decreases. In addition, in the region of higher DMMP concentration (above 20 ppm) the sensor response reaches a maximum after which it decreases before offset of the gas. The reason is ascribed to the concentration of DMMP were not distributed uniformity with the time increases. Above 20 ppm, the response time is shorter, so that the concentration of DMMP did not distribute uniformity in chamber when the sensor reached the maximum response. This appearance may be avoided, if the calibration gases are prepared by dynamic volumetric method [18].

The responses shown in Fig. 5 represent plotting the frequency shifts (Δf) against the concentrations of DMMP vapor (C). The data points represent frequency shifts from the equilibrium state in response to injected DMMP vapor. It can be seen that the frequency shifts of the sensors were linear to the vapor concentrations in the range of 1–50 ppm, and the regression curve equation can be expressed as: $\Delta f = 49.583 + 14.11C$ with a correlation coefficient $R = 0.998$. According to the slope of regression curve, the sensitivity of the sensor was nearly 14 Hz/ppm.

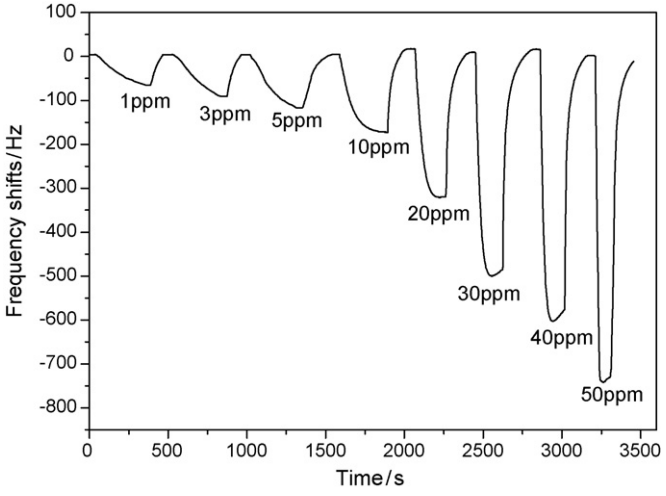

Fig. 4. The response curve of the QCM sensor to different concentrations of DMMP.

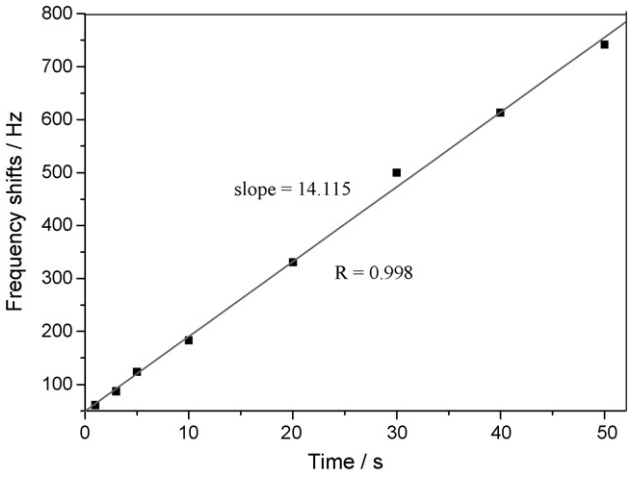

Fig. 5. The frequency shifts of QCM sensors versus DMMP concentration.

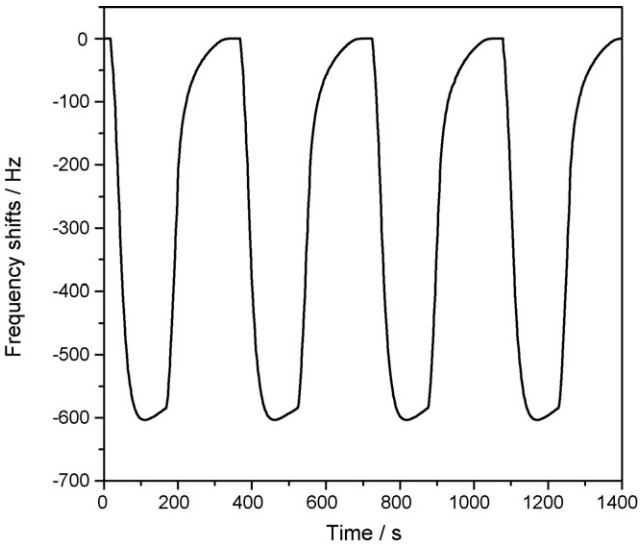

Fig. 6. Reproducibility of the QCM sensor exposed to 40 ppm DMMP.

To investigate the reproducibility of the sensor, the poly{methyl[3-(2-hydroxy-3,4-difluoro)phenyl]propyl siloxane} coated QCM sensor was repeatedly exposed to DMMP (40 ppm) and the time dependent frequency shifts were recorded (Fig. 6). From Fig. 6, it was found that the poly{methyl[3-(2-hydroxy-3,4-difluoro)phenyl]propyl siloxane} modified sensor showed reproducible results, whereas there was a little drift in each cycle. The little drifts were assumed to be caused by the concentration differences because the dilution process could not control the vapor concentration in a high accurate way.

The limit of detection (LOD) of the poly{methyl[3-(2-hydroxy-3,4-difluoro)phenyl]propyl siloxane}-coated QCM sensor was calculated by the measured sensor sensitivity (Hz/ppm).The noise level of the QCM sensor coated with poly{methyl[3-(2-hydroxy-3,4-difluoro)phenyl]propyl siloxane} was 1 Hz, and taking into account the signal-to-noise ratio of 3:1 [21], the theoretical LOD was as low as 0.21 ppm.

3.3. Sensitivity to interfering vapors

The poly{methyl[3-(2-hydroxy-3,4-difluoro)phenyl]propyl siloxane} films were also tested against several conventional volatile organic vapors, including water, acetone, ethanol, dichloroethane, *n*-hexane, dimethyl acetamide (DMA) and toluene (Fig. 7). Each organic vapor was at a saturated concentration, which may result in interference due to overlapping sensitivities. Fig. 7 demonstrates that the sensor was significantly more sensitive to DMMP vapor than to any of the interfering vapors at saturation concentrations. The sensor demonstrated the second highest sensitivity to DMA. This can be attributed to the hydrogen-bond formation between poly{methyl[3-(2-hydroxy-3,4-difluoro)phenyl]propyl siloxane}film and DMA. However, Fig. 7 clearly shows that the sensor has significantly higher sensitivity to DMMP than to DMA.

3.4. Comparison of poly{methyl[3-(2-hydroxy-3,4-difluoro)phenyl]propyl siloxane} and poly(vinylidene fluoride) (PVDF) sensitivity characteristic

The response data of the new polymer was compared with our previously studied polymer, PVDF [22], the result was shown in Fig. 8. The frequency response of the QCM coated with the new

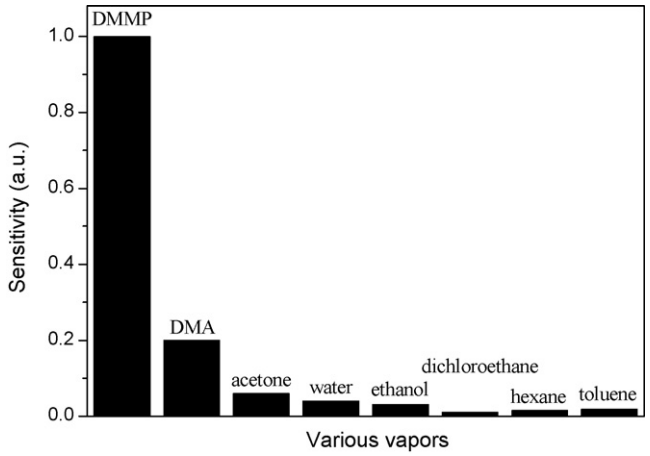

Fig. 7. Responses of the QCM sensor to DMMP and interfering vapor at saturating concentrations.

polymer shows a marked improvement in sensitivity over polymer PVDF. This can be understood by considering the structures of the polymers. PVDF is a weak hydrogen bond acidic polymer, the hydrogen atoms of PVDF exhibit acidity because of the polarization of fluorine atoms, thus the detection mechanism of QCM sensor coated with PVDF bases on the quasi-hydrogen bonding effect of the hydrogen atoms of PVDF between oxygen atoms of DMMP. But the hydroxyl groups of the new polymer exhibit stronger hydrogen bond acidity because of the electrophilic effect of aromatic ring, thus the QCM sensor coated with new polymer bases on the hydrogen bonding effect of the hydroxyl groups of new polymer between oxygen atoms of DMMP. These indicate that the sensitivity of QCM sensor increases as the hydrogen bond acidity of polymer increases.

3.5. Applications

The proposed method was applied to the determination of DMMP in fire retardant sample (Chengdu Fire retardant Paint & Coating Ltd., Chengdu China) in which DMMP was used as an additional agent. The testing gas contained DMMP was obtained by air stripping from the sample. Response measurement and calculation were performed following the analytical procedure described above. In addition, gas chromatographic method [6] was

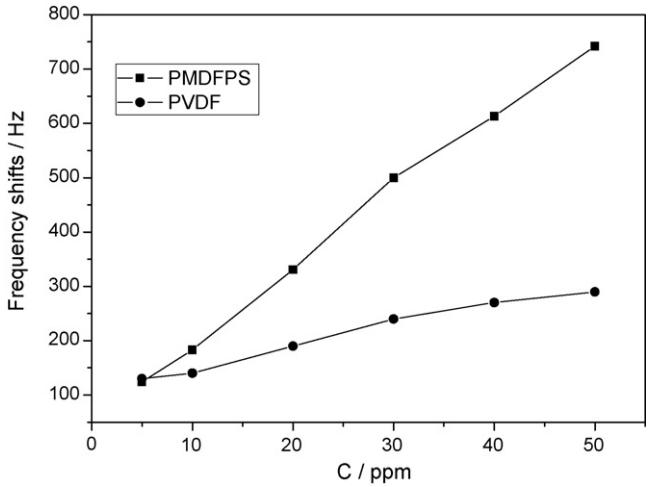

Fig. 8. Comparison of frequency shifts of QCM coated with PVDF and poly{methyl[3-(2-hydroxy-3,4-difluoro)phenyl]propyl siloxane} response to DMMP vapor.

Table 1
Determination of DMMP in fire retardant sample

Added DMMP vapor (ppm)	QCM sensor (ppm)	Gas chromatography (ppm)	Recovery (%) for QCM
0 (sample)	2.9	3.1	\
10	12.8	13.0	99.0
20	23.0	23.1	100.5
30	32.4	33.3	98.3

also used to determinate the DMMP vapor concentration to compare the accuracy of QCM sensor. The results are summarized in Table 1 (data based on the average of three determinations). From Table 1, it is obvious that the QCM sensor was of very high accuracy. Recovery tests were also carried out based on the DMMP standard sample and results show that the recoveries are acceptable.

4. Conclusions

A novel material, poly{methyl[3-(2-hydroxy-3,4-difluoro)-phenyl]propyl siloxane}, sensitive to toxic organophosphate vapor was synthesized from 2,3-difluorophenol, allyl bromide and poly methyl hydrosiloxane, via *O*-alkylation, Claisen rearrange reaction and hydrosilylation reaction. The poly{methyl[3-(2-hydroxy-3,4-difluoro)phenyl]propyl siloxane} was coated on a QCM to investigate its gas sensitive properties to DMMP vapor, a known simulant of nerve agents, as well as other potentially interfering vapors. The QCM sensor responded linearly to DMMP vapor with a slope of 14 Hz/ppm in the 1–50 ppm range with a detection limit of 0.21 ppm (S/N = 3). When tested with saturating vapors, the sensor was more than 10 times as sensitive to DMMP as to other interfering vapors. Thus, poly{methyl[3-(2-hydroxy-3,4-difluoro)phenyl]propyl siloxane} is a very promising material which has great potential as a sensitive detection material for DMMP sensors.

Acknowledgements

This work was financially supported by the National Science Foundation of China (Grant no. 604251001). Support from the State Key Lab of Electronic Thin Films and Integrated Devices is also acknowledged. Analytical assistance is greatly appreciated from Analysis and Testing Center Chengdu Branch, Chinese Academy of Science.

References

[1] Q. Xiao, B. Hu, C. Yu, L. Xia, Z. Jiang, Talanta 69 (2006) 848.
[2] F. Worek, M. Koller, H. Thiermann, L. Szinicz, Toxicology 214 (2005) 182.
[3] E.R. Menzel, L.W. Menzel, J.R. Schwierking, Talanta 67 (2005) 383.
[4] D.H. Moore, J. Physiol. (Paris) 92 (1998) 325.
[5] C.E. Kientz, J. Chromatogr. A 814 (1998) 1.
[6] C.E.A.M. Degenhardt-Langelaan, C.E. Kientz, J. Chromatogr. A 723 (1996) 210.
[7] E.W.J. Hooijschuur, C.E. Kientz, U.A.T. Brinkman, J. Chromatogr. A 928 (2001) 187.
[8] W.R. Creasy, A.A. Rodriguez, J.R. Stuff, R.W. Warren, J. Chromatogr. A 709 (1995) 333.
[9] B.A. Eckenrode, J. Am. Soc. Mass Spectrom. 12 (2001) 683.
[10] W.D. Vermillion, M.D. Crenshaw, J. Chromatogr. A 770 (1997) 253.
[11] J.W. Barlow, P.E. Cassidy, D.R. Lloyd, C.J. You, Y. Chang, P.C. Wong, J. Noriyan, J. Polym. Eng. Sci. 27 (1987) 703.
[12] D. Rebière, C. Déjousa, J. Pistré, J.F. Lipskier, R. Planade, Sens. Actuators B 49 (1998) 139.
[13] J.W. Grate, S.N. Kaganove, S.J. Patrash, R. Craig, M. Bliss, Chem. Mater. 9 (1997) 1201.
[14] C. Zimmermann, D. Rebière, C. Déjous, J. Pistré, E. Chastaing, R. Planade, Sens. Actuators B 76 (2001) 86.
[15] R.A. Mcgill, R. Chung, D.B. Chrisey, P.C. Dorsey, P. Matthews, A. Piqué, T.E. Mlsna, J.L. Stepnowski, IEEE Trans. Ultrason. Ferroelectr. Freq. Control 45 (1998) 1370.
[16] R.A. McGill, M.H. Abraham, J.W. Grate, Chemtech. 9 (1994) 27.
[17] J.W. Grate, M.H. Abraham, Sens. Actuators B 3 (1991) 85.
[18] E.J. Houser, T.E. Mlsna, V.K. Nguyen, R. Chung, R.L. Mowery, R.A. Mcgill, Talanta 54 (2001) 469.
[19] J.W. Grate, S.J. Patrash, S.N. Kaganove, Anal. Chem. 71 (1999) 1033.
[20] C.D. Nucci, A. Fort, S. Rocchi, L. Tondi, V. Vignoli, F. Di Francesco, M.B.S. Santos, IEEE. Trans. Instrum. Meas. 52 (2003) 1079.
[21] T.E. Mlsna, S. Cemalovic, M. Warburton, S.T. Hobson, D.A. Mlsna, S.V. Patel, Sens. Actuators B 116 (2001) 192.
[22] Z.H. Ying, Y.D. Jiang, X.S. Du, G.Z. Xie, J.S. Yu, H. Wang, Sens. Actuators B 125 (2007) 167.

Talanta 76 (2008) 674–679

Contents lists available at ScienceDirect

Talanta

journal homepage: www.elsevier.com/locate/talanta

A screening test for heroin based on sequential injection analysis with dual-reagent chemiluminescence detection

Lauren A. Hill, Claire E. Lenehan[1], Paul S. Francis*, Jacqui L. Adcock, Michelle E. Gange, Frederick M. Pfeffer, Neil W. Barnett

School of Life and Environmental Sciences, Deakin University, Geelong, Victoria 3217, Australia

ARTICLE INFO

Article history:
Received 9 March 2008
Received in revised form 6 April 2008
Accepted 7 April 2008
Available online 16 April 2008

Keywords:
Sequential injection analysis
Sandwich technique
Chemiluminescence detection
Acidic potassium permanganate
Tris(2,2′-bipyridine)ruthenium(III)
Opiate alkaloids
Heroin
Morphine

ABSTRACT

A sequential injection analysis procedure with dual-reagent chemiluminescence detection was applied to the screening of street drug seizure samples for the presence of heroin. The chemiluminescence reagents (acidic potassium permanganate and tris(2,2′-bipyridine)ruthenium(III)) were aspirated from either side of a sample aliquot that was sufficiently large to prevent interdispersion of the reagent zones, and therefore two different chemical reactions could be performed simultaneously at either end of the sample zone. The presence of heroin in seizure samples was indicated by a strong response with the tris(2,2′-bipyridine)ruthenium(III) reagent and confirmed by a significant increase in the response with the permanganate reagent when the sample was treated with sodium hydroxide to hydrolyse the heroin to morphine. Nicomorphine (a morphine-derived pharmaceutical) was synthesised and tested under the same conditions. The responses with the permanganate reagent were similar to those for heroin, which supports the proposed chemical basis for the test. However, the responses with tris(2,2′-bipyridine)ruthenium(III) were far lower for nicomorphine than heroin (approximately 5-fold for the samples that had not been hydrolysed).

1. Introduction

Since its inception in 1990 [1], sequential injection analysis has proven to be a highly useful and flexible protocol for manipulating a wide range of samples and reagents for chemical analysis [2,3]. The power of this approach stems from the configuration and computer control of the individual liquid handling apparatus (pump and multi-position valve), which allows the precise 'stacking' of a defined series of zones (that each contain a liquid, gas or suspended particles) within a narrow-bore conduit. This instrumental arrangement and control enables the use of complex chemical operations that would be difficult to achieve using traditional flow analysis techniques [4]. However, most procedures based on sequential injection analysis involve the detection of a single analyte within a sample and use reaction chemistry employing only one or two reagents [2,3].

Among several innovative approaches to extend sequential injection analysis to the detection of more than one compound per analytical cycle [5], Cerdà and co-workers described the aspiration of two reagents either side of a sample zone that was sufficiently large to prevent interdispersion of the reagents [6]. This 'sandwich' technique enabled two disparate chemical reactions to be performed simultaneously, resulting in two time-resolved signals when the reaction products were propelled through the detector. Although initially applied to the simultaneous determination of iron(II) and nitrite based on colour-forming reactions with *o*-phenanthroline and the Griess reagent [6], this approach has been adopted for other applications, including the determination of phosphate and silicate using vanadomolybdate and ammonium molybdate reagents [7], and the determination of nitrite and nitrate by sandwiching the sample between two zones of the Griess reagent and drawing half the total solution over a reduction column [8].

We have examined the sandwich technique using sequential injection analysis for dual-reagent chemiluminescence detection, which exploits the contrasting selectivity of two highly sensitive reagents to determine two concomitant species in a single aliquot of sample (Fig. 1). Furthermore, we have used this approach to combine two operations of a proposed qualitative screening test for heroin into a single manifold that is better suited for the development of miniaturised analytical devices.

Screening tests are vital for the rapid preliminary identification of drugs and selection of appropriate samples for analysis with confirmatory techniques such as GC–MS or HPLC–MS [9,10]. Current

* Corresponding author. Tel.: +61 3 5227 1294; fax: +61 3 5227 1040.
E-mail address: psf@deakin.edu.au (P.S. Francis).
[1] Current address: School of Chemistry, Physics and Earth Sciences, Flinders University, Adelaide 5001, Australia.

0039-9140/$ – see front matter © 2008 Elsevier B.V. All rights reserved.
doi:10.1016/j.talanta.2008.04.012

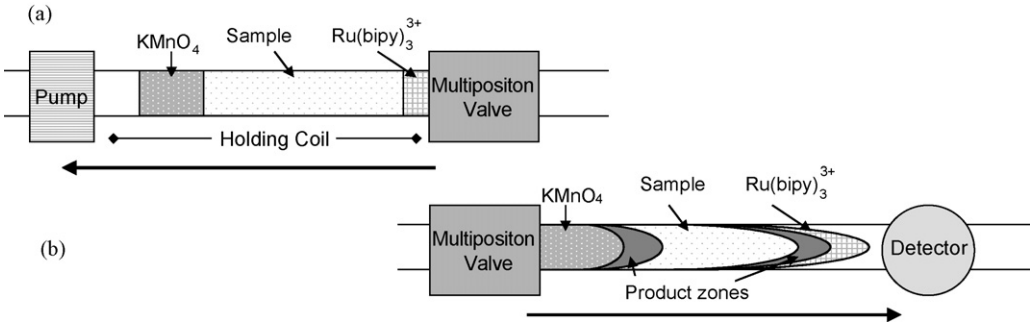

Fig. 1. (a) Stacking sample and reagents in the holding coil by operating the pump in the reverse direction; (b) dispersion of sample and reagent zones upon propulsion of the, stack, toward the detector.

tests for heroin, morphine, and other opiate derivatives involve a visual assessment of colour changes when samples are mixed with the Marquis reagent or Mecke's reagent [9,11,12]. An additional test with nitric acid can be used to distinguish between heroin and morphine [10,12]. Microcrystalline examinations have also been used as presumptive chemical tests, but require experience for adequate interpretation [9].

As depicted in Fig. 2a, the proposed screening test for heroin in street seizure samples is based on the reaction of heroin and its hydrolysis products with two chemiluminescence reagents: tris(2,2′-bipyridine)ruthenium(III) [13] and acidic potassium permanganate [14], which have both previously been used in sensitive procedures for the determination of opiate alkaloids [13,14]. Many non-phenolic morphinan-type alkaloids (and semi-synthetic derivatives) that contain tertiary amine functionality, such as codeine, thebaine and heroin, evoke an intense chemiluminescence emission with tris(2,2′-bipyridine)ruthenium(III), but a very weak emission with acidic potassium permanganate [15–18]. However, the relative intensities are reversed for certain phenolic analogues such as morphine and 6-monoacetylmorphine (the hydrolysis products of heroin; Fig. 2a) [15–18]. The characteristic response for heroin and hydrolysed heroin samples with the two chemiluminescence reagents using flow injection analysis methodology is shown in Fig. 2b [19]. Some other tertiary amines (such as codeine, strychnine and chloroquine) cause false positives with tris(2,2′-bipyridine)ruthenium(III), but do not produce the markedly increased response with the permanganate reagent after the hydrolysis procedure. Therefore, the combination of the two reagents provides an unambiguous test for heroin [19].

In addition to adapting the screening test for sequential injection analysis methodology using the sandwich technique for multi-component analysis, we have synthesised nicomorphine (a morphine-derived pharmaceutical) and examined the relative response for this compound, to further explore the proposed chemical basis for the heroin test.

2. Experimental

2.1. General instrumentation

^{1}H and ^{13}C NMR spectra were recorded on a Jeol JNM-EX 400 MHz FT-NMR spectrometer, with samples dissolved in *d*-chloroform ($CDCl_3$) and referenced against tetramethylsilane ($(CH_3)_4Si$) at 0.00 ppm. Complete characterisation of nicomorphine was performed using 2D NMR techniques. Proton peaks were recorded as follows: chemical shift δ (ppm) (integral, multiplicity (s = singlet, d = doublet, and m = multiplet), coupling constant *J* = Hz, assignment). The CH_2 protons were designated as ax = axial, eq = equatorial, qa = quasi-axial (α) and qe = quasi-equatorial (β). Mass spectra were recorded with a 6210 MSD TOF mass spectrometer (Agilent Technologies, Blackburn, Victoria, Australia) using the following conditions: drying gas, nitrogen (7 ml/min, 350 °C); nebulizer gas, nitrogen (16 psi); capillary voltage, 4.0 kV; vaporizer temperature, 350 °C; cone voltage, 60 V. The melting point of nico-

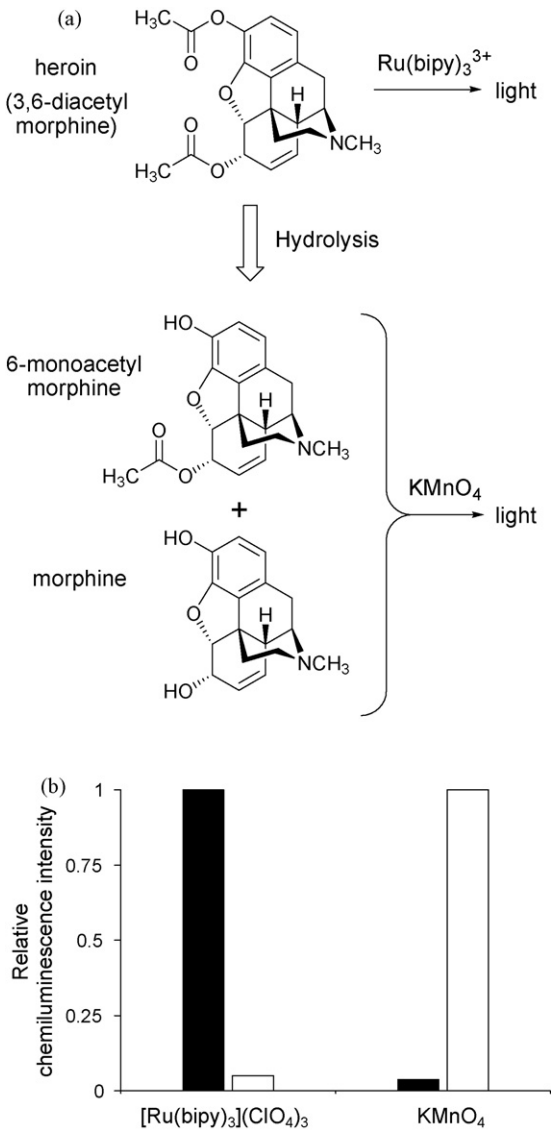

Fig. 2. (a) Concept for a rapid screening test for heroin; (b) chemiluminescence response for a non-hydrolyzed (black columns) and hydrolyzed (white columns) heroin standard with an anhydrous tris(2,2′-bipyridine)ruthenium(III) perchlorate reagent and a potassium permanganate reagent, using flow injection analysis methodology [19]. Signals were normalized for each reagent.

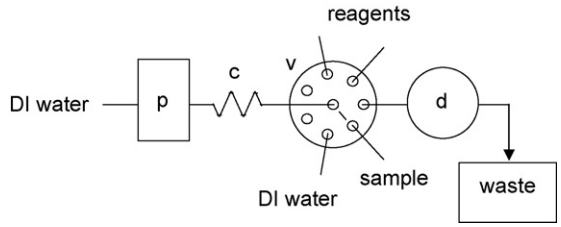

Fig. 3. Sequential injection analysis manifold. Key: p = pump, c = holding coil, v = multi-position valve, and d = detector.

morphine was obtained using a SMP3 Stuart Scientific melting point apparatus and is uncorrected.

2.2. Sequential injection analysis instrumentation

The instrument (Fig. 3) was constructed from a ten-port multiposition valve (Valco C25Z; SGE, Melbourne, Victoria, Australia), chemiluminescence detector (details below) and high precision pump. A Cavro XP-3000 syringe pump (GlobalFIA, Fox Island, Washington, USA) was used for the initial experiments (described in Section 3.1). For subsequent work, the syringe pump was replaced with a milliGAT pump (model CP-DSM-GF; GlobalFIA). The manifold tubing (0.8 mm i.d. PTFE) was purchased from Cole–Parmer (Vernon Hills, IL, USA). The flow-though chemiluminescence detector comprised a glass spiral flow cell (~80 μl, Embell Scientific, Murwillimbah, New South Wales, Australia) mounted flush against a photomultiplier tube (Electron Tubes, type 9828; ETP, Ermington, New South Wales, Australia) operated at 900 V, supplied by a stable power supply (Electron Tubes, model PM20D; ETP) via a voltage divider (Electron Tubes, model C611; ETP). The instrument was controlled with a desktop computer equipped with either LabPC 1200 or LabJack U12 data acquisition board (National Instruments, Ringwood, Victoria, Australia), and running LabVIEW software (Version 6.0, National Instruments). The instrument was initially flushed with deionised water to remove air bubbles and contaminants prior to priming of the tubing between the valve and the solution reservoirs.

2.3. Chemiluminescence reagents

A univariate optimisation of each component of the chemiluminescence reagents was conducted to achieve the best response using the SIA instrument. The optimised permanganate reagent was prepared daily by dissolving potassium permanganate (Chem-Supply, Gillman, South Australia, Australia) in 1% (m/v) sodium polyphosphate (Aldrich, St Louis, MO, USA) and adjusting the pH to 2.5 by the drop-wise addition of concentrated sulfuric acid (Merck, Kilsyth, Victoria, Australia). The tris(2,2′-bipyridine)ruthenium(III) reagent was prepared by dissolving tris(2,2′-bipyridine)ruthenium(II) chloride hexahydrate (Strem, Newbury, MA, USA) in 0.05 M sulfuric acid and oxidising the complex with solid lead dioxide (Ajax, Sydney, New South Wales, Australia). The emerald green solution was then filtered using an Acrodisc PSF syringe filter (0.45 μm Tuffyn membrane; Pall, Cheltenham, Victoria, Australia) to remove the excess oxidant prior to use.

2.4. Opiate standards

Pure heroin (3,6-diacetylmorphine) and drug seizure samples were provided by the Victoria Police Forensic Services Centre (Macleod, Victoria, Australia). Morphine, codeine and thebaine were obtained from GlaxoSmithKline (Port Fairy, Victoria, Australia). Stock solutions (1×10^{-3} M) of the alkaloids were prepared by dissolution of the free base in deionised water, aided by the addition of one or two drops of concentrated sulfuric acid per 100 ml of solution. Stock solutions of 3,6-diacetylmorphine (1×10^{-3} M) were prepared in acetic acid (BHD, Poole, England) solution (0.1%, v/v).

2.5. Sample preparation for screening test

Stock solutions of the drug seizure samples were prepared by dissolving 15 mg of the solid material into 100 ml of deionised water. The 'nonhydrolysed' samples were prepared by taking 1 ml of stock solution (3,6-diacetylmorphine, nicomorphine, or heroin drug seizure sample) and diluting to 100 ml with a 0.05% (v/v) acetic acid solution. The 'hydrolysed' samples were prepared by mixing 1 ml of stock solution with 100 μl of 1.0 M sodium hydroxide (Ajax) and then diluting the mixture to 100 ml with the 0.05% (v/v) acetic acid solution.

2.6. Synthesis of nicomorphine

A mixture of nicotinic acid (0.136 g, 1.10 mmol), morphine (0.151 g, 0.526 mmol), EDCI (0.253 g, 1.31 mmol) and 4-(dimethylamino)pyridine (DMAP) (0.0213 g, 0.174 mmol) in anhydrous *N*,*N*-dimethylformamide (DMF) (5 ml) was stirred at room temperature for 24 h under a nitrogen atmosphere (Fig. 4). A second equivalent of EDCI (0.252 g, 1.31 mmol) was added and the mixture was stirred at room temperature for a further 24 h. Chloroform ($CHCl_3$) (100 ml) was added and the contents of the flask transferred to a separatory funnel. This organic solution

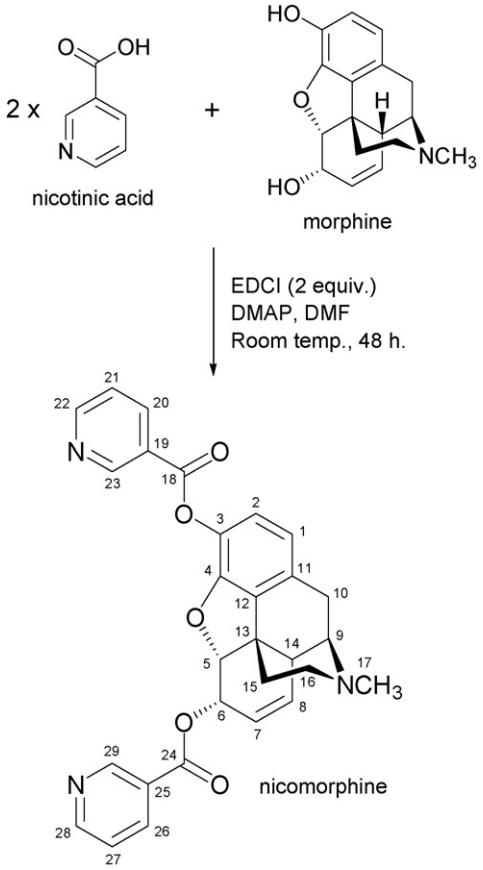

Fig. 4. Synthesis of nicomorphine.

was washed with water (2 × 100 ml), then saturated aqueous sodium chloride (2 × 100 ml). The organic was drained, dried over anhydrous magnesium sulfate, filtered and the solvent removed *in vacuo* to furnish an oily residue. Purification by column chromatography (9:1 $CHCl_3$:methanol) afforded the desired product as a solid (97.2 mg, 37% yield; mp 176.4–177.8 °C; Lit. 178–178.5 °C [20]; MS: *m*/*z* 496.20 $[M+H]^+$, calculated: 496.19).

^{1}H NMR (400 MHz; $CDCl_3$): 1.93 (1H, d, *J* = 12, $H15_{eq}$), 2.09 (1H, ddd, *J* = 12, 12, 4.8, $H15_{ax}$), 2.32–2.42 (2H, m, $H10_{qa}$, $H16_{ax}$), 2.45 (3H, s, $NCH_3$17), 2.61 (1H, dd, *J* = 3.7, 12, $H16_{eq}$), 2.84 (1H, ddd, *J* = 3.0, 3.0, 3.0, *H*14), 3.10 (1H, d, *J* = 19, $H10_{qe}$), 3.41 (1H, dd, *J* = 3.0, 5.5, *H*9), 5.26 (1H, d, *J* = 7.0, *H*5), 5.41 (1H, m, *H*6), 5.55 (1H, m, *H*8), 5.79 (1H, d, *J* = 9.9, *H*7), 6.66 (1H, d, *J* = 8.0, *H*1), 6.88 (1H, d, *J* = 8.0, *H*2), 7.22 (1H, dd, *J* = 4.8, *J* = 7.7, *H*27), 7.28 (1H, dd, *J* = 4.8, 7.7, *H*21), 8.11 (1H, d, *J* = 8.0, *H*20), 8.21 (1H, d, *J* = 8.0, *H*26), 8.65 (1H, d, *J* = 4.0, *H*28), 8.73 (1H, d, *J* = 4.0, *H*22), 9.08 (1H, s, *H*23), 9.18 (1H, s, *H*29). ^{13}C NMR (100.5 MHz; $CDCl_3$): 20.8, 35.2, 40.5, 42.7, 43.1, 46.7, 59.1, 68.6, 88.5, 119.8, 121.9, 123.1, 123.3, 125.0, 125.6, 128.2, 129.9, 131.7, 131.7, 132.8, 137.1, 137.5, 149.2, 151.2, 151.3, 153.5, 153.8, 162.8, 164.5.

3. Results and discussion

3.1. Optimisation of instrumental parameters

Preliminary investigations into sequential injection analysis with dual-reagent chemiluminescence detection were performed using standard solutions of morphine and thebaine or mixtures of the two analytes. In some cases, depending on availability, codeine was used instead of thebaine (Fig. 5).

As shown in Fig. 1a, solutions were aspirated into the holding coil in the following order: (1) permanganate reagent, (2) sample solution, and (3) tris(2,2′-bipyridine)ruthenium(III) reagent. The flow was then reversed to propel the solutions through the detector (Fig. 1b). The chemiluminescence signal from the reaction of thebaine (or codeine) with tris(2,2′-bipyridine)ruthenium(III) and the chemiluminescence signal from the reaction of morphine with acidic potassium permanganate were recorded. Under appropriate conditions, a mixture of analytes resulted in two time-resolved peaks (Fig. 6). Reversal of the aspiration order resulted in an increase in the emission from the reaction with potassium permanganate, but a relatively large decrease in the emission from the reaction with tris(2,2′-bipyridine)ruthenium(III). This was attributed to a faster light-producing pathway with tris(2,2′-bipyridine)ruthenium(III); when this reagent is aspirated first, a greater proportion of the transient emission occurs before the merging zones reach the detector.

The segregation of the two peaks (as shown in Fig. 6) is dependent on a sufficiently large volume of sample solution sandwiched between the two chemiluminescence reagents. Using our instrumental configuration and analyte concentrations of 1×10^{-5} M, a sample volume of at least 670 μl was required to prevent interdispersion of the reaction zones. Sample volumes over 1330 μl caused unnecessary decreases in intensity with the permanganate reagent due to the extended time that the sample and reagent zone were

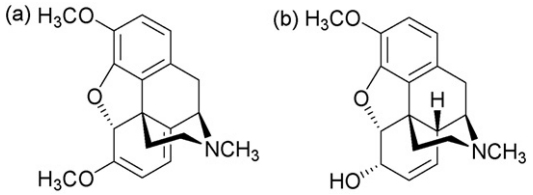

Fig. 5. The chemical structure of (a) thebaine and (b) codeine.

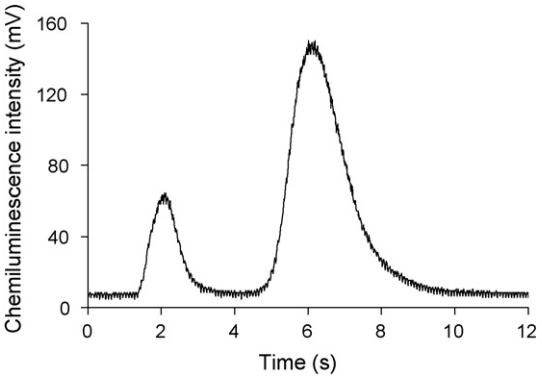

Fig. 6. Response for a sample solution containing morphine and codeine (1×10^{-5} M), using the sequential injection analysis system with two chemiluminescence reagents. The peak at ~2 s resulted from the reaction of codeine with the tris(2,2′-bipyridine)ruthenium(III) reagent and the peak at 6.5 s was due to the reaction of morphine with the permanganate reagent.

in contact within the holding coil. A sample volume of 1000 μl was used for all further experiments.

The volume of the tris(2,2′-bipyridine)ruthenium(III) reagent solution was varied between 20 and 150 μl. Volumes below 50 μl resulted in lower precision in the chemiluminescence signal for that reagent. Increasing the volume above 50 μl did not have a significant effect on precision; a small enhancement in signal intensity was observed, but this was accompanied by signal broadening. Consequently, the volume was maintained at 50 μl. For the permanganate reagent, a decrease in signal intensity was observed when the aspirated volume was reduced below 150 μl, and therefore this value was selected for all further experiments.

The effect of flow rate on the precision and signal intensity was investigated. Increasing the aspiration (reverse) rate from 0.5 to 1.25 ml min^{-1} had little effect on the precision, but improved the emission intensity, probably due to the reduced residence time in the holding coil. Increasing the rate of propulsion (forward flow) to 10 ml min^{-1} resulted in improved peak heights whilst maintaining good reproducibility (*ca.* 3% r.s.d.). Forward flow rates greater than 10 ml min^{-1} were not practicable due to the consequent high pressure. The optimised parameters are summarised in Table 1.

A series of standard solutions (1×10^{-7} to 5×10^{-5} M) was used to determine the analytical figures of merit under the optimised conditions. Quadratic curves were required for morphine ($y = -0.0001x^2 + 0.0181x - 0.0022$; $R^2 = 0.9924$) and thebaine ($y = -5 \times 10^{-5}x^2 + 0.006x + 0.1012$; $R^2 = 0.9842$) calibrations. The limits of detection (blank + 3σ) of 3×10^{-8} M morphine and 5×10^{-8} M thebaine were inferior to those obtained using single reagent zone or immobilised reagent approaches [21,22], but the proposed method is sufficiently sensitive for the application described in the following section. The relative standard deviations for the response (peak area) for 6×10^{-6} M morphine and thebaine (using ten replicates of a binary mixture) were 2.4% and 3.3%, respectively.

3.2. A screening test for heroin

We have previously developed a new approach to qualitatively screen for heroin in drug seizure samples [19], based on the response with two chemiluminescence reagents (with and without the initial addition of sodium hydroxide to the sample to rapidly convert the heroin to morphine). In that study, two flow injection analysis systems were used to combine the samples with the chemiluminescence reagents [19] and although this simple approach was convenient for the optimisation of the reaction

Table 1
Optimum parameters for the dual-reagent sequential injection analysis system

Step	Solution	Direction of flow	Volume (μl)	Flow rate (ml min^{-1})
1	Deionised water	Reverse	1500	10
2	0.5 mM $KMnO_4$ in 1% (m/v) sodium polyphosphate, adjusted to pH 2.5	Reverse	150	1.25
3	Sample	Reverse	1000	1.25
4	0.5 mM $Ru(bipy)_3^{3+}$ in 0.05 M H_2SO_4	Reverse	50	1.25
5	Holding coil contents	Forward	2700	10

chemistry, it is not ideal for the development of miniaturised devices for at-scene analysis. However, the multi-zone sequential injection analysis system allows the simultaneous reaction of the sample with both reagents within a single flow manifold.

Using the optimised parameters shown in Table 1, the chemiluminescence responses for the pure heroin solutions prepared with and without the hydrolysis step were examined. The relative responses (Fig. 7) were similar to those obtained when combining the samples with individual reagents using flow injection analysis (Fig. 2b), with the exception that a larger response was observed for the hydrolysed sample with the tris(2,2′-bipyridine)ruthenium(III) reagent. However, this was of little consequence to the overall screening procedure.

Four drug seizure samples (known to contain heroin) were obtained from the Victoria Police Forensic Services Centre and examined using the sequential injection analysis version of the screening test. The relative signal intensities (peak heights) with the tris(2,2′-bipyridine)ruthenium(III) reagent and the permanganate reagent for the non-hydrolysed and hydrolysed samples are shown in Fig. 8a and b. In the previous study (using the flow injection analysis approach), both the non-hydrolysed and hydrolysed heroin seizure samples produced the maximum instrument response with the tris(2,2′-bipyridine)ruthenium(III) reagent [19]. However, in the present study, a more judicious selection of data acquisition settings prevented any signal reaching the maximum response. The chemiluminescence signals for the hydrolysed samples were between 36% and 50% of that observed from the corresponding non-hydrolysed samples (Fig. 8a), due to the conversion of heroin to 6-monoacetylmorphine and/or morphine, which (unlike heroin) do not produce a strong signal with the tris(2,2′-bipyridine)ruthenium(III) reagent. This range was similar to the response observed for the hydrolysed sample of pure heroin, and may therefore indicate that compounds previously found to interfere with the tris(2,2′-bipyridine)ruthenium(III) aspect of the test (such as codeine, strychnine and chloroquine [19]) were not present in these seizure samples.

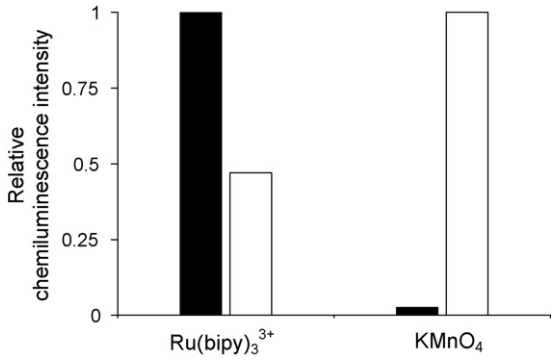

Fig. 7. Response for a non-hydrolyzed (black columns) and hydrolyzed (white columns) pure heroin standard with tris(2,2′-bipyridine)ruthenium(III) and permanganate reagents, using the sequential injection analysis approach. Signals were normalized for each reagent.

Fig. 8b shows the relative responses for the non-hydrolysed and hydrolysed heroin seizure samples with the permanganate reagent. The non-hydrolysed samples yielded chemiluminescence signals that were between 8.0% and 12.1% of that observed from the corresponding hydrolysed sample. This was similar to the response for pure heroin (8.2%). In each case a clear positive result for heroin was obtained.

3.3. Relative response for nicomorphine

Using flow injection analysis, many cutting agents (and other compounds that could be mistaken as heroin) have been tested [19]. Although several compounds containing tertiary amines produce a large signal with the tris(2,2′-bipyridine)ruthenium(III) reagent, none of those tested so far have been found to produce the large increase in the response with the permanganate reagent that is observed for heroin after the hydrolysis procedure [19]. In this study, we have examined the relative response for nicomorphine, a morphine-derived pharmaceutical with a potentially hydrolysable ester.

Nicomorphine has previously been synthesised by treating morphine with either the anhydride or acid chloride of nicotinic acid

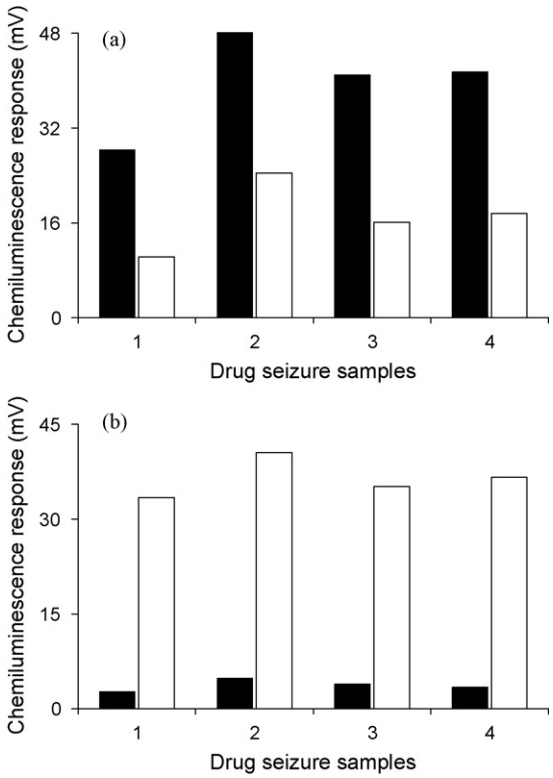

Fig. 8. Responses for non-hydrolyzed (black columns) and hydrolyzed (white columns) drug seizure samples with the (a) tris(2,2′-bipyridine)ruthenium(III) reagent and (b) the permanganate reagent, using the sequential injection analysis approach.

[23,24]. For the small-scale synthesis of nicomorphine (Fig. 4), we coupled morphine with nicotinic acid using a carbodiimide: *N*-(3-dimethylaminopropyl)-*N*′-ethylcarbodiimide hydrochloride (EDCI) as the dehydrating agent [25].

Using the dual-reagent sequential injection analysis system, we found that the responses with the permanganate reagent (with and without the initial hydrolysis procedure) were similar to those for heroin, which supports the proposed chemical basis for the heroin test (Fig. 2). However, the responses with tris(2,2′-bipyridine)ruthenium(III) were far lower for nicomorphine than heroin (approximately 5-fold for the samples that had not been hydrolysed). Large differences in the chemiluminescence intensity with tris(2,2′-bipyridine)ruthenium(III) have previously been reported for structurally related opiate alkaloids [16].

4. Conclusions

The sandwich technique enabled each sample to be simultaneously mixed with two different chemiluminescence reagents, which resulted in two time-resolved signals when the reacting mixture was propelled through the detector. This approach provided an appropriate means to simultaneously perform both steps of a proposed screening test for heroin within a single flow analysis manifold that was better suited for the development of miniaturised devices than the previously reported system. The examination of nicomorphine provided further evidence for the chemical basis of the test. Nicomorphine is not expected to be found in clandestine laboratories and therefore the positive result for this compound does not pose a problem for the screening test.

Acknowledgements

The authors thank the Australian Research Council and BioDeakin for financial support, Daniel Priebbenow for help with the synthesis of nicomorphine, and Gail Dyson and Xavier Conlan for their assistance with NMR and mass spectrometry.

References

[1] J. Ruzicka, G.D. Marshall, Anal. Chim. Acta 237 (1990) 329–343.
[2] C.E. Lenehan, N.W. Barnett, S.W. Lewis, Analyst 127 (2002) 997–1020.
[3] A. Economou, Trends Anal. Chem. 24 (2005) 416–425.
[4] G. Marshall, D. Wolcott, D. Olson, Anal. Chim. Acta 499 (2003) 29–40.
[5] V. Gómez, M.P. Callao, Trends Anal. Chem. 26 (2007) 767–774.
[6] J.M. Estela, A. Cladera, A. Munoz, V. Cerdà, Int. J. Environ. Anal. Chem. 64 (1996) 205–215.
[7] F. Mas-Torres, A. Munoz, J.M. Estela, V. Cerdà, Analyst 122 (1997) 1033–1038.
[8] A. Cerdà, M.T. Oms, R. Forteza, V. Cerdà, Anal. Chim. Acta 371 (1998) 63–71.
[9] B. Levine, in: J.A. Siegel, P.J. Saukko, G.C. Knupfer (Eds.), Encyclopedia of Forensic Sciences, Academic Press, San Diego, 2000, pp. 167–172.
[10] C.L. O'Neal, D.J. Crouch, A.A. Fatah, Forensic Sci. Int. 109 (2000) 189–201.
[11] C.C. Clark, J. Forensic Sci. 22 (1977) 418–428.
[12] OVD Inc. (Armor Forensics) website: http://www.odvinc.com/.
[13] B.A. Gorman, P.S. Francis, N.W. Barnett, Analyst 131 (2006) 616–639.
[14] J.L. Adcock, P.S. Francis, N.W. Barnett, Anal. Chim. Acta 601 (2007) 36–67.
[15] R.W. Abbott, A. Townshend, R. Gill, Analyst 111 (1986) 635–640.
[16] N.W. Barnett, T.A. Bowser, R.D. Gerardi, B. Smith, Anal. Chim. Acta 318 (1996) 309–317.
[17] J.L. Adcock, P.S. Francis, K.M. Agg, G.D. Marshall, N.W. Barnett, Anal. Chim. Acta 600 (2007) 136–141.
[18] J.W. Costin, S.W. Lewis, S.D. Purcell, L.R. Waddell, P.S. Francis, N.W. Barnett, Anal. Chim. Acta 597 (2007) 19–23.
[19] K.M. Agg, A.F. Craddock, R. Bos, P.S. Francis, S.W. Lewis, N.W. Barnett, J. Forensic Sci. 51 (2006) 1080–1084 (erratum: J. Forensic Sci. 52 (2007) 759).
[20] M.J. O'Neil, P.A. Heckelman, C.B. Koch, K.J. Roman (Eds.), The Merck Index: An Encyclopedia of Chemicals, Drugs, and Biologicals, 14th ed., Nicomorphine [639-48-5], Merck, Whitehouse Station, NJ, USA, 2006, p. 1127.
[21] B.A. Gorman, N.W. Barnett, R. Bos, Anal. Chim. Acta 541 (2004) 119–124.
[22] C.E. Lenehan, N.W. Barnett, S.W. Lewis, J. Autom. Methods Manage. Chem. 24 (2002) 99–103.
[23] A. Pongratz, K.L. Zirm, Monatsh. Chem. 88 (1957) 330–335.
[24] S. Hosztafi, I. Kohegyi, C. Simon, Z. Furst, Arzneimittelforschung 43 (1993) 1200–1203.
[25] M.K. Dhaon, R.K. Olsen, K. Ramasamy, J. Org. Chem. 47 (1982) 1962–1965.

Talanta 76 (2008) 522–527

Contents lists available at ScienceDirect

Talanta

journal homepage: www.elsevier.com/locate/talanta

Study on the retention equation in hydrophilic interaction liquid chromatography

Gaowa Jin, Zhimou Guo, Feifang Zhang, Xingya Xue, Yu Jin, Xinmiao Liang*

Dalian Institute of Chemical Physics, Chinese Academy of Sciences, Dalian 116023, China

ARTICLE INFO

Article history:
Received 23 January 2008
Received in revised form 20 March 2008
Accepted 21 March 2008
Available online 8 April 2008

Keywords:
Hydrophilic interaction liquid chromatography
Retention equation
Stationary phases
Selectivity
Nucleoside

ABSTRACT

Hydrophilic interaction liquid chromatography (HILIC) is an effective technique for separating polar compounds. But its retention equation has not been studied systematically yet. In this study, an appropriate retention equation was established by using eight nucleosides as model analytes and by comparing four retention models on six different HILIC columns. As a result, retention equation $\ln k = a + b \times \ln C_B + c \times C_B$ could be quantitatively described the retention factors with good accuracy in HILIC mode. Based on this equation, the retention times of eight nucleosides under the conditions by other mobile phase can be predicted on each column. All of the predicted relative errors of retention times were smaller than 5%. The established retention model was also successfully applied to predict retention times of the real Traditional Chinese Medicine—*Carthaus tinctorius* L. sample.

1. Introduction

Hydrophilic interaction liquid chromatography (HILIC), an alternative HPLC mode for separating polar compounds, was firstly termed by Alpert in 1990 [1]. Like normal phase HPLC (NP-HPLC), HILIC uses polar stationary phases. But the mobile phase is similar to reversed phase HPLC (RP-HPLC) mode [2–4]. It has many specific advantages over conventional NP-HPLC or RP-HPLC. For example, it is suitable for analysis of the compounds which elute near the void on reserved-phase chromatographic columns. Polar samples always have good solubility in aqueous mobile phase used by HILIC, which overcome the drawbacks of poor solubility often encountered in NP-HPLC. The expensive ion pair reagents are not required under HILIC mode, and it is conveniently coupled to mass spectrometry (MS) analysis.

Commonly, there are some polar compounds existing in the complex systems, such as metabonomic, proteinomic and Traditional Chinese Medicines (TCMs). These polar compounds are always poorly retained on RP-HPLC columns. HILIC has been proven to be an effective alternative method for analysis of these polar compounds, which has been successfully demonstrated by the analysis of carbohydrates [5,6], peptides [7–9], and polar pharmaceuticals [10,11], etc. HILIC separation employs polar stationary phases such as silica, amino or cyano phases traditionally used in NPLC [2,3,7,11,12]. Although the number of commercially available columns designed specially for HILIC is growing, there is still not a versatile stationary phase like C18 in RP-HPLC. Some novel separation materials for HILIC have attracted increasing attention in recent years [4,10,13–21]. These special separation materials for HILIC demonstrate good selectivity and reproducibility for separation of polar compounds. However, different types of separation materials for HILIC have different retention characteristics and separation selectivity. Besides, the preparation procedure is usually complicated and difficult due to the complex structures and active groups on the bonded stationary phases. Our group synthesized a series of stationary phases by "click chemistry" for separating polar compounds under HILIC mode [22,23], such as single-hydroxyl, multi-hydroxyl and β-cyclodextrin columns. The stationary phase structures of them were shown in Fig. 1.

Although the reports about HILIC increased rapidly, the retention equation is short of systematic research. Retention equation plays an important role in prediction and optimization on a given chromatographic system. There are many different retention prediction approaches in RP-HPLC. But in HILIC, most papers discussed the tendency of retention behavior affected by the mobile phase composition, but the quantitative description of retention in HILIC was not studied further [24–27]. Jinno et al. developed a retention prediction model of adrenoreceptor agonists and antagonists in HILIC using quantitative structure–retention relationships (QSRRs) equation [28–30]. This equation is complex, it shows the rela-

* Corresponding author at: Dalian Institute of Chemical Physics, Chinese Academy of Sciences, Bio-Technique Department, 457 Zhongshan Road, Dalian, Liaoning 116023, China. Tel.: +86 411 8437 9519; fax: +86 411 8437 9539.
E-mail address: liangxm@dicp.ac.cn (X. Liang).

0039-9140/$ – see front matter © 2008 Elsevier B.V. All rights reserved.
doi:10.1016/j.talanta.2008.03.042

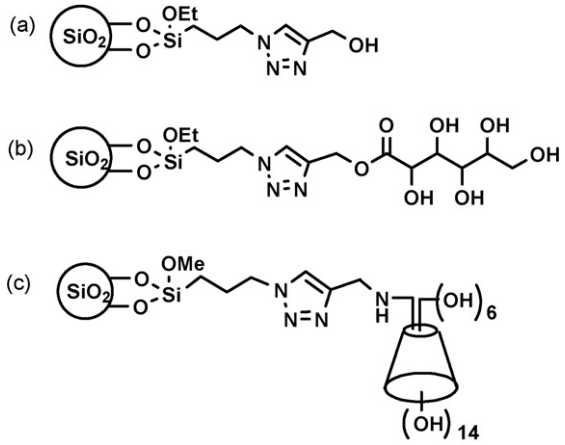

Fig. 1. The functionalized packings of single-hydroxyl (a), multi-hydroxyl (b) and β-cyclodextrin (c) columns.

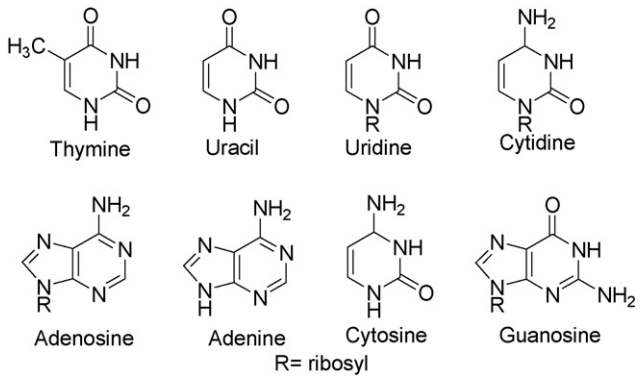

Fig. 2. The chemical structures of eight nucleosides.

tionships between the chromatographic parameters such as the logarithm of the retention factor and the descriptors accounting for the structural differences among the analytes. But for structure unknown compounds, QSRR method is not suitable. So it is necessary to establish a versatile retention equation in HILIC for further prediction and optimization.

A major objective of this article was to establish suitable retention equation in HILIC. To this end, six different polar stationary phases were selected including native silica, organic inorganic hybrid silica, single-hydroxyl, multi-hydroxyl, β-cyclodextrin and acylamide that contained different functional groups on the silica surface. The selectivity of different columns was studied. Comparing four different retention models, eight nucleosides were selected to establish suitable quantitative descriptive retention equation. Based on established equation, the retention time of each compound on each column under other mobile phase conditions was predicted. The established retention equation was also successfully applied to predict retention times of the real TCM—*Carthaus tinctorius* L. sample.

2. Experimental

2.1. Materials and chemicals

The reference substances cytidine, adenosine, guanosine, cytosine, uracil (Acros), uridine, thymine (Sinopharm Chemical Reagent Co. Ltd.) and adenine (Shanghai Bio Life Science & Technology Co. Ltd.) were diluted in acetonitrile/water to prepare a mix stock solution with 0.13 mg ml^{-1} for each compound. The chemical structures of the analytes were shown in Fig. 2. Acetic acid and ammonium acetate (Tedia, USA) were mobile phase additives. HPLC grade acetonitrile (Fisher) was filtered by 0.22 μm membrane. Milli-Q pure water (Millipore, Bedford, USA) was used throughout.

2.2. Instruments and methods

All analyses were performed on a Waters Acquity UPLC system (Waters, USA), including binary solvent manager, sample manager and PDA detector, connected to Waters Empower 2 software. The HILIC columns were single-hydroxyl column (4.6 mm × 150 mm, 5 μm, homemade), multi-hydroxyl column (4.6 mm × 150 mm, 5 μm, homemade), β-cyclodextrin column (4.6 mm × 150 mm, 5 μm, homemade), Venusil HILIC (4.6 mm × 250 mm, 5 μm, USA), Atlantis HILIC silica (4.6 mm × 250 mm, 5 μm, Waters) and BEH HILIC column (2.1 mm × 100 mm, 1.7 μm, Waters), respectively. The mobile phases were (A) acetonitrile with 200 mmol l^{-1} ammonium acetate aqueous solution and acetic acid (97.5:2.5:0.1, v/v/v); (B) water with 200 mmol l^{-1} ammonium acetate aqueous solution and acetic acid (97.5:2.5:0.1, v/v/v). The retention times were obtained at 10 isocratic conditions to establish retention equations. The 10 isocratic conditions were performed using mobile phase A by 100, 97, 93, 90, 85, 80, 75, 70, 65 and 60%, respectively. The isocratic conditions at 95% and 87% of A were used to validate the precision of prediction. The experiment for each condition was carried out in duplicate. The flow rates were 0.2 ml min^{-1} for BEH HILIC column and 1.0 ml min^{-1} for other columns. UV detection was at 260 nm. All analysis was performed at ambient temperature.

2.3. Plant material and sample preparation

C. tinctorius L. was collected from Ta County, Xinjiang Province, China. The herbs were authenticated by the China Academy of Traditional Chinese Medicine Research—Institute of Traditional Chinese Medicine. The sample used in this study was the standard fraction in item—Knowledge Innovation Project of the Chinese Academy of Science (KGCX2 – SW – 213). They were prepared as follows: the herb was dried and 100 kg was weighed and refluxed with 10-fold water twice for 2 and 1.5 h, respectively. The solution was filtered and the filtrate was concentrated and sprayed to dryness. Then 1.5 kg of residual solid was collected and diluted in 4.5 l of water and 12.6 l of 95% ethanol to produce 70% ethanol solution for deposition. The upper clear layer was evaporated to remove ethanol and the residual aqueous solution was partitioned with EtOAc and *n*-BuOH, in sequence. The *n*-butanol fraction was concentrated and the residual aqueous solution was subjected to AB-8 macroporous resin column and successively eluted with water. The fraction was collected and evaporated to dryness. In this study, an aliquot (5 mg) of the dry sample was redissolved in 1 ml of acetonitrile/water and filtered through a 0.22-μm cellulose membrane before injection into the UPLC column for analysis.

3. Results and discussion

3.1. Selectivity of the stationary phases

Selectivity is an important parameter to influence chromatographic separation. It reflects the difference between two solutes in terms of Gibbs free energy of transfer from the mobile phase to the stationary phase.

$$\alpha = \frac{k_j}{k_i}$$

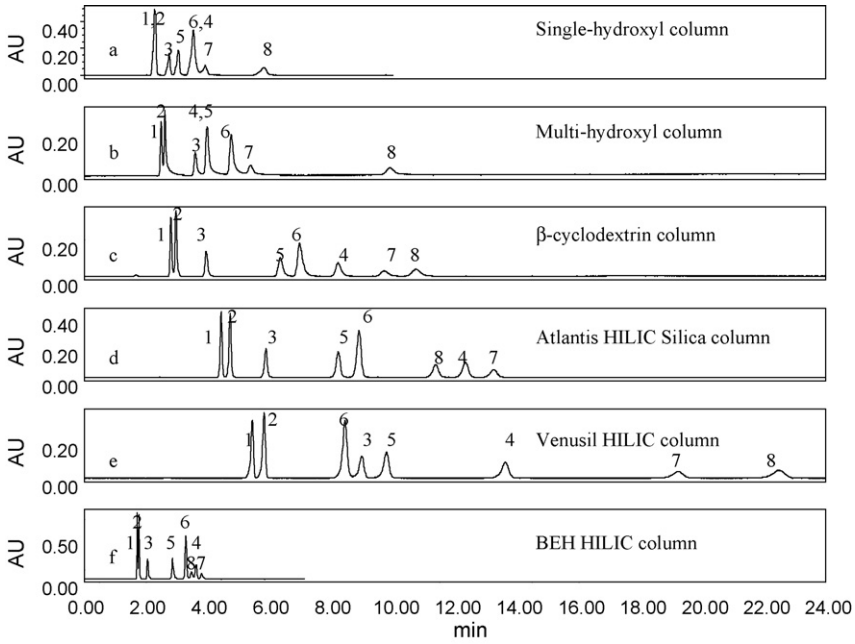

Fig. 3. Separation of eight nucleosides on: (a) single-hydroxyl column; (b) multi-hydroxyl column; (c) β-cyclodextrin column; (d) Atlantis HILIC silica column; (e) Venusil HILIC column; (f) BEH HILIC column. Mobile phase: acetonitrile with 2.5% 200 mmol l^{-1} ammonium acetate aqueous solution and 0.1% acetic acid/water with 2.5% 200 mmol l^{-1} ammonium acetate aqueous solution and 0.1% acetic (93:7, v/v). Flow rate: 1.0 ml min^{-1} (for (f) 0.2 ml min^{-1}). UV detection: 260 nm. Compounds: 1. thymine; 2. uracil; 3. uridine; 4. cytosine; 5. adenosine; 6. adenine; 7. cytidine; 8. guanosine.

where k_j and k_i are retention factors for solutes i and j. Column selectivity depends on the molecular interactions between the stationary phases and the solutes [31]. Fig. 3 is a typical chromatogram of eight nucleosides in all six columns. On single-hydroxyl, multi-hydroxyl and β-cyclodextrin columns, the elution order of eight nucleosides was similar, but their retention times were gradually increased. The reason was that the hydroxyl numbers and structures of their stationary phases were different (Fig. 1). The elution order was the same on Atlantis HILIC silica column and BEH HILIC column. The packings of their stationary phases were silica with different surface properties. The retention times of eight nucleosides on BEH HILIC column were shorter, but the good separation was achieved due to the use of 1.7 μm packings. The packings of Venusil HILIC column are acylamide bonded silica and the elution order of peaks was different relative to other HILIC columns. Then the stationary phases in HILIC have large development space. Increasing the interaction of the stationary phases, series packings can be synthesized to separate suitable compounds.

The selectivity of adenosine/guanosine on six columns was compared. The structure has small difference between two substances (Fig. 2). As shown in Fig. 4, multi-hydroxyl column has the largest selectivity for them when the water content was lower than 0.20. The selectivity decreased with increasing water content of the mobile phase for each column. When the water content was lower than 0.13, the adjustable range of the selectivity of adenosine/guanosine on six columns was large, but when the water content increased, the evolution of the selectivity changed little. The selectivity of adenosine/guanosine on β-cyclodextrin, Atlantis HILIC silica and BEH HILIC column was not obvious when the water concentration larger than 0.20. And also the selectivity between single-hydroxyl and multi-hydroxyl column was not obvious when the water concentration larger than 0.20. But the selectivity was obvious compared to the Venusil column. Uracil/cytosine and cytidine/cytosine on six columns also had obvious selectivity. The stationary phases had large effect to retention and had different selectivity. It depends on the characteristics of the stationary phases, the composition of the mobile phase and the structure of the solutes. The research of column selectivity can help to select most suitable method for separating compounds. Researches of the retention behavior of solutes in different stationary phases can help to develop expert systems that are able to predict the retention of the analytes with good accuracy. Whether versatile retention equation exists or not on these different columns was studied further.

3.2. Comparison of different retention models

HILIC separation commonly employs water and acetonitrile as the mobile phase, and requires much higher organic content. The level of organic solvent in the mobile phase has large influence on retention.

RP chromatography has its roots in liquid–liquid chromatography and retention is considered to be controlled by partitioning, the

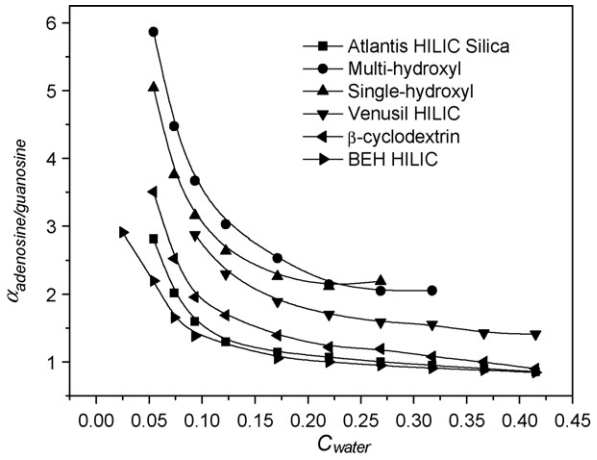

Fig. 4. Relative retention of adenosine/guanosine on six columns to the mobile phase composition. (■) Atlantis HILIC silica column, (●) multi-hydroxyl column, (▲) single-hydroxyl column, (▼) Venusil HILIC column, (◄) β-cyclodextrin column and (►) BEH HILIC column.

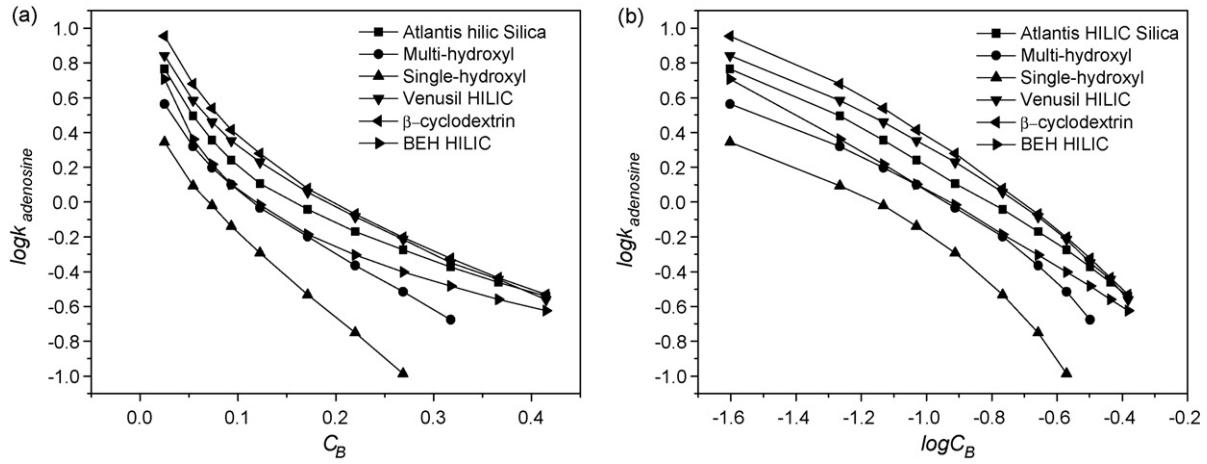

Fig. 5. Linear (a) and logarithmic (b) plots of log k vs. volume fraction of water in the mobile phase for adenosine on (■) Atlantis HILIC silica column, (●) multi-hydroxyl column, (▲) single-hydroxyl column, (▼) Venusil HILIC column, (◄) β-cyclodextrin column and (►) BEH HILIC column.

logarithm of retention factor of solute log k has good linear relationship with the composition of stronger modifier C_B in binary solvent system, see Eq. (1) [32].

$$\log k = \log k_w - SC_B \quad (1)$$

where k_w is the retention factor for the weaker eluent which only consists as mobile phase and S is a constant. So in the case of HILIC, C_B is the concentration of water in the mobile phase and log k_w is the log of the retention factor when solvent A is used pure.

The retention factor (k) of each compound in isocratic HILIC mode was calculated in accordance with the following equation:

$$k = \frac{(t_R - t_0)}{t_0}$$

in which t_R is the retention time of solute, t_0 is the dead time. The dead time was determined by injecting 2 μl methanol with the mobile phase of 100%A. The dead time was 1.76 min for multi-hydroxyl, single-hydroxyl and β-cyclodextrin columns (4.6 mm × 150 mm, 5 μm), and 3 min for Venusil HILIC and Atlantis HILIC silica columns (4.6 mm × 250 mm, 5 μm), and 1.26 min for BEH HILIC column (2.1 mm × 100 mm, 1.7 μm).

In HILIC mode, above retention model was not suitable. As shown in Fig. 5a, taking adenosine for example, the linearity between log k and C_B was not all good. It was not versatile.

For conventional NP chromatographic systems, where retention is based on surface adsorption, log k has good linear relationship with log C_B, see Eq. (2) [33,34].

$$\log k = \log k_B - \frac{A_s}{n_B} \log C_B \quad (2)$$

where k_B is the solute retention factor with pure B as eluent, A_s and n_B are the cross-sectional areas occupied by the solute molecule on the surface and the B molecules, respectively, and C_B is the concentration of water in the mobile phase here. But in HILIC mode, Eq. (2) was also not suitable to quantitatively describe retention factor. As shown in Fig. 5b, the linearity between log k and log C_B of adenosine was not good. So Eqs. (1) and (2) were not suitable for accurate calculation in HILIC.

In order to accurately describe the retention behaviors in LC, the following retention model was proposed [35,36], which is expressed in Eq. (3).

$$\ln k = a + b \ln C_B + cC_B \quad (3)$$

The regression results based on Eq. (3) were shown in Table 1. As shown in Table 1, the regression coefficients of Eq. (3) were all about 0.999. It was in accord with the requirement of precise calculation. This retention model is not only a mathematic calculation. It has theory foundation. Where a is constant and relates to the molecular volume of solutes, the interaction energy between solutes with the stationary phase and the mobile phase. b is the coefficient of ln C_B and relates to the direct analyte-stationary phase interaction. c is the coefficient of C_B in the retention equation and relates to the interaction energy between solutes and solvents. This model not only considers the adsorption between solutes and solvents on the surface of stationary phase, but also considers the interaction between solutes and solvents. It is a rational model in LC retention progress.

In RPLC, there are other suitable multi-parameter retention models to describe retention factor, indicated by Eq. (4) [37–39].

$$\ln k = c_0 + c_1 C_B + c_2 C_B^2 \quad (4)$$

Table 1
Compare of regression coefficients of Eq. (3) and Eq. (4) for each nucleoside on each column

No.	Single-hydroxyl column		Multi-hydroxyl column		β-Cyclodextrin column		Venusil HILIC column		Atlantis HILIC silica column		BEH HILIC column	
	R^2, Eq. (3)	R^2, Eq. (4)	R^2, Eq. (3)	R^2, Eq. (4)	R^2, Eq. (3)	R^2, Eq. (4)	R^2, Eq. (3)	R^2, Eq. (4)	R^2, Eq. (3)	R^2, Eq. (4)	R^2, Eq. (3)	R^2, Eq. (4)
1	0.9457	0.9655	0.9984	0.9920	0.9990	0.9881	0.9998	0.9896	0.9984	0.9771	0.9956	0.9461
2	0.9505	0.9673	0.9979	0.9933	0.9989	0.9878	0.9998	0.9894	0.9976	0.9776	0.9932	0.9462
3	0.9969	0.9947	0.9988	0.9902	0.9981	0.9849	0.9992	0.9872	0.9962	0.9705	0.9939	0.9253
4	0.9933	0.9836	0.9992	0.9899	0.9993	0.9861	0.9996	0.9860	0.9989	0.9819	0.9991	0.9758
5	0.9998	0.9978	0.9997	0.9940	0.9994	0.9921	0.9998	0.9917	0.9994	0.9855	0.9999	0.9778
6	0.9998	0.9920	0.9998	0.9883	0.9987	0.9892	0.9996	0.9909	0.9996	0.9848	0.9975	0.9866
7	0.9967	0.9892	0.9991	0.9875	0.9992	0.9892	0.9997	0.9971	0.9985	0.9808	0.9996	0.9781
8	0.9999	0.9974	0.9996	0.9942	0.9984	0.9842	0.9997	0.9966	0.9962	0.9731	0.9985	0.9751

Table 2
Results of predicted retention time of each nucleoside on each column with Eqs. (3) and (4)

No.		Single-hydroxyl column			Multi-hydroxyl column			β-Cyclodextrin column			Venusil HILIC column			Atlantis HILIC silica column			BEH HILIC column		
		Exp (min)[a]	Pre (min)[b]	Err (%)[c]	Exp (min)	Pre (min)	Err (%)	Exp (min)	Pre (min)	Err (%)	Exp (min)	Pre (min)	Err (%)	Exp (min)	Pre (min)	Err (%)	Exp (min)	Pre (min)	Err (%)
1	Eq. (3)	2.37	2.49	4.82	2.61	2.64	1.14	3.06	3.02	1.32	5.93	5.90	0.51	4.70	4.69	0.21	1.79	1.81	1.10
	Eq. (4)		2.43	2.47		2.68	2.61		3.17	3.47		6.21	4.51		4.85	3.09		1.88	4.79
2	Eq. (3)	2.43	2.54	4.33	2.76	2.80	1.43	3.28	3.26	0.61	6.37	6.36	0.16	5.07	5.01	1.20	1.85	1.88	1.60
	Eq. (4)		2.47	1.62		2.85	3.16		3.40	3.53		6.68	4.64		5.23	3.06		1.97	6.09
3	Eq. (3)	3.07	3.06	0.33	4.10	4.20	2.38	4.89	4.88	0.20	10.77	10.83	0.55	6.88	6.87	0.15	2.26	2.34	3.42
	Eq. (4)		3.12	1.60		4.41	7.03		5.30	7.74		11.81	8.81		7.48	8.02		2.67	15.36
4	Eq. (3)	4.19	4.35	3.68	4.69	4.71	0.42	10.89	10.40	4.71	17.54	17.07	2.75	16.23	15.59	4.11	4.59	4.49	2.23
	Eq. (4)		4.67	10.28		5.03	6.76		12.49	12.81		19.88	11.77		18.56	12.55		5.43	15.47
5	Eq. (3)	3.44	3.44	0.00	4.54	4.55	0.22	7.85	7.53	4.25	11.65	11.66	0.09	9.81	9.57	2.51	3.34	3.32	0.60
	Eq. (4)		3.51	1.99		4.80	5.42		8.53	7.97		12.68	8.12		10.68	8.15		3.74	10.70
6	Eq. (3)	4.06	4.07	0.25	5.61	5.51	1.81	8.27	8.03	2.99	9.83	9.68	1.55	10.41	10.29	1.17	3.93	3.75	4.80
	Eq. (4)		4.39	7.52		6.12	8.33		9.17	9.81		10.56	6.91		11.43	8.92		4.24	7.31
7	Eq. (3)	4.88	4.86	0.41	6.88	6.91	0.43	14.66	14.55	0.76	26.75	25.76	3.84	19.25	18.93	1.69	5.08	5.01	1.40
	Eq. (4)		5.37	9.12		7.86	12.47		14.49	1.17		22.18	20.60		19.17	0.42		6.31	19.49
8	Eq. (3)	8.08	8.02	0.75	14.18	14.42	1.66	17.15	17.33	1.04	31.29	31.03	0.84	16.74	16.90	0.95	4.71	4.71	0.00
	Eq. (4)		8.36	3.35		14.80	4.19		17.11	0.23		26.38	18.61		16.71	0.18		6.00	21.50

[a] Exp (min): experimental retention time.
[b] Pre (min): predicted retention time.
[c] Err (%): relative error.

c_i are regression coefficients with characteristic values for a given solute and column-solvent system.

Here, the retention factors of eight nucleosides on six HILIC columns under ten isocratic mobile phase conditions were measured to examine the accuracy of Eq. (4). The regression coefficients were shown in Table 1. The regression coefficients of Eq. (4) were between 0.94 and 0.998. It was not very good and was not suitable for prediction.

Comparing the results of Table 1, although the regression results of peaks 1 and 2 on single-hydroxyl column from Eq. (4) were a little better than them from Eq. (3), regression coefficients of other peaks on all six columns from Eq. (3) were much better than them from Eq. (4). So Eq. (3) is more suitable for high accurate calculation. Based on this model, the retention equations of eight nucleosides on six HILIC columns were established. From these equations, the retention times of solute under other mobile phase conditions can be predicted and the mobile phase composition can be optimized to get better separation. The predicted retention times can also verify the accuracy of the retention equation.

3.3. Prediction of retention times

Based on the retention data from Eqs. (3) and (4), the retention times of eight nucleosides on six HILIC columns under 95%A condition were predicted. These predicted results were also compared to the experimental values. The results were shown in Table 2. It can be seen that the predicted retention times with Eq. (4) had larger error to the data from Eq. (3). About 60% relative errors of predicted retention times were larger than 5% with Eq. (4), the largest was 21.50%. Obviously, such larger error could not be accepted for precise prediction. On the contrary, all the relative errors of predicted retention times were smaller than 5% with Eq. (3), the largest was 4.82%. The predicted errors of retention times of nucleosides on each column under 87%A also got satisfied values with Eq. (3). These results were satisfied for further accurate calculation. Eq. (3) is more suitable for describing retention equation in HILIC.

3.4. Application of retention equation to real samples

TCMs are always prepared with water, which results in many polar compounds are included in the decoction. Their separation is very important and necessary. Here, Eq. (3) was tested for the prediction of these polar compounds in real samples. The chromatogram of *C. tinctorius* L. was shown in Fig. 6. The experimental conditions were the same as the above on β-cyclodextrin column. Based on Eq. (3), the retention equation of 11 polar compounds in *C. tinctorius* L. were established. The retention times under 93%A

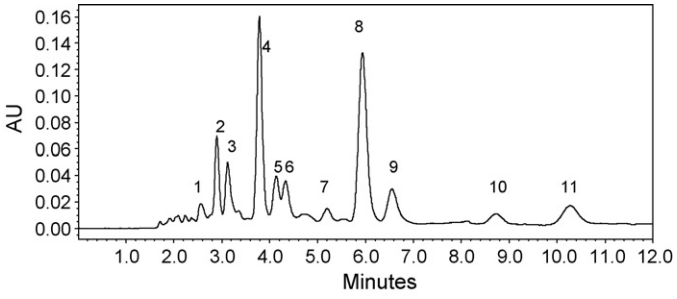

Fig. 6. The chromatogram of *Carthaus tinctorius* L. sample on β-cyclodextrin column. Mobile phase: acetonitrile with 2.5% 200 mmol l^{-1} ammonium acetate aqueous solution and 0.1% acetic acid/water with 2.5% 200 mmol l^{-1} ammonium acetate aqueous solution and 0.1% acetic (93:7, v/v). Flow rate: 1.0 ml min^{-1}. UV detection: 254 nm.

Table 3
Regression equation and results of predicted retention times of 11 compounds in *Carthaus tinctorius* L. on β-cyclodextrin column with Eq. (3)

No.	*a*	*b*	*c*	R^2	Exp (min)[a]	Pre (min)[b]	Err (%)[c]
1	−0.74	−0.13	−3.77	0.9965	2.57	2.56	0.39
2	−0.47	−0.20	−4.20	0.9945	2.89	2.96	2.36
3	−0.54	−0.30	−4.19	0.9836	3.12	3.17	1.58
4	−0.25	−0.37	−4.94	0.9993	3.79	3.84	1.30
5	−0.61	−0.55	−4.08	0.9816	4.13	4.17	0.96
6	−0.86	−0.60	−1.97	0.9982	4.34	4.33	0.23
7	−0.87	−0.78	−3.31	0.9855	5.20	5.21	0.19
8	−1.11	−0.94	−2.64	0.9998	5.94	5.98	0.67
9	−2.18	−1.35	0.23	0.9997	6.56	6.76	2.96
10	−1.76	−1.39	−1.81	0.9998	8.73	8.68	0.58
11	−0.69	−1.17	−5.13	0.9971	10.27	10.54	2.56

[a] Exp (min): experimental retention time.
[b] Pre (min): predicted retention time.
[c] Err (%): relative error.

condition were predicted. The results were shown in Table 3. Most regression coefficients of retention equations were larger than 0.99. From these equations, the relative error of predicted retention time was only 2.96%. The regression coefficients of equations and the predicted accuracy validated the application of Eq. (3) in HILIC mode. This retention equation can also be used to quantitatively describe retention factors and predict retention times of compounds in real samples.

4. Conclusion

Different stationary phases brought the different separation selectivity and then affected the elution order of solutes. Comparing to other retention models, retention equation $\ln k = a + b \times \ln C_B + c \times C_B$ was well established to quantitatively describe the retention factors in HILIC mode. It was validated that the predicted retention times were almost identical to the experimental results. The retention equation was also applied to real TCM. All the relative errors of predicted retention times were smaller than 5%. The quantitative equations laid a foundation for further prediction and optimization under gradient mobile phase conditions for both structure known and unknown compounds.

Acknowledgement

The research was supported by the Knowledge Innovation Program of DICP, CAS (K2006A3) and Project of International Cooperation Plan from Ministry of Science and Technology of China (20071816).

References

[1] A.J. Alpert, J. Chromatogr. 499 (1990) 177.
[2] R.P. Li, J.X. Huang, J. Chromatogr. A 1041 (2004) 163.
[3] Y. Guo, S. Gaiki, J. Chromatogr. A 1074 (2005) 71.
[4] P. Hemström, K. Irgum, J. Sep. Sci. 29 (2006) 1784.
[5] A.J. Alpert, M. Shukla, A.K. Shukla, L.R. Zieske, S.W. Yuen, M.A.J. Ferguson, A. Mehlert, M. Pauly, R. Orlando, J. Chromatogr. A 676 (1994) 191.
[6] S.C. Churms, J. Chromatogr. A 720 (1996) 75.
[7] A.R. Oyler, B.L. Armstrong, J.Y. Cha, M.X. Zhou, Q. Yang, R.I. Robinson, R. Dunphy, D.J. Burnisky, J. Chromatogr. A 724 (1996) 378.
[8] T. Yoshida, J. Biochem, Biophys. Methods 60 (2004) 265.
[9] Z.G. Hao, C. Lu, B.M. Xiao, N.D. Weng, B. Parker, M. Knapp, C. Ho, J. Chromatogr. A 1147 (2007) 165.
[10] M.A. Strege, S. Stevenson, S.M. Lawrence, Anal. Chem. 72 (2000) 4629.
[11] B.A. Olsen, J. Chromatogr. A 913 (2001) 113.
[12] S.D. Garbis, A. Melse-Boonstra, C.E. West, R.B. van Breemen, Anal. Chem. 73 (2001) 5358.
[13] M.A. Strege, Anal. Chem. 70 (1998) 2439.
[14] D.S. Risley, M.A. Strege, Anal. Chem. 72 (2000) 1736.
[15] V.V. Tolstikov, O. Fiehn, Anal. Biochem. 301 (2002) 298.
[16] H. Schlichtherle-Cerny, M. Affolter, C. Cerny, Anal. Chem. 75 (2003) 2349.
[17] R. Oertel, V. Neumeister, W. Kirch, J. Chromatogr. A 1058 (2004) 197.
[18] G. Karlsson, S. Winge, H. Sandberg, J. Chromatogr. A 1092 (2005) 246.
[19] H.L. Koh, A.J. Lau, E.C.Y. Chan, Rapid Commun. Mass Spectrom. 19 (2005)1237.
[20] Y. Iwasaki, M. Hoshi, R. Ito, K. Saito, H. Nakazawa, J. Chromatogr. B 839 (2006) 74.
[21] Z.J. Jiang, N.W. Smith, P.D. Ferguson, M.R. Taylor, Anal. Chem. 79 (2007) 1243.
[22] Z.M. Guo, A.W. Lei, X.M. Liang, Q. Xu, Chem. Commun. (2006) 4512.
[23] Z.M. Guo, A.W. Lei, Y.P. Zhang, Q. Xu, X.Y. Xue, F.F. Zhang, X.M. Liang, Chem. Commun. (2007) 2491.
[24] P.J. Schoenmakers, H.A.H. Billiet, L. De Galan, J. Chromatogr. 218 (1981) 261.
[25] P. Orth, H. Engelhardt, Chromatographia 15 (1982) 91.
[26] Y. Guo, A.H. Huang, J. Pharm. Biomed. Anal. 31 (2003) 1191.
[27] J.C. Valette, C. Demesmay, J.L. Rocca, E. Verdon, Chromatographia 59 (2004) 55.
[28] N.S. Quiming, N.L. Denola, Y. Saito, K. Jinno, Anal. Bioanal. Chem. 388 (2007) 1693.
[29] N.S. Quiming, N.L. Denola, I. Ueta, Y. Saito, S. Tatematsu, K. Jinno, Anal. Chim. Acta 598 (2007) 41.
[30] N.S. Quiming, N.L. Denola, A.B. Soliev, Y. Saito, K. Jinno, Anal. Bioanal. Chem. 389 (2007) 1477.
[31] A. Sándi, L. Szepesy, J. Chromatogr. A 845 (1999) 113.
[32] J.W. Dolan, D.C. Lommen, L.R. Snyder, J. Chromatogr. 535 (1990) 55.
[33] L.R. Snyder, H. Poppe, J. Chromatogr. 184 (1980) 363.
[34] P. Nikitas, A. Pappa-Louisi, P. Agrafiotou, J. Chromatogr. A 946 (2002) 33.
[35] P.Z. Lu, X.M. Lu, X.Z. Li, Y.K. Zhang, Chin. Sci. Bull. 19 (1982) 1175.
[36] P.Z. Lu, X.M. Lu, X.Z. Li, Y.K. Zhang, Chin. Sci. Bull. 21 (1982) 1307.
[37] L.X. Wang, L.F. Zhang, H.B. Xiao, X.M. Liang, Anal. Chim. Acta 476 (2003) 123.
[38] G. Vivó-Truyols, J.R. Torres-Lapasió, M.C. García-Alvarez-Coque, J. Chromatogr. A 1018 (2003) 169.
[39] A. Pappa-Louisi, P. Nikitas, P. Balkatzopoulou, C. Malliakas, J. Chromatogr. A 1033 (2004) 29.

Talanta 76 (2008) 610–616

Contents lists available at ScienceDirect

Talanta

journal homepage: www.elsevier.com/locate/talanta

Nanocrystalline In_2O_3-based H_2S sensors operable at low temperatures

V.D. Kapse [a,*], S.A. Ghosh [a], G.N. Chaudhari [b], F.C. Raghuwanshi [c]

[a] Department of Physics, Government Vidarbha Institute of Science & Humanities, Amravati 444604, India
[b] Nano Technology Research Laboratory, Department of Chemistry, Shri Shivaji Science College, Amravati 444603, India
[c] Department of Physics, Vidyabharati Mahavidyalaya, Amravati 444603, India

ARTICLE INFO

Article history:
Received 3 January 2008
Received in revised form 30 March 2008
Accepted 31 March 2008
Available online 8 April 2008

Keywords:
Indium oxide
Gas sensors
H_2S
Sensitivity
Selectivity

ABSTRACT

Nanocrystalline In_2O_3-based solid solutions, with different concentration of Co, with cubic structure were successfully prepared by a simple route. The as-prepared materials were characterized by X-ray diffraction (XRD) and transmission electron microscopy (TEM). The indirect heating structure sensors based on pure and doped In_2O_3 as sensitive materials were fabricated on an alumna tube with Au electrodes and gas-sensing properties of the sensor elements were measured as a function of concentration of dopant, operating temperature and concentrations of the test gases. The results showed that In_2O_3 had high response towards H_2S gas at an operating temperature 150 °C, while 2.5 wt.% Co-doped In_2O_3 sensor exhibited enhance response and selectivity to H_2S at rather lower operating temperature. Incorporation of platinum further improved the response, selectivity and response time towards H_2S. Platinum incorporated 2.5 wt.% Co-doped In_2O_3 (Pt: 0.5 wt.%) was able to detect 10–100 ppm of H_2S in air at an operating temperature of 100 °C. The selectivity of the sensor elements for H_2S against liquefied petroleum gas (LPG), NH_3 and H_2 gases was studied. The improved gas-sensing properties can mainly be attributed to the selectivity to oxidation of H_2S and noble metal additive sensitization.

1. Introduction

Gas sensors have been used for industrial process controls, for the detection of toxic environmental pollutants, in human health, and for the prevention of hazardous gas leaks, which comes from the manufacturing processes [1–3]. Though there are different types of gas sensors that have been used to detect several inflammable, toxic and odorless gases, the gas sensors based on metal-oxides are playing an important role in the detection of toxic pollutants and the control of industrial processes. Hydrogen sulphide (H_2S) detection is nowadays a very important target for different processes, such as coal or natural gas manufacturing. This gas can be very dangerous for human bodies when its concentration is greater than 250 ppm. Monitoring and controlling of H_2S is crucial in laboratories and industrial areas. Semiconductor gas sensors in the form of thin or thick films, based on metal-oxides like SnO_2, WO_3 and p–n heterojunctions, have been widely reported in the literature for H_2S detection [4–10].

Gas sensitivity, selectivity and durability are the most important sensor properties. In order to attain high response and excellent selectivity, different approaches such as microstructure control, additives, physical or chemical filters, operating temperature, etc. have been adopted to modify the sensing properties of semiconductor metal oxide gas sensors. It is well known that sensing mechanism is based on the surface reaction of the particles with the exposed gas (adsorption and desorption of the test gas). As the adsorption is a surface effect, one of the most important factors to change the sensitivity of the sensor material is the surface area. It is well known that the response of gas sensors can also be improved by decreasing the particle size of the gas-sensing material in order to increase the number of oxygen sites on its surfaces. So the nanosized materials are desirable to enhance the gas-sensing properties of semiconducting oxides. In nanosized materials, a large fraction of the atoms are present at the surface, and consequently, the surface properties turn out to be foremost. The use of nanosized materials in gas sensors is arousing attention in the scientific community [11–16].

Indium oxide (In_2O_3) belongs to the class of wide-bandgap metal oxides, which has a wide application in preparing transparent conducting windows [17]. Moreover, this oxide has been shown to be a promising material for semiconductor gas sensors [18,19]. As a gas-sensing material, In_2O_3 has been extensively applied to detect O_3, NO_2 and CO, etc. [20–22]. But, up till now, there are very few reports on the H_2S sensing properties of In_2O_3. Cobalt oxide, owing to its better catalytic activity, can be considered as an active additive in the base oxide matrix so as to improve its sensing performance. The sensitivity as well as selectivity of an In_2O_3-based element to

* Corresponding author. Tel.: +91 9422157790.
E-mail addresses: vdk_research@yahoo.com, ath135@rediffmail.com, vdk.nano@gmail.com (V.D. Kapse).

0039-9140/$ – see front matter © 2008 Elsevier B.V. All rights reserved.
doi:10.1016/j.talanta.2008.03.050

CO over H_2 was improved dramatically by the addition of 0.5 wt.% cobalt oxide and 0.04 wt.% Au. The doubly promoted element thus obtained has excellent CO-sensing characteristics at 250 °C [23].

In this paper, preparation of pure and Co-doped In_2O_3 nanocrystalline powders by a simple route has been reported. Their gas-sensing properties to H_2S, H_2, NH_3 and liquefied petroleum gas (LPG) were investigated. The results reveals that, in our knowledge, the In_2O_3-based H_2S sensors designed here are superior to those reported in the literature.

2. Experimental details

2.1. Preparation of nanosized pure and doped In_2O_3

All the chemicals used in this work are of AR grade (>99.9%). In a typical experiment of synthesis, aqueous solution of indium nitrate salt stirred for 30 min and subsequently transferred to Teflon lined stainless steel autoclave. The temperature of the autoclave was raised slowly to 170 °C and maintained for 12 h. Thereafter, the autoclave was allowed to cool naturally to room temperature and the resulting product washed several times with deionized water and absolute ethanol, followed by drying at 100 °C overnight and calcination at 600 °C for 6 h. Depending on the required Co-doping concentration, correspondingly Co $(NO_3)_2{\cdot}6H_2O$ salt was added to the aqueous solution of indium nitrate. Doping concentration of cobalt was varied from 0.5 to 4.0 wt.%.

2.2. Material characterization

The crystal structure of samples was characterized by X-ray diffraction (XRD) (model: Philips X'pert) with copper target, K_α radiation ($\lambda = 1.54059$ Å). The crystallite size D is calculated according to the Scherrer's equation:

$$\Delta(2\theta) = \frac{K\lambda}{D\cos\theta}$$

where $\Delta(2\theta)$ is the width at half-maximum intensity (in rad) and θ is the scanning angle, K is a constant, depending on the line shape profile; λ is the wavelength of the X-ray source. In addition, further information, about the particle size and the morphology of the synthesized powders were obtained using a transmission electron microscopy (TEM) (Model: Philips CM-200) operated at 200 kV.

2.3. Sensor fabrication and gas-sensing measurement

A stationary state gas distribution method was used for the test of gas-sensing properties. For gas-sensing properties, α-terpineol was added to the calcined powder. The resulting fresh paste was applied on alumina tube substrate equipped with two gold electrode 8 mm apart and leads. The electrodes were connected to base and Ni–Cr heating wire was inserted. Then sensor element was annealed at 500 °C for 1 h to evaporate the α-terpineol. To improve the stability and repeatability, the sensors were aged at 350 °C for 300 h in air prior to use.

The sensors were subjected to measurements of their electrical resistance in dry air or a test gas at various operating temperatures. The responses of the sensor were studied in a sealed test chamber (300 cm^3) with a gas inlet and an outlet. The test gas was injected into the test chamber through the inlet port and the resistance was measured as a function of time till a constant value was attained. Then the chamber was purged with air for about 10 min and then the experiments were repeated. The sensor's resistance was measured by using a conventional resistor in series at a circuit voltage of 10 V. The concentrations of the test gases were obtained by diluting them with fresh air. The concentration of test gases was 500 ppm for ammonia (NH_3), hydrogen (H_2) and liquefied petroleum gas (LPG) and varied from 10 to 150 ppm for hydrogen sulphide (H_2S). The change in resistance of the sensor with temperature in gas/air ambient is an important study, for a resistive gas sensor, to find an optimal sensing temperature. It is the temperature at which the maximum change in the resistance upon gas adsorption is observed. This procedure was carried out one by one for samples of all doping concentrations. The optimal temperature was obtained from the plot of sensor response as a function of operating temperature.

The sensor response to a test gas, S, is defined as follows [24]:

$$S = \frac{\Delta R}{R_a} = \frac{|R_a - R_g|}{R_a} \quad (1)$$

where R_a is the resistance of a sensor in air, and R_g is that in a test gas.

To obtain the response time, the requisite amount of gas was inleted in the test chamber keeping the sensor at the optimal temperature. The time taken by the sensor element to achieve ~90% of stable output was considered as a response time. For measuring the recovery time, sample was exposed to air ambient by keeping it at optimal temperature and the time taken by the sensor to reach to ~90% of its original value was taken as recovery time.

3. Results and discussion

3.1. Structural characterization

Fig. 1(a)–(d) depicts the XRD patterns for various concentrations of Co (0.5–4.0 wt.%) in In_2O_3 along with pure In_2O_3 powder. All the composition exhibits bixbyite-type structure (cubic-In_2O_3; space group $Ia-3$). This confirmed that the synthesis method is viable and complete. The lattice constant of the prepared powders were calculated from the XRD peaks by indexing it in a cubic space group $Ia-3$, using least square refinement. Further, average crystallite size was calculated with Debye–Scherrer formula. The average crystallite size estimated from XRD data agrees with the TEM investigations.

The XRD pattern, shown in Fig. 1(a), indicates the formation of crystalline In_2O_3 with cubic structure with average crystallite size of 35 nm. The average crystallite size of In_2O_3 is found to decrease for Co-doped samples and is minimum (25 nm) for 2.5 wt.% Co. The

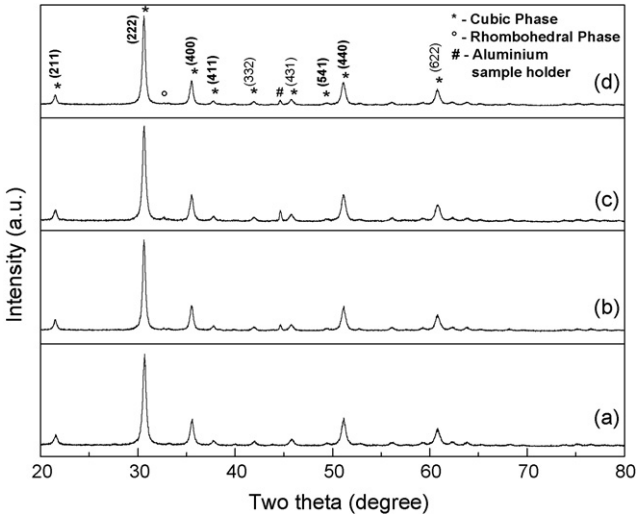

Fig. 1. XRD patterns of (a) pure In_2O_3, (b) In_2O_3: 0.5 wt.% Co, (c) In_2O_3: 2.5 wt.% Co and (d) In_2O_3: 4.0 wt.% Co.

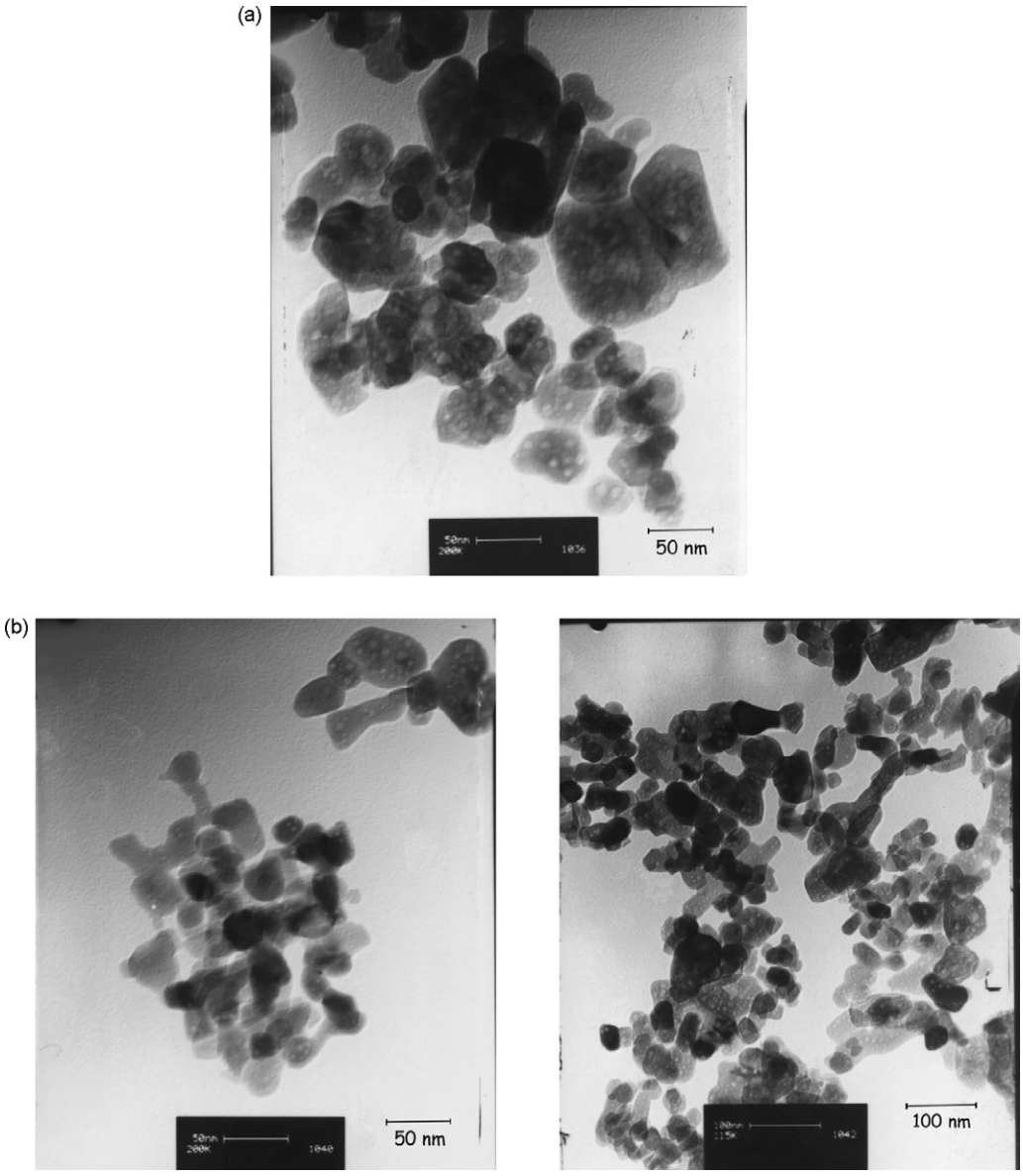

Fig. 2. TEM photographs of (a) pure In_2O_3 and (b) In_2O_3: 2.5 wt.% Co.

peaks corresponding to pure cobalt oxide (Co_3O_4 or CoO) are not observed in Fig. 1(b)–(d), indicating formation of In_2O_3-based solid solution within the concentration of respective doping investigated in this study. However, it should be noted that the lattice constant of pure In_2O_3 sample (a = 10.096(2) Å) is somewhat decreased relative to a reference value. The decrease in the lattice constant, in case of doped samples, can be caused by the formation of a substitution solid solution of Co ions in In_2O_3. Also, the traces of rhombohedral phase peak are observed and the 2.5 wt.% Co-doped composition exhibits noticeable intensity for the peak at about $2\theta = 32.6^\circ$ corresponding to rhombohedral indium oxide. When foreign atoms with a smaller ionic radius than indium were substitutionally introduced into the cubic indium oxide network, the cubic to hexagonal phase transition was supposed to be favored [25]. However, this type of phase transformation was not observed for Co doping into the In_2O_3 lattice. Fig. 2(a) and (b) shows the TEM micrographs of pure and 2.5 wt.% Co-doped In_2O_3 samples, respectively. There is a small amount of agglomeration of particles observed in the micrographs. In the case of pure In_2O_3, the particle size estimated from TEM is somewhat greater than calculated from XRD pattern. The difference might be because of the techniques as TEM provides surface topography while X-ray penetrates within and gives the average picture. It is interesting to observe large number of white spots on the surface of the nanoparticles. The formation of these defects possibly attributed because of the strong impact of gas evolution during the thermal decomposition reaction.

3.2. Gas-sensing properties

The gas-sensing responses of pure In_2O_3 to different reducing gases like ammonia (NH_3), hydrogen sulfide (H_2S), hydrogen (H_2) and liquefied petroleum gas (LPG) as a function of operating temperature were studied. It is observed that the sensing responses to different gases go through maxima at different operating temperature. For 50 ppm H_2S, it is 150 °C, while it is around 250–300 °C for other test gases. The responses of pure In_2O_3 to NH_3, H_2, LPG and 50 ppm of H_2S at 150 °C is shown in Fig. 3. Doping of In_2O_3 ceramics is an effective way to get better gas-sensing characteristics. The

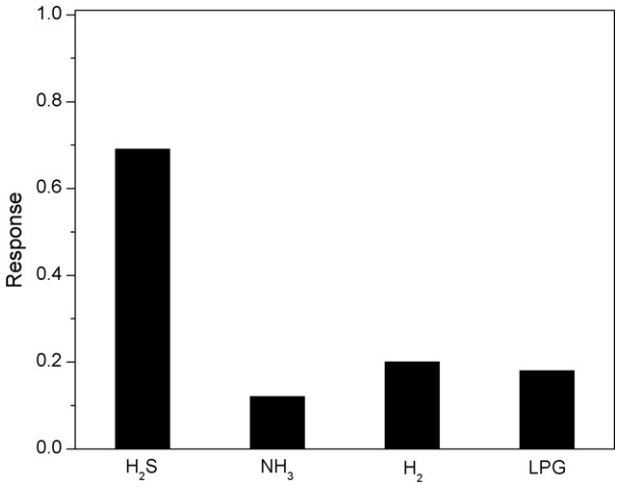

Fig. 3. Sensor response of pure In_2O_3 at 150 °C.

appropriate selection of additive may give rise to the possibility to enhance gas response to both reducing and oxidizing gases and, also, to improve selectivity of gas response. However, this effect does not have universal character. Optimizing effect depends on many factors, such as the nature of tested gas, the type and concentration of additives [26]. The responses of pure and Co-doped In_2O_3 to 50 ppm H_2S in air as a function of operating temperature are shown in Fig. 4. It can be seen that 2.5 wt.% Co-doped In_2O_3 exhibits the maximum response 0.82 to H_2S at 125 °C. The sensor elements based on pure and Co-doped In_2O_3 nanoparticles exhibited a typical n-type semiconducting behavior, as there was a drop in voltage across the sensor element on exposure to the reducing gas.

Fig. 4 depicts that the optimal operating temperature for pure In_2O_3 is 150 °C that shifts towards the lower temperature by 25 °C for 2.5 wt.% Co-doped In_2O_3 with increase in the response to H_2S. The reduction in the optimal temperature explains the oxidation of H_2S at rather lower temperature. The possible reasons for decrease in optimal temperature are the reduction in the particle size; increase in the density of surface states with the decrease in the particle size; presence of the nonstoichiometric cobalt–indium oxide phase. In addition to this, the presence of grains with rhombohedral phase in nanocrystalline 2.5 wt.% Co-doped In_2O_3 may also be responsible for the enhanced response to H_2S at rather lower operating temperature [27]. Furthermore, the catalytic activity may be at a suitable level in between 2.5 wt.% Co-doped In_2O_3 at 125 °C, so H_2S can diffuse into the inner region of the sensor element and react with the adsorbed oxygen there, giving rise to a maximum response. The decrease in the optimal operating temperature in the present investigation can be due to the catalytic activation upon Co doping. The specific area and the active site on the surface of materials also affected the sensing response; the active site can adsorb oxygen and gases to be detected. Normally, for higher specific surface area and oxygen adsorption quantity of sensor material, the gas sensitivity is higher [28]. The higher response to H_2S is also related to the active sites on the surface of the nanoparticles prepared by this method.

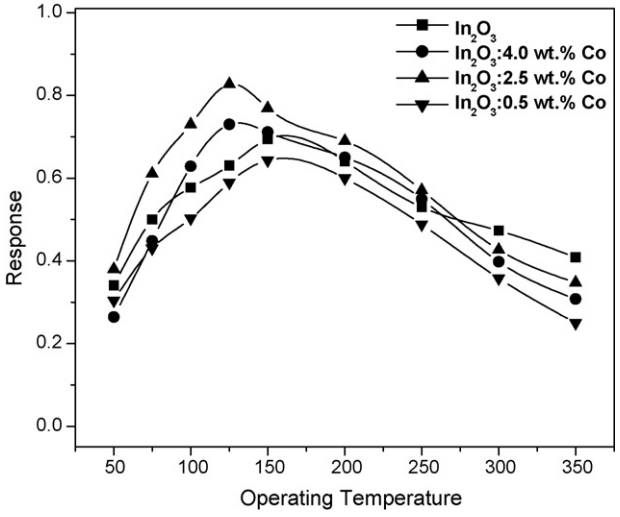

Fig. 4. Sensor responses towards 50 ppm of H_2S as a function of operating temperature.

The gas-sensing mechanism of In_2O_3, n-type semiconducting metal oxide, belong to surface-controlled type. It is well known that the surface of oxide semiconductors can adsorb oxygen and water from the atmosphere.

$$O_2\,(\text{gas}) \leftrightarrow O_2\,(\text{ads}) \quad (2)$$

$$O_2\,(\text{ads}) + e^- \leftrightarrow O_2{}^-\,(\text{ads}) \quad (3)$$

$$O_2{}^-\,(\text{ads}) + e^- \leftrightarrow 2O^-\,(\text{ads}) \quad (4)$$

$$O^-\,(\text{ads}) + e^- \leftrightarrow O^{2-}\,(\text{ads}) \quad (5)$$

Oxygen may be either physisorbed as uncharged molecules (Eq. (2)) or chemisorbed as charged species (Eq. (3)–(5)) on the indium oxide surface. The physisorbed oxygen will not affect the surface states, while the chemisorbed oxygen species act as surface acceptors, trapping electrons and decreasing surface conductivity of the indium oxide.

The inleted H_2S can react rapidly with the adsorbed oxygen and hydroxyl species, therefore releasing the captured electrons back to the bulk. Reducing gases can also react with the lattice oxygen, but the rate is much slower than the surface reaction and can be neglected. The surface reactions between the H_2S and the oxygen species can be described as

$$H_2S + 3O^{2-}\,(\text{ads}) \rightarrow H_2O\,(\text{g}) + SO_2\,(\text{g}) + 6e^- \quad (6)$$

The reactions change the density of surface states and create conduction band electrons. Therefore, the conductivity will increase when indium oxide materials are exposed to the H_2S.

Selectivity is an imperative factor in gas sensing, and the sensor have to exhibit rather high selectivity for its application. For that reason, we examined the response of 2.5 wt.% Co-doped In_2O_3 sensor towards NH_3, H_2 and LPG at different operating temperatures, provided in Fig. 5. The response values obtained at 125 °C are 0.11, 0.04 and 0.04 for NH_3 (500 ppm), H_2 (500 ppm) and LPG (500 ppm), respectively. Furthermore, the response of 2.5 wt.% Co-doped In_2O_3 to H_2S at 125 °C was measured by injecting the 50 ppm H_2S, and then, in its presence, NH_3 (500 ppm), LPG (500 ppm) and

Table 1
Response of sensor elements to H_2S and other interfering gases

Sensor element	Operating temperature (°C)	Gas species (ppm)	Response
In_2O_3: 2.5 wt.% Co	125	50 H_2S	0.82
		50 H_2S + 500 NH_3	0.86
		50 H_2S + 500 LPG	0.83
		50 H_2S + 500 H_2	0.82
In_2O_3: 2.5 wt.% Co/Pt (0.5 wt.%)	100	50 H_2S	0.92
		50 H_2S + 500 NH_3	0.94
		50 H_2S + 500 LPG	0.92
		50 H_2S + 500 H_2	0.93

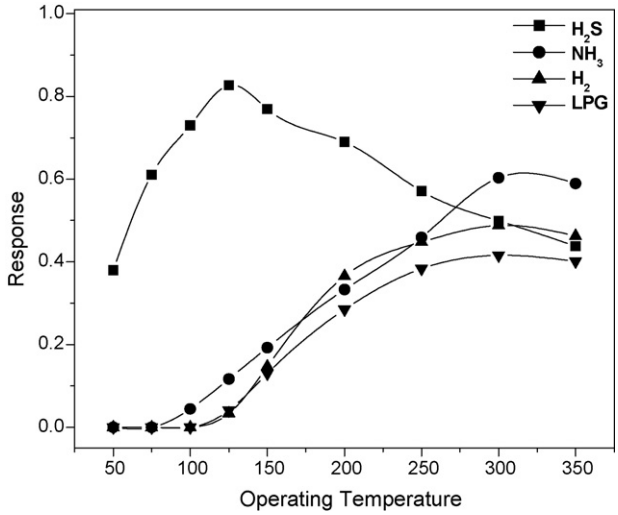

Fig. 5. Responses of 2.5 wt.% Co-doped In_2O_3 to various gases at different operating temperatures.

H_2 (500 ppm) was also injected. The results are illustrated in Table 1. It can be seen that the response of sensor elements to H_2S remains high after the introduction of interfering gases like NH_3, LPG and H_2 besides H_2S in the testing chamber. The influence of other reducing gases that are additionally present on the H_2S characteristics is minimal (0–5%) at 125 °C. Therefore, a sensor could selectively detect H_2S at lower operating temperature without serious interference from other tested reducing gases.

Using the same operating conditions, the response of In_2O_3: 2.5 wt.% Co to 50 ppm H_2S was also measured at 100 °C in the presence of other tested interfering gases. The sensor response was found to vary by 0–5%, same as obtained at 125 °C. In addition to this, the response of sensor element to 50 ppm H_2S was greater at 125 °C than at 100 °C. So, the working temperature of 2.5 wt.% Co-doped In_2O_3 sensor element to 50 ppm H_2S was considered as 125 °C.

The response of 2.5 wt.% Co-doped In_2O_3 sensors at 125 °C for various concentrations of H_2S is depicted in Fig. 6. The sensor shows an increase in response as a function of H_2S concentration up to 100 ppm and then it reaches saturation level. At a fixed-specific

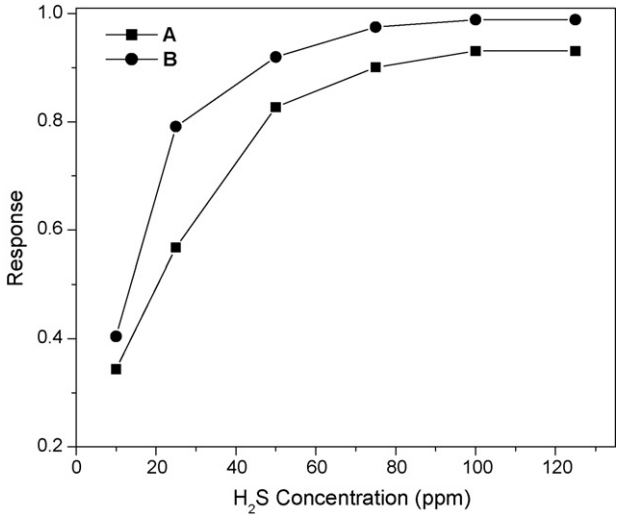

Fig. 6. The response vs. H_2S concentration of (A) 2.5 wt.% Co-doped In_2O_3 at 125 °C and (B) In_2O_3: 2.5 wt.% Co/Pt (1.0 wt.%) at 100 °C.

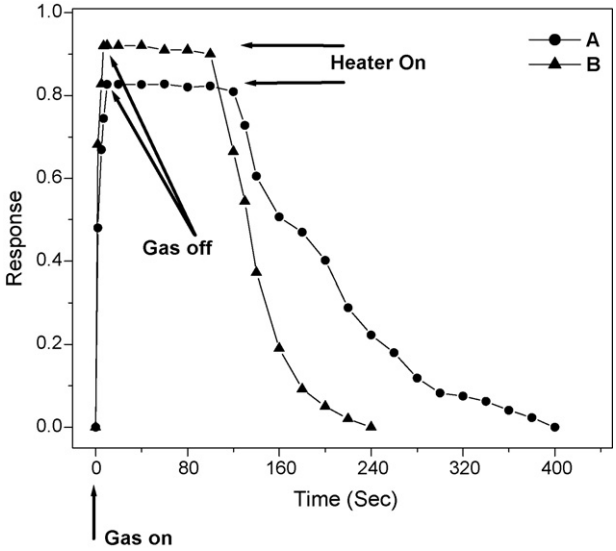

Fig. 7. Response characteristics of (A) 2.5 wt.% Co-doped In_2O_3 at 125 °C and (B) In_2O_3: 2.5 wt.% Co/Pt (1.0 wt.%) at 100 °C to 50 ppm H_2S.

surface area, a low gas concentration implies a small surface coverage of gas molecules. An increase in H_2S concentration raises the surface coverage eventually leading to a saturation level, thus determining the upper detection limit. As the response exhibits a linear increase with the H_2S concentration, which suggests that the 2.5 wt.% Co-doped In_2O_3 could meet the applications in H_2S sensing.

The variation in response to H_2S with time in seconds for 2.5 wt.% Co-doped In_2O_3 sensor at 125 °C is exhibited in Fig. 7. The sensor exhibits an excellent response of 7 s. It was further observed that after about dozens of minutes, the reduced resistance of the sensor started to increase (i.e. response decrease) but took longer time to recover to its initial value. It may be due to the difficulty in desorption of H_2O and SO_2 in Eq. (6). We succeed to recover initial state of sensor by heating it for a short time at 250 °C in air atmosphere after every H_2S sensing cycle. This has minimized the recovery time to about 5 min (Fig. 7). The sensor based on WO_3 thick films had a fast response to H_2S, but the recovery time was very long which reduced on short heating [7].

3.2.1. Effect of noble metal additives

In order to improve the gas-sensing properties of 2.5 wt.% Co-doped In_2O_3, different weight percentages (0.2, 0.5 and 1.0) of noble metals Pt and Au were incorporated in it as the additive by impregnation method. The gas-sensing characteristics of each composition to H_2S was studied. It was found that, on impregnation of the 2.5 wt.% Co-doped In_2O_3 with Pt, there was notable increase in the response to H_2S. As compared to Pt, Au modified 2.5 wt.% Co-doped In_2O_3 are found to be less sensitive to H_2S. Fig. 8 depicts the response of In_2O_3: 2.5 wt.% Co/Pt as a function of the operating temperature to 50 ppm of H_2S. It can be seen that the maximum response was obtained for In_2O_3: 2.5 wt.% Co/Pt (0.5 wt.%) with the shift in optimal operating temperature to lower side by 25 °C. To know about the selective behavior of In_2O_3: 2.5 wt.% Co/Pt (0.5 wt.%) towards H_2S at optimal operating temperature, its responses to NH_3, H_2 and LPG were also studied. The results are shown in Fig. 9. It was found that the responses towards NH_3 (500 ppm), H_2 (500 ppm) and LPG (500 ppm) were 0.06, 0.07 and 0.03, respectively. Also, it was found that the response of In_2O_3: 2.5 wt.% Co/Pt (0.5 wt.%) to 50 ppm H_2S remains high after the intro-

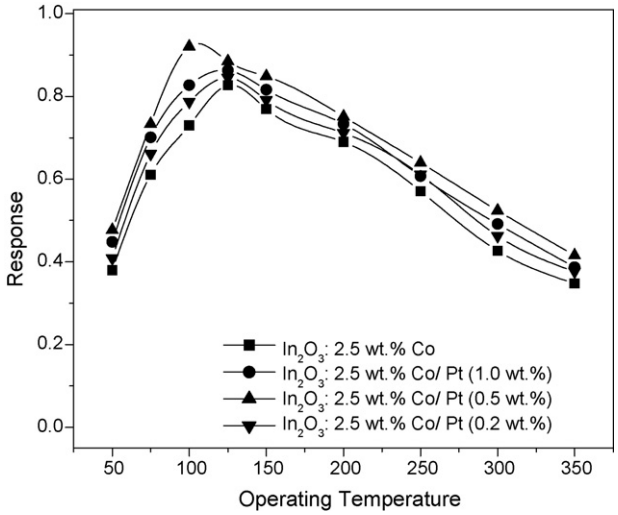

Fig. 8. Responses of In_2O_3: 2.5 wt.% Co/Pt towards 50 ppm H_2S.

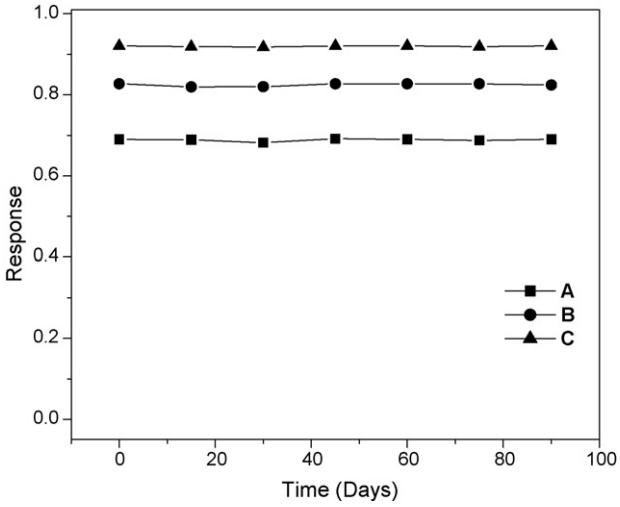

Fig. 10. Long-term stability of (A) pure In_2O_3 at 150 °C, (B) 2.5 wt.% Co-doped In_2O_3 at 125 °C and (C) In_2O_3: 2.5 wt.% Co/Pt (0.5 wt.%) at 100 °C to 50 ppm H_2S.

duction of interfering gases like NH_3, LPG and H_2 besides H_2S in the testing chamber. The results are shown in Table 1. Therefore, it may be concluded that modification of In_2O_3: 2.5 wt.% Co with Pt (0.5 wt.%) is not only effective in enhancing the response but also retaining the selectivity to H_2S.

Two types of sensitization mechanisms, chemical and electronic sensitization, were discussed commonly to explain the effect of noble metals on the gas-sensing properties of semiconductor oxides. In chemical sensitization, the sensing gas molecule gets adsorbed at the sensor surface where it is dissociated or activated due to a dopant. This dissociated molecule interacts with the semiconducting oxide at the sensor surface. This will produce a change in the resistivity at the sensor surface. On the other hand, electronic sensitization is followed by direct exchange of electrons between added dopant and the semiconductor surface. The oxidation state of dopant gets changed on contact with sensing gas molecule due to electron exchange from dopant to oxygen, which produces a change in the resistivity of the sensor surface. In the case of Pt, chemical sensitization plays a significant role in improving the resistance change and so the response of the sensor [29,30]. Pt possibly acts as specific adsorption sites to dissolve O_2 and to adsorb gas molecules to be sensed. The test gas is initially adsorbed on the surface of the noble metal particles at suitable temperature. Then the gas molecules spill over the semiconductor surface. Consequently, Pt activates H_2S to facilitate its catalytic oxidation on the surface of the sample. Hence, Pt does not have direct effect on the sensor resistance and the In_2O_3: 2.5 wt.% Co/Pt (0.5 wt.%) has the similar gas-sensing mechanism basically as the case without Pt. The additive enhances the response as it enhances the rate of the chemical process leading to a reduction in concentration of the chemisorbed oxygen species on the surface of semiconductor, which may be the dominant reason for the lower operating temperature of the In_2O_3: 2.5 wt.% Co/Pt (0.5 wt.%).

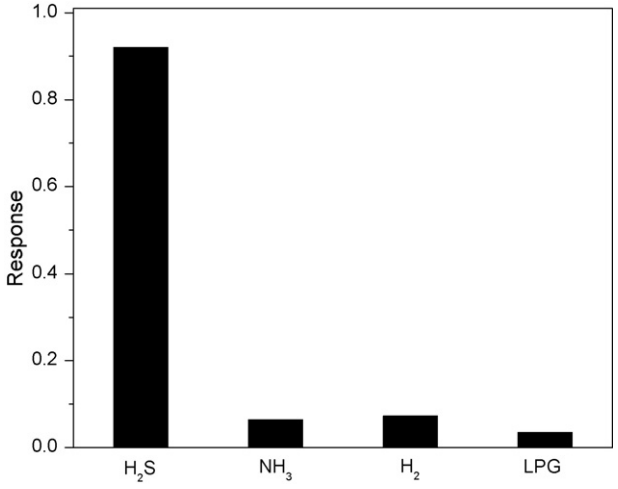

Fig. 9. Responses for different gases.

For In_2O_3: 2.5 wt.% Co/Pt (0.5 wt.%) sensor, the magnitude of response increased linearly with the H_2S gas concentration up to 100 ppm and afterward it attains saturation level (Fig. 6). The variation in response to H_2S with time in seconds for In_2O_3: 2.5 wt.% Co/Pt (0.5 wt.%) sensor at 100 °C is also studied (Fig. 7). The sensors exhibit a fast response of about 5 s but a recovery time was very long. The initial state of sensor can be obtained by providing the heating arrangement as described in the previous section. The stability of the sensor elements based on pure and doped In_2O_3 was also measured by repeating the tests up to the period of 3 months from first measurement. The results are illustrated in Fig. 10. During the tests, no considerable variations were observed indicating the good stability of the sensors.

4. Conclusions

In summary, nanocrystalline powders of pure and Co-doped In_2O_3 with n-type semiconducting behavior has been prepared successfully. The phase composition analyzed by XRD, pointed out the formation of the In_2O_3 solid solution. Compared with the undoped one, In_2O_3: 2.5 wt.% Co sensors showed high response, better selectivity and rather lower optimum operating temperature to H_2S than the undoped one. The promoting effect of the response of the sensor elements with cobalt oxide appears to be allied to the decreased particle size, selectivity to oxidation of H_2S, presence of the nonstoichiometric cobalt–indium oxide phase and the existence of rhombohedral phase. The reduction in the particle size with Co-doping may be due to the re-crystallization and dis-agglomeration effect of cobalt oxide over indium oxide.

The optimum performance was observed for In_2O_3: 2.5 wt.% Co/Pt (0.5 wt.%) to 50 ppm H_2S at 100 °C. The sensor realized the

detection of H_2S gas in the range from 10 to 100 ppm with response time in seconds and possessed good reproducibility. Thus, Pt modified Co-doped In_2O_3 can be a promising candidate for detection of H_2S in environments. However, the gas sensor needs to be further investigated to shorten the recovery times.

Acknowledgements

The authors thank to Sophisticated Analytical Instrument Facility, Indian Institute of Technology (I.I.T.), Bombay for carrying out TEM characterization and Department of Metallurgical Engineering and Materials Science, I.I.T., Bombay for providing the XRD facility. One of the authors (VDK) thanks University Grant Commission (UGC) for awarding Teacher Fellowship under Faculty Improvement Programme. The discussion with D.D. Gulwade is highly acknowledged.

References

[1] N. Guillet, R. Lalauze, J.-P. Viricelle, C. Pijolat, L. Montanaro, Mater. Sci. Eng. C 21 (2002) 97.
[2] P.S. More, Y.B. Khollam, S.B. Deshpande, S.K. Date, N.D. Sali, S.V. Bhoraskar, S.R. Sainkar, R.N. Karekar, R.C. Aiyer, Mater. Lett. 58 (2004) 1020.
[3] L. Wang, R.V. Kumar, Sens. Actuators B 98 (2004) 196.
[4] T. Maekawa, J. Tamaki, N. Miura, N. Yamazoe, Chem. Lett. 4 (1991) 575.
[5] J. Tamaki, T. Maekawa, N. Miura, N. Yamazoe, Sens. Actuators B 9 (1992) 197.
[6] D.J. Yoo, J. Tamaki, S.J. Park, N. Miura, N. Yamazoe, Jpn. J. Appl. Phys. Part 2 34 (1995) 455.
[7] J.L. Solis, S. Saukko, L.B. Kish, C.G. Granqvist, V. Lantto, Sens. Actuators B 77 (2001) 316.
[8] J.L. Solis, S. Saukko, L. Kish, C.G. Granqvist, V. Lantto, Thin Solid Films 391 (2001) 255.
[9] J.L. Solis, A. Hoel, L.B. Kish, C.G. Granqvist, S. Saukko, V. Lantto, J. Am. Ceram. Soc. 84 (2001) 1504.
[10] L.A. Patil, D.R. Patil, Sens. Actuators B 120 (2006) 316.
[11] M. Schweizer-Berberich, J.G. Zheng, U. Wermar, W. Göpel, N. Barsan, E. Pentia, A. Tomescu, Sens. Actuators B 31 (1996) 71.
[12] L.E. Depero, M. Ferroni, V. Guidi, G. Martinelli, P. Nelli, L. Sangaletti, G. Sberveglieri, Sens. Actuators B 36 (1996) 381.
[13] Z. Jin, H.J. Zhou, Z.L. Jin, R.F. Savinell, C.C. Liu, Sens. Actuators B 52 (1998) 188.
[14] M.J. Willett, V.N. Burganos, C.D. Tsakiroglou, A.C. Payatakes, Sens. Actuators B 53 (1998) 76.
[15] S. Zhao, et al., Sens. Actuators B 64 (1–3) (2000) 83.
[16] F. Lu, Y. Liu, M. Dong, X. Wang, Sens. Actuators B 66 (1–3) (2000) 225.
[17] I. Hamberg, C.G. Granqvist, J. Appl. Phys. 60 (1986) R123.
[18] H. Yamaura, J. Tamaki, K. Moriya, N. Miura, N. Yamazoe, J. Electrochem. Soc. 143 (1996) L36.
[19] A. Gurlo, N. Bârsan, M. Ivanovskaya, U. Weimar, W. Göpel, Sens. Actuators B 47 (1998) 92.
[20] G. Faglia, B. Allieri, E. Comini, et al., Sens. Actuators B 57 (1999) 188.
[21] H. Steffes, C. Imawan, F. Slozbacher, et al., Sens. Actuators B 68 (2000) 249.
[22] T.V. Belysheva, E.A. Kazachkov, E.E. Gutman, J. Anal. Chem. 56 (2001) 676.
[23] H. Yamaura, K. Moriya, N. Miura, N. Yamazoe, Sens. Actuators B 65 (2000) 39.
[24] B. Baruwati, D. Kishore Kumar, S.V. Manorama, Sens. Actuators B 119 (2006) 676.
[25] A. Gurlo, N. Barsan, U. Weimar, M. Ivanovskaya, A. Taurino, P. Siciliano, Chem. Mater. 15 (2003) 4377.
[26] G. Korotcenkov, I. Boris, A. Cornet, J. Rodriguez, A. Cirera, V. Golovanov, Y. Lychkovsky, G. Karkotsky, Sens. Actuators B 120 (2007) 657.
[27] B.-C. Kim, J.-Y. Kim, D.-D. Lee, J.-O. Lim, J.-S. Huh, Sens. Actuators B 89 (2003) 180.
[28] J.Q. Xu, Q.Y. Pan, Y.A. Shun, Z.Z. Tian, Sens. Actuators B 66 (2000) 277.
[29] C.V. Gopal Reddy, S.V. Manorama, V.J. Rao, A. Lobo, S.K. Kulkarni, Thin Solid Films 348 (1999) 261.
[30] P. Montmeat, J.C. Marchand, R. Lalauze, J.P. Viricelle, G. Tournier, C. Pijolat, Sens. Actuators B 95 (2003) 83.

Talanta 76 (2008) 540–547

Contents lists available at ScienceDirect

Talanta

journal homepage: www.elsevier.com/locate/talanta

Highly sensitive determination of iodide by ion chromatography with amperometric detection at a silver-based carbon paste electrode

Trésor Kimbeni Malongo[a,b], Stéphanie Patris[a], Pascale Macours[c], Frédéric Cotton[a,c], Jean Nsangu[b], Jean-Michel Kauffmann[a,*]

[a] Université Libre de Bruxelles, Institute of Pharmacy, Campus plaine, CP 205/06, 1050 Brussels, Belgium
[b] University of Kinshasa, Faculty of Pharmaceutical Sciences, BP 212 Kinshasa, Congo
[c] Erasme University Hospital, Clinical Chemistry Department, 808 route de Lennik, Brussels, Belgium

ARTICLE INFO

Article history:
Received 16 February 2008
Received in revised form 21 March 2008
Accepted 24 March 2008
Available online 10 April 2008

Keywords:
Iodide
Silver electrode
Carbon paste
Ion chromatography
Amperometry

ABSTRACT

A silver-based solid carbon paste electrode was developed for use as a detector in ion chromatography (IC) for the sensitive determination of iodide in real samples. Micro- and nano-particles of silver were investigated for the fabrication of different electrodes. The iodide assay was based on IC with amperometric detection (IC-AD) at a silver composite electrode polarized at +0.080 V *versus* Ag/AgCl. Free iodide and organoiodide compounds were studied. The detection process was characterized by studying the redox behavior of iodide ions at both silver and silver composite electrodes by cyclic voltammetry (CV). The presence of iodide ions in solution was found to considerably facilitate metallic silver oxidation, with response currents directly related to iodide concentration. The calibration curve at the selected silver carbon paste electrode was linear in the concentration range comprised between 0.635 μg/L and 63.5 μg/L iodide. The relative standard deviation (R.S.D.) for successive injections was below 3% for all iodide standard solutions investigated. The limit of detection (LOD) was 0.47 μg/L (3.7 nmol/L) for an injection volume of 20 μL, i.e. 74 fmol injected. The IC-AD method was successfully applied to the determination of iodide in complex real samples such as table salts, sea products and iodide bound drug compounds. The analytical accuracy was verified by the assay of iodide in milk powder from an iodide certified reference material (CRM) Community Bureau of Reference (BCR) 150.

1. Introduction

Iodine is known to be an essential micronutrient utilized by the thyroid gland for the biosynthesis of the thyroid hormones thyroxin (T4) and triiodothyronine (T3). These hormones play an important role in mental development, growth and basic metabolism. Deficiency of iodine can result in a serious delay in neurological development. An excess of iodine or iodide ingestion can produce goitre and hypothyroidism as well as hyperthyroidism [1,2]. Iodide is present in food, drug compounds and in drinking water and it is often added to table salt as a source of iodine for preventing iodine deficiency disorders [2,3].

Previous studies and more recent epidemiological investigations indicate that dietary iodine supply is still insufficient in several regions worldwide [4,5]. The determination of iodine in biological samples such as urine or serum as well as in food samples such as sea and milk products (which may be one of the main sources for iodine supply besides iodized salt) is thus, of great interest.

The analysis of iodide can be accomplished by UV–vis spectrophotometry [6–9], different electroanalytical methods [10–13], or by spectrophotometry exploiting the catalytic effect of iodide on the oxidation of As(III) by Ce(IV) [14,15] or the oxidation of chlorpromazine by H_2O_2 [16]. More elaborated instrumental techniques can been employed as well such as derivative gas chromatography–mass spectrometry [17], inductively coupled plasma-mass spectrometry (ICP-MS) [18–22] or neutron activation analysis (NAA) [22]. The latter two are very efficient techniques but require quite expensive instrumentation. An alternative to the above-cited techniques is provided by liquid chromatography with UV or electrochemical detection. Ion chromatography (IC) coupled to electrochemical (EC) detection allows selective and sensitive determination of iodide in complex samples [23–31]. Potentiometric iodide sensors have been developed for flow injection analysis [32] and chromatography [33]. Most often, though, amperometric detection (AD) of iodide is preferred because of electrode stability and sensitivity. Gold [27,28], platinum [24,28,34,35] and glassy

* Corresponding author.
E-mail address: jmkauf@ulb.ac.be (J.-M. Kauffmann).

0039-9140/$ – see front matter © 2008 Elsevier B.V. All rights reserved.
doi:10.1016/j.talanta.2008.03.053

Table 1
Comparative data of amperometric detection in liquid chromatography of iodide ions

Electrode	Mode	*E* (V) vs. Ag/AgCl	LOD (μg/L)	Stability	Linearity	R.S.D. (%)	Ref.
Ag	a. PAD b. DCA	+0.1	a. 35 b. 3.5	Sensitivity loss in 4 h			28
Ag	PAD	−0.03	5	2 weeks	0.005–10 mg/L	2.9	23
Ag	PAD	−0.05	2		0.050–8 mg/L	1.7	25
Ag	PAD	−0.05	0.5		0.050–10 mg/L	<4	25
Ag	DCA	+0.05	6		0.100–1 mg/L		29
Ag	DCA	+0.130	1		4.6–46 μg/L		30
Ag	DCA	+0.20	10		–	1	37
Ag	PAD	+0.05	0.04	45 h or 216 injections	0.0–50 μg/L		39
Ag	PAD	+0.1	1		0.025–10 mg/L	2.5	40
Ag	DCA	−0.04	7	2 weeks or 600 injections	3.2–47 μg/L	<4	This work
SCPE	DCA	+0.08	0.5	more than 600 injections	0.6–60 μg/L	<3	This work
Au	DCA	+0.8		Sensitivity loss > 40% (6 h)		6.2	28
Au	DCA	+0.0	1		2–600 μg/L	4.6	27
Pt	DCA	+0.9	127		0.127–127 mg/L	2.0	35
Pt	DCA	+0.85	0.5	Sensitivity loss > 6% (8 h)	0.5–6000 μg/L	<105	24,28
Pt	DCA	+0.8	10		0.020–12 mg/L	0.44	34
GC	DCA	+1.0	5		0.100–20 mg/L	3	31

PAD = pulsed amperometric detection, DCA = direct current amperometry, LOD = limit of detection, SCPE = silver carbon paste electrode, GC = glassy carbon.

carbon [31,36] electrodes have been utilized in amperometric or pulsed amperometric detection. The oxidation of iodide, though, requires relatively high positive potentials which is not in favor of an optimal signal *versus* noise ratio [23,24]. Yet, the strong interaction between iodide and silver ions at the silver electrode–solution interface can be exploited in amperometic detection at a low applied potential close to 0.0 V *versus* Ag/AgCl [28,29,37]. There is some confusion in the literature regarding the amperometric response mechanism at a silver electrode but it is well established that silver oxidation is facilitated in the presence of iodide ions [38]. In amperometric detection at the constant applied potential, and in agreement with Nernst equation, the consumption of silver ions by iodide arriving at the electrode solution interface implies that new silver ions must be generated to maintain the electrochemical equilibrium. Thus, the recorded current corresponds to metallic silver oxidation [23]. Some deposit of silver iodide onto the electrode surface, however, may occur leading to chromatographic postpeak distortion, poor reproducibility and a signal drift over time [27,28]. Pulsed amperometric detection at a silver electrode has been recently applied as a mean to electrochemically clean the electrode surface and improve the reproducibility of the electrode response [23,25,39–41]. Alternative strategies consist in the use of disposable silver electrodes [23,25]. A survey of several amperometric detectors and their characteristics for iodide determination is outlined in Table 1.

Here, we compare two types of silver working electrodes as amperometric detector in IC: (i) a polycrystalline silver electrode (PSE) and (ii) a micronised silver-based solid carbon paste electrode (SCPE). Silver/Kel-F composite electrodes for the electroanalysis of organic compounds were first described by Tallman and co-workers [42]. Metal-dispersed carbon paste electrodes comprising platinum, palladium or ruthenium on graphite were developed for enhanced electroanalytical performances [43]. A silver/graphite dispersed methacrylate resin electrode was described for the voltammetric assay of halogenides [44]. Recently, an electrode made of glassy carbon microparticles coated with silver nanoparticles blended in an epoxy paste was described for the cyclic voltammetric assay of bromide ions [45]. In this work, it is demonstrated that a silver-based SCPE, implemented as detector in liquid chromatography, permits reproducible repetitive assays over a long period of time with good selectivity and high sensitivity. The determination of iodide in various real samples using either external calibration or the standard addition method is described.

2. Experimental

2.1. Chemicals and reagents

All chemicals were of analytical grade or of the highest purity available from several suppliers and were used as received. High purity micronised silver was purchased from Aldrich (Steinheim, Germany), colloidal silver, solid paraffin, sodium nitrate, potassium chloride and EDTANa_2H_2, $2H_2O$ (EDTA) were obtained from Merck (Darmstadt, Germany). Ultracarbon F graphite powder was from Jonhson Matthey Chemicals. Potassium salts of iodide, chloride, thiocyanate, sulfite and iodate were obtained from VWR (Leuven, Belgium), sodium acetate was obtained from VEL (Leuven, Belgium), acetonitrile and acetic acid were from Lab-Scan (Dublin, Ireland). Potassium hexacyanoferrate was from UCB (Brussels, Belgium). Amiodarone (AMD) and iodochlorhydroxyquinoline (ICHQ) were supplied by Aldrich (Steinheim, Germany). Skim milk powder (certified reference material (CRM No. 150) was purchased from Community Bureau of Reference (BCR, Geel, Belgium) and was certified for total iodide (spiked as KI). Deionised water (reverse osmosis) was used throughout. The stock solution of iodide was prepared by dilution of iodide in deionised water stored in a refrigerator (+4 °C) and diluted before use. Exposure of iodide solutions to light should be minimized in order to avoid degradation. The working standard solutions were made by dissolving the stock solution in the selected mobile phase. Anion-exchange chromatography was performed using a mobile phase consisting of acetate buffer, EDTA, deionised water, sodium nitrate and acetonitrile.

2.2. Instrumentation

The IC system consisted of the following components connected in series: a double piston high pressure pump PM-80 (BASi West Lafayette, USA), a Rheodyne® injector Model 7125 (Cotati, CA, USA) with a 20 μL loop and an Ionospher® A Chromsep anion-exchange LC-Varian® column (Varian NV/SA Belgium). The detection was performed using a BASi cross-flow amperometric cell connected to a LC, 4B potentiostat (BASi, West Lafayette, USA). The signal was recorded with a *Y*/*t* Kip-Zonen BD 40 (Ankersmit, Belgium). The cross-flow cell consisted of a dual disk silver electrode (or a dual empty disk for silver carbon paste housing) as a working electrode (BASi), an Ag/AgCl reference electrode and a stainless steel block as auxiliary electrode.

Cyclic voltammetry was performed with a PalmSens potentiostat (Eindhoven, The Netherlands). The potentiostat and the data acquisition were computer controlled. The electrochemical cell was a conventional three electrode system consisting of an Ag/AgCl reference electrode, a platinum counter electrode and the working electrode which was either the dual disk silver electrode (BASi) or the dual disk micronised silver carbon paste electrode. Centrifugation was performed with a Beckman Microfuge B. The ICP-MS was an Element 2 instrument (Thermo Fisher Scientific, Zellik, Belgium).

2.3. Electrode preparation

2.3.1. Metal silver electrode

The dual disk silver electrode was treated, when needed, by smoothing on a polishing cloth in the presence of alumina and water and subsequently rinsed by ultrasonication in water.

2.3.2. Colloidal and micronised silver carbon paste electrodes

The micronised silver (2–3.5 μm) or colloidal silver (<150 nm) were blended, in a mortar, with graphite and the hydrophobic binding agent for the solid carbon paste preparation. This was achieved by hand-mixing an appropriate amount of graphite powder and different amounts of micronised silver (2.5–50%) or colloidal silver (2.5–5%) in the mortar for at least 10 min, i.e. until the micronised silver or colloidal silver was uniformly dispersed in the graphite powder. Then, an accurate quantity of solid paraffin, warmed beforehand, was added to the graphite–silver powder and blended until a uniform paste was obtained. The silver-based SCPE was packed in the cavity of the dual disk-working electrode. The electrode was smoothed on a filter paper until the surface had a shiny aspect. When needed, a fresh surface was obtained by removing a thin layer of paste and refilling with new paste and smoothing.

2.4. IC-AD chromatography

The isocratic chromatographic and direct current amperometric experimental parameters were fixed as indicated below. The setup was operated during working day time. A methanol/water (50:50, v/v) mobile phase was passed through the IC setup during 15 min for rinsing and kept in the system when not in use. Experiments were performed at room temperature.

2.5. Sample preparation

2.5.1. Combustion of adsorbable organic iodide

For the determination of the iodine bound to organic compounds, the Schöninger combustion method described by Schramel and Hasse [46] was applied. Samples (4.1 mg and 4.7 mg powder of ICHQ and AMD, respectively) were wrapped in a piece of ashless filter paper and placed into the platinum grid holder fixed to the Schöninger flask stopper containing 10 mL reduction solution (sodium hydroxide 1 mmol/L and sodium sulfite 25 μmol/L) and was subsequently filled with oxygen by blowing the gas through a flexible tube. The sample was then ignited with a match and the stopper was quickly fitted on the flask for oxidative combustion. Following the incineration, the flask was cooled at room temperature for 10 min and shaken vigorously for complete iodine absorption and dissolution as iodide ions. The resultant solution was diluted five times with the mobile phase and the flask was again shaken vigorously. This solution was finally diluted 1000 times with the mobile phase before analysis. This treatment was also applied for preparing the blank solution.

2.5.2. Determination of iodide in skim milk powder

A precise quantity of milk powder (0.6345 g) was inserted in a 25 mL volumetric flask and reconstituted with 4.5 mL of warm water then stirred by sonication during 15 min in the presence of 4.5 mL of 1% acetic acid solution to precipitate proteins. To this mixture, methanol (or acetonitrile) was added to the final volume. After a period of settling, the supernatant was centrifuged for 5 min. The supernatant was then passed through a carbon-based solid phase extraction column, Supel Clean Envi-Carb 6 mL (Supleco Inc., Bellefonte, USA). The eluted solution was finally filtered, via a syringe, through a 0.20 μm filter (Scheiler & Schuel, Dassel, Germany) and diluted twice with the mobile phase before injection. The quantity of iodide was determined by referring to a pre-established calibration curve. The iodide content was also estimated by the standard addition method which consisted in spiking increasing volumes of an iodide standard solution to the milk reconstituted solution.

2.5.3. Determination of iodide in seaweeds product

The commercially available distillate of seaweeds (drinkable ampoules of 10 mL) was supplied without any indication of iodide content on the label. Five ampoules were taken to constitute the sample. A 10 mL aliquot of the sample was mixed under ultrasonication with 5 mL of 1% acetic acid and adjusted to 50 mL with the IC mobile phase. The mixture was centrifuged for 10 min and then filtered through a 0.20 μm membrane filter. The filtrate was diluted 100 times with the IC mobile phase before injection. The assay was performed by the method of standard addition. The latter consisted in spiking the diluted filtrate with a standard solution of 0.01 mol/L iodide such as: (a) 0.0 μg/L (blank); (b) 12.7 μg/L; (c) 25.4 μg/L.

For ICP-MS assays, the ampoule supernatant as well as the entire sample, i.e. supernatant and particles in suspension were analyzed. The latter were dissolved in the presence of tetramethylammonium hydroxide (1:1, v/v). Five hundred microlitres of mixture were diluted in 9 mL of a 2.5 μg/L rhodium (internal standard) solution containing 0.05% (v/v) Triton. The resulting solution was then acidified by 100 μL of concentrated HCl before analysis.

2.5.4. Determination of iodide in salts

IC-AD was applied to the determination of iodide in iodized table salt and sea salt with no special sample pre-treatment. The salt (4.669 g) was first dissolved in deionised water then diluted to the appropriate concentration with the IC mobile phase before injection. The content of iodide was obtained by referring to a pre-established calibration curve.

3. Results and discussion

The study of the influence of several experimental parameters affecting the results was realized using the IC setup with the silver disks-based detector. The IC stationary phase consisted of a 5 μm diameter porous silica-based anion exchanger grafted with quaternary ammonium head groups allowing for efficient separation of iodide from interfering halogenides. Other interfering anions and surface-active species may be encountered in a complex matrix and may interfere at the amperometric sensor. For this reason, the parameters affecting both the chromatographic separation and the electrochemical detection were investigated.

The pH, the amount of organic solvent and the salt content in the mobile phase as well as the flow rate were studied as parameters exerting a major influence both on the retention characteristics of iodide and on the electrode response. The influence of the working electrode potential was examined once the previous parameters were selected.

Due to its silica-based composition, the stability of the anion exchange column was restricted to a pH range comprised between

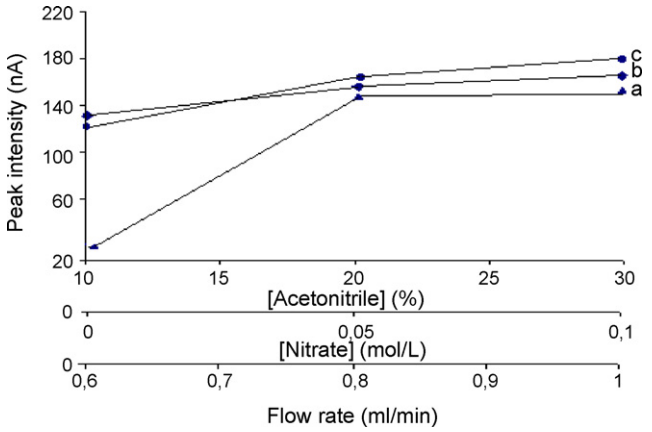

Fig. 1. Variation of the iodide peak intensity with: (a) (▲) concentration of nitrate (flow rate 0.6 mL/min, ACN 20%, v/v), (b) (♦) percentage of ACN(0.05 mol/L nitrate, flow rate 0.6 mL/min), (c) (●) flow rate (0.05 mol/L nitrate, 20% ACN). Mobile phase: $[I^-] = 96.4\ \mu g/L$; $[Cl^-] = 355$ mg/L, EDTA = 0.5 mM; acetate buffer pH 4.9. Silver electrode, $E_{app} = 0.0$ V vs. Ag/AgCl.

2 and 5. This pH range limited also the risks of silver electrode dissolution especially in oxidizing acidic media (e.g. in nitric acid) or silver oxide formation in alkaline media [23,39]. The final selected mobile phase consisted of acetate buffer pH 4.9/acetonitrile 20% (v/v) containing sodium nitrate (0.1 mol/L or 0.05 mol/L see below) and 0.5 mmol/L EDTA. The latter permitted the complexation of traces of cations which might interact with iodide ions and/or metallic silver. The standard solution studied was a mixture of iodide and chloride at 96.5 μg/L and 355 mg/L, respectively.

Nitrate acted as a competitor for the cationic sites at the stationary phase and its effect was studied over the concentration range comprised between 0.0 mol/L and 0.1 mol/L. As expected, the retention time of iodide decreased and the peak intensity increased substantially by raising the nitrate concentration from 0 mol/L to 0.05 mol/L (Fig. 1a). No substantial change was noted from 0.05 mol/L to 1 mol/L.

The effect of acetonitrile was studied in the percentage range 10–32% (v/v). The presence of ACN in the mobile phase allowed for good solvation of the stationary phase and elution of the relatively hydrophobic iodide ions. A reduction in the retention time from 9.65 min to 7.2 min and a slight increase in the signal (Fig. 1b) were observed by raising ACN to 20% with no further change above this percentage. A decrease in the resolution (Rs), however, between iodide and chloride was observed with Rs values dropping from 1.4 to 1.1.

By increasing the flow rate between 0.6 mL/min and 1.0 mL/min, the retention time decreased and peak intensity increased slightly (Fig. 1c). The Rs between iodide and chloride ions dropped from 1.1 to 1.0. There was no substantial change for both the peak retention time and the slope of the calibration curve at pH 4.7, 4.9 and 5.2.

Based on these results the chromatographic operating conditions were selected as summarized in Table 2.

3.1. Cyclic voltammetry

In order to understand the mechanism underlying the amperometric response and apply a suitable operating potential for the IC detection, cyclic voltammetry was performed both at the PSE and at the SCPE in the mobile phase as supporting electrolyte

The voltammograms were recorded starting at 0.0 V towards positive potentials At the PSE (Fig. 2), in the absence of iodide, the first run showed one oxidation wave (A) at +0.450 V which corresponded to the oxidation of silver metal. This was followed, on the reserve scan, by one peak (B) at +0.180 V attributed to the reduction of silver ions. In the presence of iodide ions, in addition to the previously mentioned peaks, a new redox couple was observed (peaks C and D) located at potentials below 0.0 V. By raising iodide concentration, peaks A and B were not significantly affected while peaks C and D raised and shifted towards more negative potentials. Based on literature data on silver iodide reduction at a silver electrode it was assumed that the newly developed redox couple C/D corresponded to adsorbed silver iodide reduction to give metallic silver and free iodide in solution (C) and reoxidation (redissolution) of the silver particles (D) [47]. These data confirm the facilitated oxidation of silver in the presence of iodide (and halogens in general) [23,38]. The interaction of iodide with silver ions occurs in a broad potential range, even at open circuit. The latter has been attributed to the oxidation of metallic silver by protons or dissolved oxygen as follows [48]:

$$Ag + I^- + H^+ (\text{or dissolved oxygen}) \rightarrow AgI\,(ads) + (1/2)H_2\,(g)$$

This has been exploited by adsorptive accumulation of halogenide ions in acidic media on silver and silver composite electrodes, under controlled potential, for the determination of those ions by anodic [49] and cathodic [38,44] stripping voltammetry.

At the SCPE, each run was realized with a fresh electrode surface (Fig. 3). The cyclic voltammetry showed one oxidation peak

Table 2
Selected conditions for IC–AD iodide determination

Parameter	Condition	
	Studied	Selected
NO_3^- (mol/L)	0.00–0.10	0.10 or 0.05
CAN (%, v/v)	10.0–30.0	20.0
EDTA (mmol/L)	–	0.5
NaAc 10.0 mM-HAc 50% (pH)	4.7–5.2	4.9
Flow rate (mL/min)	0.6–1.0	0.6
Sample volume (μL)	–	20.0
Applied potential (mV)		
PSE	−70 till +70	−40
SCPE	−100 till +100	+80

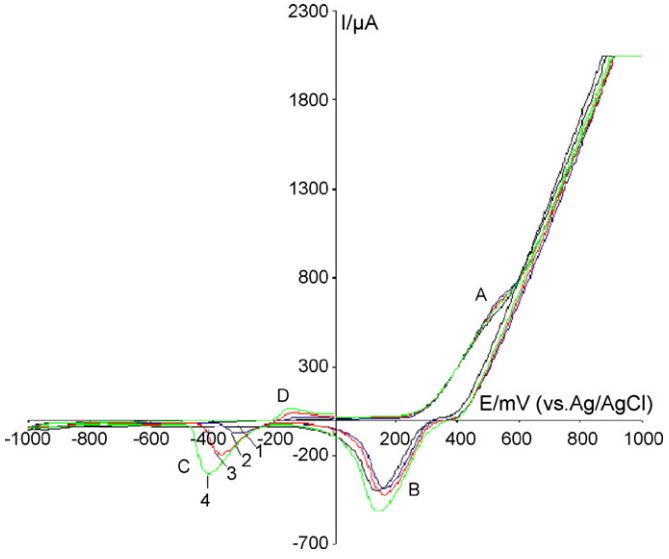

Fig. 2. CV at the PSE in mobile phase electrolyte (0.1 mol/L nitrate; ACN 20%; EDTA 0.5 mmol/L; acetate buffer pH 4.9). (1) Electrolyte; (2) electrolyte + 0.5 mmol/L iodide; (3) electrolyte + 1 mmol/L iodide; (4) electrolyte + 1.5 mmol/L iodide. Cycling from 0.0 to +1.0 back till −1.0, final 0.0 V. Scan rate 50 mV/s.

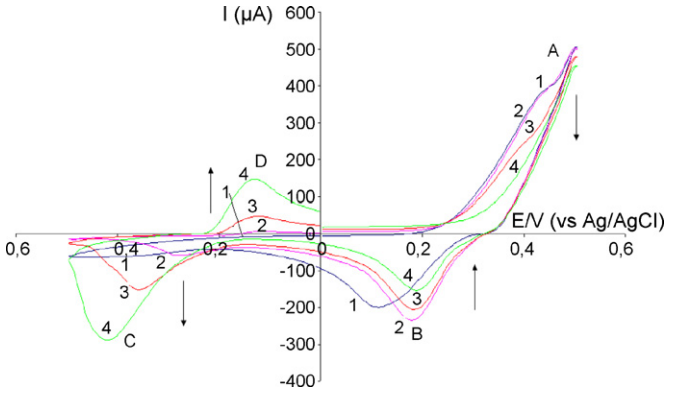

Fig. 3. CV at the SCPE in mobile phase electrolyte (0.1 mol/L nitrate; ACN 20%; EDTA 0.5 mmol/L; acetate buffer pH 4.9). (1) Electrolyte; (2) electrolyte + 0.5 mmol/L iodide; (3) electrolyte + 1 mmol/L iodide; (4) electrolyte + 2 mmol/L iodide. Cycling from 0.0 to +0.5 back till −0.5, final 0.0 V. Scan rate 50 mV/s.

(A1) starting at 0.2 V with, on the reverse scan, the corresponding reduction peak (B1) and a broad wave (C1) around −0.4 due to oxygen reduction (see below). These peaks likely corresponded to the oxidation of the silver microparticles to silver ions subsequently reduced on the reverse scan. The addition of iodide ions (0.5 mmol/L) to the electrolyte solution produced a slight decrease of peak A1 and shifted its reduction peak to more positive potentials (B2) and a new reduction peak was obtained (C2) with its corresponding oxidation peak (D2). Further addition of iodide in solution produced a decrease of the redox couple A/B and an increase of couple C/D intensity (Fig. 3). In order to assign the nature of the peaks observed, cyclic voltammetry were recorded by starting at 0.0 V towards negative potentials direction (Fig. 4). In the absence of iodide, only one broad wave due to oxygen reduction was observed around −0.4 V (C1). In the presence of iodide (0.5 mM) a double peak (two overlapping peaks) were noted (C2) in agreement with literature data on silver iodide reduction at a silver composite electrode [44] and the corresponding reoxidation peak (D2). By increasing the dissolved iodide concentration, only one broad reduction peak was obtained at −0.4 V (C3) and the corresponding reoxidation (redissolution) peak at −0.150 V (D3). The former likely corresponded to the reduction of adsorbed silver iodide and the latter to silver oxidation facilitated by the presence of iodide ions. These data are in agreement with the results obtained at the PSE, with the redox couple A/B corresponding to silver oxidation to silver ions (peak A) and subsequent silver ion reduction (peak B) in the absence of iodide. Couple C/D corresponded to the reduction of

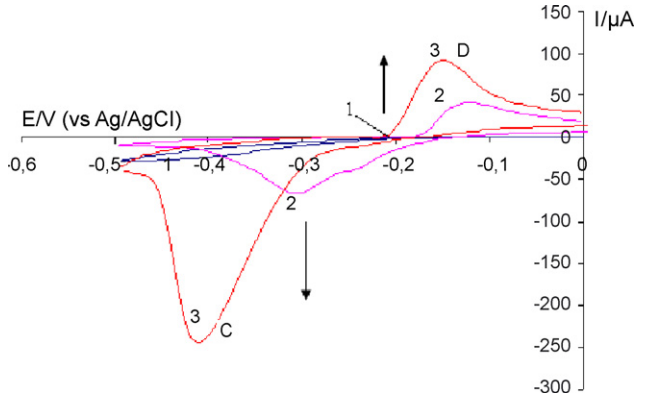

Fig. 4. CV at the SCPE. Scan cycle from 0.0 to −0.5 V and back to 0.0 V. (1) Electrolyte; (2) electrolyte + iodide 0.5 mmol/L; (3) electrolyte + iodide 2 mmol/L. Same conditions as in Fig. 3.

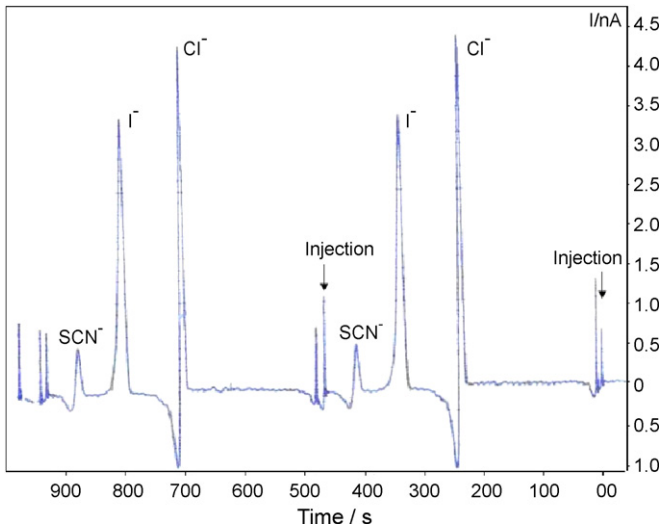

Fig. 5. Typical repetitive IC-AD(SCPE) chromatograms. Iodide (KI) = 6.35 μg/L in the presence of some interfering anions: [NaCl] = 2.92 mg/L; [KIO_3] = 107 μg/L; [KSCN] = 486 μg/L; $K_4Fe(CN)_6 \cdot 3H_2O$ = 211.2 μg/L. Experimental conditions are those reported in Table 2 with 0.1 mol/L nitrate in mobile phase.

adsorbed silver iodide (C) and reoxidation (redissolution) of silver (D) to give silver ions (as AgI or AgI_2^-). Interestingly, the anodic redissolution of deposited silver (peak D) was highly reproducible and the current linearly related to iodide concentration.

3.2. Peak intensity as a function of applied potential

Taking into account these results, the electrode response was studied by IC-AD as a function of the applied potential from −100 mV to +100 mV at both the PSE and SCPE electrodes. This was realized by injecting repetitively 25.4 μg/L and 63.5 μg/L iodide solutions. At both electrodes the current was almost of same magnitude. At potentials higher than +100 mV an increase of the baseline noise current was observed resulting in a less good S/N. Based on these data an arbitrary potential of −40 mV and +80 mV was chosen for the metal silver and micronised silver electrodes, respectively. At these potentials no special care was needed to remove dissolved oxygen.

3.3. Study of interferences

The influence of species likely present, along with iodide, in complex samples and which might be detected at the silver electrode was examined by injecting possible foreign ions separately or by injecting a mixture of iodide in the presence of interfering ions in different ratios. It was found that chloride, thiocyanate (present in biological and sea food samples), iodate (sometimes added in table salt for iodide supply), sulfite and hexacyanoferrate (anti-cracking agent often present in table salt) did not interfere. Chloride showed a strong interference when present at a relatively high concentration compared to iodide due to a negative peak with a long tailing following the chloride peak (Fig. 5). This peculiar phenomenon can be attributed to silver chloride deposits which decreased the active surface of the working electrode (i.e. drop in baseline current). The washout effect exerted by the mobile phase allowed progressive recovering of the baseline [23]. Interestingly, nitrate had a different effect on the retention of iodide and chloride ions which implied that the risk of interference by chloride ions could be solved by decreasing the concentration of nitrate in the mobile phase (Table 3).

Table 3
Effect of nitrate ion on retention time of iodide and chloride

Nitrate (mol/L)	Retention time (s)		Δt (s) between I^- and Cl^-
	Iodide	Chloride	
0.10	340	240	100
0.05	450	300	150
Gain in terms of resolution time (Δt)			50

As indicated, if the nitrate concentration dropped from 0.10 mol/L to 0.05 mol/L, the difference in resolution time between iodide and chloride peaks raised from 100 s to 150 s, allowing sufficient time for the negative chloride peak to return to the baseline. Under such conditions, the separation of iodide from the studied interfering ions was very satisfactory with a total run time of approximately 11 min.

3.4. Electrode calibration

Experiments were performed comparatively at the three silver-based electrodes. A series of iodide standard solutions at different concentrations (0.254–127 μg/L), prepared in the selected mobile phase, were injected into the IC system. It was noted that the repeatability of the amperometric response was less good at concentrations higher than 63.5 μg/L. At the metal silver electrode, a good linear relationship between signal and iodide concentration was found between 3.2 μg/L and 47 μg/L (determination coefficient of 0.9991). At the micronised silver electrode, the best characteristics were obtained with 35% (m/m) of silver (other ratios not shown) with a good linearity of the response between 0.635 μg/L and 63.5 μg/L (determination coefficient of 0.9997). With the colloidal silver electrode a linear relationship between signal and iodide concentration was found between 0.635 μg/L and 63.5 μg/L with a R^2 of 0.9995 (Table 4). The limit of detection (LOD) of iodide at the metal, colloidal and micronised electrodes were 2.2 μg/L, 0.47 μg/L and 0.47 μg/L (signal three times the baseline noise), respectively.

3.5. Short- and long-term reproducibility

The reproducibility of the iodide reponse at the different electrodes was evaluated over short-term (within 1 day) and long-term periods (14 consecutive days) by studying 3.17 μg/L, 31.7 μg/L and 63.5 μg/L standard iodide solutions. For short-term periods, better results were obtained at the micronised electrode with relative standard deviation (R.S.D.) lower than 3% at the lowest iodide concentration. Higher R.S.D.s were obtained at higher iodide concentrations, a result likely attributed to electrode surface perturbation due to silver iodide deposits. Under identical experimental conditions, the R.S.D. values at the PSE were less good than at the SCPE but still lower than 3.4% (Table 5).

The long-term reproducibility was determined by testing the response for several days in terms of slope of the calibration curve within the linear concentration domain (3 calibrations/day, 10 concentration points). The slope at both electrodes was significantly different the first day compared to the following days. This can likely be explained by a conditioning of the surface of the working electrode in the IC setup. At the SCPE, excellent reproducibility was obtained from day 2 to day 14 (average R.S.D. = 0.7), then the slope started to decrease progressively (Table 6). At the PSE, depending if one considers the assays of the first day or not, the R.S.D. values were 15% and 9%, respectively (data not shown).

For the colloidal electrode, in spite of its broad domain of linearity, it was not selected since it generated crippling problems of stability and reproducibility, a phenomenon likely related to a high dissolution rate of silver nanoparticles in the selected mobile phase (visual detection of surface erosion).

Based on these comparative results, the micronised silver carbon paste electrode was chosen for subsequent iodide determinations in real samples. This electrode, in addition to the above mentioned interesting analytical figures of merit, can be operated for more than 2 weeks of continuous use and may readily be renewed when damaged, e.g. in the presence of high concentration of halide ions or surface active species or in case of surface erosion. It was noted that at iodide concentrations higher than 25.4 μg/L the iodide peak was immediately followed by a negative peak. This perturbating effect is often reported to occur at the metallic silver-based amperometric detector and is assumed to be related to silver iodide deposits onto the electrode surface [23,24,27,28]. Under the selected conditions (Table 1) and below 25 μg/L, the iodide peak showed a symmetric profile with no tailing and no opposite peak problems.

Table 4
Dynamic response range at the metal, micronised, and colloidal silver working electrodes (y = nA, x = μg/L)

Electrode	Linear range (μg/L)	Calibration range	R^2
PSE	0.635–127	$y = 95.005x - 2.0042$	0.9941
	3.2–63.5	$y = 85.338x - 1.0576$	0.9986
	3.2–47.0	$y = 82.367x - 0.7056$	0.9991
SCPE	0.635–127	$y = 60.750x - 0.0574$	0.9993
	0.635–63.5	$y = 63.083x - 0.364$	0.9997
Colloidal	0.635–127	$y = 51.592x - 0.1764$	0.9953
	0.635–63.5	$y = 52.978x - 0.4125$	0.9995

Table 5
Short-term reproducibility (repeatability) at metal and micronised electrodes (N = 5)

Parameter	Silver electrode (PSE)			Micronised electrode (SCPE)		
	Intensity (nA)					
	3.17	31.7	63.5 (μg/L)	3.17	31.7	63.5 (μg/L)
Average	1.91	21.3	46.2	1.45	16.5	34.2
S.D.	0.06	0.59	1.55	0.04	0.28	0.57
R.S.D. (%)	3.1	2.8	3.4	2.8	2.0	2.1

Table 6
Long-term reproducibility at the SCPE

Day	Slope	R^2
1st	63.76	0.9997
2nd	54.44	0.9994
7th	54.40	0.9991
14th	53.77	0.9997
Average	56.6	54.2
S.D.	4.79 (0.37)	
R.S.D. (%)	8.5 (0.7)	

( ) = statistics without counting first day.

Table 7
Results of iodide determination in skim milk powder by standard addition method (A) and external calibration (B). Methanol treatment

Milk powder	Method	I^- found[a] (μg/g)	Recovery (μg/g)	S.D. (%)	R.S.D. (%)
	A	1.34	103.8	0.012	0.9
	B	1.32	102.3	0.014	1.1
BCR certified value: 1.29 ± 0.09 μg I^-/g milk					

[a] Average of three determinations.

Table 8
Results of iodide determination in real samples

Sample[a]			Specification	Iodide taken (μg)	Iodide found[b] ± S.D. (μg)	R.S.D. (%)	*R* (%)	Calculated value with regard to the specification
1	A		(Label) 20 mg KI/kg NaCl	93.38	68.1 ± 0.8	1.2	72.9	14.6 mg KI/kg NaCl
	B		(Label) not specified	–	4.7 ± 0.3	1.1	–	1.0 mg I^-/kg NaCl
	C		(Spiked) 20.0 mg KI/kg NaCl	93.38	98.0 ± 0.9	1.0	104.9	21.0 mg KI/kg NaCl
2	Seaweeds (ampoule 10 mL)		No label	–	190 ± 3	1.6	–	0.190 mg I^-/ampoule
3	Organoiodide drug compounds	ICHQ	n_{I^-} = 1	1700	1640 ± 20	1.2	96	–
		AMD	n_{I^-} = 2	1710	1790 ± 30	1.7	104	–

[a] Iodized table salt (1 A); sea salt (1 B); potassium iodide fortified high-purity NaCl (1C).
[b] Average of three determinations; n_{I^-} = number of iodine atoms/molecule.

3.6. Analytical applications

3.6.1. Determination of iodide in skim milk

In order to illustrate the applicability of the proposed setup, different real samples were studied. Iodide determination was realized on table salts (iodide fortified), sea products (seaweeds and sea salt), organoiodide drug compounds and certified skim milk. The latter permitted to control the accuracy of the proposed method. As reported in Table 7, the results obtained for iodide determination in skim milk CRM No. 150 were found in very good agreement with the certified value.

3.6.2. Determination of iodide in table salts (Table 8)

Results were obtained by referring to a pre-established linear calibration graph in the iodide concentration range comprised between 1.27 μg/L and 63.5 μg/L. No interference was observed by chloride and hexacyanoferrate ions (not shown). The accuracy was tested by calculating the recovery (*R*) of iodide spiked in high-purity grade sodium chloride (sample C). A recovery of 104.9% was found suggesting that the assay slightly over estimated the amount of iodide in real salt samples. A low amount of iodide was found in sea salt (sample B). The content of iodide in table salt was substantially lower than declared (sample A).

3.6.3. Determination of iodide in sea product (labeled as distillate of seaweeds)

The accuracy of the assay was checked by comparison with ICP-MS data. The latter technique gave results with a R.S.D. of 12% within the iodine dynamic concentration range, i.e. up to 20 μg/L [50]. The IC-AD developed method gave 190 μg/10 mL (Table 8) which was slightly higher than the ICP-MS result for the supernatant (166 μg/10 mL) and slightly lower than the ICP-MS result for the total digest (256 μg/mL). The latter can be explained by the fact that ICP-MS determined the total amount of iodine (free iodide and organoiodide).

3.6.4. Determination of iodide bound to organic compounds

Organoiodide compounds have been determined by LC-AD with post-column photochemical reaction with LOD in the range 1–2 μg/L [51]. The oxygen combustion method, though, was preferred in our work as the IC was developed for iodide ions. As reported in Table 8, good recoveries were obtained for both ICHQ and AMD.

4. Conclusion

A micronised silver solid carbon paste-working electrode has been found to be a very appropriate amperometric detector in IC for the sensitive and selective determination of halogenides and more specifically iodide in complex matrices. With the developed IC-AD methodology, the detector can be operated for weeks without surface cleaning or renewing and the sample treatments do not require tedious cleaning or extraction procedures. Linear responses within a broad dynamic range and detection and quantification limits down to subμg I^-/L (nmol/L) have been achieved.

Acknowledgements

Thanks are expressed to the Coopération Technique Belge and to the David et Alice Van Buuren foundation for grant and financial support to TKM.

References

[1] F. Azizi, M. Hedayati, M. Rahmani, R. Sheikloleslam, S. Allahverdian, N. Salarkia, J. Endocrinol. Invest. 28 (2005) 23.
[2] J.R. Reid, S.F. Wheeler, Am. Fam. Phys. 72 (2005) 623.
[3] P. Lind, G. Kumning, M. Heinich, I. Igerc, P. Mikosch, H.J. Gallowitsch, E. Kresnik, I. Gomez, O. Unterwegen, H. Aigner, Thyroid 12 (2002) 903.
[4] P. Vitti, F. Delange, A. Pinchera, M. Zimmermann, J.T. Dunn, Lancet 361 (2003) 1226.
[5] G. Pouessel, K. Bouarfa, B. Soudan, J. Sauvage, F. Gottrand, D. Turck, Arch. Pédiatr. 10 (2003) 96.
[6] A. Malon, A. Radu, W. Qin, A. Ceresa, M. Majzurawska, E. Bakker, E. Pretsch, J.F. van Staden, Anal. Chem. 75 (2003) 3865.
[7] K.A. Schwehr, P.H. Santschi, Anal. Chim. Acta 482 (2003) 59.
[8] R.O. Rahn, Anal. Chim. Acta 248 (1991) 595.
[9] Z. Xie, J. Zhao, Talanta 63 (2004) 339.
[10] I. Svancara, B. Ogorevc, M. Novic, K. Vytras, Anal. Bioanal. Chem. 372 (2002) 795.
[11] J. Kontoyannakos, G.J. Moody, J.D.R. Thomas, Anal. Chim. Acta 85 (1976) 47.
[12] A.K. Singh, S. Mehtab, Talanta 74 (2008) 806.
[13] D.E. David, D.E. Mulcahy, G.R. O'Connell, Talanta 37 (1990) 313.
[14] T.H.J. Postmes, J.M. Coenegracht, Clin. Chim. Acta 38 (1972) 313.
[15] D. Gamallo-Lorenzo, M. Barciela-Alonso, A. Moreda-Pineiro, A. Bermejo-Barrera, P. Bermejo-Barrera, Anal. Chim. Acta 542 (2005) 287.
[16] T. Tomiyasu, M. Nonaka, M. Uchikado, K. Anazawa, H. Sakamoto, Anal. Sci. 20 (2004) 391.
[17] F. Gu, A.A. Marchetti, T. Straume, Analyst 122 (1997) 535.
[18] K.M. Eckhoff, A. Maage, J. Food Comp. Anal. 10 (1997) 270.
[19] F. Schöne, C. Zimmermann, G. Quanz, G. Richter, M. Leiterer, Meat Sci. 72 (2006) 365.
[20] E.H. Larsen, M.B. Ludwigsen, J. Anal. Atom. Spectrom. 12 (1997) 435.
[21] B. Michalke, P. Schramel, S. Hasse, Mikrochim. Acta 122 (1996) 67.
[22] Y. Gelinas, V. Iyengar, R.M. Barnes, Fresen. J. Anal. Chem. 362 (1998) 483.
[23] J. Cheng, P. Jandik, N. Avdalovic, Anal. Chim. Acta 536 (2005) 267.
[24] T.R.I. Cataldi, A. Rubino, R. Ciriello, Anal. Bioanal. Chem. 382 (2005) 134.
[25] L. Liang, Y. Cai, S. Mou, J. Cheng, J. Chromatogr. A 1085 (2005) 37.
[26] C.M. Selavka, I.S. Krull, Anal. Chem. 59 (1987) 2704.
[27] H. Below, H. Kahlert, Fresen. J. Anal. Chem. 371 (2001) 431.
[28] T.R.I. Cataldi, A. Rubino, M.C. Laviola, R. Ciriello, J. Chromatogr. B 827 (2005) 224.
[29] J. Melichercik, L. Szijarto, A.R. Hill, J. Dairy Sci. 89 (2006) 934.
[30] W. Buchberger, K. Winsauer, Mikrochim. Acta 3 (1985) 347.
[31] K. Ito, H. Sunahara, J. Chromatogr. 502 (1990) 121.
[32] J.F. van Staden, Anal. Chim. Acta 261 (1992) 381.
[33] A.A. Almeida, X. Jun, J.L.F.C. Lima, Mikrochim. Acta 127 (1997) 55.
[34] K. Han, W.F. Koch, K.W. Pratt, Anal. Chem. 59 (1987) 731.
[35] Z. Chen, D.B. Hibbert, Anal. Chim. Acta 350 (1997) 1.
[36] J. Jakmunee, K. Grudpan, Anal. Chim. Acta 438 (2001) 299.
[37] R.D. Rocklin, E.L. Johnson, Anal. Chem. 55 (1983) 4.
[38] I. Shain, S.P. Perone, Anal. Chem. 33 (1961) 325.

[39] C. Bruggink, W.J.M. van Rossum, E. Spilkerman, E.S.E. van Beelen, J. Chromatogr. A 1144 (2007) 170.
[40] Application note 37, Determination of iodide in milk products, Dionex Corporation, 2000.
[41] C. Fan, G. Li, Y. Zhuang, J. Zhu, D. Zhu, Electroanalysis 12 (2000) 205.
[42] S.L. Petersen, D. Tallman, Anal. Chem. 60 (1988) 82.
[43] J. Wang, N. Naser, L. Angnes, H. Wu, L. Chen, Anal. Chem. 64 (1992) 1285.
[44] S. Sebkova, T. Navratil, M. Kopanica, Anal. Lett. 37 (2004) 603.
[45] B. Sljukic, R. Baron, C. Salter, A. Crossley, R.G. Compton, Anal. Chim. Acta 590 (2007) 67.
[46] P. Schramel, S. Hasse, Michrochim. Acta 116 (1994) 205.
[47] F. Fourcade, T. Tzedakis, J. Electroanal. Chem. 493 (2000) 20.
[48] G.N. Salaita, F. Lu, L. Laguren-Davidson, A.T. Hubbard, J. Electroanal. Chem. 229 (1987) 8.
[49] T.P. Aleksandrova, Y.B. Kletenik, J. Anal. Chem. 55 (2000) 590.
[50] P. Macours, J.C. Aubry, B. Hauquier, J-M. Boeynaems, S. Goldman, R. Moreno-Reyes, J. Trace Elem. Med. Biol., in press.
[51] C.-H. Wu, J.-H. Lian, J.-L. Wang, J.-G. Lo, J. Chromatogr. A 976 (2002) 423.

Talanta 76 (2008) 497–502

Contents lists available at ScienceDirect

Talanta

journal homepage: www.elsevier.com/locate/talanta

Copper(II) modified carbon paste electrodes based on self-assembled mercapto compounds-gold-nanoparticle

Mohammad Hossein Mashhadizadeh[a,*], Khadijeh Eskandari[a], Alireza Foroumadi[b], Abbas Shafiee[b]

[a] Faculty of Chemistry, Tarbiat Moallem University, Tehran, Iran
[b] Department of Medicinal Chemistry, Faculty of Pharmacy and Pharmaceutical Sciences Research Center, Tehran University of Medical Sciences, Tehran 14174, Iran

ARTICLE INFO

Article history:
Received 26 January 2008
Received in revised form 8 February 2008
Accepted 9 February 2008
Available online 26 February 2008

Keywords:
Gold nanoparticle
Self-assemble
Mercapto compound
Potentiometric sensor
Carbon paste electrode
Copper ion

ABSTRACT

Three mercapto compounds [2-mercapto-5-(1-methyl-5-nitroimidazole-2-yl)-1,3,4-thiadiazole] (MMNIT), [2-mercapto-5-(5-nitrofuran-2-yl)-1,3,4-thiadiazole] (MNFT) and [2-mercapto-5-(5-nitrothiophen-2-yl)-1,3,4-thidiazole] (MNTT) were used for self-assembled-gold nanoparticle (SAGNP) modified carbon paste electrodes. The electrodes were applied as indicator electrodes for potentiometric determination of Cu(II) ion. The prepared electrodes exhibit a Nernstian slope of 31.0 ± 0.5 mV per decade for Cu(II) ion over a wide concentration range of 7.9×10^{-9}–3.2×10^{-2}, 7.9×10^{-9}–7.9×10^{-4}, and 2.8×10^{-8}–7.9×10^{-3} mol L^{-1} for MMNIT, MNFT and, MNTT, respectively. The detection limits of electrodes were 3.5 (±0.2) × 10^{-9}, 4.1×10^{-9}, and 4.1×10^{-8} mol L^{-1} of copper ion, respectively. The potentiometric responses of electrodes based on MMNIT, MNFT, and MNTT are independent of the pH of test solution in the pH range 2.0–5.5, 2.5–7.0, and 2.0–6.5, respectively. They have quick response with response time of about 5 s. The proposed electrodes show fairly good selectivity over some alkali, alkaline earth, transition and heavy metal ions. Finally, the proposed electrodes were successfully employed to detect Cu(II) ion in hair and water samples.

1. Introduction

Copper is a natural element that is an essential micronutrient to ensure the well being of all aerobic life forms. It plays a vital part in the development and performance of the human nervous and cardiovascular systems, as well as the skin, bone, immune and reproductive systems, including gene transcription. Copper can also inhibit the growth of microbes, thus providing a measure of protection against harmful germs and bacteria in many environments. Due to environmental and biological importance of Cu(II) many sensors for the determination of this ion have been developed [1].

Metal nanoparticles play an important role in modern bioanalytical chemistry due to their usefulness for the preparation of sensors giving rise to improved responses from biological compounds with respect to those observed at conventional metal surfaces. Gold nanoparticles display electronic, chemical and physical properties that may by employ in optical and electronic devices, catalysis and sensor technology [2]. In particular, gold nanoparticles have demonstrated to be very appropriate for the development of modified electrodes. Gold nanoparticles allow the construction of electrode nanoarrays in one or several dimensions, with signal-to-noise several orders of magnitude higher than those achieved at conventional electrodes. Colloidal gold-modified electrodes have been prepared using glassy carbon [3], metal Au [4] and carbon paste [5] as electrode substrates.

The self-assemble monolayer (SAM) of sulfur-containing molecules was characterized by Nuzzo and Allara [6] almost 25 years ago. Disulfides, sulfide and thiols coordinate very strongly onto a variety of metals, e.g. gold, silver, platinum or cadmium. Nevertheless gold is the most favored because it is reasonably inert [7]. SAM provides a simple method of electrode functionalization by strong chemisorption of free anchor groups such as thiols, disulfides, amines, silanes or acids, and has found potential applications such as in sensors, corrosion inhibition, wetting control, and other biomolecular electronic devices [8].

The development of selective chemical sensor has received widespread attention during the past three decades because of their possibility use in clinical and environmental monitoring, as they provide a rapid, accurate and low cost method of analysis. Carbon pastes are well known as useful materials for the fabrication of various electrometric sensors for analytical purpose. The operation mechanism of such chemically modified carbon paste electrodes (CMCPEs) depends on the properties of the modifier which is used for important selectivity towards the target species [9]. Each measurement was performed on a new surface, obtained by a simple/polishing procedure.

* Corresponding author. Fax: +98 21 88820993.
E-mail address: mashhadizadeh@tmu.ac.ir (M.H. Mashhadizadeh).

0039-9140/$ – see front matter © 2008 Published by Elsevier B.V.
doi:10.1016/j.talanta.2008.02.019

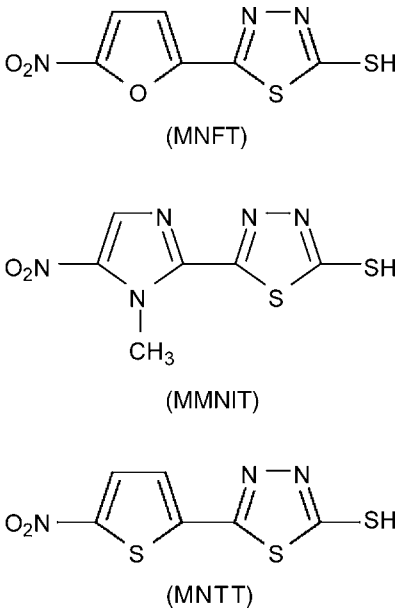

Fig. 1. Structures of mercapto compounds used as ionophore in the proposed electrodes.

Recently, we have demonstrated that some PVC membrane and carbon paste electrodes for the potentiometric determination of some heavy and transition metal ions [9–15]. We described here, three mercapto compounds MMNIT, MNFT and MNTT, recently synthesized in our laboratories [16–18] (Fig. 1), were used for self-assembled-gold nanoparticle (GNP) modified carbon paste electrodes. The electrodes were applied as indicator electrode for potentiometric determination of ultra trace amounts of Cu(II) ion.

2. Experimental

2.1. Reagents

All analytical reagent grade chemicals and distilled water were used for preparing all aqueous solutions. Hydrogen tetracholoroaurate ($HAuCl_4{\cdot}3H_2O$), trisodium citrate and copper nitrate were obtained from Merck, carbon graphite powder and paraffin oil were purchased from Fluka. Salts of metal nitrates (all from Merck) were of the highest purity available and used without any further purification except for vacuum drying over P_2O_5.

2.2. Apparatus

All potentiometric measurements were made with a pH/mV meter (Metrohm-827) using proposed sensor in conjunction with a double junction Ag/AgCl (Azar electrode, Iran) reference electrode. UV–vis absorption spectrum was recorded with a UV–vis spectrometer (Philips-PU8750).

2.3. Preparation of gold nanoparticle

Colloidal gold nanoparticles were prepared according to the literature [19–23] by adding 0.5 mL of 1% (w/v) sodium citrate solution to 50 mL of 0.01% (w/v) $HAuCl_4{\cdot}3H_2O$. All glassware used in this procedure was cleaned in freshly prepared 1:3 HNO_3–HCl and rinsed thoroughly distilled water. The two solutions were heated up to 60 °C. The final mixture of red color was boiled for 15 min. The preparation was stored in dark glass bottles at 4 °C.

2.4. UV–vis spectrum

UV–vis absorption spectrum was recorded with a UV–vis spectrometer (Philips-PU8750) in the wavelength range from 360 to 800 nm. The fresh GNPs solution without any further treatment was used as the samples for UV–vis measurement using deionized water as a blank for background correction. The UV–vis spectrum represented in Fig. 2 shows a peak at 540 nm which the indicative of the formation of gold nanoparticles in the colloidal solution [24].

2.5. Preparation of carbon paste modified electrodes

Bare CPEs were prepared by mixing 1.20 g of graphite powder, which had been heated at 700 °C in a muffle furnace for 15 s, with 800 μL of paraffin oil with a mortar and pestle. A modified paste was prepared in a similar fashion, except that the graphite powder was mixed with a desired weight of ligand and gold nanoparticle to get different composition as given in Table 1. Both unmodified and modified pastes were packed into a polyethylene tube (2.5 mm diameter), the tip of which had been cut off. Electrical contact to the paste was established via inserting a copper wire thorough flank.

The surface of fresh modified carbon paste electrode were preconditioned by exposure to a 1.0×10^{-2} mol L^{-1} Cu(II) ion solution for 2 h then, the electrode was rinsed with deionized water. A fresh electrode surface was obtained by squeezing more out. The surplus of paste was cut out with a glass rod and the exposed-end polished on a paper until the surface showed shiny appearance.

2.6. Electrodes system and emf measurement

All emf measurements were carried out with the following cell assembly:

Ag/AgCl|sample solution|CPE

All the emf observations were made relative to a double junction Ag/AgCl electrode with a pH/mV meter. The performance of the electrodes was investigated by measuring the emfs of copper nitrate solution which is prepared with a concentration rang of 10^{-1}–10^{-9} mol L^{-1} by serial dilution. Each solution was stirred and the potential reading was recorded when it became stable, and then plotted as a logarithmic function of Cu(II) activity. The activities of metal ions were based on the activity coefficient (λ), where calculated from the modified form of the Debye–Huckel equation, which

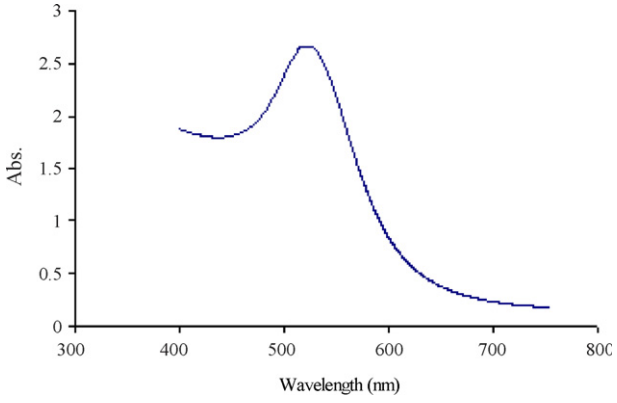

Fig. 2. UV–vis absorption spectra of Gold nanoparticle.

Table 1
Optimization of membrane ingredients of modified carbon paste electrodes

	Ligand (mg)	GP[a] (mg)	PO[b] (mg)	NP[c] (μL)	Slope mV/decade	Linear range (mol L^{-1})
1	–	50.1	27.3	–	–	–
2	–	50.0	28.0	120	–	–
3	0.5 (1)	48.2	26.9	120	21.3	3.8×10^{-7}–4.5×10^{-4}
4	2.0 (1)	45.3	26.1	120	28.4	2.0×10^{-8}–3.2×10^{-5}
5	2.5 (1)	43.3	26.3	120	29.8	7.9×10^{-9}–7.9×10^{-4}
6	2.5 (1)	43.3	26.5	–	23.6	7.8×10^{-7}–4.5×10^{-4}
7	0.5 (2)	47.7	27.4	120	24.2	3.9×10^{-7}–4.5×10^{-4}
8	2.0 (2)	48.0	27.2	120	30.8	2.0×10^{-8}–3.2×10^{-3}
9	2.5 (2)	45.2	27.4	120	31.1	7.9×10^{-9}–3.2×10^{-2}
10	2.0 (2)	45.2	27.3	–	25.2	6.0×10^{-7}–4.2×10^{-4}
11	0.5 (3)	46.0	27.1	120	25.1	4.5×10^{-7}–4.5×10^{-4}
12	2.0 (3)	44.5	27.1	120	27.4	2.0×10^{-7}–3.2×10^{-3}
13	2.5 (3)	44.4	27.2	120	31.0	2.8×10^{-8}–7.9×10^{-3}
14	2.0 (3)	44.1	27.3	–	26.2	8.2×10^{-7}–4.6×10^{-4}

Ligand 1 = [2-mercapto-5-(5-nitrofuran-2-yl)-1,3,4-thiadiazole].
Ligand 2 = [2-mercapto-5-(1-methyl-5-nitroimidazole-2-yl)-1,3,4-thiadiazole].
Ligand 3 = [2-mercapto-5-(5-nitrothiophen-2-yl)-1,3,4-thiadiazole].
[a] GP = graphite powder.
[b] PO = paraffin oil.
[c] NP = nanoparticle.

is applicable to any ion

$$\log\lambda = -0.511Z_2\left[\frac{\mu^{1/2}}{(1+1.5\mu^{1/2})-0.2\mu}\right]$$

where μ is the ionic strength and Z the valency. All measurements were carried out at $25\pm0.1\,^{\circ}C$.

2.7. Determination of selectivity coefficients

Potentiometric selectivity coefficients ($K^{pot}_{Cu,J}$) were determined by fixed interference method (FIM). In this manner, the CPE and the reference electrode was placed in 50.0 mL of 1.0×10^{-2} mol L^{-1} interference ion solution. Various volumes of 0.001, 0.01, or 0.1 mol L^{-1} of copper nitrate solution were added by microsyringe. The solution was stirred magnetically throughout and after each addition, the cell potential was recorded. In this manner, the copper ion concentration was varied over a wide range (1.0×10^{-8}–0.01 mol L^{-1}) while the interference ion (M^{n+}) concentration was kept constant without having to transfer the electrodes to new solutions. The pHs of test solutions are about 5–6.

2.8. Procedure for determination of copper in human hair

Hair samples were washed with acetone and distilled water to remove the surface contamination and dryashed in a muffle furnace at 450 °C. The residue was dissolved in nitric acid and evaporated to dryness at low heating rate. The residue dissolved in 20 mL of water and filtered. The clear solution was quantitatively transferred into a 50-mL volumetric flask and diluted to mark with water. Working solutions were prepared by taking a suitable aliquot of the sample and its copper content determined with the proposed electrodes and by a Varian Spectra AA220 atomic absorption spectrometer.

3. Results and discussion

Alkanethiols adsorb spontaneously onto the surface of coinage metals such as gold, silver, platinum and copper. Gold is the most frequently used because it does not have a stable oxide under ambient conditions. The thiol groups chemisorb onto the gold surface via the formation of a gold thiol bond to produce a densely packed, highly ordered monolayer [25].

Owing to their small dimensional size, good conductivity and excellent catalytic activity, gold nanoparticles have potential applications in the construction of electrochemical sensors and biosensors where they function as “electron antennae’ efficiently channeling electrons between the electrode and the electroactive species promoting better electron transfer between the electrode surface and the electrolyte [26–28,3]. It could not only increase the assembly amount of organothiol but also influence the structure and stability of SAM. Based on these investigations, we have used gold nanoparticles and three mercapto compounds (MMNIT, MNFT, and MNTT) to modify the carbon paste electrode and use as an ion selective electrode for potentiometric determination of copper ion.

3.1. Composition and characteristics of the electrodes

It is well known that the sensitivity, linearity and other analytical characteristics of the CPE electrodes depend significantly on the paste composition [14]. Thus, the influence of the type and amount of modifier, amount of gold nanoparticle and amount of oil on the potential response of the electrodes to Cu^{2+} ion activity were investigated and the results are summarized in Table 1. As seen, in the absence of mercapto compound modifier the electrodes have no response or low response towards copper ion.

In addition, the electrodes without gold nanoparticle gave a limited working concentration range and relative high detection limit. It is probably due to the power of gold to self-assembled, the ionophore from –SH group of mercapto compounds used as modifier. The UV–Vis absorption spectra showed that in the absence of nanoparticle the –SH groups in mercapto compounds bonded to Cu ions and a charge transfer peak appear at ~313 nm, and this peak disappear when the nanoparticle added to solution (Fig. 3). This shows that the –SH groups are bonded to gold nanoparticles. Besides, the gold nanoparticles may lead to the expanding of the surface of paste by fabrication of three-dimensional nanostructures; as well as diminish of the Ohmic resistance of the paste.

The results thus obtained indicate that the best sensitivity, detection limit, and linear ranges are obtained for pastes with the following compositions (Fig. 4).

Number 5 with a MNFT/graphite powder/paraphin oil weight ratio of 2.5/43.3/26.3 with 120 μL of GNP have a slope of 29.8 and linear range 7.9×10^{-9}–7.9×10^{-4} mol L^{-1} with a detection limit of 3.5×10^{-9} mol L^{-1}.

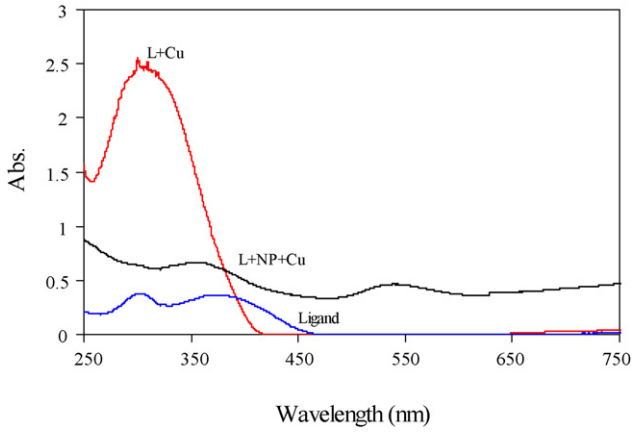

Fig. 3. UV–Vis absorption spectra of MMNT, MMNT-Cu and MMNT-GNP-Cu.

Number 9 with a MMNIT/graphite powder/paraphin oil/GNP weight ratio of 2.5/45.2/27.4 with 120 μL of GNP have a slope of 31.1, detection limit 4.1×10^{-9} mol L^{-1}, and linear range 7.9×10^{-9}–3.2×10^{-2} mol L^{-1}.

Number 13 with a MNTT/graphite powder/paraphin oil/GNP weight ratio of 2.5/44.4/27.2 with 120 μL of GNP have a slope of 31.0, detection limit 4.2×10^{-8} mol L^{-1}, and linear range 2.0×10^{-7}–3.2×10^{-3} mol L^{-1}.

These results show that addition of gold nanoparticle to the paste improves the linear range and detection limit of electrodes. Also, the mercapto modifiers were used are excellent ionophore for Cu(II) ion.

In Table 2, some important characteristics of the proposed electrodes are compared with the corresponding values previously reported for Cu(II)-selective electrodes based on different modifier [29–36]. As seen, in many cases, the proposed electrodes shows superior behaviors to the electrodes prepared previously.

3.2. Response time

We measured the average time required for the Cu^{2+} carbon paste electrodes to reach a potential within ±1 mV of the final equilibrium value after successive immersion in a series of copper(II) ion solutions, each having a 10-fold difference in concentration. In this study, the practical response time was recorded by changing the Cu^{2+} ion over a concentration range 1.0×10^{-4}–1.0×10^{-7} mol L^{-1}. The results showed that, in whole concentration range all electrodes reach their equilibrium response in a short time (~5 s). The results thus obtained are indicative of a rapid diffusion achievement of equilibrium between the aqueous layers and the carbon paste sensors, rapid complex formation, and exchange of ions in the pastes. The potentials stayed constant for ~20 min, after which only a very slow divergence within the months without any measurable change in response time, slope, or detection limit. The sensing behavior of the electrodes remained unchanged when the potentials recorded either from low to high concentrations or vice versa.

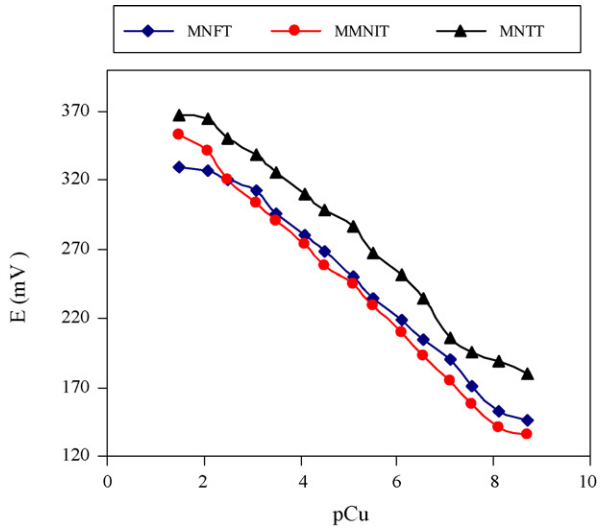

Fig. 4. Calibration curves for Cu^{2+} carbon paste electrodes based on MMNIT, MNFT, and MNTT at pH ~4–5.

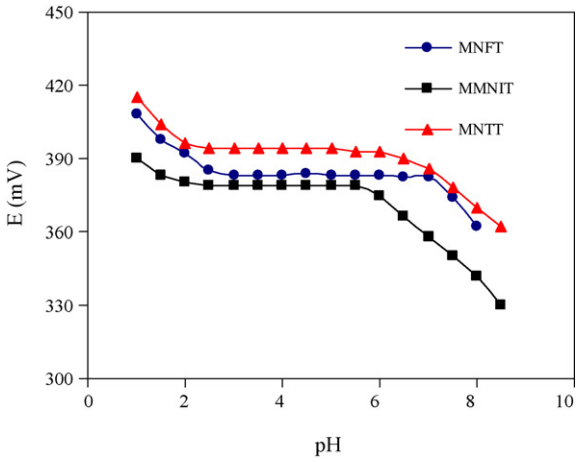

Fig. 5. Effect of pH of test solutions on the response of the proposed Cu^{2+} carbon paste electrodes.

3.3. Effect of pH

The effects of pH of test solution on the response of electrodes were investigated in a 1.0×10^{-5} M $Cu(NO_3)_2$ solution and pH adjustments in solutions were made with 0.01 M nitric acid or sodium hydroxide solutions. As shown in Fig. 5 the electrode responses are independent of pH in the range of 2–5.5, 2.5–7, and 2–6.5 for MMNIT, MNFT, and MNTT, respectively. However, the observed potential decrease at higher pH values could be due to the formation of some hydroxy complexes of Cu^{2+} ions in solution. On the other hand, at pH values lower the 2 or 2.5, the electrode potential rises. This is probably due to simultaneous response of the electrodes to H_3O^+ and Cu^{2+} ions or could be due to the protonation of the ion carrier.

3.4. Selectivity

The potentiometric selectivity coefficient of an electrode as one the most important characteristics is defined by its relative response for the primary ion over other ions present in the solution [37]. In this work, the potentiometric selectivity coefficients were determined graphically by the fixed interference method that is on the Nikolski–Eizenman equation [37,38]. From the plots of E *vs.* $\log a_{Cu}$ and using the expression $\ln K^{pot}_{A,B} = \ln(a_A/a_B^{2/Z_B})$, the selectivity coefficients were determined. The value of a_A that is estimated by determining the Cu^{2+} activity for which the linear and rising portion of the graph deviates by $2.303RT \log Z/F$ mV from the curved part and the value of a_B^{1/Z_B} (a_B and Z_B are the activity and charge of interference ion, respectively) were used to calculate

Table 2
Comparison of the response characteristics and selectivity coefficients of different Cu^{2+} ion selective electrodes

Ref.	Carrier	DL (M)	Linear range (M)	$t_{90\%}$ (s)	pH range	Selectivity coefficients ($-\log K^{pot}_{Cu,M}$)
[29]	8-Hydroxyquinoline	1.6×10^{-7}	5.0×10^{-7}–1×10^{-1}	15	3.0–9.0	Na^+(2.5), K^+(2.6), Mg^{2+}(2.3), Ca^{2+}(2.0), Ba^{2+}(2.5), Pb^{2+}(2.6), Ag^+(2.2), Co^{2+}(2.5), Ni^{2+}(2.6), Zn^{2+}(3.0), Cd^{2+}(2.7), Al^{3+}(2.8)
[30]	Dithiomacrocycle	5.6×10^{-7}	1.0×10^{-6}–1.0×10^{-2}	14	3.5–6.0	Na^+(4.2), K^+(3.2), Mg^{2+}(2.2), Ca^{2+}(1.0)
[31]	Tetraethyl thiuram disulfide	4.0×10^{-8}	6.6×10^{-8}–6.0×10^{-4}	–	<7	Co^{2+} (4), Pb^{2+} (3.35), Zn^{2+} (4), Ni^{2+} (0.47), Cd^{2+}(3.6), Mg^{2+} (1.15)
[32]	3-(2-Pyridinyl)-2Hpyrido[1,2,-a]-1,3,5-triazine-2,4(3H)-dithione	4.0×10^{-8}	5.0×10^{-8}–1.0×10^{-2}	12	3–9.5	Ca^{2+} (3.5), Mg^{2+} (4.5), Ba^{2+} (4.2), Ni^{2+} (2.9), Co^{2+} (1.1), Cd^{2+} (2.2), Pb^{2+} (1.5), Zn^{2+} (2.4), Ag^+ (0.5)
[33]	Schiff base	3.0×10^{-6}	8.0×10^{-6}–1.0×10^{-1}	15	3–6.5	Na^+ (2.9), K^+ (4.9), Ca^{2+} (2.6), Mg^{2+} (2.3), Ba^{2+} (2.1), Ni^{2+} (2.4), Co^{2+} (2.2), Cd^{2+} (2.2), Pb^{2+}(0.5), Zn^{2+} (2.3), Na^+ (3.78), Zn^{2+}(2.25)
[34]	Salens	3.1×10^{-6}	1.0×10^{-5}–1.0×10^{-1}	10	3.5–6.5	K^+ (2.02) Ca^{2+} (3.0), Ni^{2+} (2.0), Co^{2+} (2.0), Cd^{2+} (3.2), Zn^{2+} (4.0), Na^+ (3.3), Hg^{2+} (3.0), Ag^+ (2.5)
[35]	*o*-Xylene bis(dithiocarbamates)	1.4×10^{-7}	10^{-6}–10^{-1}	9	3.5–5.5	K^+(4.1), Pb^{2+} (2.3) Ca^{2+} (3.6), Ni^{2+} (3.2), Co^{2+} (4.0), Cd^{2+} (4.5), Pb^{2+} (0.7), Zn^{2+} (2.2), K^+ (2.3), Mg^{2+} (3.6), Na^+ (2.6)
[36]	3,6, 9,14-Tetrathiabicyclo [9.2.1] tetradeca-11,13-diene	3.2×10^{-7}	6.3×10^{-7}–2.5×10^{-1}	<10	5.0–7.0	Na^+(2.2), K^+(2.2), Ag^+(1.6), Mg^{2+}(3.4), Ca^{2+}(3.4), Co^{2+}(3.3), Ni^{2+}(5.0), Cd^{2+}(2.6), Zn^{2+}(3.3), Pb^{2+}(2.3)
This work	2-Mercapto-5-(1-methyl-5-nitroimidazole-2-yle)-1,3,4-thiadiazole	4.1×10^{-9}	7.9×10^{-9}–3.2×10^{-2}	5	2.0–5.5	Ca^{2+} (NR), Mg^{2+} (NR), Al^{3+} (6.3), Mn^{2+} (4.2), Ni^{2+} (3.4), Co^{2+} (3.4), Cd^{2+} (3.7), Pb^{2+} (3.5), Zn^{2+} (3.9), Ln^{3+} (4.6), Ag^+ (2.5)
This work	2-Mercapto-5-(5-nitrofuran-2-yl)-1,3,4-thiadiazole	3.5×10^{-9}	7.9×10^{-9}–7.9×10^{-4}	5	2.5–7.0	Ca^{2+} (NR), Mg^{2+} (NR), Al^{3+} (6.2), Mn^{2+} (4.2), Ni^{2+} (3.3), Co^{2+} (3.1), Cd^{2+} (3.3), Pb^{2+} (3.5), Zn^{2+} (3.6), Ln^{3+} (4.6), Ag^+ (1.7)
This work	2-Mercapto-5-(5-nitrothiophen-2-yl)-1,3,4-thidiazole	4.2×10^{-8}	2.8×10^{-8}–7.9×10^{-3}	5	2.0–6.5	Ca^{2+} (NR), Mg^{2+} (NR), Al^{3+} (7.0), Mn^{2+} (4.4), Ni^{2+} (3.9), Co^{2+} (3.7), Cd^{2+} (3.8), Pb^{2+} (3.6), Zn^{2+} (3.5), Ln^{3+} (4.7), Ag^+ (2.3)

Three new mercapto compounds [2-mercapto-5-(1-methyl-5-nitroimidazole-2-yle)-1,3,4-thiadiazole] (MMNIT), [2-mercapto-5-(5-nitrofuran-2-yl)-1,3,4-thiadiazole] (MNFT) and [2-mercapto-5-(5-nitrothiophen-2-yl)-1,3,4-thidiazole] (MNTT) were used for self-assembled-gold nanoparticle (SAGNP) modified carbon paste electrodes. The electrodes were applied as indicator electrodes for potentiometric determination of Cu(II) ion. The prepared electrodes exhibit a Nernstian slope of 31.0 ± 0.5 mV per decade for Cu(II) ion over a wide concentration range of 7.9×10^{-9}–3.2×10^{-2}, 7.9×10^{-9}–7.9×10^{-4}, and 2.8×10^{-8}–7.9×10^{-3} mol L^{-1} for MMNIT, MNFT, and MNTT, respectively. The detection limits of electrodes were $3.5\ (\pm0.2)\times10^{-9}$, 4.1×10^{-9}, and 4.1×10^{-8} mol L^{-1} of copper ion, respectively.

the potentiometric selectivity coefficients. In this work, the concentration of the copper ion is varied while that of the interfering ions is 1×10^{-2} mol L^{-1}. The resulting selectivity coefficient values thus obtained for the proposed Cu(II) sensors are given in Table 3. As it is evident, some of the interfering ions do not have any effect on the response of electrodes and most of them show low values of selectivity coefficients, indicating no interference in the performance of the carbon paste electrodes assembly. However, as seen, the selectivity coefficients for Ag^+ ion are relatively high. Although the –SH groups in modifier ligands were bonded to gold nanoparticle, and decreased the interaction between ionophors and Ag^+ ions but, it was probably occur by interaction of other soft S donor atoms in mercapto compounds with Ag^+ ions. The same problem happens for Hg^{2+} ions, but the strong interaction between S atoms and Hg^{2+} ions causes the modified paste to be destroyed in the solution containing Hg^{2+} ions.

As can be seen in Table 2, selectivity behavior of the proposed electrodes is among the most selective Cu^{2+} ion sensors reported. This indicates that the ionophors with N donors atoms assembles to gold interact selectively to copper ion compared to other cations.

Table 3
Selectivity coefficients of various ions for Cu(II) electrodes

Interference ion	$-\log K^{pot}_{A,B}$ (MNTT)	$-\log K^{pot}_{A,B}$ (MMNIT)	$-\log K^{pot}_{A,B}$ (MNFT)
K^+	>4	>4	>4
Na^+	>4	>4	>4
Ca^{2+}	>4	>4	>4
Mg^{2+}	>4	>4	>4
NH_4^+	>4	>4	>4
Co^{2+}	2.9 (±0.1)[a]	3.1 (±0.2)	2.7 (±0.3)
Cd^{2+}	2.8 (±0.1)	2.5 (±0.3)	3.7 (±0.1)
Pb^{2+}	3.0 (±0.1)	2.9 (±0.1)	2.8 (±0.4)
Ni^{2+}	3.4 (±0.4)	3.1 (±0.1)	3.2 (±0.1)
Ln^{3+}	4.5 (±0.1)	4.2 (±0.1)	4.4 (±0.1)
Al^{3+}	4.2 (±04)	4.1 (±0.3)	4.5 (±0.2)
Mn^{2+}	4.1 (±0.1)	4.0 (±0.2)	3.8 (±0.1)
Zn^{2+}	3.3 (±0.2)	3.7 (±0.1)	3.7 (±0.1)
Ag^+	1.4 (±0.1)	1.6 (±0.1)	2.2 (±0.1)

[a] Values in parentheses are R.S.D.s based on four replicate analyses.

Table 4
Recovery of copper ions from different water samples

Sample	Cu(II) ($\mu g\,L^{-1}$)		Recovery (%)
	Added	Found	
Well water	10	10.3 (0.2)[a]	103
Tap water	10	10.1 (0.1)	101
River water (Karoun)	8	7.9 (0.2)	98.8
Laboratory water	13	12.7 (0.2)	97.7

[a] Values in parentheses are R.S.D.s based on four replicate analyses.

Moreover, to investigate the effect of anions on the electrode's potential responses, the cell potentials were obtained using copper nitrate and copper sulfate. No significant change in the emf vs. *p*Cu plots was observed, indicating that these anions (NO_3^- and SO_4^{-2}) do not cause any interference.

3.5. Determination of Cu(II) in human hair

In order to illustrate these electrodes application in practical analysis, the copper content of a human hair sample was determined by the proposed electrodes. The copper content obtained from three replicate measurements was 71.0 ($\pm$1.7) $\mu g\,L^{-1}$, which was found to be satisfactory agreement with that obtained by atomic absorption spectrometry (70.5 ($\pm$1.2) $\mu g\,L^{-1}$). These electrodes were also successfully applied to direct determination of copper in different water samples and the results are given in Table 4. As can be seen, the accuracy of copper determination in different water samples is almost quantitative.

4. Conclusions

Three new mercapto compounds were used for self-assembled-gold nanoparticle (GNP) modified carbon paste electrodes and applied for potentiometric determination of copper ion. The proposed sensors have good characteristics such as; low detection limit of 4 ($\pm$1) $\times 10^{-9}$ mol L^{-1}, wide concentration range from 7.9 $\times 10^{-9}$ to 3.2 $\times 10^{-2}$ mol L^{-1}, fast response time of $\sim$5 s and good selectivity coefficient for many cations. The potentiometric responses of these electrodes are independent of the pH of the test solution in the pH range 2.5–7.

References

[1] A. Profumo, D. Merli, M. Pesavento, Anal. Chim. Acta 557 (2006) 45.
[2] V. Shumantseva, S. Carrara, V. Bavastrello, J. Riley, T. VBulko, K.G. Skryabin, A.L. Archakov, C. Nicolini, Biosens. Bioelectron. 21 (2005) 217.
[3] F. Xiao, F. Zhao, J. Li, R. Yan, J. Yu, B. Zeng, Anal. Chim. Acta 596 (2007) 79.
[4] S. Liu, L. Wang, F. Zhao, J. Electroanal. Chem. 602 (2007) 55.
[5] L. Agüi, C. Peña-Farfal, P. Yañez-Sedeño, J.M. Pingarrón, Talanta 74 (2007) 412.
[6] R.G. Nuzzo, D.L. Allara, J. Am. Chem. Soc. 105 (1983) 4481.
[7] L. Agui, G. Manso, P. Yañez-Sedeño, J.M. Pingarron, Talanta 64 (2004) 1041.
[8] F. Lucarelli, G.M. Anthony, P.F. Marco Mascini, Biosens. Bioelectron. 19 (2004) 515.
[9] M.H. Mashhadizadeh, A. Mostafavi, H. Allah-Abedi, I. Sheikhshoai, Sens. Actuators B 113 (2006) 930.
[10] M.H. Mashhadizadeh, I. Sheikhshoaie, S. Saeid-Nia, Electroanalysis 17 (2005) 648.
[11] M.H. Mashhadizadeh, I. Sheikhshoaie, N. Monadi, Talanta 64 (2004) 1048.
[12] M.H. Mashhadizadeh, I. Sheikhshoaie, S. Saeid-Nia, Sens. Actuators B 94 (2003) 241.
[13] M. Bagheri, M.H. Mashhadizadeh, S. Razee, A. Momeni, Electroanalysis 15 (2005) 1824.
[14] M.H. Mashhadizadeh, E. Pour Taheri, I. Sheikhshoaie, Talanta 72 (2007) 1088.
[15] M.H. Mashhadizadeh, M. Talakesh, M. Peste, A. Momeni, H. Hamidian, M. Mazlum, Electroanalysis 18 (2006) 2174.
[16] A. Foroumadi, A. Asadipour, M. Mirzaei, J. Karimi, S. Emami, Farmaco 57 (2002) 765.
[17] A. Foroumadi, Z. Kiani, F. Soltani, Farmaco 58 (2003) 1073.
[18] A. Foroumadi, M. Mirzaei, A. Shafiee, Pharmazie 56 (2001) 610.
[19] L. Agüi, J. Manso, P. Yañez-Sedeño, J.M. Pingarrón, Sens. Actuators B 113 (2006) 272.
[20] X.U. Dia, D. Nekrassova, M.E. Hyde, R.G. Compton, Anal. Chem. 67 (2004) 5924.
[21] Y. Zhuo, R. Yuan, Y. Chai, Y. Zhange, X. Li, N. Wang, Q. Zhu, Sens. Actuators B 114 (2006) 631.
[22] G. Jiang, L. Wang, W. Chen, Mater. Lett. 61 (2007) 278.
[23] E. Majid, S. Harpovic, Y. Liu, K.B. Male, J.H.T. Luong, Anal. Chem. 78 (2006) 762.
[24] L.M. Liz-Marzan, Langmuir 22 (2006) 32.
[25] J.J. Gooding, F. Mearns, W. Yang, J. Liu, Electroanalysis 15 (2003) 81.
[26] K.R. Brown, A.P. Fox, M.J. Natan, J. Am. Chem. Soc. 118 (1996) 1154.
[27] A.R. Raj, T. Okajima, T. Ohsaka, J. Electroanal. Chem. 543 (2003) 127.
[28] M.C. Daniel, D. Astruc, Chem. Rev. 104 (2004) 293.
[29] S.K. Mittal, A. Kumar, S.K.N. Gupta, S. Kaur, S. Kumar, Anal. Chim. Acta 585 (2007) 161.
[30] I.A. Marques de Oliveira, M. Pla-Roca, L1. Escriche, J. Casabo, N. Zine, J. Bausells, F. Teixidor, E. Crespo, A. Errachid, J. Samitier, Electrochim. Acta 51 (2006) 5070.
[31] M.J. Gismera, D. Hueso, J.R. Procopio, M.T. Sevilla, Anal. Chim. Acta 524 (2004) 347.
[32] A.K. Singh, S. Mehtab, A.K. Jain, Anal. Chim. Acta 575 (2006) 25.
[33] S. Sadeghi, M. Eslahi, M.A. Naseri, H. Naeimi, H. Sharghi, A. Shameli, Electroanalysis 15 (2003) 1327.
[34] A.R. Fakhari, T.A. Raji, H. Naeimi, Sens. Actuators B 104 (2005) 317.
[35] O. Marcin, M. Agata, M. Krzysztof, Electrochim. Acta 51 (2006) 2298.
[36] M.H. Mashhadizadeh, A. Mostafavi, R. Razavi, M. Shamsipur, Sens. Actuators B 86 (2002) 222.
[37] E. Bakker, P. Buhlmann, E. Pretsch, Chem. Rev. 97 (1997) 3038.
[38] IUPAC, Analytical chemistry division, commission on analytical electrodes, Pure Appl. Chem. 48 (1979) 127.

Talanta 76 (2008) 685–689

Contents lists available at ScienceDirect

Talanta

journal homepage: www.elsevier.com/locate/talanta

Simultaneous square-wave voltammetric determination of aspartame and cyclamate using a boron-doped diamond electrode

Roberta Antigo Medeiros, Adriana Evaristo de Carvalho, Romeu C. Rocha-Filho, Orlando Fatibello-Filho*

Departamento de Química, Universidade Federal de São Carlos, C.P. 676, 13560-970 São Carlos, SP, Brazil

ARTICLE INFO

Article history:
Received 5 February 2008
Received in revised form 8 April 2008
Accepted 9 April 2008
Available online 20 April 2008

Keywords:
Aspartame
Cyclamate
Boron-doped diamond electrode
Square-wave voltammetry

ABSTRACT

A simple and highly selective electrochemical method was developed for the simultaneous determination of aspartame and cyclamate in dietary products at a boron-doped diamond (BDD) electrode. In square-wave voltammetric (SWV) measurements, the BDD electrode was able to separate the oxidation peak potentials of aspartame and cyclamate present in binary mixtures by about 400 mV. The detection limit for aspartame in the presence of 3.0×10^{-4} mol L^{-1} cyclamate was 4.7×10^{-7} mol L^{-1}, and the detection limit for cyclamate in the presence of 1.0×10^{-4} mol L^{-1} aspartame was 4.2×10^{-6} mol L^{-1}. When simultaneously changing the concentration of both aspartame and cyclamate in a 0.5 mol L^{-1} sulfuric acid solution, the corresponding detection limits were 3.5×10^{-7} and 4.5×10^{-6} mol L^{-1}, respectively. The relative standard deviation (R.S.D.) obtained was 1.3% for the 1.0×10^{-4} mol L^{-1} aspartame solution ($n = 5$) and 1.1% for the 3.0×10^{-3} mol L^{-1} cyclamate solution. The proposed method was successfully applied in the determination of aspartame in several dietary products with results similar to those obtained using an HPLC method at 95% confidence level.

1. Introduction

Aspartame and cyclamate are artificial sweeteners widely used in the food, beverage, confectionery and pharmaceutical industries throughout the world. Aspartame (*N*-L-α-aspartyl-L-phenylalanine methyl ester), shown in Fig. 1, was accidentally synthesized in 1965 using aspartic acid, phenylalanine and methanol as start reagents. It is a white, odorless, crystalline powder with sweetness potency 180–200 times that of sucrose [1–4]. Since its approval in 1981 for use as a low-calorie sweetener in dry food, the market has grown rapidly and today aspartame is one of the most frequently used artificial sweeteners [5–7]. Cyclamate (Fig. 1) was synthesized in 1937 at the University of Illinois (USA) by graduate student Michael Sveda, who by accident discovered the compound's very sweet taste (potency 30 times that of sucrose). Although cyclamate is stabler than other sweeteners [2,7–9], it is no longer permitted as a food additive in many countries (e.g. Canada, USA, and several European countries), due to its conversion to cyclohexylamine, which is a strong carcinogen [10]. However, the results of all the different studies carried out seeking to verify the toxicity of cyclamate reported few effects even when high amounts of the sweetener were ingested [11]. After evaluation of the available toxicological studies, the use of cyclamate in foods and drinks is considered safe, being allowed in countries such as Germany, Switzerland, Brazil, and South Africa [8].

In order to control their calorie intake, consumers select low-calorie foods. In these, a sweetener may be used by itself or in combination with sugars and other sweeteners, and the latter is becoming increasingly popular in recent years owing to technical, health and commercial advantages [12]. Thus, sweeteners can be found in a variety of foods such as carbonated soft drinks, gelatin dessert mixes, pudding mixes, chewing gums, and numerous other dietary products [2,4].

Many methods have been developed for analysis of individual sweeteners, but relatively few methods capable of simultaneously analyzing several sweeteners have been reported. In recent years, the use of high performance liquid chromatography (HPLC) [5,11–19] has become the method of choice for aspartame and sodium cyclamate analysis because it is relatively simple while providing generally good qualitative and quantitative results for many types of samples. However, usually this method is costly and requires a lengthy pre-treatment of the sample prior to the chromatographic analysis.

Electrochemical techniques can be alternative methods for aspartame and cyclamate determination because they are simple, fast, and low cost. Various potentiometric or amperometric

* Corresponding author. Tel.: +55 16 33518098; fax: +55 16 33518350.
E-mail address: bello@dq.ufscar.br (O. Fatibello-Filho).

0039-9140/$ – see front matter © 2008 Elsevier B.V. All rights reserved.
doi:10.1016/j.talanta.2008.04.015

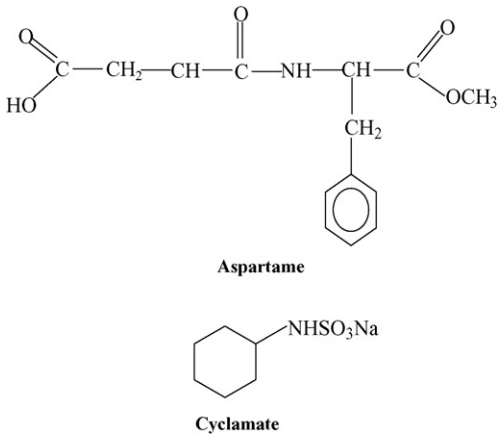

Fig. 1. Chemical structure of aspartame and cyclamate.

methods were developed for the analysis of these artificial sweeteners separately in dietary products [20–26]. Odaci et al. [23] developed a method for aspartame determination based on a bienzymatic system composed of carboxyl esterase and alcohol oxidase immobilized in a gelatin membrane, subsequently combined with the dissolved oxygen electrode. The optimum operational conditions for this enzymatic sensor were pH 8.0 and 37 °C. Xiao and Choi [22] developed another biosensor based on alcohol oxidase immobilized onto an eggshell membrane and an oxygen-sensitive optode membrane as the transducer. The analytical curve was linear in the aspartame concentration range from 5.6×10^{-5} to 3.1×10^{-3} mol L^{-1}. Fatibello-Filho et al. [25] proposed a simple procedure for cyclamate determination in dietary products, involving a biamperometric titration and flow injection (FI) procedure. For a solution containing 2.5×10^{-2} mol L^{-1} cyclamate ($n = 10$), a detection limit of 2.5×10^{-3} mol L^{-1} and a relative standard deviation of 1.7% were found. On the other hand, a sBLM-based minisensor was developed by Nikolelis and Pantoulias [26] for the determination of acesulfame-K, cyclamate and saccharin in granulated sugar products. The reported results showed that the analytically useful concentration range for cyclamate lies between 10 and 160 μmol L^{-1}, with a detection limit of 10 μmol L^{-1}. However, none of these methods is capable of simultaneously analyzing aspartame and cyclamate.

Voltammetric techniques offer the possibility of determining the analyte concentration directly in the sample without any pretreatment or chemical separation, as well as of analyzing colored materials and samples with dispersed solid particles, besides offering the possibility of the simultaneous determination of several substances [27–29]. Square-wave voltammetry (SWV) has proved to be extremely sensitive for the detection of organic molecules, with a low nonfaradaic current and high sensitivity [29]. While the conventional voltammetric techniques have detection limits of 10^{-5} mol L^{-1}, the use of SWV makes possible the obtention of detection limits three orders of magnitude lower. However, the use of SWV with BDD electrodes is not straightforward; thus, adequate choice and optimization of the experimental parameters are required in order to avoid loss of sensitivity due to kinetic limitations [30].

Boron-doped diamond (BDD) is a carbon-based electrode, which has received much attention in recent years [31–34]. In BDD, the replacement of approximately one carbon atom in a thousand by a boron atom yields a material with metallic conductivity [35]. Thus, BDD electrodes are very attractive for many potential applications due to their outstanding properties, which are significantly different from those of other conventional electrodes, e.g. glassy carbon or platinum electrode. BDD is corrosion stable in very aggressive media, has very low and stable background current, extreme electrochemical stability in both alkaline and acidic media, high response sensitivity, and a very wide working potential window, which can be larger than 3.5 V [32–39]. The boron-doped diamond electrode, compared with other electrodes such as carbon electrode materials, is very versatile and adaptable to experimental challenges [38]. On the other hand, Suffredini et al. [34] called the attention to the effect of electrochemical surface pre-treatments on the response of BDD electrodes, specifically showing that cathodic polarizations dramatically increased the electroanalytical detection limits of chlorophenols.

We recently obtained good results using SWV and a BDD electrode for aspartame [40] and cyclamate [41] determination in dietary products. For aspartame, the analytical curve was linear in the aspartame concentration range from 9.9×10^{-6} to 5.2×10^{-5} mol L^{-1} with a detection limit of 2.3×10^{-7} mol L^{-1} [40]. For cyclamate, the analytical curve was linear in the concentration range from 5.0×10^{-5} to 4.1×10^{-4} mol L^{-1}, with a detection limit of 4.8×10^{-6} mol L^{-1} [41]. Hence, the aim of this work is to couple square-wave (SW) voltammetry with the unique properties of the BDD electrode for the development and optimization of a method for the simultaneous determination of aspartame and cyclamate in several food products.

2. Experimental

2.1. Reagents and standards

All reagents were of analytical grade. Aspartame and cyclamate were obtained from Sigma; sulfuric acid, used to prepare the supporting electrolyte, was obtained from Synth. Standard aqueous 0.01 mol L^{-1} aspartame and 0.01 mol L^{-1} cyclamate solutions were prepared before use in a 0.5 mol L^{-1} sulfuric acid solution to prevent hydrolysis and/or decomposition. All solutions were prepared using deionized water. The samples of powder juice drink (A) and carbonated guaraná drinks (B) were purchased from a local market.

2.2. Construction of the analytical curve

After optimizing the experimental parameters for the proposed method, the analytical curves were constructed by addition of aliquots of the standard 0.01 mol L^{-1} aspartame and 0.01 mol L^{-1} cyclamate solutions into the measurement cell containing a 0.5 mol L^{-1} sulfuric acid solution; the SW voltammograms were obtained after each aliquot addition.

2.3. Powder juice drink (A)

An accurately weighed amount of 0.067 g was transferred to a 10-mL volumetric flask, dissolved and diluted to mark with a 0.5 mol L^{-1} sulfuric acid solution. Then 400 μL aliquots of this solution were transferred to the electrochemical cell containing 10 mL of a 0.5 mol L^{-1} sulfuric acid solution; the SW voltammograms were obtained after each aliquot addition.

2.4. Carbonated guaraná drink (B)

The carbonated guaraná drink was degassed for 5 min in an ultrasonic bath. Then, a 2.0-mL volume of it was directly transferred to the electrochemical cell containing 10 mL of a 0.5 mol L^{-1} sulfuric acid solution and the SW voltammogram was obtained.

Table 1
SW-voltammetry parameters whose influence was investigated and their optimum values for the simultaneous determination of aspartame and cyclamate

Parameter	Studied range	Optimum value
SW frequency (f)	10–150 Hz	10 Hz
SW amplitude (a)	10–80 mV	40 mV
Scan increment (ΔE_s)	0.50–5 mV	2 mV

2.5. Apparatus

Electrochemical experiments were conducted in a single-compartment glass cell provided with three electrodes and degassing facilities for bubbling N_2. The reference electrode used was an Ag/AgCl (3.0 mol L^{-1} KCl) and the counter electrode was a Pt wire. The working electrode (0.72-cm^2 exposed area) was a boron-doped (8000 ppm) diamond film on a silicon wafer from Centre Suisse de Electronique et de Microtechnique SA (CSEM), Neuchatêl, Switzerland [39]. Prior to the experiments, the BDD electrode was cathodically pre-treated by applying -1.0 A cm^{-2} for 60 s in a 0.5 mol L^{-1} sulfuric acid solution [40,41]. The voltammetric measurements were carried out using an AUTOLAB PGSTAT-30 (Ecochemie) potentiostat/galvanostat controlled with the GPES 4.0 software.

The HPLC aspartame determination was carried out using a LC-10AT Shimadzu system, with an UV–vis detector (SPD-M10-AVP) set at the wavelength of 192 nm for aspartame and 200 nm for cyclamate. A Shim-Pack CLC-ODS (60 μm × 150 mm, 5 μm) chromatographic column was used. The mobile phase was an acetonitrile/phosphate buffer (pH = 4) 14/86 v/v at a flow-rate of 0.8 mL min^{-1}, while the injection volume was 30 μL.

3. Results and discussion

3.1. Optimization of the SW voltammetry parameters

The peak current obtained in SW voltammetry is dependent on various instrumental parameters such as the SW frequency (f), scan increment (ΔE_s) and SW amplitude (a). These parameters are interrelated, having a combined influence on the peak current response. Hence, in order to establish the optimum conditions for the determination of the sweeteners under study, the influence of these instrumental parameters on the peak current response of 1.0×10^{-4} mol L^{-1} aspartame and 3.0×10^{-4} mol L^{-1} cyclamate in a 0.5 mol L^{-1} sulfuric acid solution was investigated. Table 1 shows the studied parameters and the obtained optimum values for the simultaneous determination of aspartame and cyclamate. The investigation showed that the peak current is a linear function of frequency, with a peak potential displacement towards positive potential values. According to the accepted theories for SW voltammetry [42], this behavior is typical of a totally irreversible system controlled by adsorption of the species on the electrode surface. A baseline increase was also observed when the frequency was increased. Therefore, for the subsequent analytical applications, an f value of 10 Hz was selected, because in this frequency a stable baseline and a good voltammogram definition were obtained. The pulse amplitude (a) is another parameter that strongly influences the peak current in SW voltammetry; the obtained results showed that the peak current is linearly dependent on a up to 40 mV, and reaches a plateau when a is equal to or higher than 60 mV. Therefore, an a value of 40 mV was chosen for the subsequent analytical application.

The effective rate of potential variation in SW voltammetry is the product between f and ΔE_s. Therefore, this latter parameter also will increase the signal and sensitivity of the technique. However, for large values of ΔE_s a widening of the peaks may occur, thus diminishing the resolution of the analysis [28]. In this study the peak current increased significantly for ΔE_s values up to about 3 mV, then leveling off. Hence, for the analytical applications, ΔE_s was set at 2 mV.

3.2. Simultaneous determination of aspartame and cyclamate

Initial exploratory studies of the voltammetric behavior of the artificial sweeteners were performed using SW voltammetry. The SW voltammograms presented anodic peak potentials at 1.5 (aspartame) and 1.9 V (cyclamate), with the characteristics of irreversible reactions and with a peak potential separation (ΔE_p) of about 400 mV. To further investigate the electrochemical response when aspartame and cyclamate co-exist, the SW voltammetric behavior of aspartame (or cyclamate) was tested in the presence of a large excess of cyclamate (or aspartame) in a 0.5 mol L^{-1} sulfuric acid solution. The individual determination of aspartame in the concentration range from 5.0×10^{-6} to 4.0×10^{-5} mol L^{-1} was accomplished in solutions containing cyclamate at a fixed concentration of 3.0×10^{-4} mol L^{-1}; on the other hand, the individual determination of cyclamate in the concentration range from 5.0×10^{-5} to 4.0×10^{-4} mol L^{-1} was accomplished in solutions containing aspartame at a fixed concentration of 1.0×10^{-4} mol L^{-1} (Fig. 2).

An examination of Fig. 2(A) shows that the anodic peak current for aspartame increased with an increase in aspartame concentration when the concentration of cyclamate was kept constant. Similarly, as shown in Fig. 2(B), keeping the concentration of aspartame constant, the anodic peak current for cyclamate was directly proportional to its concentration, while the one of the aspartame did not change.

The anodic peak current for aspartame was linearly dependent on its concentration (c) in the range from 5.0×10^{-6} to 4.0×10^{-5} mol L^{-1}; a linear fitting regression equation was obtained [I_{pa} (μA) = $0.435 + 1.99 \times 10^5 c$ (mol L^{-1})], with a 0.9998 correlation coefficient. The detection limit was 4.7×10^{-7} mol L^{-1}.

The anodic peak current for cyclamate was also linearly dependent on its concentration in the range from 5.0×10^{-5} to 4.0×10^{-4} mol L^{-1}; a linear fitting regression equation was obtained [I_{pa} (μA) = $1.37 + 7.59 \times 10^4 c$ (mol L^{-1})], also with a 0.9998 correlation coefficient. In this case, the detection limit was 4.2×10^{-6} mol L^{-1}.

Furthermore, the obtained results showed that neither cyclamate nor aspartame interfere with the oxidation signals of each other, thus indicating that the responses of aspartame and cyclamate at the BDD electrode are independent.

The overall easiness of using the BDD electrode for the simultaneous determination of aspartame and cyclamate was demonstrated by simultaneously changing the concentration of aspartame and cyclamate. Fig. 3 shows the SW voltammograms obtained when the concentration of both aspartame (5.0×10^{-6} to 4.0×10^{-5} mol L^{-1}) and cyclamate (5.0×10^{-5} to 4.0×10^{-4} mol L^{-1}) in a 0.5 mol L^{-1} sulfuric acid solution were simultaneously changed. The anodic peak currents for both aspartame and cyclamate increase linearly with their concentrations, and the calibration plot is linear for a wide range of concentrations, with correlation coefficients of 0.9991 and 0.9992 for aspartame and cyclamate, respectively (insets in Fig. 3). The corresponding obtained regression equations were I_{pa} (μA) = $1.36 + 2.65 \times 10^5 c$ (mol L^{-1}), for aspartame (detection limit of 3.5×10^{-7} mol L^{-1}) and I_{pa} (μA) = $2.42 + 7.14 \times 10^4 c$ (mol L^{-1}), for cyclamate (detection limit of 4.5×10^{-6} mol L^{-1}). These regression equations show that, using SW voltammetry, the sensitivity of the BDD electrode towards aspartame is nearly 3 times higher than that

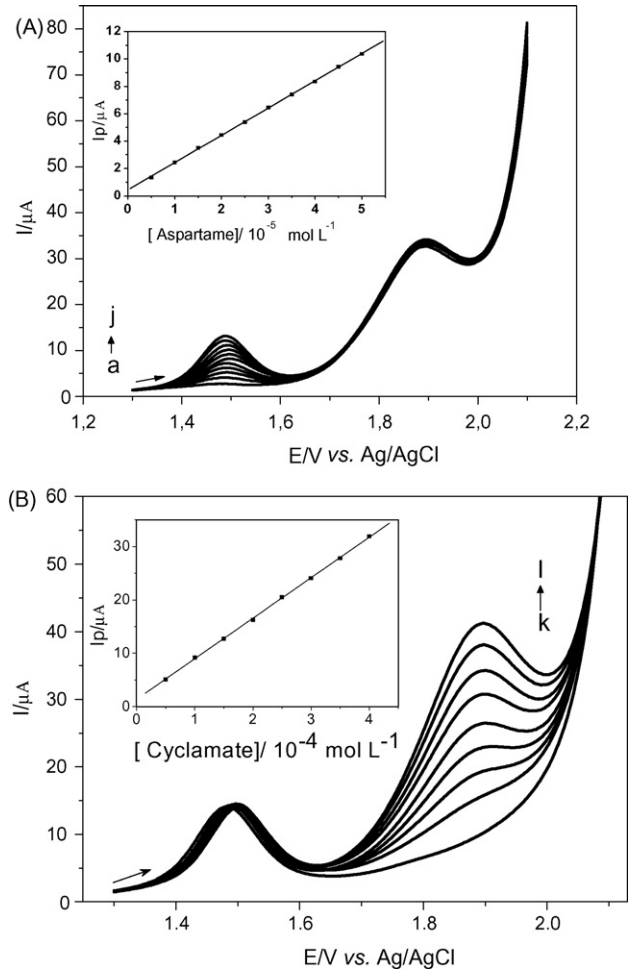

Fig. 2. (A) SW voltammograms for various concentrations of aspartame at a fixed concentration of cyclamate (3.0×10^{-4} mol L^{-1} in 0.5 mol L^{-1} H_2SO_4). Aspartame concentrations (a–j): 5.0×10^{-6} to 5.0×10^{-5} mol L^{-1}. (B) SW voltammograms for various concentrations of cyclamate at a fixed concentration of aspartame (1.0×10^{-4} mol L^{-1} in 0.5 mol L^{-1} H_2SO_4). Cyclamate concentrations (k–l): 5.0×10^{-5} to 5.0×10^{-4} mol L^{-1}. Insets are the corresponding analytical curves for the peak current corresponding to the oxidation process of aspartame or cyclamate.

towards cyclamate. By comparing the results obtained in this work with results obtained for aspartame and cyclamate determination separately [40,41], it was possible to conclude that the detection limits obtained were of the same magnitude; this indicates that the simultaneous determination of aspartame and cyclamate is as efficient as the determination of these sweeteners separately.

The repeatability was determined by successive measurements ($n = 5$) of a 1.0×10^{-4} mol L^{-1} aspartame and 3.0×10^{-3} mol L^{-1} cyclamate solution, with a relative standard deviation of 1.3% and 1.1%, respectively.

3.3. Effect of potential interferents

The selectivity of the proposed method was evaluated by the concomitant addition of possible interferents (acesulfame-K, saccharine, citric acid, ascorbic acid, sucrose, lactose, sodium benzoate, silicon dioxide, sunset yellow, tartrazine and brilliant blue) to 4.0×10^{-5} mol L^{-1} aspartame and 3.0×10^{-4} mol L^{-1} cyclamate standard solutions at the concentration ratios 1:1, 1:10, and 10:1; the obtained results were compared with that obtained using only the aspartame and cyclamate standard solution. The responses showed that these compounds do not interfere in the determination of the two sweeteners at the used working conditions. Only tartrazine presented an anodic peak potential (1.6 V) close to that of aspartame and the sweetener acesulfame-K presented an anodic peak potential (2.0 V) close to that of cyclamate; however, in the samples of dietary products analyzed the tartrazine or acesulfame-K concentration is lower than those studied in this work, thus not interfering in the simultaneous determination of aspartame and cyclamate.

3.4. Determination of aspartame and cyclamate in dietary products

First of all, addition and recovery experiments were carried out in order to evaluate the interference of matrix effects of the samples on the oxidation of aspartame and cyclamate on the BDD electrode. This study was performed by adding known amounts of standard solutions to a given sample, followed by analysis using the proposed method. Satisfactory values between 100% and 106%, for aspartame, and between 98% and 105%, for cyclamate, were obtained for their recovery, thus indicating that there are no interferences of the matrix of the samples in the proposed method and also that the proposed method is suitable for use in samples of dietary products.

Subsequently, the proposed method was used to determine the aspartame and cyclamate contents in different dietary products. Table 2 presents the aspartame and cyclamate concentrations determined simultaneously in several dietary products employing the proposed SW voltammetry method and the HPLC method [13]. The aspartame and cyclamate concentrations were obtained using the regression curves calculated with the OriginPro 7.5 software. Three determinations were done for each sample, and the standard deviations were calculated.

Applying the paired *t*-test [43] to the results obtained using both methods, the fact that the calculated *t* values (2.51 for aspartame and 2.54 for cyclamate) are smaller than the critical value (2.57, $\alpha = 0.05$) indicates that there is no difference between the obtained results at a confidence level of 95%.

Table 2
Results obtained in the simultaneous determination of aspartame and cyclamate in dietary products analyzed by HPLC and the proposed method (SWV)

Samples	Label values (mg/100 mL)	HPLC[a] (mg/100 mL)	SWV[a] (mg/100 mL)	Relative error 1 (%)[b]	Relative error 2 (%)[c]
Sample A					
Aspartame	6.8	6.6 ± 0.2	6.5 ± 0.3	−4.4	−1.5
Cyclamate	120	122 ± 5	123 ± 3	2.5	0.82
Sample B					
Aspartame	12.0	11.8 ± 0.2	12.4 ± 0.4	3.3	5.1
Cyclamate	31.0	31.5 ± 0.3	30.6 ± 0.2	−1.3	−2.8

[a] Average of 3 measurements.
[b] Relative error 1 (%) = 100 × (voltammetric value − label value)/label value.
[c] Relative error 2 (%) = 100 × (voltammetric value − HPLC value)/HPLC value.

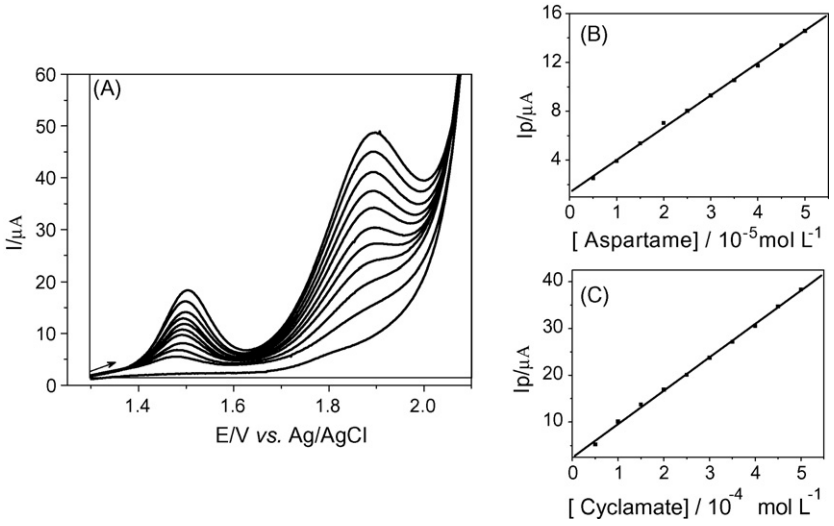

Fig. 3. (A) SW voltammograms obtained for the oxidation of aspartame and cyclamate contained in 0.5 mol L^{-1} H_2SO_4. Concentration of both aspartame (5.0×10^{-6} to 5.0×10^{-5} mol L^{-1}) and cyclamate (5.0×10^{-5} to 5.0×10^{-4} mol L^{-1}) were changed simultaneously. (B) Analytical curves for aspartame. (C) Analytical curves for cyclamate.

4. Conclusions

The present study shows that SW voltammetry using a BDD electrode can be used to simultaneously determine the concentration of aspartame and cyclamate in several dietary products dissolved in a 0.5 mol L^{-1} sulfuric acid solution. Under optimized conditions, the anodic peak current for aspartame was linearly dependent on the aspartame concentration in the range from 5.0×10^{-6} to 5.0×10^{-5} mol L^{-1} in the presence of 3.0×10^{-4} mol L^{-1} cyclamate, with a detection limit of 4.67×10^{-7} mol L^{-1}; on the other hand, the anodic peak current for cyclamate was linearly dependent on the cyclamate concentration in the range from 5.0×10^{-5} to 5.0×10^{-4} mol L^{-1} in the presence of 1.0×10^{-4} mol L^{-1} aspartame, with a detection limit of 4.2×10^{-6} mol L^{-1}. When the concentration of both aspartame (5.0×10^{-6} to 4.0×10^{-5} mol L^{-1}) and cyclamate (5.0×10^{-5} to 4.0×10^{-4} mol L^{-1}) in a 0.5 mol L^{-1} sulfuric acid solution were simultaneously changed, the detection limit was 3.5×10^{-7} (for aspartame) and 4.5×10^{-6} mol L^{-1} (for cyclamate). The proposed method was applied to the simultaneous determination of aspartame and cyclamate in samples of dietary products, yielding satisfactory addition–recovery tests; the obtained sweeteners' concentration values are similar to those obtained using a HPLC method and label values. Hence, the proposed procedure (SW voltammetry using a BDD electrode) was found to be effective for the simultaneous determination of aspartame and cyclamate, while being very simple, inexpensive, and rapid, forgoing pre-treatment of the samples.

Acknowledgements

The authors acknowledge financial support from CAPES, FAPESP and CNPq (Brazil).

References

[1] O. Fatibello-Filho, A.A. Suleiman, G.G. Guilbault, G.J. Lubrano, Anal. Chem. 60 (1988) 2397.
[2] O. Fatibello-Filho, I.C. Vieira, S.T. Gouveia, S.A. Calafatti, G.A.J.M. Santos, Quim. Nova 19 (1996) 248.
[3] B.E. Homler, Food Technol. 38 (1984) 50.
[4] W. Vetsch, Food Chem. 16 (1985) 245.
[5] B.F. Gibbs, I. Alli, C.N. Mulligan, J. Chromatogr. A 725 (1996) 372.
[6] J.J. Pesek, M.T. Matyska, J. Chromatogr. A 781 (1997) 423.
[7] M.V.S. Pinheiro, M.N. Oliveira, A.L.B. Penna, A.Y. Tamine, Int. J. Dairy Technol. 4 (2005) 193.
[8] F.E. Ahmed, D.B. Thomas, Crit. Rev. Toxicol. 22 (1992) 81.
[9] L. O'Brien, R.C. Gelardi, Chemtech May (1981) 274.
[10] N.E. Llamas, M.S. Di Nezio, M.E. Palomeque, B.S.F. Band, Anal. Chim. Acta 539 (2005) 301.
[11] J. Lawrence, Analyst 112 (1987) 879.
[12] Q. Chen, S. Mou, K. Liu, Z. Yang, Z. Ni, J. Chromatogr. A 771 (1997) 135.
[13] E.D. Çubuk, G. Ozkan, Z. Guzel-Seydim, Chromatographia 63 (2006) 91.
[14] G. Verzella, A. Mangia, J. Chromatogr. A 346 (1985) 417.
[15] G. Verzella, A. Mangia, G. Bagnasco, J. Chromatogr. A 349 (1985) 83.
[16] Z. Huang, J. Ma, B. Chen, Y. Zhang, S. Yao, Anal. Chim. Acta 555 (2006) 233.
[17] M.M.F. Choi, M.Y. Hsu, S.L. Wong, Analyst 125 (2000) 217.
[18] J. Prando, M.A. Prado, Abstracts of the "XIV Congresso Interno de Iniciação Científica", Unicamp, 2006, Campinas, Brazil.
[19] I. Casals, M. Reixach, J. Amat, M. Fuentes, L. Serra-Majem, J. Chromatogr. A 750 (1996) 397.
[20] D. Compagnone, D. O'Sullivan, G.G. Guilbault, Analyst 122 (1997) 487.
[21] U.A. Kirgoz, D. Odaci, S. Timur, A. Merkoci, S. Alegret, N. Besun, A. Telefoncu, Anal. Chim. Acta 570 (2006) 165.
[22] D. Xiao, M.M.F. Choi, Anal. Chem. 74 (2002) 863.
[23] D. Odaci, S. Timur, A. Telefoncu, Food Chem. 84 (2004) 493.
[24] M.L. Richardson, P.E. Luton, Analyst 91 (1966) 522.
[25] O. Fatibello-Filho, M.D. Capelato, S.A. Calafatti, Analyst 120 (1995) 2407.
[26] D.P. Nikolelis, S. Pantoulias, Electroanalysis 12 (2000) 786.
[27] L. Codognoto, S.A.S. Machado, L.A. Avaca, Diamond Relat. Mater. 11 (2002) 1670.
[28] D. Souza, S.A.S. Machado, L.A. Avaca, Quim. Nova 26 (2003) 81.
[29] V.A. Pedrosa, L. Codognoto, L.A. Avaca, Quim. Nova 26 (2003) 844.
[30] J. Osteryoung, R. Osteryoung, Anal. Chem. 57 (1985) 101A.
[31] Y.V. Pleskov, J. Anal. Chem. 55 (2000) 1045.
[32] M. Hupert, A. Muck, J. Wang, J. Stotter, Z. Cvakova, S. Haymond, Y. Show, G.M. Swain, Diamond Relat. Mater. 12 (2003) 1940.
[33] G.M. Swain, in: A.J. Bard, I. Rubinstein (Eds.), Electroanalytical Chemistry, vol. 22, Marcel Dekker, New York, 2004, p. 182.
[34] H.B. Suffredini, V.A. Pedrosa, L. Codognoto, S.A.S. Machado, R.C. Rocha-Filho, L.A. Avaca, Electrochim. Acta 49 (2004) 4021.
[35] C.E. Banks, R.G. Compton, Analyst 131 (2006) 15.
[36] Y.V. Pleskov, Russ. J. Electrochem. 38 (2002) 1275.
[37] Y. Zhang, S. Yoshihara, J. Electroanal. Chem. 573 (2004) 327.
[38] R.G. Compton, J.S. Foord, F. Marken, Electroanalysis 15 (2003) 1349.
[39] G.R. Salazar-Banda, L.S. Andrade, P.A.P. Nascente, P.S. Pizani, R.C. Rocha-Filho, L.A. Avaca, Electrochim. Acta 51 (2006) 4612.
[40] R.A. Medeiros, A.E. Carvalho, R.C. Rocha-Filho, O. Fatibello-Filho, Anal. Lett. 40 (2007) 3195.
[41] R.A. Medeiros, A.E. Carvalho, R.C. Rocha-Filho, O. Fatibello-Filho, Quim. Nova, in press.
[42] M. Lovric, S. Komorsky-Lovric, R.W. Murray, Electrochim. Acta 33 (1988) 739.
[43] R.L. Anderson, Practical Statistics for Analytical Chemists, Van Nostrand Reinhold, New York, 1987.

Talanta 76 (2008) 513–521

Contents lists available at ScienceDirect

Talanta

journal homepage: www.elsevier.com/locate/talanta

Fluorescence spectrometric study on the interactions of Isoprocarb and sodium 2-isopropylphenate with bovine serum albumin

Yongnian Ni[a,*], Genlan Liu[a], Serge Kokot[b]

[a] Department of Chemistry, Nanchang University, Nanchang, Jiangxi 330047, China
[b] School of Physical and Chemical Sciences, Queensland University of Technology, Brisbane, Queensland 4001, Australia

ARTICLE INFO

Article history:
Received 7 December 2007
Received in revised form 19 March 2008
Accepted 21 March 2008
Available online 8 April 2008

Keywords:
Isoprocarb
Sodium 2-isopropylphenate
Bovine serum albumin
Interactions
Three-way excitation–emission fluorescence

ABSTRACT

The binding interaction of the pesticide Isoprocarb and its degradation product, sodium 2-isopropylphenate, with bovine serum albumin (BSA) was studied by spectrofluorimetry under simulated physiological conditions. Both Isoprocarb and sodium 2-isopropylphenate quenched the intrinsic fluorescence of BSA. This quenching proceeded via a static mechanism. The thermodynamic parameters (ΔH°, ΔS° and ΔG°) obtained from the fluorescence data measured at two different temperatures showed that the binding of Isoprocarb to BSA involved hydrogen bonds and that of sodium 2-isopropylphenate to BSA involved hydrophobic and electrostatic interactions. Synchronous fluorescence spectroscopy of the interaction of BSA with either Isoprocarb or sodium 2-isopropylphenate showed that the molecular structure of the BSA was changed significantly, which is consistent with the known toxicity of the pesticide, i.e., the protein is denatured. The sodium 2-isopropylphenate, was estimated to be about 4–5 times more toxic than its parent, Isoprocarb.

Synchronous fluorescence spectroscopy and the resolution of the three-way excitation–emission fluorescence spectra by the PARAFAC method extracted the relative concentration profiles of BSA, Isoprocab and sodium 2-isopropylphenate as a function of the added sodium 2-isopropylphenate. These profiles showed that the degradation product, sodium 2-isopropylphenate, displaced the pesticide in a competitive reaction with the BSA protein.

1. Introduction

The interactions of small molecules or ligands with major biopolymers such as proteins and DNA, are numerous and their effects range from highly beneficial to deadly. *In vivo,* many ligands may compete for the same binding sites and hence, the interactions can be quite complex but are clearly important to investigate. To understand the basic processes involved in such cases, comparatively simpler *in vitro* models are commonly studied. Serum albumin (SA) and particularly the readily available purified bovine serum albumin (BSA) are often used to investigate the interactions of small molecules and proteins [1,2]. In recent years, attention has been focused on the interactions between SA and medicinal drugs [3]. The application of chemometrics for the extraction of concentration profiles of the competing species has also provided a pathway leading to deeper insights of these interactions [4,5]. In general, such studies utilized UV–vis and fluorescence spectroscopy techniques, which are sometimes supported by electrochemical methods such as cyclic voltammetry. Such investigations provide, for example, information about the binding sites, the non-covalent forces involved in the complexation reaction, the thermodynamic constants for this process, and the concentrations profiles as mentioned above [6,7]. However, literature suggests that there are only a few studies available, which investigated the interaction between pesticides and SA with the use of fluorescence spectroscopy [8]. Thus, Mourik and De Jong [9] studied the binding of the organophosphates, parathion and paraoxon, to BSA and human serum albumin (HSA) with the use of equilibrium dialysis. The concentration of the unbound organophosphates was determined from its anti-cholinesterase activity. The binding of parathion to BSA was shown to be reversible. The organophosphates interacted with only one type of binding site in BSA and HSA. The affinity constants for the interaction of BSA or HSA and parathion were found to be 2.7×10^6 and 1.5×10^6 L mol^{-1}, respectively. The affinity constants for the interaction of BSA or HSA and paraoxon were considerably lower, 6.0×10^3 and 1.6×10^4 L mol^{-1}, respectively. Lowering the pH from 7.2 to 4.8 did not significantly affect the binding parameters. The significant difference in affinity of the SA to parathion and paraoxon was discussed with respect to the fate of parathion in the body. Maliwal and Guthrie [10] studied the binding of chlori-

* Corresponding author. Tel.: +86 791 3969500; fax: +86 791 3969500.
E-mail address: ynni@ncu.edu.cn (Y. Ni).

0039-9140/$ – see front matter © 2008 Elsevier B.V. All rights reserved.
doi:10.1016/j.talanta.2008.03.037

nated hydrocarbons, carbamate, and organophosphate insecticides to HSA with the use of equilibrium dialysis, difference spectra, and fluorescence. These investigations indicated the presence of one high affinity site on the HSA as well as 4–6 binding sites of moderate affinity. The affinity was found to be inversely related to the aqueous solubility of the compounds. The interaction was regarded as primarily hydrophobic because the binding was only weakly temperature dependent. The absorption spectra of the tyrosyl and tryptophyl residues showed a shift to longer wavelengths when the pesticides were bound to HSA. The protein fluorescence was quenched to varying degrees as a result of the binding. The difference spectra and fluorescence quenching indicated that tyrosyl and tryptophyl residues were located near the binding sites of moderate affinity, although the possible role of binding-induced conformational changes could not be ruled out. Xu et al. [11] researched the interactions between the pesticide, phenthoate (PTA), and BSA. This work involved the quenching of the tryptophan residue fluorescence, and a study of the associated inhibition of acetylcholinesterase activity by PTA. The affinity of PTA for BSA was evaluated, and the results showed that the Stern–Volmer quenching constant, K_{SV} ($2.8–3.4 \times 10^4$ mol L^{-1}), was inversely correlated with temperature. This indicates that the quenching mechanism of the PTA–BSA binding reaction is probably initiated by complex formation between the ligand and the BSA. Silva et al. [12] studied interactions of methyl parathion with BSA and HSA with the use of fluorescence quenching techniques. The Stern–Volmer plots enabled the estimation of the quenching constants, and the results pointed to the formation of complexes of methyl parathion with the albumins. The association constants at 25 °C were 1.96×10^4 L mol^{-1} for BSA, and 3.07×10^4 L mol^{-1} for HAS, and at 37 °C, they were 8.16×10^3 L mol^{-1} for BSA, and 1.08×10^4 L mol^{-1} for HSA. From this work, the primary binding site for methyl parathion on albumin was suggested to be close to the tryptophan residues 214 of HSA and 212 of BSA. Yan et al. [13] studied the binding of the herbicide, paraquat, to BSA with the use of fluorescence and UV spectroscopy. Deepa and Mishra [14] investigated the binding of a rodenticide, bromadiolone to BSA, with the use of the same techniques. This compound is a coumarin, which is an anti-coagulant of blood. When compared to warfarin, which is an effective oral anti-coagulant for humans, bromadiolone is acutely toxic, and its residues can be transferred from rodent carcasses by scavengers and predators to humans with potentially catastrophic results.

From the 1970s, carbamate formulations progressively replaced the organochlorine and organophosphate pesticides in agriculture. They and their degradation products are also considered hazardous to the environment and human health [15,16], and thus, they are on the priority list of the US Environmental Protection Agency.

An example of a carbamate pesticide is Isoprocarb, which was released for agricultural and cotton spraying in 1970 [17]. In this paper, a study of the binding of the Isoprocarb (2-(1-methylethyl)phenyl-methylcarbamate) and its degradation product, sodium 2-isopropylphenate, to BSA is reported. The work was carried out with the use of fluorescence spectroscopy in order to compare the nature of the binding of the two molecules to BSA, separately and in competition with each other; in particular, the effect of Isoprocarb and sodium 2-isopropylphenate on the conformation of BSA was investigated.

2. Experimental

2.1. Apparatus

The fluorescence measurements were made on a Perkin Elmer LS-55 luminescence spectrometer equipped with a thermostatic bath (Model ZC-10, Ningbo Tianheng Instruments Factory, China) and a 10 mm quartz cuvette. The excitation and emission slits were set at 12 nm while the scanning rate was 1500 nm min^{-1}.

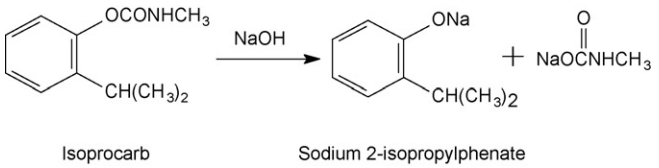

Scheme 1. Chemical equation of the Isoprocarb degradation.

2.2. Reagents

A stock solution of Isoprocarb (100 mg L^{-1}) was prepared by dissolving its crystals (0.01 g, The Pesticide Assay Station, Beijing) in a small amount of methanol (160 μL), and then diluting this solution to the required volume of 100 mL with distilled water.

Sodium 2-isopropylphenate solution was prepared by adding 10 μL of 4.0 mol L^{-1} sodium hydroxide to 10 mL of 5.18×10^{-4} mol L^{-1} Isoprocarb solution and mixed thoroughly. The mixture was allowed to stand for 12 h, and then the solution was neutralized with the addition of 8 μL of 5.0 mol L^{-1} hydrochloric acid. Under strongly basic conditions Isoprocarb undergoes a complete hydrolysis reaction, which in this work, resulted in a 5.18×10^{-4} mol L^{-1} sodium 2-isopropylphenate degradation product solution. The degradation reaction of Isoprocarb is shown in Scheme 1.

BSA (5×10^{-5} mol L^{-1}) was prepared by dissolving 0.33 g of the purified protein (M = 66,000 Da; "essentially globulin and fatty acid free" (The Huamei Biological Co. Ltd., Shanghai)) in 100 mL of 50×10^{-3} mol L^{-1} sodium chloride solution and stored at 4 °C. Its purity was 99% based on a reference absorbance value of 0.667 at 279 nm for 1.0 g L^{-1} pure BSA [2]. All experimental solutions were adjusted with the Tris–HCl buffer ((hydroxy methyl) amino methane–hydrogen chloride), pH 7.4. All other chemicals were Analytical Grade reagents, and doubly distilled water was used throughout.

2.3. Fluorescence measurements

2.3.1. Binding of Isoprocarb and BSA

45 μL of BSA (5.0×10^{-5} mol L^{-1}) and 2.0 mL Tris–HCl buffer (pH 7.4) were added to a 10 mL volumetric flask, and diluted with distilled water. An aliquot of this solution (3 mL) was transferred to a 10 mm quartz cuvette. Isoprocarb was added to this solution at different concentrations in the range of 0 to 7.77×10^{-6} mol L^{-1} in steps of 5.18×10^{-7} mol L^{-1} to give a series of 16 samples. These well-mixed solutions were allowed to stand for 5 min at 25 ± 1 and 35 ± 1 °C. The fluorescence spectra of the 16 samples were measured at the excitation wavelength of 280 nm with emission being recorded between 250 and 450 nm.

Synchronous fluorescence spectra (SFS) of BSA (1.33×10^{-7} mol L^{-1}) in the presence of Isoprocarb were measured ($\Delta\lambda$ = 60 nm; λ_{ex} = 240–320 nm). The range of Isoprocarb concentration was 0 to 1.72×10^{-6} mol L^{-1} with spectra being recorded at intervals of 0.345×10^{-6} mol L^{-1} (total: 6 samples). In addition, three-way excitation–emission fluorescence spectra of BSA (1.67×10^{-7} mol L^{-1}) in the presence of Isoprocarb were recorded (λ_{ex} = 200–500 nm (every 10 nm)) over the emission range of 250–500 nm (every 10 nm). The Isoprocarb concentration was varied from 0 to 6.45×10^{-6} mol L^{-1} with spectra being recorded at intervals of 1.29×10^{-6} mol L^{-1} (total: 6 samples).

2.3.2. Binding of sodium 2-isopropylphenate and BSA

Similar to the procedure in Section 2.3.1, the fluorescence of BSA (2.25×10^{-7} mol L^{-1}) in the presence of sodium 2-isopropylphenate (λ_{ex} = 280 nm) was recorded over the emission range of 250–450 nm. The sodium 2-isopropylphenate concentration was varied between 0 and 1.63×10^{-6} mol L^{-1} at intervals of 8.6×10^{-8} mol L^{-1} (total: 20 samples). SFS of BSA (1.33×10^{-7} mol L^{-1}) in the presence of sodium 2-isopropylphenate ($\Delta\lambda$ = 60 nm; λ_{ex} = 240–320 nm) were recorded in the range of 0 to 2.76×10^{-7} mol L^{-1} at intervals of 0.345×10^{-7} mol L^{-1} (total 9 samples). Three-way excitation–emission fluorescence spectra of BSA (1.67×10^{-7} mol L^{-1}) were recorded in the same range as Isoprocarb (Section 2.3.1), in the presence of sodium 2-isopropylphenate in the range of 0 to 1.3×10^{-6} mol L^{-1} and at intervals of 4.3×10^{-7} mol L^{-1} (total: 4 samples).

2.3.3. Competitive reaction of Isoprocarb and sodium 2-isopropylphenate with the BSA protein

45 μL of BSA (5.0×10^{-5} mol L^{-1}), 60 μL of Isoprocarb (5.18×10^{-4} mol L^{-1}) and 2.0 mL of Tris–HCl buffer (pH 7.4) were added to a 10 mL volumetric flask, and diluted to the mark with distilled water. This solution was thoroughly mixed and allowed to equilibrate at 25 ± 1 °C for 10 min. Then, 3 mL of this solution were transferred to a 10 mm quartz cuvette. Sodium 2-isopropylphenate was added in different concentrations in the range of 0 to 1.29×10^{-6} mol L^{-1} in steps of 0.86×10^{-7} mol L^{-1}, to give a series of 16 samples. Samples were measured in the excitation range of 200–400 nm (every 10 nm), and emission range of 250–450 nm (every 0.5 nm). Thus, the three-way excitation–emission fluorescence matrix (EEM) obtained, has the dimensions of 21 (λ_{ex}) × 401 (λ_{em}) × 16 (samples), as defined by the $I \times J \times K$ dimensions (Section 2.4).

2.4. Parallel factor analysis algorithm (PARAFAC)

Parallel factor analysis is a multi-way chemometrics method [18], which can overcome the well-known rotational freedom problem present with bilinear methods [19]. A PARAFAC model of a three-way array is given by three loading matrices, ***A***, ***B*** and ***C***, with elements a_{if}, b_{if} and c_{kf}, respectively, and is expressed by the following equation:

$$x_{ijk} = \sum_{f=1}^{F} a_{if} b_{if} c_{kf} + e_{ijk} \quad (1)$$

where x_{ijk} is an element of the trilinear data set ***X***, and e_{ijk} represents the elements of the three-way array ***E***, which is a residual error term of the same dimensions as ***X***. The trilinear model is optimized to minimize the sum of squares of the residuals, e_{ijk}. The algorithm employed to solve the trilinear model is the alternating least squares (ALS) [19], which uses loadings values in two models to estimate the unknown set of parameters of the third model. Iterations are performed until convergence.

A second-order fluorescence EEM data are produced by modulating individual data points of an excitation spectrum according to the emission wavelength. Then, a three-way fluorescence EEM array is produced by stacking several second-order EEM spectra in order of the concentration, which facilitates the extraction of the estimated curves of relative concentration of the chemical components. This results in a three-way data cube that can be mathematically modeled by PARAFAC [18,19]. In the case of EEM spectra, x_{ijk} represents the fluorescence intensity of a sample k (k = 1, 2, ..., K), at an excitation wavelength i (i = 1, 2, ..., I), and emission wavelength j (j = 1, 2, ..., J). F is the number of independently varying fluorescence contributions (analyte components) in the sample solution, and it is a user-selected number. The columns of ***A***, ***B*** and ***C*** are the estimates of the excitation, emission and relative concentration curves, respectively. Thus, the EEM array stacks should have dimensions of $I \times J \times K$. PARAFAC can be utilized to resolve overlapping spectra and decompose the three-way data sets, even if no unique spectral data exists; such data processing eliminates or minimizes the need for laboratory sample pretreatment and separation. If the data is indeed trilinear, the true underlying spectra will be found, and as the solutions are unique, the estimated spectra should be very similar to the measured ones if the appropriate number of analyte components is selected [19].

3. Results and discussion

3.1. Interactions between Isoprocarb, sodium 2-isopropylphenate and BSA

When excited by radiation at 280 nm, the BSA protein naturally fluoresces at 350 nm, and this fluorescence is attributed to a tryptophan residue [20]. Binding of small molecules with BSA can quench this effect, and this is illustrated by the interaction of BSA (0.225×10^{-6} mol L^{-1}) with the Isoprocarb pesticide (Fig. 1A), as well as by a separate experiment with sodium 2-isopropylphenate (Fig. 1B).

In the case of the Isoprocarb molecule, the BSA fluorescence band shifts to shorter wavelengths, and a new Isoprocarb fluorescence peak develops at about 310 nm with increase in the concentration of the added pesticide (0–7.77×10^{-6} mol L^{-1}). An isoactinic point forms at ca. 340 nm, and indicates an equilibrium between the free Isoprocarb and the molecule bound to BSA (340 nm).

Stern–Volmer [21] linear plots for this equilibrium system show decreasing slopes with increase in temperature (Table 1). This indicates a static quenching mechanism [22] during the interaction between Isoprocarb and BSA.

This conclusion is supported by the results from the application of the dynamic quenching equation [23]:

$$\frac{F_0}{F} = 1 + K_{SV}[Q] = 1 + K_q \tau_0 [Q] \quad (2)$$

where K_q is the quenching rate constant and τ_0 is the fluorescence lifetime value. K_q decreased with increasing temperature (Table 1). Generally, τ_0 (biopolymer) is taken as 10^{-8} s^{-1} [24], and when combined with the value of K_{SV} ($\sim 10^4$) gives a K_q in the order of 10^{12}. This value is much larger than that of the maximum scatter collision-quenching rate constant, K_q, of various quenchers with a biopolymer (2.0×10^{10} L mol^{-1} s^{-1}). This observation essentially indicates that the BSA–Isoprocarb binding cannot be associated with the dynamic fluorescence quenching mechanism but rather with the static one, which originates from the formation of the BSA–Isoprocarb complex. Therefore, the quenching data were analysed according to the modified Stern–Volmer equation [25]:

$$\frac{F_0}{(F_0 - F)} = \frac{1}{(fK\,[Q])} + \frac{1}{f} \quad (3)$$

where f is the fraction of accessible fluorescence and K is the effective quenching constant for the accessible fluorophores. The K is analogous to the associative binding constants for the quencher–acceptor system. K values show a decreasing trend with increasing temperature (Table 1). This observation is in accordance with the temperature dependence of the K_{SV} values noted previously.

In general, a similar behaviour of the fluorescence bands is observed in a separate experiment on the addition of

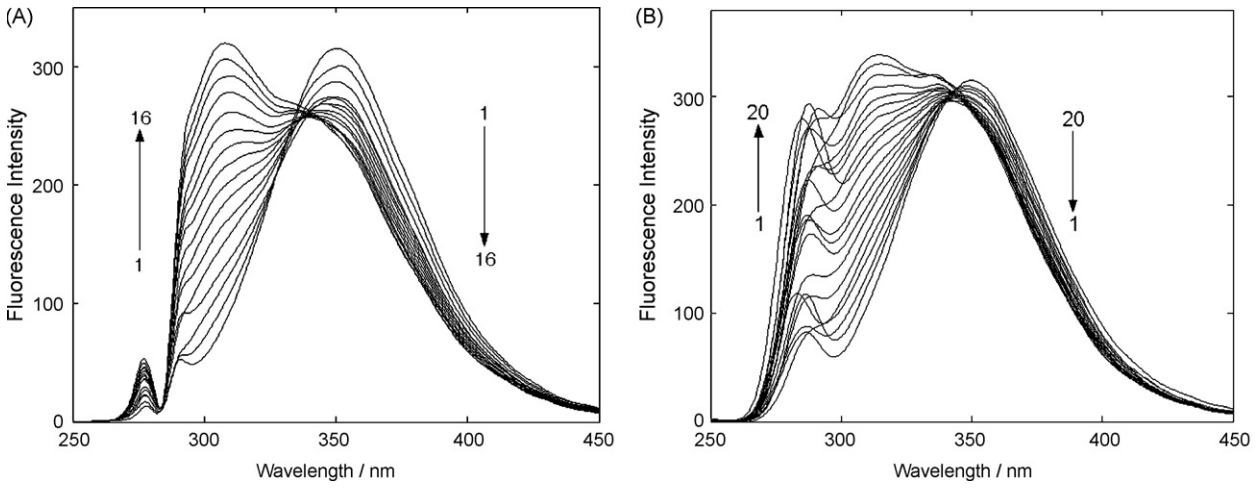

Fig. 1. (A) Fluorescence emission spectra of BSA (2.25×10^{-7} mol L^{-1}) in the presence of different concentrations of Isoprocarb (1–16): [Isoprocarb] = 0 to 7.77×10^{-6} mol L^{-1} at intervals of 5.18×10^{-7} mol L^{-1} (1–16); λ_{ex} = 280 nm; (B) fluorescence emission spectra of BSA (2.25×10^{-7} mol L^{-1}) in the presence of different concentrations of sodium 2-isopropylphenate (1–20): [sodium 2-isopropylphenate] = 0 to 1.63×10^{-6} mol L^{-1} at intervals of 8.6×10^{-8} mol L^{-1} (1–20); λ_{ex} = 280 nm.

the sodium 2-isopropylphenate (0–1.38×10^{-6} mol L^{-1}) to BSA (0.225×10^{-6} mol L^{-1}, Fig. 1B). The λ_{max} of the fluorescence band of the BSA (350 nm) initially appears to be quenched due to the ligand–BSA complex formation, and the band shifts to shorter wavelength (~340 nm). A new fluorescence peak, attributed to the addition of sodium 2-isopropylphenate can be observed to form roughly at 310 nm. This trend continues to develop until about the 1.2×10^{-6} mol L^{-1} addition of the ligand. Up to this stage an isoactinic point is at about 340 nm, which indicates an equilibrium between the free ligand (~310 nm) and its bound form with BSA [26]. Thereafter, on addition of the next two aliquots of the ligand, a peak with distinctly three weak but growing maxima forms (~310, 325 and 335 nm). These three bands appear to coalesce and grow in parallel with intensities at about 310 and 335 nm.

The shift of λ_{max} towards the shorter wavelengths and the decrease in fluorescence intensity suggested that the polarity around the tryptophan residues decreased and the hydrophobicity increased [27]. The fluorescence intensity of sodium 2-isopropylphenate between 300 and 330 nm (Fig. 1) was much stronger than the one from the Isoprocarb. This is supported by a comparison of spectral intensities taken at the same concentration, i.e., 1.55×10^{-6} mol L^{-1}, of Isoprocarb and sodium 2-isopropylphenate.

The previously noted K_{SV}, K_q, and K constants estimated on the basis of the Stern–Volmer models (Table 1) support the above conclusion, which indicates that the quenching mechanism of the interaction between sodium 2-isopropylphenate and BSA was initiated by the formation of a complex rather than by dynamic collision.

The spectral bands, which behave erratically, and are observed in the range of 270–290 nm (Fig. 1B), are attributed to the Rayleigh scattering given that the excitation line was at 280 nm.

3.2. Thermodynamic analysis and the nature of the binding forces

In general, the binding forces between a small molecule and a biomacromolecule may include hydrophobic forces, electrostatic interactions, van der Waals interactions, and hydrogen bonds. The thermodynamic parameters associated with a binding reaction provide evidence for the nature of the binding [25]. If the enthalpy change (ΔH°) does not vary significantly over the temperature range studied, then it can be approximated from Eq. (4), while the free-energy change (ΔG°) and the entropy change (ΔS°) of the binding reaction follow Eqs. (5) and (6), respectively.

$$\ln\left(\frac{K_2}{K_1}\right) = \left(\frac{1}{T_1} - \frac{1}{T_2}\right)\left(\frac{\Delta H^\circ}{R}\right) \quad (4)$$

$$\Delta G^\circ = -RT \ln K^\circ \quad (5)$$

$$\Delta G^\circ = \Delta H^\circ - T\Delta S^\circ \quad (6)$$

where K_1 and K_2 are the binding constants (i.e. K in Eq. (3)) at the corresponding temperature T_1 and T_2, and R is the universal gas constant. For the binding of the Isoprocarb and sodium 2-isopropylphenate to BSA, negative ΔH° and ΔG° values were obtained (Table 1). Ross and Subramanian [28] have characterized the sign and magnitude of the thermodynamic parameters associated with various individual kinds of interaction. Accordingly, the negative ΔG° and ΔH° indicate that the binding process is spontaneous and the formation of the Isoprocarb–BSA and sodium 2-isopropylphenate–BSA complexes, respectively, is exothermic. Thus, the negative ΔH° and ΔS° values for the Isoprocarb and BSA system in an aqueous medium suggest the presence of intermolecular hydrogen bonds. On the other hand, the relatively small and positive ΔS° for the sodium 2-isopropylphenate and BSA interaction, indicates the presence of hydrophobic interactions. In addition, a specific electrostatic interaction between ionic species

Table 1
Binding constants and thermodynamic parameters

T (K)	K_{SV} (L mol^{-1})	K_q (L mol^{-1} s^{-1})	K (L mol^{-1})	ΔH° (kJ mol^{-1})	ΔS° (J mol^{-1} K^{-1})	ΔG° (kJ mol^{-1})
Isoprocarb						
298	4.76×10^4	4.76×10^{12}	9.64×10^4	−102.3	−248.0	−28.4
308	4.00×10^4	4.00×10^{12}	2.52×10^4	−102.3	−247.7	−26.0
Sodium 2-isopropylphenate						
298	8.40×10^4	8.40×10^{12}	2.99×10^6	−23.1	46.3	−36.9
308	8.00×10^4	8.00×10^{12}	2.21×10^6	−23.1	46.4	−37.4

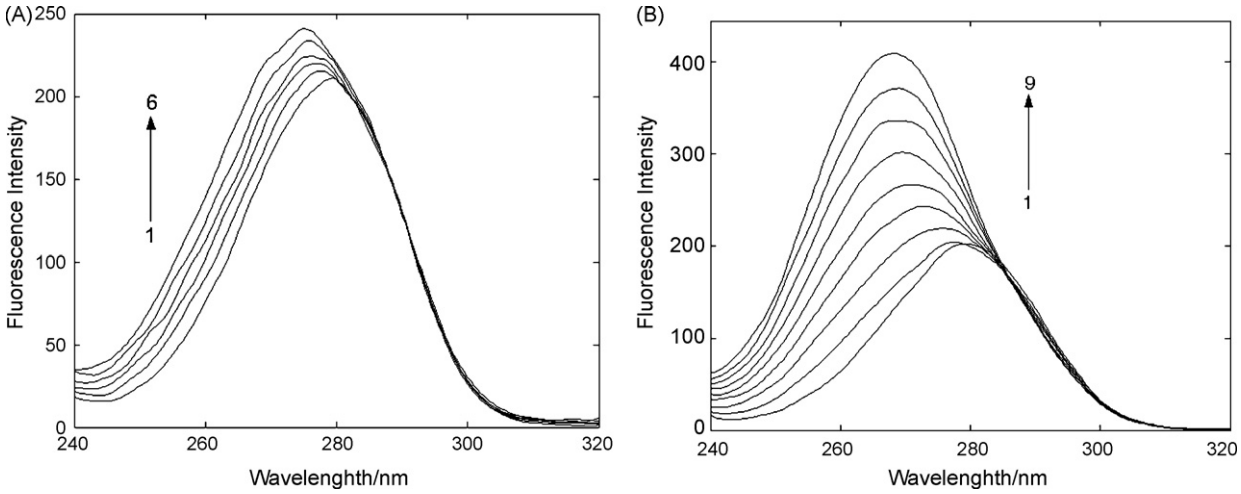

Fig. 2. (A) Synchronous fluorescence spectra of BSA (1.33×10^{-7} mol L^{-1}) in the presence of different concentrations of Isoprocarb (1–6): [Isoprocarb] = 0, 0.35, 0.69, 1.04, 1.39 and 1.73×10^{-6} mol L^{-1} (1–6); $\Delta\lambda$ = 60 nm; (B) synchronous fluorescence spectra of BSA (1.33×10^{-7} mol L^{-1}) in the presence of different concentrations of the sodium 2-isopropylphenate (1–9): [sodium 2-isopropylphenate] = 0, 0.35, 0.69, 1.04, 1.38, 1.73, 2.07, 2.42 and 2.76×10^{-7} mol L^{-1} (1–9); $\Delta\lambda$ = 60 nm.

in an aqueous solution is characterized by a negative ΔH° value and positive ΔS° value [25]. Sodium 2-isopropylphenate can exist as ions under the experimental conditions (pH 7.4). Thus, there is potential for electrostatic interaction. However, this is unlikely to contribute strongly given the nature of the binding sites on the BSA as discussed below.

BSA is characterized by two tryptophan residues: Trp-134, which is thought to be located on the surface (sub-domain IA), and Trp-212, which is considered to be located within a hydrophobic pocket [23,29]. This latter site is in a well-characterized binding cavity (sub-domain IIA) for small charged aromatic molecules. The crystallographic analysis of SA also revealed that the major ligand binding sites are identified within this region [30]. Thus, it is likely that the sodium 2-isopropylphenate molecule interacts via its hydrophobic aromatic part of its molecule at the binding site located in sub-domain IIA of the BSA. This supports the previous suggestion that hydrophobic interaction plays a major role in the interaction of sodium 2-isopropylphenate with BSA.

3.3. Conformation investigation

Spectroscopy is a useful tool to observe conformational changes in proteins because it allows non-intrusive measurements of substances, which are in low concentration under physiological conditions [29]. Tryptophan side chain residues are highly sensitive to their local environment in the BSA protein, and there will be a substantial spectral shift of the fluorescence, λ_{em}, if the environment is changed [31]. In addition, the spectral profile depends on the degree of exposure of the tryptophan side chain to the polar aqueous medium, and also, on this residue's proximity to specific quenching groups.

Kragh-Hansen et al. [32] suggested synchronous fluorescence spectroscopy (SFS) as a useful method to study the environment of amino acid residues. It involves the measurement of any shift in the emission maximum, λ_{em}, on addition of ligand molecules. Such shifts reflect the changes of polarity around the chromophore molecule. Thus, it was demonstrated that when the $\Delta\lambda$ was fixed at 60 nm, the SFS provided information characteristic of the changes to the tryptophan residues [33].

The SF spectra may be obtained by simultaneously scanning the excitation and emission monochromators [34]. Thus, the relationship for SF intensity is given by [35]:

$$F = kcdE_{ex}(\lambda_{em} - \Delta\lambda)E_{em}(\lambda_{em}) \quad (7)$$

where F is the relative intensity of SF, k is characteristic constant, c is analytical concentration, d is pathlength of the sample cell, E_{ex} is excitation function at the given excitation wavelength, $\Delta\lambda = \lambda_{em} - \lambda_{ex}$ is a constant, and E_{em} is the normal emission function at the corresponding emission wavelength, which includes the instrumental factor and related parameters. Since the relationship of the SF intensity (F) and the concentration of Isoprocarb and sodium 2-isopropylphenate should follow Eq. (7), F should be directly proportional to the concentration of either the Isoprocarb or the sodium 2-isopropylphenate.

When the wavelength interval ($\Delta\lambda$) is fixed at 60 nm, the SF has the same intensity as the emission fluorescence, which follows the excitation at 280 nm, and only the λ_{em} maximum and the peak shapes change. Thus, the SF measurements can be applied to calculate the association constants in a similar manner to that used with the emission fluorescence measurements, and consequently the binding mechanism may be investigated [36].

In this work, SF spectra of BSA with various amounts of either Isoprocarb or sodium 2-isopropylphenate were recorded at $\Delta\lambda$ = 60 nm (Fig. 2) in order to explore any structural changes of the protein molecule on addition of the pesticides. The resulting spectra may be analysed in the form of a three-way excitation–emission spectral array, which is related to the fluorescence characteristics of the reagent, and which contains the fluorescence intensity changes as a function of both the emission and excitation wavelengths [37,38].

The fluorescence contour plots of BSA in the presence of different concentrations of either Isoprocarb or sodium 2-isopropylphenate (Figs. 3 and 4), respectively, as well as the information in Table 2, were derived from the three-way excitation–emission spectral array. They demonstrate that the Stokes shift and fluorescence intensity related to Peak 1 (λ_{em} (BSA); Figs. 3 and 4, and Table 2) decreases and the peak maximum shows a blue shift. This blue shift effect indicates that conformational changes have occurred in the BSA structure as the polarity around the tryptophan residues decreases and the hydrophobicity increases [25]. For Peak 2, the Stokes shift does not change, and the fluorescence intensity increases in the presence of different concentrations of Isoprocarb; but the Stokes shift decreases, and the fluorescence intensity increases in the presence of different concentrations of sodium 2-isopropylphenate (Table 2). However, when the concentration of the sodium 2-isopropylphenate is lower than that of Isoprocarb, Peak 1 disappears (Table 2); on the other hand, at the same time,

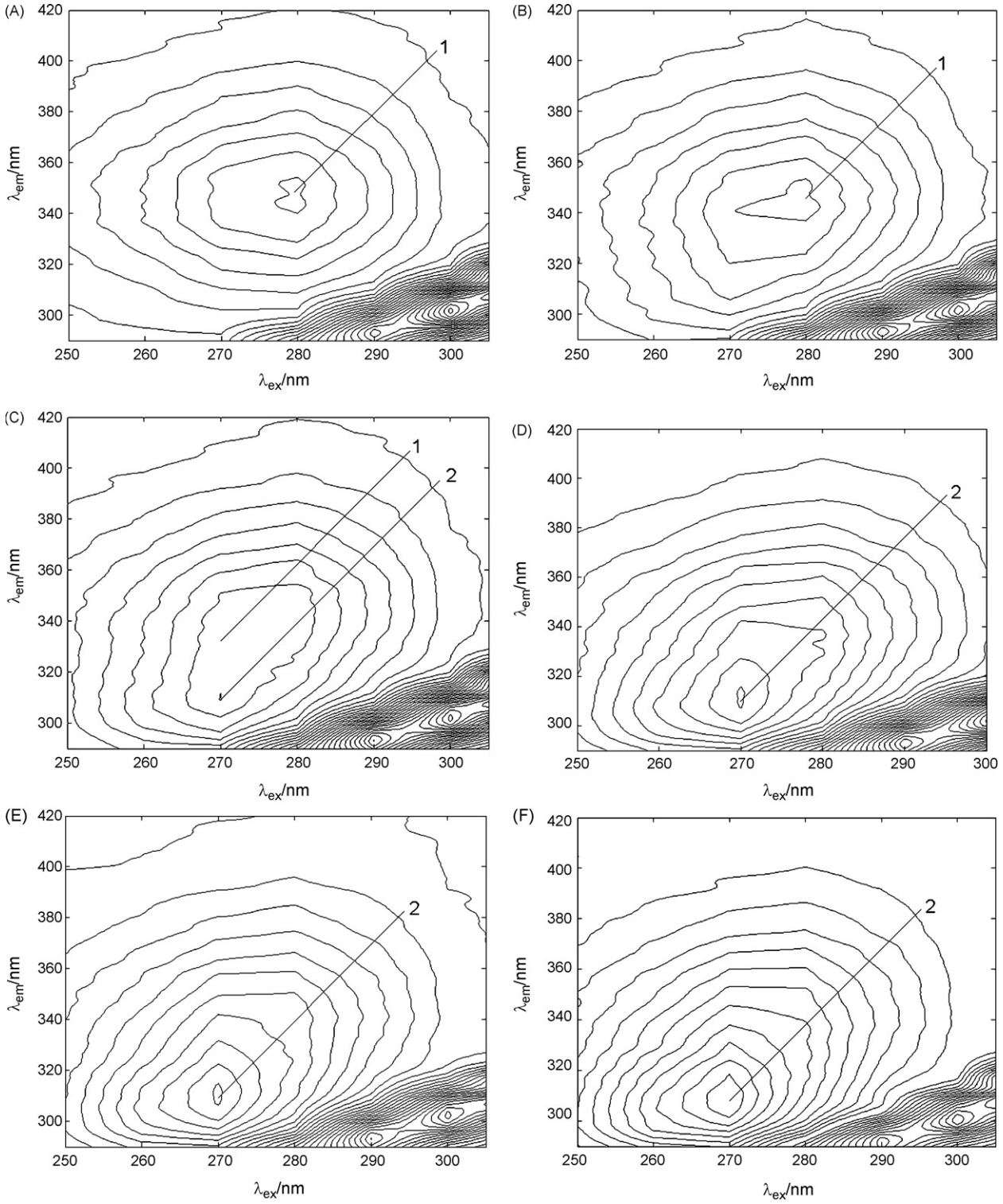

Fig. 3. Contour plot of BSA (1.67×10^{-7} mol L^{-1}) in the presence of different concentrations of Isoprocarb: [Isoprocarb] = 0, 12.9, 25.8, 38.7, 51.6 and 64.5×10^{-7} mol L^{-1} (A–F).

the intensity of Peak 2 for sodium 2-isopropylphenate is larger than that of the Isoprocarb. These observations indicate that the effect of sodium 2-isopropylphenate on BSA is larger than that of the Isoprocarb. This result suggests that the conformational changes have occurred on the BSA molecule and that it has been denatured by the interaction with either Isoprocarb or sodium 2-isopropylphenate. Interestingly, in reference to the discussion in Section 3.2, there is evidence to suggest that binding of small molecules in sub-domain IIA affects conformational changes [29].

Given that the pesticides are generally regarded as toxic to humans and animals, this result may be interpreted as evidence of such toxicity, and it may be possible to estimate the relative toxicity of the two substances by comparing the quenching of the BSA-

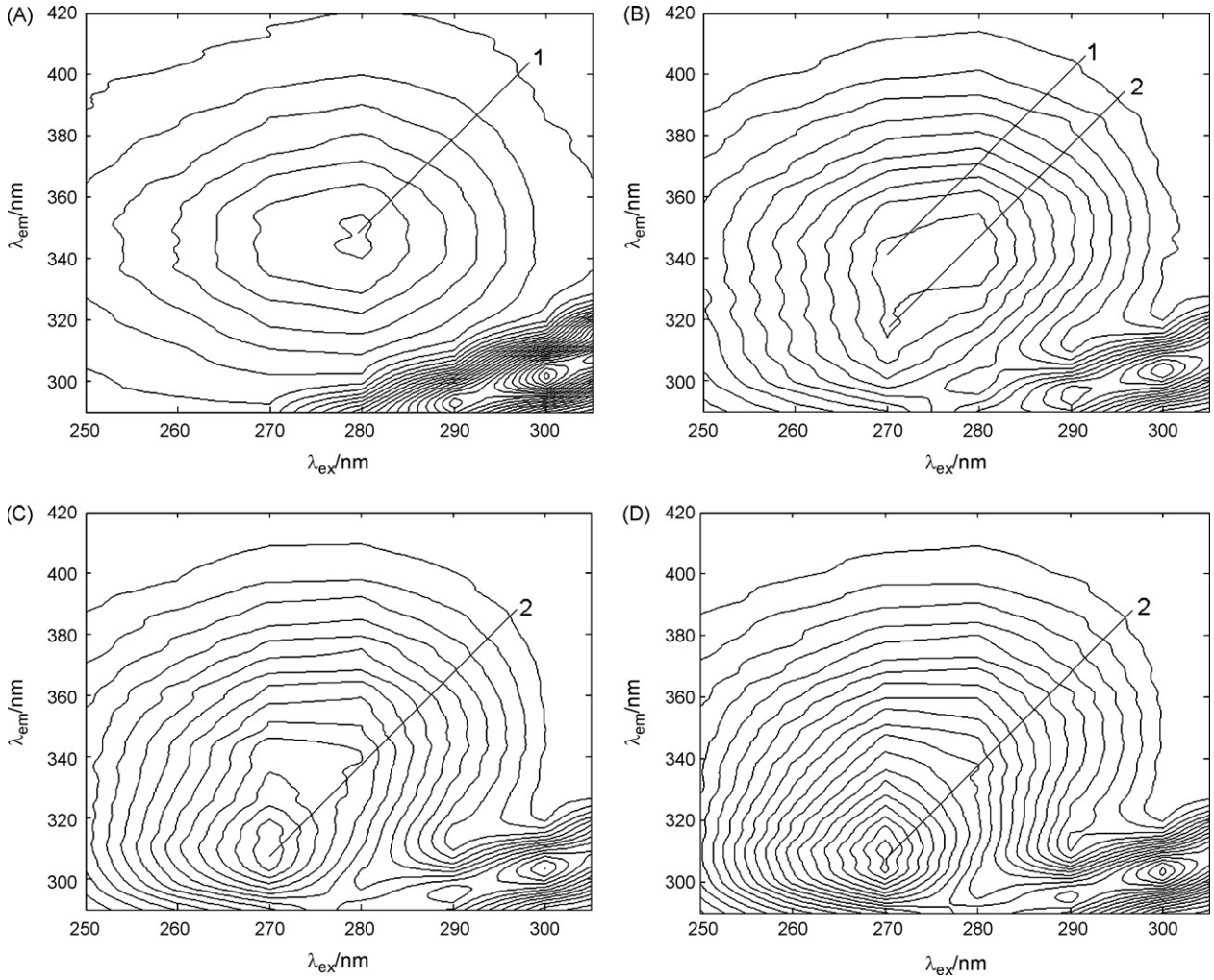

Fig. 4. Contour plot of BSA (1.67×10^{-7} mol L^{-1}) in the presence of different concentrations of sodium 2-isopropylphenate: [sodium 2-isopropylphenate] = 0, 4.3, 8.6 and 12.9×10^{-7} mol L^{-1} (A–D).

derived fluorescence. Thus, Peak 1 effectively disappears (Fig. 3) at the Isoprocarb concentration of ca. 38.7×10^{-7} mol L^{-1}, while the same Peak 1 of the sodium 2-isopropylphenate (Fig. 4) is completely quenched at a concentration of about 8.6×10^{-7} mol L^{-1}. The concentration ratio for Peak 1 at the point of complete quenching, i.e., Isoprocarb/sodium 2-isopropylphenate, is 4.5, which suggests that in terms of denaturation or BSA protein toxicity, sodium 2-isopropylphenate is about 4–5 times more effective than Isoprocarb.

The above results were obtained by studying the interactions of BSA with either Isoprocarb or sodium 2-isopropylphenate. Clearly, an experiment which investigates the competition of the two ligands with BSA could add significantly to the understanding of the above interactions.

Table 2
Characteristic parameters of the three-way excitation–emission fluorescence spectra

System	Concentration (mol L^{-1})	Fluorescence peak 1[a]			Fluorescence peak 2[a]		
		$\lambda_{ex}/\lambda_{em}$ (nm/nm)	Intensity	Stokes shift ($\Delta\lambda$ (nm))	$\lambda_{ex}/\lambda_{em}$ (nm/nm)	Intensity	Stokes shift ($\Delta\lambda$ (nm))
BSA–Isoprocarb							
A	0	280/351	205.9	71			
B	12.9×10^{-7}	280/343	191.1	64	270/309	190.8	39
C	25.8×10^{-7}				270/309	250.8	39
D	38.7×10^{-7}				270/309	294.2	39
E	51.6×10^{-7}				270/309	294.2	39
F	64.5×10^{-7}				270/309	340.3	39
BSA–sodium 2-isopropylphenate							
A	0	280/351	205.9	71			
B	4.3×10^{-7}	270/340.5	204.6	70.5	270/315	204.5	45
C	8.6×10^{-7}				270/307	312.9	37
D	12.9×10^{-7}				270/307	413.5	37

[a] Peak 1 is the fluorescence emission peak of BSA and Peak 2 is the fluorescence emission peak of Isoprocarb or sodium 2-isopropylphenate.

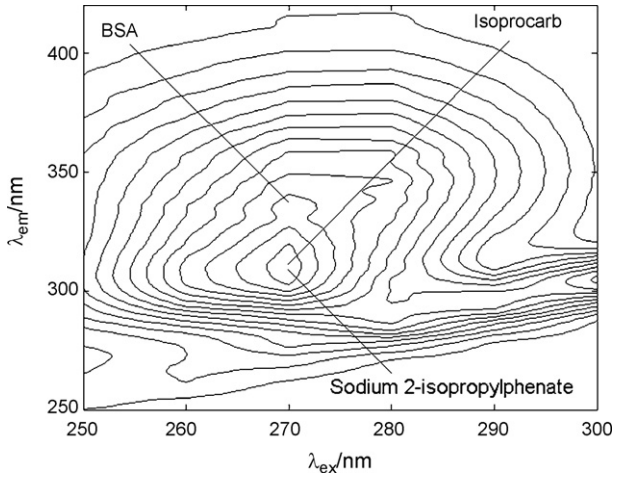

Fig. 5. Contour plot of the complex mixture of BSA, Isoprocarb and sodium 2-isopropylphenate. [BSA] = 2.25×10^{-7} mol L^{-1}, [Isoprocarb] = 3.11×10^{-7} mol L^{-1} and [sodium 2-isopropylphenate] = 5.16×10^{-7} mol L^{-1}.

3.4. Decomposition of the three-way fluorescence EEM stack arrays by PARAFAC

A contour plot (Fig. 5) extracted from the seventh spectral profile of the competitive reaction experiment (Section 2.3.3) reflects the complex system of the mixture of Isoprocarb, sodium 2-isopropylphenate and BSA, in which the concentrations of the three analytes were 3.11×10^{-7}, 5.16×10^{-7} and 2.25×10^{-7} mol L^{-1}, respectively. It was found that there were only two fluorescence peaks because the peaks of Isoprocarb (λ_{em} = 309 nm, λ_{ex} = 270 nm) and sodium 2-isopropylphenate (λ_{em} = 307 nm, λ_{ex} = 270 nm) overlapped severely and any apparent intermediate band was the result of such overlapping.

The loading matrix, ***C***, resolved by PARAFAC refers to the relative concentrations for each of the three individual chemical analytes, i.e., Isoprocarb, sodium 2-isopropylphenate and BSA. It contains information about the trends of the concentration changes of the three analytes at equilibrium in the reaction process. Thus, the concentration of the BSA decreased (Fig. 6) because some of the added sodium 2-isopropylphenate was bound to the free protein; the free Isoprocarb concentration increased gradually with increasing concentration of the added sodium 2-isopropylphenate, which is present in excess. Moreover, the concentration of the free Isoprocarb increased from 0 to 1.5×10^{-8} mol L^{-1} when it was replaced by added sodium 2-isopropylphenate from the Isoprocarb–BSA complex. Thus, these results indicate that Isoprocarb and sodium 2-isopropylphenate bond to the same site on BSA. This is supported by the observation that Isoprocarb is displaced from the BSA–Isoprocarb complex, and it would appear that the binding forces of sodium 2-isopropylphenate binding to BSA are somewhat stronger than those for the Isoprocarb ligand. This conclusion, in turn, is supported by the thermodynamic parameters in Table 1.

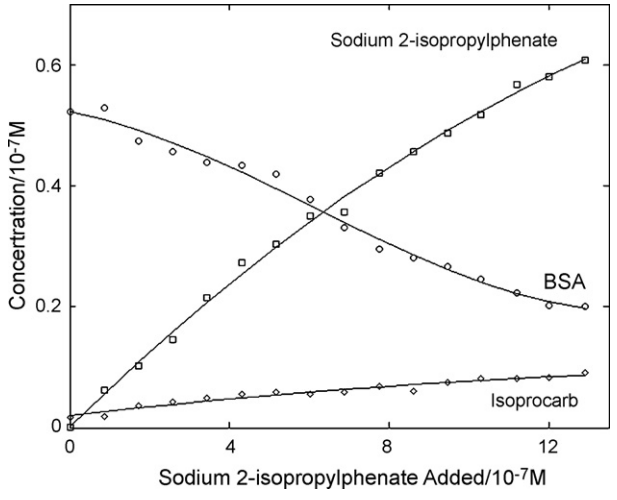

Fig. 6. Relative concentrations for BSA, Isoprocarb and sodium 2-isopropylphenate as extracted by PARAFAC and plotted against different concentrations of sodium 2-isopropylphenate.

4. Conclusion

In this paper, the interaction of Isoprocarb and sodium 2-isopropylphenate with bovine serum albumin (BSA) was studied by fluorescence spectroscopy.

- Isoprocarb and sodium 2-isopropylphenate quenched the BSA fluorescence mainly through a static quenching mechanism, the binding reaction is spontaneous and hydrogen bonds play a major role in the binding of Isoprocarb to BSA.
- In contrast, the weaker hydrophobic interactions are apparently principally involved in the binding of sodium 2-isopropylphenate to BSA.
- Other fluorescence experiments showed that the secondary structure of the BSA molecule changed significantly on interaction with either of the two small pesticide molecules, i.e., the protein was denatured.
- From a comparison of fluorescence emission intensities of Isoprocarb and sodium 2-isopropylphenate, it was estimated that the degradation product, sodium 2-isopropylphenate, is about 4–5 times more toxic than its parent, Isoprocarb.
- Synchronous fluorescence spectroscopy and the resolution of the three-way excitation–emission fluorescence spectra by the PARAFAC method extracted the relative concentration profiles of (a) BSA, (b) Isoprocab and (c) sodium 2-isopropylphenate as a function of the added sodium 2-isopropylphenate.
- It was shown that the degradation product displaced the Isoprocarb pesticide in a competitive reaction with BSA.

Acknowledgements

The authors gratefully acknowledge the financial support of this study by the Natural Science Foundation of China (NSFC20562009), the State Key Laboratories of Electroanalytical Chemistry of Changchun Applied Chemical Institute (SKLEAC2004-3) and Chemo/Biosensing and Chemometrics of Hunan University (SKLCBC2005-22), the Jiangxi Province Natural Science Foundation (JXNSF0620041), and the Program for Changjiang Scholars and Innovative Research Team in Universities (IRT0540).

References

[1] S. Ercelen, A.S. Klymchenko, Y. Mely, A.P. Demchenko, Int. J. Biol. Macromol. 35 (2005) 231–242.
[2] T. Peter, All About Albumin. Biochemistry Genetics and Medical Applications, Academic Press, San Diego, CA, 1996, 9–75.
[3] Y.N. Ni, S.J. Su, S. Kokot, Anal. Chim. Acta 580 (2006) 206–215.
[4] Y.N. Ni, D.Q. Lin, S. Kokot, Talanta 65 (2005) 1295–1302.
[5] O. Divya, A.K. Mishra, Anal. Chim. Acta 592 (2007) 82–90.
[6] J.N. Tian, J.Q. Liu, X. Tian, Z.D. Hu, X.G. Chen, J. Mol. Struct. 691 (2004) 197–202.
[7] Y.Q. Wang, H.M. Zhang, G.C. Zhang, W.H. Tao, S.H. Tang, J. Lumin. 126 (2007) 211–218.
[8] Y. Wang, Y. Cheng, H.F. Sun, Chin. Chem. Lett. 11 (2000) 247–250.
[9] J. Mourik, L.P.A. De Jong, Arch. Toxicol. 41 (1978) 43–48.
[10] B.P. Maliwal, F.E. Guthrie, Mol. Pharmacol. 20 (1981) 138–144.

[11] C. Xu, A.P. Zhang, W.P. Liu, Pest. Biochem. Physiol. 88 (2007) 176–180.
[12] D. Silva, C.M. Cortez, J. Cunha-Bastos, S.R.W. Louro, Toxicol. Lett. 147 (2004) 53–61.
[13] C.N. Yan, H.X. Zhang, Y. Liu, P. Mei, K.H. Li, J.Q. Tong, Acta Chim. Sin. 63 (2005) 1727–1732.
[14] S. Deepa, A.K. Mishra, J. Pharm. Biomed. Anal. 38 (2005) 556–563.
[15] D.S. Saunders, C. Harper, in: A.W. Hayes (Ed.), Principles and Methods of Toxicology, Raven Press, New York, 1994, p. 389.
[16] R.C. Gupta, J. Toxicol. Environ. Health 43 (1994) 383–418.
[17] http://www.pesticideinfo.org/index.html.
[18] R.A. Harshman, Foundations of the PARAFAC procedure: models and conditions for an 'explanatory' multi-mode factor analysis, UCLA Working Papers in Phonetics, 16, 1970, pp. 1–84.
[19] R. Bro, Chemom. Intel. Lab. Sys. 38 (1997) 149–171.
[20] B.F. Pan, F. Gao, L.M. Ao, J. Magn. Magn. Mater. 293 (2005) 252–258.
[21] J.R. Lakowicz, G. Weber, Biochemistry 12 (1973) 4161–4170.
[22] J.B. Xiao, J.W. Chen, H. Cao, F.L. Ren, C.S. Yang, Y. Chen, M. Xu, J. Photochem. Photobiol. A 191 (2007) 222–227.
[23] P.B. Kandagal, S.M.T. Shaikh, D.H. Manjunatha, J. Seetharamappa, B.S. Nagaralli, J. Photochem. Photobiol. A 189 (2007) 121–127.
[24] T.G. Dewey, Biophysical and Biochemical Aspects of Fluorescence Spectroscopy, Plenum Press, New York, 1991, 1–41.
[25] J.H. Tang, F. Luan, X.G. Chen, Med. Chem. 14 (2006) 3210–3217.
[26] F. Moreno, J. Gonzalez-Jimenez, Chem. Biol. Interact. 121 (1999) 237–252.
[27] A. Tricerri, B.C. órsico, J.D. Toledo, H.A. Garda, R.R. Brenner, Biochim. Biophys. Acta 1391 (1998) 67–78.
[28] D.P. Ross, S. Subramanian, Biochemistry 20 (1981) 3096–3102.
[29] Y.J. Hu, Y. Liu, R.M. Zhao, J.X. Dong, S.S. Qu, J. Photochem. Photobiol. A 179 (2006) 324–329.
[30] D.C. Carter, X.M. He, Science 249 (1990) 302–303.
[31] Y.L. Wei, J.Q. Li, C. Dong, S.M. Shuang, D.S. Liu, C.W. Huie, Talanta 70 (2006) 377–382.
[32] U. Kragh-Hansen, F. Hellec, B. de Foresta, M. le Maire, J.V. Moller, J. Biol. Phys. 80 (2001) 2898–2911.
[33] J.N. Miller, Proc. Anal. Div. Chem. 16 (1979) 203–208.
[34] O. Divya, A.K. Mishra, Talanta 72 (2007) 43–48.
[35] S. Rubio, A. Gomez-Hens, M. Ualcarcel, Talanta 33 (1986) 633–640.
[36] J. Jin, X. Zhang, J. Lumin. 128 (2008) 81–86.
[37] T.T. Ndou, I.M. Warner, Chem. Rev. 91 (1991) 493–507.
[38] Y. Yan, J.G. Xu, G.Z. Chen, Sci. China (Series B) 27 (1997) 16–22 (in Chinese).

Talanta 76 (2008) 557–563

Contents lists available at ScienceDirect

Talanta

journal homepage: www.elsevier.com/locate/talanta

Ratiometric sensing of CO_2 in ionic liquid modified ethyl cellulose matrix

Ozlem Oter*, Kadriye Ertekin, Sibel Derinkuyu

University of Dokuz Eylul, Faculty of Arts and Sciences, Department of Chemistry, 35160 Tinaztepe, Izmir, Turkey

ARTICLE INFO

Article history:
Received 15 November 2007
Received in revised form 20 March 2008
Accepted 25 March 2008
Available online 8 April 2008

Keywords:
CO_2 sensing
Optic sensor
HPTS
Ionic liquid
$EMIMBF_4$

ABSTRACT

In this study emission-based ratiometric response of ion pair form of 1-hydroxy-3,6,8-pyrenetrisulfonate (HPTS) to gaseous CO_2 has been evaluated in ionic liquid (IL) containing ethyl cellulose (EC) matrix. The ionic liquid: 1-ethyl-3-methylimidazolium tetrafluoroborate ($EMIMBF_4$); provided longer storage time and highly stable microenvironment for the HPTS molecule due to the buffering effect. The utilization of ionic liquid in ethyl cellulose matrix resulted with superior spectral characteristics. The excitation spectra of HPTS exhibited an atypical isoemmissive point in modified EC matrix at 418 nm which allows ratiometric processing of the signal intensities.

$EMIMBF_4$-doped sensor films exhibited enhanced linear working range between 0 and 100% pCO_2. The signal changes were fully reversible and the shelf life of the $EMIMBF_4$-doped films was extended from 15 to 95 days.

1. Introduction

The monitoring of CO_2 levels in the atmosphere is of vital importance because of the threat of global warming. Over the past two decades, the optical CO_2 sensors based on the absorbance or fluorescence changes of pH indicators have been developed [1–6]. Usually they contain a chemical sensing layer, mostly a pH indicator, at the tip of a fiber which changes the absorbance or fluorescence intensity in response to CO_2. A number of investigations of pCO_2 sensor designs have resulted in commercialization of the products [1–4]. Amao and Nakamura [5] designed an optical CO_2 sensor based on overlay of the CO_2-induced absorbance change of the pH indicator dye α-naphtholphthalein with the fluorescence of tetraphenylporphyrin using ethyl cellulose and polystyrene membranes. They obtained 53.9% signal change from 100% N_2 to 100% CO_2. Neurauter et al. measured gaseous CO_2 levels with an ethyl cellulose-based sensor in the concentration range of 0–30 hPa [7]. They reported a storage lifetime of several weeks. The pH-sensitive fluorescent dye HPTS has been exploited in many previously described carbon dioxide optical sensors [8–13]. Weigl and Wolfbeis proposed a method based on ion pairing between HPTS and a quaternary ammonium cation. The ion pair is dissolved in various kinds of silicone rubbers, and the resulting materials are shown to be useful for optically sensing carbon dioxide over the 0–100 hPa (0–75 Torr) partial pressure range. The reported operational lifetime was in the order of 2 months [8]. Ertekin et al. designed a fiber optic sensing device in a capillary reservoir employing the ion pair form of the fluorescent indicator HPTS, in solution form of ethyl cellulose [13]. They reported 16.2% drift in relative signal change over a period of 5 days when the sensors were stored in a desiccator. Nivens et al. prepared HPTS containing base catalyzed sol–gel layers for pH, carbon dioxide and ammonia measurements [14]. Although the sensor had a long life time of 12 months, the linearized working range was between 0 and 8% pCO_2.

Most of the ethyl cellulose-based sensors using HPTS as indicator material have suffered from limited storage lifetimes arising from photobleaching of the dye, evaporation of their trace amount of water content and degradation of their quaternary hydroxide constituent [5–13]. Therefore, choice of matrix material is important and may be effective to overcome some of these problems. Several investigations have shown that ionic liquids provide better stability for the embedded dye and higher CO_2 adsorption capacity with respect to currently used polymeric materials [15–19]. CO_2 is reversibly soluble in imidazolium-based ionic liquids [20–24]. Additionally, CO_2 is found to be the most soluble gas among ethane, methane, oxygen, nitrogen, argon, hydrogen and carbon monoxide in 1-butyl-3-methylimidazolium tetrafluoroborate [25]. Here, we report a stable solid-state optical sensor prepared by employing $EMIMBF_4$ with ion pair form of HPTS in ethyl cellulose matrix for gaseous CO_2 measurements. As far as we know, there are a few

* Corresponding author. Present address: Dokuz Eylul Universitesi Fen-Edebiyat Fakultesi, Kimya Bolumu 35160, Tinaztepe Buca, Izmir, Turkey.
Tel.: +90 232 412 86 89; fax: +90 232 453 41 88.
E-mail address: ozlem.oter@deu.edu.tr (O. Oter).

0039-9140/$ – see front matter © 2008 Elsevier B.V. All rights reserved.
doi:10.1016/j.talanta.2008.03.047

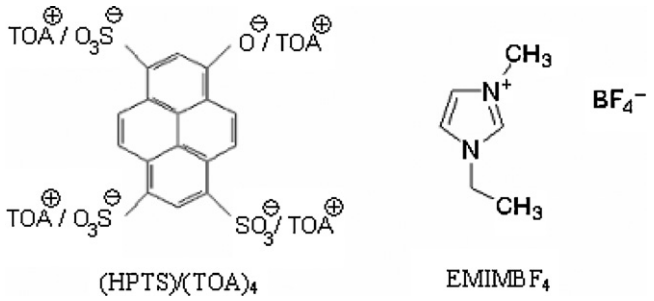

Fig. 1. Chemical structure of the ion pair (HPTS)/$(TOA)_4$ and the RTIL; 1-ethyl-3-methylimidazolium tetrafluoroborate ($EMIMBF_4$).

reported studies employing ionic liquids in solid thin films for CO_2 sensing purposes. Borisow et al. used ionic liquid in silicon matrix and reported excellent linearity for their calibration plots [26].

Our sensor design combines the advantages of both liquid-RTILs and the solid-ethyl cellulose matrix providing better spectral characteristics, wide dynamic range and long shelf life.

2. Experimental

2.1. Materials

All solvents and chemicals were of analytical grade and purchased from Merck, Fluka, and Riedel. The pH and CO_2 sensitive fluorescent dye, 8-hydroxypyrene-1,3,6-trisulfonic acid trisodium salt was from Fluka and used in the ion pair form. The ion pair was prepared by the reagent tetraoctyl ammonium bromide (TOABr) which was obtained from Sigma. The polymer ethyl cellulose was from organics with an ethoxy content of 48%. The plasticizer, dioctyl phthalate (DOP) was from Aldrich. The additive tetraoctyl ammonium hydroxide (TOAOH) was from Fluka; in the form of 20% solution in methanol. The ionic liquid, 1-ethyl-3-methylimidazolium tetrafluoroborate ($EMIMBF_4$) was supplied from Fluka. Cylinders of carbon dioxide and nitrogen gas of 99.99% purity were obtained from Linde Gas, Izmir, Turkey. The schematic structures of the employed ion pair and the ionic liquid were shown in Fig. 1.

2.2. Instrumentation and gas measurements

Steady-state fluorescence emission and excitation spectra were measured using Varian Cary Eclipse Spectrofluorometer with a Xenon flash lamp as the light source. Fluorescence measurements were carried out with fiber optic probe (2 m long) and solid sample tip accessories constructed on the spectrofluorometer. For instrumental control, data acquisition and processing of time-based measurements; the software package of the spectrofluorometer was used. The tip of the bifurcated fiber optic probe was interfaced with the sensing film in a sealed small beaker. Gas mixtures were introduced on the sensing membrane via a diffuser needle under ambient conditions. The humidification of the gases was accomplished by bubbling the gas stream through thermostated wash bottles filled with water at 25 °C at constant relative humidity level of 100% (see Fig. 2).

Gaseous CO_2 and N_2 were mixed in the concentration range of 0–100% in a Sonimix 7000A gas blending system. The output flow rate of the gas mixture was maintained at 550 mL min^{-1}. All of the gas measurements were performed with at least three different films for the same experiment and the error bars show the standard deviations.

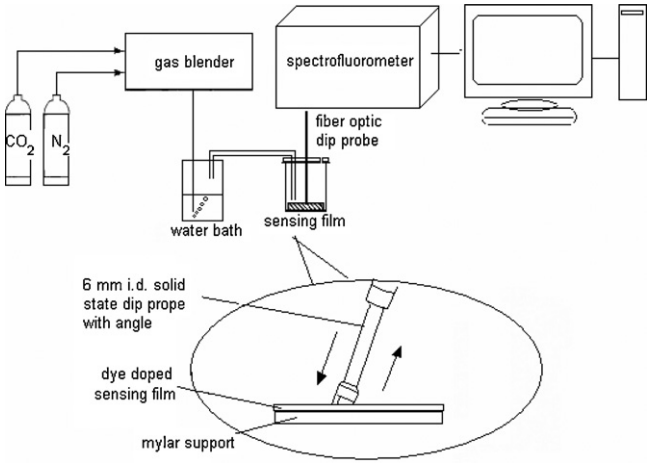

Fig. 2. Schematic illustration of experimental set-up used for CO_2 sensing.

2.3. Synthesis of ion pair

The ion pair between anionic form of the HPTS and the tetraoctylammonium counterion (TOA^+) has the composition (HPTS)/$(TOA)_4$ (Fig. 1) and was prepared according to the following literature method [8,13]: 200 mg of the trisodium salt of HPTS and the fourfold molar quantity of TOABr (834 mg) were dissolved in 30 mL of water containing 1% sodium carbonate and 30 mL of CH_2Cl_2, respectively, and were mixed in a separatory funnel. After a few minutes the ion pair was completely extracted from the aqueous phase into the organic phase. The organic phase was washed three times with 0.05 M NaOH and separated. After the evaporation of organic solvent under vacuum, the ion pair was obtained. The ion pair is less subject to leaching from the polymer matrix than the HPTS sodium salt owing to its greater affinity to the ethyl cellulose matrix.

2.4. Cocktail preparation procedures

The effect of the ionic liquid on CO_2 sensitivity was examined for the plasticizer free (C-1–C-3) and plasticizer containing (C-4–C-5) sensor films. The prepared cocktails contained in the range of 33–80% $EMIMBF_4$ by weight. Cocktail 5 was prepared by mixing 0.06 g of ethyl cellulose and 0.06 g of DOP in 0.75 mL of tetrahydofuran (THF). 200 μL of the TOAOH and 1 mg of ion pair (HPTS)/$(TOA)_4$ were added into the mixture and mixed in a glass vial. Then 0.12 g of $EMIMBF_4$ was added into the sensor composition. Other cocktails were prepared by the similar procedure. All of the cocktail compositions were shown in Table 1.

Prior to the experiments, the employed cocktails were completely converted to the basic form. The resulting mixtures were spread onto a 125 μm polyester support (Mylar TM type) with a spreading device. Thickness of the films were measured using Tencor Alpha Step 500 Prophylometer and found to be 5.10 mm. This result was an average of eight measurements and exhibited a standard deviation of ±0.081.

Table 1
Compositions of the cocktails used as CO_2-sensing agents

Cocktail name	EC (g)	THF (mL)	DOP (g)	TOAOH (μL)	Ionic liquid (g)
C-1	0.06	0.75	–	200	0.12
C-2	0.06	0.75	–	200	0.24
C-3	0.06	0.75	–	200	0.06
C-4	0.06	0.75	0.06	200	0.06
C-5	0.06	0.75	0.06	200	0.12
C-6	0.06	0.75	0.06	200	–

Table 2
Comparison of response characteristics of newly offered sensor and literature information

pH sensitive dye	Matrix material	Storage conditions	Storage time	Dynamic working range	Ref.
HPTS$(TOA)_4$ ion pair	Ethyl cellulose and ionic liquid	Ambient laboratory conditions	95 days	1–100% CO_2	Current sensor
HPTS$(TOA)_4$ ion pair	Ethyl cellulose and Teflon AF	In refrigerator	Several days	0.05–7 hPa pCO_2	[12]
HPTS $(CTA)_3$ ion pair	Ethyl cellulose	In a drying chamber at 90 °C	About 6 h	1–50% CO_2	[10]
	Ethyl cellulose with additive ionic cellulose	In water or in humid air	Over 5 months	2–100% CO_2	
Thymol blue ion pair + (Ru(dph-bpy)3-(TMS)2)	Ethyl cellulose	In air and exposed to sunlight	A few days	0–30 hPa pCO_2	[7]
		In sealed bags containing sodium carbonate	2 months		
HPTS$(TOA)_4$ ion pair	Ethyl cellulose	In a desiccator containing sodium carbonate and silica gel	5 days	1–20 hPa pCO_2	[13]
HPTS ion pair + Ru(dpp)3TMS2)	Ethyl cellulose and black silicone rubber	In the dark, under a CO_2 atmosphere, free of other acidic gases.	Not mentioned	0–10 hPa CO_2	[29]

The polyester support was optically fully transparent, ion impermeable and exhibited good adhesion to EC. The most important function of the polyester was to act as a mechanical support because the thin EC films were difficult to handle. All of the thin films were kept in a closed box in the ambient air of the laboratory. In order to obtain the emission spectra, the film was placed into a sealed beaker and the excitation and corrected emission spectra were recorded with fiber optic probe.

3. Results and discussion

3.1. Choice of matrix material

In most previous sensor designs quaternary hydroxides were added into the sensing cocktail as a counter ion to increase sensitivity and storage time [7–10,13,27]. These quaternary hyroxides are neutralized by uptake of carbon dioxide from the air and forms a lipophilic hydrogencarbonate buffer in the polymer. The excess quaternary hydroxides were neutralized by atmospheric carbon dioxide, forming a hydrogen carbonate buffer in the matrix and this can be used to tune the sensitivity and to improve the storage stability of the sensor. However, the presence of quaternary hydroxides alone is not enough for long-term stability of the ethyl cellulose-based CO_2 sensing films. Several authors explained the slow decay of the quaternary ammonium hydroxides via Hofmann degradation [27,28]. Schröder and Klimant attributed the short storage times to the presence of other acidic gases like NO_x or SO_2 which can permeate through the sensor membrane and irreversibly protonate the indicator [29]. However, many such sensors are reported to be stable for a prolonged time when stored in the absence of acidic gases (see Table 2). Neurauter et al. used the pH-indicator HPTS with TOAOH in the ethyl cellulose matrix and reported the storage time as several days when the sensor films were kept in a refrigerator [12]. In another work, Neurauter et al. reported stable signals for their sensor films over weeks if stored in sealed bags along with sodium carbonate in the dark [7]. Wolfbeis et al. stated 5 months of storage lifetime for electrostatically bound HPTS to the surface of particles of aminocellulose in silicone polymer [10].

In our offered matrix, TOAOH was used together with the ionic liquid: 1-ethyl-3-methylimidazolium tetrafluoroborate as an internal buffering system which resulted with increased storage times even under ambient air of the laboratory.

Additionally, the $EMIMBF_4$ provides an increased solubility for CO_2 in the sensing membrane. Gas molecules are believed to occupy 'molecular cavities' within ionic liquids. 10 to 20 times higher solubilities were reported for CO_2 in water miscible ionic liquids than that of in conventional solvents, polymer matrices, or water. According to the literature the high solubility of CO_2 in RTILs arises

Table 3
Spectral characteristics of HPTS or (HPTS)/$(TOA)_4$ in phosphate buffer, in ethyl cellulose and in C-1,C-2, C-3, C-4 and C-5

	Excitation, acidic form (nm)	Emission, acidic form (nm)	Excitation, basic form (nm)	Emission, basic form (nm)	Isoemissive point (nm)
HPTS in phosphate buffer	404, 382, 368(s)	510	457, 395, 369(s)	510	EX 417 EM 510
(HPTS)/$(TOA)_4$ in ethyl cellulose film	402, 382(s), 369	429	468, 458(s), 402, 370	515	– –
(HPTS)/$(TOA)_4$ in C-1	401, 383, 372	423	465, 404, 375	511	EX 418 EM–
(HPTS)/$(TOA)_4$ in C-2	401, 383, 372	422	465, 405, 374	512	EX 418 EM–
(HPTS)/$(TOA)_4$ in C-3	401, 383, 372	422	465, 405, 376	513	EX 418 EM–
(HPTS)/$(TOA)_4$ in C-4	401, 383, 372	422	465, 406, 377	514	EX 418 EM
(HPTS)/$(TOA)_4$ in C-5	401, 383, 372	421, 518	465, 406, 379	518	EX 418 EM–

(s) denotes shoulder on peak.

from formation of weak Lewis acid–base complexes between CO_2 (the electron-pair acceptor) and anion of the RTIL (the electron-pair donor) [21,22].

Hydration of CO_2 and subsequent protolysis is also essential for the functionality of the optical CO_2 sensors [27,30]. It has been reported that the presence of F^- in hydrated molten ammonium salts results in facilitated transport of CO_2 via a catalyzed bicarbonate reaction [15,21,22]. In the presence of trace amounts of water, $[PF_6]^-$ decomposes into HF and subsequently catalyzes the HCO_3^- formation in accordance with the reaction:

$$2F^- + H_2O + CO_2 \leftrightarrow HCO_3^- + HF_2^-$$

Similarly, it is expected that the $[BF_4]^-$ anion of $EMIMBF_4$ would decompose into HF and F^- ions and would catalyze the bicarbonate formation.

3.2. Excitation and emission spectra of HPTS in the presence of $EMIMBF_4$

The emission-excitation spectra related data of the sensing films were gathered in Table 3. $(HPTS)/(TOA)_4$ in $EMIMBF_4$-doped ethyl cellulose (C-3) was excited at 468 nm which is identical with the excitation wavelength of $(HPTS)/(TOA)_4$ in $EMIMBF_4$-free ethyl cellulose matrix. Increasing amounts of the ionic liquid in the membrane (C-1 and C-2) created a 3 nm of blue shift in the excitation wavelength with respect to the IL-free membranes. This blue shift is referred to the increasing hydrophilic character of the IL-doped membrane. Nevertheless, the HPTS is excited at a lower wavelength; at 457 nm in aqueous media. Therefore the IL-doped matrix cannot be concluded as polar as water.

The most attractive result obtained from the spectral data of $(HPTS)/(TOA)_4$ in $EMIMBF_4$-doped EC films was the occurrence of an isoemmissive point at 418 nm in the excitation spectra. This makes the IL-doped ethyl cellulose matrix superior with respect to the IL-free one allowing ratiometric measurements.

The imidazolium-based ionic liquids have non-negligible absorption beyond 300 nm and unusual shifting fluorescence. This fluorescence behavior arises from the presence of energetically different associated forms of the imidazolium ions [18]. We therefore investigated the possibility of interference of the intrinsic fluorescence of $EMIMBF_4$ with the fluorescence of $(HPTS)/(TOA)_4$. Fig. 3 reveals that the observed fluorescence of the studied ionic liquid-doped HPTS free film is negligible and does not limit the sensing ability of the films containing $(HPTS)/(TOA)_4$.

3.3. Gaseous CO_2 sensing

Most of the CO_2 sensing films contain the ion pair form of HPTS and the quaternary ammonium base (TOAOH) in ethyl cellulose matrix. TOA^+OH^- is usually added as a counter ion stabilizing the anionic (deprotonated) form of the HPTS in the lipophilic matrix. In such designs, the sensing scheme is based on two processes, the first

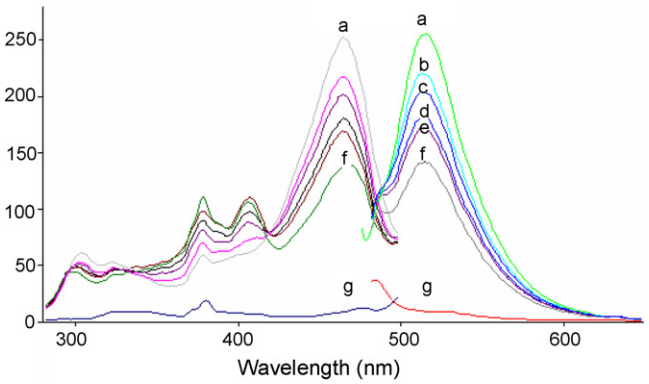

Fig. 3. Emission and excitation spectra of $(HPTS)/(TOA)_4$ in the sensing film prepared from C-5: (a) 0%, (b) 20%, (c) 40%, (d) 60%, (e) 80%, (f) 100% CO_2 and the blank film containing $EMIMBF_4$ (λ^{ex}_{max} = 465 nm, 406 nm; λ^{em}_{max} = 518 nm; isoemissive point at excitation spectra: 418 nm).

being the diffusion of CO_2 through the membrane into the sensing region, the second being the reaction of the gas with anionic and highly fluorescent HPTS phenolate anion. The indicator is functional owing to the water content of the ion pair, which causes the formation of carbonic acid with CO_2. Hydration of CO_2 and subsequent protolysis decreases the fluorescence intensity of HPTS at 518 nm and converts fluorescent HPTS anion (Dye^-) into the less fluorescent HPTS (Dye) form. The following equation is used to describe the reaction:

$$TOA^+/Dye^- + xH_2O + CO_2 \rightleftharpoons_< TOA^+/HCO_3^- + (x-1)H_2O + \text{H-Dye}$$

In our approach, ionic liquid: 1-ethyl-3-methylimidazolium tetrafluoroborate was used as an internal buffering system together with TOAOH. Fig. 4 shows the response characteristics of $[EMIM]BF_4$ containing plasticizer free matrices after exposure to CO_2. The composition C-1 exhibited high sensitivity and gradient up to 20% CO_2 concentrations. However, deviation from linearity was observed

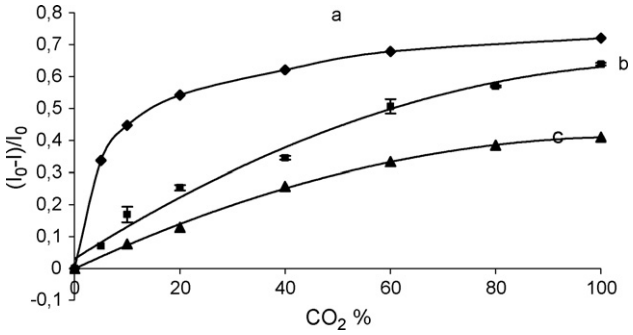

Fig. 4. Plots of $(I_0 - I)/I_0$ versus carbon dioxide concentration for the ionic liquid-doped plasticizer-free cocktails: (a) C-1, (b) C-2 and (c) C-3.

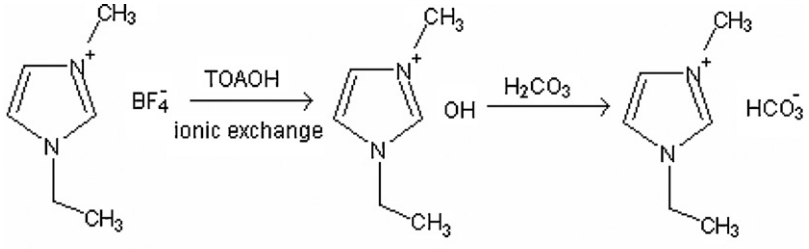

Scheme 1. The anion exchange scheme between TOAOH and $EMIMBF_4$ and consequent interaction with H_2CO_3.

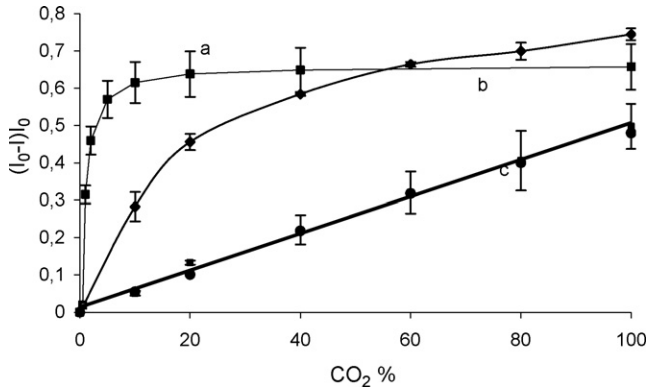

Fig. 5. Plots of $(I_0 - I)/I_0$ versus carbon dioxide concentration for the plasticizer containing ionic liquid free cocktails of (a) C-6 and ionic liquid-doped, (b) C-4 and (c) C-5.

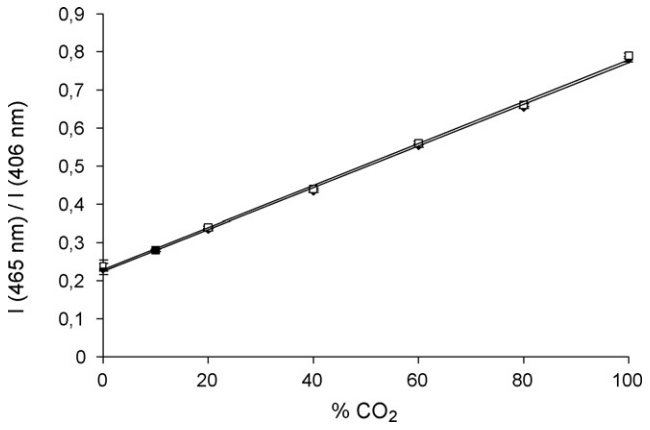

Fig. 6. Ratiometric calibration plots for the freshly prepared and stored (68 days) sensing films.

when exposed to the high partial pressures of CO_2. The C-2 which has the highest amount of ionic liquid exhibited better linearity with respect to C-1 and C-3.

In our case, [EMIM]OH moieties are produced by anion exchange with the present TOAOH in the sensing composition according to the following reaction (see Scheme 1). The ([EMIM]OH) forms a buffer-like system by neutralization with the hydrated CO_2 or carbonic acid (H_2CO_3) which is in accordance with the literature information. The resulting product is [EMIM]HCO_3 [31]. Formation of such a buffer system tunes the sensitivity of the sensor and enhances the long-term stability since it slowly acts as a sink for acidic species. Therefore the well known hyperbolic response [5,7,13] of the (HPTS)/$(TOA)_4$ in ethyl cellulose matrix becomes linear. The stoichiometry of TOAOH/[EMIM]BF_4 is critical and tunes the sensitivity of the sensor via the formation of [EMIM]OH moieties. In this work 1:1 (C-3), 1:2 (C-1) and 1:4 (C-2) mol ratios were employed for TOAOH and $EMIMBF_4$, respectively (see Table 1 and Fig. 4). After a threshold value (1:2) the addition of [EMIM]BF_4 does not enhance the sensor response. This result can be attributed to the slight intrinsic acidic–basic characteristics of the employed ionic liquid. Additionally, presence of excess amounts of $EMIMBF_4$ results with increased polarity, poor optical transparency and unadequate adhesion of thin film to Mylar support.

Fig. 5 shows the response characteristics of [EMIM]BF_4-free and [EMIM]BF_4 containing plasticized matrices after exposure to CO_2. The cocktail compositions of C-4, C-5 and C-6 contain 33, 25 and 50% plasticizer by weight which covers convenient applications for polymer-based sensors [10]. After exposure to CO_2, the C-3 and C-4 exhibited relative signal changes of 40% and 75%, respectively. As expected, in presence of plasticizer (C-4), the accessibility of the CO_2 molecules into the membrane become easier due to the increased permeability of the polymer films. The sensor membrane prepared from C-5 exhibited completely linear response to CO_2 in the concentration range of 0–100% CO_2 with a correlation coefficient of $R^2 = 0.9948$ (Fig. 5). The attained relative signal change was 53% in the direction of a decrease in emission intensity upon exposure to 100% CO_2. The increase in the linear working range and accompanying decrease in the relative signal change can be attributed to the above discussed buffering effect of the ionic liquid; $EMIMBF_4$.

In addition, the occurrence of an isoemmissive point at 418 nm in the excitation spectra of (HPTS)/$(TOA)_4$ allows the construction of the calibration graph with ratiometric data (Fig. 3). Ratiometric measurements are desirable for sensor applications, due to the enhanced accuracy of the data processing [32]. The technique depends on the measurement of the ratio of the fluorescence intensity at two wavelengths. Such systems are not affected from changes in fluorophore concentrations arising from photobleaching or leaching of the indicator dye from matrix [33]. Furthermore, they are not influenced by fluctuations in excitation light source intensities. Fig. 6 shows the calibration plots of freshly prepared and stored films after ratiometric data processing. (I_{406}/I_{465}) refers to the fluorescence intensity ratios of the sensing films at 406 and 465 nm, respectively. The regression coefficient of the plot for fresh films was $R^2 = 0.9990$. Additionally, the utilization of the ratiometric data processing resulted with smaller standard deviations with respect to the conventional data processing.

3.4. Response time and recovery characteristics

The τ_{90} response time (the time to achieve 90% of the overall signal change) of C-5 was in the range of 20–54 s on exposure to CO_2 (see Fig. 7). The reported response times of the employed films include the dead volume of gas tubings rather than the true response times. The system used here was for characterization purposes only, and a significantly lower tubing volume or a micro flow cell is required for shorter response times.

The initial signal intensities for the sensing films could be completely recovered and no drift was observed even after the 9th cycle. Between the 1st and 9th cycles the level of reproducibility of upper signal levels was 672 ± 5 ($n = 9$). The regeneration time was 180 s. This long regeneration time can be attributed to the low solubility of

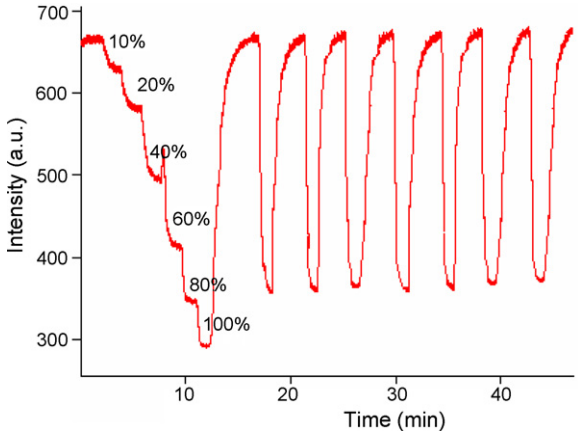

Fig. 7. Kinetic response of the sensing films prepared from C-5.

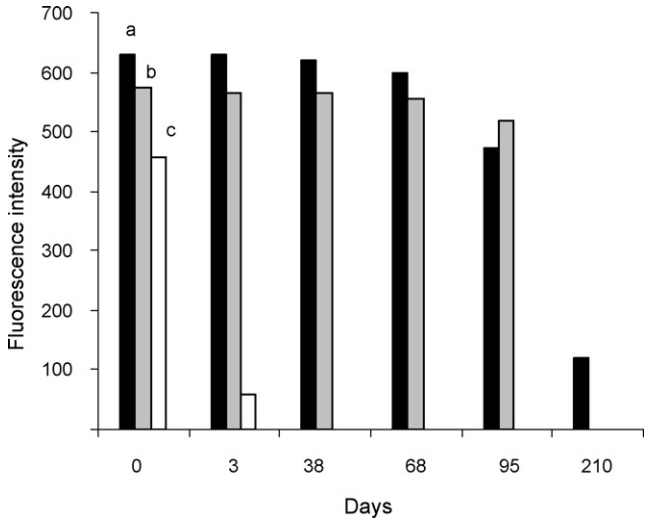

Fig. 8. Long-term stability of the sensing films prepared from (a) C-5, (b) C-1 and (c) C-6.

the regeneration agent, N_2, in ionic liquid containing media as well as experimental setup. The reported solubility of CO_2 is 374-fold of the solubility of N_2 in butylmethylimidazolium hexafluorophosphate ([bmim][PF_6] [24].

Due to the different gas sorption–desorption dynamics of $EMIMBF_4$, desorption of CO_2 by vacuuming may be faster.

3.5. Sensor stability

Fig. 8 illustrates the stability of the sensing films prepared from C-1, C-5 and C-6 which were stored in ambient laboratory conditions. No significant decrease in the fluorescence intensity of the films was observed after 95 days for the ionic liquid containing cocktails; C-1 and C-5. 95 days later, the $(HPTS)/(TOA)_4$ in C-1 and C-5 had lost its original fluorescence intensity by 10 and 24%, respectively but still had efficient luminescence for CO_2 measurements. However after 210 days, the 80% of luminescence of $(HPTS)/(TOA)_4$ in C-5 was lost and the sensor was incapable for CO_2 measurements. The IL-free composition; C-6; had completely lost its sensing capability within 3 days (see Fig. 8).

In our earlier studies [34], we have reported the storage stability time for HPTS in pure ionic liquid media as 212 days. In the newly employed solid-state approach, the considerable amount of ionic liquid (50%, w/w) was mixed with ethyl cellulose and the sensing films were prepared. The currently reported storage time of the ion pair form of HPTS is between the storage time of this dye in ethyl cellulose and in pure $EMIMBF_4$. The stability of the sensors increases by increasing amounts of the doped ionic liquid into the matrix.

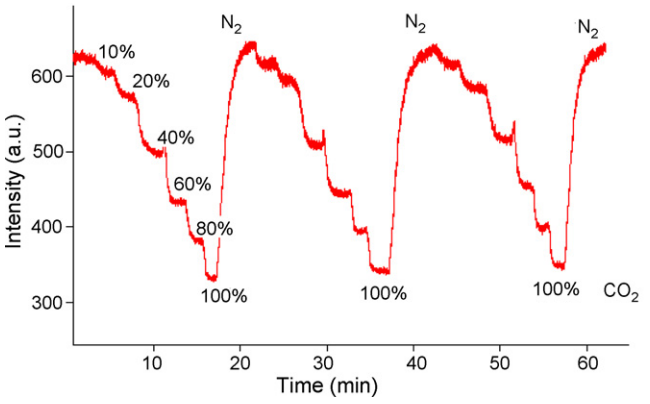

Fig. 9. Kinetic response of the sensing films prepared from C-5 after storage of 68 days.

Fig. 9 illustrates the kinetic response of the sensing film prepared from C-5 after a storage time of 68 days. The linearized calibration plots of the freshly prepared and stored sensor membranes can be described by the equations $y = 0.0055x + 0.2294$ ($R^2 = 0.9983$) and $y = 0.0055x + 0.2246$ ($R^2 = 0.9990$), respectively (see Fig. 6). We have demonstrated that the $EMIMBF_4$-doped sensor membranes exhibited a stable and reproducible response for carbon dioxide measurements.

4. Conclusion

Here we report a RTIL-doped ethyl cellulose matrix for gaseous carbon dioxide sensing. $EMIMBF_4$ can be effectively used as an additive in ethyl cellulose matrix for gas phase measurements. RTILs are discussed as green solvents. Several unique properties of the ILs, mainly their reversible CO_2 solubility and selectivity, negligible vapor pressure, dye-dissolution properties, water-miscible characteristics and optical transparency, make them promising matrix materials or additives for CO_2 sensor design. The $EMIMBF_4$ employing sensor exhibited a storage time of longer than 3 months, enhanced repeatability; wide dynamic range (between 0 and 100% CO_2) and better spectral characteristics allowing ratiometric measurements with more precise data. The offered sensor is unsuitable for monitoring of CO_2 in physiologically important CO_2 concentrations because of its relatively lower sensitivity between 0 and 5% CO_2 but can be a potential for environmental monitoring and food packaging technology in which usually high carbon dioxide levels up to 100% are desirable.

Acknowledgements

Funding for this research was provided by the TUBITAK-(Kariyer Project-104M268) and Scientific Research Funds of Dokuz Eylul University (04 kb Fen 104 and 04.kb. Fen.019).

References

[1] M. Yafuso, J.K. Suzuki, Gas sensors, US Patent 4,824,789 (1989).
[2] J.E. Alderete, A.D. Olstein, S.C. Furlong, US Patent 5,714,121 (1998).
[3] W. Adrian, B.S. Mark, A.G. Novartis, US Patent 6,338,822 (2002).
[4] S.C. Furlong, US Patent 5,672,515 (1997).
[5] Y. Amao, N. Nakamura, Sens. Actuators B 100 (2004) 347.
[6] B. Müller, P.C. Hauser, Analyst 121 (1996) 339.
[7] G. Neurauter, I. Klimant, O.S. Wolfbeis, Anal. Chim. Acta 382 (1999) 67.
[8] B.H. Weigl, O.S. Wolfbeis, Anal. Chim. Acta 302 (1995) 249.
[9] C. Bültzingslöwen, K.A. McEvoy, C. McDonagh, B.D. MacCraith, I. Klimant, C. Krause, O.S. Wolfbeis, Analyst 127 (2002) 1478.
[10] O.S. Wolfbeis, B. Kovacs, K. Goswami, S.M. Klainer, Microchim. Acta 129 (1998) 181.
[11] C. Malins, B.D. MacCraith, Analyst 123 (1998) 2373.
[12] G. Neurauter, I. Klimant, O.S. Wolfbeis, Fresenius J. Anal. Chem. 366 (2000) 481.
[13] K. Ertekin, I. Klimant, G. Neurauter, O.S. Wolfbeis, Talanta 59 (2003) 261.
[14] D.A. Nivens, M.V. Schiza, S.M. Angel, Talanta 58 (2002) 543.
[15] L.A. Blanchard, D. Hancu, E.J. Beckman, J.F. Brennecke, Nature 399 (1999) 28.
[16] L.A. Blanchard, Z.Y. Gu, J.F. Brennecke, J. Phys. Chem. B 105 (2001) 2437.
[17] C. Cadena, J.L. Anthony, J.K. Shah, T.I. Morrow, J.F. Brennecke, E. Maginn, J. Am. Chem. Soc. 126 (2004) 5308.
[18] P. Scovazzo, D. Camper, J. Kieft, J. Poshusta, C. Koval, R.D. Noble, Ind. Eng. Chem. Res. 43 (2004) 6855.
[19] D. Camper, P. Scovazzo, C. Koval, R.D. Noble, Ind. Eng. Chem. Res. 43 (2004) 3049.
[20] S.N.V.K. Aki, B.R. Mellein, E.M. Saurer, J.F. Brennecke, J. Phys. Chem. B 108 (2004) 20355.
[21] J.L. Anthony, E.J. Maginn, J.F. Brennecke, J. Phys. Chem. B 106 (2002) 7315.
[22] E.D. Bates, R.D. Mayton, I. Ntai, J.H. Davis, J. Am. Chem. Soc. 124 (2002) 926.
[23] A.P.S. Kamps, D. Tuma, J. Xia, G. Maurer, Chem. Eng. Data 48 (2003) 746.
[24] J.L. Anthony, E.J. Maginn, J.F. Brennecke, J. Phys. Chem. B 105 (2001) 10942.

[25] J. Jacquemin, M.F.C. Gomes, P. Husson, V. Majer, J. Chem. Thermodyn. 38 (2006) 490.
[26] Borisov, Waldhier, Klimant, Wolfbeis, Chem. Mater. 19 (2007) 6187.
[27] A. Mills, Q. Chang, N. McMurray, Anal. Chem. 64 (1992) 1383.
[28] A. Waldner, S.M. Barnard, Optical carbon dioxide sensors, US Patent 6,338,822 (2002).
[29] C.R. Schröder, I. Klimant, Sens. Actuators B 107 (2005) 572.
[30] W. Stumm, J.J. Morgan, Aquatic Chemistry, 2nd ed., Wiley, New York, 1981.
[31] G. Ou, M. Zhu, J. She, Y. Yuan, Chem. Commun. (2006) 4626.
[32] H.R. Kermis, Y. Kostov, P. Harms, G. Rao, Biotechnol. Prog. 18 (2002) 1047.
[33] A. Song, S. Parus, R. Kopelman, Anal. Chem. 69 (1997) 863.
[34] O. Oter, K. Ertekin, D. Topkaya, S. Alp, Anal. Bioanal. Chem. 386 (2006) 1225.

Talanta 76 (2008) 485–496

Contents lists available at ScienceDirect

Talanta

journal homepage: www.elsevier.com/locate/talanta

Review

Potentiometric transducer based biomimetic sensors for priority envirotoxic markers—An overview

T. Prasada Rao*, R. Kala

Inorganic and Polymer Materials, National Institute for Interdisciplinary Science & Technology (CSIR), Trivandrum 695019, India

ARTICLE INFO

Article history:
Received 5 February 2008
Received in revised form 23 March 2008
Accepted 24 March 2008
Available online 4 April 2008

Keywords:
Imprinted polymers
Potentiometric sensors
Envirotoxic markers
Cation/anion/molecular recognition

ABSTRACT

Most of the potentiometric sensing electrodes offer detection limits of the order of ~1 μmol L^{-1} rarely stretching down to 0.1 μmol L^{-1}. Recent advances have made it possible to bring these levels down to 0.01–10 nmol L^{-1} for some inorganic ions. Most of these electrodes (barring a few) have come up to expectations in terms of selectivity in spite of significant strides made in the design and synthesis of novel chemical receptors. Imprinted polymers or plastic antibodies which rely on lock and key mechanism can, in principle, selectively rebind and sense a particular analyte in a host of other analogous species of similar size, shape and geometry. Thus, the integration of imprinted polymers with potentiometric transducers has immense potentialities in the fabrication of commercial sensing devices. This review gives an overview of research efforts made so far in this direction, critically discusses the virtues and vices and presents the futuristic scenario on imprinted polymer based potentiometric sensors.

Contents

1. Introduction

Analytical chemistry started as an art and then developed into full-fledged science. The two important stages of analytical method development include classical and instrumental methods. The instrumental method passes through phases of analog, digital, microprocessor and computer controlled, in that order. Even though there is no clear cut demarcation, it is understood that "*trace analysis*" pertains to μg mL^{-1} or ppm level determination of various analytes or measurands and "*ultratrace analysis*" refers to ng mL^{-1} or ppb and lower. Depending on the volume of sample employed in particular analysis, it is termed "*micro*", "*semimicro*" and "*macro*" analysis. The importance of detection and quantification of toxicants at ultratrace levels in complex environmental

* Corresponding author. Tel.: +91 471 2515317; fax: +91 471 2491712.
E-mail address: tprasadarao@rediffmail.com (T. Prasada Rao).

0039-9140/$ – see front matter © 2008 Elsevier B.V. All rights reserved.
doi:10.1016/j.talanta.2008.03.044

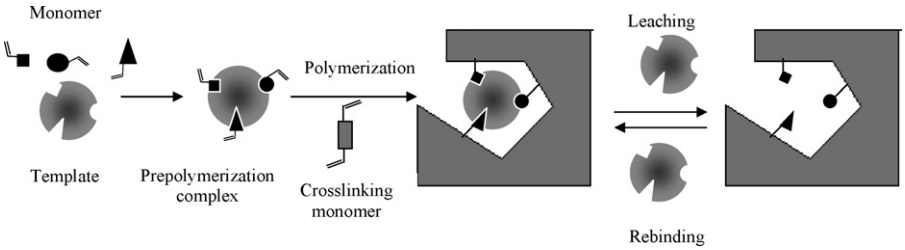

Fig. 1. Schematic representation of imprinting process.

samples is now well recognized. In addition, the demand from other branches of science such as metallurgy, geology, biology, agriculture, archaeology, medicine, forensic science, etc., has brought forth many a powerful analytical tools for quantification of both inorganic and organic analytes. Thus, spectral, electrochemical, X-ray, radiochemical and mass spectrometric techniques either singularly or in combination with prior separation (i.e. coupled or hyphenated techniques) have come into existence and many have found applications for a given analytical demand. In turn, analytical chemistry has played a key role and contributed immensely to the growth of other branches of sciences as mentioned above. As each technique provides a different and unique approach for quantification of toxic analytes in environmental samples—"ENVIROTOXIC MARKERS", the choice of a particular technique depends primarily on criteria such as "*Sensitivity*", "*Selectivity*" and "*Accuracy and precision*" and auxiliary criteria such as cost of equipment, time of analysis, scope, sampling and standards requirements [1].

1.1. Sensors

Gas/high performance liquid chromatography mass spectrometry (GC/HPLC-MS) and inductively coupled plasma-MS are undoubtedly highly sensitive and selective for various organic and inorganic envirotoxic markers. But, these are laboratory based instruments, require skilled technicians, demand tedious transportation and storage protocols and often need time consuming separation/clean-up methodologies. In addition, long analysis time and extensive sample handling with multiple washing steps are other limitations. Hence, design and development of "PORTABLE SENSORS" are highly desirable for facilitating the task of on-site monitoring and field studies. The quality and efficacy of sensors are determined by selectivity, sensitivity (high signal-to-noise ratio), quality and stability of various components of sensing device, effective integration with transducer, affordability, non-toxicity, reusability and response time. Thus, sensors find widespread application in research, agriculture (diagnosis of plant and animal diseases, agricultural chemical monitoring, quality control of meat and plant products), chemical and pharmaceutical industry (fermentation monitoring, food processing and drug development) and in environment (remote/continuous/point source monitoring of air, water and solids), medicine and pharmacology (drug screening and in vivo monitoring), defence (chemical and biological warfare agents), deep ocean and space exploration (in extreme environments) [2].

1.2. Molecularly imprinted polymers

Molecularly imprinted polymers (MIPs) are crosslinked polymers with specific binding for a particular analyte [3,4]. These binding sites are tailor made in situ by the copolymerization of functional and crosslinking monomers in the presence of a print molecule called the "*template*". After polymerization, the removal of template leaves recognition sites that are complementary to the print molecule in terms of size, shape and functionality (see Fig. 1). So, ideally a molecular memory is introduced in the polymer by the imprinting process, which results in selective rebinding of the template in preference to other closely related molecules [5–7]. Thus, MIPs are synthetic polymers or plastic locks for template keys having predetermined selectivity for a particular analyte comparable to antibodies. In addition, MIPs unlike biological counterparts are highly stable against mechanical stress, elevated temperatures and high pressures, resistant to harsh environments such as acids, bases and organic solvents. The different strategies of molecular imprinting include (i) "*covalent*" or "*pre-organized*", (ii) "*non-covalent*" or "*self-assembly*", (iii) "*semi-covalent*" or "*sacrificial spacer*" (iv) "*metal ion*" and (v) "*metal-chelate*" and have been used in various fields

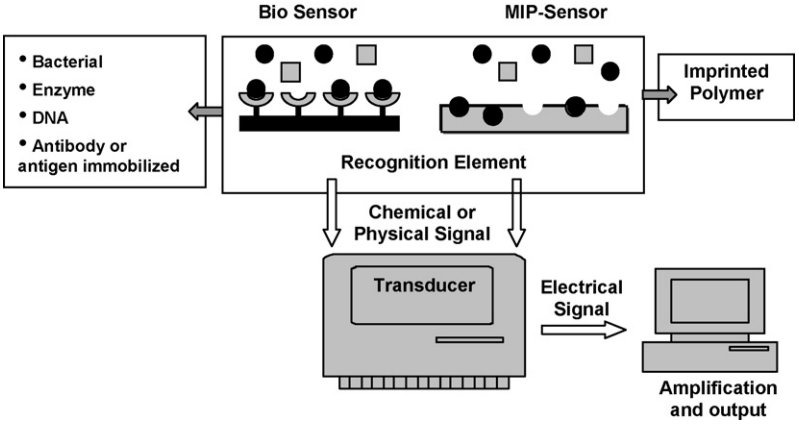

Fig. 2. Schematic representation of a MIP-based biomimetic sensor vis-à-vis biosensor.

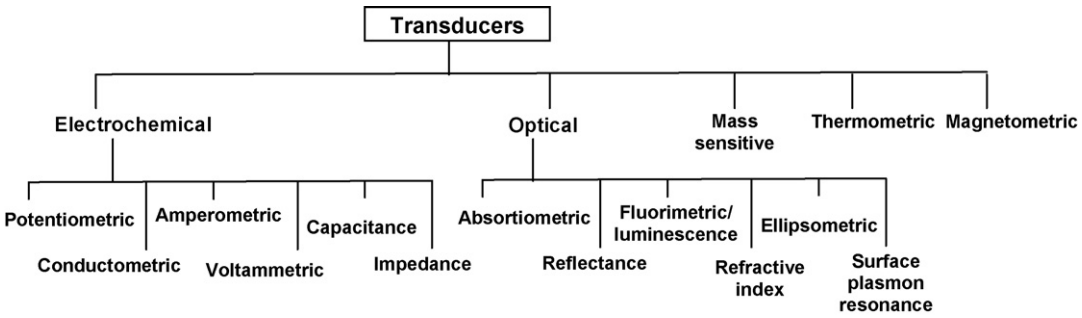

Fig. 3. Popular transducers employed in MIP-based biomimetic sensors.

including sensors. The possibility of using tailor made, highly selective and low cost artificial receptors, with good mechanical, thermal and chemical properties have paved the way for the development of a new generation of chemical sensors, using imprinted polymers as recognition elements [8–14]. As in the case of biosensors, a signal is generated upon the binding of analyte to the recognition element. The transducer then translates the signal into a quantifiable output signal (see Fig. 2). Until recently, most of the published accounts on sensors describe novel concept based sensors in each of the imprinting strategies but not the actual sensing device. The difficulty in fabrication of sensing devices with imprinted polymers lies in integrating the MIP recognition membrane with signal transduction. Fig. 3 depicts various transducers employed in conjunction with MIP based recognition elements. Of these, methods based on spectral and electrochemical transducers are widely employed [15]. Thus, the combination of imprinting and transduction selectivities can result in sensing devices which exclusively recognize target analyte and not the interfering species [8]. MIP based sensors employing spectral transducers have been extensively reviewed [3,4,16]. Table 1 presents the highlights of book chapters and reviews that deal with electrochemical transducer based MIP sensors [3,8,15–29].

2. Potentiometric transducer based imprinted polymer sensors

Potentiometry is one of the simplest instrumental techniques that many chemists encounter. However, its basic simplicity does not mean that the applications are limited. Potentiometric sensors provide an exciting and achievable opportunity to perform biomedical, environmental and industrial analyses away from a centralized laboratory since these make it possible to combine the ease of use and portability with simple, inexpensive fabrication techniques. Ion selective electrodes, in particular have expanded the range of applications of potentiometry. Whilst potentiometry has been used for many years, the advances in the field of ion-selective electrodes makes it such a valuable technique in the modern laboratory. An ideal ion selective sensing would take place in a simple single-stage operation involving no elaborate apparatus, be rapid, require little or no pretreatment of the aqueous phase, involve an agent that is insoluble in aqueous phase and entail minimal cost. Potentiometry makes use of the development of electrical potential at the surface of sensor membrane when dipped in solution containing ions (ion sensing electrodes) [17] or on binding with template (molecular sensing electrodes). For the development of MIP sensors, it is important that the creation of membrane potential between sample and inner filling solutions do not require the template to be extracted from the membrane. This is an advantage, because extraction of the template to leave recognition sites ready for binding is a cause for uncertainty at the determination or a sensitivity limiting factor [27]. Another unique feature of potentiometry is that the species do not have to diffuse through the membrane, so that there is no size restriction on the template compound. Despite all these advantages, only a very few MIP based sensors have been reported using potentiometric transducer [15,16,24,25].

2.1. Ion sensing electrodes (ISEs)

Ion sensing electrodes are broadly classified into primary, compound or multiple membrane (multilayer) and metal contact or all solid state ISEs. Barring a few, all of them are beset with problems of selectivity (though projected to be specific when introduced) and have sensitivities far inferior to other analytical techniques. The limits of detection of most of ISEs are in the range 0.1–1 μmol L^{-1}. During last 5–6 years, there is a significant break through in pushing the LODs down to 10 pmol L^{-1} [30]. However, there remains a scope in improving the selectivity inspite of significant strides made in the designing of novel synthetic strategies for the preparation of tailor made chemical receptors. In view of the proven potentialities of MIPs for enhancing the selectivity via specific binding of analyte, there are opportunities in developing commercial sensing devices by integrating MIPs with potentiometric transducer.

2.1.1. ISE—virtues

Ion sensing electrodes are part of a group of relatively simple and inexpensive analytical tools. The use of ion sensing electrodes in environmental analysis offers several advantages over other methods of analysis. ISEs are relatively inexpensive, simple to use and have an extremely wide range of applications and wider concentration range compared to many other analytical techniques. They are very robust and durable and ideal for use in either field or laboratory environments. They are invaluable for the continuous monitoring of changes in concentration, for example, in potentiometric titrations or monitoring the uptake of nutrients or the consumption of reagents. With careful use, frequent calibration and an awareness of the limitations, they can achieve accuracy and precision levels of ± 2 or 3% for some ions and thus compare favorably with analytical techniques, which require far more complex and expensive instrumentation. ISEs are one of the few techniques which can measure both positive and negative ions, are unaffected by sample colour or turbidity and can be used in aqueous solutions over a wide temperature range.

2.1.2. ISE—vices or limitations

For many applications, the ISEs are sensitive to some other ions to some extent. In some extreme cases, the electrode is far more sensitive to the interfering ion than to the primary ion and can only be used if the interfering ion is present in trace quantities

Table 1
Highlights of book chapters and reviews on electrochemical transducer based MIP sensors

	Title [reference]	Salient features
Book chapters		
1	Biomimetic electrochemical sensors based on molecular imprinting—Chapter 18 of "Molecularly imprinted polymers" [15]	Compiles (i) types of transducers with a special emphasis on electrochemical ones, (ii) various recognition elements and presents an over view of electrochemical sensors utilizing molecularly imprinted recognition sites
2	Ionic sensors based on molecularly imprinted polymers—Chapter 19 of "Molecularly imprinted polymers" [17]	Enumerates different steps of the process of producing an ion-selective MIPs for the construction of ISEs and optical sensors
3	Metal ion selective molecularly imprinted materials—Chapter 22 of "Molecularly imprinted materials" [3]	Describes the subject of metal ion imprinting, providing a guide to the current methods for making molecularly imprinted metal ion complexing polymers and attempts to follow the progress in metal ion imprinting
4	Molecularly imprinted polymers as recognition elements in sensors: mass and electrochemical sensors—Chapter 26 of "Molecularly imprinted materials" [18]	Focuses on theoretical and practical aspects of the application of molecularly imprinted polymers in sensors, with special emphasis on electrochemical and acoustic sensors and explains some experimental protocols with the help of examples
Reviews		
1	Biomimetic sensors for toxic pesticides and inorganics based on optoelectronic/electrochemical transducers—an over view [16]	Deals with survey of synthetic strategies and characterization of MIPs, transducers that convert binding event into a detectable signal, integration strategies of MIP and transducer and compiles of reports on MIP based sensors for toxic pesticides and heavy metals
2	Metal ion imprinted polymers—novel materials for selective recognition of inorganics [19]	Summarizes ion imprinted polymer based sensors in addition to applications of IIPs in areas such as solid phase extraction and membrane separation
3	Towards separation free electrochemical affinity sensors by using antibodies, aptamers and MIPs—a review [20]	Presents an over view of the main recognition elements such as antibodies, aptamers and MIPs and measuring principles used in electrochemical affinity assays and sensors
4	Impedence spectroscopy: over 35 years of electrochemical sensor optimization [21]	Reviews some of the work that has been undertaken using electrochemical impedance spectroscopy (EIS) for characterization of electrode–electrolyte interface processes (i.e. membrane-transducer) over past 35 years and also evaluates the power of EIS in characterizing electrochemical sensor systems
5	Electrochemical sensing with electrodes modified with MIP films [22]	Summarizes work on the development of voltammetric sensors based on MIP membranes cast by electropolymerization, drop coating and in situ means or MIP composite membranes
6	Electrochemical sensors based on MIPs [23]	Highlights recent achievements in molecular imprinting related to the area of sensor technology pertaining to electrochemical transducers and problems and possible solutions
7	New materials for electrochemical sensing IV.MIPs [24]	An over view of MIPs for the design of electrochemical sensors based on different signal-transduction schemes is presented
8	Electrochemical sensors based on MIPs [25]	Examines the literature on non-covalent MIP based electrochemical sensors over the period 1993–2003
9	Electrochemical and piezoelectric enantioselective sensors and biosensors [26]	Lists out the developments in electrochemical and piezoelectric enantioselective sensors during 1992–2004
10	MIPs and their use in biomimetic sensors [8]	A compresensive and highly informative review and first of its kind dedicated fully to MIP based sensors as on 2000
11	Progress in the development of MIP sensors [27]	Examines the combination of fibre-optical based luminescence and MI to create highly sensitive chemical sensors
12	MIP for the selective sequestering and sensing of ions [28]	Documents studies conducted at John Hopkins Laboratory (as on 1997) the polymeric resins developed for sequestering (resulting in possible removal/purification of a variety of chemicals) and sensing of ions in aqueous solutions (using ISEs)
13	Molecular imprinting: selective materials for separations, sensors and catalysis [29]	First of this kind on MIP based sensors published in 1995 in addition to separations and catalysis

or even completely absent. In some systems, the interfering ion can be removed by chemical means (chiefly by precipitation or complexing) before using, but this can be a laborious and time consuming process and most analysts prefer to avoid this, if possible.

2.1.3. ISE—theory [31]

Ion selective potentiometry is a routine analytical technique, in which the cell voltage is measured as a function of the activity of the analyte in the sample. The electrochemical notation of the potentiometric cell of a biomimetic sensor in analogy with conventional

heterogenous polymer membrane electrode is given by

$$\underset{\varepsilon_1}{\mathrm{Ag}} \mid \underset{\varepsilon_2}{\mathrm{AgCl}} \mid \underset{\varepsilon_3}{\mathrm{KCl}} \,||\, \underset{\varepsilon_j}{\text{salt bridge}} \,||\, \underset{\varepsilon'}{\text{sample solution}} \mid \underbrace{\text{membrane}}_{\varepsilon_M} \mid_{\varepsilon''} \text{inner filling solution} \mid \underset{\varepsilon_4}{\mathrm{AgCl}} \mid \underset{\varepsilon_5}{\mathrm{Ag}} \quad (1)$$

in which phase boundaries are indicated by vertical lines and the two parallel lines mark a liquid–liquid interface. The total potential difference measured between the two terminal electrodes is evidently composed of a considerable number of local potential differences taken from right to left across the interfaces

$$E = (\varepsilon_1 + \varepsilon_2 + \varepsilon_3 + \varepsilon_4 + \varepsilon_5) + \varepsilon_j + (\varepsilon' + \varepsilon'') = E_o + \varepsilon_j + \varepsilon_M \quad (2)$$

in which E_o is a constant potential term comprising the potential contributions ε_1 to ε_5, which arises within the system from the two reference electrodes in the cell, ε_j is the liquid junction potential and ε_M is the membrane potential. We usually seek electrolyte combinations for the reference electrode in which ε_j is nearly zero. The essential part of an ISE is the ion-sensitive membrane that is commonly placed between two aqueous phases, for example, the sample and the inner filling solution. Typically, the membrane potential is divided into three separate potential contributions—the phase boundary potentials at both interfaces (ε' and ε'') and the diffusion potential within the ion-sensing membrane [32–34]. However, the membrane's internal diffusion potential is zero, if there is no concentration gradient within the membrane. The basic equation for the interfacial potentials ε' and ε'' is

$$E = \frac{RT}{z_i F} \ln \frac{k_i a_i}{\overline{a_i}} \quad (3)$$

in which R is the gas constant, T is the absolute temperature, F is the Faraday constant, z_i is the charge number of the primary ion i, k_i is the single-ion partition coefficient, and a_i and $\overline{a_i}$ are the primary ion solution and membrane activities, respectively. The phase boundary potential is a simple function of the sample ion activities only when $\overline{a_i}$ is not influenced significantly by the sample. Accordingly, for an ideally selective membrane, the membrane potential is directly related to the respective activities in the contacting solutions.

$$\varepsilon_M = \frac{RT}{z_i F} \ln \frac{a_i(1)}{a_i(2)} \quad (4)$$

in which $a_i(1)$ and $a_i(2)$ are the ion activities in the sample and the inner filling solution, respectively. A Nernstian response is expected in a potentiometric cell when the liquid junction potential can be neglected and the inner filling solution of the electrode is kept constant [31]:

$$E = \text{constant} + \frac{RT}{z_i F} \ln a_i \quad (5)$$

2.1.4. ISE—primary evaluation criteria

The primary or chief criteria for the evaluation of MIP based ISE as in the case of any sensing device are "*Sensitivity*", "*Selectivity*" and "*Response time*".

2.1.4.1. Sensitivity [30]. Assuming linear concentration gradients across the membrane phase and the aqueous Nernst diffusion layer at the sample side, and considering Fick's first law of diffusion for a one-dimensional system, the problem may be illustrated with the following steady-state relationship [35].

$$\frac{C_{L.aq}(\text{pb}) - C_{L.aq}(\text{bulk})}{C_{IL.org}(\text{inside}) - C_{IL.org}(\text{pb})} = q = \frac{D_{org}\delta_{aq}}{D_{aq}\delta_{org}} \quad (6)$$

where $C_{L.aq}$ is the aqueous concentration of the analyte ion at the sample—membrane phase boundary (pb) and in the bulk sample (bulk) and $C_{1L.org}$ is the membrane phase boundary (pb). The parameter q incorporates the ratio of the diffusion coefficients of the analyte ion in both phases (D_{org} and D_{aq}) and the diffusion-layer thicknesses of the membrane and aqueous phase (δ_{org} and δ_{aq}). At the LOD, $C_{L.aq}$(bulk) is negligible and $C_{L.aq}$(pb) is equal to the LOD, DLI. Eq. (6) may therefore be rewritten as

$$\text{DLI} = \frac{D_{org}\delta_{aq}}{D_{aq}\delta_{org}}(C_{IL.org}(\text{inside}) - C_{IL.org}(\text{pb})) \quad (7)$$

where DLI is the limit of detection.

Clearly, six different parameters may influence the LOD under steady-state conditions. The lowering of LODs is possible by addressing any one of the above six parameters for MIP based ISEs as well.

2.1.4.2. Selectivity. Selectivity is the degree of recognition of analyte or primary ion (A) over interferent ion (B, etc.). Internationally accepted selectivity coefficient, $K^{Pot}_{A,B}$ is calculated by employing Nicholsky–Eisenman equation which is given by an expression [36].

$$E = \text{constant} + \frac{2.303RT}{z_i F} \log[a_A + K^{Pot}_{A,B} \cdot a_B^{z_A/z_B}] \quad (8)$$

Among the five different methods for quantifying $K^{Pot}_{A,B}$ such as fixed interferent ion, fixed analyte ion, separate solutions, mixed solution and matched potential method, IUPAC has recommended the last method for obtaining accurate $K^{Pot}_{A,B}$ values as it is independent of Nicholsky–Eisenman equation and is applicable even when the charges of primary and interferent ions are different. In matched potential method, the $K^{Pot}_{A,B}$ is defined as the activity (concentration) ratio of primary ion and the interfering ion which gives the same potential change in a reference solution [37].

$$K^{Pot}_{A,B} = \frac{\Delta a_A}{\Delta a_B}, \quad \text{where } \Delta a_A = a_{A'} - a_A \quad \text{and} \quad \Delta a_B = a_{B'} - a_B \quad (9)$$

2.1.4.3. Response time. The response time, t^0 or t^{90}, was measured at the first instant at which the potential of the potentiometric cell reaches steady state value or 90% of the above value. The use of the a suitably chosen value of differential quotient($\Delta E/\Delta t$) was recommended in 1994. But several researchers still use t^0 or t^{90} [38]. The latest recommendation of 0.5 mV min^{-1} by IUPAC has to be rigorously followed by all researchers to have quick evaluation of response times of several analogous ISEs reported in literature [38].

2.1.4.4. Pathways for an ideal sensing device. Various factors that contribute to an ideal sensing device are higher sensitivity and better selectivity in terms of lower and lower limits of detection and $K^{Pot}_{A,B}$ values, respectively, with faster response times. The additional features desired for an ideal sensing device as mentioned in Introduction are reusability, stability, non-toxic nature and proper integration with transducer. The lower detection limits of heterogeneous polymeric membrane and pressed pellets or insoluble precipitates are in the μmol L^{-1} range except when ion activities are adjusted by using ion buffers, which maintain low and constant activity via. superimposed complexation or solubility equilibra [39]. Larger improvement of the lower detection limit can be obtained (i) by incorporating chelators of analyte ion or ion exchange resins or lipophilic interfering ion to internal filling solution, (ii) by reducing the thickness of the Nernst diffusion layer (via stirring of sample or using a rotating electrode configuration or a wall-jet system), (iii) by increasing the thickness of the diffusion layer on the inner side of the membrane, (iv)

by reducing plasticizer content or covalently attaching ionophore and (v) by partially blocking the sample side of membrane (via embedding inert lipophilic microparticles during membrane construction) as shown in case of conventional ionophore based ISEs [30]. The major bottleneck of all ISEs had been lack of selectivity. The major research programs were hitherto aimed at designing novel chemical receptors based on newer synthetic protocols but not with great success. Approaches such as doping of complexing agents [40] and application of anodic current density [41] to conducting polymer membranes has also resulted in lowering of LODs of ISEs. Alternate approaches in improving the selectivity search for new carriers with anti-Hofmeister response patterns and supramolecular and host–guest chemistry [42]. On the other hand, MIPs with all its virtues analogous to biological counterparts can result in improving the selectivity of potentiometric transducer based sensors by using simpler, low cost and off-the-shelf ionophores.

2.1.5. Cation imprinting

2.1.5.1. Inorganics. Potentiometric transducer based MIP sensors reported so far has been summarized in Table 2. Mosbach's group has reported the first imprinted ISE for Ca(II) and Mg(II) analytes [43]. The imprinting process enabled enhanced selectivity for Ca(II) by factors of 6 and 1.7 on Ca(II) binding using Ca(II) and Mg(II) imprinted polymer materials over a non-imprinted polymer blank. Johns Hopkins University team led by Prof. Murray, way back in 1995 [28,44,17] developed lead and uranyl imprinted polymer inclusion membrane (IPIM) based sensors wherein the metal ion imprinted polymer materials were dispersed in polyvinyl chloride in presence of plasticizer. However, the imprinting effect has not been demonstrated as per the available information. Furthermore, a binary metal-polymerizable vinyl ligand complex is mixed with functional and crosslinking monomers and initiator during synthesis. The rebinding (after leaching of template) is by complexation with ligand chemically immobilized onto polymer matrix. Our group has successfully demonstrated the fabrication of stable and reusable IPIM sensor for uranium [45] which employs binary or ternary complex, viz. uranium-non-polymerizable ligand or uranium-non-polymerizable and polymerizable ligands during the synthesis of IIP materials. The non-polymerizable ligands investigated include 5,7-dichloroquinoline-8-ol (DCQ), succinic acid and salicylaldoxime. The polymerizable ligand is 4-vinylpyridine (VP). The sensors constructed based on the above materials were evaluated based on the sensitivity and selectivity criteria. Of these, DCQ-VP material based sensor exhibited superior performance [45]. It is pertinent to mention here that in addition to unequivocally demonstrating the imprinting effect by comparing imprinted and non-imprinted polymer materials based IPIM sensors, the linear dynamic range and LOD of DCQ-VP based sensor is better compared to the vinyl benzoate or vinyl-salicylaldoxime based ones [17,28]. It is not out of context to mention here that the non-polymerizable ligand is trapped within the polymer matrix (quite different from trapping of template while rebinding with washed or leached MIP or IIP materials) resisting mineral acid attack. This enables the selective rebinding of uranyl ion. The incorporation of complexing agents, viz. EDTA or Na_2CO_3 resulted in pushing the LOD of uranyl biomimetic sensor by 2 orders to $\sim 1 \times 10^{-8}$ mol L^{-1}. Our group again reported for the first time the MIP based potentiometric sensor (IPIM format) for a lanthanide, i.e. dysprosium [46]. By using off-the shelf and low cost chemicals, it was proved that the MIP based ISEs of Dy [46] and U [45] have lower $K^{Pot}_{A,B}$ values determined for Dy or U over various alkali, alkaline earth and transition metal ions when compared to the respective best ionophore sensors reported. Baghel et al. [47] in their recent paper made an observation (based on chronopotentiometric study), that on increase of copper concentration from 10^{-8} to 10^{-4} mol L^{-1} resulted in 0 and 40 mV change with NIPIM and IPIM sensors constructed on the lines similar to lead, uranyl or dysprosium sensors reported previously [15,28,44–46]. These authors have utilized Cu-acrylamide complex during synthesis of copper imprinted materials. However, detailed sensor evaluation has not been undertaken.

2.1.5.2. Organics. Agostino et al. [48] have reported for the first time atrazine imprinted potentiometric sensor, wherein the recognition membrane was cast in situ by placing the glass tube (containing pre polymerization mixture) in oven at 70 °C for 17 h. As the ISE responds for atrazinium ion, the response profile is dependent on pH. For example, at pH 4.0 and 1.5, the slopes are zero and 25 mV/decade, respectively. This result cannot be explained as the reported pK_a value of atrazine is 1.7. In contrast, the atrazine sensor reported from our group based on IPIM format responds in Nernstian manner, corresponding to monoprotonated atrazinium ion at a pH of 2.7 ± 0.2 [49]. Again, the IPIM sensor has wide linear dynamic range (1×10^{-7} to 1×10^{-2} mol L^{-1}) compared to in situ sensor (3×10^{-5} to 1×10^{-3} mol L^{-1}) and lower limit of detection (5×10^{-7} mol L^{-1} as against 1.2×10^{-5} mol L^{-1}). Levamisole imprinted potentiometric sensor fabricated via IPIM format again offers wide linear dynamic range (2.5×10^{-6} to 1×10^{-1} mol L^{-1}) with Nernstian slope of 57.0 mV/decade corresponding to its monoprotonated form [50]. Unlike Atrazine IPIM sensor, faster response time of 15 s was reported by these authors.

2.1.6. Anion imprinting

2.1.6.1. Inorganics. The only potentiometric transducer based inorganic anion sensor todate was reported by Hutchins and Bachas [51] way back in 1995. This was based on the electropolymerization of pyrrole onto glassy carbon electrode in presence of $NaNO_3$. The resulting sensor gave near Nernstian slope of 56.0 ± 1 mV/decade over a concentration range of 5.0×10^{-5} to 5×10^{-1} mol L^{-1} with a LOD of 2×10^{-5} mol L^{-1}. Unlike commercially marketed conventional nitrate ISE, the imprinted sensor offers much higher selectivity—to the tune of 4 orders of magnitude better over perchlorate and iodide.

2.1.6.2. Organics. Zhou et al. [52–54] have surface imprinted MIP films onto indium tin oxide coated glass plate for templates such as methyl phosphonic acid, dipicolinic acid and *N*-carbobenzoxy aspartic acid. As expected of the availability of cavities on the surface compared to conventional polymerization techniques, the response times are very low, i.e. ~a few seconds except for the last one which is ~2 min just like IPIM sensors described above. The authors have not cited any specific reasons for this observation. Prathish et al. [55] have designed and developed IPIM sensor for methyl phosphonic acid which gives Nernstian response in contrast to the one reported by Zhou et al. [52]. The sensitivity of this IPIM sensor developed by us is 3 orders lower. However, the steady state response for incremental addition of MPA takes about 5 min against a few seconds. IPIM sensors were fabricated by dispersing PMP imprinted polymer materials prepared by bulk, precipitation and suspension methods [56]. Based on the sensitivity and selectivity criteria, the order of performance of the IPIM sensors fabricated by the above materials lies in the order bulk > suspension > precipitation. Again, the imprinting effect is more pronounced in the case of bulk material based IPIM sensor compared to others as visualized by $K^{Pot}_{A,B}$ values.

Fig. 4 shows the SEM pictures of the three sets of materials as well as IPIM (surface view) casted after dispersing the polymer materials synthesized by the bulk, precipitation and suspension

Table 2
Potentiometric transducer based MIP sensors realized to date

Analyte or measurand (1)	Imprinting strategy (2)	Chelating ligand and membrane composition (3)	Demonstration of imprinting effect and improved selectivity (4)	Linear dynamic range (mol l^{-1}) (5)	LOD (mol L^{-1}) (6)	Response time (7)	Reference (8)
IPIMs							
Ca(II)	Cation	*N*,*N*′-Dimethyl-*N*,*N*′-bis(4-vinylphenyl)-3-oxapentadiamide, PVC, BEHC potassium tetrakis(*p*-chlorophenyl)borate	Yes	–	–	–	[43]
Mg(II)	Cation	*N*,*N*′-Dimethyl-*N*,*N*′-bis(4-vinylphenyl)-3-oxapentadiamide, PVC, BEHC potassium tetrakis(*p*-chlorophenyl)borate	Yes	–	–	–	[43]
Pb(II)	Cation	Vinyl benzoate; styrene, DVB, PVC	No	1×10^{-6} to 510^{-2}	1×10^{-6}	–	[44,28]
U(VI)	Cation	Vinyl benzoate or vinyl salicylaldoxime; styrene, DVB, PVC, NPOE/DOP	No	1×10^{-6} to 5×10^{-2}	8×10^{-7}	–	[17,28]
U(VI)	Cation	5,7-Dichloroquinoline-8-ol, 4-vinyl pyridine; PVC, NPOE, NaTPB, EDTA/Na_2CO_3	Yes	1×10^{-8} to 1×10^{-2}	2×10^{-8}	2 min	[45]
Dy(III)	Cation	5,7-Dichloroquinoline-8-ol, 4-vinyl pyridine, PVC, NPOE, NaTPB	Yes	8×10^{-6} to 1×10^{-1}	2×10^{-6}	10 s	[46]
Cu(II)	Cation	Acrylamide; PVC, NPOE	Yes	Chromopotentiometric study	–	–	[47]
Levamisole	Cation	MAA, DVB; PVC, DBS	-	2.5×10^{-6} to 1×10^{-1}	1×10^{-6}	15 s	[48]
Atrazine	Cation	MAA, EGDMA; PVC, DOP	Yes	1×10^{-7} to 1×10^{-2}	0.5×10^{-6}	2 min	[49]
In situ							
Atrazine	Cation	MAA, EGDMA; in situ	Yes	3×10^{-5} to 1×10^{-3}	1.2×10^{-5}	1.2×10^{-5}	[50]
Conducting polymers							
NO_3^-	Anion	Polypyrrole, electropolymerization in presence of NO_3^-	–	5×10^{-5} to 5×10^{-1}	2×10^{-5}	–	[46]
Surface imprinting							
MPA	Anion	Indium tin oxide	Yes	5×10^{-5} to 0.62	5×10^{-5}	50 s	[52]
Dipicolinic acid	Anion	Indium tin oxide	–	1.5×10^{-6} to 0.0194	1.5×10^{-6}	25 s	[53]
N-Carbo benzoxy asparatic acid	Anion	Indium tin oxide	Yes	5×10^{-6} to 8×10^{-3}	1.4×10^{-3} to 1×10^{-2}	2 min	[54]
IPIMs							

Table 2
(*Continued*)

Analyte or measurand (1)	Imprinting strategy (2)	Chelating ligand and membrane composition (3)	Demonstration of imprinting effect and improved selectivity (4)	Linear dynamic range (mol l^{-1}) (5)	LOD (mol L^{-1}) (6)	Response time (7)	Reference (8)
MPA	Anion	MAA, EGDMA; PVC, NPOE	Yes	5×10^{-8} to 1×10^{-4}; 1×10^{-3} to 1×10^{-1}	5×10^{-8}	5 min	[55]
PMP	Anion	MMA, EGDMA; PVC, NPOE	Yes	4×10^{-8} to 1×10^{-5}; 1×10^{-5} to 1×10^{-3}	4×10^{-8}	0.5 min	[56]
Immunosensor							
Serotonin	Anion	MAA, EGDMA	–	1×10^{-6} to 1×10^{-2}	1×10^{-10}	12 s	[57]
IPIMs							
Phorate	Non-covalent	MAA, EGDMA; PVC, NPOE	Yes	1×10^{-9} to 1×10^{-6}; 1×10^{-6} to 1×10^{-5}	1×10^{-9}	5 min	[63]
DCP	Non-covalent	HEMA, EGDMA; PVC, NPOE	Yes	1×10^{-4} to 1×10^{-2}	1×10^{-4}	5 min	[64]
DCP	Covalent	HEMA, 4-vinylaniline, EDGMA	Yes	1×10^{-5} to 1×10^{-2}	1×10^{-5}	5 min	[64]
In situ							
DCP	Non-covalent	HEMA, EGDMA; PVC, NPOE	Yes	1×10^{-5} to 1×10^{-2}	1×10^{-5}	2 min	[64]
DCP	Covalent	HEMA, 4-vinylaniline, EGDMA	Yes	1×10^{-6} to 1×10^{-2}	1×10^{-6}	2 min	[64]
Indirect							
Glucose	Metal-chelate	Copper-methyl-β-glucopyranoside, sensing of liberated H^+	–	–	–	–	[65]
3-Chloro-1,2-propanediol (MCPD)	Covalent	4-Vinyl phenylboronic acid, EGDMA; sensing of liberated H^+ on addition of MCPD with glass electrode	Yes	$0–3.2 \times 10^{-3}$	–	–	[66]
Carbaryl	Non-covalent	MAA, EGDMA; flow injection column sensor; deprotonation of carbaryl in alkaline medium and subsequent monitoring with glass electrode	–	10–100	10 μg/ml		[67]

Abbreviations: IPIM, imprinted polymer inclusion membrane; PVC, polyvinyl chloride; DVB, divinyl benzene; NPOE, *o*-nitrophenyl octyl ether; DOP, dioctyl phthalate; EDTA, ethylene diamine tetraacetic acid; NaTPB, sodium tetraphenyl borate; MAA, methacrylic acid; DBS, dibutyl sebaccate; EGDMA, ethylene glycol dimethacrylate; HEMA, 2-hydroxy ethylmethacrylate.

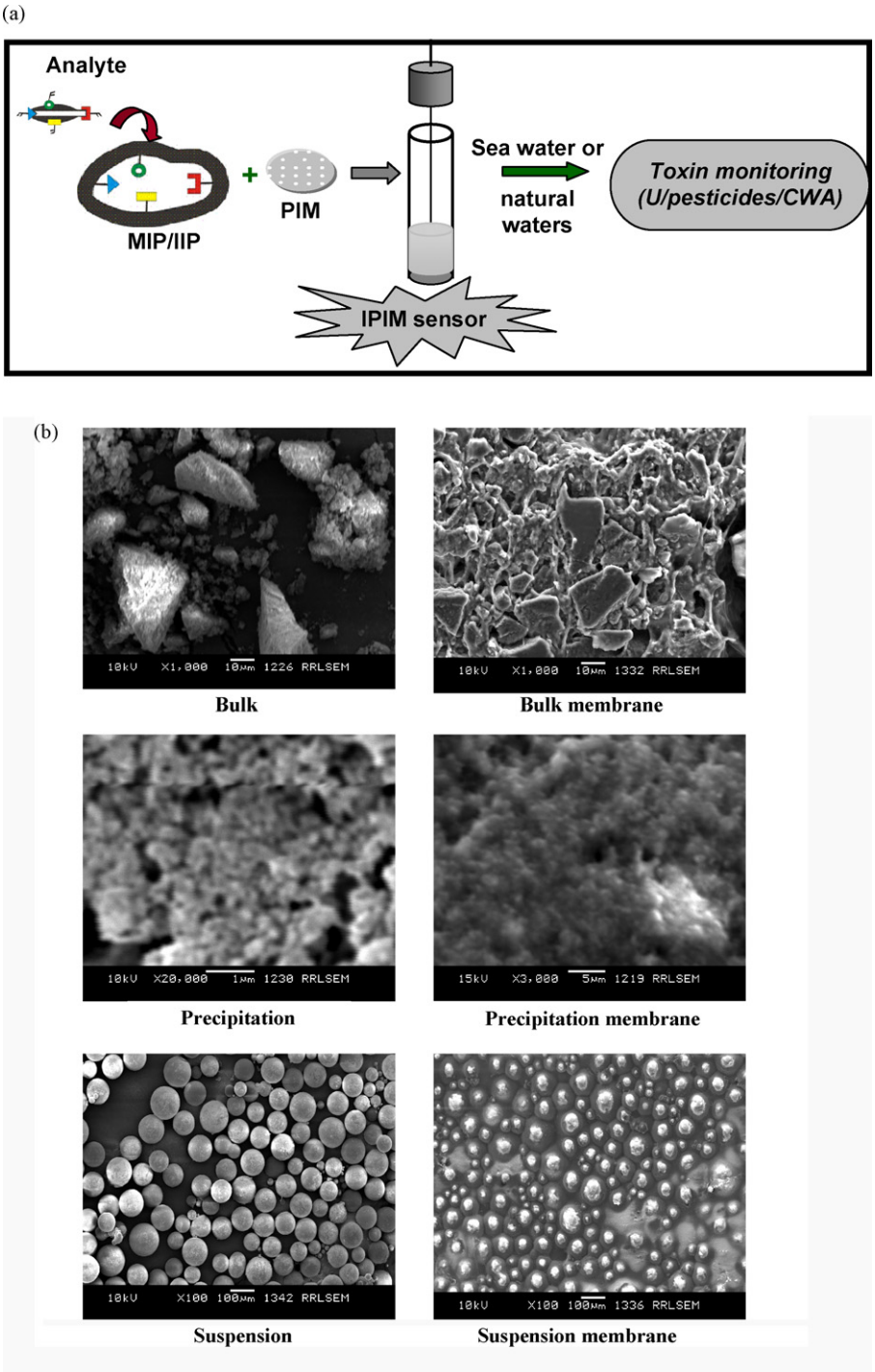

Fig. 4. Imprinted polymer inclusion membrane based sensor. (a) Schematic diagram and (b) SEM micrographs of imprinted polymer materials and surface view of IPIM membranes.

methods in THF solution of PVC. For the bulk imprinted material, the morphology of the crushed polymer is shown while in other cases, the polymers in the form of beaded materials were shown as such. The bulk imprinted materials show an agglomerated appearance with irregular shape in the size range 50–200 μm. In the suspension method, the material crystallizes into perfect uniform spherical beads (10–100 μm). In case of precipitation polymerization, the materials were of nanometer range and slightly irregular in shape. Thus, based on different polymerization approaches, different kinds of materials were obtained, viz. large irregular sized particles (bulk), microspheres (suspension) and nanospheres (precipitation). Also, one can clearly visualize from the SEM pictures that eventhough we have dispersed polymeric materials separately in the PVC matrix, the IPIM membranes obtained were of almost uniform in nature.

Kitade et al. [57] have reported a potentiometric artificial immunosensor based on MIP, which detects as low as 100 pmol L^{-1} of serotonin and distinguishes from structurally related species such as tryptamine, acetaminophen or procainamide and the response is fast [t^{95} = 12 s).

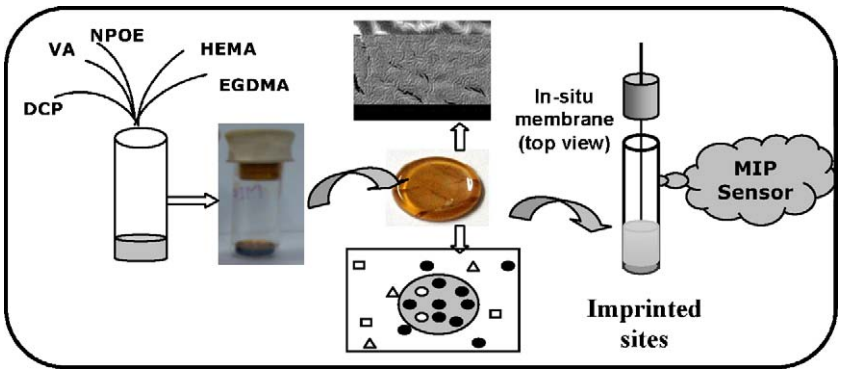

Fig. 5. Sequence of steps in design and development of IPIM (phorate) and in situ (DCP) membrane based sensing devices.

2.1.7. Molecule sensing electrodes (MSEs)

Piletsky et al. [58] have observed that the electroconductivity increases with increase in concentration of atrazine solution (buffered at pH 8.0 with Tris–HCl buffer). To explain this and subsequent observations, Piletsky et al. [59,60] proposed a "*Gate effect*" model. In the "*Gate*" analogy, the template may correspond to the "*key*" and the site in MIP for specific binding with template may correspond to the "*Keyhole*". The MIP based potentiometric sensing electrodes described above essentially sense either inorganic or organic ions which include both cations and anions as well. However, the partial shrinking of MIP on rebinding increases the size of the micro- and macropores affecting the diffusion of uncharged species analogous to Co- and counter-ions [58]. The enhancement of anodic current for theophylline in cyclic voltammetry [61], increase in impedance or decrease in capacitance in capacitive detection of glucose again [62] can be attributed to similar "*Gate effect*" which results in increase in diffusive permeability in the presence of template. Thus, the potentiometric sensing of template molecules is also possible as shown by us in case of phorate [63] diethyl chlorophosphate sensor [64]. The potential responses to phorate or diethyl chlorophospate in IPIM sensors can be explained by invoking *Gate effects* (see Fig. 5a). Biomimetic field monitoring sensing device for phorate have linear dynamic range and LOD of 1×10^{-9} to 1×10^{-5} and 1×10^{-9} mol L^{-1}, respectively [63]. The selectivity of the above sensing device for phorate over various common organophosphorous or chlorophenoxy acetic acid

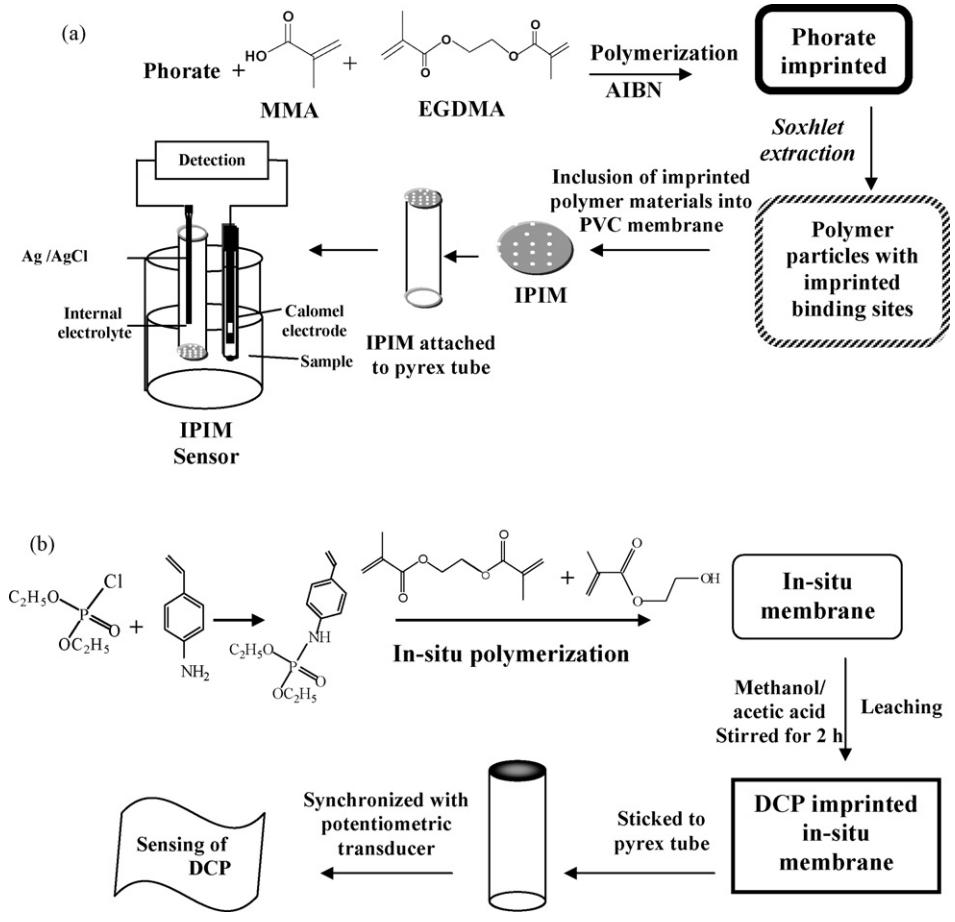

Fig. 6. Schematic diagram of in situ membrane based sensor.

pesticides and atrazine herbicides is remarkable mainly because of the imprinting effect. In our recent work, we have designed and developed IPIM sensors for DCP template by both non-covalent and covalent strategies (see Fig. 5b) [64]. In covalent strategy, a second functional monomer, viz. 4-vinyl aniline is incorporated in the pre-polymerization mixture in addition to 2-hydroxyethyl methacrylate. Alternately, both covalent and non-covalent strategy based in situ membranes were obtained by a single pot synthesis (See Fig. 6 for schematic diagram). The above recognition membranes on integration with potentiometric transducer selectively senses DCP over structurally similar molecules and selected degradation products of chemical warfare agents. The performance of the above fabricated sensors lies in the order covalent in situ > non-covalent in situ ~ covalent inclusion > non-covalent inclusion based on the essential sensor criteria, viz. LOD, $K^{Pot}_{A,B}$, linear dynamic range and magnitude of imprinting effect. The possible reasons for sensing of DCP and relative sensing characteristics of biomimetic sensors were explained by invoking "*Gate concept*" proposed by Piletsky et al. [58–60] and extending the concepts outlined by Bakker and Pretsch for lowering of LODs of ionophore based sensors [30].

2.2. Indirect sensing electrodes

In addition to ion and molecule sensing electrodes, there is a set of electrodes wherein the rebinding of template by imprinted polymer releases H^+ ions which can be sensed by a pH electrode, i.e. the sensing of analyte is done indirectly by monitoring the product formed either by displacement or alkaline hydrolysis or deportation. This class of electrodes can be termed as potentiometric chemosensors. Arnold and co-workers [65] have described glucose sensor by following the pH of sample solution with pH electrode as the replacement of OH^- and H_2O molecules of copper-methyl-β-glucopyranoside complex imprinted material is proportional to glucose concentration. Similar phenomenon was employed to indirectly monitor 3-chloro-1,2-propane-diol also [66]. Authors have unequivocally demonstrated the imprinting effect also by comparing with non-imprinted potentiometric sensor. Hantash et al. [67] have for the first time demonstrated an in-line MIP based sensor, which employs potentiometric transducer. Even here, the sensing of carbaryl is made possible only by indirect means, i.e. by monitoring liberated H^+ ions with pH electrode during deprotonation of carbaryl in alkaline medium. This sensor eliminates lengthy and expensive extraction steps when dealing with determination of a pesticide (in this case carbaryl) in complex biological samples.

3. Future outlook

The limitation of the imprinted polymer based potentiometric sensors is the long response time which is of the order of ~5 min. This situation is partly because of the synthetic protocols adopted which essentially pertain to bulk polymerization. This has to be addressed by employing surface imprinting cocktails in the coming years. Another important issue which has to be addressed in near future is the multi-analyte or multi-measurand analysis. This assumes importance as the real environmental samples are complex containing toxins ranging from heavy metals to pesticides to toxic drug metabolites. In view of the high selectivity, one can visualize potentiometric sensors consisting of sensing devices of several analytes and hooked onto multichannel electronic output data station. If necessary, chemometric approaches can also be adopted to resolve the multi-measurand sensor output signal. There is only one report on flow through sensor, i.e. analysis of carbaryl—but it is only an indirect method [67]. The coming years are likely to witness the design and development of on-line flow through sensors for detection and quantification of envirotoxic markers which are amenable for routine process monitoring and control. Another concern that has to be addressed, as in the case of ionophore based potentiometric sensors, is the problem encountered in the dependence of sensor output on changes in composition of complex environmental samples. As mentioned earlier, the potentiometric transducer on integration with analyte specific biomimetic or imprinted polymer recognition membrane can result in multitude of "*Portable sensing devices*". These will have immense global market potential and will most probably be the futuristic goal of researchers working in this discipline.

Acknowledgements

One of the authors Dr. T. Prasada Rao thanks Council of Scientific and Industrial Research (CSIR), New Delhi, India, for the sanctioning of a Network Project (NWP0010) on "SPECIALITY INORGANIC MATERIALS". Ms. R. Kala wishes to acknowledge CSIR, New Delhi, for awarding Senior Research Fellowship.

References

[1] G.H. Morrison, Trace Analysis, Interscience Publishers, New York, 1065.
[2] A.G. Mayes, M.J. Whitcombe, Adv. Drug Deliv. Rev. 57 (2005) 1742.
[3] G.M. Murray, G.E. Southard, in: M. Yan, G. Ramstrom (Eds.), Molecularly Imprinted Materials Science and Technology, Marcel Dekker, New York, 2005, p. 579.
[4] B. Sellergren, F. Lanza, Molecularly Imprinted Polymers, Elsevier, New York, 2001, p. 355.
[5] E. Yilmaz, K. Haupt, K. Mosbach, Angew. Chem. Int. Ed. 39 (2000) 2115.
[6] B. Sellergren, Angew. Chem. Int. Ed. 39 (2000) 1031.
[7] S.C. Zimmerman, N.G. Lemcoff, Chem. Commun. (2004) 5.
[8] K. Haupt, K. Mosbach, Chem. Rev. 100 (2000) 2495.
[9] P.J. Hudson, Curr. Opin. Biotechnol. 9 (1998) 395.
[10] G. Winter, A.D. Griffiths, R.E. Hawkins, H.R. Hoogenboom, Annu. Rev. Immunol. 12 (1994) 433.
[11] R.J. Ansell, O. Ramstrom, K. Mosbach, Clin. Chem. 42 (1996) 1506.
[12] K. Haupt, Analyst 126 (2001) 747.
[13] A.P.F. Turner, Biosens. Bioelectron. 16 (2001) 609.
[14] L.M. Kindschy, E.C. Alocilja, Trans. ASAE 47 (2004) 1375.
[15] D. Kriz, R.J. Ansell, in: B. Sellergren, F. Lanza (Eds.), Molecularly Imprinted Polymers, Elsevier, New York, 2001, pp. 417–440.
[16] T. Prasada Rao, K. Prasad, R. Kala, J.M. Gladis, Crit. Rev. Anal. Chem. 37 (2007) 191.
[17] G.M. Murray, O.M. Uy, in: B. Sellergren, F. Lanza (Eds.), Molecular Imprinted Polymers, Elsevier, New York, 2001, pp. 441–465.
[18] K. Haupt, in: M. Yan, O. Ramstrom (Eds.), Molecularly Imprinted Materials, Science and Technology, Marcel Dekker, New York, 2005, pp. 685–700.
[19] T. Prasada Rao, R. Kala, S. Daniel, Anal. Chim. Acta 578 (2006) 105.
[20] A. Warsinke, B. Nagel, Anal. Lett. 39 (2006) 2507.
[21] B. Pejcic, R. De Marco, Electrochim. Acta 51 (2006) 6217.
[22] M.C. Blanco-Lopez, S. Gutierrez-Fernandez, M.J. Lobo-Castanon, A.J. Miranda-Ordiers, P. Tunon-Blanco, Anal. Bioanal. Chem. 378 (2004) 1922.
[23] S.A. Piletsky, A.P.F. Turner, Electroanalysis 14 (2002) 317.
[24] A. Merkoci, S. Alegret, Trends Anal. Chem. 21 (2002) 717.
[25] M.C. Blanco-Lopez, M.J. Lobo-Castanon, A.J. Miranda-Ordieres, P. Tunon-Blanco, Trends Anal. Chem. 23 (2004) 36.
[26] M. Trojanowicz, M. Wcislo, Anal. Lett. 38 (2005) 523.
[27] B.R. Arnold, A.C. Euler, A.L. Jenkins, O.M. Uy, G.M. Murray, Johns Hopkins APL Tech. Digest 20 (1999) 190.
[28] G.M. Murray, A.L. Jenkins, A. Bzhelyansky, O.M. Uy, Johns Hopkins APL Tech. Digest 18 (1997) 464.
[29] S. Vidyasankar, F.H. Arnold, Curr. Opin. Biotechnol. 6 (1995) 218.
[30] E. Bakker, E. Pretsch, Trends Anal. Chem. 24 (2005) 199.
[31] E. Lindner, R.P. Buck, Anal. Chem. 72 (2000) 336A.
[32] T. Teorell, Proc. Soc. Natl. Acad. Sci. U.S.A. 21 (1935) 152.
[33] T. Teorell, Proc. Soc. Exp. Biol. Med. 33 (1935) 282.
[34] K.H. Meyer, J.F. Sievers, Helv. Chim. Acta 19 (1936) 649.
[35] T. Sokalski, T. Zwickl, E. Bakker, E. Pretsch, Anal. Chem. 71 (1999) 1204.
[36] R.P. Buck, E. Lindner, Pure Appl. Chem. 66 (1994) 2527.
[37] R.P. Buck, E. Lindner, Pure Appl. Chem. 67 (1995) 507.
[38] C. Macca, Anal. Chim. Acta 512 (2004) 183.
[39] T. Sokalski, A. Ceresa, T. Zwickl, E. Pretsch, J. Am. Chem. Soc. 119 (1997) 11347.
[40] A. Konopka, T. Sokalski, A. Michalska, A. Lewenstam, M. Maj-Zurawska, Anal. Chem. 76 (2004) 6410.
[41] A. Michalska, J. Dumanska, K. Maksymiuk, Anal. Chem. 75 (2003) 4964.
[42] R.Q. Yu, Z.R. Zhang, G.L. Shen, Sens. Actuators B 65 (2000) 150.

[43] T. Rosatzin, L.I. Andersson, W. Simon, K. Mosbach, J. Chem. Soc., Perkin Trans. 2 (1991) 1261.
[44] X. Zeng, G.M. Murray, Sep. Sci. Technol. 31 (1996) 2403.
[45] P. Metilda, K. Prasad, R. Kala, J.M. Gladis, T. Prasada Rao, G.R.K. Naidu, Anal. Chim. Acta 582 (2007) 147.
[46] K. Prasad, R. Kala, T. Prasada Rao, G.R.K. Naidu, Anal. Chim. Acta 566 (2006) 69.
[47] A. Baghel, M. Boopathi, B. Singh, P. Pandey, T.H. Mahato, P.K. Gutch, K. Sekhar, Biosens. Bioelectron. 22 (2007) 3326.
[48] G.D. Agostino, G. Alberti, R. Biesuz, M. Pasavento, Biosens. Bioelectron. 22 (2006) 145.
[49] K. Prasad, K.P. Prathish, J.M. Gladis, G.R.K. Naidu, T. Prasada Rao, Sens. Actuators B 123 (2007) 65.
[50] S. Sadeghi, F. Fathi, J. Abbasifar, Sens. Actuators B 122 (2007) 158.
[51] R.S. Hutchins, L.G. Bachas, Anal. Chem. 67 (1995) 1654.
[52] Y. Zhou, B. Yu, E. Shiu, K. Levon, Anal. Chem. 76 (2004) 2689.
[53] Y. Zhou, B. Yu, K. Levon, Biosens. Bioelectron. 20 (2005) 1851.
[54] Y. Zhou, B. Yu, K. Levon, Chem. Mater. 15 (2003) 2774.
[55] K.P. Prathish, K. Prasad, T. Prasada Rao, M.V.S. Suryanarayana, Talanta 71 (2007) 1976.
[56] V. Vishnuvardhan, K.P. Prathish, G.R.K. Naidu, T. Prasada Rao, Electrochim. Acta 52 (2007) 6922.
[57] T. Kitade, K. Kitamura, T. Konishi, S. Takegami, T. Okuno, M. Ishikawa, M. Wakabayashi, K. Nishikawa, Y. Muramatsu, Anal. Chem. 76 (2004) 6602.
[58] S.A. Piletsky, E.V. Piletskaya, A.V. Elgersma, K. Yano, I. Karube, Y.P. Parhometz, A.V. El'skaya, Biosens. Bioelectron. 10 (1995) 959.
[59] S.A. Piletsky, E.V. Piletskaya, T.L. Panasyuk, A.V. El'skaya, R. Levi, I. Karube, G. Wulff, Macromolecules 31 (1998) 2137.
[60] S.A. Piletsky, E.V. Piletskaya, K. Yano, A. Kugimiya, A.V. Elgersma, R. Levi, U. Kahlow, T. Takeuchi, I. Karube, T.I. Panasyuk, A.V. El'skaya, Anal. Lett. 29 (1996) 157.
[61] Y. Yoshimi, R. Ohdaira, C. Liyama, K. Sakai, Sens. Actuators B 73 (2001) 49.
[62] Z. Cheng, E. Wang, X. Yang, Biosens. Bioelectron. 16 (2001) 179.
[63] K. Prasad, K.P. Prathish, J.M. Gladis, G.R.K. Naidu, T. Prasada Rao, Electroanalysis 19 (2007) 1195.
[64] V. Vishnuvardhan, K.P. Prathish, T. Prasada Rao, J. Eelectroanal. Chem. (communicated).
[65] G. Chen, Z. Guan, C.T. Chen, L. Fu, V. Sundaresan, F.H. Arnold, Nat. Biotech. 15 (1997) 354.
[66] M.K.P. Leung, B.K.W. Chiu, M.H.W. Lam, Anal. Chim. Acta 491 (2003) 15.
[67] J. Hantash, A. Bartlcett, P. Oldfield, G. Denes, R. O'Rielly, F. David, Anal. Bioanal. Chem. 387 (2007) 351.

Talanta 76 (2008) 642–650

Contents lists available at ScienceDirect

Talanta

journal homepage: www.elsevier.com/locate/talanta

Identification and quantification of ibuprofen, naproxen, ketoprofen and diclofenac present in waste-waters, as their trimethylsilyl derivatives, by gas chromatography mass spectrometry

Á. Sebők[a,b], A. Vasanits-Zsigrai[a], Gy. Palkó[c], Gy. Záray[a,b], I. Molnár-Perl[a,*]

[a] Institute of Chemistry, Department of Analytical Chemistry, L. Eötvös University, Hungary
[b] Cooperative Research Center of Environmental Sciences, H-1518, Budapest 112, P.O. Box 32, Hungary
[c] Budapest Sewage Works Limited, 1087 Budapest, Asztalos Sándor Street 4, Hungary

ARTICLE INFO

Article history:
Received 11 December 2007
Received in revised form 1 April 2008
Accepted 7 April 2008
Available online 16 April 2008

Keywords:
GC–MS
Trimethylsilylation
Ionization technique
Mass fragmentation
Non-steroidal anti-inflammatory drugs
Waste-water

ABSTRACT

This paper reports a derivatization, mass fragmentation study relating to the most common, non-steroidal anti-inflammatory drugs (NSAIDs), such as ibuprofen, naproxen, ketoprofen and diclofenac, identified and quantified in the aquatic environment. Derivatizations have been performed with four silylation reagents in order to select the most proper one, taking into account analytical and financial points of view, equally. The tested reagents were *N*,*O*-bis(trimethylsilyl)trifluoroacetamide (BSTFA), *N*-methyl-*N*-(trimethylsilyl)trifluoroacetamide (MSTFA), *N*-methyl-*N*-*tert*-butyldimethylsilyl-trifluoroacetamide (MTBSTFA) and for this purpose at the first time, hexamethyldisilazan (HMDS) + trifluoroacetic acid (TFAA). Varying derivatization time and temperature, taking into consideration chemical and financial advantages, HMDS + TFAA proved to be the optimum selection. Responses of derivatives have been compared, as a function of the ionization technique (external/internal ionization), as well as on the treatment of compounds' selective fragment ions (SFIs): (i) extracting the corresponding, characteristic *m*/*z* masses from TIC elutions and (ii) from SIM elutions, in parallel. Reproducibilities of measurements, expressed in relative standard deviation percentages (R.S.D.%), including the nanogram and the low picogram levels of injected derivatives, provided an average between 0.93 R.S.D.% and 4.11 R.S.D.%. NSAIDs' enrichment was performed with solid-phase extraction (SPE), applying the Oasis HLB (Waters) cartridges: recoveries in the 1–6 $\mu g\,L^{-1}$ range varied between 84% and 111%, with an average reproducibility of 6.4 R.S.D.%. The utility of the optimized derivatization method is presented, on monthly basis, by the identification and quantitation of the ibuprofen, naproxen, ketoprofen and diclofenac content of the influent and effluent waste-water samples obtained from a Hungarian waste-water treatment plant.

1. Introduction

In order to identify and quantify several functional group containing compounds, simultaneously – like in case of pharmaceuticals, personal care products and their metabolites (further on: pollutants), present in waste, in river and in drinking waters – gas chromatographic mass spectrometric (GC–MS) analysis was accepted as a preferred technique [1–3]; Due to the fact that our selected four pollutants (ibuprofen, naproxen, ketoprofen and diclofenac) are all carboxylic acids (Fig. 1), they were identified and quantified by GC–MS as methyl [4–11], butyl [12], pentafluoropropyl [13], pentafluorobenzyl [14–18] and silyl [19–30] esters. Silyl derivatives were prepared with various silylating reagents, under different conditions.

Subsequently to solid-phase extractions (SPE) [19–28] a two-step procedure was introduced applying in the first step *N*-methyl-*N*-(trimethylsilyl)trifluoroacetamide (MSTFA) at room temperature, for 30 min, in the second step acetylation of the OH groups (if any) with *N*-methyl-bis(trifluoroacetamide) (MBTFA) at 60 °C, for 5 min [19–21]. Derivatizations with MSTFA alone were carried out at room temperature in dark, on a shaker for 12 h [22], or at 60 °C for 10 min with an additional 35 min reaction time at an ambient temperature [23,24]. *N*-Methyl-*N*-*tert*-butyldimethylsilyl-trifluoroacetamide (MTBSTFA) was used at 60 °C for 1 h [25,26] or, at 60 °C for 90 min [27].

Recently [28], four different silylating reagents {(1)–(4)} were compared, at various temperatures applying different reaction times, as follows:

* Corresponding author at: Institute of Chemistry, Department of Analytical Chemistry, L. Eötvös University, 2H-1518, P.O. Box 32, 112 Budapest, Hungary.
Tel.: +36 1 372 2616; fax: +36 1 372 2592.
E-mail address: perlne@chem.elte.hu (I. Molnár-Perl).

0039-9140/$ – see front matter © 2008 Elsevier B.V. All rights reserved.
doi:10.1016/j.talanta.2008.04.008

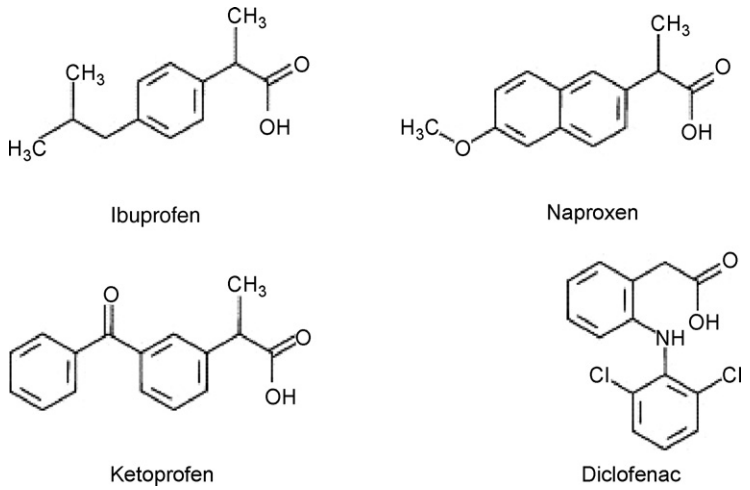

Fig. 1. Chemical structures of ibuprofen, naproxen, ketoprofen and diclofenac.

(1) *N,O*-Bis(trimethylsilyl)trifluoroacetamide (BSTFA) + 1% trimethylchlorosilane (TMCS) at 60 °C and 70 °C, for 10 min and 20 min;
(2) MSTFA + 1% TMCS at 23 °C and 60 °C, for 15 min and 30 min;
(3) Trimethylsilylimidazole (TMSI) at 23 °C and 70 °C, for 20 min, 30 min and 60 min;
(4) TMSI:*N,O*-bis(trimethylsilyl)acetamide (BSA):TMCS = 3:3:2 at 60 °C, for 180 min and 360 min. As a result of this comparison [28] BSTFA + 1% TMCS was selected as the most effective reagent at 70 °C, for 20 min, applying it with pyridine (PYR) at a (v/v) ratio of BSTFA:PYR = 2:1.

Derivatizations with BSTFA at 40 °C, for 1 h [29] and with MTBSTFA at room temperature, for 30 min performing on-fiber silylation, [30] were carried out in both cases, subsequently to solid-phase microextraction (SPME) enrichments [29,30].

To authors' knowledge, hexamethyldisilazane catalyzed by trifluoroacetic acid, in the analysis of non-steroidal anti-inflammatory drugs (NSAIDs), for the time being has not been applied. According to authors' experience [31–35] HMDS + TFA combined with PYR (containing hydroxylamine hydrochloride to label free carbonyl groups) proved to be in particular advantageous in the analysis of a wide scale of natural matrices. This derivatization condition ensures the intimate mixing/dissolving of the analyte(s) and reagents, providing quantitative silylation for the different, active proton containing functional groups.

The goal of this paper was

(a) to compare derivatization conditions for the commonly used reagents (MSTFA, BSTFA and MTBSTFA), including the suggested HMDS + TFA,
(b) to show the differences in responses—obtained by the internal and external ionization techniques, as well as,
(c) to perform TIC and SIM elutions, in parallel, in order to select the preferred one,
(d) to document the reproducibilities of the TMS (oxime) ester derivatives of ibuprofen, naproxen, ketoprofen and diclofenac, in the picogram concentration ranges, both from model solutions and from waste-water samples,
(e) to give an overview on the content of these four NSAIDs measured in the influent and effluent samples of a Hungarian waste-water treatment plant under a 16-month period of time and
(f) to compare the efficiency of their removal under the waste-water treatment process in comparison to those obtained in different other countries.

2. Experimental

2.1. Instrumentation

The apparatus consisted of a Varian 4000 GC–MS/MS system (Varian, Walnut Creek, CA, USA), equipped with a Varian CP-8400 AutoSampler, and with the septum-equipped programmable injector (SPI). The column used was a product of SGE (Victoria, Australia); SGE forte capillary: 30 m × 0.25 mm; d.f. = 0.25 μm. The temperature of the transfer line, ion trap and manifold were, in order of listing 280 °C, 210 °C and 80 °C, respectively.

SPE extractions were performed on the Visiprep DL Vacuum Manifold for 12 samples (Cat No. 57044) from Supelco (Bellefonte, PA, USA).

Extracts were dried on a Büchi Rotavapor R-200 by means of Büchi Vacuum pump, V-700, both from Büchi (Flawil, Switzerland).

2.2. Materials and reagents

All were of an analytical reagent grade. Pyridine, hydroxylamine·HCl from Reanal (Budapest, Hungary). Hexane, methanol, ethyl acetate, hexamethyldisilazane, bis-(trimethylsilyl)trifluoroacetamide, *N*-methyl-*N*-(trimethylsilyl)-trifluoroacetamide, *N-tert*.-Butyldimethylsilyl-*N*-methyltrifluoroacetamide trifluoroacetic acid (TFA) and model compounds such as, ibuprofen {α-methyl-4-(isobutyryl)phenyl acetic acid}, naproxen {(+)-6-methoxy-α-methyl-2-naphtalene acetic acid}, ketoprofen {2-(3-benzoylphenyl)propionic acid} and diclofenac sodium salt {2-[(2,6-dichlorophenyl)-amino]benzeneacetic acid sodium salt} were all from Sigma (St. Louis, MO, USA). Glass microfiber filters (GF/A 125 mm, ∅, Cat No. 1820–125) were from Whatman (Maidstone, UK). Cartridges (Oasis, HLB 6cc), for solid-phase extraction, were from Waters (Milford, MA, USA).

2.3. Solid-phase extraction

Cartridges, prior to extractions were treated with 5 mL hexane, 5 mL ethyl acetate, 10 mL methanol and 10 mL distilled water. Before the SPE enrichment, river and waste-water samples were filtered on glass microfiber paper. Water samples (0.25–1.0 L) were adjusted to

pH 4 and extractions were followed without or by adding different amounts of standard solutions, with a rate of 4–5 mL min^{-1}. Cartridges have been dried by vacuum, and elutions were performed, in order of listing with 5 mL hexane, 5 mL ethyl acetate, and with 14 mL methanol. The unified eluents were reduced in volume, evaporated to dryness by means of a rotary evaporator at 30–40 °C (further on: extract).

2.4. Preparation of the TMS/TBDMS (oxime) derivatives

Model compounds (20–25 mg 100 mL^{-1}, weighed with analytical precision were dissolved in water or in water/ethanol = 1/1 (v/v) solution and further diluted for 10×, 100×, 1000×. Model solutions (10–500 μL) and the extracts were rotary evaporated to dryness at 30–40 °C. The residues were treated with 125 μL pyridine (in case of oximation with 125 μL hydroxylamine·HCl containing pyridine {2.5 g hydroxylamine·HCl 100 mL^{-1}}) + 225 μL HMDS + 25 μL TFAA, or 150 μL pyridine + 150 μL BSTFA, or 150 μL pyridine + 150 μL MSTFA and 150 μL pyridine + 150 μL MTBSTFA in 2–4 mL Reacti vials. Vials were heated in oven, at 60 °C, 70 °C and 80 °C for 30 min, 60 min, 90 min and 120 min. Finally as optimum derivatization condition 70 °C and 90 min were selected. At each stage samples were taken for the analysis, e.g., after dilutions with the corresponding derivatization agent 1 μL of the diluted solutions was injected into the GC–MS system.

2.5. Separation of the TMS/TBDMS derivatives

Under gradient conditions, the optimized temperature programs different for both the column and the SPI were as follows:

(a) injections were made at 100 °C, and held at 100 °C for 1.0 min, then heated to 270 °C (200 °C min^{-1}), with a 3 min hold at 270 °C and
(b) column temperature starts at 100 °C, for 1 min, then heated up to 300 °C (20 °C min^{-1}), with a 5.5 min hold at 300 °C.

3. Results and discussion

3.1. Derivatization

Derivatization conditions have been optimized with four NSAIDs, such as ibuprofen, naproxen, ketoprofen and diclofenac, in order to clear up different conditions found in literature proposals.

The efficiency of trimetylsilylations has been compared, applying HMDS + TFA, BSTFA and MSTFA, under strictly the same conditions. At the beginning of our study we used the external ionization technique and reactions have been followed at 60 °C, 70 °C and at 80 °C, for 30 min, 60 min, 90 min and 120 min (Table 1).

On the basis of these experiences we could confirm that

(a) after 90 min reaction time there was no temperature dependence at all and
(b) at 70 °C temperature, between 60 min and 120 min reaction times, quantitative labeling has been obtained. 30 min reaction time proved to be unsatisfactory also at 70 °C: out of twelve cases in eight (Table 1, italic printed responses). Consequently, remaining on the safer side and taking into consideration also our next goal [36], which means we plan to use the same derivatization protocol for multiresidue analysis (including also compounds that do need extended derivatization time for quantitative labeling), thus, as optimum condition for trimethylsilylation 70 °C temperature and 90 min reaction time has been selected.

Table 1
Derivatization study of the non-steroidal anti-inflammatory drugs: response values obtained from model solutions, depending on the silylating agent and on the reaction time, determined on the basis of their selective fragment ions (m/z, SFIs)[a], by gas chromatography mass spectrometry (GC–MS)

at 70 °C		Integrator units 1^{-1} pg model compound, based on the total of SFIs			
Reagent	Reaction time, min	ibuprofen Inj. pg: 222 m/z=161±1 m/z=234±1 m/z=263±1 m/z=278±1	naproxen Inj. pg: 255 m/z=185±1 m/z=243±1 m/z=287±1 m/z=302±1	ketoprofen Inj. pg: 283 m/z=267±1 m/z=282±1 m/z=311±1 m/z=326±1	diclofenac Inj. pg: 314 m/z=214±1 m/z=242±1 m/z=277±1 m/z=368±1
HMDS	30	*2608* (3.13)	4823 (2.53)	*756* (5.33)	*2703* (9.3)
	60	2851 (1.49)	4944 (3.53)	807 (2.41)	4171 (5.1)
	90	2828 (1.67)	5098 (4.34)	781(3.67)	3853 (5.9)
	120	2802 (2.25)	4823 (4.62)	781 (5.0)	3980 (6.8)
BSTFA	30	*2608* (2.12)	5020 (1.85)	*770* (1.50)	4045 (0.41)
	60	2758 (1.24)	4823 (1.13)	816 (2.73)	4012 (2.62)
	90	2909 (1.44)	4862 (3.84)	795 (7.62)	3821 (4.37)
	120	2829 (1.93)	4902 (0.82)	812 (1.80)	*3566* (5.3)
MSTFA	30	2873 (0.77)	*4352* (11)	*922* (2.70)	*4713* (1.40)
	60	2779 (1.92)	5294 (1.58)	830 (4.11)	4426 (0.55)
	90	2909 (2.39)	5176 (0.68)	798 (1.23)	4333 (1.68)
	120	2838 (2.43)	4823 (5.1)	765 (4.94)	*3566* (12)
Av.		2837 (1.78)	4963 (3.30)	798 (2.54)	4080 (5.3)

Indications: inj. pg, injected pg; SFIs, taking into account averages of three separate derivatizations; in parentheses, R.S.D.%; italic printed values have been omitted from the mean. Naproxen (Mw = 230.3); m/z = 302 = $[M]^{\ddagger}$; m/z = 287 = $[M-CH_3]^+$; m/z = 243 = $[M-(COO+CH_3)]^+$; m/z = 185 = [M−TMSCOO]. Ketoprofen: (Mw = 254.3), m/z = 326 = $[M]^{\ddagger}$; m/z = 311 = $[M-CH_3]^+$. m/z = 282 = $[M-COO]^+$; m/z = 267 = $[M-(COO+CH_3)]^+$. Diclofenac(Na): (Mw = 318.13; m/z = 368 = $[M]^{\ddagger}$; m/z = 277 = $[M-TMSOH_2]^+$. m/z = 242 = $[M-(TMSOH+HCl)]^+$; m/z = 214 = $[M-(TMSCOOH+HCL)]^+$. [a]As trimethylsilyl (TMS) derivatives obtained with the HMDS, BSTFA and MSTFA reagents; ibuprofen (Mw = 206.3); m/z = 278 = [M]; $[M-CH_3]^+$ = 263; m/z = 234 = $[M-COO]^+$; m/z = 161 = $[M-TMSCOO]^+$.

Later on, reverting to the considerable higher responses furnishing internal ionization technique (details in section entitled "Comparison of the external and internal ionization techniques"), HMDS and MTBSTFA labeling was also compared. In this case at 70 °C, only, as a function of the reaction time (Table 2). Response values obtained with MTBSTFA revealed that,

(a) in case of our selected NSAIDs also *tert*-butyldimethylsilylation proved to be quantitative after 30 min derivatization time and
(b) TBDMS derivatives furnish considerable higher responses compared to the TMS ones (Table 2, last column: response ratio values).

As to the selection of the silylating agents, out of the four reagents tested, for our further studies trimethylsilylation with HMDS + TFA was preferred. Since

(a) this reagent ensures the same efficiency as MSTFA and BSTFA (Table 1),
(b) MTBSTFA does not react unambiguously with the sterically hindered groups, such as estrogens [37–39] (being target compounds in our multiresidue analysis system: under preparation [36]) and in addition
(c) HMDS + TFA is the most cost-effective reagent: according to 2006–2007 Sigma Catalogues. The price of 1 mL HMDS, BSTFA, MSTFA and MTBSTFA, in order of their listing, they cost €0.19, €3.44, €8.08 and €21.6 respectively. It means that the price of MTBSTFA is more than hundredfold higher (21.6/0.19 = 113.7) compared it to the price of the HMDS reagent.

Table 2
Responses calculated on the total of selective fragment ions (SFI) of derivatives obtained by HMDS + TFA and MTBSTFA at 70 °C, as a function of the reaction time

Compounds⇓		Response values: Integrator units (Iu) pg^{-1}												Response ratios:
		HMDS+TFAA						MTBSTFA						
Reaction time, ⇒ min		30	60	90	120	Ave-rage	RSD %[a]	30	60	90	120	Ave-rage	RSD %[a]	MTBSTFA/ HMDS
Ibuprofen	Iu pg^{-1}	17227	17591	17955	17273	17512	1.92	49545	50455	47727	48182	48977	0.20	48977/17512= **2.8**
	RSD%[b]	3.90	2.59	2.84	2.44			6.12	2.60	2.39	1.45			
Naproxen	Iu pg^{-1}	40323	39597	39777	38992	39672	1.38	77823	76210	79839	79839	78428	2.24	76539/39672= **1.9**
	RSD%[b]	9.1	1.54	6.13	2.79			3.24	4.20	1.62	1.42			
Ketoprofen	Iu pg^{-1}	16418	16028	15816	15425	15924	2.60	67376	70921	65248	68840	68096	3.51	68096/15924= **4.3**
	RSD%[b]	2.18	1.53	6.65	5.04			3.20	0	0.54	6.9			
Diclofenac	Iu pg^{-1}	31975	31348	30251	30012	30897	2.99	44201	44828	42006	41379	43104	3.87	43104/30897= **1.4**
	RSD%[b]	7.74	1.89	8.0	4.50			3.51	2.01	4.66	0.88			

Response values for the TMS derivatives were calculated on the masses of selective fragment ions as detailed in Table 1, while for the TBDMS ones, as follows: ibuprofen (Mw = 206.3); $m/z = 320.6 = [M]^{\ddagger}$; $[M-15]^+ = 305$; $[M-57]^+ = 263$; $m/z = 161 = [M-TBDMSCOO]^+$. Naproxen: (Mw = 230.3); $m/z = 344.5 = [M]^{\ddagger}$; $m/z = 329 = [M-CH_3]^+$; $m/z = 287 = [M-57)]^+$; $m/z = 185 = [M-TBDMSCOO]$. Ketoprofen: (Mw = 254.3), $m/z = 368.5 = [M]^{\ddagger}$; $m/z = 311 = [M-57]^+$; $m/z = 295 = [M-(57+16)]^+$; $m/z = 267 = [M-(COO+57)]^+$. Diclofenac(Na) (Mw = 318.13; $m/z = 410 = [M]^{\ddagger}$; $m/z = 353 = [M-57]^+$; $m/z = 242 = [M-TBDMSCOO]$; $m/z = 214 = [M-(TBDMSCOOH+HCl)]^+$.
[a]Indications: reproducibility of responses obtained after various derivatization times.
[b]Reproducibility of responses obtained from parallel derivatizations.

3.2. Comparison of the external and internal ionization techniques

In order to exhaust the possibilities of our ionization system the two ionization techniques have been compared on the basis of the responses of the NSAID content of a waste-water sample (Fig. 2). (Note: it is worth to remark that ionization techniques' have been compared with a new (6 months old) apparatus, within 2 weeks: it means at the same GC–MS conditions. The main difference between the internal and external ionizations might be similar to that which exists between the ion trap and quadrupole techniques resulting in higher response/sensitivity provided by the ion trap ionization compared to the quadrupole one. In addition, according to the structure of the Varian 4000 MS detector, the way of ions forced to get to the multiplier are considerably longer in the case of external ionization in comparison to the way of ions intended to reach the ring electrodes of the ion trap.)

Response values, compared in arbitrary units corresponding to the ng L^{-1} concentrations of samples revealed that internal ionization technique provided by ~15–25 times higher responses compared to the corresponding external one. It means that

(a) the internal ionization technique (Fig. 2: black columns), at the 10–104 ng L^{-1}, 12–119 ng L^{-1}, 13–133 ng L^{-1}, and 15–147 ng L^{-1} ranges, provides commensurable responses
(b) as obtained by the external ionization technique (Fig. 2: gray columns), at considerable higher concentrations, at

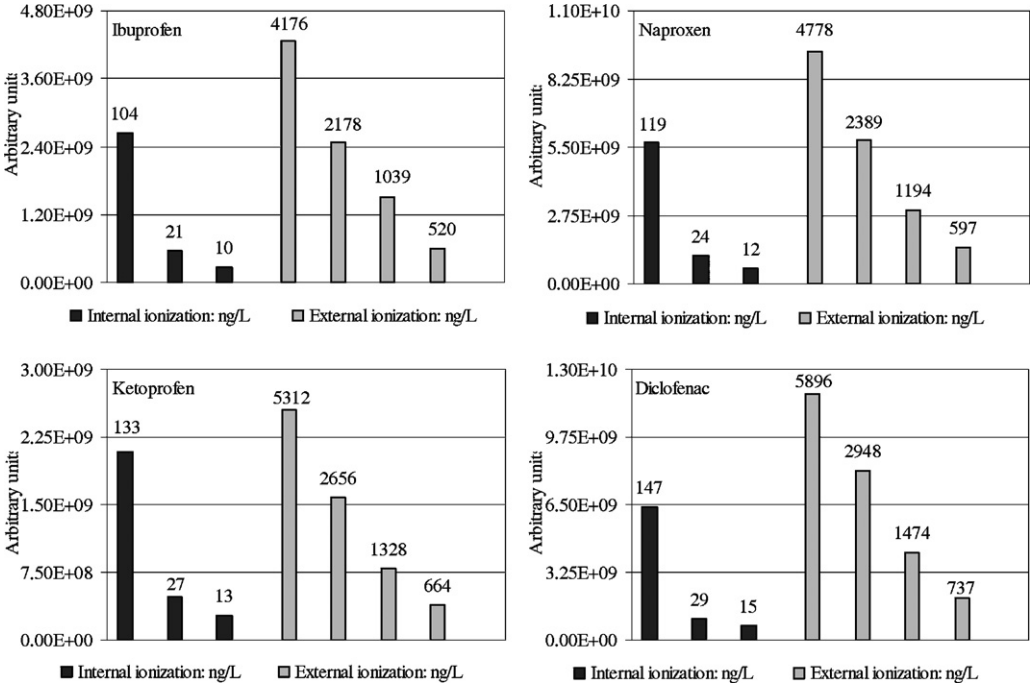

Fig. 2. Comparison of responses obtained for the trimethylsilyl derivatives of ibuprofen, naproxen, ketoprofen and diclofenac, determined by internal (dark gray columns) and by external (light gray columns) ionization techniques.

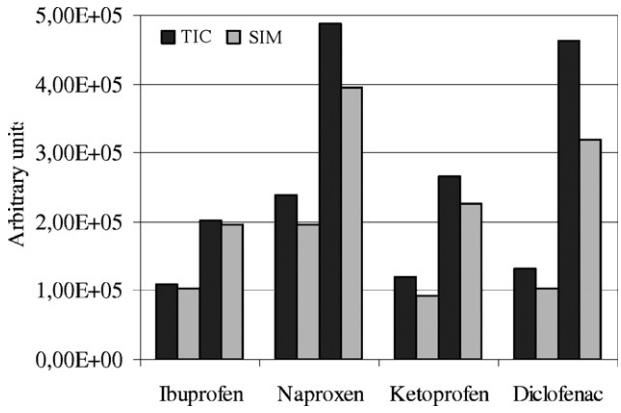

Fig. 3. Comparison of responses obtained for the trimethylsilyl derivatives of ibuprofen, naproxen, ketoprofen and diclofenac, evaluated on the basis of the same selective fragment ions (Table 1) subtracting from TIC (dark gray columns) chromatograms and obtained by SIM (light gray columns) elutions.

the 520–4176 ng L^{-1}, 597–4778 ng L^{-1}, 664–5312 ng L^{-1} and 737–5896 ng L^{-1} ranges. Consequently, all further studies were carried out applying the internal ionization technique.

Comparison of response values evaluated on the basis of the total ion current (TIC) and of the selective fragment ion monitoring (SIM) elutions.

In this context the behavior of our four target compounds was tested, in the low concentration ranges (Fig. 3: 5–10 pg injected amounts). Comparing the response ratios (TIC/SIM), evaluated on the basis of the same ions (detailed in Table 1), by subtracting selective fragments ions from TIC elutions (black columns) and in parallel from SIM elutions (gray columns) (*note: total ion current chromatogram is also called as reconstructed ion chromatogram (RIC)).

Evaluating responses it turned out that in all cases tested, in terms of waste-water solutions' analysis TIC elutions should be preferred. For two reasons:

Table 3
Recovery of the non-steroidal, anti-inflammatory drugs from a waste-water influent sample fortified with various amounts of ibuprofen, naproxen, ketoprofen and diclofenac: subsequently to SPE treatment, derivatized, ionized and evaluated under optimum conditions

Derivatized* ⇓	µg/l L compound, based on the total of SFIs**			
	ibuprofen	naproxen	ketoprofen	diclofenac
Influent sample, no addition	0.410 (10)	1.910 (2.7)	1.780 (4.5)	5.504 (3.1)
Influent sample, fortified with	Recovery %			
1. 4 -6µg/L	98	101	106	103
2. 2-3µg/L	104	84	101	93
3. 1-1.5µg/L	98	105	93	103
Average of 1. -3. (RSD%)	100.0 (3.5)	96.7 (11)	100.0 (6.6)	99.7 (5.8)

Indications: as in Tables 1 and 2, as well as: in parentheses = R.S.D. percentages obtained from 3 parallel derivatizations and/or from the recovery of samples fortified with three different amounts of NSAIDs; Derivatized amounts.
[a]Weighed with analytical precision, into 1 L sample.
[b]SFIs detailed in Table 1.

(1) responses subtracted from TIC elutions provided higher values in cases of 5 pg and 10 pg injected compounds, equally (providing without exception a signal to noise ratio ≥10). In the order of their listing, response ratios of TIC/SIM responses proved to be for ibuprofen (1.04, 1.22), for naproxen (1.23, 1.22), for ketoprofen (1.17, 1.20) and for diclofenac (1.44,1.36) and
(2) because of TIC elutions'main advantage. This means TIC elutions, in archived form, are available for the identification and quantifications of further compounds from the same chromatogram, in case of future interest.

3.3. Extraction of NSAIDs from waste-water samples

Prior to the chromatographic analysis in case of all waste-water samples an introductory, pollutants' enrichment step needs to be inserted. According to the literature, as the best choice for this

Table 4
Reproducibility in the quantitation of ibuprofen, naproxen, ketoprofen and diclofenac on the basis of their selective fragment ions: (A) from model solutions and (B) from an influent waste-water sample, as their trimethylsilyl (oxime) ester derivatives obtained under optimum derivatization, ionization and evaluation conditions

Compounds ⇓ (m/z values)	**A** Response values from model solutions: Integrator units/pg; (RSD%[a])						**B** Obtained (pg) from the influent waste-water samples in 1µL injected stock solution; (RSD%[a])					
Injected: in 1 µL stock solution ⇒	6.93-9.83	13.85-19.65	27.70-39.30	55.40-78.60	Average	RSD %[b]	waste-water, L 0.25	0.50	1.0	Average[c]	RSD %[d]	Corresponds to: µg L^{-1}**
Ibuprofen (161+263+234+278)	7873 (2.38)	8311 (1.53)	8017 (2.80)	8133 (0.10)	8084	2.29	49.23 (3.70)	114.2 (5.2)	231.3 (0.74)	4.11	8.9	4.11
Naproxen (185+243+287+302)	14266 (1.35)	14284 (5.2)	14393 (2.48)	14795 (3.23)	14435	1.71	46.48 (3.08)	84.52 (2.62)	170.4 (3.48)	3.29	5.4	3.29
Ketoprofen (oxime) (207+398+413)	18150 (10)	18361 (0.99)	18164 (0.71)	17514 (0.06)	18047	2.04	not found					
Diclofenac (214+242+277+368)	15402 (3.63)	15369 (1.62)	15140 (1.89)	15140 (1.28)	15263	0.93	41.41 (1.99)	81.24 (1.85)	155.3 (4.15)	3.03	3.1	3.03

Indications: response values for the TMS derivatives were calculated on the masses of selective fragment ions as detailed in Table 1, except for the ketoprofen' s oxime: $m/z = 413 = [M]$, $m/z = [M-15]^+ = 398$, $m/z = 207 = [M-(TMSO + TMSCOO)]^+$; not found = <5 pg per injection.
[a]Reproducibility of responses obtained from parallel extractions and derivatizations.
[b]Reproducibility of responses obtained from different extracted and derivatized amounts of NSAIDs.
[c]Average = related to 1 µL waste-water sample, obtained from 0.25 L, 0.50 L and 1.0 L extracted and derivatized waste-water.
[d]Reproducibility of NSAID content of waste-water, obtained from three different amounts (0.25 L, 0.5 L and 1 L)
[e]ng L^{-1} = taking into consideration that from 0.25 L, 0.5 L and 1 L waste-water samples, uniformly 375 µL derivatized stock solutions were prepared, before injection diluted fifty folds: injected 1 µL (corresponds to 13.3 µL, 26.6 µL and 53.2 µL original waste-water samples).

purpose, we selected solid-phase extraction applying the porous polymer Oasis® HLB cartridges [4–7,12,13,25–27,29,30].

Our experiences, in accordance with the literature, confirmed an acceptable recovery (Table 3), which served as the reassuring basis for the reliable and reproducible analysis of the NSAID contents of our influent and effluent waste-water samples: recoveries from the fortified influent waste-water samples (added amounts in the 1–6-$\mu g\,L^{-1}$ range) varied between 84% and 106%, with an average recovery of 99% and with an average reproducibility of 6.7 R.S.D.%.

3.4. Reproducibility studies

On the basis of our optimized extraction, derivatization (HMDS + TFA), ionization (internal ionization) and mass evaluation (TIC) processes we defined the reproducibility values of our target compounds, both from model solutions and from waste-water samples (Table 4, Fig. 4a and b).

In the frame of these studies, in favor of the carbonyl group containing ketoprofen, the two-step derivatization process has been introduced: prior to the trimethylsilylation the oximation step was inserted. This combined derivatization protocol leaded to the particularly characteristic double peak of the TMS-syn and anti-oximes of ketoprofen (Fig. 4b, spectrum 1A), with a ≥3 times higher response values of TMS(oxime)–ketoprofen compared to the TMS–ketoprofen's one.

The peak profile and mass spectra of a standard and an influent waste-water sample are shown in Fig. 4a,b by spectra 1A, 2A and 3A, 4A.

As seen, data evaluations have been performed on the basis of selective fragment ions, detailed fragment composition in Table 1 (except TMS (oxime)–ketoprofen), as follows:

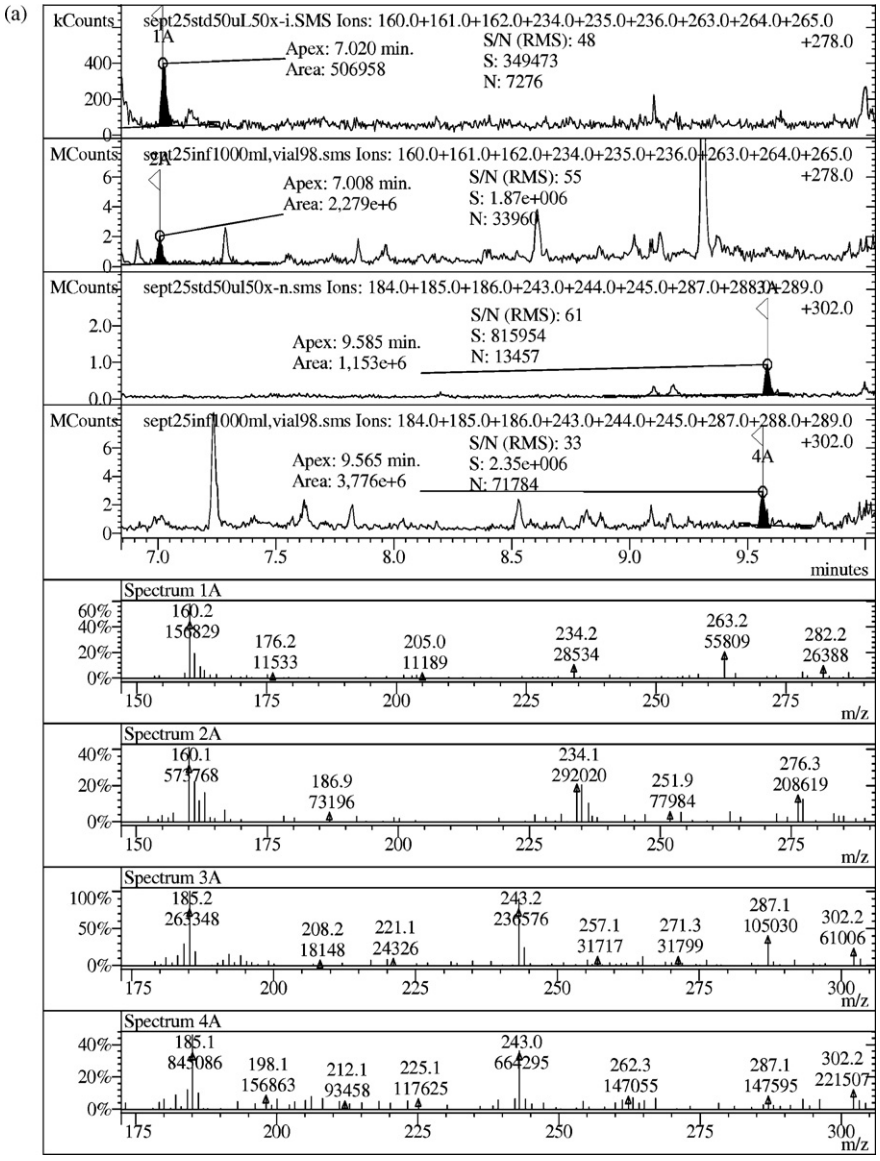

Fig. 4. (a) The peak profile and mass spectra obtained for the trimethylsilyl (oxime) derivatives of ibuprofen and naproxen. Spectra 1A and 3A, from standard solutions; spectra 2A and 4A, from influent waste-water samples. From standard solutions the peaks represent 55.4 pg ibuprofen, 63.7 pg naproxen, from the influent waste-water sample 231.3 pg ibuprofen, 170.4 pg naproxen (detailed data in Table 4). (b) The peak profile and mass spectra obtained for the trimethylsilyl (oxime) derivatives of ketoprofen and diclofenac. Spectra 1A and 3A, from standard solutions; spectra 2A and 4A, from influent waste-water samples. From standard solutions the peaks represent 70.84 pg ketoprofen, 78.6 pg diclofenac, from the influent waste-water sample <5 pg ketoprofen and 155.3 pg diclofenac (detailed data in Table 4).

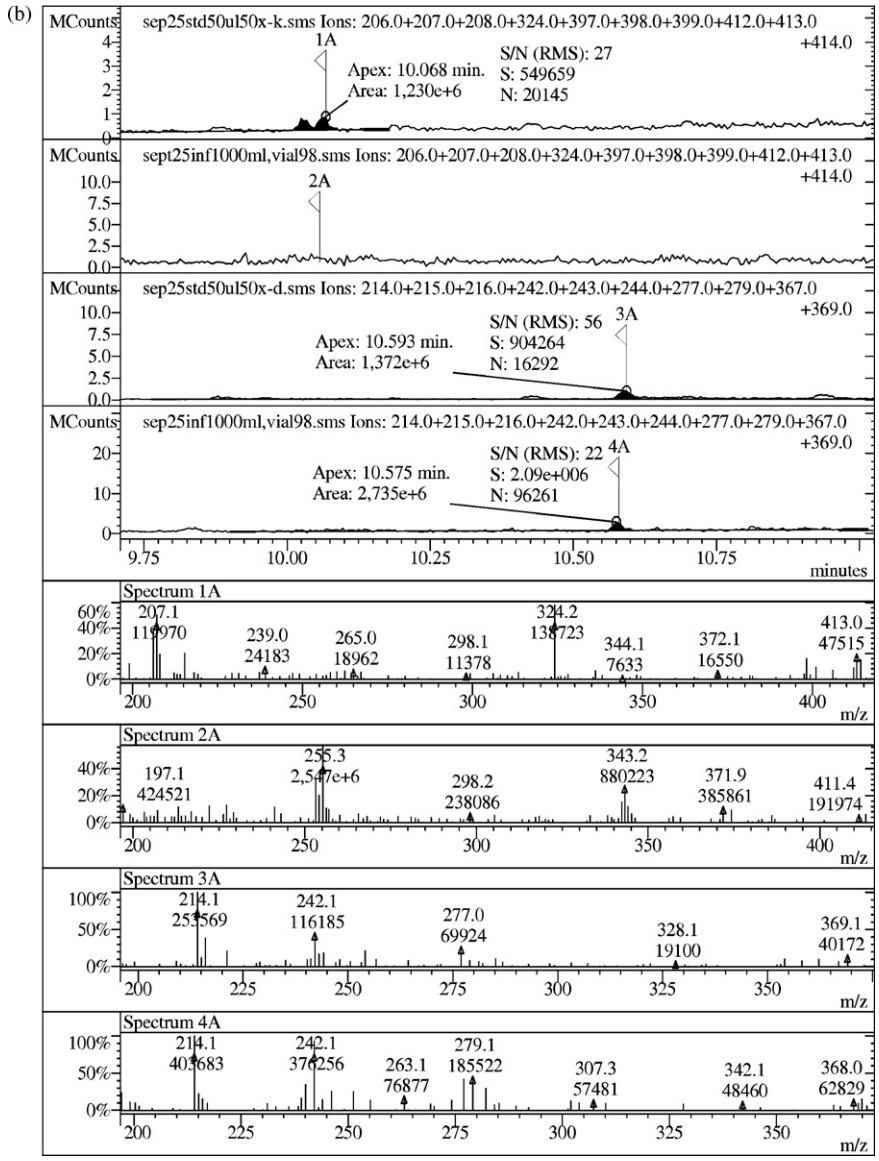

Fig. 4. (*Continued*).

TMS-ibuprofen by ions at $m/z = 161$, at $m/z = 234$, at $m/z = 263$ and $m/z = 278$ (Fig. 4a, spectra 1A and 2A),
TMS-naproxen by ions at $m/z = 185$, at $m/z = 243$, at $m/z = 287$ and $m/z = 302$ (Fig. 4a, spectra 3A and 4A),
TMS(oxime)–ketoprofen by ions at $m/z = 207$, at $m/z = 324$, at $m/z = 398 = [M-CH_3]^+$ and at $m/z = 413 = [M]^+$ (Fig. 4b, spectrum 1A; according to spectrum 2A influent waste-water did not contain ketoprofen) and
TMS–diclofenac by ions at $m/z = 214$, $m/z = 242$, $m/z = 277$ and $m/z = 368$ (Fig. 4b, spectra 3A and 4A).

Reproducibilities obtained from model solutions:

(a) applying parallel derivatizations of the same amounts of compounds (Table 4A: R.S.D.%[a]) varied between 0.06 and 5.2 R.S.D.%, while
(b) in cases of different amounts of the NSAIDs, in the 6.93–78.6 pg range (Table 4A: R.S.D.%[b]), differences proved to be between 0.93 R.S.D.% and 2.46 R.S.D.%.

Reproducibilities from three different amounts of influent waste-water samples (12 September 2007: 0.25 L, 0.50 L and 1 L):

(a) performing extraction and derivatization from the same amounts of influent waste-waters (Table 4B: R.S.D.%[a]) varied between 0.74 and 5.2 relative standard deviation percentages, while
(b) performing extractions and derivatizations from various amounts of influent waste-water samples (0.25 L, 0.50 L and 1.0 L, Table 4B: R.S.D.%[d]), varied between 3.1 R.S.D.% and 8.9 R.S.D.%.

3.5. The NSAID content of a Hungarian waste-water treatment plant's influent and effluent samples

Under a 17-month period (from May 2006 to September 2007) influent and effluent waste-water samples have been analyzed 16 times (Fig. 5: 2007 Augustus sampling was omitted).
Results revealed that

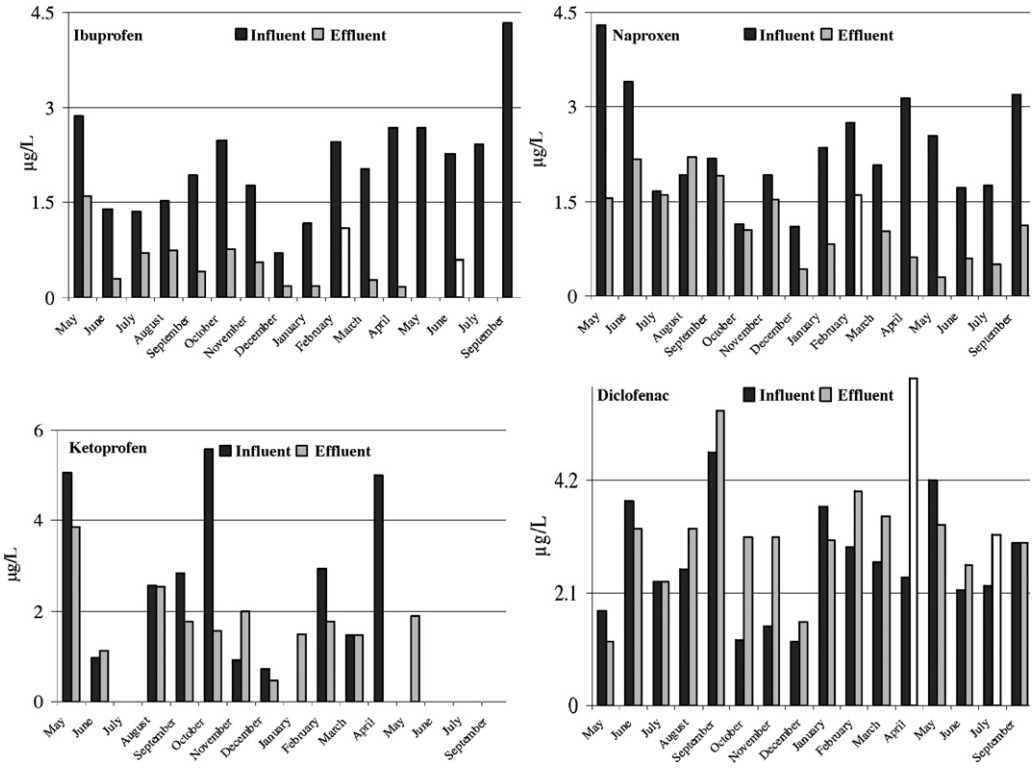

Fig. 5. The NSAID content of a Hungarian waste-water treatment plant's influent and effluent waste-water samples, in the period of May 2006–September 2007.

(a) all influent samples (Fig. 5) did contain ibuprofen, naproxen and diclofenac, while out of sixteen cases in five ketoprofen was not found.
(b) The composition of the effluent samples reflects unambiguous removal of ibuprofen and naproxen, altering removal of ketoprofen, and out of 16 cases in 10 surpluses of the particularly stable diclofenac.

Removals' percentages of ibuprofen and naproxen varied from 44% to 100% (ibuprofen) and from 9% to 81% (naproxen). The reason(s) of the higher diclofenac contents of effluent waste-waters in comparison to the influent ones might be attributed to the hydrolysis of diclofenac-glucoronides under the treatment process.

3.6. Comparison of the NSAID content of the influent and effluent waste-water samples reported from different countries

In order to evaluate the differences and/or the similarities of the NSAID contents of waste-waters, treated throughout the globe and measured according to different protocols [13,17,25,30,40], literature data are compiled in Table 5. In this term results, including our ones (determined at the first time in Hungary) were reassuring. Since, data proved that

(a) the NSAIDs' level and the efficiency of their removal are comparable: considerable differences have not been reported. Very likely due to the fact that
(b) the use of these NSAIDs are – everywhere on the globe uniformly – popular, and also
(c) treatment processes applied in the waste-water treatment plants are the conventional mechanical, biological and chemical cleaning procedures.

Table 5
The contamination of influent and effluent waste-waters with ibuprofen, naproxen ketoprofen and diclofenac determined in different countries

Country/Town [Ref]	No/Pe	I/E/D	NSAIDs: µg L^{-1}			
			Ibuprofen	Naproxen	Ketoprofen	Diclofenac
Canada/Ontario [13]	3/ month	I	6.77	2.76	0.08	0.17
		E	0.31	0.82	0.05	0.11
		D	6.46 (**95**)	1.84 (**67**)	0.03 (**38**)	0.06 (**35**)
USA/Baltimore [17]	1	I	1.90	3.20	1.20	0.11
		E	0.25	0.38	0.28	0.09
		I	1.65 (**87**)	2.82 (**88**)	0.92 (**77**)	0.02 (**18**)
Spain/city of 1×10^5 inhabitants [25]	2/ month	I	4.29	3.50	-	-
		E	1.50	1.51	-	-
		I	2.79 (**65**)	1.99 (**57**)	-	-
Spain/Santiago de Compostela [30]	1	I	2.75	2.18	-	-
		E	0.55	0.16	-	-
		I	2.20 (**80**)	2.02 (**93**)	-	-
Croatia/city unknown [41]	1	I	0.52	0.099	0.45	0.25
		E	0.27	0.108	0.32	0.22
		D	0.25 (**48**)	0.009 (**9**)*	0.13 (**29**)	0.03 (**12**)
Hungary/Budapest [this paper]	16/ month	I	2.01	2.33	1.75	2.65
		E	0.58	1.19	1.12	3.27
		D	1.43 (**71**)	1.14 (**50**)	0.63 (**36**)	0.52 (**20**)*

Indications: No/Pe = number of sampling/period of time, month; I/E/D = concentrations in influent (I), in effluent (E) samples and the difference (D) between them (bold printed values in parentheses represent the removal of pollutants, expressed in percentages); –, no data available.
[a]Surplus, reason unknown.

4. Conclusions

(1) Reliable, reproducible fast and cost-effective gas chromatographic mass spectrometric method has been developed for the identification and quantification of four non-steroidal anti-inflammatory drugs as their trimethylsilyl(oxime) ester derivatives.

(2) Derivatization, ionization and data evaluation methods have been studied and optimized: it was shown that
   (a) trimethylsilylation with HMDS + TFA ensures the same efficiency as MSTFA and BSTFA (strictly under the same conditions) and
   (b) it is also the most cost-effective reagent.
(3) It was demonstrated that internal ionization technique furnished 15–25 times higher responses in comparison to the external one.
(4) On the basis of parallel TIC and SIM elutions, performing data evaluations evaluations with the same the same selective fragment ions, in the case of waste-water analysis, TIC elutions were preferred. Since, TIC elutions
   (a) provide higher responses and
   (b) are available in archived form for future interest.
(5) Reproducibilities in the quantitation of ibuprofen, naproxen ketoprofen and diclofenac, both from model- and from waste-water solutions, in the 7–250-pg ranges proved to be between 0.93 and 4.11 R.S.D.%.
(6) The four NSAIDs' contents determined in the influent and effluent waste-waters of a Hungarian waste-water treatment plant were followed under a 17-month period of time. Our results, in accordance with those measured in Canada, in the United States, in Spain and in Croatia revealed uniformly, that both

(a) the level of these four NSAIDs and
(b) the efficiency of their removal do not differ significantly: due to the worldwide popularity of these NSAIDs, and to the very similar elimination processes applied for their removal.

Acknowledgement

This work was supported by the Hungarian Academy of Sciences (Project No. OTKA T0-47199).

References

[1] M. Petrovic, S. Gonzales, D. Barceló, Trends Anal. Chem. 22 (2003) 685–696.
[2] L.M. Hewitt, C.H. Marvin, Mut. Res. 589 (2005) 208–232.
[3] M. Farré, M. Petrovic, D. Barceló, Anal. Bioanal. Chem. 387 (2007) 1203–1214.
[4] S. Öllers, H.P. Singer, P. Fassler, S.R. Müller, J. Chromatogr. A 911 (2001) 225–234.
[5] S.S. Verenitch, C.J. Lowe, A. Mazumder, J. Chromatogr. A 1116 (2006) 193–203.
[6] S. Weigel, R. Kallenborn, H. Hühnerfuss, J. Chromatogr. A 1023 (2004) 183–195.
[7] M. Stumpf, T.A. Ternes, K. Haberer, P. Seel, W. Baumann, Vom Wasser 86 (1996) 291–303.
[8] T.A. Ternes, M. Stumpf, B. Schuppert, K. Haberer, Vom Wasser 90 (1998) 295–309.
[9] C. Zwiener, F.H. Frimmel, Sci. Total. Environ. 309 (2003) 201–211.
[10] S. Weigel, J. Kuhlmann, H. Hühnerfuss, Sci. Total Environ. 295 (2002) 131–141.
[11] M. Petrovic, Z. Debeljak, N. Blazevic, J. Pharm. Biomed. Anal. 39 (2005) 531–534.
[12] W.C. Lin, H.C. Chen, W.H. Ding, J. Chromatogr. A 1065 (2005) 279–285.
[13] H.B. Lee, T.E. Peart, M.L. Svodoba, J. Chromatogr. A 1094 (2005) 122–129.
[14] B. Soulet, A. Tauxe, J. Tarradellas, Int. J. Environ. Anal. Chem. 82 (2002) 659–667.
[15] K. Reddersen, Th. Heberer, J. Chromatogr. A 1011 (2003) 221–226.
[16] V. Koutsouba, Th. Heberer, B. Fuhrmann, K. Schmidt-Baumler, D. Tsipi, A. Hiskia, Chemosphere 51 (2003) 69–75.
[17] J.T. Yu, E.J. Bouwer, M. Coelhan, Agric. Water Manage. 86 (2006) 72–80.
[18] F. Sacher, F.T. Lange, H.J. Brauch, I. Blankenhorn, J. Chromatogr. A 938 (2001) 199–201.
[19] T.A. Ternes, R. Hirsch, J. Mueller, J.K. Haberer, Fresen. J. Anal Chem. 362 (1998) 329–340.
[20] T.A. Ternes, Water Res. 32 (1998) 3245–3260.
[21] S. Wiegel, A. Aulinger, R. Brockmeyer, H. harms, J. Löffler, H. Reincke, R. Schmidt, B. Stachel, W. von Tümpling, A. Wanke, Chemosphere 57 (2004) 107–126.
[22] T. Kosjek, E. Heath, A. Krbavcic, Environ. Int. 31 (2005) 679–685.
[23] O.A.H. Jones, N. Voulvoulis, J.N. Lester, Chromatographia 58 (2003) 471–477.
[24] O.A.H. Jones, N. Voulvoulis, J.N. Lester, Environ. Pollut. 145 (2007) 738–744.
[25] I. Rodriguez, J.B. Quintana, J. Carpinteiro, A.M. Carro, R.A. Lorenzo, R. Cela, J. Chromatogr. A 985 (2003) 265–274.
[26] M. Carballa, F. Omil, J.M. Lema, M. Llompart, C. García-Jares, I. Rodrígues, M. Gómez, T. Ternes, Water Res. 38 (2004) 2918–2926.
[27] Z. Yu, S. Peldszus, P.M. Huck, J. Chromatogr. A 1148 (2007) 65–77.
[28] S.L. Rice, S. Mitra, Anal. Chim. Acta 589 (2007) 125–132.
[29] M. Moeder, S. Schrader, M. Winkler, P. Popp, J. Chromatogr. A 873 (2000) 95–106.
[30] I. Rodríguez, J. Carpinteiro, J.B. Quintana, A.M. Carro, R.A. Lorenzo, R. Cela, J. Chromatogr. A 1024 (2004) 1–8.
[31] I. Molnár-Perl, Rev. J. Chromatogr. A 845 (1999) 181–195.
[32] I. Molnár-Perl, Rev. J. Chromatogr. A 891 (2000) 1–32.
[33] I. Molnár-Perl, Zs. Füzfai, Rev. J. Chromatogr. A 1073 (2005) 201–227.
[34] I. Boldizsár, Z. Szűcs, Zs. Füzfai, I. Molnár-Perl, J. Chromatogr. A 1133 (2006) 259–274.
[35] Zs. Füzfai, I. Molnár-Perl, J. Chromatogr. A 1149 (2007) 88–101.
[36] Á. Sebők, A. Vasanits-Zsigrai, A. Helenkár, Gy. Záray, I. Molnár-Perl, Presented at the Riva del Garda Symposium, J. Chromatogr. A (2008), in preparation.
[37] A. Shareef, C.J. Parnis, M.J. Angove, J.D. Wells, B.B. Johnson, J. Chromatogr. A 1026 (2004) 295–300.
[38] A. Shareef, M.J. Angove, J.D. Wells, J. Chromatogr. A 1108 (2006) 121–128.
[39] H. Noppe, K. Verheyden, W. Gillis, D. Courtheyn, P. Vanthemsche, H.F. De Brabander, Anal. Chim. Acta 586 (2007) 22–29.
[40] M. Gros, M. Petrovic, D. Barceló, Talanta 70 (2006) 678–690.

Talanta 76 (2008) 680–684

Contents lists available at ScienceDirect

Talanta

journal homepage: www.elsevier.com/locate/talanta

Simultaneous determination of eight pesticide residues in coconut using MSPD and GC/MS

Maria Geovânia Dantas Silva, Adriano Aquino, Haroldo Silveira Dórea, Sandro Navickiene*

Departamento de Química, Universidade Federal de Sergipe, Av. Marechal Rondon s/no, 49100-000 São Cristóvão, SE, Brazil

ARTICLE INFO

Article history:
Received 5 January 2008
Received in revised form 7 April 2008
Accepted 8 April 2008
Available online 20 April 2008

Keywords:
MSPD
Coconut pulp
Lipophilic matrix
Pesticides
GC/MS

ABSTRACT

A simple and effective extraction method based on matrix solid-phase dispersion (MSPD) was developed to determine dimethoate, malathion, lufenuron, carbofuran, 3-hydroxycarbofuran, thiabendazole, difenoconazole and trichlorfon in coconut pulp using gas chromatography–mass spectrometry with selected ion monitoring (GC/MS, SIM). Different parameters of the method were evaluated, such as type of solid-phase (C_{18}, alumina, silica-gel and Florisil), the amount of solid-phase and eluent (dichloromethane, acetone, ethyl acetate, acetonitrile, *n*-hexane and *n*-hexane:ethyl acetate (1:1, v/v)). The best results were obtained using 0.5 g of coconut pulp, 1.0 g of C_{18} as dispersant sorbent, 1.0 g of Florisil as clean-up sorbent and acetonitrile saturated with *n*-hexane as eluting solvent. The method was validated using coconut pulp samples fortified with pesticides at different concentration levels (0.25–1.0 mg kg^{-1}). Average recoveries (four replicates) ranged from 70.1% to 98.7%, with relative standard deviations between 2.7% and 14.7%, except for lufenuron and difenoconazole, for which recoveries were 47.2% and 48.2%, respectively. Detection and quantification limits for coconut pulp ranged from 0.02 to 0.17 mg kg^{-1} and from 0.15 to 0.25 mg kg^{-1}, respectively.

1. Introduction

Brazil possesses good environmental conditions for coconut cultivation, with the northeast of the country responsible for 83% of Brazilian production. By-products of coconut pulp, such as coconut oil and coconut milk, have been commercialized and are widely employed in the food and cosmetic industries [1]. Pesticides are extensively used in this culture at various stages of cultivation to control pests and diseases that might cause yield reduction. As a result, the Brazilian government has established maximum residue limits for 18 compounds in coconuts [2]. Those most extensively used in Brazil belong to the organophosphorus, benzimidazoles and triazoles categories, and are mainly malathion, dimethoate, difenoconazole, lufenuron, carbofuran, 3-hydroxycarbofuran, trichlorfon and thiabendazole. Following application, pesticide residues may remain in the crop and constitute a health risk due to their toxicity. Therefore, the monitoring of pesticide residues in coconut pulp is of particular concern from the consumer safety perspective. Notably, studies have suggested that malathion and dimethoate may act as potential endocrine disruptors [3–5]. To our knowledge, the literature does not describe chromatographic methods for the determination of pesticide residues in coconut pulp, with the exception of coconut water [6,7]. The determination of pesticides in foodstuffs is usually accomplished using chromatographic techniques and involves many preliminary steps including sampling, extraction and clean-up [8–11]. Matrix solid-phase dispersion (MSPD) is an extraction method that provides a good alternative to traditional extraction techniques for chromatographic analysis [12–14]. MSPD can be carried out simultaneously with sample homogenization, extraction and clean-up and it requires only a small sample size and small amounts of solvent. It avoids the drawbacks generally associated with liquid–liquid extraction, such as the use of large volumes of solvent, the occurrence of troublesome emulsions, and slow speed [15–19].

The present work reports a simple methodology for simultaneous determination of dimethoate, malathion, lufenuron, trichlorfon, carbofuran, 3-hydroxycarbofuran, difenoconazole and thiabendazole in coconut pulp using matrix solid-phase dispersion and gas chromatography–mass spectrometry (GC/MS).

2. Materials and methods

2.1. Standards, reagents and supplies

Dichloromethane, ethyl acetate, acetone, acetonitrile and *n*-hexane were nanograde (Mallinckrodt Baker, Paris, KY, USA). Cer-

* Corresponding author. Tel.: +55 79 21056654; fax: +55 79 21056651.
E-mail address: sandnavi@ufs.br (S. Navickiene).

0039-9140/$ – see front matter © 2008 Elsevier B.V. All rights reserved.
doi:10.1016/j.talanta.2008.04.018

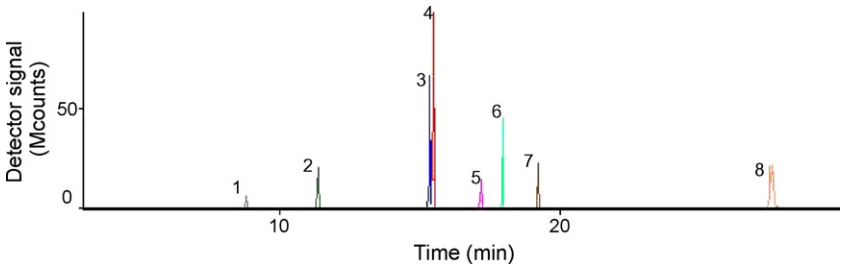

Fig. 1. GC/MS (SIM) chromatogram of standard solution of the pesticides at 1.0 mg kg^{-1}. Peak identification: 1, trichlorfon; 2, lufenuron; 3, dimethoate; 4, carbofuran; 5, 3-hydroxycarbofuran; 6, malathion; 7, thiabendazole; 8, difenoconazole.

tified standards of trichlorfon, dimethoate, malathion, lufenuron, carbofuran, 3-hydroxycarbofuran, difenoconazole and thiabendazole were purchased from Dr. Ehrenstorfer (Augsburg, Germany). All standards were at least 98.5% pure. The individual standard stock solutions of the analytes were prepared in dichloromethane at 500 μg mL^{-1} and stored at −18 °C. The working standard solutions were prepared by diluting the stock solutions in dichloromethane as required. Matrix-matched standards were prepared at the same concentrations as those of calibration solutions by adding appropriate amounts of standards to the control matrix extract. Analytical grade anhydrous sodium sulfate was supplied from Mallinckrodt Baker (Paris, KY, USA). Research grade Florisil (80–100 mesh) was supplied from Sigma (Büchs, Switzerland). C_{18}-bonded silica (50 μm) was obtained from Phenomenex (Torrance, CA, USA), silica-gel 60 (70–230 mesh) from Merck (Darmstadt, Germany), and neutral alumina (70–290 mesh, activity I) from Macherey-Nagel (Düren, Germany).

2.2. Apparatus

A Shimadzu system (Kyoto, Japan), consisting of a QP-5050*A* mass spectrometer equipped with a GC-17A gas chromatograph with a split/splitless injector, was used for the identification and quantification of the pesticides studied. A fused-silica column DB-5MS (5% phenyl–95% polydimethylsiloxane; 30 m × 0.25 mm ID, 0.25 μm), supplied by J&W Scientific (Folsom, CA, USA), was employed, with helium (purity 99.999%) as carrier gas at a flow rate of 1.8 mL min^{-1}. The column temperature was programmed as follows: 60 °C for 1 min, then directly to 300 °C at 10 °C min^{-1} and holding for 3 min. The solvent delay was 5 min. The injector port was maintained at 250 °C, and 1 μL sample volumes were injected in splitless mode (0.7 min). The data were acquired and processed using Shimadzu class 5000 software. The total analysis time was 28 min.

The eluent from the GC column was transferred via a transfer line heated at 280 °C, and fed into a 70 eV electron impact ionization source, also maintained at 280 °C. The analysis was performed in the selected ion monitoring (SIM) mode. For the first acquisition window (5.00–10.00 min), the ions monitored were *m*/*z* 84, **109** and 145 (trichlorfon). For the second acquisition window (11.00–20.00 min), ions with *m*/*z* 122, 149 and **164** (lufenuron), *m*/*z* 87, **125** and 229 (dimethoate), *m*/*z* 147, **162**, and 180 (carbofuran), *m*/*z* 87 and 125 (3-hydroxycarbofuran), *m*/*z* **127**, 158 and 173 (malathion) and *m*/*z* **129**, 174 and 201 (thiabendazole) were monitored. For the third acquisition window (20.00–28.00 min) *m*/*z* **265.1**, 323.1 and 325.1 (difenoconazole) were monitored. Values of *m*/*z* in bold type correspond to the quantification ion for each analyte.

2.3. Sample preparation and fortification

The coconut samples used for method development were obtained from an organic farm (pesticide free) located in the municipality of Aracaju, state of Sergipe, Brazil. A representative portion of coconut pulp (100 g) was homogenized using a household blender and stored in jars at −18 °C until used for analysis. Fortified samples were prepared by adding 500 μL of different standard solutions to 1 g of sample resulting in final concentrations ranging from 0.25 to 1.0 mg kg^{-1} of pesticides in the sample. The fortified coconut pulps were left to stand for 30 min before extraction to allow the spike solution to penetrate into the matrix. Four replicates were analyzed at each fortification level. The extraction procedure was as described below.

2.4. Extraction procedure

An aliquot of coconut pulp (0.5 g) was placed into a glass mortar (*ca.* 50 mL) and 1.0 g of C_{18} was added. The coconut pulp was then gently blended into the C_{18} material with a glass pestle, until a homogeneous mixture was obtained (*ca.* 1 min). The homogenized mixture was introduced into a 100 mm × 20 mm ID polypropylene column, filled with 0.1 g of silanized glass wool at the base, followed by, in order, 1.0 g of anhydrous Na_2SO_4 and 1.0 g of Florisil. The column was lightly tapped to remove air pockets. A 40 mL portion of acetonitrile saturated with *n*-hexane was added to the column and the sample was allowed to elute dropwise. The eluent was collected into a graduated conical tube and concentrated to a volume of 1 mL, using first a rotary vacuum evaporator (40 °C), followed by a gen-

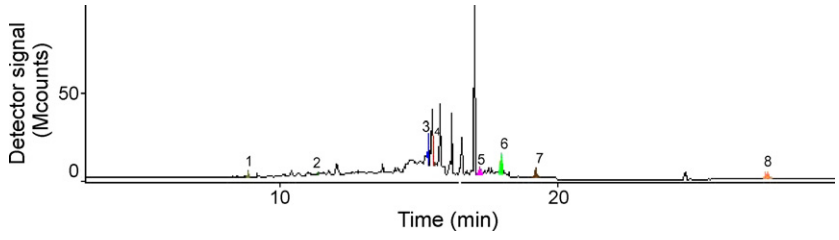

Fig. 2. GC/MS (SIM) chromatogram of extract of coconut pulp spiked at 0.25 mg kg^{-1}. Peak identification: 1, trichlorfon; 2, lufenuron; 3, dimethoate; 4, carbofuran; 5, 3-hydroxycarbofuran; 6, malathion; 7, thiabendazole; 8, difenoconazole.

tle flow of nitrogen. A 1 μL portion of the extract was then directly analyzed by GC/MS.

3. Results and discussion

3.1. GC/MS conditions

Pesticide peak retention times and resolutions were optimized in full scan mode, using a 5 $\mu g\,mL^{-1}$ standard solution and varying the oven temperature and carrier gas flow rate. In these evaluations, the characteristic ions were chosen for quantification of each pesticide. Matrix components can provide variation in the detector response to pesticides. Therefore, the matrix effect was evaluated by comparing the detector response for pesticide standards prepared in dichloromethane with that for standards prepared in coconut pulp extract. When standards were prepared by spiking blank coconut pulp samples with known amounts of pesticides, higher peak areas were obtained for the same pesticide concentrations. Consequently, the quantification of pesticide residues was carried out using matrix-matched standards. Selection of the ions for SIM acquisition was based on the best S/N ratios. Figs. 1 and 2 show chromatograms obtained for pesticide standard solutions and spiked coconut pulp, using the GC/MS system in SIM mode. The chromatographic resolution was satisfactory. Since difenoconazole is a diastereomer, two peaks were detected corresponding to its *cis* and *trans* configuration. The former configuration was selected for quantification.

3.2. MSPD procedure

The extraction method proposed is based on the MSPD procedure. The most suitable extraction parameters were evaluated to achieve the highest recoveries for carbofuran, 3-hydroxycarbofuran, malathion, dimethoate, trichlorfon, thiabendazole, lufenuron and difenoconazole from the coconut pulp. The polarities of the sorbent and the elution solvent are known to be key factors in MSPD, since they determine both the efficacy of the extraction and the purity of the final extracts [19]. Preliminary investigations for optimization of the MSPD procedure for the extraction of pesticides from coconut pulp were performed using coconut pulp samples spiked with pesticides at 0.5 $mg\,kg^{-1}$, and C_{18} and Florisil as solid-phase sorbents. To evaluate the influence of the eluting solvent, dichloromethane, ethyl acetate, *n*-hexane:ethyl acetate (1:1, v/v), and dichloromethane:acetone (9:1; 1:9; 1:4; 2:3, v/v, mixtures) were tested using a solid-phase sorbent to coconut pulp matrix ratio of 1:2 (m/m). This solid-phase sorbent/matrix ratio was evaluated first, since C_{18} is an expensive sorbent. Tables 1 and 2 show the percentage recoveries obtained using different eluting solvents with C_{18} and Florisil. When comparing the data obtained, rather different results were found for the solvents tested. Dichloromethane presented the cleanest extracts for the pesticide extraction from the coconut pulp matrix, while elution of the MSPD column with ethyl acetate, dichloromethane:acetone (9:1; 1:9; 1:4; 2:3, v/v) or *n*-hexane:ethyl acetate (1:1, v/v) mixture produced not only an enhancement of recoveries, but also a higher background and more interfering peaks from the coconut pulp, compared to dichloromethane. In some of these assays, a co-column (1 g) of alumina, silica or Florisil was packed in the base of the C_{18}:coconut pulp matrix blend to obtain further fractionation and to assist in sample clean-up using these same eluting solvents. The extraction column prepared with C_{18}:coconut pulp blend produced an extract that showed minimal interferences for most of the pesticides studied, while the use of C_{18} as support in the MSPD method produced recoveries ranging from 0% to 212%, similar to those obtained with Florisil, considering the same proportion between solid-phase and coconut pulp matrix. The higher peak areas can be explained by a matrix effect that enhances the chromatographic response to pesticides, as previously reported for the matrix effect in the determination of pesticides in different foodstuffs [19–21]. Other sorbent:coconut pulp matrix ratios (1:1, 2:1 and 3:1, m/m) were used in an attempt to optimize the MSPD method. The results obtained show that the best recoveries were obtained using 1.0 g of C_{18} to 0.5 g of coconut pulp matrix (2:1, m/m), and any further increase of C_{18} did not improve the recovery of the pesticides studied. These tests demonstrated that only the assay using the C_{18}/Florisil and dichloromethane:acetone (9:1, v/v) system resulted in reasonable recoveries, ranging from 41% to 147% for the pesticides studied, with the exception of lufenuron (19%). Therefore, in order to obtain satisfactory recoveries, acetonitrile, and combinations of acetonitrile and ethyl acetate or *n*-hexane (saturation point of *n*-hexane = 4 mL), were assayed as

Table 1
Influence of elution solvents on pesticide recovery using Florisil as solid-phase sorbent in the MSPD procedure (2.0 g of coconut pulp + 1.0 g of sorbent)

Pesticide	Recovery (%)[a]				
	Florisil				
	Dichloromethane:acetone (v/v)				Dichloromethane
	1:9	1:4	2:3	9:1	
Trichlorfon	56	182	17	283	–
Lufenuron	7	5	0.6	8	6
Dimethoate	26	21	7	61	30
Carbofuran	56	35	10	104	3
3-Hydroxycarbofuran	137	7	7	152	12
Malathion	42	22	5	70	28
Thiabendazole	12	63	39	97	–
Difenoconazole	49	17	5	40	–

[a] Coconut sample fortified at 0.5 $mg\,kg^{-1}$ ($n = 2$).

Table 2
Influence of C_{18} as solid-phase sorbent on pesticide recovery in the MSPD procedure (2.0 g of coconut pulp + 1.0 g of sorbent)

Pesticide	Recovery (%)[a]					
	Dichloromethane:acetone (9:1, v/v)				*n*-Hexane:ethyl acetate (1:1, v/v)	Ethyl acetate
	C_{18}	C_{18}/alumina	C_{18}/silica	C_{18}/Florisil	C_{18}	C_{18}
Trichlorfon	212	56	17	100	–	–
Lufenuron	5	7	0.6	19	25	25
Dimethoate	21	26	7	41	13	13
Carbofuran	35	56	10	69	10	12
3-Hydroxycarbofuran	7	137	7	147	9	14
Malathion	22	42	5	65	7	6
Thiabendazole	63	12	39	124	–	–
Difenoconazole	17	49	5	48	–	–

[a] Coconut sample fortified at 0.5 $mg\,kg^{-1}$ ($n = 2$).

Table 3
Influence of acetonitrile ratio as elution solvent on pesticide recovery in the MSPD procedure using C_{18} and Florisil (co-column) solid-phase sorbents

Pesticide	Recovery (%)[a]				
	C_{18}/Florisil				
	Acetonitrile (mL)			Acetonitrile:*n*-hexane (saturated)	Acetonitrile:ethyl acetate (1:1, v/v)
	20	30	40		
Trichlorfon	145	134	150	93	192
Lufenuron	31	41	42	36	52
Dimethoate	33	45	102	99	78
Carbofuran	68	109	133	81	280
3-Hydroxycarbofuran	41	104	120	85	112
Malathion	33	65	132	76	103
Thiabendazole	0	0	0	60	24
Difenoconazole	13	30	81	57	44

MSPD column: 2.0 g of coconut pulp + 1.0 g of sorbent.
[a] Coconut sample fortified at 0.5 mg kg^{-1} ($n = 2$).

extractants. In addition, three volumes of acetonitrile (20, 30 and 40 mL) were tested. According to these tests, the elution of the pesticides using different volumes of acetonitrile showed a response enhancement ranging from 13% to 150% for lufenuron, dimethoate, difenoconazole, trichlorfon, carbofuran, 3-hydroxycarbofuran and malathion. However, thiabendazole showed zero recovery in all tests. Steven et al. [22] previously reported an inadequate recovery for thiabendazole using acetonitrile. The occurrence of a high recovery ($R\% > 100\%$) can be attributed to the presence of interfering endogenous compounds. The use of acetonitrile:ethyl acetate (1:1) or acetonitrile saturated with *n*-hexane was investigated in order to ensure the removal of these interfering compounds and obtain a good recovery of thiabendazole. The second approach gave the best results: all pesticides were recovered almost quantitatively, and with good reproducibility, using the acetonitrile saturated with *n*-hexane mixture. Recovery values varied between 36% and 99%. The lower values obtained for lufenuron (36%) and difenoconazole (54%) can be ascribed to their partial binding to the lipophilic matrix. This possibility is supported by the high K_{ow} (octanol/water partition coefficient) values for lufenuron and difenoconazole, $10^{5.12}$ and $10^{4.20}$, respectively [23]. Because of their high liposolubility, these two pesticides can be absorbed and retained by the waxes of the coconut pulp. Table 3 summarizes the recoveries obtained using pure acetonitrile, and two acetonitrile mixtures as eluting solvent. All analyses were carried out in duplicate. Overall results indicate that the combination of C_{18} as solid-phase, Florisil as clean-up layer and acetonitrile saturated with *n*-hexane as elution solvent is a suitable extraction procedure for determination of dimethoate, malathion, trichlorfon, lufenuron, carbofuran, 3-hydroxycarbofuran, thiabendazole and difenoconazole in a complex matrix such as coconut pulp.

3.3. Recovery study

Once the factors that affect the MSPD procedure had been optimized, validation of the method was performed. Recovery data were calculated by comparison with the appropriate working standard solutions. The untreated coconut pulps were fortified at different concentrations (0.25–1.0 mg kg^{-1}), and residues were quantified using the external standards method. Standard solutions were injected after every 10 samples to monitor changes in chromatographic conditions. Fortification concentrations were selected to reach the maximum residue levels (MRLs) for pesticides in coconut, according to Brazilian legislation, which range from 0.2 to 0.5 mg kg^{-1} [2]. Table 4 presents recoveries of the eight pesticides at three concentration levels for the coconut pulp tested. Average recoveries ranged from 70.1% to 98.7%, with relative standard deviation (RSD) values of 2.7–14.7%, except for lufenuron and difenoconazole (recoveries of 47.2% and 48.3%, respectively), which show lower recoveries for lipophilic samples [20]. Each recovery analysis was repeated 4 times. The precision and accuracy were considered adequate for validating the method according to the validation criteria. Accuracy was calculated as the percent ratio between the measured and known concentrations, and precision was determined as the percentage coefficient of variation (%RSD), which is the ratio between standard deviation and mean measured concentration [24].

3.4. Linearity, and detection and quantification limits

The detector response was linear within the concentration range studied. Linearities for all compounds were determined using blank coconut pulp samples fortified at concentration levels ranging from 0.09 to 10.0 μg mL^{-1}. The slope and intercept values, together with

Table 4
Percentage recoveries and relative standard deviations obtained by MSPD procedure of the fortified coconut pulp for the pesticides studied ($n = 4$)*

Pesticide	Concentration level (mg kg^{-1})	Mean recuperation (%)*	RSD (%)
Trichlorfon	0.25	87.7	10.0
	0.50	81.1	10.1
	1.00	70.2	11.8
Lufenuron	0.25	47.2	12.1
	0.50	36.8	9.0
	1.00	25.1	9.2
Dimethoate	0.25	98.7	12.1
	0.50	90.7	2.7
	1.00	91.7	13.2
Carbofuran	0.25	79.7	9.7
	0.50	71.0	8.6
	1.00	70.1	9.1
3-Hydroxycarbofuran	0.25	78.2	10.4
	0.50	76.9	12.4
	1.00	82.9	11.2
Malathion	0.25	77.2	11.4
	0.50	87.7	14.1
	1.00	82.6	11.6
Thiabendazole	0.25	88.4	5.9
	0.50	80.2	4.5
	1.00	74.1	14.7
Difenoconazole	0.25	48.2	9.8
	0.50	45.6	14.5
	1.00	38.3	9.1

Table 5
Retention times, calibration data, LOD and LOQ of the pesticides analyzed by GC/MS

Pesticide	Retention time (min)	Calibration data		LOD (mg kg^{-1})	LOQ (mg kg^{-1})
		Equation	Determination coefficient		
Trichlorfon	8.87	$y = 10974.3x + 4081.6$	0.9977	0.15	0.25
Lufenuron	11.40	$y = 120794.7x + 6265.5$	0.9977	0.11	0.25
Dimethoate	15.45	$y = 399118.5x - 46448$	0.9972	0.17	0.25
Carbofuran	15.56	$y = 194172x + 3160$	0.9976	0.02	0.15
3-Hydroxycarbofuran	11.91	$y = 241532.1x + 9092$	0.9933	0.12	0.24
Malathion	17.98	$y = 220380.1x - 73.9$	0.9992	0.16	0.25
Thiabendazole	19.26	$y = 321929.3x - 51637$	0.9979	0.08	0.18
Difenoconazole	27.55	$y = 16770.51x - 19198.51$	0.9990	0.11	0.25

their standard deviations, were determined using regression analyses. Linear regression coefficients for all pesticides ranged from 0.9933 to 0.9992.

The limits of detection (LOD) for the pesticides studied were calculated considering the standard deviation of the analytical noise (a value of 7 times the standard deviation of the blank) and the slope of the regression line, and ranged from 0.02 to 0.11 mg kg^{-1}. The limits of quantification (LOQ) were determined as the lowest concentration giving a response of 10 times the average of the baseline noise, calculated using seven unfortified samples. The LOQ values for these compounds ranged from 0.15 to 0.25 mg kg^{-1} [24]. These data are summarized in Table 5.

3.5. Real samples

The MSPD procedure developed was applied to the determination of pesticides in coconut pulps. Four different samples of coconut pulp, obtained from local markets in the city of Aracaju (Brazil), and originating from conventional agriculture, were analyzed using this procedure. No pesticide residues, at concentrations above the detection limit, were found in these samples.

4. Conclusions

The proposed MSPD procedure followed by GC/MS (SIM) can be applied to determine carbofuran, 3-hydroxycarbofuran, lufenuron, trichlorfon, thiabendazole, difenoconazole, malathion and dimethoate in coconut pulp. The method uses C_{18}-based on the MSPD column, with Florisil as co-column, and acetonitrile saturated with *n*-hexane as elution solvent. The results demonstrate that the accuracy, precision and selectivity of the proposed method are acceptable for multiresidue analyses of pesticides, and that the LOQs achieved by the method are in good agreement with the limit values established by Brazilian legislation. In addition, the method requires only a small sample size, and offers considerable savings in terms of solvent consumption, cost of materials, sample manipulation and analysis time. Detection of the presence of pesticides in coconut pulp can be achieved within 50 min following sample receipt, after suitable adjustment of chromatographic conditions.

Acknowledgements

The authors wish to thank CNPq/MCT (proc. no. 502334/2005-3) and FAPITEC-SE/FUNTEC (proc. no. 35.0073/2004-0) for a fellowship and financial support of this study.

References

[1] J.M.S. Ferreira, D.R.N. Warwick, L.A. Siqueira, A Cultura do Coqueiro no Brasil, second ed., Embrapa-SPI, Brasília, 1998.
[2] Pesticide residues in food, http://www.anvisa.gov.br/toxicologia/monografias/index.htm.
[3] C.M. Bruhn, Food Chem. 16 (2005) 487.
[4] B.L.L. Tan, M.A. Mohd, Talanta 61 (2003) 385.
[5] L.P. Walsh, D.R. Webster, D.M. Stocco, J. Endocrinol. 167 (2000) 253.
[6] N.M. Brito, S. Navickiene, R.B. Abakerli, L. Polese, E.F.G. Jardim, M.L. Ribeiro, J. Chromatogr. A 957 (2002) 201.
[7] L. Leite, S. Ogawa, M.L. Ribeiro, H.S. Dórea, S. Navickiene, J. Liq. Chromatogr. Relat. Technol. 29 (2006) 1833.
[8] K. Ridway, S.P.D. Lalljie, R.M. Smith, J. Chromtogr. A 1153 (2007) 36.
[9] Y. Picó, M. Fernández, M.J. Ruiz, G. Font, J. Biochem. Biophys. Methods 70 (2007) 117.
[10] D.A. Lambropoulou, T.A. Albanis, Anal. Bioanal. Chem. 389 (2007) 1663.
[11] E.M. Kristenson, U.A.T. Brinkman, L. Ramos, Trends Anal. Chem. 25 (2006) 96.
[12] S.A. Barker, J. Chromatogr. A 885 (2000) 115.
[13] S.A. Barker, J. Chromatogr. A 880 (2000) 63;
S. Wang, Y. Xu, C. Pan, S. Jiang, F. Liu, Anal. Bioanal. Chem. 387 (2007) 673.
[14] S.A. Barker, J. Biochem. Biophys. Methods 70 (2007) 151.
[15] T.F.S. Santos, A. Aquino, H.S. Dórea, S. Navickiene, Anal. Bioanal. Chem. 390 (2008) 1425.
[16] C. Sánchez-Brunete, E. Miguel, J.L. Tadeo, Talanta 74 (2008) 1211.
[17] M.S. Dopico-García, P. Valentão, A. Jagodziñska, J. Klepczyñska, L. Guerra, P.B. Andrade, R.M. Seabra, Talanta 74 (2007) 20.
[18] R. Rial-Otero, E.M. Gaspar, I. Moura, J.L. Capelo, Talanta 71 (2007) 503.
[19] C.F. Poole, J. Chromatogr. A 1158 (2007) 241.
[20] B. Albero, C. Sanchez-Brunete, J.L. Tadeo, J. Agric. Food Chem. 52 (2004) 5828.
[21] S. Bogialli, A. Di Corcia, J. Biochem. Biophys. Methods 70 (2007) 163.
[22] J. Steven, K.M. Lehotay, J. Seon, J. AOAC Int. 88 (2005) 630.
[23] C. Tomlin (Ed.), The Pesticide Manual, 10th ed., British Crop Protection Publications, London, 1994.
[24] A. Hill, Quality Control Procedures for Pesticide Residues Analysis—Guidelines for Residues Monitoring in the European Union, European Community, Brussels, 2000.

Talanta 76 (2008) 602–609

Contents lists available at ScienceDirect

Talanta

journal homepage: www.elsevier.com/locate/talanta

Classification of data with missing elements and outliers☆

I. Stanimirova, B. Walczak*

Department of Chemometrics, Institute of Chemistry, Silesian University, 9 Szkolna Street, 40-006 Katowice, Poland

ARTICLE INFO

Article history:
Received 22 December 2007
Received in revised form 26 March 2008
Accepted 28 March 2008
Available online 8 April 2008

Keywords:
Expectation-maximization
Robust SIMCA
Robust PCA
Projection to model plane

ABSTRACT

Missing elements and outliers can often occur in experimental data. The presence of outliers makes the evaluation of any least squares model parameters difficult, while the missing values influence the adequate identification of outliers. Therefore, approaches that can handle incomplete data containing outliers are highly valued. In this paper, we present the expectation-maximization robust soft independent modeling of class analogy approach (EM-S-SIMCA) based on the recently introduced spherical SIMCA method. Several important issues like the possibility of choosing the complexity of the model with the leverage correction procedure, the selection of training and test sets using methods of uniform design for incomplete data and prediction of new samples containing missing elements are discussed. The results of a comparison study showed that EM-S-SIMCA outperforms the classic expectation-maximization SIMCA method. The performance of the method was illustrated on simulated and real data sets and led to satisfactory results.

1. Introduction

The present paper addresses the problem of classification of experimental data in which both missing elements and outliers occur. The lack of measurement values in the data may be caused by a failure of analytical instruments, incapability of accomplishing an expensive sampling procedure, unexpected changes of experimental conditions, etc. Outliers are samples for which the parameters measured differ to a great extent in comparison with the majority of samples in the data. Usually, they can be samples with unique characteristics or they appear as the result of gross analytical error. The presence of outliers strongly influences the estimation of any least squares model parameters, while incompleteness in the data disturbs the proper identification of outliers. Therefore, chemometric methods, which can handle incomplete data with outliers, are sorely needed. Several approaches for exploring [1,2] and modeling [3] of such types of data have already been proposed in the literature.

In this paper, the possibility to extend the recently introduced robust soft independent modeling of class analogy (S-SIMCA) approach [4] to work with incomplete data is discussed. S-SIMCA was shown to have virtually the same performance in comparison with the other robust SIMCA (R-SIMCA) method [5]. It was preferred over R-SIMCA because of its conceptual simplicity and computational efficiency. In the strategy proposed, the S-SIMCA approach is embedded in the self-consistent iterative procedure called expectation-maximization [6] that allows with incomplete data to be dealt with. Although the proposal seems straightforward, there are a few important issues that arise, namely, (i) how to choose representative training and test sets, (ii) how to quickly evaluate the complexity of the model and (iii) how to make a prediction for the incomplete independent test set. For clarity in the further discussion, we will elaborate the above-mentioned issues briefly.

The goal of S-SIMCA is to create boundaries for each class separately by using spherical principal component analysis (spherical PCA (S-PCA)) [7] applied to the set of training samples of a given class. Prior to construction of the model, there are several possible ways to select the training set. The easiest and least problematic is to perform a random selection. However, such a selection does not guarantee the representativeness of the subset. Consequently, the model built using a randomly selected training set can lead to either over-optimistic or over-pessimistic predictions. On the other hand, uniform designs like the Kennard and Stone [8] and duplex [9] allow the selection of a representative training set, but cannot be applied directly to incomplete data.

To assess the complexity of the S-SIMCA model a leave-one object out cross-validation procedure can be used. This is possible due to the special weighting scheme employed in S-PCA that diminishes the influence of outliers on the model. However, the leave-one object out cross-validation is a time-consuming step when the S-PCA model is incorporated into the expectation-maximization

☆ This publication reflects only the author's views and the European Commission is not liable for any use that may be made of the information contained herein.

* Corresponding author. Tel.: +48 32 359 2115; fax: +48 32 259 9978.
E-mail address: beata@us.edu.pl (B. Walczak).

0039-9140/$ – see front matter © 2008 Elsevier B.V. All rights reserved.
doi:10.1016/j.talanta.2008.03.049

framework. Therefore, to speed up the computations, a modified validation method based on leverage correction [10] was adopted.

Once the class models of definite complexity are built, the new samples are projected into the spaces spanned by the individual principal components and are assigned to the class into which they fit best. Often, the new sample data can also contain missing elements. To obtain their scores, several approaches have been used so far. These were the trimmed score method (TRI), the iterative imputation method, a single-component projection method (SCP), a method minimizing the squared prediction error (SPE), the trimmed scores regression (TSR), a regression method using known data (KDR) and a method of projection to the model plane (PMP). A good overview of all these methods can be found in [11]. In our study, the PMP approach, which has been shown to be equivalent to the iterative imputation method, was preferred because of its low computational cost.

To demonstrate the performance of the expectation-maximization S-SIMCA (EM-S-SIMCA) method proposed, it was further compared with classic SIMCA incorporated into the expectation-maximization algorithm. The comparison was illustrated using simulated and real data sets.

The following section describes the theoretical basis of SIMCA, S-SIMCA and the corresponding EM-SIMCA and EM-S-SIMCA methods. In Section 3, the properties of the classic and robust SIMCA methods for incomplete data with outliers are discussed. The results of a simulation study and applications of both algorithms to a real data set are also presented. Finally, the conclusions of the study follow in Section 4.

2. Theory

2.1. Classic SIMCA

Soft independent modeling of class analogy, SIMCA [12], belongs to the group of classification techniques, the classification rules of which are created by constructing a PCA model of definite complexity (f) for each class separately. The PCA model for the kth class of m samples characterized by n parameters, $\mathbf{X}_k$ ($m \times n$), can be expressed as follows:

$$\mathbf{X}_k = \mathbf{T}_k \mathbf{P}'_k + \mathbf{E}_k \tag{1}$$

In the equation above, matrix $\mathbf{T}$ ($m \times f$) holds f principal components (PCs); $\mathbf{P}_k$ ($n \times f$) contains the model's loadings and $\mathbf{E}_k$ ($m \times n$) is the matrix of the model's residuals. It should be noted that $\mathbf{X}_k$ is a column-wise centered matrix.

The optimal complexity (f) of the model is usually determined on the basis of a cross-validation procedure often performed in a leave-one object out manner [13]. To define the boundaries of the kth class, the critical value of the class residual standard deviation, σ_{crit}, should be calculated. The residual standard deviation, σ_k, can be determined in two equivalent ways. One is to estimate the sum of squared residuals from the PCA model with f PCs for all objects and the other is to consider the sum of squared scores for the principal components that are not used in the model construction.

$$\sigma_k = \sqrt{\sum_{i=1}^{m}\sum_{j=1}^{n} \frac{e_{ij}^2}{(r-f)(m-f-1)}} = \sqrt{\sum_{i=1}^{m}\sum_{i=1}^{r} \frac{t_{ij}^2}{(r-f)(m-f-1)}} \tag{2}$$

In the given expression, e_{ij} is the residual element from the ith row and jth column of matrix $\mathbf{E}_k$, t_{ij} is the element of the score matrix $\mathbf{T}_k$ and r is the maximum number of PCs (corresponding to the rank of $\mathbf{X}_k$) that can be found for $\mathbf{X}_k$. No matter which method of defining the class boundaries is chosen, to determine the σ_k value, cross-validated scores should be considered in order to reduce the probability of the incorrect rejection of objects from the model. An important assumption in SIMCA is that the residuals of objects follow the normal distribution, which allows using the F-test with $(r-f)/(r-f)(m-f-1)$ degrees of freedom and definite level of significance, to determine the critical value of σ_k as

$$\sigma_{\text{crit}} = \sqrt{F_{\text{crit}}}\sigma_k \tag{3}$$

Once new samples are available, their scores in the kth PCs space are found and their residuals are compared with the critical value of the residual standard deviation. A new sample with a residual standard deviation smaller than σ_{crit} is assigned to the kth class.

In our study, the samples were classified using a distance–distance plot. For each sample the Mahalanobis distance in the score space and the orthogonal distance from the PCA model were considered. The Mahalanobis distance for samples of kth class, $\mathbf{MD}_k$ ($m \times 1$), can be found according to the following expression:

$$\mathbf{MD}_k = \sqrt{\mathbf{T}_k \mathbf{V}_k^{-1} \mathbf{T}'_k} \tag{4}$$

where the elements of the diagonal matrix $\mathbf{V}_k$ are the f eigenvalues of $\mathbf{X}_k$.

The orthogonal distances for the samples of the kth class, $\mathbf{OD}_k$ ($m \times 1$) are computed as

$$\mathbf{OD}_k = \sqrt{\sum_{j=1}^{n} e_{ij}^2} = \sqrt{\sum_{j=f+1}^{r} t_{ij}^2} \tag{5}$$

Please note that both distances are constructed assuming a certain complexity of the PCA model. To define the cut-off values for both distances, the so-called z-scores are used. z-Scores are obtained by centering each distance around its mean and dividing it by the corresponding standard deviation. For the Mahalanobis and orthogonal distances represented as z-scores, the cut-off value can be set at three, which means that 99.90% of the centered distances of samples can be found within the three times standard deviation of the distances. With this criterion, the assumption for normally distributed residuals of samples from a given class is fulfilled. Moreover, using the distance–distance plot, one can easily distinguish between regular samples and three categories of atypical observations. Regular samples are the samples that have z-scores smaller than three for both distances. Good leverage samples have a large z-score value for the Mahalanobis distance, but a small value for the orthogonal distance while large z-score values for both distances are found for bad leverage observations. High residual samples are characterized by a large z-score value for the orthogonal distance, but a small value for the Mahalanobis distance.

In general, each sample is fitted to each of the kth models and is assigned to the model for which its z-scores for the Mahalanobis and orthogonal distances are smaller than three. Thus, it can happen that the sample belongs to one class, to more than one class or to none of the classes, which is actually the meaning of the 'soft' classification rule. Of course, a 'hard' classification rule can also be considered by assigning each sample to only one group for which the minimal value of the weighted sum of its Mahalanobis and orthogonal distances are found [4]. However, this possibility is no longer pursued here.

2.2. The robust SIMCA method based on S-PCA (S-SIMCA)

The robust classification rules in S-SIMCA [4] are created using the spherical PCA approach. As mentioned before, this method is chosen because of its simplicity, computational efficiency and its

capability to handle outliers (high breakdown point). In S-PCA, the samples of the kth class are centered about the L_1-median center [14,15] and are then weighted according to the inverse of their Euclidean distances from the robust data center. This weighting of objects can be regarded as a projection of samples onto a hyper sphere with the unit radius and the center at the L_1-median. Introducing small weights for samples that are far away from the majority of data diminishes their negative influence on the final PCA model. The robust scores for samples are further obtained by means of the classic PCA carried out on the weighted data. Due to the specific weighting scheme, the complexity of the final model can again be chosen using the leave-one object out cross-validation. As before, the classification of samples can be performed with the help of the distance–distance plot.

For this purpose, the Mahalanobis distances of samples are calculated according to Eq. (4), in which the classic scores and the corresponding eigenvalues are replaced with the robust scores and the robust eigenvalues. When estimating the orthogonal distances using Eq. (5), the residuals of the robust PCA model are taken into account. To determine the cut-off values at three, the z-scores for both distances should be obtained. In this case, the distances are centered about their medians and are divided by their robust scales. As a robust scale estimate, the Q_n estimator [16] was applied. The Matlab code for spherical PCA can be found in [4].

2.3. Expectation-maximization versions of SIMCA and S-SIMCA

To obtain expectation-maximization versions of SIMCA (EM-SIMCA) and S-SIMCA (EM-S-SIMCA), PCA and S-PCA were incorporated into the expectation-maximization procedure. With EM, the PCA or S-PCA model was constructed using only the data observed, and the missing elements were iteratively replaced with values that fit the final model perfectly. This concept works well for data with a high correlation structure. The EM-SIMCA algorithm starts with initialization of missing elements by means of the corresponding row and column means. Then, the scores and loadings are found according to the PCA model (see Eq. (1)) and the initial estimates for the missing elements are replaced with the values predicted by the currently constructed PCA model with f factors. In the following iterations, this mechanism is repeated until the sum of squared differences calculated for the re-filled values of missing elements in two consecutive iterations is smaller than, e.g. 10^{-8}. The main steps of the EM-SIMCA algorithm can be summarized as follows:

1. initialize the missing elements with the mean of the corresponding column and row means of $\mathbf{X}_k$,
   for $f = 1{:}r$ (where r is the maximum number of PCs to be calculated)
   2. preprocess the data (column-wise centering or autoscaling),
   3. perform principal component analysis according to Eq. (1),
   4. predict $\mathbf{X}_k$ using f principal components and f loading vectors,
   5. replace missing values with the estimates predicted with the PCA model with f PCs,
   6. go to step 2 until the convergence criterion is not fulfilled,
   7. perform fast cross-validation (based on leverage correction) to obtain mean square errors (MSEs) for the PCA model with f PCs,
   end
8. select the final complexity of the model,
9. perform standard leave-one object out cross-validation for the model with the selected complexity to define the boundaries for the kth class,
10. find the scores for the test samples and samples from the other classes.

The presented scheme allows for the constriction of a SIMCA model using the principle 'one class versus the other(s)'. The preprocessing of data should be done within the steps of EM. In this way, the mean and the standard deviation are re-estimated together with refilling in the values predicted for the missing elements. The leverage correction concept was chosen to decide on the complexity of the PCA model similar to the way this could be done for the calibration models [10]. The so-called leverage for the ith object can be expressed in the following way:

$$h_i = \frac{1}{m} + \sum_{f=1}^{r} \frac{t_{if}^2}{\mathbf{t}_f' \mathbf{t}_f} \tag{6}$$

To estimate MSE, the residuals from the PCA model constructed with f components were calculated for the observed elements only. Then the residuals were divided by the factor $1 - h_i$, summed and finally divided by the number of objects. Since the leverage correction does not include all the variation in $\mathbf{T}$ that is involved in the cross-validation process, the standard leave-one object out cross-validation procedure was performed on the model of definite complexity. The cross-validated scores obtained in this way were further used to estimate the Mahalanobis and orthogonal distances for the training samples and to define the class borders. The final step was to find the scores, $\mathbf{T}_{\text{new}}$ ($l \times f$, $l \neq m$), for l samples, $\mathbf{X}_{\text{new}}$ ($l \times n$) which were not involved in the model construction (test samples, new samples or samples from the other classes). As mentioned before, this could be done in several possible ways. We used the projection to model plane method [11]. After preprocessing $\mathbf{X}_{\text{new}}$ with the mean and/or standard deviation obtained from the training set, it is projected onto the model's loadings, $\mathbf{P}_k$ ($n \times f$) as

$$\mathbf{T}_{\text{new}} = \mathbf{X}_{\text{new}} \mathbf{P}_k (\mathbf{P}_k' \mathbf{P}_k)^{-1} \tag{7}$$

The PMP scores are obtained only for the elements observed in $\mathbf{X}_{\text{new}}$ and are used to calculate the orthogonal and Mahalanobis distances for new samples on the bases of which their classification is performed.

The EM algorithm of S-SIMCA follows almost the same steps as the algorithm previously described. The initialization of missing elements (step 1) was done using the medians of the row and column medians. A robust centering with the L_1-median estimator (step 2) was then performed on the data. If a scaling of the data is required, the Q_n estimator is applied. To find the optimal complexity of the robust PCA model, the fast cross-validation procedure based on leverage correction was again chosen. MSE (step 7) was calculated by taking the median of the residuals, which were divided by $1 - h_i$. The following steps remain the same as in the classic algorithm. Finally, the robust scores of new upcoming samples were found by projecting them on the robust loadings.

3. Results and discussion

3.1. A simulation study

In order to demonstrate the efficiency of the EM-S-SIMCA method in handling incomplete data, a two-class data set of definite complexity was simulated. For each class, a training set, $\mathbf{X}_m$ (50×30), and a test set, $\mathbf{X}_t$ (50×30), the elements of which were drawn from the normal distribution, $N(0, 1)$, were constructed. The training set was centered and decomposed by means of PCA. It was then reconstructed according to Eq. (1) using the f principal components. In general, the number of principal components can be chosen by the user. In our study, two PCs were used. A normally distributed noise was added to the reconstructed $\mathbf{X}_m$, and to keep its level low, the elements of the noise matrix (50×30) were multiplied by 0.05. To fit the test objects to the space spanned by the selected number of principal components, $\mathbf{X}_t$ was centered by the mean of the training set and projected onto the chosen number of loading vectors. The scores obtained were further used to reconstruct $\mathbf{X}_t$. Similar to $\mathbf{X}_m$, a matrix of dimension (50×30), the elements of which were generated from the normal distri-

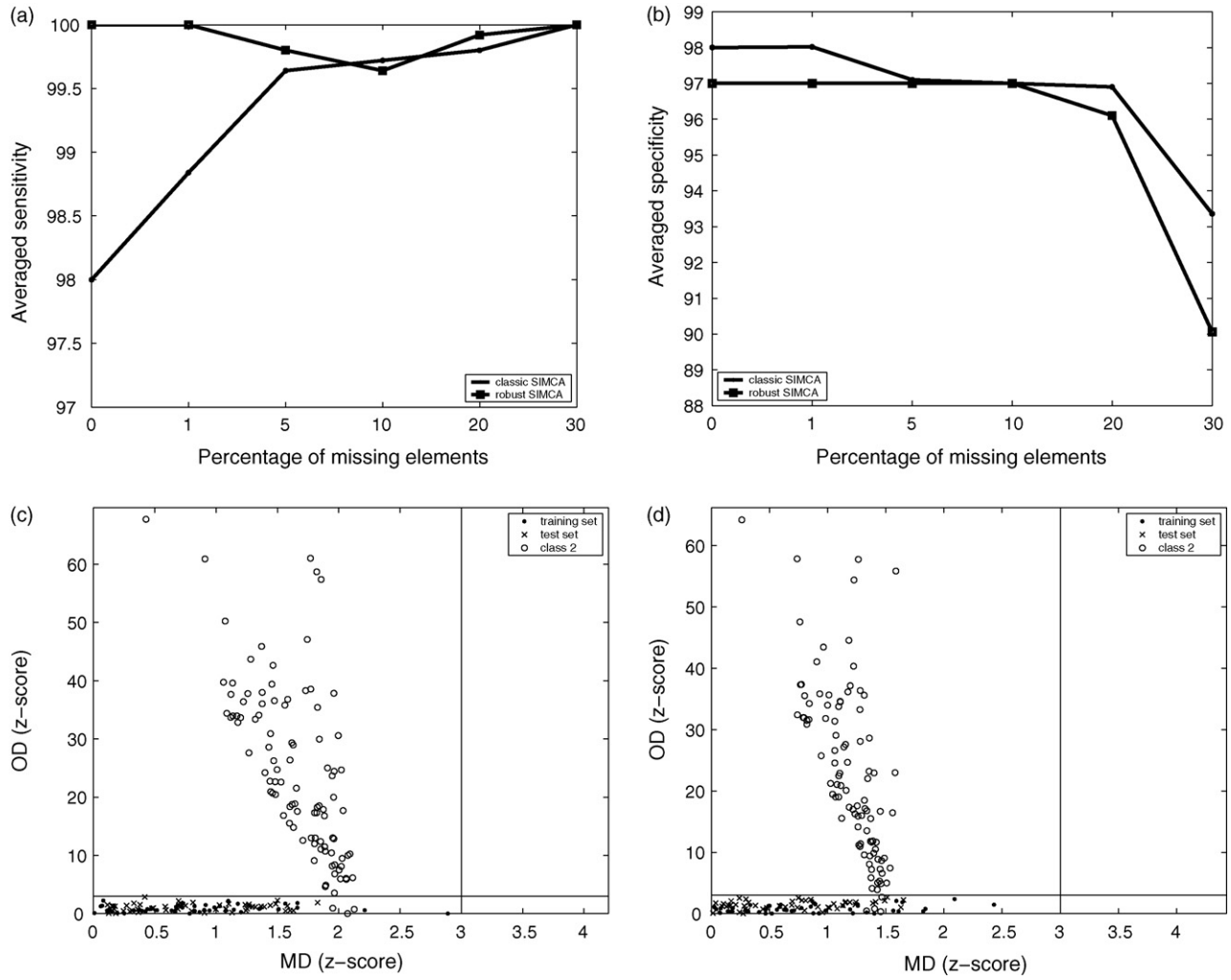

Fig. 1. Performances of the expectation-maximization SIMCA and expectation-maximization S-SIMCA methods applied to a normally distributed two-class data set. The models were built using a training set in which various percentages (1, 5, 10, 20 and 30) of elements were deleted: (a) sensitivity of the models obtained as an average of 50 runs of the algorithms, (b) specificity of the models obtained as an average of 50 runs of the algorithms, (c) distance–distance plot of a two-component EM-SIMCA model built for a training set containing 20% of missing elements with a sensitivity of 100% and a specificity of 97% and (d) distance–distance plot of a two-component EM-S-SIMCA model built for the same training set as (c) with a sensitivity of 100% and a specificity of 96%.

bution and multiplied by 0.05, was added. The data of the other class (100×30) were simulated in the same way, but with a different population mean. To trace the changes in the classification results with the number of elements deleted in the training set, two figures of merit, e.g. sensitivity and specificity were used. Sensitivity is defined as the percentage of class objects that are accepted by the class-model correctly, while specificity is the percentage of objects from the other classes that are rejected by the class-model.

Various percentages (1, 5, 10, 20, and 30) of elements were deleted from the training set completely at random and the SIMCA and robust SIMCA models were constructed. In general, the performances of the methods depend on the pattern of missing elements. Therefore, the deletion of a given number of elements was repeated 50 times. The sensitivities and specificities of the models with optimal complexity were estimated as the average of 50 repetitions. The results are presented in Fig. 1. To enable easy comparison, the models for the data without missing elements are also displayed.

The key assumption in the study of the efficiency is that EM-S-SIMCA should detect the same outliers in the test set as the EM-SIMCA approach for normally distributed data. Fig. 1a shows that the averaged sensitivities of the EM-SIMCA models increase with an increasing percentage of missing elements. This means that a large percentage of test samples are correctly classified in comparison with the EM-SIMCA model built without missing elements. This can be explained by the fact that the Mahalanobis and orthogonal distances are calculated only for the elements observed and therefore, wider borders are set in comparison with the model without missing elements. The wider borders suggest that a larger number of samples from the other class fall into the class box. An indication of this is the decrease of specificity with an increasing percentage of missing elements (see Fig. 1b). A similar tendency is observed for the EM-S-SIMCA models. Although the sensitivity does not change much with an increasing percentage of missing elements, it is higher than that observed for EM-SIMCA. On the other hand, the specificities decrease to a greater degree with the increasing percentage of missing elements in comparison with the EM-SIMCA models (compare Fig. 1a with Fig. 1b). This suggests that with the robust model wider borders are constructed than with the classic one. Therefore, the probability that objects from the other class can be assigned as members of the class-model is higher for the robust model. It should be emphasized that the robust models do not perform optimally for normally distributed data and worse results can be expected. As an example, the distance–distance plots

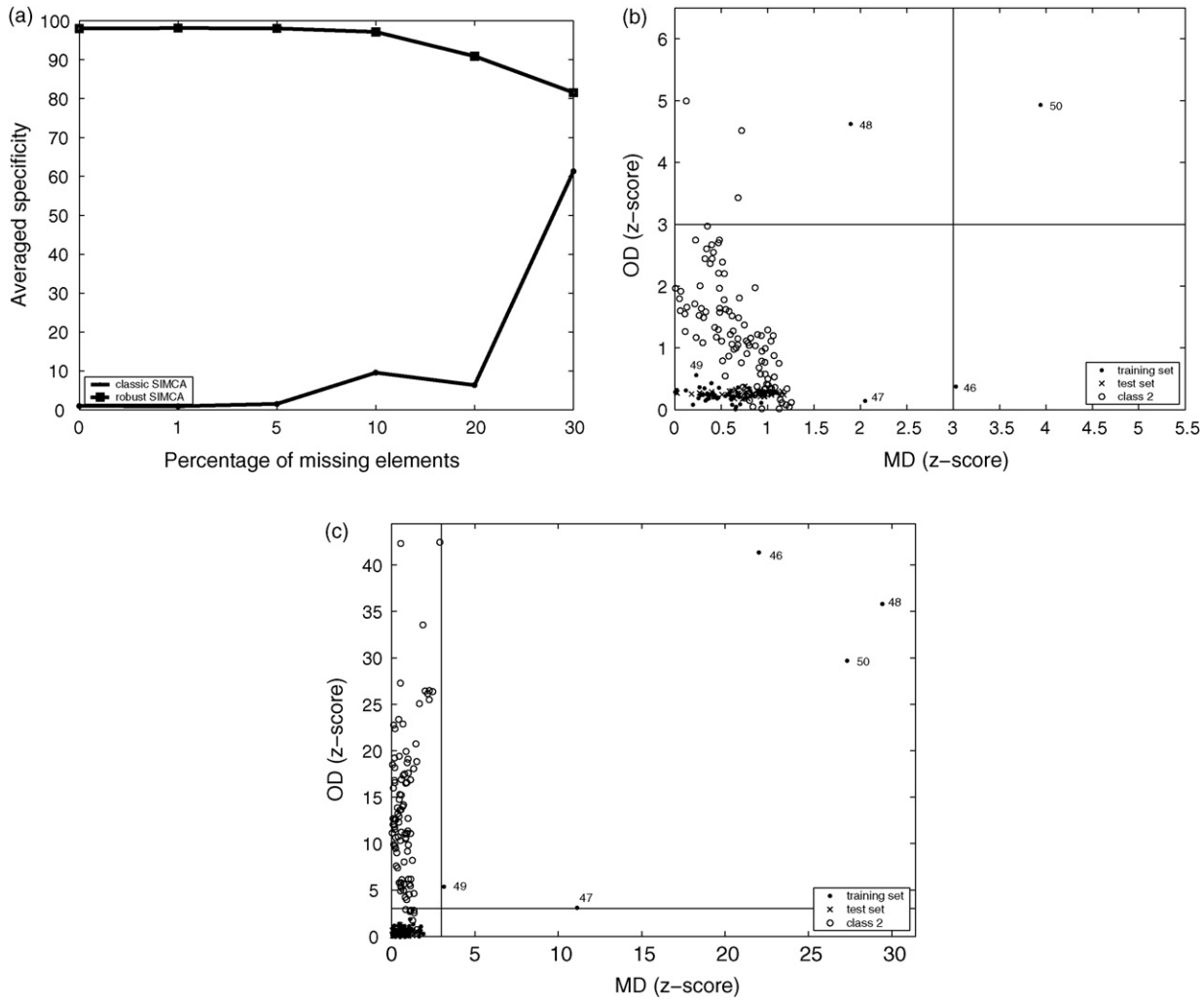

Fig. 2. Performances of the expectation-maximization SIMCA and expectation-maximization S-SIMCA methods applied to a two-class data set containing outliers. The models were built using a training set in which various percentages (1, 5, 10, 20 and 30) of elements were deleted: (a) specificity of the models obtained as an average of 50 runs of the algorithms, (b) distance–distance plot of a five-component EM-SIMCA model built for a contaminated training set containing 20% of missing elements with the highest possible sensitivity of 100%, but a quite poor specificity of 3% and (c) distance–distance plot of a four-component EM-S-SIMCA model built for the same training set with a sensitivity of 100% and a fairly high specificity of 92%.

built in a single run of EM-SIMCA and of EM-S-SIMCA for data with 20% of missing elements are presented in Fig. 1c and d, respectively. Both models show sensitivity of 100%, but a lower specificity (96%) of 1% is found for the EM-S-SIMCA model in comparison with the specificity (97%) obtained from EM-SIMCA for the same data. The complexity of the models is 2.

To demonstrate the performances of both methods for incomplete data with outliers, 10% of objects in the training set, $\mathbf{X}_m$ (50×30), were drawn from the Student's t-distribution with two degrees of freedom. Additionally the elements of these objects were multiplied by a constant with a magnitude of 0.5. Objects with nos. 46, 47, 48, 49 and 50 are the outliers in $\mathbf{X}_m$. The remaining objects in $\mathbf{X}_m$ and $\mathbf{X}_t$ are simulated in the same way as described before. Again, different percentages (1, 5, 10, 20 and 30) of elements were deleted from the training set. The deletion process was not restricted only to the data with normal distribution. This means that there is a possibility that the outlying objects contain missing elements. The sensitivities and specificities of the models built for the particular number of missing elements are calculated as averages of 50 runs of both algorithms, i.e. 50 different patterns of missing elements were again simulated. The optimal complexity of the models varies depending on the pattern of missing elements and on the method applied. The results are presented in Fig. 2.

One can clearly see that the EM-S-SIMCA approach outperforms the EM-SIMCA method when a model using an incomplete training set with outliers is built. The sensitivities of all the models constructed are equal to 100%. Compared to EM-S-SIMCA, the specificities of the EM-SIMCA models are considerably worse. This shows the large influence of the outliers on the classic SIMCA approach. As expected, the specificities of the robust model decrease with an increasing percentage of missing elements. On the contrary, the specificities of the EM-SIMCA models increase with an increasing percentage of missing elements. This might be related to the smaller number of observed elements that is used to construct the model and consequently to the lesser influence of the outliers due to which the class borders become narrower. As an illustration, the five-component EM-SIMCA model built for a contaminated training set with 20% of missing elements has a fairly high sensitivity of 100%, but a very poor specificity of 3%. The distance–distance plot in Fig. 2b shows the strong influence of outliers. The four-component EM-S-SIMCA model presents a sensitivity of 100% and a high specificity of 92% and successfully identifies objects nos. 46, 47, 48, 49 and 50 as outliers (see Fig. 2c).

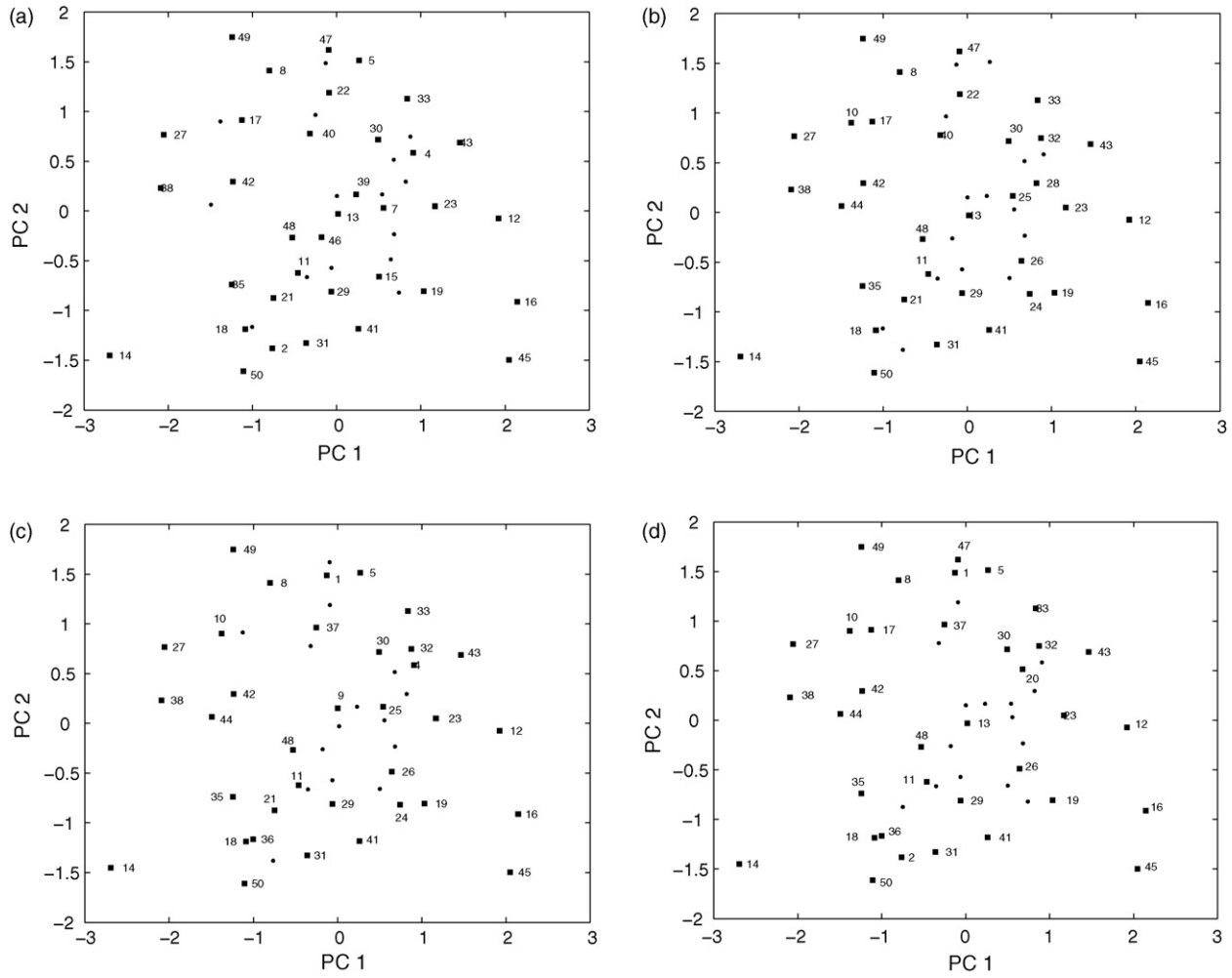

Fig. 3. Selection of the training (■) and test (●) sets using the Kennard and Stone method for data (a) without missing elements, (b) with 5% of missing elements, (c) with 10% of missing elements and (d) with 20% of missing elements.

Concerning the convergence properties of the EM-SPCA algorithm, it generally depends on the distribution and the number of missing elements and correlation structure of the data. Moreover, the higher the correlation among the variables, the faster convergence is reached [1].

Another important issue to discuss is how to create a uniform design with the help of the Kennard and Stone [8] or duplex [9] method. As mentioned before, random selection is not problematic. With the Kennard and Stone method (KS), the samples in the training set are sequentially selected according to the largest Euclidean distance calculated among each of the candidate samples and the samples already included in the training set. Once the user-specified number of samples is selected in the training set, the remaining ones form the test set. This selection method guarantees the representativeness of the training set (i.e., all possible sources of variance are enclosed in the training set).

Using the 'duplex' algorithm, one can ensure the representativeness of both subsets. This is achieved by a parallel scheme of selecting samples for the training and test sets. Firstly, a pair of the most distant samples is chosen and included in the training set. Then, another pair of the most distant samples is found and added into the test set. The selection procedure continues until a specified number of samples are found. At each selection step, a new sample found as the furthest from the samples selected with respect to the currently considered subset is included into the training and test sets, respectively.

For classification purposes, the selection of training and test sets is done for the objects of each class separately. It should be noted

Table 1
Sensitivities (in%) and specificities (in%) obtained from expectation-maximization SIMCA (EM-SIMCA) and expectation-maximization S-SIMCA (EM-S-SIMCA) for contaminated wine data with 10% of missing elements

	EM-SIMCA			EM-S-SIMCA		
	Sensitivity	Specificity	Complexity	Sensitivity	Specificity	Complexity
Barolo vs. others	100.0	10.80	8	50.0	91.60	9
Grignolino vs. others	90.48	3.74	4	90.48	49.53	8
Barbera vs. others	7.14	71.53	11	64.29	99.23	8

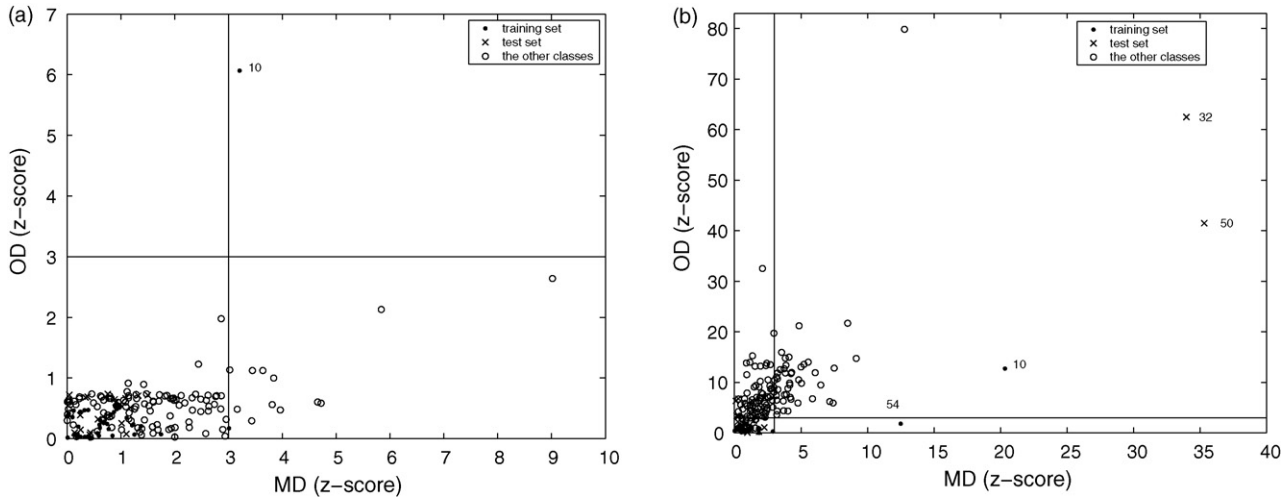

Fig. 4. Distance–distance plots of the (a) EM-SIMCA and (b) EM-S-SIMCA models built for the contaminated 'Barolo' class with 10% of missing elements.

that the uniform selection done on the original complete data is the same as that performed on the full rank score matrix. Therefore, when the data contain missing elements, EM-PCA can be used to obtain the maximum number of scores which then must be input in the Kennard and Stone or 'duplex' algorithm. An example of the application of the Kennard and Stone to simulated data (50×30) of definite complexity with and without missing elements is presented in Fig. 3. The training set (■) contained 70% of samples while the test set (●) included 30% of samples.

From Fig. 3, one can see that the objects included in the training set change with an increasing percentage of missing elements (see Fig. 3b–d) in comparison with the objects selected in the training set for complete data (see Fig. 3a). Moreover, these changes are not dramatic and still the training set can be considered representative for the data.

3.2. Application of EM-SIMCA and EM-S-SIMCA to a real data set

The data set contained 178 samples of wine that were characterized by the 13 parameters measured [17]. The samples represented three types of wine, namely Barolo (59 samples), Grignolino (71 samples) and Barbera (48 samples). The data had already been used in several studies [17,18]. The goal was to see whether the three types of wine could be distinguished using the selected set of parameters. Moreover, the original data did not contain outliers and missing elements. To demonstrate the strategy for analyzing contaminated data with missing elements in our study, several outliers were introduced in the wine data and 10% of the elements were then deleted. The elements were deleted completely at random. The aim was to compare the performance of EM-SIMCA with the EM-S-SIMCA approach for classification of the different types of wine. The training and test sets were chosen using the 'duplex' method applied to the full rank score matrix of each class as this was done for the simulated data. The selection was performed on the autoscaled data to avoid the influence of the different ranges and units of variables when estimating the Euclidian distances among objects. Duplex was preferred here because it allowed for the selection of representative training and test sets. It should be noted that both subsets designed with duplex contain, by definition, outliers due to the selection scheme applied. Again, the training set contained 70% of samples from each class, while the test set included 30% of samples from each class. The results for sensitivities and specificities of models are presented in Table 1.

Four outliers were included in the class 'Barolo'. These were sample nos. 10, 32, 50 and 54 in the original data. Two of them were selected in the training set and the other two in the test set. Table 1 and Fig. 4a show that the EM-SIMCA model has a fairly high sensitivity of 100% since all the Barolo test samples were classified correctly, but a very poor specificity of 10.80% was observed.

Only one outlier was identified in the model, namely, object no. 10. When the robust version of EM-SIMCA was applied, specificity increased to 91.6%. However, sensitivity was 50% for the test samples that were classified correctly. The two outliers in the test nos. 32 and 50 were correctly rejected (see Fig. 4b). From Fig. 4, it can clearly be seen that the EM-S-SIMCA outperforms the EM-SIMCA approach, since in the former the construction of the class boundaries is not affected by the presence of outliers. The outliers in the model were also identified properly. A similar tendency was observed for the other two models for Grignolino and Barbera wines. Sensitivities were unchanged or increased while the specificities of the models increased. This means that with the robust model a higher percentage of samples from the other classes were correctly rejected by the class-model. In general a classification model, which yields considerably high sensitivity and specificity parameters, is to be favored over a model with a high sensitivity and a low specificity.

4. Conclusions

In this paper, we proposed an expectation-maximization S-SIMCA based on the spherical PCA method. It was shown that the method can be used to construct a model for contaminated data with missing elements. Its performance was illustrated on simulated data sets with and without contamination as well as on real data. The influence of missing elements on the model built was discussed. Special care was taken during the model validation, selection of training and test sets and making predictions for new samples. In this context, a modified version of the leverage correction procedure was implemented to quickly choose the complexity of the model constructed. The selection of training and test samples for incomplete data should be done on the full rank score matrix obtained from the expectation-maximization PCA approach, which allows for an optimal selection of the training and test sets using either the Kennard and Stone or duplex method. Furthermore, the prediction for samples with missing elements was done using the PMP method and offered satisfactory results.

Acknowledgement

The authors are grateful for the financial support concerning scientific activities within the Sixth Framework Programme of the European Union, project TRACE—"TRAcing food Commodities in Europe" (project no. FOOD-CT-2005-006942).

References

[1] I. Stanimirova, M. Daszykowski, B. Walczak, Talanta 72 (2007) 172–178.
[2] S. Serneels, T. Verdonck, Comput. Stat. Data Anal. 52 (2008) 1712–1727.
[3] I. Stanimirova, S. Serneels, P.J. Van Espen, B. Walczak, Anal. Chim. Acta 581 (2007) 324–332.
[4] M. Daszykowski, K. Kaczmarek, I. Stanimirova, Y. Vander Heyden, B. Walczak, Chemometr. Intell. Lab. Syst. 87 (2007) 121–129.
[5] K. Vanden Branden, M. Hubert, Chemometr. Intell. Lab. Syst. 79 (2005) 10–21.
[6] A.P. Dempster, N.M. Laird, D.B. Rubin, J. Roy. Stat. Soc. Ser. B: Stat. Methodol. 39 (1977) 1–38.
[7] N. Locantore, J.S. Marron, D.G. Simpson, N. Tripoli, J.T. Zhang, K.L. Cohen, Test 8 (1999) 1–74.
[8] R.W. Kennard, L.A. Stone, Technometrics 11 (1969) 137–148.
[9] R.D. Snee, Technometrics 19 (1977) 415–428.
[10] H. Martens, T. Naes, Multivariate Calibration, John Wiley & Sons, Gulford, Great Britain, 1989.
[11] F. Arteaga, A. Ferrer, J. Chemometr. 16 (2002) 408–418.
[12] S. Wold, Pattern Recogn. 8 (1976) 127–139.
[13] B.G.M. Vandeginste, D.L. Massart, L.M.C. Buydens, S. de Jong, P.J. Lewi, J. Smeyers-Verbeke, Handbook of Chemometrics and Qualimetrics, Part B, Elsevier, Amsterdam, The Netherlands, 1998.
[14] P.J. Huber, Robust Statistics, Wiley, New York, The USA, 1981.
[15] O. Hössjer, C. Croux, J. Nonparametr. Stat. 4 (1995) 293–308.
[16] P.J. Rousseeuw, C. Croux, J. Am. Stat. Assoc. 88 (1993) 1273–1283.
[17] M. Forina, C. Armanino, M. Castino, M. Ubigli, Vitis 25 (1986) 189–201.
[18] R. Todeschini, Anal. Chim. Acta 348 (1997) 419–430.

Talanta 76 (2008) 617–620

Contents lists available at ScienceDirect

Talanta

journal homepage: www.elsevier.com/locate/talanta

Use of a capacitance measurement device for surrogate noncontact conductance measurement

Masaki Takeuchi [a], Qingyang Li [a], Bingcheng Yang [a], Purnendu K. Dasgupta [a,*], Vincent E. Wilde [b]

[a] Department of Chemistry and Biochemistry, The University of Texas at Arlington, Arlington, TX 76019-0065, United States
[b] Department of Chemistry and Biochemistry, Texas Tech University, Lubbock, TX 79409-1061, United States

ARTICLE INFO

Article history:
Received 10 February 2008
Received in revised form 31 March 2008
Accepted 1 April 2008
Available online 10 April 2008

Keywords:
Contactless conductivity
Capacitance
Ion chromatography

ABSTRACT

A capacitance to digital converter (AD7746) is used in the same mode as noncontact conductance detectors. The detector output is linearly proportional to specific conductance (σ) at low σ values but becomes nonlinear and reaches a plateau value at $\sigma \sim$>0.75 mS/cm, regardless of the nature of the electrolyte. For all applications at sub- to low-mM concentrations, the device, available as an evaluation board, provides a very affordable nothing-else-required means of contactless surrogate conductivity detection from capillary scale to larger bore conduits. For the same measurement cell volume, the detector provides virtually the same limits of detection (LODs) as a standard galvanic contact conductivity detector in conventional scale suppressed conductometric ion chromatography. The detection limits deteriorate as the conduit inner diameter deceases.

1. Introduction

There has been a great deal of recent interest in impedance-related measurements in miniature flow-through detectors without imposing direct solution–electrode contact. Gas et al. [1] described the first flow-through nongalvanic conductivity detector with a differential measurement based on four electrodes; the basic concept can be traced to at least 1965 [2]. However, the 1998 papers by Zemann et al. [3] and da Silva and do Lago [4] really brought attention to this area by demonstrating noncontact conductivity measurements from outside a capillary with one transmitter and one receiver electrode. In capillary electrophoresis (CE), galvanic measurements are made difficult by the presence of the high voltage electrophoretic field and this became particularly useful. The approach was soon adapted to on-chip measurements [5], with probe voltages as high as 500 V to improve sensitivity [6] and a return to four electrode systems [7]. Reviews, or papers that contain an excellent review section, are available [8–11]. Simplicity, small size, and ease of use have led to new uses, e.g., to monitor flow velocities [12,13] and photothermal absorbance detection [14].

Capacitively coupled contactless conductance detectors (C^4D) have been modeled. The two electrodes are each envisioned to form a capacitor with the inside of the capillary, which are connected by a resistor represented by the solution resistance [8]. If the electrodes are close and the free-space capacitance between the electrodes is significant, this capacitance, parallel to the resistance represented by the cell must also be considered. However, this will be negligible for the thin-walled tubular electrodes at probe frequencies less than 100 kHz. The serial capacitors remain important. All the factors that affect this interfacial capacitance at each electrode have never been delineated. Under conditions where the interfacial capacitance values are significantly controlled by the ionic concentration in the wall double layer, the output of any capacitance measurement device will de facto depend on the ionic concentration of the solution. Recently integrated circuit chips that measure capacitance from floating sensors with 21-bit resolution with a range of 4 pF and a resolution of 4 aF (AD7746), have become inexpensively available [15]. A similar device with a range of 8 pF is also available (AD7747). These devices can measure the capacitance of a single capacitive input or the difference between two sets of inputs and provide a digital output. They are also available as evaluation boards with a Universal Serial Bus (USB) interface (US$ 120–150). It was of interest to see how the output of such a device, designed to measure capacitance at 32 kHz, varies with solution conductance and if it could be used effectively as a surrogate C^4D. Here we compare the performance of an AD7746 evaluation board with a conventional state-of-the-art galvanic bipolar pulse conductance detector for suppressed ion chromatography (IC) applications.

* Corresponding author. Tel.: +1 817 272 3171.
E-mail address: Dasgupta@uta.edu (P.K. Dasgupta).

0039-9140/$ – see front matter © 2008 Elsevier B.V. All rights reserved.
doi:10.1016/j.talanta.2008.04.001

2. Experimental

The capacitance-to-digital converter was obtained as the evaluation board (EVAL-AD7746EB-ND, www.digi-key.com). It was used in the simplest configuration, without external voltage reference or temperature sensors. The sensor was connected to floating tubular electrodes (*vide-infra*) placed on a glass or polyimide-coated fused silica flow-through tube. The vendor supplied software permits output of data at frequencies between 10 and 90 Hz. The data output is already averaged within the reporting interval; there is no advantage of getting data out at a higher frequency and averaging externally, unless higher frequency data are needed. Vendor software supports either graphic display or acquisition of the data but not both. A routine to simultaneously acquire and display the data in MS Excel™ was written in-house. Unless otherwise stated, sensor output data reported were collected at 10 Hz and then averaged to 1 s; data from the galvanic conductance detector was collected with a 1 Hz frequency for comparability. The intrinsic response of the sensing circuitry is faster than 10 Hz, but this response speed is not needed for the flow injection or ion chromatography applications of interest to us. As such, averaging was used to improve S/N ratio.

Chromatography was carried out both with standard scale commercial equipment and with homebuilt capillary scale instrumentation. Suppressed anion chromatography was conducted with a DX-600 IC system that comprised of (a) a GS-50 pump, (b) an EG-40 electrodialytic eluent generator, (c) a loop injector (25 μL), (d) AG-20 (4 mm × 50 mm) and AS-20 (4 mm × 250 mm) guard and analytical columns, (e) an ASRS-Ultra 4-mm suppressor (operated in the eluent recycle mode with a drive current of 100 mA), (f) an LC-30 chromatography oven to house *c-e* and a conductivity detection cell connected to (g) a CD-25 conductivity detector. All components were from Dionex Corp. (Sunnyvale, CA). Potassium hydroxide (32 mM) was used as the eluent at a flow rate of 0.6 mL/min. The capacitance detection cell was designed to match the cell volume of the conventional conductivity cell as closely as possible. It consisted of a 1.45 mm i.d. glass tube of 320 μm wall thickness as the flow conduit. Two 2-mm long stainless steel tubular segments (2.1 mm i.d., 2.54 mm o.d.; HTX 12-1/2R, www.smallparts.com) that fit snug on the glass tube were placed on the latter, 1 mm apart, resulting in a cell volume of 1.65 μL. The free ends of the shielded cables terminate at one end in subminiature version B (SMB) connectors (J1836-ND, www.digi-key.com) and connect the sensor inputs to the board. The other ends were affixed to the stainless tube segments by conductive epoxy adhesive. The tube/detection cell and cable assemblies were put in a small metal enclosure with appropriate holes drilled in for entry/exit of the tube and the cables. No shielding (metal foil, etc.) was put between the electrodes; this is regarded to be important at least in some publications on high-frequency contactless conductivity measurements which find that otherwise peak shapes become distorted [9].

In one set of experiments, a similar chromatographic system as above was used, except with a pump head and suppressor optimized for 2-mm bore columns and after the suppressor, the effluent flow of 150 μL/min was split in two equal flow rate streams, one to proceed through a conventional galvanic contact bipolar pulse conductance detector (CD 25) and the other to proceed through a capacitance detector. The general arrangement is given in Supplementary Fig. S1. This capacitance detection cell is similar to the larger glass tube based cell described above but based on a 365 μm o.d. fused silica capillary, with 10 mm long stainless steel sleeves (410 μm i.d., 660 μm o.d., HTX-22R) placed 1 mm apart. Supplementary Fig. S2 shows photographs of the cell—this design was used with capillaries varying in i.d. from 50 to 250 μm, as specified.

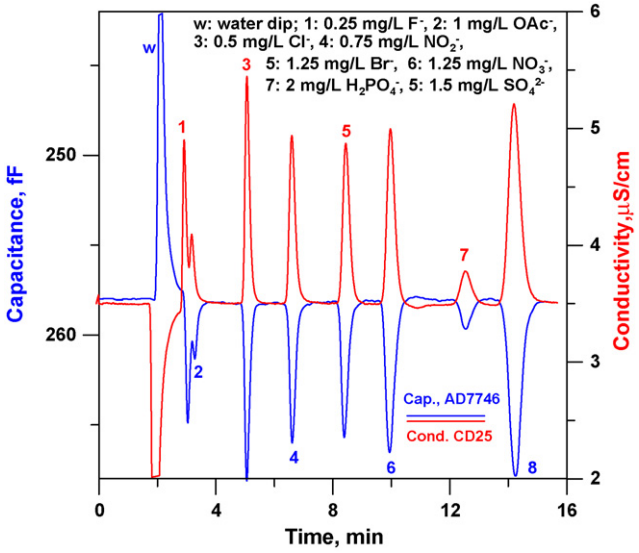

Fig. 1. Superimposed chromatograms obtained with conventional conductivity and present capacitance detector. 4-mm bore AG-20/AS-20 anion exchange columns, 32 mM KOH at 0.6 mL/min. Sample volume 25 μL.

Capillary chromatography was conducted with a 48,000-step syringe pump (Type V6, P/N 54022) equipped with a high pressure valve assembly (P/N P0753) syringe of 500 μL capacity (P/N P1147, all from www.kloehn.com). Some experiments were conducted in the nonsuppressed mode, the details of which for example, appear in ref. [16] and chromatograms in that mode with the present capacitance detector has already been presented therein. Presently, chromatography was conducted on a 380 μm × 300 mm column containing AS-19 packing (Dionex Corp). The column was operated with a 200 nL sample injector (P/N CI4W.2, VICI), and 15 mM KOH eluent at 10 μL/min. The eluites were detected after suppression with a prototype capillary scale membrane suppressor [17].

3. Results and discussion

3.1. General behavior and performance at low concentrations

The sensor output, obtained in terms of measured capacitance, increased with increasing electrolyte concentration. At low and typical concentrations encountered in IC, the capacitance detector produced a chromatogram that is essentially identical to the conductivity based chromatogram, as shown in Fig. 1. An inverted ordinate axis is used for the test sensor to permit comparison without overlap. Taking chloride as an example, over the low concentration range of 0–500 μg/L (lowest non-blank concentration 50 μg/L), the conventional galvanic conductometric peak height response was linear (r^2 = 0.9902, slope 14.6 ns/cm/(μg/L)), with a baseline noise of ~13 nS/cm. The response from the present sensor (1.45 mm i.d. cell) was also linear (r^2 = 0.9986, slope 794 aF/(μg/L)) with a baseline noise of 0.67 fF. In effect, a signal of 1 μS/cm on the conductivity detector was equivalent to ~54 fF (or 1 fF = 18.5 nS/cm) measured by the AD 7746 sensor and both detectors showed approximately the same limit of detection (LOD), ~2.6 μg/L Cl^-. Linear correlation coefficients alone are not a full descriptor of linearity or linear range. A Cassidy plot (sensitivity vs. concentration) with a logarithmic abscissa is shown in Fig. 2. It will be observed that the detector output remains linear with concentration (constant sensitivity) up to about ~700 μg/L and thereafter the response continues to decrease. Response over a large concentration range is discussed in greater detail in a later section.

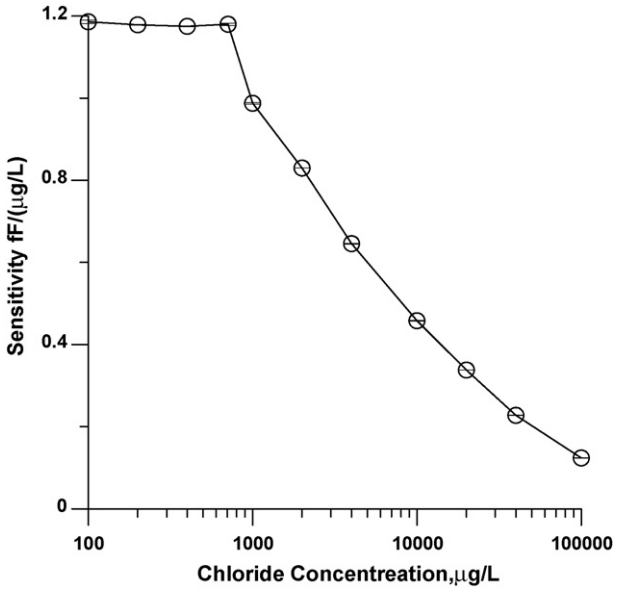

Fig. 2. Response per unit concentration of chloride as a function of concentration [25] over a large concentration range; note logarithmic abscissa.

The noise of both detectors, filled with deionized water was also measured in a static (no-flow) mode, after allowing for thermal equilibration. The galvanic conductivity detector had a measured noise of 0.13 nS/cm, close to the manufacturer's specifications, while the capacitance detector had a measured noise level of 6 aF (which is equivalent to ~0.11 nS/cm, based on the comparison above), close to the manufacturer's resolution specification of 4 aF. The two detectors thus produced comparable results at the low concentration end.

We found the detector to be equally applicable to capillary scale anion chromatography applications. Fig. 3 shows a trace level capillary chromatogram where 4 pmol of each analyte (200 nL, 20 μM) was injected. The LOD in this case is not as good as that for galvanic conductance detectors, compared for example to the data of Boring et al. [18], the LODs in absolute amounts are a factor of 5–8x worse. However, the data of Boring et al. pertain to gradient conditions.

3.2. Signal and noise as a function of conduit diameter

Our experience with galvanic conductivity measurements in a chromatographic context ranges from 4 mm columns to 75 μm bore capillaries [19–22]. We find that cell dimensions have very little on the attainable S/N until the cell constant gets too large and the corresponding cell current becomes too small. Although this has not been documented as such in the literature, others have had similar findings (Srinivasan, Dionex Corp., personal communication, 2008). In suppressed IC, the detector background is nearly pure water with a high specific resistivity. The present sensor measured background capacitance values in the sub-pF range. We thought that with a larger bore cell, the background noise would decrease because of the larger cell current. However, experimentally the background noise with various tube inner diameters (50, 75, 100, 180 and 250 μm) did not show any consistent pattern as a function of diameter. In fact, they did not vary a great deal: the lowest and highest noise values were within <2.5x of each other.

The equation that describes the capacitance of a capacitor with two parallel electrodes [23] is virtually identical to one that describes the conductance of a similar cell filled with an electrolyte. Whereas the capacitance is given by the product of the permittivity and the cell constant, the conductance is the product of the

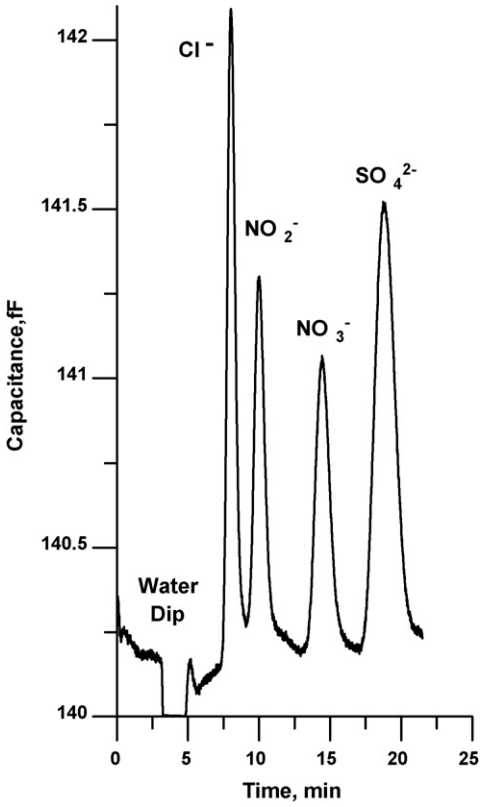

Fig. 3. Capillary scale detection with capacitance detector. Sample: 20 μM of each anion, 200 nL. 0.38 mm × 300 mm AS-19 column, 15 mM KOH, 10 μL/min. Detector on 100 μm i.d. tube.

specific conductance and the cell constant [24]. In both cases, the cell constant is defined to be the electrode area divided by the distance separating them. In the present case, the electrodes can be thought of as infinitely thin parallel rings (the distance of separation was held constant at 1 mm) and the capacitance should thus be directly proportional to the electrode perimeter or the diameter. However, this diameter is not the physical inner diameter of the steel electrodes (410 μm for all of the 50–250 μm capillaries) but the corresponding virtual electrodes as the field first penetrate into the solution. The virtual electrode diameter thus corresponds to the inner bore of the capillary. The signal or the measured capacitance value should increase linearly with the capillary diameter. This was observed. Over the entire 50–1450 μm diameter range, the observed capacitance was linearly related to the capillary diameter with an r^2 value of 0.9992 for a 0.4 mM KCl solution (see Supplementary Fig. S3 for detailed data).

3.3. Response behavior over a large concentration range

Although at low concentrations the response of the capacitance detector was linear with concentration, there were indications that this may not be true over a large concentration range. We examined both the conductivity and the capacitance (250 μm bore cell) of 0–6 mM HCl and 0–16 mM KCl solutions; the results are shown in Fig. 4. It is clear that the conductivity response is linear in both cases. But not only is the measured capacitance value nonlinearly related to concentration, it reaches a plateau at specific conductance values ~>0.75 mS/cm and thereafter actually decreases, for both electrolytes. These conductance values are generally much larger than what would normally be encountered in IC applications, but would be of interest in the future to characterize this behavior.

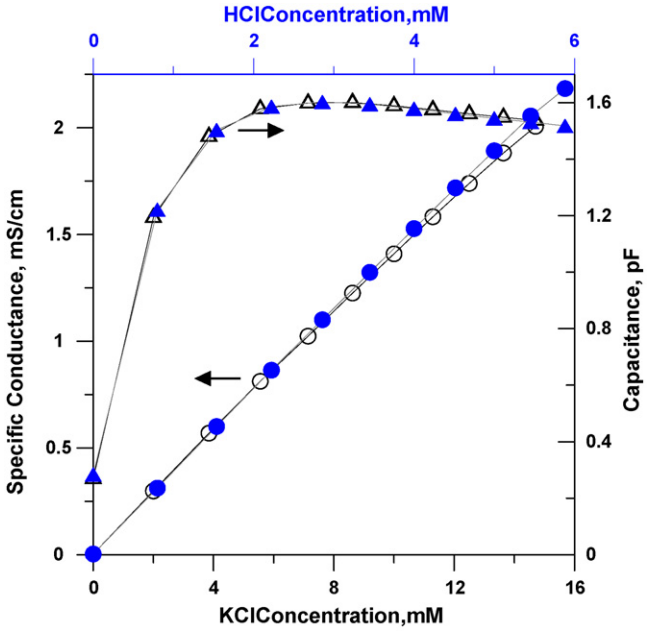

Fig. 4. Specific conductance (left ordinate) vs. capacitance (measured in a 250 μm bore cell, right ordinate) for KCl (bottom abscissa) and HCl (top abscissa) solutions. The experimental arrangement of Supplementary Fig. S1, without the chromatographic columns and large volume injection to read plateau values was used for the measurements.

Granted that the system consists of a capacitor–resistor–capacitor serial combination, we hypothesize that at low specific conductance levels, the capacitance of each of the capacitors actually increases in value as the wall double layer ionic population increases. But this levels out at increased ionic strength and no further increase is observed. At high enough ionic strength, the observed capacitance actually decreases as the double layer thickness begins to decrease. It is possible that the decrease in the observed capacitance at high electrolyte concentrations is influenced also by the decreasing value of the interconnecting resistor.

Whether the above hypothesis is correct or not, we have shown that an off-the-shelf relatively inexpensive capacitance measurement device can be readily used as an on-tube noncontact detector that responds to the conductivity of electrolyte solutions; at low specific conductance values, the output of this device is linearly related to the specific conductance of the solution. With a polynomial based calibration relationship, the device can be actually used to much higher conductivities.

Acknowledgements

This research was supported by National Science Foundation grant CHE-05198652 and by a grant from the Dionex Corporation. We thank Yan Liu for the AS-19 capillary column.

Appendix A. Supplementary data

Supplementary data associated with this article can be found, in the online version, at doi:10.1016/j.talanta.2008.04.001.

References

[1] B. Gas, M. Demjanenko, J. Vacik, J. Chromatogr. 190 (1980) 253–257.
[2] E. Pungor, Oscillometry and Conductometry, Pergamon Press, New York, 1965.
[3] A.J. Zemann, E. Schnell, D. Volgger, G.K. Bonn, Anal. Chem. 70 (1998) 563–567.
[4] J.A.F. da Silva, C.L. do Lago, Anal. Chem. 70 (1998) 4339–4343.
[5] M. Pumera, J. Wang, F. Opekar, J. Jelıĭnek, J. Feldman, H. Lowe, S. Hardt, Anal. Chem. 74 (2002) 1968–1971.
[6] J. Tanyanyiwa, P.C. Hauser, Anal. Chem. 74 (2002) 6378–6382.
[7] F. Laugere, R.M. Guijt, J. Bastemeijer, G. van der Steen, A. Berthold, E. Baltussen, P. Sarro, G.W.K. van Dedem, M. Vellekoop, A. Bossche, Anal. Chem. 75 (2003) 306–312.
[8] P. Kubáň, P.C. Hauser, Electrophoresis 25 (2004) 3387–3397.
[9] P. Kubáň, P.C. Hauser, Electrophoresis 25 (2004) 3398–3405.
[10] R.M. Guijt, C.J. Evenhuis, P.R. Haddad, M. Macka, Electrophoresis 25 (2004) 4032–4057.
[11] S.E. Johnston, K.E. Fadgen, L.T. Tolley, J.W. Jorgenson, J. Chromatogr. A. 1094 (2005) 148–157.
[12] A.D. Jerkovich, J.S. Mellors, W. Thompson, J.W. Jorgenson, Anal. Chem. 77 (2005) 6292–6299.
[13] R.M. Saito, C.A. Neves, F.S. Lopes, L. Blanes, J.G.A. Brito-Neto, C.L. do Lago, Anal. Chem. 79 (2007) 215–223.
[14] S.E. Johnston, K.E. Fadgen, J.W. Jorgenson, Anal. Chem. 78 (2006) 5309–5315.
[15] Analog Devices, Inc., 24-bit Capacitance-to-Digital Converter with Temperature Sensor, AD 7745/AD7746, http://www.analog.com/en/prod/0%2C2877%2CAD7746%2C00.html.
[16] B.C. Yang, M. Takeuchi, P.K. Dasgupta, P.K.T. Umemura, Y. Ueki, K. Tsunoda, Anal. Chem. 79 (2007) 769–772.
[17] P. Kuban, P.K. Dasgupta, C.A. Pohl, Anal. Chem. 79 (2007) 5462–5467.
[18] C.B. Boring, P.K. Dasgupta, A. Sjögren, J. Chromatogr. 804 (1998) 45–54.
[19] H. Shintani, P.K. Dasgupta, Anal. Chem. 59 (1987) 802–808.
[20] D. Qi, T. Okada, P.K. Dasgupta, Anal. Chem. 61 (1989) 1383–1387.
[21] P.K. Dasgupta, L. Bao, Anal. Chem. 65 (1993) 1003–1011.
[22] S. Kar, P.K. Dasgupta, H. Liu, H. Hwang, Anal. Chem. 66 (1994) 2537–2543.
[23] C.R. Nave, Hyperphysics, Parallel Plate Capacitors, Georgia State University, http://hyperphysics.phy-astr.gsu.edu/hbase/electric/pplate.html.
[24] H. Small, Ion Chromatography, Plenum, New York, 1989, p. 151.
[25] R.M. Cassidy, L.C. Chen, LC·GC Mag. 10 (1992) 692–696.

Talanta 76 (2008) 533–539

Contents lists available at ScienceDirect

Talanta

journal homepage: www.elsevier.com/locate/talanta

Voltammetric study and electrochemical detection of hexavalent chromium at gold nanoparticle-electrodeposited indium tinoxide (ITO) electrodes in acidic media

Ming-Chih Tsai, Po-Yu Chen*

Faculty of Medicinal and Applied Chemistry, Kaohsiung Medical University, Kaohsiung City 807, Taiwan

ARTICLE INFO

Article history:
Received 1 February 2008
Received in revised form 24 March 2008
Accepted 24 March 2008
Available online 4 April 2008

Keywords:
Gold
Nanoparticle
Hexavalent chromium
Indium tinoxide
Modified electrode

ABSTRACT

The voltammetric behavior of hexavalent chromium species (Cr(VI)) was respectively studied at ITO, bulk Au, and Au-electrodeposited electrodes in 0.01 M NaCl aqueous solutions containing 0.01 M HCl. It was found that performance degradation of the ITO electrodes toward the reduction of Cr(VI) can be suppressed by modifying the electrode surface with gold nanoparticles (AuNPs), which were formed on ITO electrodes by potential-sweeping or potential-step electrodeposition in a 0.01 M Na_2SO_4 solution containing 1 mM $HAuCl_4{\cdot}3H_2O$ and 0.01 M H_2SO_4. After the modification, the surface of ITO electrodes turned to the characteristically red or blue color exhibited by AuNPs. The gold nanoparticle-electrodeposited indium-tinoxide electrode (AuNP-ITO) demonstrates unique catalytic behavior, higher sensitivity and stability in the reduction of Cr(VI). Cr(VI) species was detected by either cyclic voltammetry or hydrodynamic amperometry. By cyclic voltammetry, the dependence of cathodic peak current on concentration was linear from 5 to 100 μM with a detection limit of 2 μM ($\sigma = 3$), and linearity was obtained from 0.5 to 50 μM by hydrodynamic amperometry where a constant potential of +0.2 V (*vs.* Ag/AgCl) was applied and a batch-injection cell was employed. For hydrodynamic amperometry, the detection limit was 0.1 μM ($\sigma = 3$).

1. Introduction

In aqueous systems, the dominate species of chromium are Cr(VI) and Cr(III) that are present in the wastewater drained from leather tanning, textile, electroplating, and electronic industries, timber treatment [1], and steel manufacturing [2]. Depending on the concentration of Cr(VI) and solution pH, Cr(VI) can be present in anionic forms such as CrO_4^{2-}, $Cr_2O_7^{2-}$ or their protonized forms that have been reported as being 100–1000 times more toxic than Cr(III) [3] because of its strongly oxidizing potency. In addition, Cr(VI) is a well-known carcinogen, and highly mobile in the environment while Cr(III) is readily precipitated or adsorbed by many organic or inorganic substances. The effluent containing Cr(VI), therefore, produces serious impact to our environment and organisms. The determination and treatment of Cr(VI) species are thus important tasks and attractive topics.

Cr(VI) can be reduced to less toxic Cr(III) by adding chemical reagents, and then the Cr(III) species can be precipitated in the form of hydroxides. However, the additive chemicals would be consumed and might not be recovered for reuse. Instead, the more attractive technique is electrochemical reduction. In fact, there are many reports corresponding to the electrochemical treatment of water that contains Cr(VI) [4–8]. Conducting polymers have been employed, however, degradation of polymer and/or electrode itself are(is) encountered [9–12].

The selective detection of Cr(VI) is relatively easier based on electrochemical techniques because the reduction potentials of Cr(VI) and Cr(III) are different from each other. The electrochemical detection of Cr(VI) has been reported at mercury electrodes [13–17], and a good detection limit was obtained. However, the toxicity of mercury limits its application in analytical chemistry, and solid electrodes were then employed. The reduction of Cr(VI) has been studied at gold and platinum electrodes, respectively [18–20]. These literatures indicate that the electrochemical behavior of Cr(VI) significantly depends on the electrode material and compositions of supporting electrolytes. Different results obtained might be explained partially by the highly corrosive property of Cr(VI), or passivation of electrodes. In contrast, gold electrodes are more stable toward corrosion and passivation [18]. Modification at platinum and gold electrodes has been employed for more sensitive detection of chromium [21–26]; nevertheless, to the best of our knowledge, metallic nanoparticle-modified electrodes have not been used for Cr(VI) detection and it should be highly interesting.

How to prepare an aqueous solution containing gold nanoparticles (AuNPs) is well-known. However, this solution is not very appropriate for modifying untreated electrode surface because

* Corresponding author. Tel.: +886 7 3121101x2587; fax: +886 7 3125339.
E-mail address: pyc@kmu.edu.tw (P.-Y. Chen).

0039-9140/$ – see front matter © 2008 Elsevier B.V. All rights reserved.
doi:10.1016/j.talanta.2008.03.043

aggregation of gold particles usually happens if dip-coating is employed. AuNPs can be attached to the electrode surface through self-assembled monolayer (SAM) and the results have been reported [27–30]. However, the molecules used for bridging the AuNPs and the electrode surface should be carefully selected in order to maintain smooth electron transfer. In addition, it is not very convenient to modify the electrode surface with AuNPs by the two-step or even multi-step process. More seriously, these functionalized molecules employed for attaching or protecting the AuNPs may reduce their catalytic activity or inhibit electron transfer [29]. To prepare AuNPs-modified electrodes in one step is definitely more straightforward. Electrodeposition seems to be a proper method for this purpose because the mechanism of electrodeposition is very similar to crystallization. It is possible to stop at the right moment at which the dimensions of the electrodeposited crystals fall in nanoscale. Unfortunately, the relevant studies are relatively rare. The more popular way to form nanostructure by electrodeposition is to use suitable templates [31–34]; however, the disadvantage of this method is also inconvenient even though the nanoparticles prepared from this technique may be more stable. AuNPs have been formed on electrode surfaces by direct electrodeposition without using templates [35–37]. In those reports, AuNPs were formed by potential-step electrodeposition and were used for electrocatalytic reduction of oxygen or for the study of optical and spectroscopic properties. According to those studies, electrodeposition might be a convenient method for AuNPs formation; however, the density, size, and distribution regularity of the particles are not very ideal.

In this study, AuNPs were formed by either potential-sweeping or potential-step electrodeposition at indium-tinoxide electrodes in order to prepare the gold nanoparticle-electrodeposited indium-tinoxide electrodes (AuNP-ITO). Compared with ITO and regular gold-electrodeposited ITO (Au-ITO), the AuNP-ITO exhibits excellent stability toward the reduction of Cr(VI). The detection of Cr(VI) was performed by using cyclic voltammetry and hydrodynamic amperometry at the AuNP-ITO in acidic media. The surface morphology of the AuNP-ITO was analyzed by a scanning electron microscope (SEM) that equips a energy dispersive spectrometer (EDS). The AuNP-ITO was also studied by a UV–vis spectrophotometer in order to observe the characteristic absorption of AuNPs.

2. Experimental

2.1. Apparatus and chemicals

All electrochemical experiments were performed with a CHI 621A electrochemical analyzer (CH Instruments, Inc.) in conjunction with a Bioanalytical Systems (BAS) model C-2 electrochemical cell in which a three-electrode system is employed. The three-electrode system consists of an indium-tin oxide (ITO)-coated glass electrode with or without electrodeposited gold particles, an Ag/AgCl (saturated NaCl) reference electrode, and a platinum spiral counter electrode. A large piece of ITO electrode was cut into smaller pieces with individual area of $0.6 \times 1.2\,cm^2$. They were soaked supersonically in acetone, and then in deionized water, and dried in a vacuum oven at room temperature before experiments would be carried out. The conducting area of each electrode was restricted in $0.6 \times 0.6\,cm^2$ by wrapping the electrode with Teflon tape. The surface morphology and elemental compositions of the AuNP-ITO were investigated with the FEI Quanta 400 F environmental scanning electron microscope (ESEM) coupled with a energy dispersive spectrometer (EDS).

The hydrochloric acid (J.T. Baker, 38%), sulfuric acid (SHOWA, 97%), sodium chloride (J.T. Baker, 99.9%), sodium sulfate (TEDIA), potassium chromate (KANTO, 98.5%), and hydrogen tetrachloroaurate(III) trihydrate (ACROS) were used as received without further purification. All solutions were prepared with deionized water purified by the Milli-Q Gradient system (Millipore).

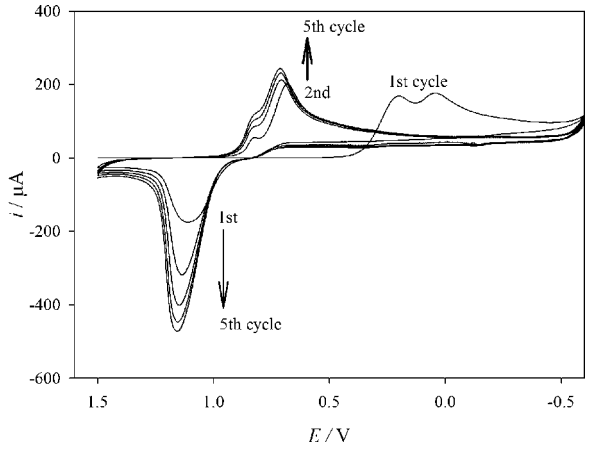

Fig. 1. Staircase cyclic voltammograms recorded at an ITO electrode immersed in the 0.01 M Na_2SO_4 solution containing 0.01 M H_2SO_4 and 1 mM $HAuCl_4{\cdot}3H_2O$. Scan rate: 100 mV/s. Number of potential cycle was indicated.

2.2. Fabrication of gold-electrodeposited ITO electrodes

A 0.01 M Na_2SO_4 aqueous solution containing 0.01 M H_2SO_4 and 1 mM $HAuCl_4{\cdot}3H_2O$ was used for electrodeposition of gold particles at ITO electrodes. Gold particles were electrodeposited upon ITO electrodes by either potential-step or potential-sweeping electrodeposition. For potential-step electrodeposition, a fixed potential of −0.20 V was applied at ITO electrodes for a particular period of time and the solution was stirred steadily during the entire process of electrodeposition. AuNPs formed through this technique were bigger in diameter and the electrode surface exhibits blue color. Smaller AuNPs can be formed on the ITO electrodes by cycling the potential of the working electrode between +1.50 V and −0.60 V for one or five cycles. The cyclic voltammograms of this process are shown in Fig. 1. The resulting AuNP-ITO reveals the typically red color exhibited by AuNPs.

3. Results and discussion

3.1. Fabrication and characteristics of AuNP-ITO electrodes

Fig. 1 shows the continuous cyclic voltammograms recorded at an ITO electrode in the bath of gold electrodeposition. In order to avoid the interference contributed by dissolved oxygen, the bath was sparged by highly pure argon gas. The applied potential at the electrode was initially scanned from +1.50 V to negative direction at a sweep rate of 100 mV/s. The reduction waves of Au(III) occurred at more negative potentials in the first cycle and then shifted to more positive potentials in the subsequent four cycles. Besides, a current loop was observed in the first cycle and it disappeared during the following potential scans. This phenomenon indicates that higher overpotential and nucleation processes were needed for electrodeposition of gold at a fresh ITO electrode. Once the gold particles have been formed on the electrode surface, a much lower potential was needed for subsequent gold electrodeposition. The reduction waves of Au(III) were accompanied with typical stripping waves observed during the reverse scans, indicating that electrodeposited Au particles can be reoxidized; however, by careful observation, the area of each stripping wave was found smaller than its relevant reduction counterpart, and the cathodic peak current of Au(III) increased

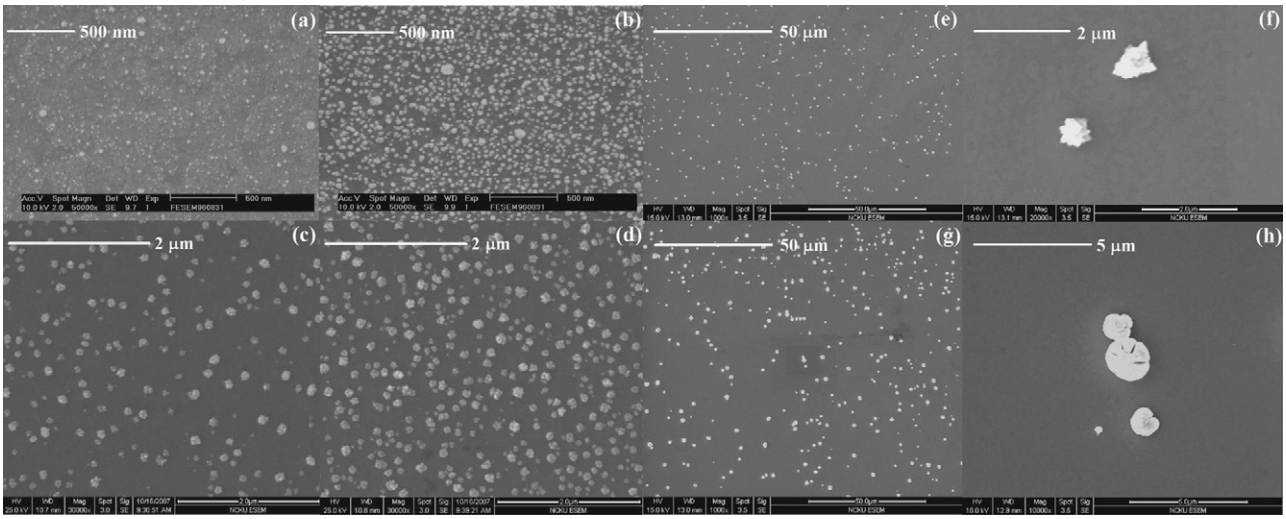

Fig. 2. SEM micrographs of the ITO electrodes that were electrodeposited with gold by potential-sweeping electrodeposition for one cycle and five cycles ((a) and (b)), by potential-step electrodeposition at −0.2 V for 10 and 30 s ((c) and (d)) or at +0.2 V for accumulating charges of 1.4 and 14 mC, respectively ((e) and (g)). (f) and (h) are the magnified images of (e) and (g), respectively.

continuously. These features imply that electrodeposited Au cannot be completely reoxidized and the active surface area for gold electrodeposition increased with continuous potential scans.

The surface of the AuNP-ITO electrodes prepared by above procedures was characterized with SEM and the micrographs are shown in Fig. 2(a) and (b), respectively. The electrode shown in Fig. 2(a) was fabricated by potential-sweeping electrodeposition and a single cycle was performed; five cycles of potential scan were applied at the electrode shown in Fig. 2(b). Apparently, raising the cycle number of potential scan can increase the density and size of AuNPs. This characteristic is coincidental to the voltammetric behavior of gold electrodeposition in which the electrodeposited Au was found unable to be completely reoxidized and the active area of electrode increased continuously. Regardless of few bigger particles, the AuNPs shown in Fig. 2(b) are near 20–30 nm in diameter. This electrode was also analyzed with a spectrophotometer in the visible wavelengths and a specific absorption maximum of AuNPs was observed near 555 nm (Fig. 3(a)). The photograph of the AuNP-ITOs is shown in the inset of Fig. 3(a), the characteristically red color of AuNPs is apparent.

Electrodeposition of AuNPs was also carried out by applying a fixed potential of −0.2 V for a particular period of time at ITO electrodes. Under this condition, the electrodeposition of Au should be diffusion-controlled. In order to avoid deficiency of surface concentration, the electrodeposition solution was firmly stirred. The SEM micrographs of these electrodes are represented in Fig. 2(c) and (d), respectively. As can be seen, increasing deposition time enlarged particle size and enhanced particle density. The AuNPs formed by potential-step electrodeposition, however, were less uniform and the particle size is between 100 and 150 nm in diameter. One of such electrodes was studied with a spectrophotometer and the spectrum is shown in Fig. 3(b). An absorption maximum was observed near 630 nm, indicating bigger AuNPs. The inset of Fig. 3(b) shows the photograph of the AuNP-ITO electrodes; blue instead of red color is observed.

For comparison, regular gold particle-electrodeposited ITO electrodes (Au-ITO) were prepared by electrodeposition at +0.2 V and their relevant SEM micrographs are shown in Fig. 3(e)–(h). Particles in micrometer-domain instead of nanoparticles were obtained based on the above processes. Moreover, increasing the electrodeposition time at this applied potential simply increased particle size rather than enhancing particle density.

3.2. Voltammetric behavior of Cr(VI)

The cyclic voltammograms of Cr(VI) were individually recorded at bulk gold, bare ITO, Au-ITO, and AuNP-ITO electrodes in the aqueous solutions containing 0.01 M NaCl, 0.01 M HCl, and 50 μM K_2CrO_4 (Fig. 4). This electrolyte composition was determined to be employed because higher stability and sensitivity were obtained.

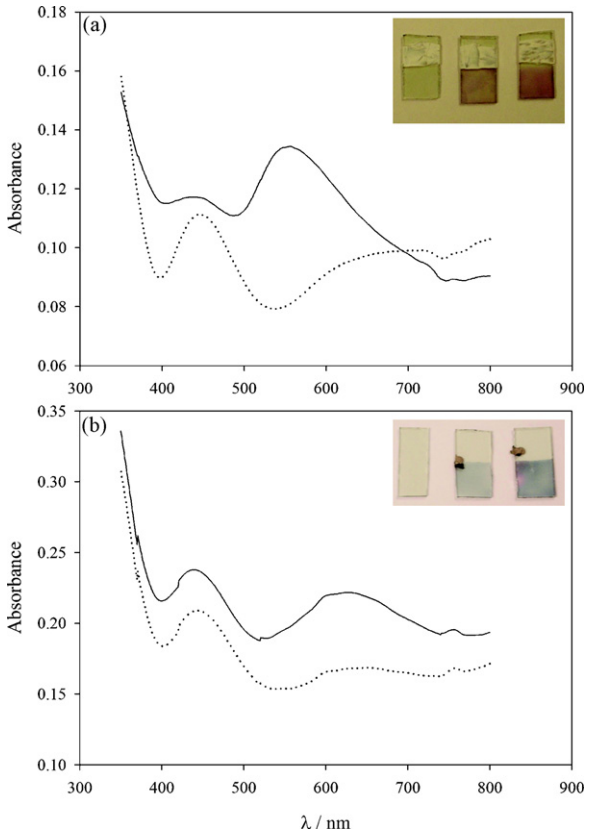

Fig. 3. The electron absorption spectra of (—) AuNP-ITO electrodes and (···) bare ITO electrodes, respectively. The AuNP-ITO electrodes were fabricated by (a) potential-sweeping electrodeposition or (b) potential-step electrodeposition. The photographs of the AuNP-ITO electrodes are shown in the insets.

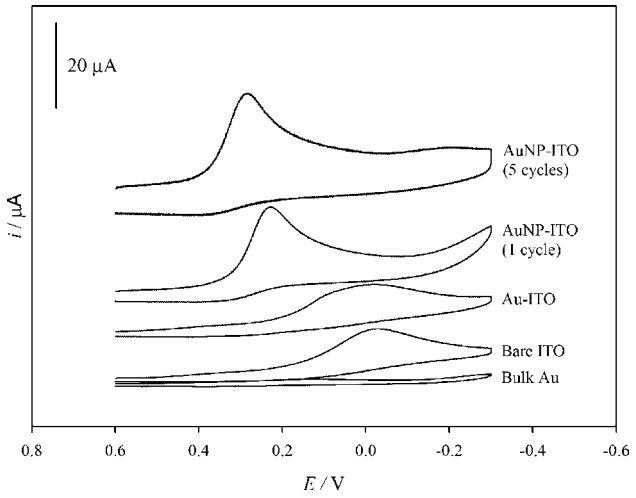

Fig. 4. Staircase cyclic voltammograms recorded at different electrodes that were indicated in the figure. The solution contained 50 μM Cr(VI), 0.01 M NaCl, and 0.01 M HCl. Scan rate: 100 mV/s. The numbers shown in the brackets indicate the number of potential cycle used for potential-sweeping electrodeposition.

Under various pH ranges, the dominant species of CrO_4^{2-} in solutions is different and $HCrO_4^-$ is the principal species [38] under the experimental condition in this study. Fig. 4 indicates that $HCrO_4^-$ can be reduced electrochemically regardless of the electrode material. The reduction current of Cr(VI) at the bulk gold electrode is very low because of its small conductive area. In order to compensate the effect of electrode area, current densities were compared and the bulk gold electrode still reveals worse performance than the AuNP-ITO electrodes. As can be seen in Fig. 4, the shape and position of the reduction wave of Cr(VI) at a Au-ITO were very similar to those recorded at a bare ITO regardless of the broader reduction wave occurring at the former electrode. Bulk gold electrode, however, reveals less extent of overpotential necessary for the reduction of Cr(VI) because the cathodic peak potential was observed at the more positive value (+0.2 V). This tendency was considerably enhanced when AuNP-ITO electrodes were employed. Moreover, the cathodic peak potential of Cr(VI) has a correlation with the processes used for forming the AuNP-ITO; for example, the cathodic peak potential occurred at the most positive position if the AuNP-ITO is fabricated by five cycles potential-sweeping electrodeposition. The AuNP-ITO reveals somehow an electrocatalytic

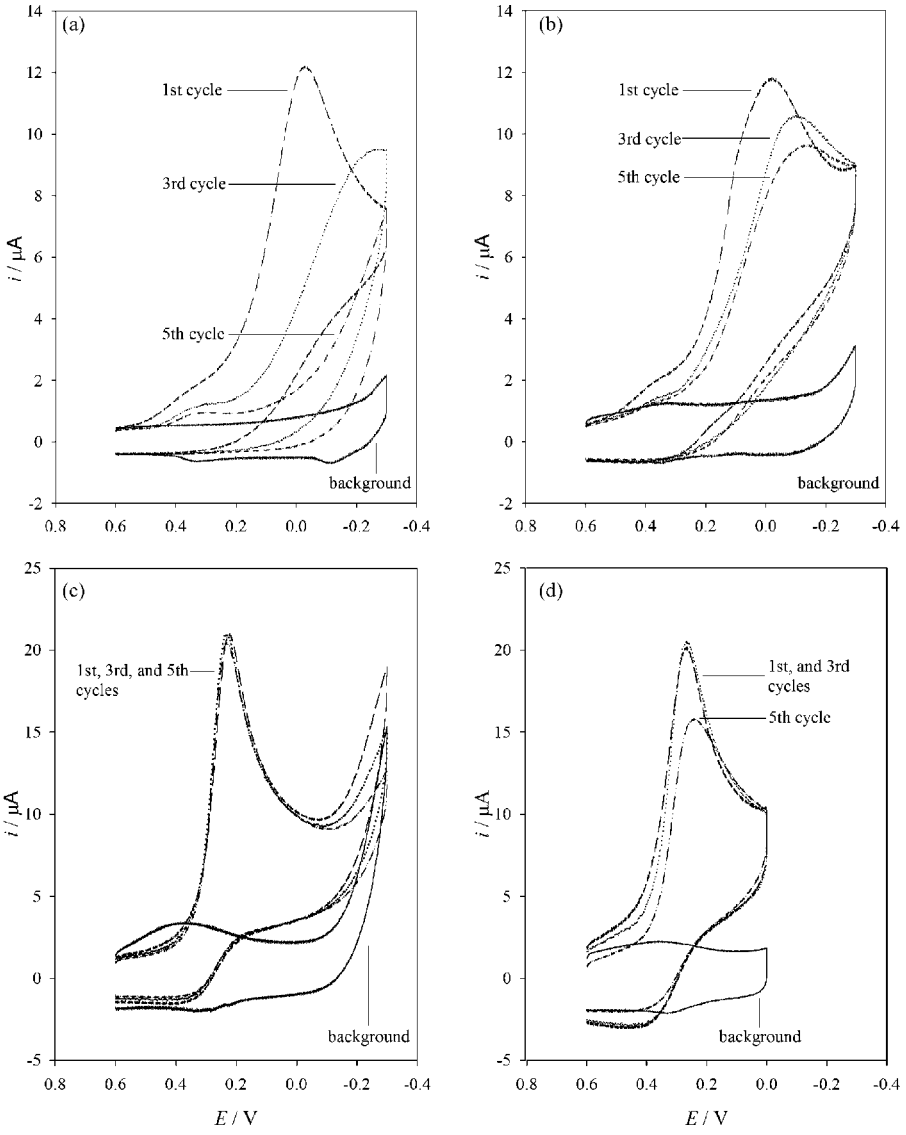

Fig. 5. Staircase cyclic voltammograms recorded at (a) bare ITO, (b) Au-ITO, (c) AuNP-ITO fabricated by potential-sweeping electrodeposition for five cycles, and (d) AuNP-ITO fabricated by potential-step electrodeposition for 30 s in 0.01 M NaCl solution containing 0.01 M HCl and 50 μM Cr(VI).

behavior toward the reduction of Cr(VI). Higher specific surface area exhibited by AuNP-ITOs may be one of the reasons; however, more experiments will be needed in order to investigate this behavior. At gold electrode, Cr(VI) is believed to be reduced to Cr(V) and the following homogeneous chemical reactions convert Cr(V) to Cr(III) [38]. The chemical reactions depend on the level of H^+ because proton transfer is involved in the reaction mechanism. In this study, the same reaction mechanism is supposed to occur at the AuNP-ITO electrodes; however, peak splitting that was discussed in the published paper [38] was not encountered in the solution used for this study. Additionally, the reduction wave of Cr(VI) that was observed at the AuNP-ITO electrodes occurred at the more positive potential (+0.3 V) than that (+0.2 V) at bulk Au electrode, implying a catalytic feature.

The AuNP-ITO electrodes exhibit not only higher sensitivity but better stability toward the reduction of Cr(VI). The first, third, and fifth cycle of the cyclic voltammograms recorded at a bare ITO electrode in the Cr(VI) solution are shown in Fig. 5(a). Between each cycle, the solution was stirred completely in order to restore the surface concentration of Cr(VI) to its bulk level. Obviously, the bare ITO electrode degraded seriously during the multiple potential scans, and the electrode was thoroughly passivated because the reduction current was no longer observed even after the electrode has been cleaned with a lot of deionized water or by soaking in acidic media. Degradation of performance was suppressed within a certain degree if the bare ITO is modified with regular gold particles formed by potential-step electrodeposition. The reduction current of Cr(VI), however, still decayed apparently with continuous scans (Fig. 5(b)). No degradation was observed at the AuNP-ITO electrodes fabricated by potential-sweeping electrodeposition (Fig. 5(c)); however, those prepared by potential-step electrodeposition still degraded at the fifth cycle (Fig. 5(d)). For the AuNP-ITO electrodes prepared by potential-sweeping electrodeposition, there was approximately no noticeable decrement of cathodic peak current of Cr(VI) among the successive 20 cycles (not shown here). Thus, the electrode stability is obviously related to the size and density of AuNPs. In this study, it has been found that bigger AuNPs would induce not only a negative shift of peak potential and a smaller peak current but also worse stability. This phenomenon has been reported [30] and the reason might be attributed to the blockage of electron communication between the solution species and electrode if the electrode surface is modified with enlarged AuNPs. The AuNP-ITO electrode shown in Fig. 5(c) demonstrates distinguished stability toward the reduction of Cr(VI), compared with the bare ITO, and Au-ITO electrodes. Based on this fact, the AuNP-ITO electrode fabricated by potential-sweeping electrodeposition should be more appropriate for electrochemical treatment of Cr(VI) wastewater or for Cr(VI) detection.

3.3. Calibration

The AuNP-ITO electrode mentioned in Fig. 5(c) was employed to detect Cr(VI) in acidic media by cyclic voltammetry and hydrodynamic amperometry, respectively. Both techniques were carried out in a batch-injection cell where the standard solutions or sample solutions were injected through the pinhole on the sidewall. The acidic media in which Cr(VI) was detected composed of 0.01 M NaCl and 0.01 M HCl. The acidic media stood steadily for cyclic voltammetry measurements; however, it was stirred firmly in order to obtain limiting current when amperometric measurements were carried out.

The upper inset of Fig. 6 illustrates the cyclic voltammograms recorded at a AuNP-ITO electrode in the acidic media containing 5, 10, 20, 50, and 100 μM of Cr(VI), respectively. The dependence of the cathodic peak current on the concentration of Cr(VI) was shown in Fig. 6. This calibration curve reveals linearity from 5 to

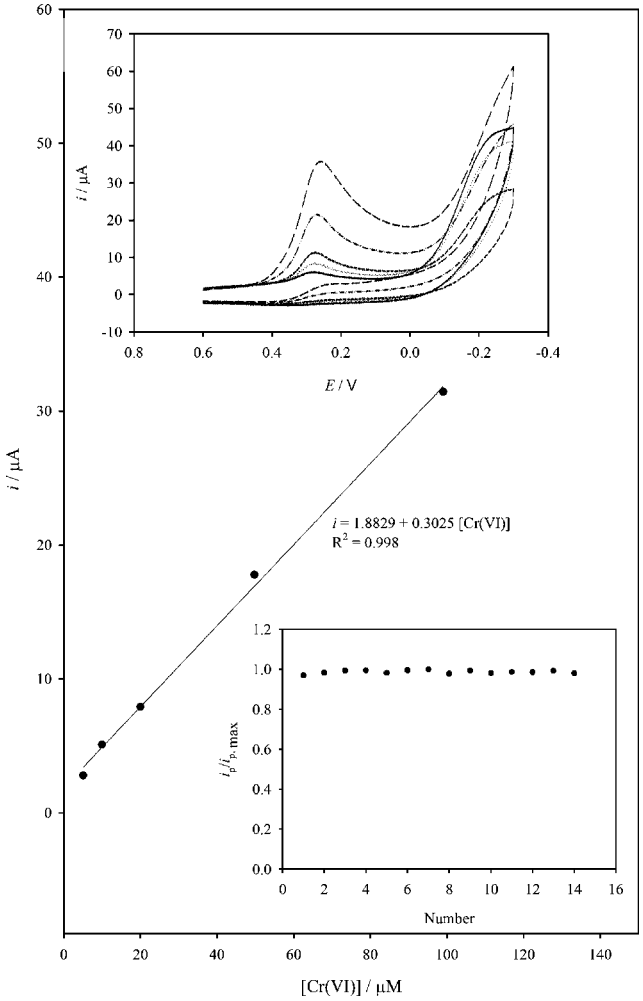

Fig. 6. The calibration curve of Cr(VI). It was established based on the peak current response taken from the cyclic voltammograms that are shown in the upper inset. The inset in the bottom shows the current ratios obtained from successive 14 detections of 50 μM Cr(VI).

100 μM with a slope of 0.3025 μA/μM and a regression coefficient of 0.998. The detection limit is 2 μM ($\sigma = 3$). In Fig. 6, it was also found that the cathodic peak potential of Cr(VI) shifted a little bit to negative direction with increasing the concentration of Cr(VI). The uncompensated resistance of the solution may cause this behavior because the reduction of Cr(VI) at gold electrode should proceed via a reversible one-electron and one-proton reaction to Cr(V), which disproportionates to Cr(IV) and Cr(VI) species [38]. The inset shown in the bottom of Fig. 6 represents the short-term stability of the AuNP-ITO, which was employed to detect 50 μM Cr(VI) for 14 times and the current ratios ($i_p/i_{p,max}$) fall in 0.97–1 and the relative standard deviation (R.S.D.) is about 0.8%, indicating good stability. A recovery test was performed in the same acidic media and the results were collected in Table 1.

Another electrochemical technique, amperometry, was also employed for detecting Cr(VI) in the acidic media. For amperometric measurements, a fixed potential of +0.2 V was applied at the AuNP-ITO electrode immersed in the firmly stirred solution. The standard solution of Cr(VI) was successively injected and a limiting current was obtained after each injection (the inset of Fig. 7). The value of the limiting current was employed to build the calibration curve that is shown in Fig. 7. The dependence of the limiting current on concentration of Cr(VI) is linear from 0.5 to 50 μM with a slope

Table 1
Determination of Cr(VI) in several water samples

	Deionized water		Tap water		Stream water		Sea water	
	CV[a]	HA[b]	CV	HA	CV	HA	CV	HA
Detected value, original (μM)	ND	ND	ND	ND	ND	ND	ND	ND
K_2CrO_4 added (μM)	29.9	2.5	29.9	2.5	29.9	2.5	29.9	2.5
K_2CrO_4 found after addition (μM)	32.2 ± 1.3[c]	2.5 ± 0.2[c]	30.0 ± 1.3[c]	2.7 ± 0.02[c]	29.8 ± 0.7[c]	2.5 ± 0.1[c]	28.9 ± 0.5[c]	3.2 ± 0.2[c]
Recovery (%)	107.7 ± 4.3	100 ± 8.0	100.1 ± 4.4	108 ± 0.9	99.6 ± 2.3	101.7 ± 1.8	96.5 ± 1.6	125.9 ± 7.7

[a] CV: cyclic voltammetry.
[b] HA: hydrodynamic amperometry.
[c] Three samples were assayed in order to obtain the standard deviation.

of 0.3553 μA/μM and a regression coefficient of 0.999. The detection limit is 0.1 μM ($\sigma = 3$). The limit of quantitation (LOQ) obtained by amperometry was much lower (0.5 μM) than that obtained by cyclic voltammetry (5 μM). A recovery test was also carried out by hydrodynamic amperometry and the results were collected in Table 1.

3.4. Determination of Cr(VI) in water samples

The analytical application of AuNP-ITO was demonstrated by employing it to determine the concentration of Cr(VI) in tap water, stream water, and sea water. No Cr(VI) can be detected in the original water samples. Therefore, a recovery test was performed by introducing known concentration of Cr(VI) into the water samples in order to verify the feasibility of this entire method. For each sample, two electrochemical techniques, cyclic voltammetry (CV) and hydrodynamic amperometry (HA), were employed to obtain the electrochemical signals. The experimental results are collected in Table 1 and the percentages of recovery higher than 95% were obtained. The recovery ratio obtained by hydrodynamic amperometry in sea water is somehow not good. A more serious fluctuation of current observed during the experiment might be one of the reasons. It must be emphasized that 0.01 M NaCl and 0.01 M HCl were introduced into each water sample except only 0.01 M HCl was dissolved in the samples of sea water.

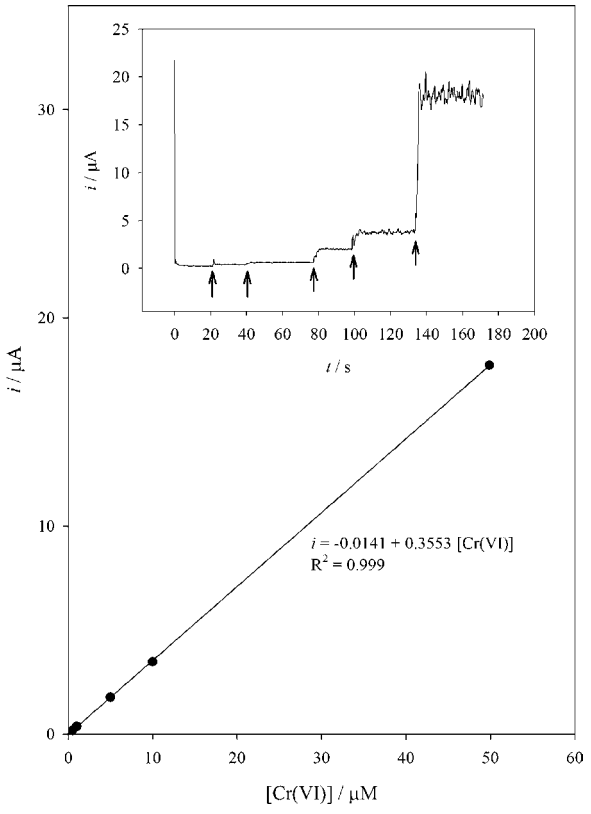

Fig. 7. The calibration curve of Cr(VI). It was established based on the limiting current response taken from the current transient that is shown in the inset.

4. Conclusion

AuNPs can be formed on ITO electrodes by potential-sweeping or potential-step electrodeposition in the Na_2SO_4 solution containing H_2SO_4 and $HAuCl_4 \cdot 3H_2O$. Compared with bare ITO electrodes, AuNP-ITO electrodes demonstrate electrocatalytic activity because the cathodic peak potential of Cr(VI) was observed at a more positive value when AuNP-ITO electrode was employed. Both the reduction current response of Cr(VI) and the stability of the AuNP-ITO electrodes depend on the size and the density of the electrodeposited AuNPs, respectively. In this study, it was found that potential-sweeping electrodeposition generates smaller AuNPs with higher distribution density on ITO surface. Such electrodes exhibit better sensitivity and stability. Although the results are not shown here, it was found that AuNPs can also be formed at glassy carbon electrodes by the identical procedures mentioned in this study. It implies that substrate may be not a crucial factor for AuNP electrodeposition and the proposed method may be a good way for fabricating disposable AuNP-modified electrodes that exhibit acceptable short-term stability. It is probably still a long way to improve the long-term stability for the present electrodes. By using simple template electrodeposition, a more rigid nanostructure and a long-term stability, however, may be obtained. Actually, the work is proceeding currently.

Acknowledgement

The important financial support provided from National Science Council of the Republic of China (Taiwan) was sincerely acknowledged (Grant number: NSC 96-2113-M-037-014-MY2).

References

[1] D. Golub, Y. Oren, J. Appl. Electrochem. 19 (1989) 311.
[2] R.J. Kieber, J.D. Willey, S.D. Zvalaren, Environ. Sci. Technol. 36 (2002) 5321.
[3] R.M. Cespon-Romero, M.C. Yebra-Biurrun, M.P. Bermejo-Barrera, Anal. Chim. Acta 327 (1996) 37.
[4] C.C. Sanders, Waste Manage. 16 (1996) 683.
[5] L.A.M. Ruotolo, A.A. Liao, J.C. Gubulin, J. Appl. Electrochem. 34 (2004) 1259.
[6] J. Guzman-Pantoja, J.G. Ibanez, R.C. Vasquez-Medrano, M.T. Oropeza-Guzman, Bull. Electrochem. 20 (2004) 107.
[7] L.A.M. Ruotolo, J.C. Gubulin, Chem. Eng. J. 110 (2005) 113.
[8] L.A.M. Ruotolo, D.S. Santos-Júnior, J.C. Gubulin, Water Res. 40 (2006) 1555.
[9] R. Senthurchelvan, Y. Wang, S. Basak, K. Rajeshwar, J. Electrochem. Soc. 143 (1996) 44.
[10] M.A. Alatorre, S. Gutiérrez, U. Páramo, J.G. Ibañez, J. Appl. Electrochem. 28 (1998) 551.
[11] A. Malinauskas, R. Holze, Ber. Bunsenges. Phys. Chem. 102 (1998) 982.
[12] A. Malinauskas, R. Holze, J. Appl. Pol. Sci. 73 (1999) 287.
[13] S.T. Crosmun, T.R. Mueller, Anal. Chim. Acta 75 (1975) 199.

[14] C. Harzdorf, G. Janser, Anal. Chim. Acta 165 (1984) 201.
[15] J.A. Cox, J.L. West, P.J. Kulesza, Analyst 109 (1984) 927.
[16] M. Boussemart, C.M.G. van den Berg, M. Ghaddaf, Anal. Chim. Acta 262 (1992) 103.
[17] M.A. Ghandour, S.A. El-Shatoury, A.M.M. Aly, S.M. Ahmed, Anal. Lett. 29 (1996) 1431.
[18] F.I. Danilov, V.S. Protsenko, Russ. J. Electrochem. 34 (1998) 276.
[19] L.D. Burke, P.F. Nugent, Electrochim. Acta 42 (1997) 399.
[20] S.B. Faldini, S.M.L. Agostinho, H.C. Chagas, J. Electroanal. Chem. 284 (1990) 173.
[21] J.A. Cox, P.J. Kulesza, M.A. Mbugwa, Anal. Chem. 54 (1982) 787.
[22] J.A. Cox, P.J. Kulesza, Anal. Chim. Acta 154 (1983) 71.
[23] H. Ge, J. Zhang, G.G. Wallace, Anal. Lett. 25 (1992) 429.
[24] I. Turyan, D. Mandler, Anal. Chem. 69 (1997) 894.
[25] F. Tian, V.I. Boiadjiev, L.A. Pinnaduwage, G.M. Brown, T. Thundat, J. Vac. Sci. Technol. A 23 (2005) 1022.
[26] L.P. Singh, J.M. Bhatnagar, S. Tanaka, H. Tsue, M. Mori, Anal. Chim. Acta 546 (2005) 199.
[27] E.W.L. Chan, L. Yu, Langmuir 18 (2002) 311.
[28] J. Zhong, Z. Qi, H. Dai, C. Fan, G. Li, N. Matsuda, Anal. Sci. 19 (2003) 653.
[29] M. Yang, Z. Zhang, Electrochim. Acta 49 (2004) 5089.
[30] N. Zhou, J. Wang, T. Chen, Z. Yu, G. Li, Anal. Chem. 78 (2006) 5227.
[31] M.D. Pérez, E. Otal, S.A. Bilmes, G.J.A.A. Soler-Illia, E.L. Crepaldi, D. Grosso, C. Sanchez, Langmuir 20 (2004) 6879.
[32] J.-M. Moon, A. Wei, J. Phys. Chem. B 109 (2005) 23336.
[33] L. Yang, Q. Cai, Y. Yu, Inorg. Chem. 45 (2006) 9616.
[34] B.G. McMillan, L.E.A. Berlouis, F.R. Cruickshank, P.F. Brevet, J. Electroanal. Chem. 599 (2007) 177.
[35] M.S. El-Deab, T. Ohsaka, Electrochem. Commun. 4 (2002) 288.
[36] M.S. El-Deab, T. Okajima, T. Ohsaka, J. Electrochem. Soc. 150 (2003) A851.
[37] W. Plieth, H. Dietz, A. Anders, G. Sandmann, A. Meixner, M. Weber, H. Kneppe, Surf. Sci. 597 (2005) 119.
[38] C.M. Welch, O. Nekrassova, R.G. Compton, Talanta 65 (2005) 74.

Talanta 76 (2008) 635–641

Contents lists available at ScienceDirect

Talanta

journal homepage: www.elsevier.com/locate/talanta

On the re-assessment of the optimum conditions for the determination of platinum, palladium and rhodium in environmental samples by electrothermal atomic absorption spectrometry and microwave digestion

George Z. Tsogas, Dimosthenis L. Giokas*, Athanasios G. Vlessidis, Nicholaos P. Evmiridis

Laboratory of Analytical Chemistry, Department of Chemistry, University of Ioannina, 45110, Greece

ARTICLE INFO

Article history:
Received 23 November 2007
Received in revised form 2 April 2008
Accepted 7 April 2008
Available online 16 April 2008

Keywords:
Environmental samples
Certified materials
GFAAS
Microwave extraction
Platinum-group elements

ABSTRACT

The experimental conditions for the determination of platinum, palladium and rhodium by graphite furnace atomic absorption spectrometry (GFAAS) are re-assessed. A certified material (BCR-723) was used as a working sample and analyzed using various extraction and atomization procedures in order to find the optimal experimental conditions that enable the quantitative and reproducible detection of platinum, palladium and rhodium in environmental matrices. Evidently, literature observations regarding the atomization conditions were proven fairly adequate. However, the provision of the optimum extraction conditions revealed several parameters that lie behind the reported uncertainties. The appropriate combination between extraction conditions and atomization programs afforded a considerable improvement in the recoveries and analytical features of platinum, palladium and rhodium determination with GFAAS. Cross-examination of the analytical data with various CRMs (certified reference materials) was used to validate the robustness of the method in heterogeneous matrices bearing different element levels. Under the optimum experimental conditions the method permits the determination at concentrations as low as ($LOD_{3S/N}$) 1.9 ng g^{-1}, 0.45 ng g^{-1} and 0.6 ng g^{-1} for Pt, Pd and Rh, respectively affording recoveries in the range of 93–101%. The method was successfully applied to the assessment of Pt, Pd and Rh accumulation in real road dust and soil samples in Greece.

1. Introduction

Since the introduction of catalytic converters in modern automobiles, the determination of platinum-group elements (PGE), mainly platinum, rhodium and palladium, has received increasing attention due to their release into the environment and their cytotoxic and allergic properties [1–3]. Although numerous research studies have been carried out ever since, on developing reliable analytical methods for accurate determinations of traces of PGEs in different materials, their reliable determination is still a difficult task due to their particular properties (low reactivity towards single chemical reagents, great chemical similarities, numerous oxidation states, formation of polynuclear complexes, etc.), their extremely low environmental concentrations and the significant interaction with sample matrix components.

The most crucial step in the analysis of PGEs is the selection of the appropriate analytical technique [4]. Most sensitive analytical techniques, such as graphite furnace atomic absorption spectrometry (GFAAS) [5–9], instrumental neutron activation analysis (INAA) [10], adsorptive stripping voltammetry (ASV) [11], inductively coupled plasma-atomic emission spectrometry (ICP-AES) [12] and inductively coupled plasma-mass spectrometry (ICP-MS) [13–18] have been used for that purpose. For many years, GFAAS has been a popular method for the determination of PGEs but the very low detection limits and the multielement capability of ICP-MS have made it the most popular technique in the environmental monitoring of PGEs at the ng l^{-1} levels [4,19]. However, despite the advantages of ICP-MS, the accurate determination of PGEs at trace levels is not a facile undertaking due to many interferences from abundant matrix constituents and gases used during the atomization process forming oxides, and polyatomic and double charged ions like HfO^+, SrO^+, RbO^+, $ArCu^+$, $ArZn^+$, Cd^{+2}, Pb^{+2}, etc. [4,15,16,20,21]. Mathematical correction, based on the evaluation of the contribution of interferent signal in that one for analyte, was successfully applied for the elimination of spectral interferences occurring during the determination of Pt [15,16,22], but was proven to be inefficient for Pd and in some cases for Rh [15,16,23]. Hence, in order to obtain accurate results chemical separation of Pt and Pd from the sample matrix has been deployed involving

* Corresponding author. Tel.: +30 26510 98400; fax: +30 26510 98781.
E-mail address: dgiokas@cc.uoi.gr (D.L. Giokas).

0039-9140/$ – see front matter © 2008 Published by Elsevier B.V.
doi:10.1016/j.talanta.2008.04.007

various procedures like solid phase extraction based on adsorption [24], ion-exchange [25,26] chelation onto solid sorbents [27], etc. As a result, the pre-concentration step usually required to bring the detection limits within the dynamic measuring range of the GFAAS detector has not been overcome. Furthermore, all methods employed for the pre-concentration of PGEs, do not enable their selective isolation and other elements may be retained simultaneously which reiterates the problem of interferences either due to competition with PGEs for the available reactive (or chelation) sites or due to spectral interferences during the detection step, as previously discussed [12,28].

In the majority of methods published hitherto, emphasis is being given to the removal of interferences mainly through the optimization of the atomization conditions and less frequently to the optimization of the extraction procedure. Although microwave assisted extraction (MAE) has been the most popular digestion procedure for the dissolution of PGEs [4,13,14], there is a severe literature fragmentation regarding the optimum extraction conditions possibly due to the different detector set-up, the large matrix heterogeneity and the methods used to overcome the interferences. In most occasions where detector optimization or mathematical correction is employed, optimization of the extraction conditions is disregarded and vise versa. As a consequence, various extraction conditions have been reported as optimum although similar acid digestion mixtures have been used (and vise versa) [13,14,15,26,29,30]. Another source of error is the use of model solutions or site-specific real samples in order to optimize the experimental protocol which is then validated and corrected against a certified reference material (CRM) [14,29]. Although BCR-723 (road dust, Institute of Reference Materials and Measurements,) has brought a significant reduction in the uncertainty surrounding the representativity of certified materials, this validation procedure still does not ensure the robustness of the results because of error propagation induced by matrix heterogeneity among samples (sample vs. sample, sample vs. CRM, etc.).

Motivated by a monitoring campaign for the assessment of pollution state of Ioannina city (NW, Greece) from PGEs, an analytical optimization study was set forth. At the beginning of this investigation, various analytical methods involving microwave digestion and electrothermal atomic absorption spectrometry were examined for the extraction and determination of the most important PGEs emitted from catalytic converters abrasion, that are platinum, palladium and rhodium. Evidently, preliminary results suffered from poor repeatability, moderate recoveries and high background signals attributed to unknown sources. To cope with these problems, a re-examination of all factors that may influence the extraction and detection procedure was decided. In order to ensure the robustness of the analytical results, a certified material was used as a working sample. BCR-723 (road dust) was selected for that purpose since it has been an integral component of quality control/quality assurance procedures in most environmental laboratories measuring PGEs and its values have been verified through numerous studies [31]. The results suggest that factors related to atomization and detection conditions are well-established and may provide an accurate estimate of platinum, palladium and rhodium in environmental matrices and at the ng l^{-1} levels. However, the extraction conditions were found to significantly affect the analytical results re-defining the optimum extraction and digestion conditions and shedding some more light on the reasons behind the reported uncertainities in the determination of platinum, palladium and rhodium in environmental samples. Cross-examination of the method's efficiency using various certified materials was used to validate the universal applicability of the method to heterogeneous matrices prior to its application in real samples. Some initial conclusions from the first monitoring survey of platinum, palladium and rhodium in roadside soils and dust samples in Greece (Ioannina city, NW Greece) are also provided.

2. Experimental

2.1. Reagents and materials

All reagents were of analytical grade and free from PGEs traces. Stock solutions of 1000 mg l^{-1} of Pt, Pd and Rh were prepared by dissolving appropriate amounts of K_2PtCl_4 (Fluka, 99.99%), $Pd(NO_3)_2$ (Aldrich, >99.9%) and $RhCl_3{\cdot}3H_2O$ (Sigma, >99.9%) in doubly distilled water acidified with 1 M HCl and stored for no longer than 3 weeks in thoroughly cleaned quart vessels [2] at 4 °C, protected from light. Working standards were prepared daily by appropriate dilution. For the decomposition of the samples concentrated, HNO_3 (65%, Merck, analytical grade), HCl (30%, Merck, analytical grade) and HF (40%, Merck, analytical grade), were used.

The certified reference material BCR-723 (road dust, Institute of Reference Materials and Measurements, EU Joint Research Center, Geely, Belgium) was used for method development. The CRMs, UMT-1 (mill tailings from the nickel–copper mines, Canadian Certified Reference Materials Project, CANMET-MMSL, Ontatio, Canada) and Jsd-2 (stream sediment, Geological Survey of Japan, Geochemical References Samples, Tsukuba, Ibaraki, Japan) were used to evaluate the efficiency of the method.

2.2. Instrumentation

A microwave oven, equipped with a 6-sample tray with power feedback/controls was used for the extraction of PGEs from the solid matrices. Savillex (France) screw top Teflon bombs were used throughout the experiments following the safety precautions of the manufacturer. A Shimandzu AA-6800 atomic absorption spectrophotometer with hollow cathode lamps operating at 10 mA, 14 mA and 12 mA for Pd, Pt and Rh, respectively were used throughout measurements which were made at 247.6 nm, 266.0 nm and 343.5 nm, respectively with dual background correction D_2. Electrothermal atomization was performed with a Shimadzu GFA-6500 longitudinally heated graphite atomizer, using pyrolytic-coated graphite tubes. The output signals were collected and processed in continuous peak height mode [32]. Prior to each measurement, the instrument was calibrated with standard solutions using the external calibration curve method, according to the instructions of the manufacturer. The calibration curve was linear from 0–100 ng g^{-1}, 0–20 ng g^{-1} and 0–16 ng g^{-1} for Pt, Pd and Rh respectively.

2.3. Samples

Six sampling sites from the city of Ioannina (NW Greece) were selected in relation to traffic intensity, diurnal traffic variation, and driving styles and identified to represent a cross-section of traffic volumes. Site 1 is located near traffic lights on the most heavily used route intersecting the city center. Site 2 is located near traffic lights in a main motorway with maximum traffic burden during the day. Site 3 is located in a local road near the city Lake. Although no traffic lights exist, it is the most popular road during the night with many parking sites and continues stop/start cycles due to the high traffic density. In this road, the traffic reaches a peak during the night, whereas during the day the traffic is sparse. Site 4 is located in the central highway which is a major route into and out of the city. Site 5 (University drive) is located in a popular roadway parallel to the central highway. The last sampling site (site 6) is located just after the nearest tollbooths. For procedural blanks, samples were also collected from a non-populated forest area 50 km away from the city.

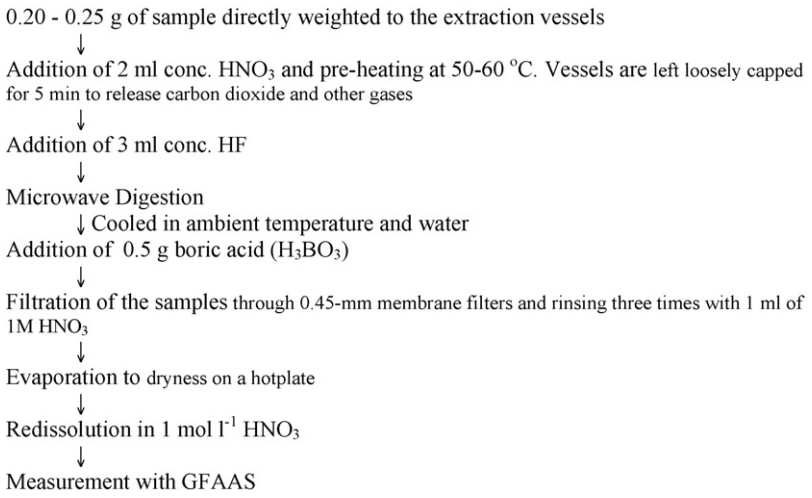

Fig. 1. Experimental procedure for the determination of PGEs.

Soil samples were collected by scraping up the superficial soil (0–5 cm depth) with an acid-washed plastic (HDPE) trowel while road dust was hand-brushed with disposable plastic brushes along the kerbstones. All samples were placed in plastic sample bags for transportation to the laboratory. The samples were dried at 40 °C in a vacuum drying oven (Vacucell, MMM Medcenter Einrichtungen, GmbH), homogenized, sieved into 2 mm, 2 mm–63 μm and 63 μm fractions and stored at room temperature in sealed secure polypropylene (PP) containers to avoid contamination. All analysis was performed to the silt (<63 μm) fraction which was grounded to highly homogeneous finepowder with an agate polytetrafluoroethylene (PTFE) ball mill. For homogeneity reasons all certified materials (BCR-723, UMT-1 and Jsd-2) were exposed to the same pre-treatment procedure before analysis.

2.4. Procedure

The procedure for the determination of PGEs in road dust, soil and CRM samples is depicted in Fig. 1. Approximately 200 mg of sample weight was used throughout the experimental work in order to reduce imprecision due to the nugget effect [31]. The final extract (1 ml) consists of an aquatic solution of 1 mol l^{-1} HNO_3 and is used to re-dissolve the concentrated PGEs. All samples were delivered to the auto-sampler (Shimadzu ASC-6100) of GFAAS and analyzed at least three times (confidence level 95%).

Blank samples were prepared using the analytical procedure of Fig. 1 without the addition of sample.

3. Results and discussion

3.1. Effect of acid type and concentration

Three acids (HCl, HNO_3 and HF) were selected in this study due to their frequency of application in the extraction of PGEs. Addition of HF was adopted irrespectively of the initial acid igestion mixture due to its distinct role in the decomposition of silicates that are insoluble in other acids.

Aqua regia is one of the most frequently applied acid mixtures for matrix decomposition. However, the data depicted in Fig. 2a indicate that moderate recoveries were attained for all PGEs (<80%) in BCR-723 irrespectively of *aqua regia* concentration. This came as no surprise, especially for Pt, were signal depression has been reported both in the presence of *aqua regia* [4], and HCl [20]. For Pd on the other hand, although recoveries were slightly better they

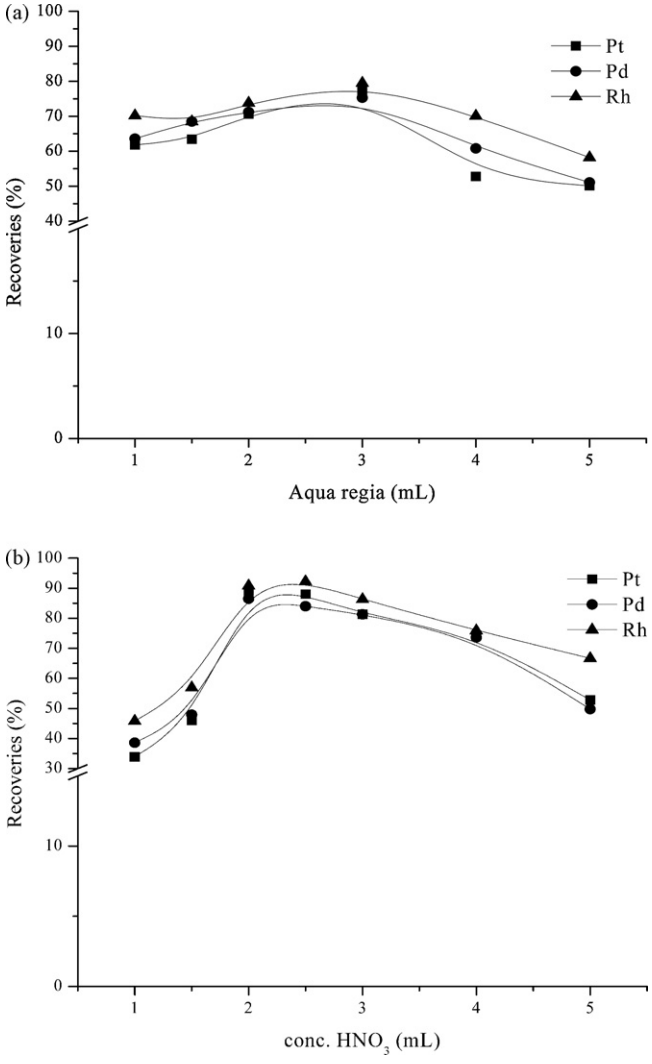

Fig. 2. Effect of the acid type and concentration on the recovery of Pt, Pd and Rh from BCR-723.

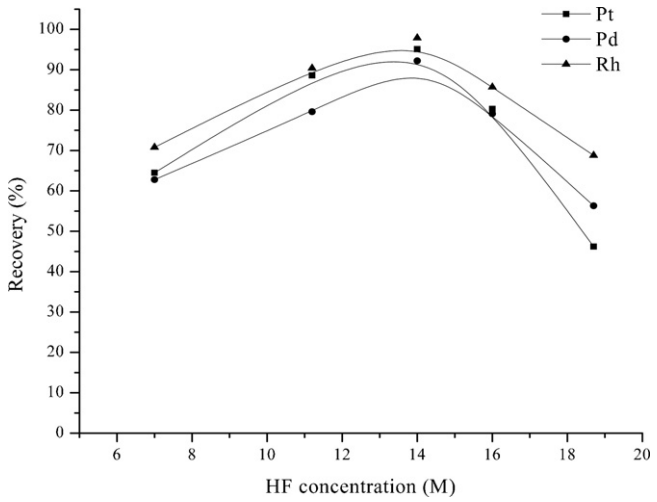

Fig. 3. Effect of hydrofluoric acid concentration on the recovery of Pt, Pd and Rh from BCR-723.

were still inefficient for trace analysis. Considering previous studies that observed an increase in Pd signal by HCl, as a function of acid concentration [20], the measured recoveries of Pd are rather controversial.

With the above observations in mind, the potential influence of each acid in the recovery of the target metal species was examined using various mixtures of HCl and HNO_3. Evidently, decreasing HCl concentration improved analyte's recoveries as a function of HNO_3 concentration. The reason for this change of sensitivity in the presence of HCl probably lies with the intense formation of analyte chlorides and spectral and/or vapour-phase interferences (formation of a metal chlorocomplex in the gas phase, occlusion of the target element in the matrix, etc.) [33–35].

Based on the above observations, HCl was omitted from the extraction mixture and the effect of HNO_3 was separately investigated. The use of HNO_3 brought about a reduction in the background adsorption signal and improved precision (about 2–5% depending on the target element) which resulted in improved recoveries (Fig. 2) and up to 90% with almost half HNO_3 volume (compared to the respective volume of *aqua regia* needed to obtain maximum recovery).

Despite this improvement, HNO_3 was not able to promote complete recovery of PGEs from the sample matrix. This can be attributed to the inadequate mineralization of the sample matrix because HNO_3 cannot decompose silicates that may carry a small metal burden or interfere with the analysis. The concentration of HF was therefore the next parameter studied for its effect on the recovery of PGEs. To avoid losses, especially of Pt and Pd during the evaporation step, and promote the dissolution of sparingly soluble fluorides [36] boric acid was added to mask fluoride ions as tetrafluoroborate (Fig. 1). The HF concentration profile depicted in Fig. 3 reveals that at the optimum value of 14 mol l^{-1} the recoveries of all PGEs are improved. Lower concentrations yielded reduced recoveries especially for Pt and Pd (~60%) probably due to Pt signal suppression by Si and occlusion of Pd to silicate matrices [37,38].

Examination of the optimum boric acid concentration shows maximum recovery at 0.6 g 5 ml^{-1} digestion mixture. This concentration is adequate to mask fluoride ions as tetrafluoroborate as well as deter the stepwise hydrolysis of tetrafluoroborate to hydroxofluoroborates and the re-formation of hydrofluoric acid. Under the optimum HF and boric acid concentrations the recoveries of PGEs were 93.1 ± 5.3% for Pt, 92.2 ± 6.6% for Pd and 94.0 ± 6.4% for Rh.

Table 1
Microwave digestion program for the extraction of PGEs from environmental samples

Time (min)	Power (W)
5	270
1	0
4	450
2	0
2	630
5	0
4	450

3.2. Effect of the microwave digestion conditions

Before exposing the samples to microwave irradiation they were pre-heated with HNO_3 in order to release carbon dioxide and other gases. Subsequently, HF was added and the mixture was heated in a microwave oven for various time intervals and different power settings to establish the conditions that promote the most effective dissolution. Based on literature data, irradiation times were examined in the range of 1–12 min at power settings of 270–900 W while interim cooling times (in ambient air) were tested in the range of 1–5 min. Twelve program combinations were tested for each of the target elements. The observed recoveries were ranging from 82.9–97.6% for Pt, 76.3–94.8% for Pd and 80.7–96.1% for Rh. The final program that maximizes analyte recoveries in shown in Table 1. In the first step power is held at 270 W for 5 min to assist the mineralization of the remaining organic components. In step 2 lower amounts of gaseous reaction products are formed and therefore, the resulting pressure increases gradually with the rise in temperature. The energy input is preceded more steeply and a higher maximum power step is performed. A final step involving sample exposure to 450 W was applied to ensure complete decomposition. Since no pressure sensor was installed in our system, between each step, the vessels were cooled in ambient air in order to avoid over-pressure that could endanger vessels venting. At the end of the digestion procedure the vessels were cooled prior to opening and subsequent treatment. The final recoveries accomplished under the optimum dissolution conditions were 97.6 ± 4.7% for Pt, 94.8 ± 6.4% for Pd and 96.1 ± 5.8% for Rh.

3.3. Pre-concentration procedure

Due to the low abundance of PGEs in many environmental samples at concentrations ranging from ng g^{-1} to low μg g^{-1} levels, direct determination with GFAAS is not always feasible necessitating sample pre-concentration in order to increase sensitivity.

Following microwave digestion the samples were filtered through 0.45-μm membrane filters to remove the dark brown organic residue. This residue can be attributed either to incomplete oxidation of recalcitrant organic compounds that cannot be decomposed by the acid mixture but do not contain significant amounts of metals and do not interfere with subsequent metal determinations [39] or to NO_2^- ions [40] or even both. Although this residue does not contain any significant amounts of metals, it was decided to rinse the residue with dilute HNO_3 (1 M) in order to ensure quantitative elution of platinum, palladium and rhodium and avoid analyte loss on the filter or on the glassware surface, an observation concurrent with previous studies regarding the interaction of PGE solutions with laboratory vessels [41]. The combined filtrates were then placed into flatbed pyrex plates and evaporated on a hotplate at 80 °C, for 1 h, until dryness. The dried residue was re-dissolved in different inorganic (HNO_3, H_2SO_4, HCl) and organic solvents (methanol, ethanol) and mixtures of them in different proportions. The results suggest that nitric acid was the most efficient

Table 2
Average recoveries (%) of Pt, Pd and Rh with various dissolution solvents

Concentration (M)[a]	Solvent				
	HNO_3	H_2SO_4	MeOH	MeOH/HNO_3[b]	EtOH
0.2	82.5	66.4	45.6	70.6	48.8
0.5	88.3	69.8	67.4	74.3	70.6
1.0	94.6	70.4	59.6	80.6	79.1
2.0	86.4	74.5	63.8	75.9	69.9
4.0	70.1	45.6	40.1	58.0	58.2

[a] Final volume 1 ml. MeOH, methanol; EtOH, ethanol.
[b] Concentration of HNO_3 in pure methanol.

Table 3
Experimental conditions employed for the optimization of GFAAS

		Temperature (°C)	Time (s)
Drying	Ramp	120–150	20
Ashing	Ramp	250	15–50
Ashing	Ramp	600	10
Ashing	Step	600–1000	10–20
Ashing	Step	1300–1600	3–5
Atomization	Step	2200–2700	3
Cleaning	Step	2600–2800	3

dissolution agent (Table 2). Of the three elements, Pd was the most crucial factor in this investigation since lower HNO_3 concentrations led to relatively moderate recoveries possibly due to the formation of polycondensated Pd products while a similar trend was observed at concentrations above 1 mol l^{-1} possibly due to the formation of insoluble $Pd(OH)_2$ precipitates [42]. To accomplish maximum pre-concentration and quantitative recovery of all species, 1 ml of 1 mol l^{-1} HNO_3 was selected.

3.4. Optimization of atomization conditions

The instrumental conditions examined for their effect on the analytical signal of PGEs are summarized in Table 3 and the optimum conditions decided are gathered in Table 4. In contrast to pure aqueous solutions, increased pyroslsis temperatures were necessary for Pt and Pd in order to reach acceptable recoveries (>90%). This was attributed to the fact that the BCR-723 used for optimization contains various metallic ions beyond the target elements [43] that affect the analytical signal. Pb line at 247.638 nm causes background overcorrection when measuring Pd 247.642 nm while the same phenomenon occurs for Pt (265.945-nm) due to the near neighboring Al line at 266.039 nm [27,44]. In the case of Pd the presence of iron which has a stabilizing effect on Pb, necessitates the increase of pyrolysis temperature to secure full removal of Pb before the atomization step [44]. For Pt, both increased pyrolysis and atomization temperature were necessary in order to accomplish acceptable recoveries and repeatability and eliminate possible interferences from concomitant elements. For Rh, several transition metals (some of which present in BCR-723 like Cu and Fe), have also been reported to interfere with the GFAAS determination of Rh to a very diverse extent [45]. However, investigation of Rh recovery under variable pyrolysis and atomization temperatures showed no significant improvement compared to the initial program proposed by the manufacturer.

Table 5
Analytical features of the method for the determination of platinum, palladium and rhodium in environmental samples

	Pt	Pd	Rh
Linear range (ng g^{-1})	0–100	0–20	0–16
Linearity (R^2)	0.9998	0.9995	0.9996
LOD (ng g^{-1}, 3S/N)	1.90	0.45	0.60
LOQ (ng g^{-1}, 10S/N)	6.40	1.50	2.00
Precision, % (n = 5)	5.52	14.90	9.67
Accuracy (%) (n = 5)	−4.58	−5.31	−2.46
Reproducibility (%)[a]	12.6 ± 4.0	11.1 ± 3.2	11.8 ± 3.9
Error variance (variability within samples)	3.048	0.015	0.114
Recoveries ± S.D.	95.6 ± 4.5	94.4 ± 5.5	97.3 ± 4.8

[a] Average values ± S.D. (standard deviation) from the analysis of BCR-723 (n = 35) in 3 months.

3.5. Analytical features and method validation

The analytical characteristics of the proposed experimental protocol are gathered in Table 5. As can be seen, good linearity was achieved yielding detection limits at the low ng g^{-1} levels which are fairly adequate for the determination of PGEs in real samples. The precision of the method, was checked by means of repeated assays (n = 5) of BCR-723, and the coefficients of variation were calculated between 5.52% and 14.8% which is satisfactory and statistically equivalent with previous studies using BCR-723 [31]. Furthermore, the method affords good day-to-day repeatability (about 12%) as evidenced by sequential analysis of BCR-723 (n = 35) in a total period of 3 months.

Despite the fact that the use of a certified material for the investigation of the optimum extraction and measurement conditions could reduce analytical errors and improve analyte recoveries, it could not ensure the universal applicability of the method to real samples. That is because the nature of CRMs along with their PGE levels differ from that found in various environmental compartments (e.g. road dust, airborne particulate matter, etc.). This induces a certain degree of uncertainty which may lead to biased results when they are used as reference for the quality control of environmental samples. To validate the applicability of the method to various sample matrices two more certified materials were analyzed for their content in PGEs under the optimum experimental conditions established above. UMT-1 and Jsd-2 were selected for that purpose due to the different matrix composition and levels of PGEs compared to BCR-723.

The results gathered in Table 6 present PGEs recoveries from the analysis of various certified reference materials. Uncorrected recoveries were in range of 92.6–98.2% while the corrected recoveries were further improved ranging from 98.0–101.4%, depending

Table 4
Optimum furnace programs for the determination of PGEs

		Temperature (°C)	Time (s)	Temperature (°C)	Time (s)	Temperature (°C)	Time (s)
		Pt		Pd		Rh	
Drying	Ramp	120	20	150	20	120	20
Ashing	Ramp	250	30	250	20	250	10
Ashing	Ramp	600	10	1200	10	600	10
Ashing	Step	600	15	1200	10	600	3
Ashing	Step	1600	3	1200	3	2500	3
Atomization	Step	2600	3	2700	3	2500	3
Cleaning	Step	2600	3	2800	3		

Table 6
Evaluation of the method with various certified materials and cross-examination of analyte recoveries

Certified material	Element	Certified value (ng g^{-1})	Found (ng g^{-1})	Recovery (%)	Correction factor	Corrected values for BCR-723 (ng g^{-1})[a]	Corrected values for UMT-1 (ng g^{-1})[a]	Corrected values for Jsd-2 (ng g^{-1})[a]
	Pt	81.3 ± 2.45	77.8 ± 3.3	95.7	1.045	–	81.5 (100.3)	81.5 (100.3)
BCR-723	Pd	6.0 ± 1.83	5.65 ± 0.6	94.2	1.062	–	6.07 (101.2)	6.0 (100)
	Rh	12.8 ± 1.22	12.4 ± 0.8	96.8	1.032	–	12.6 (98.6)	–
	Pt	129.0 ± 5.0	123 ± 5.4	95.3	1.048	128.30 (99.4)	–	129 (100.0)
UMT-1	Pd	106.0 ± 3.0	98.2 ± 5.0	92.6	1.079	103.9 (98.0)	–	104.1 (98.2)
	Rh	9.50 ± 1.1	9.33 ± 0.9	98.2	1.018	9.61 (101.2)	–	–
	Pt	16.70 ± n.a.	15.90 ± 1.1	95.2	1.050	16.58 (99.3)	16.6 (99.4)	–
Jsd-2[b]	Pd	21.20 ± n.a.	20.0 ± 1.5	94.0	1.060	21.16 (99.8)	21.5 (101.4)	–

[a] Values in parenthesis indicate (%) recoveries. Correction factor = certified concentration/measured concentration.
[b] Provisional values, n.a.: not available.

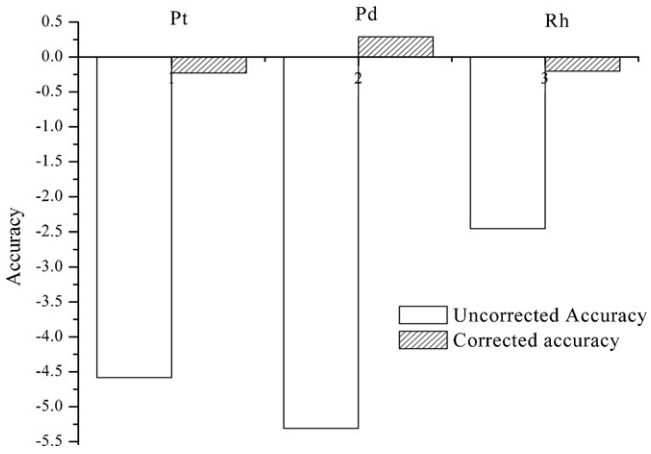

Fig. 4. Bar-plots of platinum-group element accuracy from the analysis of three CRMs.

on the certified material used for correction, suggesting quantitative determination of PGEs. The mean correction factors (CF) required to obtain a quantitative accurate result were (mean ± S.D.) 1.047 ± 0.003 for Pt, 1.067 ± 0.01 for Pd and 1.025 ± 0.01 for Rh which is in agreement with our previous observations suggesting higher CF for Pd and lower for Rh. This indicates that recoveries decrease according to the order Pd < Pt < Rh. This is in concurrent with the results obtained with BCR-723 (Table 5). *T*-test analysis to the data suggests that there are statistically significant differences in the mean recoveries of Pt and Pd among the corrected and the uncorrected values ($t_{Pt} = 11.3$; $t_{Pd} = 6.23 > t_{(0.05,25)} = 2.060$) while no difference was detected for Rh ($t_{Rh} = 1.62 < t_{(0.05,25)} = 2.060$). On the other hand, no differences among the mean corrected recoveries were detected for all PGEs suggesting that all three CRMs produce statistically equivalent results.

With regards to accuracy, both the uncorrected and corrected accuracy values were not biased, as the non-parametric sign test indicated that there were no statistically significant differences from zero. The bar-plots of Fig. 4 indicate a considerable improvement in the accuracy of the corrected values emphasising the need for a CRM to improve the quality of the analytical results.

3.6. Measurement of road dust and soil samples

Six road dust and soil samples were taken from the city of Ioannina, Greece and were assessed for their content in platinum, palladium and rhodium. For evaluation reasons the data were corrected with the available CRMs and analyzed for equivalency of means with the aid of *t*-test analysis. In concurrence with our previous findings no statistically significant differences were observed for all corrected data although some differences were detected between the corrected and the uncorrected values.

The data gathered in Table 7 show that the levels of PGEs were significantly higher than those usually found in upper crust suggesting non-natural inputs [46]. High concentrations were observed in high density roads were high speed and catalyst temperatures enhance attrition and emission of PGEs (sites 4 and 5). Sites exposed to stop/start cycles generally tend to accumulate more PGEs, but the levels are not only determined by the driving conditions but also from the diurnal variation of the traffic volume. In the city center (site 1) and in the toll road (site 6) higher concentrations were observed compared to the motorway (site 2), despite the fact that the converters have previously reached maximum temperature (before the traffic lights) due to the fact in site 2 that traffic is significantly reduced during the night. A contradictory

Table 7
Determination of PGEs in road dust and soil samples from Ioannina city (NW Greece)[a]

Sampling site	Road dust			Soil		
	Pt	Pd	Rh	Pt	Pd	Rh
1	87.2 ± 2.0	7.0 ± 0.3	12.7 ± 0.6	53.7 ± 2.6	5.5 ± 0.5	10.8 ± 1.0
2	77.4 ± 2.1	13.7 ± 1.8	19.7 ± 0.3	46.8 ± 1.8	7.3 ± 0.8	15.0 ± 0.9
3	74.1 ± 4.1	6.6 ± 0.3	31.3 ± 0.7	109.4 ± 6.0	3.8 ± 0.4	11.7 ± 1.3
4	69.3 ± 1.9	8.9 ± 0.6	29.1 ± 1.7	79.8 ± 3.9	6.2 ± 0.2	13.4 ± 0.8
5	131.6 ± 5.1	8.8 ± 0.5	42.8 ± 8.6	113.2 ± 5.8	6.3 ± 0.3	15.8 ± 1.3
6	119.2 ± 6.3	8.5 ± 0.3	13.4 ± 0.2	83.7 ± 5.5	6.5 ± 0.5	15.4 ± 0.6

[a] Corrected values with BCR-723. Concentrations in ng g^{-1}.

pattern was observed in site 3 were traffic also exhibits a significant diurnal cycle with maximum intensity during the night. However, this road is not designed for high density traffic which results in continues traffic jam. Thus, the high concentrations reflect PGEs emission from the continues stop/start cycle as well as the release during engine ignition. In site 5, PGE levels were lying in the middle of the other sampling sites reflecting emission during moderate speed driving.

4. Conclusions

In this work the experimental conditions for the determination of platinum-group elements in environmental samples was reassessed. A certified material (BCR-723) was used as a real sample in order to find the optimum extraction and atomization conditions. The results suggest that ETAAS conditions are well documented and can efficiency by employed for the determination of these elements in environmental samples. On the other hand, the provision of the optimal extraction conditions revealed several factors that may influence the extraction performance as a function of sample matrix components. Based on these observations, an experimental protocol that affords the determination of Pt, Pd and Rh in heterogenous matrices was developed and evaluated thought cross-examination of various certified materials with different matrix composition and variable PGE content. The method was successfully applied to the first monitoring survey of PGEs accumulation in the urban environment as a function of autocatalyst converter emissions in Ioannina (Greece).

Acknowledgments

This research was co-funded by the European Union in the framework of the program "Pythagoras I" of the "Operational Program for Education and Initial Vocational Training" of the 3rd Community Support Framework of the Hellenic Ministry of Education, funded by 25% from national sources and by 75% from the European Social Fund (ESF).

References

[1] F. Zereini, F. Alt (Eds.), Anthropogenic Platinum-Group Element Emissions, Springer, Berlin, 1999, p. 310.
[2] K. Ravindra, L. Bencs, R. Van Grieken, Sci. Total Environ. 318 (2004) 1.
[3] R. Merget, G. Rosner, Sci. Total Environ. 270 (2001) 165.
[4] L. Bencs, K. Ravindra, R. Van Grieken, Spectrochim. Acta Part B 58 (2003) 1723.
[5] J. Komarek, P. Krasensky, J. Balcar, P. Rehulka, Spectrochim. Acta Part B 54 (1999) 739.
[6] X. Su, M. Wang, Y. Zhang, J. Zhang, H. Zhang, Q. Jin, J. Anal. At. Spectrom. 16 (2001) 1341.
[7] J. Begerow, M. Turfeld, L. Duneman, Anal. Chim. Acta 340 (2002) 277.
[8] K. Boch, M. Schuster, G. Risse, M. Schwarzer, Anal. Chim. Acta 459 (2002) 257.
[9] S. Zimmermann, C.M. Menzel, D. Stuben, H. Taraschewski, B. Sures, Environ. Pollut. 124 (2003) 1.
[10] X. Dai, C. Koeberl, H. Fröschl, Anal. Chim. Acta 436 (2001) 79.
[11] M. Georgieva, B. Pihlar, Fresenius J. Anal. Chem. 357 (1997) 874.
[12] P. Kovacheva, R. Djingova, Anal. Chim. Acta 464 (2002) 7.
[13] F. Petrucci, B. Bocca, A. Alimonti, S. Caroli, J. Anal. At. Spectrom. 15 (2000) 525.
[14] M. Niemelä, P. Perämäki, J. Piispanen, J. Poikolainen, Anal. Chim. Acta 521 (2004) 137.
[15] R. Djingova, H. Heidenreich, P. Kovacheva, B. Markert, Anal. Chim. Acta 489 (2003) 245.
[16] M.B. Gomez, M.M. Gomez, M.A. Palacios, Anal. Chim. Acta 404 (2000) 285.
[17] M. Resano, E. Garcia-Ruiz, M.A. Belarra, F. Vanhaecke, K.S. McIntosh, Trends Anal. Chem. 26 (2007) 385.
[18] M. Muzikar, C. Fontas, M. Hidalgo, J. Havel, V. Salvado, Talanta 70 (2006) 1081.
[19] R.R. Barefoot, Trends Anal. Chem. 18 (1999) 702.
[20] B. Godlewska-Zyłkiewicz, Spectrochim. Acta Part B 58 (2003) 1531.
[21] B. Gomez, M.A. Palacios, M. Gomez, J.L. Sancez, G. Morrison, S. Rauch, C. McLeod, R. Ma, S. Caroli, A. Alimonti, F. Petrucci, B. Bocca, P. Schramel, M. Zischka, C. Petterson, U. Wass, Sci. Total Environ. 299 (2002) 1.
[22] M. Moldovan, M.M. Gomez, M.A. Palacios, J. Anal. At. Spectrom. 14 (1999) 1163.
[23] P. Schramel, M. Zischka, H. Muntau, B. Stojanik, R. Dams, M. Gomez Gomez, Ph. Quevauviller, J. Environ. Monit. 2 (2000) 443.
[24] R. Vlasankova, V. Otruba, J. Bendl, M. Fisera, V. Kanicky, Talanta 48 (1999) 839.
[25] K. Kanitsar, G. Kollensperger, S. Hann, A. Limbeck, H. Puxbaum, G. Stingeder, J. Anal. At. Spectrom. 18 (2003) 239.
[26] B.A. Lesniewska, B. Godlewska-Zyłkiewicz, A. Ruszczynska, E. Bulska, A. Hulanicki, Anal. Chim. Acta 564 (2006) 236.
[27] A.G. Coedo, M.T. Dorado, I. Padilla, F. Alguacil, Anal. Chim. Acta 340 (1997) 31.
[28] M. Brzezicka, I. Baranowska, Spectrochim. Acta Part B 56 (2001) 2513.
[29] F. Sánchez Roja, C. Bosch Ojeda, J.M. Cano Pavón, Anal. Chim. Acta 64 (2004) 230.
[30] I. Jarvis, M.M. Totland, K.E. Jarvis, Chem. Geol. 143 (1997) 27.
[31] R.A. Sutherland, Anal. Chim. Acta 582 (2007) 201.
[32] C. Bosch Ojeda, F. Sancez Rojas, J.M. Cano Pavon, Food control 17 (2006) 365.
[33] M. Hoenig, Talanta 54 (2001) 1021.
[34] S. Bektas, S. Akman, T. Balkis, Anal. Sci. 5 (1989) 439.
[35] J.D. Whiteley, F. Murray, Sci. Total Environ. 341 (2005) 199.
[36] M.M. Totland, I. Jarvis, K.E. Jarvis, Chem. Geol. 124 (1995) 21.
[37] A. Limbeck, J. Rendl, H. Puxbaum, J. Anal. At. Spectrom. 18 (2003) 161.
[38] P. Schramel, I. Wendler, G. Knapp, Fresenius J. Anal. Chem. 356 (1996) 512.
[39] D.H. Loring, R.T.T. Rantala, Earth Sci. Rev. 32 (1992) 235.
[40] H. Polkowska-Motrenko, B. Danko, R. Dybczynski, A. Koster-Ammerlaan, P. Bode, Anal. Chim. Acta 408 (2000) 89.
[41] B. Godlewska-Zyłkiewicz, Microchim. Acta 147 (2004) 189.
[42] E. Camacho Frias, H. Pitsch K, J. Ly, C. Poitrenaud, Talanta 42 (1995) 1675.
[43] M. Zischka, P. Schramel, H. Muntau, A. Rehnert, M.G. Gomez, B. Stojanik, G. Wannemaker, R. Dams, P. Quevauviller, E.A. Maier, Trends Anal. Chem. 21 (2002) 851.
[44] M. Brzezicka, E. Szmyd, Spectrochim. Acta Part B 54 (1999) 883.
[45] K. Slonawska, K. Brajter, J. Anal. At. Spectrom. 4 (1989) 653.
[46] K.H. Wedepohl, Geochim. Cosmochim. Acta 29 (1995) 1217.

Talanta 76 (2008) 509–512

Contents lists available at ScienceDirect

Talanta

journal homepage: www.elsevier.com/locate/talanta

Determination of cross-linking residues in a pharmaceutical polymer by liquid chromatography–high resolution full scan mass spectrometry

T. Zhang[a], D.G. Watson[a,*], Duo Lu[a], D. Carr[b], L. Trager[b]

[a] Strathclyde Institute for Pharmacy and Biomedical Science, 27 Taylor Street, Glasgow G4 0NR, UK
[b] Controlled Therapeutics, Peel Park Campus, East Kilbride G74 5PB, UK

ARTICLE INFO

Article history:
Received 16 November 2007
Received in revised form 17 March 2008
Accepted 21 March 2008
Available online 11 April 2008

Keywords:
Cross-linking residue
Manufacturing impurities
Fourier transform mass spectrometry
Ion suppression

ABSTRACT

A liquid chromatography–mass spectrometry (LC–MS) method was developed as limit test for an amine cross-linking residue in a pharmaceutical polymer. The method was based on full scan data with extracted ions for the accurate masses of dicyclohexylmethane-4, 4′-diamine (DMDA) and the internal standard 1,12-diaminododecane (DADD) obtained by Fourier transform MS. Dicyclohexylmethane-4,4-diisocyanate (DMDI) the reactive form of the cross-linking residue was determined as it decomposition product DMDA. Calibration curves for quantification of DMDA were linear in the range 2–100 ng/ml, the LOD was 1 ng/ml or 10 pg on column. Precisions/recoveries for spiked samples at the level of the limit of 1 ppm for DMDA and DMDI were ±9.6%/38.6% and ±14.5/10.0% (n = 3), respectively. Unpredictable recovery was found in the extraction of polymer samples because of the complexity of the matrix and the reactivity of dicyclohexylmethane-4,4-diisocyanate (DMDI). PEG residues extracted from the polymer were found to cause ionization suppression and also affected the chromatography, these effects were reduced by using a gradient program. By using this method the level of amine residues in samples from different batches of polymers were determined to be much lower than the limit of 1 ppm. The method allowed comparison of the results obtained from the polymer before and after purification indicating that the residual DMDA could be decreased by a washing procedure.

1. Introduction

Isocyanates or diisocyanates (–N=C=O) are widely used in the production of polyurethane (PUR). According to the molecular structure, they can be categorized into two groups: aromatic and aliphatic. It is well known that exposure to isocyanate is irritating to the skin, mucous membranes, eye and respiratory tract. There is increasing evidence that skin exposure can be an essential route of isocyanate sensitization in animal models [1–3] and skin exposure may be especially important with the less volatile aliphatic diisocyanates [4]. Recently a case of allergic contact dermatitis from dicyclohexylmethane-4, 4′-diisocyanate (DMDI) was reported and even its decomposed amine dicyclohexylmethane-4, 4′-diamine (DMDA) was also suspected to be a potent skin sensitizer [5]. A water-swellable cross-linked polyurethane polymer synthesised by reacting poly (ethylene glycol) (PEG), diol and dicyclohexylmethane-4,4-diisocyanate (DMDI) was invented at the University of Strathclyde and has been successfully developed as a polymer matrix for controlled drug release systems by Controlled Therapeutics (Scotland) Ltd. [6]. Considering the route of administration of the retrievable vaginal pessary manufactured from this polymer, the residues of DMDI and DMDA in the polymer matrices must be controlled carefully. A method was developed previously in order to test for residual of DMDI by determination of its decomposition product DMDA employing gas chromatography–mass spectrometry (GC–MS) in the negative ion chemical ionization mode (NICI). Solid phase extraction (SPE) and chemical derivatization were necessary for the sample preparation in this method [7]. Due to the complexity of the matrix and the reactivity of DMDI unpredictable recovery was demonstrated in the previous study.

In the current paper we report on the development of a method using LC combined with high resolution Fourier transform mass spectrometry (FT-MS) in the positive full-scan mode, without the need SPE and derivatization, for monitoring the level of DMDI/DMDA in the pharmaceutical polymers. Extraction recovery and ion suppression effects were investigated in detail.

* Corresponding author. Tel.: +44 1415482651; fax: +44 1415522651.
E-mail address: d.g.watson@strath.ac.uk (D.G. Watson).

0039-9140/$ – see front matter © 2008 Published by Elsevier B.V.
doi:10.1016/j.talanta.2008.03.054

2. Experimental

2.1. Chemicals and materials

1,12-Diaminododecane (DADD), 4,4′-diaminodicyclohexylmethane (DMDA), dicyclohexylmethane-4,4′-diisocyanate (DMDI) were purchased from Sigma–Aldrich Chemical Co. (Dorset, UK); HPLC grade methanol, acetonitrile and water were obtained from Rathburn Chemicals Ltd. (Walkerburn, Scotland). HPLC grade formic acid was obtained from VWR International Ltd. (Leicestershire, UK). The polymer pessaries were batches of product from Controlled Therapeutics (East Kilbride, Scotland).

2.2. Solution preparation

Stock solutions of DADD (internal standard) and DMDA (1 mg/ml) were prepared by dissolving 50 mg of the standard compound in 50 ml of methanol. Instead of methanol 50 ml of acetonitrile was used for dissolving 50 mg of DMDI standard to give a 1 mg/ml stock solution. The working standard solutions for the preparation of a calibration series for DMDA were prepared by diluting the stock solution with methanol to the concentrations of: 10, 5, 2, 1, 0.5, 0.2 and 0.1 ug/ml. For the recovery test the DMDI stock solution was diluted to 10, 1 and 0.1 μg/ml with acetonitrile. The stock solution of DADD was also diluted to 10 μg/ml with methanol before using.

2.3. Sample preparation

Pessaries were chopped by using a laboratory blender and 2 g of chopped polymer was added into 20 ml of 0.1% formic acid with spiking 200 μl of DADD internal standard solution (10 μg/ml). The polymers were left to swell in the buffer at 60 °C for 1 h and the remaining solutions were the filtered and the filtrate collected. For the recovery test 200 μl of DMDI or DMDA standard solution at the appropriate concentration was also spiked into the buffer before extraction. For the standard calibration series for determination of DMDA 200 μl aliquots of working standard solutions were added to 20 ml amounts of 0.1% formic acid in order to dilute the final concentrations of the test solutions to 100, 50, 20, 10, 5, 2, and 1 ng/ml.

2.4. Recovery test

2.4.1. Recovery of DMDI and DMDA

Recovery of DMDI and DMDA in the extraction was tested at three concentrations of 0.2, 0.1 and 0.05 ug/ml for spiking into solutions and equally 2, 1 and 0.5 ppm for samples spiked onto polymers using condition 1 described below.

2.4.2. Investigation of extraction conditions.

Recovery of DMDI (analysed as its decomposition product DMDA) was investigated under four extraction conditions: (1) spiking 200 μl of DMDI standard solution (10 μg/ml) onto 2 g of pessary (1 ppm) followed by extraction with 20 ml of 0.1% (v/v) formic acid by sonication at 60 °C for 60 min, and then 200 μl of DADD internal solution was added at the end. (2) The same as the conditions used in 1 except no polymer was added. (3) The same as the conditions used in one except that 2 ml of methanol was added and allowed to evaporate before extraction carried out as described in 1. (4) The same as the conditions used in three except that no polymer was added and the spiked DMDI was allowed to dry onto the glass surface of a beaker.

Table 1
Gradient programme used for reduction of effect of PEG oligomers *A* = 0.1% (v/v) formic acid and *B* = methanol

Time (min)	*A* (%)	*B* (%)	Flow rate (ml/min)
0	70	30	0.7
5	70	30	0.7
6	0	100	0.7
11	0	100	0.7
12	70	30	0.7
15	70	30	0.7

2.5. Effect of PEG oligomers extracted from the polymer

A sample solution was prepared by using the standard extraction method and was tested in order to determine the retention times of PEG oligomers running up to 60 min. The effect of the accumulation of PEG oligomers in causing ion suppression was demonstrated by continuously injecting the above sample 12 times using a short isocratic run. The removal of this effect by using a modified chromatographic method was demonstrated by using the gradient programme shown in Table 1.

2.6. Instrumentation

The LC–MS system consisted of a Finnigan Surveyor Plus HPLC System and a Finnigan LTQ-Orbitrap hybrid mass spectrometer equipped with an electrospray ionization (ESI) source. Chromatographic separations were performed on an ACE C18 column (100 mm × 4.6 mm; 5 μm; HiChrom, Reading, UK). The mobile phase conditions used were as shown in Table 1. Ionization was generated in positive mode at a spray voltage and capillary temperature of 4 kVand 200 °C, respectively. Sheath and auxiliary nitrogen gas were applied to help the evaporation of the solvent at a flow rate of 60 and 40 arbitrary units, respectively. The mass spectrometer was performed in full scan mode with the range between *m*/*z* 195 and *m*/*z* 250. The mass range *m*/*z* 211.21–211.22 was extracted for monitoring DMDA and the mass range of *m*/*z* 201.23–201.24 was monitored for DADD. DMDI was determined as its decomposition product DMDA.

3. Results and discussion

3.1. Linearity and recovery

Fig. 1 shows the mass spectrum of DMDA and DADD obtained from spiking approximate 2 μg of each compound into 20 ml of 0.1% formic acid solution. The mass spectrum of each compound was dominated by its $[M+H]^+$ ion. The chromatographic peaks

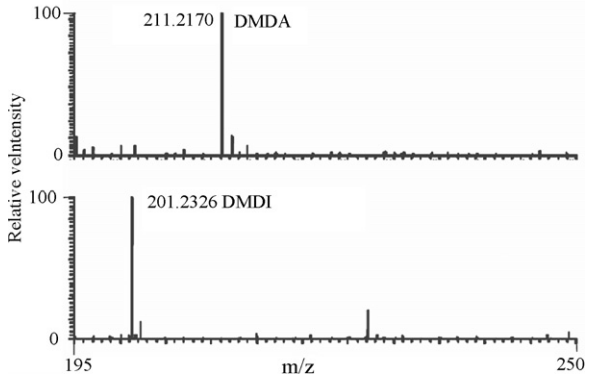

Fig. 1. Mass spectrum of DMDA and DADD in the full scan mode (*m*/*z* 195–250).

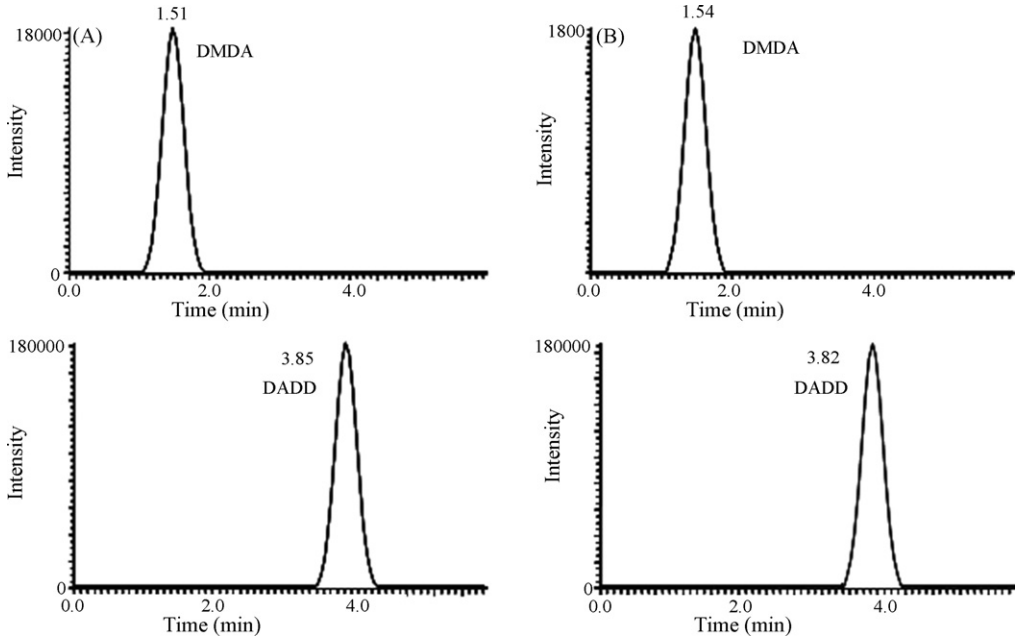

Fig. 2. Extracted ion chromatographs of (A) 0.2 ng DMDA and 2 ng DADD and (B) 0.02 ng DMDA and 2 ng DADD.

were obtained by integrating the signals in an extremely narrow mass range (m/z 211.21–211.22 for DMDA and m/z 201.23–201.24 for DADD). Fig. 2 shows the chromatographs of 10 ng/ml (A) and 1 ng/ml (B) of DMDA and 100 ng/ml of DADD. Very "clean" chromatographs were achieved by using the extremely narrow range extracted ion window and the limit of detection for DMDA was regarded as an irregular observation of the signal which was ca. 10 pg on column or 10 μl from a 1 ng/ml solution as opposed to a particular signal to noise ratio which was usually infinite until the signal disappeared. The linearity of the method was also confirmed by the fact that the R^2 value was more than 0.998 ($n = 5$) of the calibration curve ($y = 0.5699 \pm 0.0142x - 0.0171 \pm 0.0093$) from 2 to 100 ng/ml for DMDA. The levels of recovery of DMDI and DMDA are shown in Table 1. Such a low and inconsistent recovery of DMDI suggested that there was decomposition during the extraction to products other than DMDA. Therefore the recovery of DMDI was investigated further under four extraction conditions as described above (Section 2.4.2) and the results are shown in Table 2. The recovery was calculated as the ratio of: area of DMDA/area of DADD, the DMDA being formed from DMDI (1 ppm) spiked into the polymer and the one obtained from standard DMDA (1 ppm) spiked directly into buffer solution. It was evident that the recovery of DMDI analysed after its conversion into DMDA was very poor unless it was spiked directly into the extraction medium (Table 3) where the recovery was 38.0%. This might be explained by the fact that at such low levels contact with moisture will promote the decomposition of DMDI into DMDA and the DMDA formed will tend to react with remaining DMDI to form a polyurea compound (reaction of DMDI with amines is much more rapid than its reaction with water). In addition the DMDI spiked directly onto the polymer will tend to react with free hydroxyl groups in the polymer (Table 3).

Table 3
Recovery test of DMDI under four different conditions

	Area of DMDA/area of DADD			
	Condition 1	Condition 2	Condition 3	Condition 4
Spiked DMDI (1 ppm)	0.0629	0.081	0.336	0.165
Standard DMDA (1 ppm)	0.885	0.885	0.885	0.885
Recovery	7.1%	9.2%	38.0%	18.6%

3.2. Investigation of Ion suppression effects

In the course of developing the method it was observed that after a few runs using an isocratic method DMDA and the DADD internal standard could no longer be observed in spiked samples and also as the runs continued the chromatographic peaks of the analytes became distorted. Since Polyethylene glycol (MW more than 8000) was used as one of main ingredients during the manufacture of the pessaries the potential for an ion suppression effects caused by PEG were investigated and led to the chromatographic method being modified to include a gradient step. Identification of ion suppression effects of PEG and the strategies to minimise the effects have been already published [8,9]. Table 4 shows the m/z values and elution times of observed PEG oligomers within mass range 200–1000 and a running time of 60 min. The results were quite similar to the observations in Refs. [9,10] which observed that the individual PEG oligomers covered a broad range of lipophilicities. The effect

Table 2
Recovery test of DMDI and DMDA ($n = 3$)

	DMDI (area of DMDA/area of DADD)				DMDA (area of DMDA/area of DADD)			
	Standard	Extracted	Recovery (%)	R.S.D. (%)	Standard	Extracted	Recovery (%)	R.S.D. (%)
2 ppm	1.153	0.105	9.1	12.2	1.654	0.665	40.2	3.7
1 ppm	0.562	0.056	10.0	14.5	0.885	0.342	38.6	9.6
0.5 ppm	0.285	0.037	13.0	19.81	0.466	0.184	39.5	8.2

Table 4
Observed PEG oligomers and their retention times

PEG oligomer (*n*)	*m*/*z*	Retention time (min)
5	239.15	2.0–2.5
6	283.17	2.2–2.9
7	327.2	2.5–3.4
8	371.23	3.0–4.0
9	415.25	3.6–5.2
10	459.28	4.4–6.6
11	503.3	5.4–8.6
12	547.33	6.8–11.4
13	591.36	8.5–14.8
14	635.38	11.0–19.9
15	679.41	14.1–26.4
16	723.43	18.4–36.1
17	767.46	24.0–48.4
18	811.48	31.5–60

Table 5
Cumulative effect of PEG on analyte detection over 12 consecutive injections without (part 1) and with (part 2) flushing with 100% methanol at the end of each run

	DMDA		DADD		Ratio
	Retention time	Peak area	Retention time	Peak area	
Part 1					
First	1.54	154004	3.74	431602	0.356819
Sixth	1.32	55382	2.99	213565	0.259322
Twelfth	1.28	42147	–	0	0
Part 2					
First	1.51	160220	3.79	452839	0.353812
Sixth	1.51	144559	3.84	425870	0.339444
Twelfth	1.51	151685	3.84	443426	0.342075

of accumulation of PEG oligomers in the isocratic chromatographic method on the peak areas of DMDA and DADD is shown in Table 5, part 1. Under isocratic conditions all peak areas decrease with the number of consecutive injections ($n = 12$ and 5 min for each run). The ion suppression effect was clearly reflected by the significant reduction of the peak areas of DMDA and DADD and "modification" of the stationary phase could also be observed in the change of the retention times of the analytes. These effects were attributed to the accumulation of the PEG oligomers from each injection. In order to reduce the effects of the oligomers a gradient chromatographic method (Table 1) was used in which elution with 100% methanol (5 min) at the end of each run was used to wash out any oligomers which would be likely to co-elute with the analytes. Although this required an increase in running time more accurate and precise areas and chromatographic values were achieved for 12 consecutive injections (Table 4, part 2). An alternative clean up procedure would have been to use strong cation exchange extraction which we found in previous work to give very clean extracts, however, this additional time consuming step is best avoided if possible.

3.3. Limit test for DMDI

Although the recovery of DMDI was poor and unpredictable Fig. 3 indicates that it is highly unlikely that low levels of isocyanate

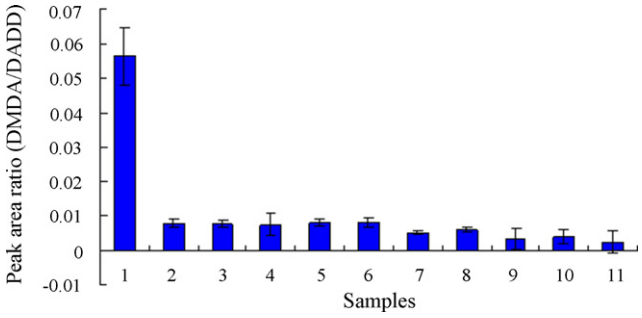

Fig. 3. Comparison of corresponding values (peak area ratio of DMDA/DADD) of DMDI in spiked and unspiked batches of polymer. Column 1, spiked DMDI polymer at the limit of 1 ppm; Columns 2–6, blank polymer samples from the batches 1–5; Columns 7–11, purified polymer samples from the batches 1–5.

would survive in the polymer before either decomposing to DMDA or polymerizing with itself or the polymer. Column 1 represents the value of peak area ratio of DMDA and DADD obtained from DMDI spiked into the polymer at the limit of 1 ppm and columns 2–6 and columns 7–11 demonstrate the values obtained from blank and purified polymers in five batches. It is clear that the all values obtained from sample polymers were much lower than those obtained from spiked polymer and a slight decrease in the values obtained from purified samples was also observed.

The advantage of using full scan MS for this type of analysis were quite apparent since unlike the more widely used tandem MS methods it is possible to directly observe ion suppressing compounds in the background matrix which are screened out the ion selection used in tandem MS. It is likely that MS will be increasingly required for the type of analysis described in this paper and guidelines has been recently released regarding the control of genotoxic impurities which include isocyanates [10]. The current paper demonstrates that the isocyanate in the hydrogel pessaries is far below levels which would give rise to concern [10], if it is present at all, even when the pessary is ground to a fine powder before extraction. The method has proved to be quantitatively robust during 1 year of usage.

References

[1] M.H. Karol, B.A. Hauth, E.J. Riley, C.M. Magreni, Toxicol. Appl. Pharmcol. 58 (1981) 221.
[2] I. Erjefalt, C.G. Persson, Clin. Exp. Allergy 22 (1992) 854.
[3] N.J. Rattray, P.A. Botham, P.M. Hext, D.R. Woodcock, I. Fielding, R.J. Dearman, I. Kimber, Toxicology 88 (1994) 15.
[4] Y.C. Liu, M.D.J. Sparer, S.R. Woskie, M.R. Cullen, J.S. Chung, C.T. Holm, C.A. Redlich, Am. J. Ind. Med. 37 (2000) 265.
[5] M. Frick, B. Björkner, N. Hamnerius, E. Zimerson, Contact Dermatitis 48 (2003) 305.
[6] M.E. McNeill, N. Graham, J. Control. Release 1 (1984) 99.
[7] D.G. Watson, L.L. Xin, J.M. Midgley, D. Carr, J. Pharm. Biomed. Anal. 19 (1999) 917.
[8] D. Temesi, B. Law, N. Howe, J. Pharm. Sci. 92 (2003) 2521.
[9] R. Weaver, R.J. Riley, Rapid Commun. Mass Spectrom. 20 (2006) 2559.
[10] European Medicines Agency. Guideline on the Limits of Genotoxic Impurities. June 2006.

Talanta 76 (2008) 690–697

Contents lists available at ScienceDirect

Talanta

journal homepage: www.elsevier.com/locate/talanta

Simultaneous determination of monoamine and amino acid neurotransmitters in rat endbrain tissues by pre-column derivatization with high-performance liquid chromatographic fluorescence detection and mass spectrometric identification

Xian-En Zhao[a,b], You-Rui Suo[a,*]

[a] Northwest Institute of Plateau Biology, Chinese Academy of Sciences, Xining 810001, China
[b] Graduate School of the Chinese Academy of Sciences, Beijing 100039, China

ARTICLE INFO

Article history:
Received 6 December 2007
Received in revised form 31 March 2008
Accepted 12 April 2008
Available online 22 April 2008

Keywords:
Neurotransmitter
HPLC–MS
Fluorescence detection
Rat endbrain
Pre-column derivatization
1,2-Bbenzo-3,4-dihydrocarbazole-9-ethyl chloroformate

ABSTRACT

A sensitive and efficient method for simultaneous determination of glutamic acid (Glu), γ-amino-butyric acid (GABA), dopamine (DA), 5-hydroxytryptamine (5-HT) and 5-hydroxyindole acetic acid (5-HIAA) in rat endbrains was developed by high-performance liquid chromatography (HPLC) with fluorescence detection and on-line mass spectrometric identification following derivatization with 1,2-benzo-3,4-dihydrocarbazole-9-ethyl chloroformate (BCEOC). Different parameters which influenced derivatization and separation were optimized. The complete separation of five neurotransmitter (NT) derivatives was performed on a reversed-phase Hypersil BDS-C_{18} column with a gradient elution. The rapid structure identification of five neurotransmitter derivatives was carried out by on-line mass spectrometry with electrospray ionization (ESI) source in positive ion mode, and the BCEOC-labeled derivatives were characterized by easy-to-interpret mass spectra. Stability of derivatives, repeatability, precision and accuracy were evaluated and the results were excellent for efficient HPLC analysis. The quantitative linear range of five neurotransmitters were 2.441–2 × 10^4 nM, and limits of detection were in the range of 0.398–1.258 nM (S/N = 3:1). The changes of their concentrations in endbrains of three rat groups were also studied using this HPLC fluorescence detection method. The results indicated that exhausting exercise could obviously influence the concentrations of neurotransmitters in rat endbrains. The established method exhibited excellent validity, high sensitivity and convenience, and provided a new technique for simultaneous analysis of monoamine and amino acid neurotransmitters in rat brain.

1. Introduction

Neurotransmitters (NT) widely distribute in central neural system, brain tissues and body fluids of mammals. They consist of amino acid neurotransmitters (AANT), such as glutamic acid (Glu) and γ-amino-butyric acid (GABA), and monoamine neurotransmitters (MANT), such as dopamine (DA), 5-hydroxytryptamine (5-HT) and 5-hydroxyindole acetic acid (5-HIAA). The monitoring of NT is an essential tool in elucidating normal and pathological neural system functions [1]. Trace level measurements in the brain are especially important in studying the role of NT in neurophysiology, behavioral effects, pathology, disease diagnosis and control since their changes have been associated with various diseases and disorders such as Parkinson's disease [2–4], Alzheimer's disease [5–7], Down's syndrome, Huntingdon's disease [8], schizophrenia, epilepsy and cocaine addiction [9].

Up to now, there have been many reports about relationship between exercise and NT. Blomstrand et al. reported that exhausting exercise caused an increase of MANT (e.g. 5-HT, DA) in hypothalamic area of rats [10]. Hokfelt et al. reported that the concentrations of AANT were a hundred times more than those of MANT in brain [11]. Researches have shown that the concentration changes of Glu, GABA, 5-HT and DA, and the ratio change of Glu/GABA in rat brain were related with the development of exercise fatigue [12,13]. Davis reported that exhausting exercise resulted in concentration changes of 5-HT and 5-HIAA in whole brain or its part region. Therefore, it was much more accurate to evaluate the formation of exercise fatigue using the ratio of 5-HT/5-HIAA [14].

HPLC or capillary electrophoresis (CE) coupled with various detection methods, such as UV detection [15], fluorescence detection (FLD) [16–21], electrochemical detection (ECD) [22–24,9],

* Corresponding author. Tel.: +86 971 6143857; fax: +86 971 6143857.
E-mail address: yrsuo@163.com (Y.-R. Suo).

0039-9140/$ – see front matter © 2008 Elsevier B.V. All rights reserved.
doi:10.1016/j.talanta.2008.04.032

laser-induced fluorescence detection (LIFD) [25–29] and mass spectrometry (MS) [30–34], have been widely developed for the determination of AANT and MANT. These methods have more or less limitations. UV detection is not sensitive and selective for monoamines and helpless for amino acids. Electrochemical detection tends to lack reproducibility mainly because of hysteretic degradation of the electrode [35]. CE-LIFD is limited for analyzing MANT in biological fluids containing complex mixtures due to the similar electrophoretic behavior of these compounds [36]. HPLC– or CE-MS methods have higher detection limits than FLD or ECD [31,34]. Recently, some new methods have been brought forward for the detection of NT, such as microfluidic electrophoresis chip for AANT [1], intramolecular fluorescence resonance energy transfer detection for MANT [35], microchip electrophoresis for MANT or AANT [29,36–37], monolithic column chromatography coupled with chemiluminescence detection [38]. However, they are just tentative as new techniques for few interested AANT or MANT.

As a matter of fact, pre-column derivatization coupled with HPLC-UV or HPLC-FLD has been successfully used for the determination of MANT and AANT in microdialysates, brain tissue extracts and other biochemical samples [19–21,39,40]. Some fluorescent derivatization reagents has been synthesized and applied in this field including *o*-phthalaldehyde-2-mercaptoethanol (OPA-2-ME) [35,40], benzylamine and 1,2-diphenylethylenediamine (BA + DPE) [39] and 6-aminoquinolyl-*N*-hydroxysuccinimidyl carbamate (AQC) [19]. Many other derivatization reagents which are not fluorescent ones have also been developed for NT analysis, such as dansyl chloride (Dns-Cl) [41], 5-furoylquinoline-3-carboxaldehyde (FQ) [25], fluorescein-5-isothiocyanate (FITC) [27], naphthalene-2,3-dicarboxaldehyde (NDA) [28] and 5-(4, 6-dichloro-striazin-2-ylamino) fluorescein (DTAF) [29]. However, these pre-column derivatization reagents have more or less limitations in their applications, such as poor stability, low detection sensitivity, tediously analytical procedure, or serious interferences in chromatogram [8,22].

In our previous studies [42,43], we described the synthesis of 1,2-benzo-3,4-dihydrocarbazole-9-ethyl chloroformate (BCEOC) and its applications for analysis of aliphatic amines, amino acids and peptides in environmental and biological samples. In this paper, a HPLC-FLD method using BCEOC as pre-column derivatization reagent was developed for the simultaneous determination of AANT and MANT. This method was also used to study the changes of NT in rat endbrains at three states (quiet state, at exercise exhaustion, 12 h after exercise exhaustion) and the relationship between NT concentration and exercise fatigue. To the best of our knowledge, BCEOC is firstly studied for the analysis of NT and shows some advantages including mild derivatization conditions, ease-of-handling and high detection sensitivity.

2. Experimental

2.1. Instrumentation

HPLC separation, MS identification and analysis of samples were performed using Agilent 1100 Series high-performance liquid chromatography/mass spectrometry (HPLC–MSD ion Trap SL, a complete LC–MS/MS). All the HPLC system devices were from the Agilent 1100 series and consisted of an online vacuum degasser (model G1322A), a quaternary pump (model G1311A), an autosampler (model G1329A), a thermostated column compartment (model G1316A), a fluorescence detector (FLD) (model G1321A) and a diode array detector (DAD) (model G1315A). The HPLC system was controlled by HP Chemstation software (Version B.01.01). The mass

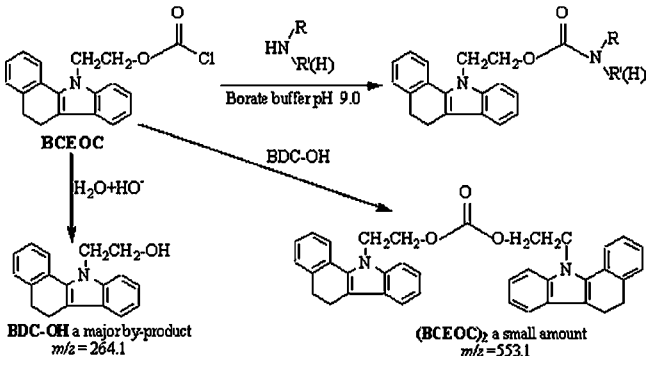

Fig. 1. Scheme of derivatization reaction of BCEOC and neurotransmitters.

spectrometer LC/MSD Trap-SL (ion trap) was from Bruker Daltonik (Bremen, Germany) equipped with an electrospray ionization (ESI) source and controlled by Esquire-LC NT software (Version 5.3). Ion source conditions: ESI in positive ion mode, nebulizer pressure 241.3 kPa, dry gas temperature 350 °C, dry gas flow 9.0 L/min and capillary voltage −3500 V. Derivatives were separated on a reversed-phase Hypersil BDS-C_{18} column (100 mm × 4.6 mm, 5 μm i.d., Dalian Elite Analytic Instruments Co. Ltd., Dalian, China) by a gradient elution. Fluorescence excitation and emission spectra were obtained on a 650-10S fluorescence spectrophotometer (Hitachi, Tokyo, Japan). Excitation and emission bandpass were both set at 10 nm. A Paratherm U2 electronic water-bath (Hitachi, Tokyo, Japan) was used to control temperature. The mobile phase was filtered through a 0.2 μm membrane.

2.2. Chemicals and materials

1,2-Benzo-3,4-dihydrocarbazole-9-ethyl chloroformate was synthesized in our laboratory [42,43]. Glutamic acid, γ-aminobutyric acid, 5-hydroxytryptamine and 5-hydroxyindole acetic acid were purchased from Sigma (St. Louis, MO, USA). Dopamine was purchased from Fluka (Buchs, Switzerland). Spectroscopically pure acetonitrile was purchased from Merck (Darmstadt, Germany). Water was purified using a Millipore system (Bedford, MA, USA). Other reagents were of analytical grade.

2.3. Preparation of standard solutions

Individual stock solution (1.0×10^{-2} M) of NT was prepared in acetonitrile/water mixed solution (v/v, 1:1). The mixed standard solutions of NT for HPLC analysis were prepared by diluting the stock solutions with acetonitrile/water to the individual concentration of 200, 100, 50, 25, 12.5, 6.25, 3.125, 1.5625, 0.7813, 0.3906, 0.1953, 0.09766, 0.04883 and 0.02441 μM. The BCEOC solution (1.0×10^{-3} M) was prepared by dissolving 3.26 mg BCEOC in 10 mL of acetonitrile. The low concentration derivatization reagent solutions were obtained by dilution with acetonitrile. Borate buffer solution (0.2 M) was prepared by dissolving borax in water and pH was adjusted using hydrochloric acid or sodium hydroxide solution to different values in 4.0–11.0 for derivatization. When not in use, all standards were stored at 4 °C in a refrigerator.

2.4. Derivatization procedure

Derivatization reaction scheme is shown in Fig. 1. The BCEOC–NT derivatization proceeded in acetonitrile/water solution in basic medium. 50 μL solution of mixed standard NT, 95 μL acetonitrile, 200 μL borate buffer (pH 9.0) and 150 μL BCEOC solution were orderly and successively added into a 2-mL vial. The vial was then

sealed and allowed to stand for 10 min at 40 °C in a thermostatic water-bath. After derivatization, to the solution was added 5 μL 50% acetic acid/water until the final pH 7.0. Then 10 μL derivatized sample solution was directly injected into the HPLC system for analysis.

2.5. High-performance liquid chromatography

HPLC separation of NT derivatives was carried out on the reversed-phase Hypersil BDS-C_{18} column by a gradient elution. Eluent A was 30% of acetonitrile consisting of 30 mM ammonium formate buffer (pH 3.7); B was 100% of acetonitrile. The gradient elution program was as follows: 0 min = 15% B, 5 min = 15% B, 15 min = 25% B, 25 min = 100% B and 30 min = 100% B. Before injecting the next sample, the column was equilibrated with the initial mobile phase for 10 min. The flow rate was constant at 1.0 mL/min and the column temperature was set at 30 °C. The fluorescence excitation and emission wavelengths were set at λ_{ex} 333 nm and λ_{em} 390 nm, respectively. The derivatives were quantified by fluorescence detector, and identified simultaneously through HPLC retention time of standards and on-line ESI/MS structure identification.

2.6. Animals

Male Wistar rats were purchased from experimental animal center of Lu Nan Pharmacy Group Joint-stock Ltd. (180–220 g). Exercise training and endbrain samples separation were performed by Prof. Liu Hongzhen (College of Sports Education, Qufu Normal University). Twenty-four rats were adaptively trained on electric drive treadmills for 1 week (rate 10 m/min, training time 20 min/d). Then, the rats were separated at random into three groups (Group A, B and C, eight rats of each group) by avoirdupois. Endbrain tissues were collected at three states corresponding to three groups as follows: quiet state without exercise (Group A, the control group), at exercise exhaustion (Group B, judgment standard: the rats could not hold up to exercise; stimulation and drive were of no effect; when the rats were taken down from electric drive treadmills and upturned, they could not turn over by themselves), 12 h after exercise exhaustion (Group C).

2.7. Extraction of NT in rat endbrain tissues

Male Wistar rats were decapitated at corresponding states of three groups. The whole brain were immediately taken out and washed by ice-cooled physiological salt solution. Endbrains were separated on a glass plate. To a hard glass tube, 1.2 mL 0.1 M ice-cooled $HClO_4$ solution and the weighted endbrain tissue (about 0.1 g) were added and slurried for 20 min. The slurried solution was centrifuged (18,000 rpm for 30 min at 4 °C). The supernatant was separated and added 20% NaOH solution to neutralize the excess amount of $HClO_4$ to pH 8.0–9.0. The resulting solutions were made up to total volume of 2.0 mL with deionized water and stored at −80 °C until HPLC analysis.

2.8. Quantitative analysis

Quantitative conversion of NT from rat endbrains to their BCEOC-labeled derivatives was guaranteed by using an excess of BCEOC. All NT were quantified using external standard method with fluorescence detection at 390 nm. The calibration curves for each BCEOC–NT derivative were obtained by linear regression plotting peak area versus injection amount.

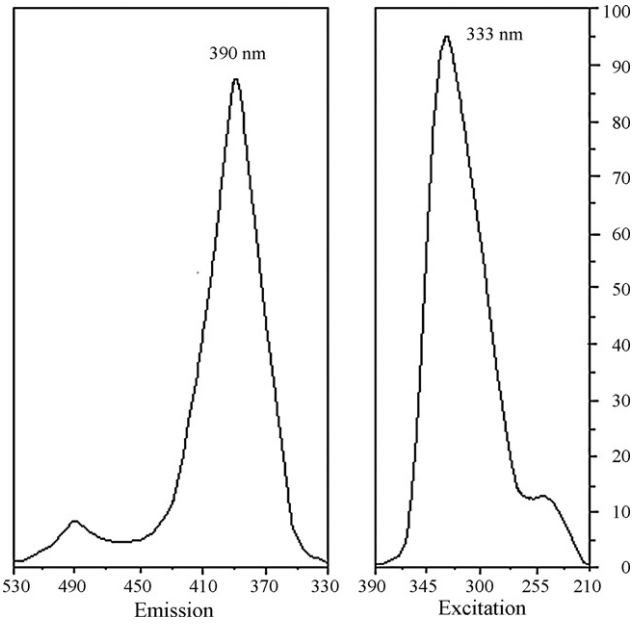

Fig. 2. Fluorescence excitation and emission spectra of BCEOC-GABA derivative.

2.9. Data statistic

All the data statistic work was accomplished with SPSS 13.0. The results were expressed in the form of "average ± standard deviation" ($\overline{X} \pm S$). Data were analyzed with independent sample *T*-test and one-way analysis of variance. Significant difference level was $P < 0.05$.

3. Results and discussion

3.1. Fluorescence spectra of BCEOC–NT derivatives

Maximum excitation and emission wavelengths which were set in HPLC fluorescence detector were important for the detection sensitivity of NT derivatives. To determine the fluorescence spectra of five NT derivatives, every BCEOC–NT sample was prepared by individual derivatization and purification on a solid-phase extraction column (ODS C_{18}, Dalian Elite Analytic Instruments Co. Ltd., Dalian, China), and scanned on the 650-10S fluorescence spectrophotometer. The maximum excitation and emission wavelengths for five BCEOC–NT derivatives were 333 and 390 nm, respectively. The representative fluorescence excitation and emission spectra of BCEOC-GABA was shown in Fig. 2.

3.2. Optimization of derivatization conditions

The main factors affecting derivatization yields were pH value of buffer, reaction time, temperature and concentration of BCEOC. Several kinds of basic media were tested including carbonate buffers, phosphate buffers and borate buffers. The maximum peak area was obtained with borate buffer in aqueous acetonitrile. However, high concentration buffers (>0.3 M) yielded a slight reduction of peak area. In the following experiments, 0.2 M borate buffer was used. The effect of pH was investigated in the pH range of 4.0–11.0. Derivatization reaction did not occur in the range of pH < 7.0, while peak areas of five derivatives obviously increased along with the increasing of pH value in the pH range of 7.0–9.0. At higher pH values (>9.0), the derivatives exhibited some hydrolysis and partially

converted to their mono-substituted ones. Therefore, all subsequent derivatization reaction was performed at pH 9.0. The effects of reaction temperature and time on the derivatization yields were evaluated from 30 to 90 °C and 1–30 min, respectively. Maximal and constant peak areas were achieved when NT standards were derivatized at 40 °C for 10 min. This indicated that BCEOC reacted rapidly and smoothly with NT under mild conditions. In addition, the effect of BCEOC concentration on derivatization yields was investigated. The peak areas of BCEOC-derivatives increased along with the increasing amounts of BCEOC. Maximal peak areas were achieved when the molar reagent was six times in excess. Accordingly, six times excess of molar reagent was taken in our following experiment. To an unknown concentration of real sample, such as the extracted endbrain tissue, complete derivatization was guaranteed by using excess BCEOC until constant peak area for detector responses was reached. After derivatization reaction completed, the solution was neutralized to pH 5.0–7.0 by adding 5 μL 50% acetic acid/water in order to avoid the degradation of NT derivatives.

3.3. HPLC separation

Several mobile phases of methanol or acetonitrile aqueous mixtures with different compositions were tested for the separation of derivatives. The results indicated that five NT derivatives could be completely separated on a Hypersil BDS-C_{18} column when (A) 30% acetonitrile (pH 3.7) containing 30 mM ammonium formate and (B) 100% acetonitrile were used as eluents. The pH value of mobile phase could significantly affect the resolution of five derivatives. Operation at pH 6.0–8.0 of mobile phase A resulted in obviously increase of retention time about 5–11 min for all derivatives. With the optimal pH 3.7, all derivatives were best separated giving appropriate retention time and good peak shape. Furthermore, the acidic eluents could provide hydrogen proton to enhance the ESI ionization efficiency of NT derivatives. Since the ammonium formate itself was volatile, the high dry gas temperature (350 °C) and abundant dry gas flow (9.0 L/min) could effectively reduce its residue in ESI source. Before injected into ESI source, the eluents was splited (split ratio = 1:1) by a three-way valve, a diverter designed in Agilent 1100 HPLC-ESI/MS system. This means that only 50% of eluents was injected into ESI source, namely the flow rate was 0.5 mL/min and only half of ammonium formate was used. That was allowable in the service manual of Agilent 1100 HPLC–MS system and did not cause contamination to ESI source. The effect of the concentration of ammonium formate was also investigated to verify whether it caused ion suppression to ESI source. Eluents A containing different concentration ammonium formate (0, 10, 20, 30 and 40 mM) were prepared and tested under the same conditions. The results indicated that MS total ion current intensities of five NT derivatives obviously increased from 0 to 30 mM ammonium formate and leveled off above 30 mM. Moreover, the intensities obtained at 30 mM ammonium formate were about two times stronger than those at 0 mM. Therefore, 30 mM ammonium formate was favorable for MS detection. Under optimum conditions, five NT derivatives were separated with a good baseline resolution as shown in Fig. 3(a). Blank experimental chromatogram obtained by derivatizing the same volume acetonitrile/water without NT standard is shown in Fig. 3(b).

The major disturbances in standard chromatogram were 1, 2-benzo-3,4-dihydrocarbazole-9-ethanol (BDC-OH, m/z 264.1) and bis-(1,2-benzo-3,4-dihydrocarbazole-9-ethyl) carbonate ($(BCEOC)_2$, m/z 553.1) which were two by-products formed in derivatization reaction because of the hydrolysis of BCEOC (see Fig. 1). Fortunately, the presence of BDC-OH and $(BCEOC)_2$ did not interfere with the separation of NT derivatives under the proposed method.

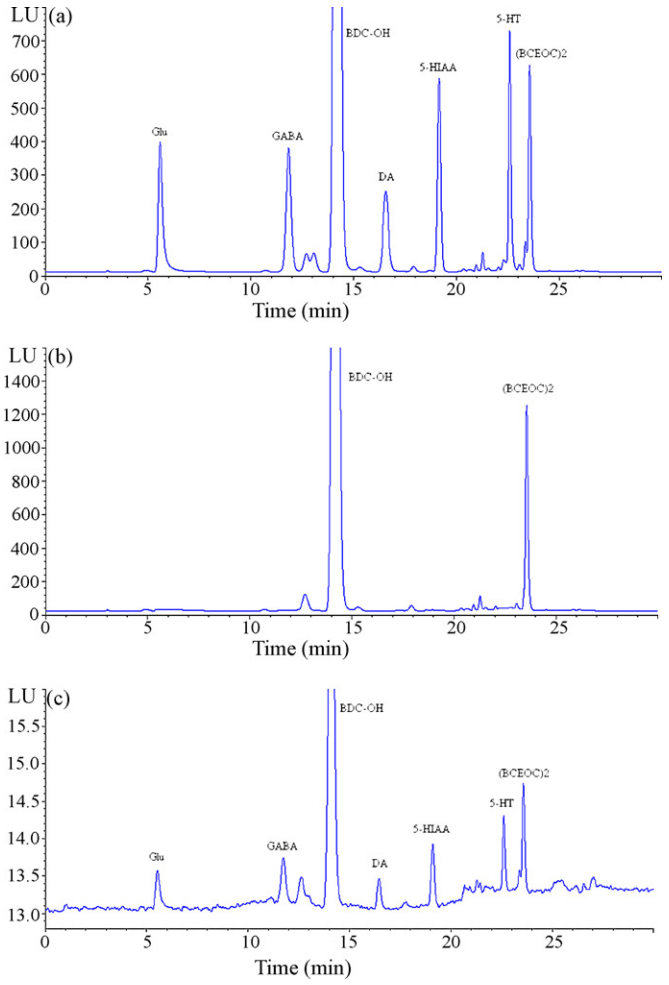

Fig. 3. Chromatogram of BCEOC-labeled (a) neurotransmitters standard (100 pmol in 10 μL), (b) blank experiment and (c) neurotransmitters standard at 2.441 nM. *Chromatographic conditions*: column, Hypersil BDS-C_{18}, 100 mm × 4.6 mm, 5 μm i.d.; flow rate = 1.0 mL/min; column temperature 30 °C; excitation wavelength λ_{ex} 333 nm; emission wavelength λ_{em} 390 nm. Gradient elution conditions were described in Sections 2.5 and 3.2. Derivatization of blank experiment was performed without neurotransmitter standard solution which was replaced by the same volume acetonitrile/water solution. *Peaks*: Glu: glutamic acid; GABA: γ-aminobutyric acid; DA: dopamine; 5-HT: 5-hydroxytryptamine; 5-HIAA: 5-hydroxyindole acetic acid; BDC-OH: 1,2-benzo-3,4-dihydrocarbazole-9-ethanol; $(BCEOC)_2$: bis-(1,2-benzo-3,4-dihydrocarbazole-9-ethyl) carbonate.

3.4. Comparison of BCEOC with reported derivatization reagents

The overall comparison of BCEOC with reported derivatization reagents for NT analysis including derivatization, separation and detection is given in Table 1. Derivatization reaction for BCEOC with NT was more simple and rapid than those reagents except OPA and AQC. But OPA and AQC were incapable of secondary amines (e.g. 5-HIAA). Moreover, the derivatives of OPA were very unstable as a result of difficulty in quantitation [22]. HPLC separation conditions for BCEOC derivatives including column, mobile phase and elution program were more facile than other methods described in Table 1. And it also brought rapid and complete resolution of NT derivatives. In addition, the fluorescence detector coupled to HPLC was easy to gain, and the higher detection sensitivity of BCEOC–NT derivatives was satisfactory.

Table 1
Comparison of BCEOC with reported derivatization reagents for neurotransmitter analysis including derivatization, separation and detection

Reagent[a]	Analytes	Derivatization	Separation	Detection	LODs (nM)	Reference
OPA-2-ME	MANT	In methanol and borate buffer (pH 11.0), at room temperature for 10–15 min	Isocratic elution on YMC-Pack reversed-phase column using acetonitrile–methanol-diluted acetic acid as mobile phase, 60 min	HPLC-FLD, Ex: 340 nm, Em: 445 nm	1.5–11.5	[35]
BA + DPE	MANT	Two-step reaction, initiated with BA in CAPA buffer (pH 10.0, 2 min 24 °C) and followed by DPE in glycine buffer (pH 10.0, 20 min 50 °C)	Isocratic elution on a C18 column (150 mm × 1.5 mm, 5 μm) using acetonitrile and acetate buffer (pH 4.5) as mobile phase, 45 min	HPLC-FLD, Ex: 345 nm, Em: 480 nm	0.12–0.85	[39]
AQC	AANT	In acetonitrile and borate buffer (pH 8.8), at room temperature within 1 min	Gradient elution on a 150 mm × 3.9 mm AccQ-Tag column, eluent A (pH 5.05) and B (pH 5.50) were aqueous acetate phosphate buffer, C and D acetonitrile and water, 25 min	HPLC-FLD, Ex: 250 nm, Em: 395 nm	3.3–7.6	[19]
Dns-Cl	AANT	In acetonitrile and lithium carbonate buffer (pH 9.5), at room temperature in darkness for 1 h	Gradient elution on a waters ODS column (150 mm × 4.6 mm), eluent A and B were methanol/water (0.6% acetic acid) and water (0.008% triethylamine), 60 min	HPLC-UV 254 nm	151–155	[41]
FQ	16 amino compounds	In borate buffer (pH 9.2) with KCN, at 65 °C in the dark for 16 min	On a 40 cm × 50 μm × 140 μm capillary column, running buffer was 20 mM borate (pH 9)/60 mM SDS, 18 min	CE-LIFD	1–80	[25]
FITC	AANT	In borate buffer (pH 9.6) and acetone, at 20 °C in the dark for 16 h	On a 57 cm × 75 mm capillary column, running buffer was 15 mM borate at pH 9.2, 18 min	CE-LIFD	0.021–0.42	[27]
NDA	AANT and catecholamines	On-line derivatization, in acetonitrile/water and borate buffer (pH 8.7)/NaCN solution	In two single figures for AANT and catecholamines with capillary column in 10 and 4 min, respectively	CE-LIFD	1–420	[28]
DTAF	Amino acids	In DMSO and borate buffer (pH 9.2), at 38 °C for 30 min	On two novel microchip, OP-chip and PVA-chip, using borate buffer (pH 8), 100 s	CE-LIFD	1600–7000	[29]
NBD-F	AANT	In acetonitrile and borate buffer (pH 9.0), at 65 °C for 20 min	On a chiral capillary column, isocratic elution with methanol/water/TFA, 40 min	ESI–MS/MS	653–963	[30]
BCEOC	AANT and MANT	In acetonitrile and borate buffer (pH 9.0), at 40 °C for 10 min	On a BDS C18 reversed-phase column, gradient elution with acetonitrile/water containing ammonium formate (pH 3.7) and acetonitrile, 25 min	HPLC-FLD Ex: 333 nm, Em: 390 nm	0.398–1.258	This work

[a] The abbreviations of these reagents were shown in Section 1 NBD-F was 7-fluoro-4-nitrobenzoxadiazole.

3.5. MS identification by ESI/MS

The structure identification of NT derivatives was carried out by on-line mass spectrometry with ESI source in positive ion mode. The MS and MS/MS spectra of representative BCEOC-labeled 5-HT derivative are shown in Fig. 4(a) and (b). The cleavage mode of protonated molecular ion of 5-HT derivative is also shown in Fig. 4(c). The molecular ions (MS, $[M+H]^+$ ion) and specific fragment ions (MS/MS) of five BCEOC-labeled derivatives are listed in Table 2. All the NT derivatives produced intense molecular ion peaks at $[M+H]^+$ ions, which should be attributed to the introduction of an alkalescent nitrogen atom in BCEOC molecular core. The collision-induced dissociation spectra (MS/MS) of molecular ions (MS, $[M+H]^+$ ion) produced intense and stable fragment ions at m/z 264.1, m/z 246.1 and m/z 218.1 corresponding to the cleavages of NCH_2CH_2O–CO, NCH_2CH_2–OCO and N–CH_2CH_2OCO bonds, respectively. The selected reaction monitoring, which was based on the $[M+H]^+$ ion → m/z 264.1, m/z 246.1 and m/z 218.1 transition, was specific for BCEOC-labeled NT derivatives. There was no detectable signal from blank deionized water sample. Although other endogenous amino compounds present in real samples were presumably co-extracted and derivatized by BCEOC reagent, no interference was observed due to the highly intense molecular ions and the characteristic fragment ions at m/z 264.1, m/z 246.1 and m/z 218.1.

3.6. Method validation

3.6.1. Linearity, limit of detection (LOD) and its comparison with other methods

Under the optimum experimental conditions, 14 standard NT solutions (0.02441–200 μM) were derivatized and analyzed. The calibration graphs were established with peak area (Y) versus NT injection amounts (X, pmol). Injected amount of each NT was from 24.41 fmol to 200.0 pmol with injection volume of 10 μL, namely the linear range of each NT was 2.441–20000 nM with an 8193-fold concentration range. Linear regression equations, correlation coefficients, limits of detection and limits of quantitation (LOQs) for all NT by HPLC-FLD were shown in Table 2. All NT derivatives gave excellent linear responses over this range with correlation coefficients of 0.9997–0.9998. The LODs of BCEOC-labeled NT were calculated at S/N = 3:1 from the standard chromatogram (Fig. 2(c)) and were in the range of 0.398–1.258 nM. The LOQs of BCEOC-labeled NT were in the range of 2.42–2.46 nM (S/N = 10:1).

LODs of BCEOC–NT derivatives by ESI/MS detection were in the range of 10.5–23.2 nM (10.5 for 5-HIAA, 11.8 for 5-HT, 14.3 for DA, 22.4 for GABA, 23.2 for Glu), which were determined by injecting standard BCEOC–NT derivatives at 48.82 nM and calculated at S/N = 10:1 (R.S.D. < 4.0%, n = 3). The LODs by ESI/MS were higher about 20 times than those by HPLC-FLD. For further comparison of HPLC-FLD and ESI/MS detection, six replicative injections (10 μM,

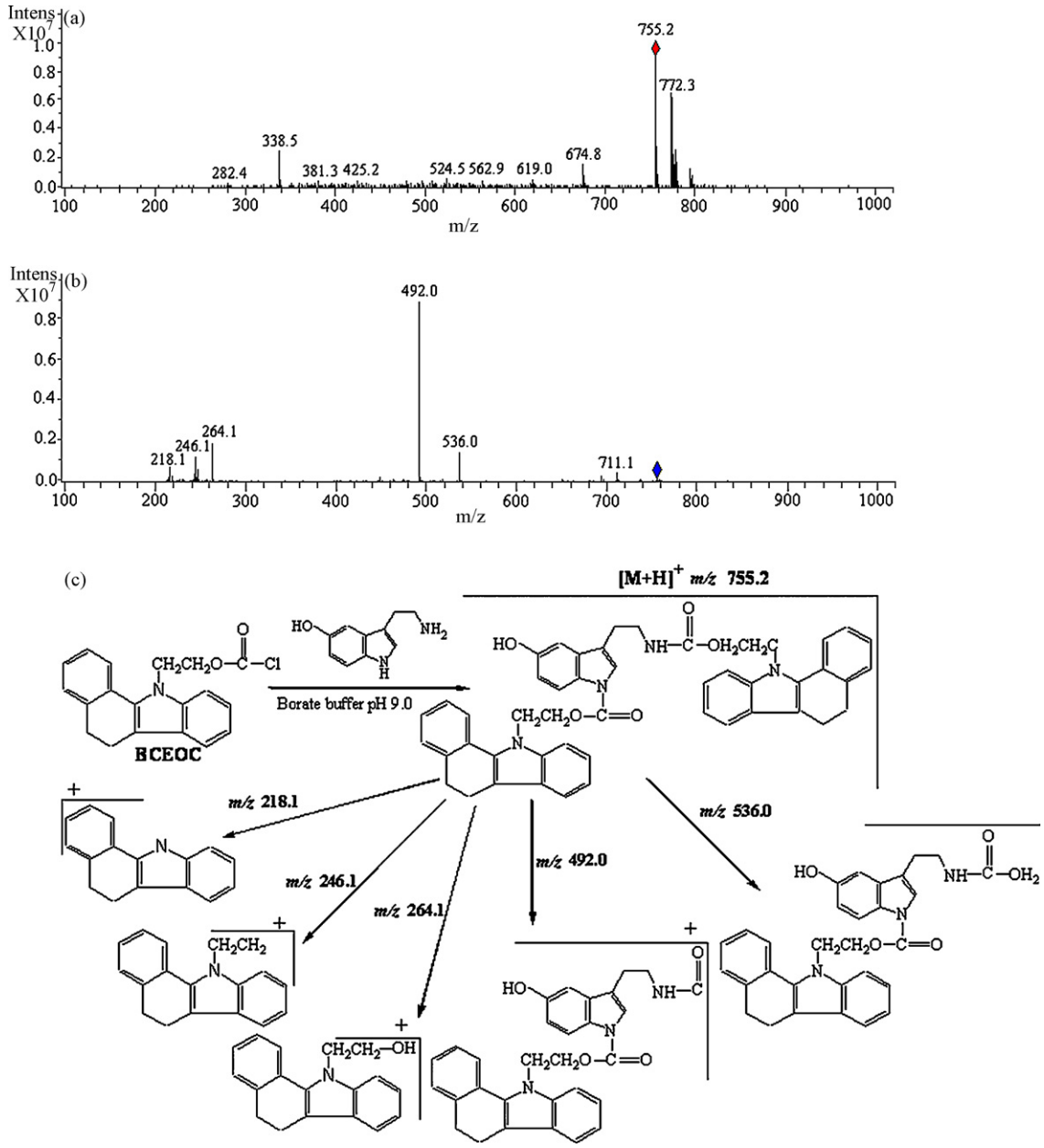

Fig. 4. MS spectra of representative BCEOC-labeled 5-HT derivative: (a) molecular ion MS, (b) MS/MS and (c) the cleavage mode of protonated molecular ion. Scanning range from 100 to 1000 amu under ESI positive ion mode; derivatives were isolated from a Hypersil BDS-C_{18} column and into the on-line mass spectrometer.

Table 2
Linearity, LODs and its comparison with reported methods, LOQs, MS and MS/MS of five BCEOC–NT derivatives by HPLC-FLD

NT	$Y = AX + B$[a]	Correlation coefficients	LODs[b] (nM)	HPLC-ECD [23,44] (nM)	HPLC–MS [31] (nM)	CE-LIFD [25] (nM)	HPLC-FRET [35] (nM)	LOQs[c] (nM)	MS $[M+H]^+$	MS/MS specific fragment ions
Glu	$Y = 61.85X + 13.52$	0.9998	0.687	No	No	10	No	2.45	437.1	418.9, 390.9, 264.1, 246.1, 218.1
GABA	$Y = 65.12X + 28.05$	0.9997	0.799	No	No	2	No	2.43	393.2	375.0, 264.1, 246.1, 218.1
DA	$Y = 37.59X + 6.764$	0.9998	1.258	2.5	42.4 (6.5 ng/mL)	80	4.65	2.42	443.1	424.2, 368.1, 307.1, 264.1, 246.1, 218.1
5-HIAA	$Y = 67.41X + 29.99$	0.9997	0.483	0.6	No	No	No	2.46	481.2	462.3, 434.9, 264.1, 246.1, 218.1
5-HT	$Y = 62.96X + 27.36$	0.9997	0.398	1.0	4.4 (0.78 ng/mL)	1	0.85	2.44	755.2	711.1, 536.0, 492.0, 264.1, 246.1, 218.1

No: not reported.

[a] Linear regression equations; Y: peak area; X: injected amount (pmol).

[b] LODs were calculated at S/N = 3:1, the injection volume was 10 μL.

[c] LOQs were obtained when S/N = 10:1, the injection volume was 10 μL.

10 μL) were analyzed. R.S.D.s of peak area were in the range of 1.95–2.86% for HPLC-FLD and 6.84–13.45% for ESI/MS detection, respectively. According to the comparison mentioned above, HPLC-FLD was better than ESI/MS detection.

In addition, LODs of our HPLC-FLD method was compared with those of reported methods (Table 2). It indicated that LODs of the proposed HPLC-FLD method were lower about 2–60 times than those of reported methods. LODs of our BCEOC method were also compared with those of other derivatization reagents in Table 1. LODs of BCEOC method were comparable with those of BA + DPE method [39] and FITC method [27], and were obviously lower than those of other seven reagents.

3.6.2. Stability

A standard solution containing of 50 pmol NT derivatives was analyzed by HPLC-FLD after being placed at room temperature for 0, 1, 2, 4, 8, 16, 24 and 48 h, respectively. R.S.D.s of peak area were 3.2%. Thus the stability of BCEOC–NT derivatives was satisfactory for chromatographic analysis.

3.6.3. Repeatability

Derivatization repeatability was examined by measuring peak area and retention time of six replicative derivatizations of mixed NT at 1.0 μM. R.S.D. values of retention time and peak area were in the range of 0.31–0.46% and 2.36–2.93%, respectively. It indicated that the BCEOC-labeling derivatization reaction was of high reproducibility.

3.6.4. Precision and accuracy

Endbrain tissue of male Wistar rat was collected from the same species as described in Section 2.6 and then was divided into two equal parts. To one part was spiked known amount NT standard which had similar concentration with rat endbrain tissue (Glu, 500 μg/g; GABA, 300 μg/g; DA, 20 μg/g; 5-HIAA, 4 μg/g; 5-HT, 4 μg/g) and to the other part was spiked nothing. Pre-treatment and derivatization of endbrain samples were the same as described in Sections 2.7 and 2.4. Six replicative analyses ($n = 6$) were performed. The precisions were expressed as R.S.D.s (%). The accuracies were expressed as recovery and calculated as follows: recovery (%) = $100(a - b)/c$, where a was the measured concentration obtained from the extracted tissue solutions which were spiked standard, b was the concentration of NT in the matrix and c was the added known concentration to the matrix. R.S.D. values of peak area and retention time were in the range of 2.56–3.85% and 0.38–0.74%, respectively. Accuracies (i.e. recoveries, %) were in the range of 91.8–105.6%. The results demonstrated that the pre-treatment and derivatization of our HPLC-FLD method were satisfactory for the quantification of NT in real samples.

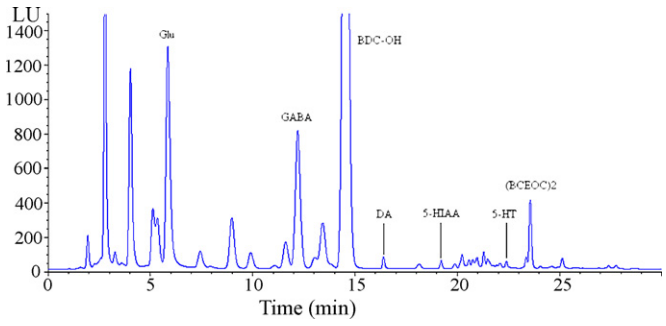

Fig. 5. Representative chromatogram of BCEOC-labeled neurotransmitters in rat endbrain tissues. Chromatographic conditions and peaks as Fig. 3.

Table 3
Concentrations and ratios of NT in rat endbrains of three groups at different states ($\overline{X} \pm S$, $n = 8$, μg/g)

NT	Group A (at quiet state without exercise)	Group B (at exercise exhaustion)	Group C (12 h after exercise exhaustion)
GLU	532.47 ± 54.9	606.41 ± 43.2[a]	586.37 ± 58.9[a]
GABA	317.05 ± 13.1	321.10 ± 24.5	281.25 ± 49.4[a]
DA	20.24 ± 1.77	19.87 ± 2.39	18.68 ± 2.41[a]
5-HIAA	3.72 ± 0.58	4.03 ± 0.67	4.32 ± 0.80[a]
5-HT	4.39 ± 0.56	5.37 ± 0.68[a]	5.94 ± 1.06[a]
5-HT/5-HIAA	1.21 ± 0.30	1.38 ± 0.35[a]	1.39 ± 0.21[a]
DA/5-HT	4.66 ± 0.59	3.76 ± 0.75[a]	3.19 ± 0.43[a]
Glu/GABA	1.68 ± 0.16	1.90 ± 0.24[a]	2.03 ± 0.39[a]

[a] Compared with Group A (the control group) with significant differences ($P < 0.05$).

3.7. Application to rat endbrain tissues analysis

Under the optimum experimental conditions mentioned above, concentrations of NT in endbrain tissues of Group A, B and C corresponding to three states were determined. The peaks were doubly identified by chromatographic retention time and on-line MS identification. Typical chromatogram of NT derivatives from rat endbrain is shown in Fig. 5 (peaks as Fig. 3). The concentrations of five NT and ratios of 5-HT/5-HIAA, DA/5-HT and Glu/GABA in endbrains were shown in Table 3. The concentration changes and the ratio changes of AANT and MANT in rat endbrains at corresponding states of three groups were in accordance with the papers reported before [11–14].

4. Concluding remarks

In this study, a new HPLC-FLD-ESI/MS method using BCEOC as pre-column derivatization reagent for the simultaneous determination of MANT and AANT in rat endbrain tissues has been developed and validated. Two most attractive advantages of this method are high detection sensitivity and convenience. All excellent characteristics allow for the development of a highly sensitive and specific method for the quantitative analysis of NT in brain tissues and other biological samples.

Acknowledgments

The authors thank Prof. Jinmao You (College of Chemical Science, Qufu Normal University, Qufu, Shandong 273165, China) for technical assistance and valuable suggestions. This work was supported by the National Natural Science Foundation of China (No. 20075016, Beijing, China).

References

[1] Z.D. Sandlin, M.S. Shou, J.G. Shackman, R.T. Kennedy, Anal. Chem. 77 (2005) 7702.
[2] S.L. Ho, A.L. Kapadi, D.B. Ramsden, A.C. Williams, Ann. Neurol. 37 (1995) 403.
[3] J.H. Kurth, M.C. Kurth, S.E. Poduslo, J.D. Schwankhaus, Ann. Neurol. 33 (1993) 368.
[4] M. Ebadi, S. Sharma, S. Shavali, H.E.L. Refaey, J. Neurosci. Res. 67 (2002) 285.
[5] J. Soto, I. Ulibarri, J.V. Jauregui, J. Ballesteros, J.J. Meana, J. Psychiatr. Res. 33 (1999) 251.
[6] W.J. Burke, S.W. Li, C.A. Schmitt, P. Xia, H.D. Chung, K.N. Gillespie, Brain Res. 816 (1999) 633.
[7] C. Bruhlmann, F. Ooms, P.A. Carrupt, B. Testa, M. Catto, F. Leonetti, C. Altomare, A. Carotti, J. Med. Chem. 44 (2001) 3195.
[8] A.J. Shaha, F. Crespib, C. Heidbrederb, J. Chromatogr. B 781 (2002) 151.
[9] S.K. Lunsford, H. Choi, J. Stinson, A. Yeary, D.D. Dionysiou, Talanta 73 (2007) 172.
[10] E. Blomstrand, D. Perrett, M. Parry-Billings, E.A. Newsholme, Acta Physiol. Scand. 136 (1989) 473.
[11] T. Hokfelt, O. Johansson, A. Ljungdahl, J.M. Lundberg, M. Schultzberg, Nature 284 (1980) 515.
[12] X.M. Zhong, H.E. Yao, Chin. J. Sports Med. (Chinese) 19 (2000) 404.

[13] J.M. Davis, S.P. Bailey, Med. Sci. Sports Exerc. 29 (1997) 45.
[14] J.M. Davis, Am. J. Clin. Nutr. 72 (2000) 573.
[15] M. Kele, R. Ohmacht, J. Chromatogr. A 730 (1996) 59.
[16] G.P. Jackman, V.J. Carson, A. Bobic, H. Skews, J. Chromatogr. 182 (1980) 277.
[17] J.P.M. Wielders, J.K. Mink, J. Chromatogr. 310 (1984) 379.
[18] M.K. Lakshmana, T.R. Raju, Anal. Biochem. 246 (1997) 166.
[19] H.J. Liu, M.C. Sanuda-Pena, J.D. Harvey-White, S. Kalra, S.A. Cohen, J. Chromatogr. A 828 (1998) 383.
[20] G. Clarke, S. O'Mahony, G. Malone, T.G. Dinan, J. Neurosci. Methods 160 (2007) 223–230.
[21] J. Peris-Vicente, J.V.G. Adelantado, M.T.D. Carbo, R.M. Castro, F.B. Reig, Talanta 68 (2006) 1648.
[22] J.A.M. McKenzie, C.J. Watson, R.D. Rostand, I. German, S.R. Witowski, R.T. Kennedy, J. Chromatogr. A 962 (2002) 105.
[23] W. Zhang, X.N. Cao, Y.F. Xie, S.Y. Ai, L.T. Jin, J.Y. Jin, J. Chromatogr. B 785 (2003) 327.
[24] P.C. Gunaratna, K.K. Cadle, C.B. Kissinger, J. Neurosci. Methods 155 (2006) 143.
[25] Z.H. Chen, J. Wu, G.B. Baker, M. Parent, N.J. Dovichi, J. Chromatogr. A 914 (2001) 293.
[26] D.M. Zhang, J.M. Zhang, W.Y. Ma, D.Y. Chen, H.W. Han, H.J. Shu, G.Q. Liu, J. Chromatogr. B 758 (2001) 277.
[27] H. Li, H. Wang, J.H. Chen, L.H. Wang, H.S. Zhang, Y. Fan, J. Chromatogr. B 788 (2003) 93.
[28] S. Parrot, V. Sauvinet, V. Riban, A. Depaulis, B. Renaud, L. Denoroy, J. Neurosci. Methods 140 (2004) 29.
[29] Y. Xiao, X.D. Yu, K. Wang, J.J. Xu, J. Huang, H.Y. Chen, Talanta 71 (2007) 2048.
[30] Y. Song, Y.Z. Feng, M.H. LeBlanc, S.L. Zhao, Y.M. Liu, Anal. Chem. 78 (2006) 8121.
[31] V. Carrera, E. Sabater, E. Vilanova, M.A. Sogorb, J. Chromatogr. B 847 (2007) 88.
[32] M.Y. Zhang, Z.A. Hughes, E.H. Kerns, Q. Lin, C.E. Beyer, J. Pharm. Biomed. 44 (2007) 586.
[33] K. Lanckmans, S. Sarre, I. Smolders, Y. Michotte, Talanta 74 (2008) 458.
[34] M.E.P. Hows, L. Lacroix, C. Heidbreder, A.J. Organ, A.J. Shah, J. Neurosci. Methods 138 (2004) 123.
[35] M. Yoshitake, H. Nohta, H. Yoshida, T. Yoshitake, K. Todoroki, M. Yamaguchi, Anal. Chem. 78 (2006) 920.
[36] M. Vlčková, M.A. Schwarz, J. Chromatogr. A 1142 (2007) 214.
[37] H. Yu, F.-Y. He, Y. Lu, Y.-L. Hu, H.-Y. Zhong, X.-H. Xia, Talanta 75 (2008) 43.
[38] J.L. Adcock, N.W. Barnett, J.W. Costin, P.S. Francis, S.W. Lewis, Talanta 67 (2005) 585.
[39] T. Yoshitake, J. Kehr, S. Yoshitake, K. Fujino, H. Nohta, M. Yamaguchi, J. Chromatogr. B 807 (2004) 177.
[40] A.V. Hemelrijck, S. Sarre, I. Smolders, Y. Michotte, J. Neurosci. Methods 144 (2005) 63.
[41] M.V. Naval, M.P. Gómez-Serranillos, M.E. Carretero, C.D. Arce, J. Chromatogr. A 1121 (2006) 242.
[42] X.E. Zhao, J.M. You, Y.R. Suo, J. Liq. Chromatogr. Related Technol. 30 (2007) 1963.
[43] J.M. You, Y.F. Ming, Y.W. Shi, X.E. Zhao, Y.R. Suo, H.L. Wang, Y.L. Li, J. Sun, Talanta 68 (2005) 448.
[44] W. Zhang, F.L. Wan, Y.F. Xie, J. Gu, J. Wang, K. Yamamoto, L.T. Jin, Anal. Chim. Acta 512 (2004) 207.

Talanta 76 (2008) 528–532

Contents lists available at ScienceDirect

Talanta

journal homepage: www.elsevier.com/locate/talanta

Optimization of Pb(II) biosorption by *Robinia* tree leaves using statistical design of experiments

Javad Zolgharnein*, Ali Shahmoradi, Mohammad Reza Sangi

Department of Chemistry, Faculty of Science, Arak University, 38156-876 Arak, Iran

ARTICLE INFO

Article history:
Received 17 December 2007
Received in revised form 19 March 2008
Accepted 22 March 2008
Available online 8 April 2008

Keywords:
Biosorption
Pb(II)
Robinia tree leaves
Doehlert design

ABSTRACT

The present study introduces *Robinia* tree leaves as a novel and efficient biosorbent for removing Pb(II) from aqueous solutions. In order to reduce the large number of experiments and find the highest removal efficiency of Pb(II), a set of full 2^3 factorial design with two blocks were performed in duplicate (16 experiments). In all experiments, the contact time was fixed at 25 min. The main interaction effects of the three factors including sorbent mass, pH and initial concentration of metal-ion were considered. By using Student's *t*-test and analysis of variances (ANOVA), the main factors, which had the highest effect on the removal process, were identified. Twenty-six experiments were designed according to Doehlert response surface design to obtain a mathematical model describing functional relationship between response and main independent variables. The most suitable regression model, that fitted the experimental data extremely well, was chosen according to the lack-of-fit-test and adjusted R^2 value. Finally, after checking for possible outliers, the optimum conditions for maximum removal of Pb(II) from aqueous solution were obtained. The best conditions were calculated to be as: initial concentration of Pb(II) = 40 mg L^{-1}, pH 4.6 and concentration of sorbet equal to 27.3 g L^{-1}.

1. Introduction

Industrial wastes and fertilizers can add excessive amount of heavy metals to the environment. Heavy metals even at very low concentrations are highly toxic, and pose a serious threat to biota and the environment [1]. Among the heavy metals lead has the most damaging effects on human health. It can enter a human body through uptake of food (65%), water (20%) and air (15%) [2]. Continuous absorption of lead may cause serious injuries to health such as encephalopathy, kidney damage and several others [3,4]. Several methods for the removal of toxic metals from wastewaters have been introduced and tried out [5]. Techno-economic considerations have restricted the wide scale application of these methods [6,7]. However, application of biosorption has been proved to be an effective way to heavy metal ions pollutions [1,3–6]. Successful metal biosorption, with a variety of biological materials including, microalgae, seaweeds, bacteria, fungi, crop residues, and papaya wood have been reported [8–10]. This study verifies a new biomass as metal sorbent, and demonstrates its potential for efficient removal of Pb(II) from aqueous solution. *Robinia* tree leaves are in great supply, inexpensive and easily available in countries such as Iran. These leaves have no commercial usage and are not eaten by livestock. Factors affecting metal ions uptake by a sorbent in a batch system include sorbent mass (*s*), acidity of medium (pH), metal-ion and the sorbent contact time (*t*), initial metal-ion concentration (*m*), speed of shaking, etc. [10]. Thus several factors should be optimized. Here the major concern is the large number of experimental runs. To resolve this problem, some variables can be arbitrarily fixed. The application of statistical design especially, Dohelert design for optimization of biosorption process has comparatively rarely been reported in literatures than other approaches such as industrial process or analytical research [10–13]. This study tries to develop an efficient method for achieving maximum removal of Pb(II) ion in aqueous solutions. For this purpose, by using Dohelert design and response surface methodology (RSM) an optimized response model was proposed [12–15].

2. Experimental

2.1. Materials

2.1.1. Biosorbent materials

The *Robinia* tree leaves were gathered from twigs into clean plastic bags, washed with doubly distilled water and dried on a clean table. The dried leaves were ground and sieved to 40–50 mesh, then stored into plastic bag.

* Corresponding author. Tel.: +98 861 4173400; fax: +98 861 4173406.
E-mail address: J-zolgharnein@araku.ac.ir (J. Zolgharnein).

0039-9140/$ – see front matter © 2008 Elsevier B.V. All rights reserved.
doi:10.1016/j.talanta.2008.03.039

Table 1
Factors and levels used in the factorial design

Factor	Low	High
Biosorbent mass (g)	0.1	0.3
Initial pH	2	5
Pb(II) initial concentration[a] ($mg\,L^{-1}$)	40	200

[a] A sample volume of 10 mL was used in either case.

2.1.2. Metal solution

The stock solution of Pb(II) was prepared by dissolving appropriate quantities of $Pb(NO_3)_2$ salt in 5% (v/v) HNO_3. All the chemicals were of analytical grade and obtained from Merck. Doubly distilled water was used throughout. Ten milliliters of Pb(II) solution was poured into 100 mL Erlenmeyer. A known amount of dried biomass was added to each sample solution. The pH of solution was adjusted with HNO_3 or NaOH before addition of biosorbent. Fresh dilutions were made for each study. Based on pervious experiences, the biosorption process is very fast in its earlier stages and reaches its equilibrium state at about 15–25 min and the following passage of time has no or marginal effect on removal efficiency improvement [16,17]. So, the contact time was chosen to be 25 min. Samples were filtered through 0.45 μm Whatman filter paper. The factors and levels used in factorial design are presented in Table 1.

2.2. Metal analysis

The concentration of Pb(II), remaining in solution after biosorption was determined by using PerkinElmer 2380 atomic absorption spectrophotometer [7]. Instrumental conditions were adjusted as recommended by manufacturer applying a current 10.0 mA. The sensitive wavelength for lead at 283.3 nm was used with slit bandwidth of 0.7 nm.

2.2.1. Removal efficiency

Percent of removal efficiency is defined as

$$R = \frac{(m-f)}{m} \times 100 \quad (1)$$

m and f stand for the initial and final concentration of Pb(II) in the solution, respectively.

2.3. Optimization

2.3.1. Optimization design

The optimization procedure of any analytical assay can be performed in two different ways: univariate and multivariate. In first approach, the optimum values for all of the variables are found one at a time. This method of optimization requires greater amounts of reagent and time to be accomplished. In addition, possible interactions among variables are not considered. In contrast, the multivariate optimization methodology considers the possible interactions and is also faster, more effective and economical. Simultaneous optimization of several variables is also possible by this approach [11–15]. Full factorial design is one of the most frequently employed chemometrics technique used for preliminary evaluation of significant variables [14,15,18]. After identification of significant factor(s), response surface methodology (RSM) is used for closer inspection of the relationship between the identified significant factors and the response variable. RSM can be done by several models including central composite design (CCD) [12–15], Box-Behnken [19,20] and Doehlert design [12,13,21,22]. The Doehlert design is a less known but very useful type of design offering advantages with respect to the other two ones [13,21]. It describes a spherical experimental domain but with less points than CCD and emphasizes uniformly space filling. Apart from its uniformity, the most important advantage is its sequentially potential. One can reuse experiments when the boundaries were not well chosen at first, provided that the old and new considered boundaries are adjacent [15]. Thus, Doehlert matrix design was chosen as the multilevel optimization strategy to have a forecast of high quality. According to it, the total number of treatment combinations was $2^k + 2k + n_0$, where k is the number of independent variables and n_0 is the number of replications of central point [12,23,24]. In Doehelrt design, the number of the levels is not the same for all variables. Generally, the levels are assigned to the factors according to their significance in such a way that the highest level is for the variable with greatest effect and lowest level for the factor of least effect [15]. In this way, the most valuable information of the system under study is obtained. Values in Doehlert design are given in coded units and should be decoded to give the real values. Decoding was performed according to the following equation:

$$z_i^* = z_i^{\max} - \frac{\left(x_i^{\max} - x_i^*\right)\left(z_i^{\max} - z_i^{\min}\right)}{2x_i^{\max}} \quad (2)$$

where x_i and z_i are the values of the factors of interest in coded and uncoded (real) units with the maximum and minimum value represented by $x_i^{\max}$ and $x_i^{\min}(x_i^{\max} = -x_i^{\min})$ for coded form and $z_i^{\max}$ and $z_i^{\min}$ for real form, respectively [14].

2.3.2. Regression analysis

Determination of regression equation which is a mathematical relation between dependent factor(s) and independent variables is the most important aim of analysis. After performing experiments required for optimization, one needs to do a regression analysis to find the desired function. Here factorial optimization and algebraic calculations were done by using MINITAB Version 14 for windows and MAPLE Version 10, respectively.

2.3.3. Model criticism and selection

A statistical method such as regression analysis is based on certain assumptions. The accuracy of the analysis and the results obtained depends critically on the validity of these assumptions. Regression analysis is viewed as an iterative process, in which the outputs are used to diagnose, validate, criticize and possibly modify input data. The process is repeated until a satisfactory result has been obtained. A good model satisfies the regression assumptions well and its lack of fit is not significant at certain confidence level [25].

3. Results and discussion

3.1. Factorial design for variable screening

To identify effective factors and interactions, a 2^3 full factorial design was performed [18,26]. The results are listed in Table 2. All the experiments were done in duplicate and random order to evaluate pure error of the method and to minimize the effect of possible uncontrolled variable(s), respectively. The blocks were performed on two different working days.

The obtained results through ANOVA showed that all the main factors, pH, initial concentration of Pb(II) (m), amount of sorbent (s) and their interactions were statistically significant ($P < 0.05$), while blocks were not effective ($P > 0.05$). This is a very important finding, since biosorption was not influenced by the day of performing the measurement and this shows robustness of biosorption process. The effects, regression coefficients, standard errors, T and P are shown in Table 3. The increase of the removal of metal-ion as the pH increases can be explained based on decreases in competition

Table 2
2^3 full factorial design results

StdOrder	RunOrder	CenterPt	Blocks	pH	m (mg L^{-1})	s (gr)	R
6	1	1	1	5	40	0.3	96.92
5	2	1	1	2	40	0.3	95.47
1	3	1	1	2	40	0.1	74.82
7	4	1	1	2	200	0.3	90
4	5	1	1	5	200	0.1	81.17
8	6	1	1	5	200	0.3	92.7
2	7	1	1	5	40	0.1	95
3	8	1	1	2	200	0.1	50.33
13	9	1	2	2	40	0.3	95.6
16	10	1	2	5	200	0.3	92.7
9	11	1	2	2	40	0.1	74.7
11	12	1	2	2	200	0.1	50.5
10	13	1	2	5	40	0.1	95
14	14	1	2	5	40	0.3	97
15	15	1	2	2	200	0.3	90.2
12	16	1	2	5	200	0.1	81.17

Variables are in uncoded units.

Table 3
Statistical parameters for 2^3 designs

Term	Effect	Coef	SE Coef	T	P
Constant		84.58	0.01892	4471.36	0.000
Block		−0.029	0.01892	−1.52	0.172
pH	13.755	6.878	0.01892	363.58	0.000
m	−11.968	−5.984	0.01892	−316.33	0.000
s	18.488	9.244	0.01892	488.68	0.000
pH × m	2.923	1.461	0.01892	77.25	0.000
pH × s	−11.743	−5.871	0.01892	−310.39	0.000
s × m	7.12	3.56	0.01892	188.2	0.000
pH × m × s	−2.335	−1.168	0.01892	−61.72	0.000

between protons and metal ions for the same functional groups. It also decreases the positive surface charge resulting in a lower electrostatic repulsion between the surface of biomass and metal ions [27]. Fig. 1 illustrates the interactions between main factors and reveals that there is an interaction between s and pH, s and m, pH and m. The presence of interaction means, the factors may affect the response interactively and not in an independent way, i.e., their combined effect is greater or less than that expected for the straight addition of the effects [28,29]. These synergistic effects would not be detected in a univariate optimization of the system. The unparallel effect lines for pH × s and m × s interaction illustrates that there is rather a strong two-way interaction between pH × s and m × s. Meanwhile, the interaction between pH and m is relatively weak, because the effect lines are nearly parallel. It also can be concluded

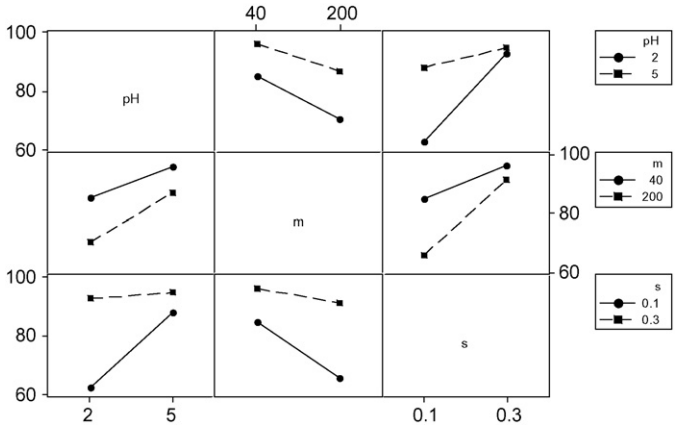

Fig. 1. Interaction effects plot. The unit of the parameters is as the main effect plot.

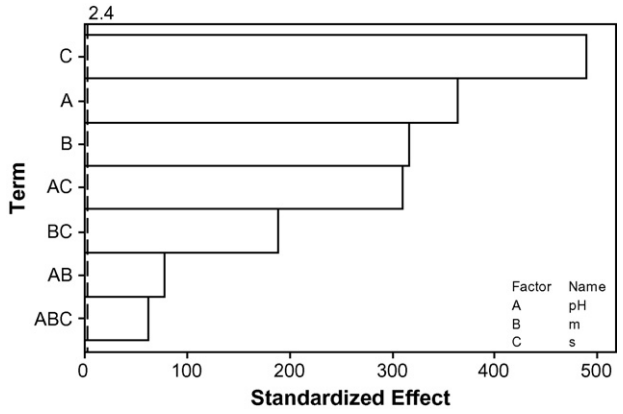

Fig. 2. Pareto chart of the main effects and related interactions. The vertical dashed line indicates the 95% confidence interval.

when sorbent mass is in its lower level; increasing the pH of solution has greater effect. This is a reasonable result, because a lower weight of sorbent implies less number of biosorption active sites and in this case proton–metal-ion competition for occupation of active sites becomes more critical. It can also be concluded when initial metal-ion concentration is high, increasing sorbent mass has grater effect. This result is also justifiable, because in the case of low initial metal-ion concentration, even low mass of sorbent can remove it sufficiently and therefore increasing the sorbent mass has marginal positive effect. The evaluation of the effect of each variable on the removal efficiency may also be verified from the Pareto chart (Fig. 2). For 95% confidence level and 8 d.f., the t-value for two-sided test is equal to 2.4. The vertical dashed line indicates minimum statistically significant effect magnitude for a 95% confidence level. Horizontal column lengths are proportional to Student's t-test values for each effect. Any effect or interaction that exceeds vertical line is considered operative. The significance of the factors can also be confirmed from the normal probability plot displayed in Fig. 3. When the effects present a large deviation from the normal distribution, they probably are significant and are obviously not related to experimental random errors. In this sense, all the points deviated from the straight line on the probability plot, are the same as those introduced as significant factors by Pareto chart, confirming the results obtained from it. The normal probability method is especially useful for analyzing the effects in experiment without replicates [14].

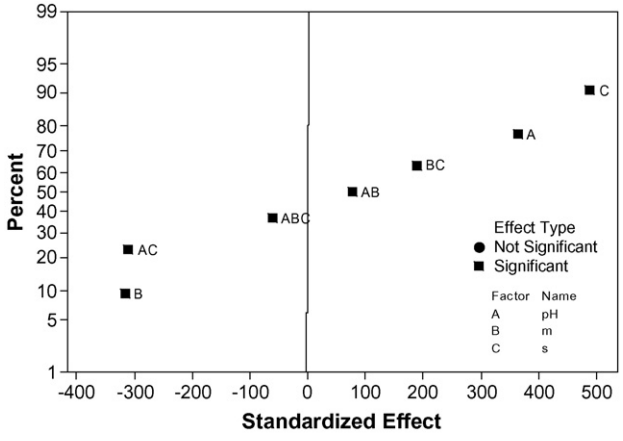

Fig. 3. Normal probability plot for standardized effects.

Table 4
Doehlert matrix response surface design and results obtained for Pb(II) biosorption using *Robinia* tree leaves

Experiment	Coded values			Real values			%R		Predicted R	Residuals	
	X_1	X_2	X_3	pH	s (gr)	m (mg L^{-1})	Rep[a]. 1	Rep. 2		Rep. 1	Rep. 2
1	0	0	0	3.5	0.2	120	90.67	91.05	90.86	−0.19	0.19
2	1	0	0	5	0.2	120	92.21	91.18	91.69	0.52	−0.52
3	0.5	0.866	0	4.25	0.3	120	93.1	92.33	92.73	0.37	−0.37
4	0.5	0.289	0.816	4.25	0.233	200	87.61	88.16	87.87	−0.26	0.29
5	−1	0	0	2	0.2	120	91.46	91.46	91.46	0	0
6	−0.5	−0.866	0	2.75	0.1	120	84.38	83.87	84.11	0.27	−0.24
7	−0.5	−0.289	−0.816	2.75	0.167	40	94.3	94.5	94.41	−0.11	0.09
8	0.5	−0.866	0	4.25	0.1	120	87.46	86.69	87.06	0.4	−0.37
9	0.5	−0.289	−0.816	4.25	0.167	40	95.08	94.69	94.9	0.18	−0.21
10	0	0.577	−0.816	3.5	0.267	40	95.86	95.47	95.64	0.22	−0.17
11	−0.5	0.866	0	2.75	0.3	120	91.46	91.59	91.54	−0.08	0.05
12	−0.5	0.289	0.816	2.75	0.233	200	85.89	86.13	86	−0.11	0.13
13	0	−0.577	0.816	3.5	0.133	200	81.59	81.13	81.38	0.21	−0.25

[a] Replicate.

Table 5
Analysis of variance for suggested third-order model

Source	d.f.	SS	MS	F	P
Regression	11	457.72	41.611	324.35	0.000
Residual error	14	1.796	0.128		
Lack of fit	1	0.004	0.004	0.03	0.867
Pure error	13	1.792	0.138		
Total	25	459.516			

3.2. Final optimization using Doehlert design

pH, s and m all were determined as effective factors and should be optimized. At this point, they were optimized according to Doehlert matrix. Seven levels were used for s, since this factor presented higher effect than the other two ones. pH and m were given five and three levels, respectively according to their effects importance (Table 4).

3.3. Finding the best model using regression analysis

An appropriate model can be expressed as

$$R = 135 - 33.9\,\mathrm{pH} - 0.271\,m + 26.4\,s + 20.8\,\mathrm{pH}\,s + 0.0527\,\mathrm{pH}\,m + 0.950\,s\,m - 0.222\,\mathrm{pH}\,s\,m - 218\,s^2 + 8.42\,\mathrm{pH}^2 - 0.771\,\mathrm{pH}^3 - 2\times10^{-7}\,m^3 \quad (4)$$

R represents percent of removal efficiency.

ANOVA test results are illustrated in Table 5. The estimated effects and coefficients for this model are listed in Table 6. The results showed that the lack of fit is not significant ($P > 0.05$) and regression is meaningful ($P < 0.05$). Goodness-of-fit for this model was also evaluated by the coefficient of determination. In this case, in fact, fitting is very well ($R^2 = 0.993$) and only 0.7% of total variance was not explained by the model. The high value of adjusted regression coefficient (0.997) is also an indication for high significance of the proposed model [30]. The residuals also had to be examined for normal distribution. Anderson–Darling test is a powerful statistical means that generates normal probability plot and performs a hypothesis test to examine whether the observations follow a normal distribution.

Table 6
Estimated effects and coefficients for suggested third-order model

Predictor	Coef	SE Coef	T	P
Constant	134.97	11.04	12.22	0.000
pH	−33.915	5.884	−5.76	0.000
m	−0.27081	0.06352	−4.26	0.001
s	26.4	39.44	0.67	0.514
pH × s	20.8	10.86	1.91	0.076
pH × m	0.05269	0.01803	2.92	0.011
s × m	0.9501	0.3144	3.02	0.009
pH × s × m	−0.22224	0.08944	−2.48	0.026
s^2	−217.94	23.26	−9.37	0.000
pH^2	8.418	1.294	6.51	0.000
pH^3	−0.7714	0.1225	−6.29	0.000
m^3	-2×10^{-7}	9×10^{-8}	−2.3	0.038

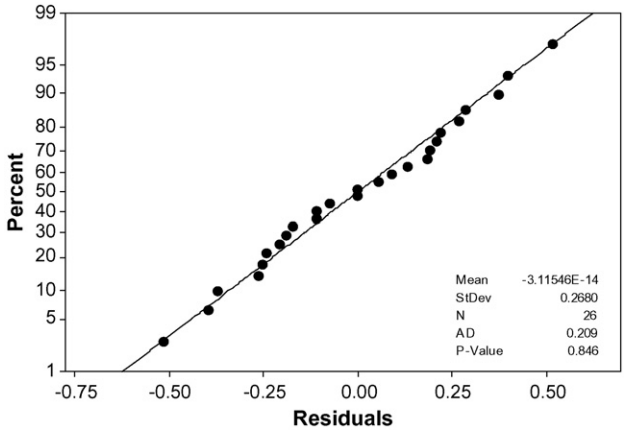

Fig. 4. Normal probability plot for residuals.

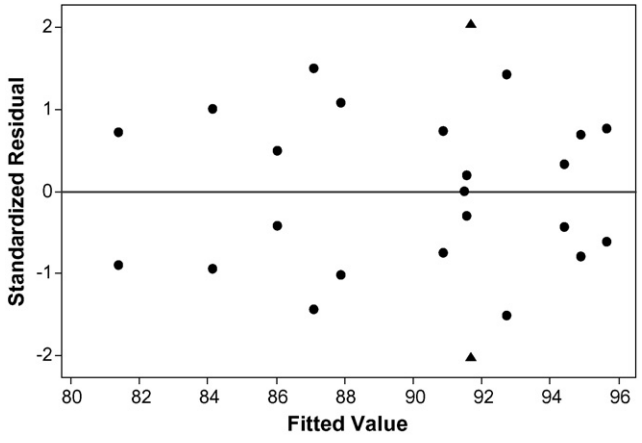

Fig. 5. Standardized residuals vs. plotted fitted values.

The result obtained by Anderson–Darling test for residuals is shown in Fig. 4. The P value for test ($0.846 > 0.05$) shows that the null hypothesis could not be rejected and it concludes that residuals follow the normal distribution. Plot of standardized residuals vs. predicted values indicates the possible existence of outliers (Fig. 5). If a point lies far from the majority of points, it may be an outlier. It is important to identify the outliers, because they can significantly influence the model, providing potentially misleading or incorrect results. Except for two points (marked with triangle) all other points were found to fall in the range of +1.5 to −1.5. Points corresponding to these runs were slightly out of this range (standardized residual = 2). However, elimination of these points did not reduce lack of fit but increased it. This shows that they were not really outliers. Application of Cochran's test for variances gives 0.296 with $n = 2$ and $k = 13$, which is smaller than Cochran's critical value of 0.515 and emphasizes the homoscedasticity numerically [15]. All these verify the fact that the model does not violate regression assumptions.

3.4. Model validation

A model is valid when it has good predictability. The low value for PRESS (6.45832) and high value for predicted R^2 (98.59%) showed the high predictive ability of the model.

By using optimization toolbox in MAPLE, the best conditions for suggested model was found to be 97.3% as maximum removal efficiency in pH = 4.6, $s = 0.27$ gr and $m = 40\ \mathrm{mg\ L^{-1}}$. Replicating the experiment twice under this condition led to an average of 96.8 ± 1.2 at 95% confidence level for removal percent of Pb(II), which is in very good agreement with the predicted value. This shows that the model has high prediction ability.

3.5. Capacity of sorbent and effect of other ions

The maximum capacity of sorbent was found to be $144.1\ \mathrm{mg\ g^{-1}}$. Interference effects due to Mg^{2+}, Ca^{2+}, Na^{+} and K^{+} at 10-fold excess were also studied. It was found that under these conditions, there is no significant adverse effect on removal efficiency. This can be attributed to high affinity of this sorbent to Pb(II) [16,17].

3.6. Application

The major interest of this study was to show the feasibility of biosorption of Pb(II) by *Robina* tree leaves through a typical mathematical model [12]. Since the concentration of Pb(II) in various industrial wastes varies drastically, thus for each case, it is recommended that researcher treat each problem individually and find its appropriate model.

4. Conclusions

Factorial experimental design is time saving and economic, because only significant effects are optimized and unnecessary experiments avoided. Interactions among the factors are also considered. It was clearly shown the feasibility of biosorptive process as a low cost and effective method for removal of Pb(II) from aqueous solutions by *Robinia* tree leaves. The calculated optimum conditions for this process were in good agreement with experimental results.

Acknowledgement

The authors would like to thank Dr. H. Yazdani for final editing of the manuscript.

References

[1] B. Volesky, Hydrometallurgy 59 (2001) 203.
[2] http://www.lenntech.com/Periodic-chart-elements/Pb-en.htm.
[3] T.W. Clarkson, L. Friberg, G.F. Nordberg, P.R. Sager, Biological Monitoring of Toxic Metals, Kluwer Academic Publishers, New York, 1998.
[4] W.N.L. dos Santos, C.M.M. dos Santos, J.L.O. Costa, H.M.C. Andrade, S.L.C. Ferreira, Microchem. J. 77 (2004) 123.
[5] B. Volesky, S. Schiewer, in: M.C. Flickinger, S.W. Drew (Eds.), Encyclopedia of Bioprocess-Engineering, Wiley, New York, 1999.
[6] A. Saeed, M.W. Akhtar, M. Iqbal, Sep. Purif. Technol. 45 (2005) 25.
[7] M.D.A. Korn, J.B. de Andrade, D.S. de Jesus, V.A. Lemos, M.L.S.F. Bandeira, W.N.L. dos Santos, M.A. Bezerra, F.A.C. Amorim, A.S. Souza, S.L.C. Ferreira, Talanta 69 (2006) 16.
[8] S. Schiewer, B. Volesky, in: D.R. Lovely (Ed.), Environmental Microbe–Metal Interactions, ASM Press, Washington, DC, 2000 (Chapter 14).
[9] A. Saeed, M. Iqbal, M.W. Akhtar, Pak. J. Sci. Ind. Res. 45 (2002) 205.
[10] E.C. Lima, B. Royer, J.C.P. Vaghetti, J.L. Brasil, N.M. Simon, A.A. dos Santos Jr., F.A. Pavan, S.L.P. Dias, E.V. Benvenutti, E.A. da Silva, J. Hazard. Mater. 140 (2007) 211.
[11] L.A. Portugal, H.S. Ferreira, W.N.L. dos Santos, S.L.C. Ferreira, Microchem. J. 8 (2007) 77.
[12] P. Vanloot, J.L. Boudenne, L. Vassalo, M. Sergent, B. Coulomb, Talanta 73 (2007) 237.
[13] S.L.C. Ferreira, W.N.L. dos Santos, C.M. Quintella, B.B. Neto, J.M. Bosque-Sendra, Talanta 63 (2004) 1061.
[14] D.C. Montgomery, Design and Analysis of Experiments, fifth edn., Wiley, New York, 2001.
[15] D.L. Massart, B.G.M. Vandeginste, L.M.C. Buydens, S. DE Jong, P.J. Lewi, J. Smeyers Verbeke, Handbook of Chemometrics and Qualimetrics, Part A, Elsevier, Amsterdam, 1997.
[16] M.R. Sangi, A. Shahmoradi, J. Zolgharnein, G. Azimi, M. Ghorbandoost, J. Hazard. Mater., in press.
[17] M.R. Sangi, A. Shahmoradi, M. Ghorbandoost, J. Zolgharnein, G. Azimi, Desalination, in press.
[18] M. Soylak, I. Narin, M.D.A. Bezerra, S.L.C. Ferreira, Talanta 65 (2005) 895.
[19] G.E.P. Box, W.G. Hunterand, J.S. Hunter, Statistics for Experimenters, Wiley, New York, 1978.
[20] S.L.C. Ferreira, R.E. Bruns, H.S. Ferreira, G.D. Matos, J.M. David, G.C. Brandao, E.G.P. da Silva, L.A. Portugal, P.S. dos Reis, A.S. Souza, W.N.L. dos Santos, Anal. Chim. Acta 597 (2007) 179.
[21] A.F. Barbosa, M.G. Segatelli, A.C. Pereira, A.D.S. Santos, L.T. Kubota, P.O. Luccas, C.R.T. Tarley, Talanta 71 (2007) 1512.
[22] A. Gustavo González, D. González-Arjona, Talanta 49 (1999) 433.
[23] F. Hellal, M. Dachraoui, Talanta 63 (2004) 1089.
[24] R.E. Santelli, M. de Almeida Bezerra, O.D. de SantAna, R.J. Cassella, S.L.C. Ferreira, Talanta 68 (2006) 1083.
[25] S. Chatterjee, A. Hadi, Regression Analysis by Example, fourth edn., John Wiley & Sons, Inc., Hoboken, New Jersey, 2006.
[26] F.A. Pavan, Y. Gushikem, A.C. Mazzocato, S.L.P. Dias, E.C. Lima, Dyes Pigments 72 (2007) 256.
[27] Z. Reddad, C. Gerente, Y. Anders, P. LeCloires, Environ. Sci. Technol. 36 (2002) 2067.
[28] R.L. Anderson, Practical Statistics for Analytical Chemists, Van Nostrand Reinhold, New York, 1987.
[29] J.N. Miller, J.C. Miller, Statistics and Chemometrics for Analytical Chemistry, fourth edn., Dorset Press, Dorchester, 2000.
[30] M. Elibol, Process Biochem. 38 (2002) 667.